Doctoral Thesis

From the Department of Pharmacology

University of the Basque Country

The endocannabinoid system in experimental models of Alzheimer´s disease

ALBERTO LLORENTE OVEJERO

2017

Alberto Llorente received a predoctoral fellowship from the regional Basque Government (GV/EJ) for a period of four years beginning in January 2012. This work was supported by the Departments of Economic Development (Elkartek KK-2016/00045) and Education (IT584-13) of the Basque Government. Technical and human support provided by General Research Services SGIker [University of the Basque Country (UPV/EHU), Ministry of Economy and Competitiveness (MINECO), Basque Government, European Regional Development Fund (ERDF) and European Social Fund (ESF)] is gratefully acknowledged.

A mi familia

Este trabajo ha sido realizado en el Departamento de Farmacología de la Universidad del País Vasco y es fruto de la ayuda y colaboración de muchas personas. Quisiera en las siguientes líneas mostrar mi gratitud a todas ellas esperando no olvidarme de nadie.

Quiero dar las gracias en primer lugar a mi director de tesis, el Dr. Rafael Rodríguez Puertas, por abrirme las puertas de su laboratorio, acogerme en su grupo de investigación y ofrecerme la oportunidad de participar en diversos proyectos, de asistir a multitud de congresos y de colaborar y aprender junto a un maravilloso grupo de compañeros de los que hablaré más adelante. Gracias Rafa por confiar en mí desde el principio y por darme la autonomía suficiente que me ha permitido adquirir una parte fundamental de mi formación científica.

También quisiera destacar la ayuda que me ha brindado la Dra. María Teresa Giralt Rué, ejemplo insuperable de tenacidad, profesionalidad y, sobre todo, compañerismo. He pasado por momentos difíciles en esta etapa de formación y, gracias a su apoyo, me ha resultado todo mucho más fácil cuando más cuesta arriba se ponía. Hace casi seis años que entré en este laboratorio, y conviene recordar aquí que cuando yo te pregunté por un grupo al que poderme incorporar no dudaste en presentarme al grupo de Neuroquímica y Neurodegeneración. Fue todo un acierto, como todo lo que haces a diario. La carrera investigadora que comienzo nunca habría sido igual si no te hubiera conocido. No lo olvidaré nunca. Gracias Teresa.

Aprovecho estas líneas para agradecer la labor de mis compañeros, los que con su esfuerzo diario contribuyen a completar los objetivos y a obtener resultados sensacionales. Al Dr. Iván Manuel por los valiosos consejos que me ha dado, por ese fino humor que nos hace empezar cada día con una sonrisa y sobre todo, por su solidaridad con el grupo y por estar siempre disponible para lo que haya hecho falta. A la Dra. Laura Lombardero por facilitarme la incorporación al grupo, por el valioso tiempo empleado en enseñarme las técnicas que han permitido la elaboración del presente trabajo y por acordarte siempre de todos nosotros. A la Dra. Estíbaliz González de San Román por ese optimismo que consigue contagiar al grupo, por su autenticidad y por ser un ejemplo de profesionalidad para todos. A Marta por ofrecerme siempre su ayuda, por estar hombro con hombro durante interminables días de experimentación y por habernos mantenido alimentados en esos extenuantes días. A la Dra. María Dolores García, con quien empecé este camino, cuyo esfuerzo diario y capacidad de superación ha supuesto un ejemplo en el que fijarme y, finalmente, a mi compañero Jonatan por sus conocimientos en lipidómica que han contribuido a la realización de este trabajo y sobre todo por contribuir al buen clima en el grupo. Gracias a todo el equipo por el apoyo recibido, este trabajo también es vuestro.

También quisiera agradecer a la Dra. Lydia Giménez Llort, colaboradora habitual y muy querida por nuestro grupo, por los ratones 3xTg-AD proporcionados y por contribuir en el análisis de los resultados. Y al personal del BIC de Bordeaux por hacer que mi estancia allí fuera inolvidable, Jonas, Ettiene, Melina y al Dr. Marc Landry. Gracias por supuesto a todos aquellos que han pasado por el laboratorio y de alguna manera han contribuido a la realización de este trabajo. Incluyo aquí al Dr. Gabriel Barreda y a Tarson y, a todos los técnicos que han hecho más fácil nuestro día a día. Tampoco me quiero olvidar de las personas de la Facultad que me han dado ánimos cada vez que han tenido ocasión, Cristina Miguélez, Teresa, Igor, Cristina Bruzos, Pilar, Irrintzi, Luisa, Isabel. Agradecer también la asistencia técnica proporcionada por Ricardo y Alex a través de SGIKER, a la Dra. Susana Mato y al Dr. Carlos Matute por los anticuerpos y las muestras proporcionados, y al profesor Juan Bilbao por sus valiosos consejos sobre análisis estadísticos.

Fuera del ámbito científico, debo comenzar agradeciendo a Cris, mi compañera de viaje, por su apoyo constante y por mostrarme el lado bueno de las cosas en los momentos de flaqueza. Gracias por tu generosidad y paciencia en esta dura etapa. Te quiero y te debo mucho. Gracias a todos mis amigos por esos momentos de ocio que han ayudado a aligerar la mochila, especialmente a Ana, Héctor, Álvaro, Silvia, Tito y Txema por vuestro cariño, y a mis primos uruguayos de los que nunca me faltó su apoyo. Finalmente, quisiera mostrar un especial agradecimiento a toda mi familia de la que me siento enormemente orgulloso. A mis padres, a mi hermano y a mi amama, y por supuesto a mis primos y tíos, por ofrecerme siempre vuestro apoyo, por confiar en mí y por todo lo demás.

Index

Introduction

1. Central cholinergic neurotransmission

The presence of cholinergic transmission in the central nervous system (CNS) was hypothesized by Henry Dale from his demonstration of the evanescence of the action of acetylcholine (ACh) by the action of the acetylcholinesterase (AChE) (EC-3.1.1.7) in the CNS (Dale, 1937). Nevertheless, Otto Loewi in 1921 had demonstrated the existence of cardiac neurotransmission by a substance that he called "vagusstoff", and which was later identified as ACh. These findings led Felderg (1945) to postulate that “the central nervous system is built of cholinergic and non-cholinergic neurons”, distributed in a particular and organized fashion. Further studies demonstrated the presence of ACh and choline acetyltransferase (ChAT) (EC-2.3.1.6), ACh synthesis and release in the CNS, and the central and peripheral effects of muscarinic agonists and anticholinesterases (Stedman and Stedman, 1937; Feldberg, 1945, 1950; Karczmar, 1967; Barker et al., 1972).

1.1. Acetylcholine metabolism

The main components of ACh synthesis are acetyl coenzyme A (acetyl-CoA), choline (Ch), Ch uptake system and ChAT whose gene is located in human chromosome 10q11.23 (Figure 1). ChAT is the enzime responsible for the synthesis of ACh from acetyl-CoA and choline in the neuronal perikarya. This reaction is reversible, but under conditions of equilibrium, the concentrations of ACh and CoA are higher than the concentrations of choline and acetyl-CoA (reviewed in Blusztajn and Wurtman, 1983). At physiological concentrations of acetyl-CoA and Ch, the activity of ChAT is much lower than its maximal rate of activity at saturation concentrations of the substrates. Thus, it is possible that, under certain conditions, ChAT activity may be insufficient to maintain the rate of ACh synthesis that would be needed to compensate for ACh release at high levels of synaptic activity (Tucek, 1984).

Choline originating from released ACh

The ACh released from cholinergic terminals can bind to cholinergic receptors and be hydrolyzed in the synaptic cleft by the enzyme AChE. Although ACh can be spontaneously hydrolyzed, the metabolic process is 100 million times faster when it is degraded by the enzyme AChE (each molecule of AChE is able to degrade about

25,000 molecules of ACh per second). AChE is found in high concentrations in the postsynaptic membrane, and is expressed in neurons, erythrocytes and lymphocytes (Brimijoin, 1983). Once the ACh is bound to AChE, the hydrolytic reaction occurs at a region of the active site called the esteratic subsite. Here, the ester bond of ACh is broken and acetate and Ch are released. Ch is then immediately uptaken by the sodium-dependent high affinity Ch uptake (SDHACU) system located on the presynaptic membrane (Figure 1). Acetate, however, becomes covalently bonded to serine residues within the esteratic subsite, forming a temporary acetylated form of AChE

Choline from diet

Nerve tissue needs sufficient amounts of "external" Ch for effective release of ACh, and Ch obtained from the diet is needed for homeostatic nerve function. High levels of dietary Ch and/or certain phospholipids increase the levels of plasma Ch which is then transported across the blood-brain barrier into the brain itself, and this is consistent with findings which show that an increased intake of Ch leads to behavioral and functional benefits (Wurtman, 1987).

Choline from brain phospholipids

The synthesis of ACh depends on the levels of Ch, and when it is in short supply, membrane phospholipids must provide an alternative source from which Ch can be synthesized *de novo* (Millington and Wurtman, 1982). Phospholipids present in the brain include phosphatidylethanolamine (PE), phosphatidylcholine (PC) and phosphatidylserine (PS) among other related compounds, and, as will be seen later, all of them can be potential sources for the *de novo* synthesis of Ch via complex enzymatic pathways (Hattori and Kanfer, 1984). Changes in the composition of membrane phospholipids caused by neurodegenerative processes may affect Ch availability for the synthesis of ACh.

Choline transport and uptake

There are two Ch reuptake systems, one with high affinity for Ch and the other with low affinity. The high affinity Ch transporter is an integral membrane protein with 13 transmembrane (TM) segments, which belongs to the Na^+/glucose co-transporter family, and which captures Ch for the synthesis of ACh (Haga, 1971; Okuda and Haga, 2003) (Figure 1). The second reuptake system captures Ch with very low affinity, displays its maximum capacity of transportation independently of Na^+, and does not

use Ch in the synthesis of ACh. The availability of the irreversible inhibitor of both transporters, hemicholinium-3 (HC-3), demonstrated the presence of both types of Ch transporters (Yamamura and Snyder, 1973; Haga and Noda, 1973). The low affinity transporters are ubiquitous and are found in multiple cell types, whereas the SDHACU is specific to cholinergic terminals (Misawa et al., 2001; Kobayashi et al., 2002). The early observation that SDHACU levels were decreased in the hippocampus after dennervation of the septo-hippocampal pathway and that most of the Ch transported via SDHACU was converted to ACh, suggested that SDHACU is not only a unique constituent of cholinergic nerve terminals, but also a rate-limiting component for synaptic ACh synthesis and availability (Amara and Kuhar, 1993).

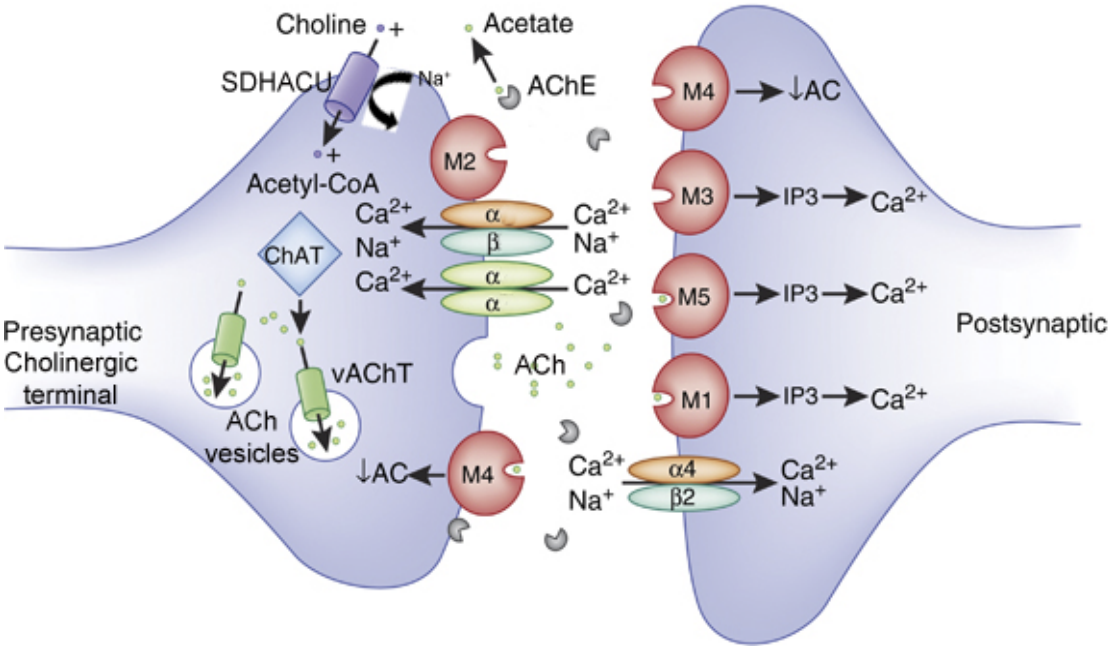

Figure 1. Schematic representation of a cholinergic synapse. The endogenous ligand, ACh, is synthesized in cholinergic neurons (left neuron) by the enzyme ChAT and can be stored in synaptic vesicles by the vesicular ACh transporter (vAChT). The ACh released into the synaptic cleft can bind to pre- and postsynaptic receptors, and be hydrolysed by AChE. Choline uptake is mediated by presynaptic SDHACU. (Modified from Jones et al., 2012).

1.2. Central cholinergic pathways

The central cholinergic pathways have been studied and described over the last decades by detection of the presence and activities of ChAT and AChE, or by analysing drug binding to cholinergic receptors, and by using different experimental models, e.g., specific cholinergic lesions and retrograde staining techniques. *In vivo* neuroimaging techniques such as the PET scanner, functional magnetic resonance

imaging and tensor diffusion tractography in humans, monkeys, apes, marmosets, raccoons, chickens, rabbits, rodents, and cats have also been applied to the study of the cerebral cholinergic pathways, and have shown a high conservation between different animal species (Mesulam et al., 1983a,b; Mesulam, 2004; van Dalen et al., 2016).

The cholinergic cells in the brain include projection neurons that innervate distal areas and local interneurons that are intermingled with their cellular targets. Cholinergic projection neurons are grouped in nuclei throughout the brain, such as in the pedunculopontine and laterodorsal tegmental areas (PPTg and LDTg), the medial habenula (MHb) (Ren et al., 2011) and the basal forebrain complex (reviewed in Woolf et al., 1991). These cholinergic neurons project widely and diffusely, innervating cortical and subcoprtical regions throughout the CNS (Figure 2; pathways in purple and in green). Cholinergic interneurons are typified by the tonically active ACh neurons of the striatum and nucleus accumbens (Mesulam, 1995; Benagiano et al., 2003; von Engelhardt et al., 2007) (Figure 2; pathways in blue).

Mesulam proposed a useful way of subdividing the cholinergic system in the brain of mammals into 8 “major sectors” named Ch1 to Ch8 (Mesulam et al., 1983a; Mesulam, 1990). The cholinergic neurons from the different Ch1 to Ch8 subdivisions differ in size and shape, are interspersed among non-cholinergic neurons, the ratio of cholinergic versus non-cholinergic neurons differs among sectors and the perikarya of the cholinergic neurons, as well as non-cholinergic radiations to these neurons, contain AChE.

Basal forebrain cholinergic system

The Ch1 to Ch4 clusters of cholinergic cells constitute the basal forebrain cholinergic system (Mesulam et al., 1983a). The basal forebrain cholinergic neurons (BFCN) located in the Ch1 to Ch4 subdivisions provide the main source of cortical and hippocampal cholinergic innervation. Ch1 neurons are contained in the medial septal nucleus or medial septum (MS), particularly along the midline and the outer edge of the septum and 80% of them are non-cholinergic (Mesulam et al., 1983a). Ch1 form a bean-shaped continuum with the Ch2 sector, which consists of neurons located within the vertical limb of the diagonal band of Broca (VDB); more than 70% of Ch2 neurons are BFCN. The main projections of the Ch1-Ch2 BFCN are to the hippocampus, hypothalamus and occipital cortex. The Ch3 sector is comprised of neurons of the horizontal limb of the diagonal band of Broca (HDB), with approximately 25% of neurons displaying a cholinergic phenotype innervating the olfactory bulb. The Ch4 sector of both human and monkey brain is the major source of cholinergic projections

to the cortical mantle (Mesulam et al., 1983b) (Figure 2; pathways in purple). The Ch4 sector is also denominated nucleus basalis of Meynert (nbM) and it has been described as containing the cells which are most vulnerable to neurodegeneration in Alzheimer's disease patients. The nbM is explained in detail later and specifically analyzed in the present manuscript.

Pedunculopontine, laterodorsal tegmental and habenular areas

The Ch5 sector is a heterogeneous nucleus located in the pontomesencephalic reticular formation and is comprised of neurons within the pedunculopontine nucleus. The Ch5 sector radiates to several thalamic nuclei and sends a minor projection to the neocortex. The Ch6 cluster, which is located in the laterodorsal tegmental nucleus, innervates various thalamic nuclei (Mesulam et al., 1989). The Ch7 sector is located in the medial habenula and projects to the interpeduncular nucleus (Kasa, 1986). Finally, the Ch8 sector corresponds to the parabigeminal nucleus of the pontomesencephalic region, and its neurons project to the superior colliculus and the lateral geniculate (Mesulam et al., 1989) (Figure 2; pathways in green).

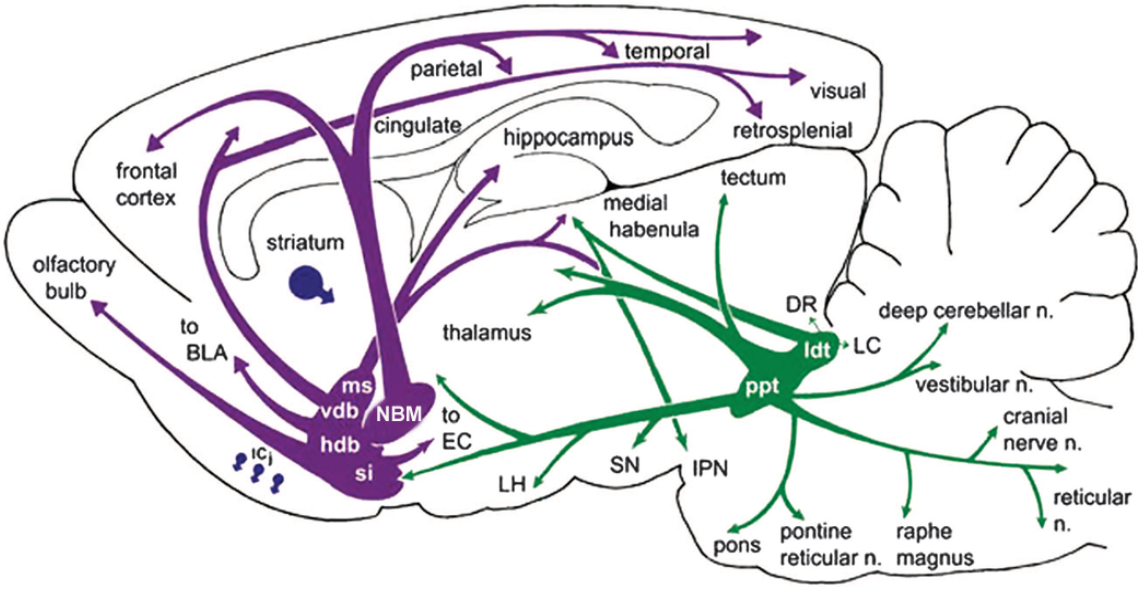

Figure 2. Basal forebrain cholinergic nuclei and networks in rodent CNS. NBM, nucleus basalis magnocellularis; BLA, basolateral amygdala; DR, dorsal raphe; EC, entorhinal cortex; HDB, horizontal diagonal band nucleus; Icj, islands of Calleja; IPN, interpeduncular nucleus; LC; locus ceruleus; ldt, laterodorsal tegmental nucleus; LH, lateral hypothalamus; MS, medial septal nucleus; PPN, pedunculopontine nucleus; SI, substantia innominata; SN, substantia nigra; VDB, vertical diagonal band nucleus. (Modified from Woolf et al., 1997).

1.3. The nucleus basalis of Meynert

Anatomy and histology of Ch4

More than 100 years ago Theodor Meynert first described a group of magnocellular hyperchromic neurons located in the human basal forebrain, naming it the nucleus of the ansa lenticularis (Meynert, 1872). This structure was later renamed as the nucleus basalis of Meynert and was considered to be homologous with the nucleus basalis magnocellularis (NBM) of the rat (Kölliker, 1896). The nbM is distributed in the sagittal plane extending from the anterior tubercle to the most rostral parahippocampal gyrus, and has the greatest cross-sectional diameter in the substantia innominata (Mesulam and Geula, 1988). The HDB (Ch3) is the inferior and rostral limit. Dorsally, the nbM is limited by the ventral globus pallidus, and laterally by the anterior commissure (Figures 2 and 3) (Gratwicke et al., 2013). The nbM is evolutionarily conserved in human and non-human primates, as well as in rodents. Although it is a well-defined anatomical structure, in rodents it is more rudimentary, and BFCN are more interspersed with other neuronal types inside the globus pallidus (Gorry, 1963). Histochemical studies in humans reveal the predominant presence of BFCN which are estimated to be 210,000 cells in each hemisphere (Gilmor et al., 1999). These are cholinergic magnocellular hyperchromic neurons, fusiform to multipolar in shape and 40–50 × 60–70 μm in size, with no particular pattern of dendritic arborisation (Mufson et al., 2003; Mesulam and Geula, 1988). Immunochemical studies show that 90% of the magnocellular neurons in the nbM express ChAT, AChE and the low affinity nerve-growth factor receptor ($p75^{NTR}$), revealing their cholinergic phenotype. Moreover, a mosaic of smaller non-cholinergic, non-galaninergic but GABAergic neurons are also present (Gritti et al., 1993; Mesulam and Geula, 1988; Mufson et al., 2003).

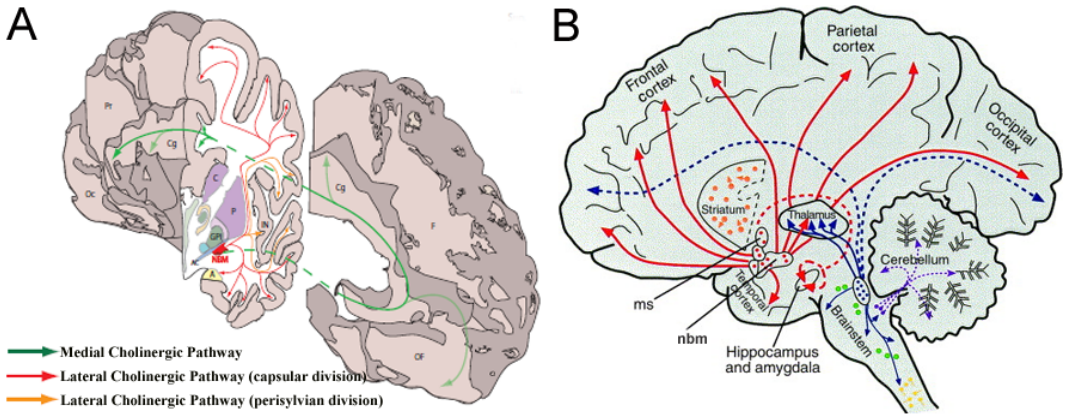

Figure 3. (A) Anatomical diagram of the left hemisphere showing the location of the nbM and its major projecting cholinergic pathways in the human brain. A = amygdala; AC = anterior commissure (lateral aspect); C = caudate; Cg = Cingulate gyrus; F = frontal lobe (medial surface); GPi = globus pallidus (internal part); IN = insular cortex; nbM = nucleus basalis of Meynert; Oc = occipital lobe (medial surface); OF = orbitofrontal cortex; P = putamen; Pr = parietal lobe (medial surface). (Modified from Gratwicke et al., 2013). (B) Anatomical diagram of the human brain showing the location of the medial septum (ms) which innervates the hippocampus and the amygdala (red dashed line), and the nucleus basalis of Meynert which innervates the entire cortical mantle (red line) (Modified from Perry et al., 1999).

Connectivity. Afferent projections to the nbM

Direct axonal tracing experiments in non-human primates and in rodents reveal the preponderance of efferent innervations to the almost entire cortical mantle and amygdala. However, the afferent connections which reach to the nbM are not symmetrical and are restricted to several well-known limbic and paralimbic areas (i.e. parahippocampal and entorhinal regions, amygdala, hypothalamus, septal nuclei and nucleus accumbens) (Figure 4) (Jones et al., 1976; Mesulam and Geula, 1988; Mesulam and Mufson, 1984; Russchen et al., 1985). Immunohistochemical studies in rodents reveal a substantial number of catecholaminergic projections from the ventral tegmental area and substantia nigra pars compacta, serotonergic projections from the dorsal raphe and ventral tegmental area and cholinergic innervations from the pedunculopontine nucleus and laterodorsal tegmental area (Figure 4) (Jones and Cuello, 1989). The afferent projections to the nbM were demonstrated at the subcellular level by the ultrastructural localization of different markers. Dendrites of Ch4 BFCN receive innervations from cholinergic (ChAT-positive), GABAergic (glutamic acid decarboxylase-positive) and dopaminergic (tyrosine hydroxylase-positive) neurons (Smiley and Mesulam, 1999; Reviewed in Mesulam, 2013). The cholinergic contacts usually form asymmetric synapses and could represent local collaterals or projections from Ch5–Ch6. The GABAergic input occurs through symmetric synapses and could represent input from inhibitory neurons within the basal forebrain. The human nbM contains numerous dopaminergic, serotonergic, and noradrenergic axons from the

neurons of the ventral tegmental area/substantia nigra, the midbrain raphe and the nucleus locus coeruleus, respectively. In the rat, all of these nuclei, together with the cholinergic Ch5–Ch6 cell groups, have been shown to project to Ch4 (Jones and Cuello, 1989). Galanin, glutamate and estrogen receptors have also been found in the human Ch4 sector as postsynaptic components of extrinsic afferents to Ch4 (Mufson et al., 2003).

Connectivity. Efferent projections from the nbM

The human and primate nbM and the NBM in rodents provides the main source of cortical cholinergic innervation (Mesulam et al., 1983a,b). Thus, both electrical or optogenetic stimulation of the rodent NBM evokes the release of ACh in neocortex (Kurosawa et al., 1989, Kalmbach et al., 2012). Moreover, specific depletion of BFCN in the Ch4 of rodents and primates significantly reduces the cortical densities of ACh and AChE (Wenk et al., 1994; McGeer et al., 1986). At present, the cortical cholinergic innervation is being topographically segmented in subsectors of the nbM by using retrograde tracing experiments, BFCN lesion models, neuropathological studies in brain samples from AD patients and in anatomical studies carried out with diffusion tensor imaging and tractography (van Dalen et al., 2016). The most rostral sector, designated as the Ch4a, is born posterior to the olfactory tubercle and can be divided into anteromedial (Ch4am), anterolateral (Ch4al) and anterointermediate (Ch4ai) subsectors. The intermediate sector (Ch4i), which can be segmented into superior/dorsal (Ch4id) and inferior/ventral (Ch4iv) subsectors, is caudally limited by the ansa peduncularis (ventral amygdalofugal pathway). The most posterior sector (Ch4p) is limited by the parahippocampal gyrus (Mesulam and Geula, 1988; Mesulam et al., 1983a,b).

Ch4a mainly innervates the most rostral part of the brain. The neurons from Ch4am provide the major cholinergic innervation to frontal, parietal and cingulate cortices. A more modest number of projections are directed to the inferior parietal lobule including hypothalamus, hippocampus, somatosensory cortex, amygdala and parahippocampal regions among others. The Ch4al subsector mainly projects to the frontoparietal cortex and the amygdala and, to a lesser degree, to the olfactory bulb, motor cortex, ventrolateral orbital cortex, insular and parahippocampal areas. The BFCN of the Ch4i subsector are located in the middle of the nucleus and send projections to orbital, insular, periarcuate, peristriate, inferotemporal and parahippocampal areas, and to the inferior parietal lobule, but project more modestly to the medial frontal pole, dorsomedial motor cortex, amygdala, anterior auditory cortex and the temporal pole. Lastly, the BFCN from the Ch4p subsector mainly innervate the

superior temporal pole and few projections are directed to inferotemporal and posterior insular regions (Jones et al., 1976; Mesulam and Geula, 1988; Mesulam et al., 1983b). The same regions can be innervated by different Ch4 subsectors which show that there is a considerable overlap among BFCN from individual subsectors. The lack of anatomical separation of BFCN in discrete subpopulations would represent a challenge for the identification of the degeneration of a specific Ch4 subsector if we were able to observe pathological alterations in a particular innervated area of the basal forebrain cholinergic system. Immunohistochemical studies in *postmortem* brain samples from human subjects show that cholinergic innervations from the nbM are mostly unmyelinated (Wainer and Mesulam, 1990) and leave the nucleus in two highly discrete organized fibre bundles which form the medial and lateral cholinergic pathways (Figure 3A) (Selden et al., 1998).

Axonal tracing experiments must be performed *in vivo* or *ex vivo* in animals but the recently developed diffusion tensor tractography technique allows us to identify the brain´s anatomical connections *in vivo* in human subjects, and the use of this technique has revealed that there are similar connectivity patterns in humans as those observed in non-human species. Both the studies in *postmortem* samples and those performed *in vivo* in healthy volunteers demonstrate that the medial pathway leaves the nbM anteriorly and enters through the cingulum, travels posteriorly to the splenium and enters the retrosplenial white matter, where it merges with fibres of the lateral pathway in the occipital lobe, thereby innervating almost the entire cortical mantle (Hong and Jang, 2010; Selden et al., 1998). Moreover, the pathways from the nbM to the cortex have been tracked in 87 cognitively impaired patients in an attempt to clarify the relationship between symptoms of cholinergic deficiency and degradation of the cortical cholinergic projections (van Dalen et al., 2016). Therefore, it is reasonable to compare human connectivity with that found in primates and rodents and, indeed, human pathological data give indirect support to this assumption (Mesulam and Geula, 1988). The cholinergic innervation fibres form a dense plexus in all regions of the human neocortex displaying synaptic specializations, as they are often in close contact with cortical cholinoceptive neurons (Mesulam and Geula, 1988). Overall, the heterogeneous neural input to the nucleus from predominantly limbic structures, combined with the massive cholinergic output to the almost entire neocortical mantle, makes the nbM the principal candidate for the modulation or influence of several aspects of complex and organized behavior such as learning, executive functions and working memory (Mesulam, 1987; Gratwicke et al., 2013).

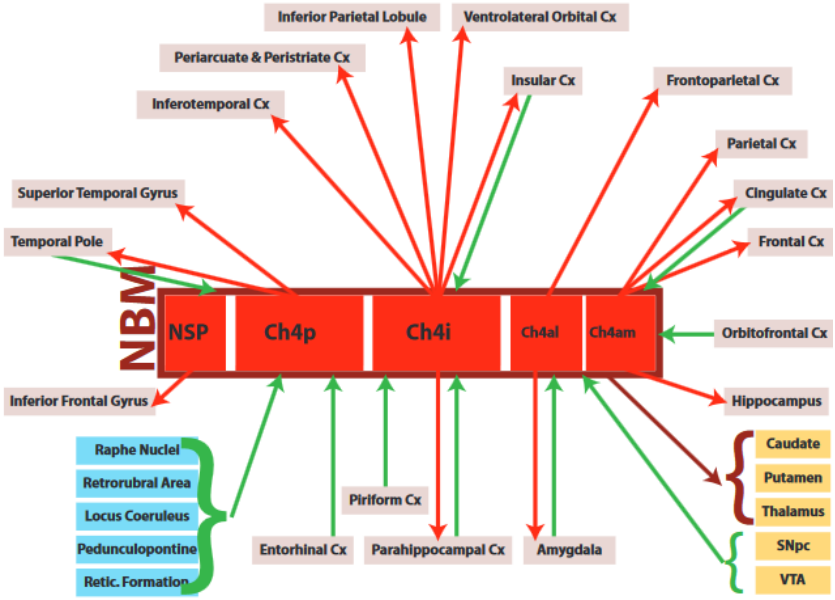

Figure 4. The proposed major connections of the human nbM with cortical and subcortical structures. Major afferent projections (bright green arrows) are inputs to the nbM as a whole: catecholaminergic, serotonergic and cholinergic projections. Major efferent projections (bright red arrows) are shown according to their subsector of origin. All efferent projections are cholinergic. Cx = cortex; Retic. Formation = brainstem reticular formation; SNpc = substantia nigra pars compacta; VTA = ventral tegmental area. (Extracted from Gratwicke et al., 2013).

1.4. Central cholinergic signaling

The acetylcholine receptors are divided into metabotropic muscarinic receptors and ionotropic nicotinic receptors.

Muscarinic acetylcholine receptors

Structure of muscarinic acetylcholine receptors

Muscarinic ACh receptors (mAChR) are constituted by seven-transmembrane (TM) spanning domains and belong to the guanine nucleotide-binding protein coupled receptor (GPCR) superfamily. There are five subtypes of mAChR which mediate multiple actions of ACh in the CNS and the periphery. All five subtypes of mAChR are expressed in the CNS and are thought to play a relevant role in the signaling mechanism for learning and memory processes, REM sleep, attention, control of movement and thermoregulation. Riker and Wescoe (1951) suggested the existence of different subtypes of mAChR when they observed a cardioselective inhibition of mAChR by gallamine and a few years later, some cholinergic compounds were described as showing selectivity for mAChR located in sympathetic ganglia (Roszkowski, 1961). The introduction of the antagonist pirenzepine demonstrated the selectivity of this compound for mAChR subtypes in radioligand binding and functional

assays, thereby demonstrating the existence of at least two distinct mAChR subtypes (Hammer et al., 1980; Brown et al., 1980; Hammer and Giachetti, 1982).

Muscarinic acetylcholine receptor subtypes

M_1 and M_2 mAChR subtypes were the first to be cloned (Kubo et al., 1986), followed by the cloning of the M_3, M_4 and M_5 genes (Bonner et al., 1987, 1988), which confirmed that the mAChR are glycoproteins which belong to the superfamily of GPCR (Hulme et al., 1990; Wess, 1993). The chromosomal localization of the human mAChR genes are as follows: M_1, 11q12–13; M_2, 7q35–36; M_3, 1q43–44; M_4, 11p12–11.2; M_5, 15q26, and phylogenetic analyses reveal that the mAChR have evolved from a common ancestor (Bonner et al. 1991; Horn et al., 2000). The amino acid composition of the human mAChR subtypes ranges from 460 amino acids for M_1, 466 for M_2, 589 for M_3, 479 for M_4, to 532 for M_5. Primary sequence alignment reveals that the individual subtypes share approximately 145 invariant amino acid residues and show between 89% and 98% common amino acid identity in various mammalian species (Wess, 1993; Bonner, 1989). Within the TM segments, there is 63% common identity in all mAChR subtypes, but it is even higher among the M_1, M_3, and M_5, and between the M_2 and M_4 subtypes.

In addition, the preferential coupling of M_1, M_3 and M_5 subtypes is to $G\alpha_{q/11}$ proteins activates phospholipase C (PLC). PLC hydrolyzes phosphatidylinositol 4,5-bisphosphate (PIP_2) to diacyl glycerol (DAG) and inositol trisphosphate (IP_3) which act as intracellular secondary messengers; DAG activates protein kinase C (PKC) and IP_3 contributes to the phosphorylation of some proteins and the movilization of intracellular Ca^{2+}.

M_2 and M_4 mAChR subtypes are preferentially coupled to $G\alpha_{i/o}$ proteins, whose activation mainly inhibits the cAMP dependent pathway by inhibiting adenylate cyclase activity which decreases the activity of cAMP-dependent protein kinases (Caulfield and Birdsall, 1998) (Figures 1 and 5).

Distribution of muscarinic acetylcholine receptor subtypes

Radioligand binding, immunoprecipitation, immunohistochemistry and *in situ* hybridization techniques have contributed to determining the precise anatomical localization and relative abundance of mAChR in the CNS. The earliest studies focused on the distribution of central mAChR subtypes were performed by means of radioligand binding using the non-subtype selective compound [^{3}H] quinuclidinyl benzilate ([^{3}H] QNB) (Snyder et al., 1975). Subsequent refinements in the radioligand-based approach to map specific mAChR subtypes involved the use of the radioligand [^{3}H] N-

methylscopolamine ([^{3}H] NMS), as well as [^{3}H] QNB, in conjunction with relatively subtype-selective antagonists (see Ehlert et al., 1994). *In situ* hybridization and quantitative autoradiographic studies with optimized labeling conditions have also significantly contributed to quantifying and anatomically locating the mAChR subtypes in the CNS (Smith et al., 1991; Rodriguez-Puertas et al., 1997; Flynn et al., 1995). The combination of both kinetic and equilibrium labeling approaches provides selective labeling of the five mAChR subtypes by using specific cocktails of subtype-selective antagonists to "mask" the presence of all mAChR subtypes except the desired receptor. Although mRNA-based techniques are very sensitive, the levels and the location of mRNA measured cannot be precise since the presence of mRNA does not mean that the protein is specifically expressed at an equivalent level in that location or that it will be transported to its final destination. The generation of mAChR subtype-selective antibodies has permitted us to establish the anatomical distribution in discrete brain regions and cell compartments and has provided us with a more profound understanding of their physiological role in relation to neuronal networks (Levey et al., 1991).

M_1 mAChR mRNA transcript is mainly localized in the cerebral cortex, hippocampus, thalamus, caudate-putamen, amygdala, olfactory bulb, olfactory tubercle and dentate gyrus, whereas M_2 mAChR mRNA is more abundantly detected in the basal forebrain, caudate-putamen, hippocampus, hypothalamus, amygdala and pontine nuclei (Buckley et al., 1988; Vilaro et al., 1994). At the cellular level, M_1 mAChR-immunoreactivity is restricted to neuronal bodies and neurites which is consistent with its role as the major postsynaptic mAChR subtype. In the basal forebrain, M_2 mAChR is expressed at high levels in the BFCN which suggests that M_2 mAChR can act as an autoreceptor. However, M_2 mAChR is also present in non-cholinergic cortical and subcortical structures, thus providing evidence that this subtype may presynaptically modulate the release of ACh and other neurotransmitters and may also operate postsynaptically (Levey et al., 1991, 1995). Quantitative autoradiographic experiments reveal the highest levels of M_1 mAChR in the hippocampus, nucleus accumbens and caudate-putamen. More modest labeling is also noted in the molecular layer of the dentate gyrus and in the olfactory tubercle (Flynn et al., 1997). M_2 mAChR labeling is observed in the occipital region of the cerebral cortex, the dorsal region of the caudate, the olfactory tubercle, the nucleus accumbens, the superficial layers of the superior and inferior colliculi, the pontine and parabrachial nuclei, the motor trigeminal and the facial nuclei in the brainstem, and some labeling is also present in the cerebellum. In general, these findings are consistent with previous studies (Mash and Potter, 1986; Levey et al., 1991), but not with *in situ* experiments that failed to find M_2

mRNA in the cortex and striatum (Buckley et al, 1988; Vilaro et al., 1994). M_3 mRNA transcription occurs in the olfactory tubercle, cerebral cortex, hippocampus, thalamus, caudate-putamen, and amygdala, whereas M_4 mRNA is highest in the olfactory bulb, olfactory tubercle, hippocampus, and striatum (Buckley et al., 1988; Caulfield, 1993), which is consistent with the quantitative autoradiographic results obtained by Flynn et al. (1997), and with those of immunohistochemical studies carried out by Levey et al. (1991). M_5 mRNA has been detected in the substantia nigra pars compacta (Weiner et al., 1990). M_5 mAChR binding is observed in the most external layers of the cortex, in the caudate-putamen, nucleus accumbens, CA1 and CA2 hippocampal regions and in the polymorphic layer of the dentate gyrus (Flynn et al., 1997; Reever et al., 1997).

Nicotinic acetylcholine receptors

Nicotinic acetylcholine receptors (nAChRs) are ligand-gated ion channels, sensitive to activation by nicotine and whose activity is induced in the micro- to submicrosecond range. They can be divided into two types; muscle receptors, which are found at the skeletal neuromuscular junction where they mediate neuromuscular transmission, and neuronal receptors, which are found throughout the peripheral and central nervous systems where they are involved in fast synaptic transmission (Gotti et al., 2004).

Structure of nicotinic acetylcholine receptors

nAChRs are pentameric structures that are made up of combinations of individual subunits closely related to an extended family of cDNAs that in mammals encode 16 structurally homologous subunits with primary structural identity. All subunits have the following: 1) an extracellular large NH_2-terminal domain of ~200 amino acids; 2) three TM domains; 3) a cytoplasmic loop of variable size and an amino acid sequence; and 4) a fourth TM domain with a relatively short and variable extracellular COOH-terminal sequence (Lukas et al., 1999). Neuronal nAChRs can be homopentamers or heteropentamers composed of different subunits of α2, α3, α4, α5, α6, α7, α9, and α10; and 3 non-α subunits (termed β2, β3, and β4), which have been cloned from neuronal tissues (Gotti et al., 2004). The receptor channel is also permeable to selected ions such as Na^+, K^+, Ca^{2+} and Mg^{2+} (Figures 1 and 5).

Localization and distribution of nicotinic ACh receptors

nAChRs can be located at the cell soma, dendrites, preterminal axon regions, axon terminals and myelinated axons (reviewed in Albuquerque et al, 2009). Binding experiments in human brain have been performed by using [^{3}H]-nicotine, [^{3}H]-cytisine,

[^{3}H]-methylcarbamylcholine and, in a few cases, [^{125}I]α-bungarotoxin. Nicotine labels all nAChRs; cytisine labels those containing the α3, α4 and β2 or β4 subunits; α-bungarotoxin labels α7 receptors. [^{3}H]-nicotine and [^{3}H]-cytisine binding studies show the highest density of nAChR in the periacqueductal grey matter, putamen, substantia nigra pars compacta, dentate gyrus of hippocampus, thalamus and dorsal raphe, and moderate densities in the cortex, claustrum, cingulated gyrus, hippocampal pyramidal and molecular layers, subiculum, tegmentum, nbM, parahippocampal area, cerebellum and substantia nigra pars reticulata. [^{125}I]α-bungarotoxin binding studies show high density in the sympathetic ganglia; moderate density in the hippocampal granular layer, subiculum, cerebellum, cortex, medial and lateral geniculate and reticular thalamic nucleus; and low density in the stratum lacunosum molecular, entorhinal cortex and cerebellum (Reviewed in Gotti et al., 1997). The distribution of nAChR has also been analyzed in the human CNS by using *in situ* hybridization and PET and these techniques have reported a similar distribution to that described using binding studies (Rubboli et al., 1994; Nordberg at al., 1992, 1995).

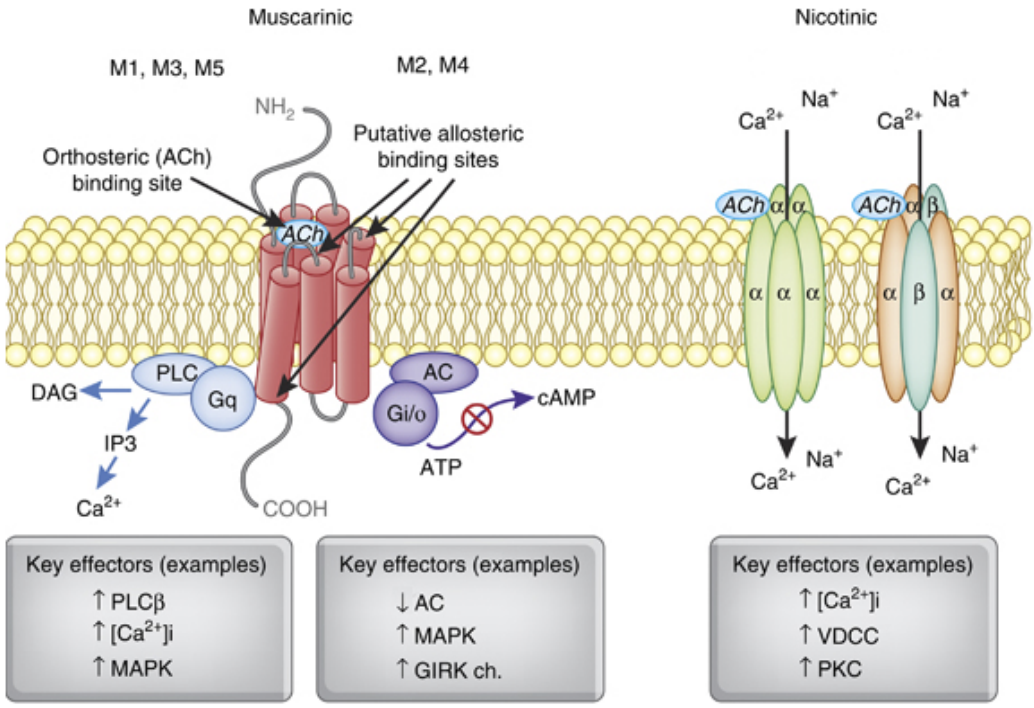

Figure 5. Structure and intracellular signaling of mAChR and nAChR. Each mAChR subtype is a seven-TM protein, which belongs to two major functional classes based on the different G-protein coupling. The M_1, M_3, and M_5 mAChR are selectively coupled to the $G\alpha_{q/11}$-type G-proteins resulting in the generation of IP_3 and DAG through activation of the phosphoinositide-specific PLCβ, leading to increased intracellular Ca^{2+} levels. The M_2 and M_4 mAChR preferentially activate $G\alpha_{i/o}$-type G-proteins, thereby inhibiting adenylate cyclase, reducing intracellular concentration of cAMP and prolonging the potassium channel opening (Modified from Jones et al., 2012).

2. The endocannabinoid system

Marijuana, a derivative of the plant *Cannabis sativa*, has been used for recreational and therapeutic purposes for thousands of years. Ancient Indian and Chinese medical writers described the physiological and psychological effects of this plant (Mechoulam, 1986). The therapeutic value of cannabis was scientifically assessed for the first time in the early 19th century, demonstrating the clinical utility of cannabis in several disorders including cholera, rheumatic diseases, delirium tremens and infantile convulsions (O'Shaughnessy, 1843). O'Shaughnessy's work probably marks the beginning of 'endocannabinoid research' (Di Marzo, 2006).

The mechanism of action and therapeutic possibilities of cannabis would not have been discovered if its active principles had not been purified and chemically characterized. At the end of the 19th century resin extraction from *Cannabis sativa* allowed to isolate cannabinol, whose structure was then further elucidated, leading to the full chemical characterization of this compound (Wood et al., 1899; Jacob and Todd, 1940). However, Δ^9-tetrahydrocannabinol (Δ^9-THC) would prove to be the most pharmacologically interesting compound of cannabis since it is responsible for its psychotropic activity. Δ^9-THC was isolated from hashish and its chemical structure was established by the pioneering studies of Gaoni and Mechoulam (1964).

The affinity of Δ^9-THC for lipid membranes and its properties of lipid solubility erroneously suggested that its effects were induced by a direct modification of cell membrane fluidity, rather than by the activation of cell-surface specific receptors (Lawrence and Gil, 1975). Experience with opioid receptors and enkephalins led to the idea that endogenous cannabinoid ligands and the associated enzymatic machinery must be present in mammalians, because such receptors would not have been selected by evolution merely to be activated by a plant product (Freund et al., 2003). The existence of specific cannabinoid-receptor interaction was confirmed when Howlett showed decreased cAMP levels in Δ^9-THC-treated neuroblastoma cultures, suggesting the existence of functional coupling to G proteins of the $G\alpha_{i/o}$ subtype (Howlett and Fleming, 1984; Howlett, 1984; 1985; Howlett et al., 1986). In 1988 the presence of high-affinity binding sites for cannabinoid agonists in rat brain membranes was described and, indeed, this was coupled to the inhibition of adenylyl cyclase activity which confirmed the findings of Howlett´s pioneering work (Devane et al., 1988; Howlett et al., 1990). In 1990 the first receptor for cannabinoids was cloned, thereby identifying a DNA sequence encoding for a GPCR (Matsuda et al., 1990). [^{3}H]CP55,940 autoradiography showed the first CB_1 receptor distribution in mammalian

brain (Herkenham et al., 1990). A second cannabinoid receptor expressed in immunitary cells, at present known as the CB_2 receptor, was cloned a few years later and pharmacologically characterized as an inhibitor of adenylyl cyclase activity (Munro et al., 1993; Galiegue et al., 1995).

Binding studies in rat brain slices demonstrated the displacement of [^{3}H]CP55,940 binding elicited by the Ca^{2+}-induced release of an endogenous cannabinoid ligand, but failed to detect and characterize it (Evans et al., 1992 and 1994). Based on the reasoning that endogenous cannabinoids could well be as hydrophobic as Δ^9-THC, the fractioned lipid extract from porcine brain was used to search for cannabinoid-like binding activity. The researchers were able to isolate and characterize the first endogenous lipid-based cannabinoid-like component (endocannabinoid; eCB) which was given the name of “anandamide” (AEA) and which had similar *in vitro* pharmacological effects to those observed for cannabinoid agonists (Devane et al., 1992; Fride and Mechoulam, 1993). However, additional lipid fractions from the rat brain contained cannabinoid-binding activity in addition to AEA and, a second eCB, 2-araquidonoylglycerol (2-AG), was simultaneously isolated from cat gut and rat brain (Mechoulam et al., 1995; Sugiura et al., 1995). The distribution of eCB in the CNS has been investigated using different approaches, e.g. by exposing rat brain slices to [^{14}C]-AEA and measuring the distribution of radioactivity by autoradiography (Giuffrida et al., 2001). Other compounds which produce the classical cannabimimetic effects *in vivo* may also serve as eCB, like O-arachidonoylethanolamine (virodhamine), isolated from rat brain, which weakly activates CB_1 receptors (Hanus et al., 2001; Porter et al., 2002). Other possible eCBs are 2-arachidonoilglycerol ether (noladin ether) isolated from porcine brain, N-arachidonoyldopamine (NADA), N-dihomo-γ-linolenoylethanolamine and N-docosatetraenoylethanolamine (Bisogno et al., 2000; Pertwee, 2005).

2.1. Endocannabinoids

Lipid signaling molecules (neurolipids) are emerging as key modulatory elements in CNS neurotransmission in which GPCR for multiple neurolipid systems are being identified. Lipids represent the main structural components of the cell membranes, but some phospholipid species present in the membranes of neurons, glia and other cells may serve as precursors for the synthesis of neurolipids, such as the eCB. The eCB are defined as endogenous compounds, generated by different tissues and organs, capable of binding to and activate cannabinoid receptors. They are synthesized through cleavage of phospholipid precursors and may be released on demand when evoked by postsynaptic depolarization or GPCR activation (Di Marzo et al., 1994; Maejima et al., 2001). The molecular structure of the eCB share two common structural motifs: a polyunsaturated fatty acid moiety i.e., arachidonic acid (AA) and a polar head group consisting of ethanolamine or glycerol.

Biosynthesis, reuptake and degradation of AEA

AEA belongs to the family of the N-acylethanolamines, which are biosynthesized via a membrane phospholipid-dependent pathway, i.e. the enzymatic hydrolysis of the corresponding N-acyl-phosphatidylethanolamines (NAPE) by a phospholipase D selective for NAPE (NAPE-PLD); (EC-3.1.4.4) (Schmid et al. 1996; Hansen et al. 1998). The AEA precursor (NAPE) is produced from the transfer of an acyl group such as AA, from the sn-1 position of phospholipids (e.g., PC) to the N-position of PE, catalyzed by a Ca^{2+}-dependent trans-acylase (Di Marzo et al. 1994). The finding of a similar distribution of N-arachidonoyl-phosphatidylethanolamine (NArPE; the NAPE precursor of AEA) and AEA in nine different brain areas (Bisogno et al. 1999), and of increasing levels of both NArPE and AEA in rat brain at different stages of development (Berrendero et al. 1999), confirms a precursor/product relationship for the two compounds, and suggest that this pathway is probably the one mainly responsible for AEA biosynthesis. In addition, the Ca^{2+} sensitivity of both the trans-acylase and NAPE-PLD is in agreement with the fact that AEA biosynthesis is triggered by neuronal depolarization and other Ca^{2+}-mobilizing stimuli. However, an alternative way for NAPE to be transformed into AEA involves both phospholipase A1 (PLA1) and the secretory phospholipase A2 (PLA2), with the formation of N-acyl-1-acyl-lyso-PE, followed by the action of a lyso-PLD enzyme distinct from the already known NAPE-PLD (Sun et al. 2004). Finally, two additional pathways for the AEA release from NAPE have been proposed; a sequential double deacylation of NAPE by

alpha/beta-hydrolase domain-containing 4 (ABHD4), followed by the cleavage of glycerolphosphoanandamide to yield AEA and the hydrolysis of NAPE to yield phosphoanandamide by PLCβ, plus a subsequent dephosphorilation by phosphatases (Fisar, 2009) (Figure 6).

Although most of the neurotransmitters are water-soluble and require specific TM proteins to transport them across the cell membrane, the eCB are non-charged lipids that readily cross lipid membranes and it is reasonable to hypothesize that there is no need for an eCB carrier. However, several structural analogs of AEA have been reported to inhibit the AEA uptake (Beltramo et al., 1997), but there is some controversy about AEA reuptake since the molecular identity of the carrier has not yet been clarified (Beltramo et al., 1997). Nevertheless, AEA transport meets four key criteria of a carrier-mediated process: saturability, fast rate, temperature dependence and substrate selectivity (reviewed in Freund et al., 2003). The uptake of AEA does not require cellular energy or external Na^+, suggesting that it is mediated through facilitated diffusion and its immediate intracellular hydrolyzation probably contributes to the rate of AEA transport. To date, four models have been proposed: 1) AEA uptake occurs by facilitated diffusion through a membrane carrier; 2) AEA crosses the membrane by enzyme-mediated cleavage of AEA; 3) AEA undergoes endocytosis through a caveolae-related uptake process; 4) Simple diffusion driven by intracellular sequestration of AEA (reviewed in Di Marzo, 2008).

The enzymatic degradation of AEA was first reported in neuroblastoma and glioma cells as anandamide amidase (Deutsch and Chin, 1993). Later it was identified as anandamide amidohydrolase in the brain, and finally renamed as fatty acid amide hydrolase (FAAH) (EC-3.5.1.99) when purified and cloned from rat liver (Cravatt et al., 1996). Rat, mouse, and human FAAH proteins are all 579 amino acids in length and the gene was mapped to human chromosome 1p34-p35. FAAH is detected in many organs including brain and recognizes a variety of fatty acid amides, but its preferred substrate is AEA. FAAH also catalyzes the hydrolysis of the ester bond of 2-AG *in vitro*. FAAH-knockout mice, created by Cravatt et al. (2001), exhibit an increased responsiveness to exogenous administration of AEA, further demonstrating the direct involvement of FAAH in AEA degradation.

Biosynthesis, uptake and degradation of 2-AG

The levels of 2-AG in tissues, cells or cerebrospinal fluid (CSF) are usually much higher than those of AEA, and may be sufficient to permanently activate cannabinoid receptors (Sugiura et al. 1995; Stella et al. 1997). Similarly to AEA, the enhancement of intracellular Ca^{2+} induces the synthesis of 2-AG. However, several

stimuli have been shown to induce the biosynthesis of 2-AG in intact neuronal and non-neuronal cells, including lipopolysaccharides (in macrophages), glutamate or carbachol (in neurons), carbachol or thrombin (in endothelial cells), endothelin (in astrocytes) or the platelet activating factor (in macrophages) (reviewed in Sugiura et al., 2002). The most important biosynthetic precursors of 2-AG are the sn-1-acyl-2-arachidonoylglycerols (DAG) from membrane phospholipids. Two metabolic pathways lead to 2-AG biosynthesis in neurons; hydrolysis of membrane lipids containing AA by the action of diacylglycerol lipase (DAGL-α) and the hydrolysis of lysophospholipids by lyso-PLC activity (Sugiura et al., 1995). In most cases, the DAG necessary for 2-AG biosynthesis is obtained from the hydrolysis of 2-arachidonate-containing phosphoinositides, catalyzed by a phosphoinositide-selective PLCβ or, alternatively, from the hydrolysis of 2-arachidonate-containing phosphatidic acid, catalyzed by a phosphohydrolase (Di Marzo et al., 1996; Bisogno et al. 1999) (Figure 6).

The main enzyme responsible for the degradation of 2-AG is the monoacylglycerol lipase (MAGL) (EC-3.1.1.23), identified by Tornqvist and Belfrage (1976) (Dinh et al., 2002). The MAGL was cloned from a mouse adipocyte cDNA library (Karlsson et al., 1997). The 303 amino acid length sequence of the MAGL is well conserved in different mammalian species such as mouse, rat, and human (Karlsson et al., 1997). Several studies suggest the existence of additional 2-AG hydrolyzing enzymes in brain microglial cells (Muccioli et al., 2007). A functional proteomic strategy estimates that MAGL hydrolyzes 85% of 2-AG, whereas the remaining 15% is mostly catalyzed by two serine hydrolases; alpha/beta-hydrolase domain-containing 6 (ABHD6) and alpha/beta-hydrolase domain-containing 12 (ABHD12) (Blankman et al., 2007).

The mechanism for 2-AG uptake is also unclear. Some studies propose that that 2-AG and AEA are transported by the same system (Piomelli et al., 1999; Bisogno et al., 2001). Evidence for this assumption is that cold 2-AG prevents [^{3}H]-AEA uptake, suggesting that both eCB may compete for the same transport system. AEA and 2-AG also share similar kinetic properties, and their transport is inhibited by AM404, (reviewed in Freund et al. 2003).

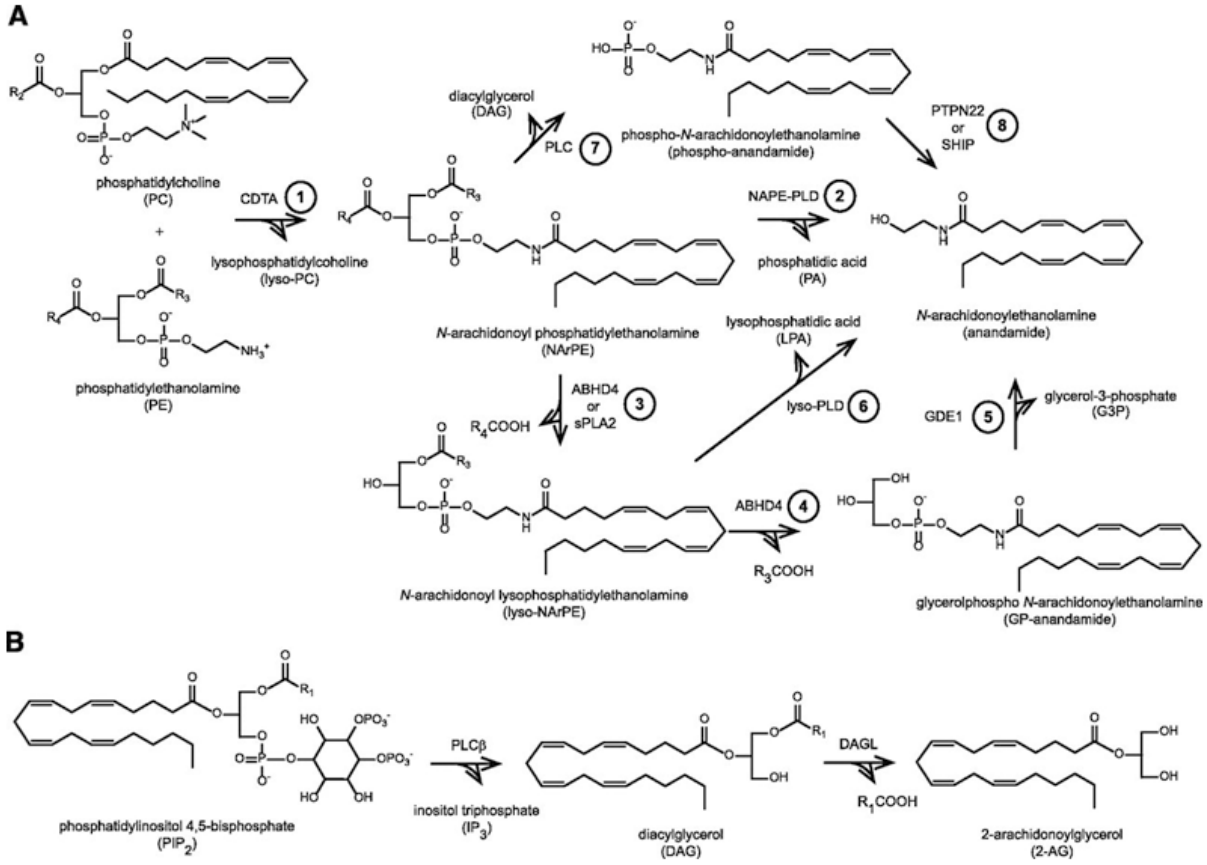

Figure 6. (A) AEA biosynthesis begins with the formation of NArPE by the transfer of AA from phosphatidylcholine (PC) to the primary amine of PE acting a Ca^{2+}-dependent trans-acylase (step 1). Multiple pathways have been postulated for the release of AEA from NArPE (steps 2–8). (B) 2-AG is generated from PIP_2 by PLC*β* followed by cleavage of DAG by DAGL*α* and DAGL*β* (Extracted from Blankman and Cravatt, 2013).

2.2. CB_1 receptor

Subtype 1 of cannabinoid receptors (CB_1 receptor) is a member of the rhodopsin-like family of seven TM domain receptors that are coupled to G proteins at their intracellular surface. This receptor was initially cloned in the rat brain (473 amino acids) and subsequently in human (472 amino acids) and in mouse (473 amino acids) sharing a 97-99% amino acid sequence homology (Matsuda et al., 1990; Gerard et al., 1990; Chakrabarti et al., 1995). The gene for the CB_1 receptor in humans is located in the 6q14-q15 chromosome (Gerard et al., 1990).

CB_1 receptor distribution in the CNS and its physiological relevance

Howlett (1984) provided the first evidence for the existence of specific receptors sensitive to cannabinoid compounds, but the subsequent development of highly

selective synthetic cannabinoid agonists accelerated the pharmacological characterization of the CB_1 receptor (Devane et al., 1988; Gerard et al., 1991). The development of the [^{3}H]CP55,940 radioligand allowed the anatomical localization of cerebral cannabinoid receptors by using autoradiographic techniques (Herkenham et al., 1990). The mapping of [^{3}H]CP55,940 binding sites showed a preferential localization of CB_1 receptors in specific areas of gray matter, thereby predicting the action of cannabinoids reported in behavioral experiments, and this led to intense research into eCB signaling (Freund et al., 2003). The highest levels of [^{3}H]CP55,940 binding were observed in the olfactory bulb, the nigrostriatal pathway including the globus pallidus, the cerebellar molecular layer and specific layers of the hippocampus. Ligand binding pointed to CB_1 receptors as one of the most abundant GPCR in CNS.

Regarding the physiological actions mediated by CB_1 receptors, the tetrad test has been used for screening drugs that induce cannabimimetic effects, consisting of four behavioral components: spontaneous activity, catalepsy, hypothermia and analgesia (Little et al., 1988). Two brain regions that are intimately involved in the control of movement, the basal ganglia and the cerebellum, display very high densities of cannabinoid binding sites which are compatible with the effects of cannabinoids on both motor and cognitive functions, according to the first behavioral paradigm of the tetrad test. The moderate levels of CB_1 receptors reported in basal forebrain-emerging pathways, including the frontal, parietal, and cingulated cortices, septum and amygdala may be an indication of the effects of the cannabinoids on cognitive functions, such as learning, memory and emotional behavior.

On the other hand, the moderate levels of binding in the hypothalamus, lateral subnucleus of interpeduncular nucleus, parabrachial nucleus, nucleus of solitary tract and spinal dorsal horn are probably related to the potent analgesic and antihyperalgesic properties of cannabinoid agonists and their orexigenic effects (Freund et al., 2003). In contrast, the reported low levels of cannabinoid ligand binding in the brainstem areas that control cardiovascular and respiratory functions may explain the tolerability to high doses of cannabinoids (Kano et al., 2009, Mailleux et al., 1992). These overall binding properties are preserved in mammals (Herkenham et al., 1990). During the last decade, there has been increasing evidence of the presence of CB_1 receptors at other locations such as postsynaptic terminals, intracellular organelles, such as the mitochondria which regulate cell metabolism and memory (Hebert-Chatelain et al., 2016), and also in astrocytes which regulate gliotransmission (Navarrete and Araque, 2008).

CB_1 receptor-mediated signaling in the CNS

Intracellular signaling pathways

Agonist stimulation of CB_1 receptors activates multiple signal transduction pathways mainly through the $G\alpha_{i/o}$ family of G proteins, and is responsible for decreases in cAMP and protein kinase A (PKA) activity (reviewed in Howlett et al., 2002). CB_1 receptors have shown a measurable constitutive activity, indicative of G protein activation in the absence of agonists, which could be related to their high abundance and localization in the presynaptic axon terminals (Kendall and Yudowski, 2017). Therefore, inverse agonists specific for CB_1 receptors such as SR141716A, have also been described (Bouaboula et al., 1997; Nie and Lewis, 2001).

The coupling of CB_1 receptors to G_s and the consequent increase in cAMP levels may also be possible in specific conditions, suggesting that different types of adenylyl cyclase isoforms may influence the outcome of CB_1 receptor activation (Glass and Felder, 1997; Maneuf and Brotchie, 1997; Rhee et al., 1998). However, a reduced activation of $G\alpha_{i/o}$ attenuating the inhibitory tone on the major isoforms of adenylyl cyclase, could partially explain the apparent coupling of CB_1 receptors to G_s proteins (Eldeeb et al., 2016). The signaling promiscuity of CB_1 receptors may be related to the agonist trafficking exhibited by structurally different classes of cannabinoid compounds that could be selective for specific intracellular signaling pathways, depending on the CB_1 receptor conformation that they induce (Hudson et al., 2010). The complexity of eCB signaling can be explained by the phenomena of functional selectivity or biased agonism i.e., the ability of ligands to activate a subset of the full repertoire of signaling cascades available to individual GPCR (Urban et al., 2007). Moreover, prolonged activation of CB_1 receptors results in rapid attenuation of behavioral responsiveness due to a decrease in the ability of the receptor to activate effector pathways (i.e., desensitization) and/or a reduction in the population of cell surface-expressed GPCR (i.e., internalization), leading to the development of tolerance in humans as well as in animal models (Howlett et al., 2004).

The internalized GPCR finally become a substrate for specific phosphorilation processes through unique GPCR kinases, and they are converted to high affinity targets for β-arrestins (Jin et al., 1999). CB_1 receptors and β-arrestins mediate the activation of several signaling cascades, including ERK1/2, JNK1/2/3, CREB and P38a, and the consequent regulation of gene expression and protein synthesis (Delgado-Peraza et al., 2016).

To further increase the complexity of eCB signaling, CB_1 receptors frequently associate with other GPCR to form heteromeric complexes, as has been detected by

fluorescence resonance energy transfer or bioluminescence resonance energy transfer (reviewed in Pertwee et al., 2010). Heterodimers of CB_1 receptors have been observed with dopamine D_2 receptors (Kearn et al., 2005), μ-opioid receptors (Rios et al., 2006) or OX_1 orexin receptors (Ellis et al., 2006). Other studies suggest that CB_1 receptors may form additional receptor heteromers based upon pharmacological cross-talk data, pointing to $GABA_B$ receptors (Pacheco et al., 1993), α_2-adrenoceptors and somatostatin receptors (Pan et al., 1998; Vásquez and Lewis, 1999). The recent crystallization of the CB_1 receptor bound to the antagonist AM6538 should not only provide new opportunities to better understand the structure-function relationship of this receptor, but should also be helpful when designing specific new drugs (Hua et al., 2016).

CB_1 receptor activation also stimulates different enzymes such as the mitogen activated protein kinase (MAPK) pathway which leads to immediate early gene expression (Howlett et al., 2002; Bouaboula et al., 1995). The activation of CB_1 receptors is critically involved in many cellular functions such as cell growth, transformation and apoptosis (Galve-Roperh et al., 2002), but the CB_1 receptor also activates other intracellular kinases including the phosphatidylinositol 3-kinase (Bouaboula et al., 1997), the focal adhesion kinase (Derkinderen et al., 1996), and some enzymes involved in energy metabolism (Guzmán et al., 2001; Guzmán and Sanchez, 1999). CB_1 receptor activation is also able to evoke a transient Ca^{2+} elevation that may be related to phospholipase C (PLC) activity modulated by $G\alpha_{i/o}$ or $G\alpha_{q/11}$ proteins (Sugiura et al., 1997; Lauckner et al., 2005). Moreover, the CB_1 receptor modulates various types of ion channels and enzymes in a cAMP-dependent or –independent manner, such as A-type, inwardly rectifying K^+ currents and inhibition of N- and P/Q-type Ca^{2+} currents (Mackie et al., 1995; Twitchell et al., 1997).

The particular distribution of CB_1 receptors and the biosynthesis of eCB in the CNS induced after the activation of multiple signaling systems e.g., dopaminergic (Giuffrida et al., 1999), cholinergic (Kim et al., 2002; Ohno-Shosaku et al., 2003), glutamatergic (Ohno-Shosaku et al., 2002) or GABAergic (Wilson and Nicoll, 2001; Wilson et al., 2001), further support the involvement of the eCB system in the modulation of CNS neurotransmission and control of neuronal network activity. To better understand the specific mechanisms of eCB signaling, it is necessary to determine the precise localization of CB_1 receptors at cellular, subcellular and ultrastructural levels in relation to other systems of neurotransmission.

Presynaptic localization of neuronal CB_1 receptors

GPCR, such as the CB_1 receptor, are embedded within the lipid bilayer of the plasma membrane. Indirect anatomical evidence was first provided by *in situ* hybridization (Matsuda et al., 1990) and receptor binding experiments (Herkenham et al., 1990), which showed the somatic distribution of CB_1 receptor mRNA in the neurons within the striatum (Matsuda et al., 1990), whereas [^{3}H]CP55,940 binding displays the highest densities of the whole brain in the globus pallidus and the substantia nigra pars reticulata (Herkenham et al., 1990), suggesting that the axonal terminals are the final destination of CB_1 receptors (Freund et al., 2003).

The first clues about the presynaptic localization of CB_1 receptors were obtained after provoking specific lesions in the CNS. Ibotenic acid lesioning of the rat striatum produced a marked decrease in cannabinoid receptor binding in the globus pallidus and the substantia nigra pars reticulata (Herkenham et al., 1991). Similarly, cannabinoid receptor binding decreased in the dorsal horn of the spinal cord after resection of the dorsal root (Hohmann et al., 1999a,b). Different immunohistochemical studies indicated that CB_1 receptors are predominantly found in axon terminals, where they may be involved in the presynaptic regulation of neurotransmitter release (reviewed in Freund et al., 2003). The first light microscopy studies revealed the existence of numerous CB_1 receptor-immunoreactive fibers in basket-like formations around CB_1 receptor-negative cell bodies throughout the brain, which largely coincides with the findings of radioligand binding experiments (Egertova and Elphick, 2000). At the ultrastructural level, the first electron microscopy studies carried out in rodents, as well as in human CNS, suggested that CB_1 receptors are located in specific types of axon terminals (Katona et al. 1999, 2000, 2001). Boutons engaged in asymmetrical (excitatory) synapses seem to be devoid of CB_1 receptors, whereas symmetrical (inhibitory) synapses display a profuse distribution of CB_1 receptors, indicating that GABAergic, but not glutamatergic, axon terminals contain CB_1 receptors. However, further studies demonstrated that CB_1 receptors are also present in glutamatergic synapses, but at much lower levels (Katona et al., 2006; Kawamura et al., 2006).

ECB mediated retrograde synaptic modulation

Although anatomical studies may reveal the precise localization of CB_1 receptors, they only enable us to make predictions about their functional role. Pharmacological, electrophysiological and neurochemical studies have all shown that CB_1 receptors are located presynaptically and regulate the release of certain types of neurotransmitters. CB_1 receptor-mediated suppression of neurotransmitter release leads to several forms of synaptic plasticity such as transiently short-term depression

(STD) or persistently long-term depression (LTD) and long-term potentiation (LTP) Both, STD and LTD are mediated by 2-AG (Figure 7).

Ca^{2+}-driven eCB release-dependent STD

STD which is dependent on Ca^{2+}-driven eCB release requires a large Ca^{2+} elevation in postsynaptic neurons induced by the activation of voltage-gated Ca^{2+} channels or NMDA receptors which leads to postsynaptic eCB synthesis in a DAGLα-dependent manner. 2-AG is then released, binds to presynaptic CB_1 receptors whose activation suppresses transmitter release by inhibiting presynaptic voltage-gated Ca^{2+} channels (Figure 7a). This form of eCB-mediated synaptic plasticity includes the following mechanisms: 1) Depolarization-induced suppression of inhibition (DSI) (Llano et al., 1991; Pitler and Alger, 1992; Wilson and Nicoll, 2001); 2) Depolarization-induced suppression of excitation (DSE) (Kreitzer and Regehr, 2001); 3) Presynaptic suppression caused by Ca^{2+} influx through NMDA-type glutamate receptors (Ohno-Shosaku et al., 2007).

1) DSI or modulation of GABAergic neurotransmission via CB_1 receptor activation

The inhibitory effects of cannabinoids on GABA release were first reported in neurons in the basal ganglia, hippocampus, cerebellum, amygdala, nucleus accumbens and cortex. Evidence of these effects is further supported by the fact that cannabinoid agonists modulate presynaptic GABA release, decrease amplitude and frequency of $GABA_A$ receptor-mediated inhibitory postsynaptic currents and fail to block the postsynaptic response induced by GABA or muscimol. This process is specifically mediated by CB_1 receptor-dependent activation because it is blocked by two independent antagonists of CB_1 receptors, e.g., rimonabant (SR141716A) and AM251, and is completely absent in CB_1 receptor knockout mice (see reviews from Freund et al., 2003; Kano et al., 2009; Kano, 2014). The lack of effect of FAAH inhibitors (increased endogenous levels of AEA) in the hippocampal DSI indicates that AEA is apparently not involved in the CB_1 receptor-mediated modulation of GABA release (Kim and Alger, 2004). On the other hand, the genetic inhibition of MAGL (increased levels of 2-AG) enhances short-term synaptic depression or DSI (Pan et al., 2011) whereas the genetic inactivation of DAGL-α (decreased levels of 2-AG) completely abolishes all forms of eCB-mediated synaptic plasticity in the prefrontal cortex (Yoshino et al., 2011), hippocampus (Gao et al., 2010), striatum and cerebellum (Tanimura et al., 2010). Taking into account that DAGL-α is mainly located postsynaptically in several brain areas, whereas MAGL is consistently found presynaptically in axon terminals throughout the CNS (see review from Katona and Freund, 2012), 2-AG is

synthesized and released postsynaptically to bind to CB_1 receptors located presynaptically. These findings point to 2-AG as the eCB which is most probably responsible for DSI.

2) DSE or modulation of glutamatergic neurotransmission by CB_1 receptor activation

Kreitzer and Regehr (2001) discovered that depolarization of cerebellar Purkinje cells induced a transient suppression of excitatory transmission by a presynaptic CB_1-mediated mechanism. Cannabinoid agonists failed to reduce postsynaptic responses to glutamate or kainate and SR141716A prevented the suppression of excitatory transmission (Shen et al., 1996; Auclair et al., 2000). DSE has also been reported in many other brain regions including the hippocampus, cerebral cortex, hypothalamus, ventral tegmental area and dorsal cochlear nucleus (reviewed in Kano et al., 2014). Surprisingly, cannabinoid agonists are able to reduce glutamatergic-mediated responses in CB_1 receptor knockout mice to the same levels as they do in wild-type mice (Hájos et al., 2001), suggesting that glutamatergic axon terminals must contain a novel cannabinoid-sensitive site which is indeed blocked by SR141716A, but it would be molecularly distinct from the cloned CB_1 receptor (Freund et al., 2003).

3) Presynaptic suppression caused by Ca^{2+} influx by NMDA-type glutamate receptors

In addition to DSE, the stimulation of NMDA receptors induces a transient suppression of inhibitory transmission in cultured hippocampal neurons which requires postsynaptic eCB synthesis in a Ca^{2+}-dependent manner and CB_1 receptor activation (Ohno-Shosaku et al., 2007).

GPCR-driven eCB release-dependent STD

The synthesis and release of eCB in a Ca^{2+} independent manner can be induced by the postsynaptic activation of $G\alpha_{q/11}$-coupled GPCRs such as Group I metabotropic glutamate receptors ($mGluR_1$ and $mGluR_5$). The activation of Group I mGluR leads to a transient suppression of the excitatory transmission to Purkinje cells which can be abolished when the $G\alpha_{q/11}$-signaling pathway is blocked by the application of GTPγS or GDPβS, whereas no effects are observed with high concentrations of the Ca^{2+} chelator BAPTA (Maejima et al., 2001). The mGluR-driven eCB-STD has been reported in many regions of the brain, including the hippocampus, striatum, nucleus accumbens, medial nucleus of the trapezoid body, and periaqueductal gray (reviewed in Kano, 2014). The same phenomenom occurs with other $G\alpha_{q/11}$-coupled GPCRs including M_1/M_3 mAChR ($mAChR_1$ and $mAChR_1$) (Kim et al., 2002), 5-HT_2-type serotonin receptors ($5HT_2R$) (Best and Regehr, 2008), orexin

receptors (Haj-Damene and Shen, 2005) and oxytocin receptors (Hirasawa et al., 2004). When postsynaptic $G\alpha_{q/11}$-coupled GPCRs are stimulated, DAG is produced through PLCβ, and converted to 2-AG by DAGL-α (reviewed in Kano et al., 2009; Katona and Freund, 2012; Kano, 2014). 2-AG is then released, activates presynaptic CB_1 receptors and the transmitter release is suppressed by inhibiting presynaptic voltage-gated Ca^{2+} channels.

Ca^{2+} assisted GPCR-driven eCB release-dependent STD

This form of short-term plasticity induces the synthesis and release of eCB by a small increase in Ca^{2+} and a weak $G\alpha_{q/11}$-coupled GPCR activation, including that of $mGluR_1$ and $mGluR_5$, $mAChR_1$ and $mAChR_3$, (Kim et al., 2002; Narushima et al, 2007; Hashimotodani et al., 2005; Maejima et al., 2001; Maejima et al., 2005). This phenomenom shares similar molecular mechanisms of eCB synthesis and release as those described immediately above.

The eCB release-dependent LTD

Long-term synaptic plasticity phenomenon which occurs in both inhibitory and excitatory synapses is mainly induced by repetitive afferent stimulation with or without postsynaptic depolarization, but also by postsynaptic firing. Presynaptic release of glutamate activates AMPA receptors and mGluR on the postsynaptic membrane and induces 2-AG release which activates CB_1 receptors in the same presynaptic terminals which release glutamate (homosynaptic) or neighboring presynaptic terminals (heterosynaptic). This phenomenon has not only been observed in excitatory synapses in the dorsal striatum, nucleus accumbens, cerebral cortex, dorsal cochlear nucleus, cerebellum, and hippocampus, and in inhibitory synapses in the hippocampus, amygdala and ventral tegmental area, but also in cholinergic synapses (reviewed in Heifets and Castillo, 2009) (Figure 7b).

The eCB release-dependent LTP

CB_1 receptor-mediated short-term DSI and DSE may contribute to additional forms of neuronal plasticity and synaptic strengthening, such as in LTP (Carlson et al. 2002). The development of cell-type specific CB_1 receptor-knockout models has helped us to study how eCB signaling in specific neuronal circuits (i.e. CB_1 receptor-mediated regulation of GABAergic or glutamatergic transmission) contributes to neuronal network activity, synaptic plasticity and behavior. Some studies have revealed that the lack of CB_1 receptors in glutamatergic neurons (Glu-CB_1-KO) facilitates hippocampal LTP formation (Monory et al., 2015), or the inactivation of CB_1 receptors exclusively in

forebrain GABAergic neurons (GABA-CB_1-KO) leads to diminished hippocampal LTP formation (Monory et al., 2015). The activation of CB_1 receptors specifically in GABAergic neurons inhibits LTD in the amygdala (Marsicano et al., 2002). Moreover, object exploration (Häring et al., 2011), impulsiveness (Lafenêtre et al., 2009), feeding response (Bellocchio et al., 2010), and active fear coping (Metna-Laurent et al., 2012), are decreased in Glu-CB_1-KO animals, whereas these behavioral outcomes are increased in GABA-CB_1-KO animals.

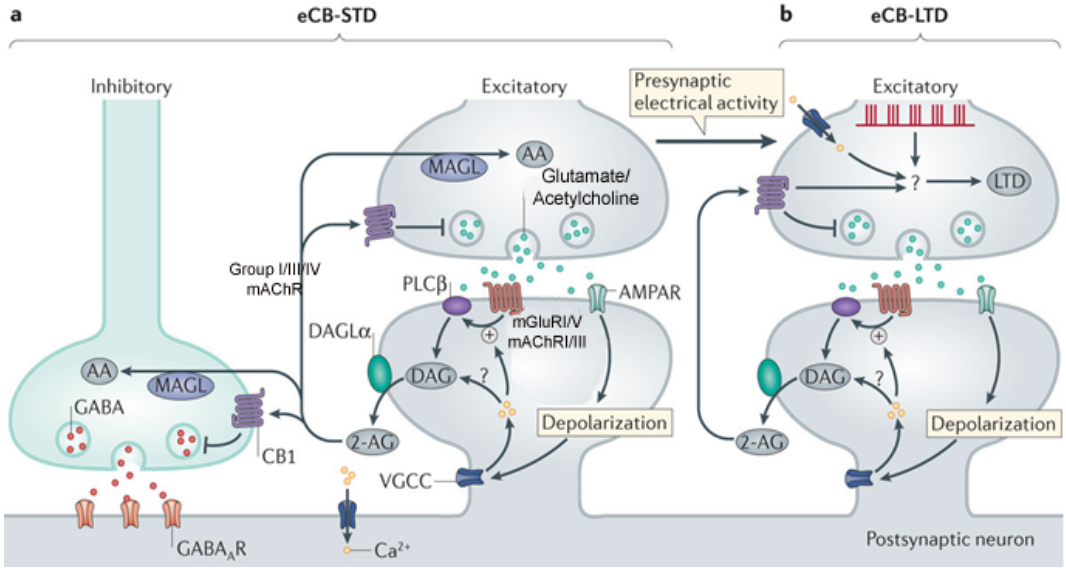

Figure 7. Schematic diagram of eCB-mediated contol of retrograde signaling. a) In Ca^{2+}-driven eCB-STD, Ca^{2+} influx through voltage-gated Ca^{2+}-channels (VGCC) stimulates an unidentified enzymatic pathway (denoted by a question mark) to produce DAG. In GPCR-driven eCB-STD, activation of $G\alpha_{q/11}$-coupled receptors stimulates PLCβ1 to yield DAG. In eCB-STD and eCB-LTD, DAG is converted to 2-AG by DAGL-α activates presynaptic CB_1 receptors to transiently suppress transmitter release and is degraded by MAGL. In synaptically driven eCB-STD, glutamate released from excitatory presynaptic terminals causes Ca^{2+} influx through both AMPA receptors and VGCC, and/or activation of group I mGluR or mAChR1/3 inducing 2-AG release which binds to CB_1 receptors located either on the stimulated terminals releasing glutamate (homosynaptic) or on neighboring terminals (heterosynaptic). b) The released 2-AG activates CB_1 receptors on either of the stimulated terminals releasing glutamate. In addition to CB_1 receptor activation, presynaptic electrical activity, Ca^{2+} influx through VGCCs and Ca^{2+} influx through NMDA-type glutamate receptors (not shown) can each play a part in the induction of eCB-mediated long-term depression (eCB-LTD). (Modified from Soltesz et al., 2015).

2.3. Modulation of cholinergic neurotransmission through CB_1 receptors

Since cortical cholinergic innervation controls cognitive processes, which can be strongly modulated by cannabinoid agonists, the crosstalk between eCB and cholinergic systems has been analyzed by different approaches. There is both histological and pharmacological evidence of the eCB-driven modulation of cholinergic neurotransmission through CB_1 receptor activation.

Histological evidence

BFCN mediated control of learning and memory processes suggests the existence of finely-tuned modulations of synaptic transmission involving eCB signaling. There are only a few immunohistochemical studies in which the anatomical distribution of the different elements of the eCB system in the mammalian central cholinergic system is described. These studies indicate that rodent BFCN of the NBM are devoid of CB_1 receptors, but contain the AEA degrading enzyme FAAH and display a fine receptor fiber meshwork surrounding the perikarya which further suggests that BFCN may utilize eCB for the retrograde control of neurotransmission (Harkany et al., 2003). Similar results were obtained in the gray mouse lemur, revealing evolutionarily conserved networks (Harkany et al., 2005). However, there are controversial anatomical data regarding the CB_1 receptor expression in BFCN (Freund et al., 2003). Previous light and electron microscopy studies reported a dense labeling of CB_1 receptors in ChAT positive neurons in monkey, and the existence of differentiated BFCN in the medial septum of the rat where cholinergic innervation of the hippocampus originates, some of which express CB_1 receptors (Lu et al., 1999; Nyíri et al., 2005).

Pharmacological evidence

There is pharmacological evidence of the eCB-driven modulation of cholinergic neurotransmission through CB_1 receptor activation by mAChR-driven eCB release-dependent STD and mAChR-driven eCB release-dependent LTD.

mAChR-driven eCB release-dependent STD

A significant decrease of electrically evoked ACh release in rodent brain can be induced by various cannabinoid receptor agonists (Gifford et al., 1996; Kathman et al., 2001). This effect is completely blocked by the CB_1 receptor antagonists SR141716A and AM281, and absent in CB_1 receptor knockout mice (Gifford et al., 2000). Moreover, the eCB-mediated ACh release is increased in “knockdown” experiments with antisense oligonucleotides complementary to CB_1 receptor mRNA and in the hippocampus and the neocortex of CB_1 receptor knockout mice (Kathmann et al., 2001). Comparable effects had been described in hippocampal slices in a CB_1 receptor activation-dependent manner (Gifford and Ashby, 1996). However, *in vivo* administration of cannabinoid compounds reveals contradictory results; e.g., the administration of Δ^9-THC or the synthocannabinoid WIN55,212-2 reduces hippocampal ACh release (Gessa et al., 1997; Carta et al., 1998), whereas Acquas et al. (2000, 2001) report increased rates of ACh release. Interestingly, cannabinoid agonists, in a

dose-dependent manner, trigger biphasic effects on functional responses (Margulies and Hammer, 1991), cortical evoked potentials (Turkanis and Karler, 1981), locomotion (Sulcova et al., 1998) and on the CB_1 receptor-mediated release of ACh (Tzavara et al., 2003a). This study shows that a low dose of WIN55,212-2 (0,5 mg/kg) induces a transient stimulation, whereas a higher dose (5 mg/kg) triggers persistent inhibition of hippocampal ACh release, probably involving dopamine D_1 and D_2 receptors. Such an "inverted U" dose-response relationship requires further investigation, but may be explained by the activation of CB_1 receptors located on non-described local neuronal networks which may enhance or reduce the intrinsic activity of BFCN (Freund et al., 2003).

On the other hand, the cholinergic agonist carbachol transiently suppresses inhibitory synaptic transmission in CA1 pyramidal cells in a CB_1 receptor activation-dependent manner (Kim et al., 2002), specifically through mAChRs with the involvement of nitric oxide (Makara et al., 2007). Moreover, in genetically modified mice lacking each subtype of mAChR, it has been demonstrated that $G\alpha_{q/11}$-coupled mAChR activation is responsible for the PLCβ-mediated stimulation of 2-AG synthesis, which finally induces short-term plasticity (DSI) in cholinergic synapses (Fukudome et al., 2004). The mAChR-driven eCB-mediated STD is also found in hippocampal excitatory synapses and in striatal inhibitory synapses, leading to the phenomena of DSE and DSI, respectively (Straiker and Mackie, 2007; Narushima et al., 2007).

mAChR-driven eCB release-dependent LTD

CB_1 receptor-mediated LTD dependent on mAChR stimulation has been described in both inhibitory synapses (Younts et al., 2013), and excitatory synapses (Zhao and Tzounopoulos, 2011). A recent study provides evidence of a 2-AG mediated LTD of glutamatergic synaptic transmission in the prefrontal cortex induced by specific stimulation of M_1 mAChR, since it is abolished by selective M_1 mAChR antagonism (Martin et al., 2015).

The above mentioned findings represent different examples of the crosstalk between both systems which reveal the CB_1 receptor-mediated short- and long term cholinergic synaptic plasticity, pointing to 2-AG as the eCB responsible for these phenomena.

2.4. CB_2 receptor

In 1993 the second subtype of cannabinoid receptors, named the CB_2 receptor was identified (Munro et al., 1993). A human cDNA cloning revealed that it is a GPCR consisting of 360 amino acids, located in chromosome 1p35-p36 and that it shares a 44% homology with the human CB_1 receptor. It was subsequently cloned in several mammalian species, including mouse (347 amino acids) (Shire et al., 1996) and rat (410 amino acids) (Brown et al., 2002).

Distribution of CB_2 receptors

CB_2 receptors are widely distributed in peripheral tissues, and particularly in immune system cells. CB_2 mRNA has been identified in many immune tissues displaying the highest levels in macrophages, CD4+ T cells, CD8+ T cells, B cells, natural killer cells, monocytes and polymorphonuclear neutrophils. Interestingly, CB_2 mRNA has been found in CNS microglia, regulating its migration (Walter et al., 2003), with variations in CB_2 receptor level expression depending on the state of activation of the cell in response to specific damage such as neurodegenerative processes (Ashton and Glass, 2007). In healthy brain, microglia does not express the CB_2 receptor (Stella, 2004). However, CB_2 receptors can be detected in neuritic plaque-associated microglia in AD brain tissue (Benito *et al.*, 2003). In addition, there is molecular and pharmacological evidence of the distribution of CB_2 receptors in several tissues including pulmonary endothelial cells, bone tissue, the gastrointestinal system, mouse spermatogonias, mature and precursor adipocytes, cirrhotic liver, cardiomyocytes, pancreas and spleen (reviewed in Atwood and Mackie, 2010).

Regarding CB_2 receptor expression in the CNS, data obtained during the CB_2 receptor knockout mouse characterization confirmed earlier reports, which led to the conclusion that it is absent in the intact CNS. When CB_2 was first cloned, *in situ* hybridization demonstrated the absence of a CB_2 mRNA signal in rat brain (Munro et al., 1993; Hohmann and Herkenham, 1999b; Howlett et al., 2002; Beltramo et al., 2006). Consistent with these observations, northern blot analyses on mouse and rat brain also failed to detect CB_2 receptors (Schatz et al., 1997). Further RT-PCR-based studies reported undetectable levels of CB_2 in human brain and in the pituitary gland (Galiegue et al., 1995), or in mouse brain using RT-PCR/southern blot analysis (McCoy et al., 1999). In addition to the above mentioned molecular evidence, pharmacological approaches based on receptor binding and GTPyS binding studies also failed to detect CB_2 receptors or G protein-mediated activity in the rat CNS (Griffin et al., 1999).

In summary, the distribution of CB_2 in the CNS remains controversial. In addition to its expression in the microglia under particular circumstances, more recent studies provide immunohistochemical, pharmacological and physiological evidence of its presence in astrocytes (Sanchez et al., 2001), brainstem neurons (Van Sickle et al., 2005) and in culture neurons of Purkinje and granular cells of mice cerebellum (Skaper et al., 1996), as well as in neural progenitor cells (Palazuelos et al., 2006). The presence of CB_2 receptors in the CNS at detectable and functionally relevant levels has been detected in rodent and human whole brain, brainstem, cerebellum, cortex, hippocampus, thalamus, olfactory bulb, thalamic nuclei and in several additional brain regions (reviewed in Atwood and Mackie, 2010). Interestingly, recent work also indicates that CB_2 receptors expressed in neurons modulate the rewarding sensations obtained from cocaine (Xi et al., 2011) and mediate hippocampal synaptic function (Stempel et al., 2016).

CB_2 receptor-mediated signaling pathways

Similarly to CB_1, the CB_2 receptor has been characterized by different research groups as a $G\alpha_{i/o}$ coupled receptor (Bayewitch et al., 1995; Felder et al., 1995; Slipetz et al., 1995; Gonsiorek et al., 2000; Sugiura et al., 2000). The CB_2 receptor-mediated intracellular signaling mechanisms include MAPK and PI3K activation, gene transcription and ceramide production, which is associated with a decrease in proliferation and apoptosis (Bouaboula et al., 1996; Shire et al., 1996; Guzmán et al., 2001a,b; Howlett et al., 2002; Herrera et al., 2005; Romero-Sandoval et al., 2009). One of the main differences in relation to CB_1 receptors, is that CB_2 receptors appear to poorly modulate Ca^{2+} channels or inwardly rectifying K^+ channels (Felder et al., 1995).

2.5. Phytocannabinoids, synthocannabinoids and indirect agonists

Phytocannabinoids

Cannabis plants produce a unique mixture of chemical constituents; the most well-known of which are the C_{21} terpenophenolic compounds, collectively called phytocannabinoids. Detailed chemical analysis has identified approximately 70 molecular species (ElSohly and Slade, 2005). Δ^9-THC was isolated by Yechiel Gaoni and Raphael Mechoulam (1964), and its psychotropic effects were assessed in primates (Mechoulam et al., 1970). Using the chemically defined Δ^9-THC molecule, researchers were able to obtain qualitatively and quantitatively reproducible pharmacological, physiological or behavioral data which led to the uncovering of the

neurobiological substrates of eCB signaling. Another important phytocannabinoid based on its abundance in the plant (up to 40% plant extract) is cannabidiol. The absence of affinity for cannabinoid receptors, together with modest cannabimimetic actions and its lack of toxicity, point to this compound as a promising therapeutic agent. Some studies suggest possible interactions with other GPCR e.g., antagonist of GPR55 (Ryberg et al., 2007), the partial agonist of 5-HT_{1A} receptor (Russo et al., 2005), or the allosteric modulator of δ-opioid receptors (Kathmann et al., 2006).

Synthocannabinoid agonists

Synthetic cannabinoid agonists or synthocannabinoids can be divided into four groups according to their chemical structures. The first group (classical cannabinoids) involves dibenzopyran derivatives that are both natural constituents of cannabis (e.g., Δ^9-THC and Δ^8-THC) and their synthetic analogues (HU 210). The first generation of classical cannabinoids lacked CB_1/CB_2 receptor selectivity, as they were synthesized by inducing minor modifications of the Δ^9-THC molecule. CB_2 receptor-selective agonists such as JWH-133 and HU-308 were also synthesized (Hanuš et al., 1999; Huffman et al., 1996). The second group (non-classical cannabinoids) was developed as bicylic and tricyclic analogues of Δ^9-THC lacking the pyran ring (Melvin et al., 1993). This group includes CP55,940, which binds to both CB_1 and CB_2 receptors with a similar affinity. The administration of CP55,940 in mouse revealed that it is 10 to 50 times more potent than Δ^9-THC (Johnson and Melvin, 1986). CP55,940 is a full agonist for both receptor types and significantly contributed to both the *in vitro* and *in vivo* pharmacological characterization of CB_1 receptors. The third group of cannabimimetic compounds consists of the aminoalkylindoles. This series is represented by WIN55,212-2 which also displays a high affinity for both cannabinoid receptors. Some of these aminoalkylindoles, such as JWH-015, display significant selectivity for the CB_2 receptors (Showalter et al., 1996). The prototype of the fourth eicosanoid group, which involves arachidonic acid derivatives, is AEA, the first eCB isolated from mammalian brain (Devane et al., 1992). Some examples of eicosanoid-based cannabinoid agonists are AM356, arachidonyl-2´-chloroethylamide (ACEA) and arachidonylcyclopropyl-amida (ACPA).

Some synthetic agonists display more selectivity for the CB_1 receptor subtype including (+)-methanandamide, ACEA and ACPA. Examples of the CB_2 receptor-selective agonists most frequently used are JWH-133, HU-308, JWH-015 and AM-1241 (Reviewed in Pertwee, 2008).

Synthocannabinoid antagonists

The first specific cannabinoid antagonist developed and pharmacologically characterized was SR141716A (Rinaldi-Carmona et al., 1994). It blocks the actions of various cannabinoid agonists both *in vitro* and *in vivo* (see reviews from Kano et al., 2009; Freund et al., 2003). This compound is a pure antagonist at nanomolar concentrations but it is not CB_1 receptor-specific and it blocks both CB_1 and CB_2 receptors (Pertwee, 1999). It displays inverse agonism under certain experimental conditions. Two analogues of SR141716A have also been developed, AM251 and AM281 (Howlett et al., 2002). Some selective antagonists for CB_2 receptors are SR144528, AM630 and surinabant, which display considerably more affinity for CB_2 receptors than for CB_1 receptors (Rinaldi-Carmona et al., 1998). However, most of the pharmacodynamic features were studied in cell cultures which overexpressed CB_2 receptors, but not by using *in vivo* experiments. One *in vivo* experiment on cannabinoid-induced antinociception demonstrated that low doses of both SR141716A and SR144528 contributed to prolonging and enhancing pain induced by tissue damage, which indicates that peripheral CB_1 and CB_2 receptors are participating in the intrinsic control of pain (Calignano et al., 1998).

Indirect agonists

Inhibitors of AEA and 2-AG degradation offer an alternative strategy to stimulate the eCB system. Indeed, despite the structural similarity shared by AEA and 2-AG, distinct enzymes inactivate these lipids and serve as key points of control over specific eCB signaling events *in vivo*. FAAH knockout mice or animals treated with selective FAAH inhibitors exhibit more than ten-fold elevations in brain levels of AEA and other N-acyl ethanolamines, but no alterations in 2-AG. Conversely, mice treated with selective MAGL inhibitors show 8 to 10-fold increases in brain 2-AG levels without changes in AEA content. Pharmacological studies have revealed that selective FAAH and MAGL inhibitors produce an intriguing subset of the behavioral effects observed with direct CB_1 receptor agonists. To date several FAAH and MAGL and dual FAAH/MAGL inhibitors have been developed (see review from Blankman and Cravatt, 2013).

AEA degradation inhibitors. The FAAH inhibitors with improved selectivity and *in vivo* activity can be divided into α-ketoheterocycles (OL-135), carbamates (URB597, URB694), alkylsufonylfluorides (AM3506) and aryl ureas, (PF-3845, LY-2183240).

2-AG degradation inhibitors. The first generation of MAGL inhibitors were carbamates that displayed low potencies and included URB602, NAM and OMDM169. The next O-aryl carbamates showed more capacity to increase brain 2-AG levels.

JZL184, which will be used in this work, is about 100-fold more selective for MAGL than for FAAH, and has been extensively used to further understand the physiological roles of 2-AG (Long et al., 2009). One of the most recently developed MAGL inhibitors is based on O-hexafluorisopropyl carbamates is KML29.

Dual AEA and 2-AG degradation inhibitors. Dual FAAH/MAGL inhibitors include organophosphates (isopropyl-dodecylfluorophosphonate), O-aryl carbamates (JZL195) and O-hydroxyacetamide carbamates (SA-57).

Blockers of eCB uptake. Some of the molecules that seem to block the uptake of eCB include AM404, UCM707, VDM11 and OMDM-2.

3. Neurotransmission in AD

The hypothesis which links age-related memory loss to cholinergic neurotransmission impairment was originally based on the observation that cognitive deficits related to learning and memory were pharmacologically induced when cholinergic neurotransmission was blocked. Antagonists of mAChR disrupt higher cognitive functions and induce transient amnestic states. When scopolamine, a centrally active and non-selective mAChR antagonist, was administered to young adult volunteers, the drug caused selective deficits in recent memory (Drachman and Leavitt, 1974). The basal forebrain cholinergic pathways play functional roles in conscious awareness, attention, working memory and additional mnemonic processes (Perry et al., 1999). In addition, a specific cholinergic deficit involving the projections from the basal forebrain to the cortex, hippocampus and amygdala, is consistently found in *postmortem* material from AD patients and in *in vivo* neuroimaging studies (Whitehouse et al., 1982; McGeer et al., 1986).

This anatomical and pharmacological evidence indicated a pivotal role for cholinergic dysfunction in age-related memory disturbances and lead to the "cholinergic hypothesis of geriatric memory dysfunction" (Bartus et al., 1982). The cholinergic brain areas involved in the control of the cognitive processes impaired in AD patients include the basal forebrain and its main afferent and efferent pathways to the cortex, hippocampus and amygdala.

3.1. The cholinergic neurotransmitter system in AD

The cholinergic pathways affected in AD

Morphological (Hedreen et al., 1984; McGeer, 1986), neurochemical (Sparks et al., 1992) and functional studies (Neary et al., 1986; Collerton, 1986; McGeer et al., 1986) showed that the atrophy of nbM, designated as the Ch4 cell group (Mesulam et al., 1983a), played a significant role in the progression of AD. *Postmortem* and *in vivo* studies have reported marked alterations related to all components of the cholinergic neurotransmission system in AD. The loss of BFCN in the nbM is one of the main hallmark features of AD brains and was originally described by Davies and Maloney (Davies and Maloney, 1976), and corroborated in subsequent studies (Whitehouse et al., 1981, 1982; Arendt et al 1983; Vogels et al., 1990; Lehericy et al., 1993; Cullen and Halliday, 1998; Geula et al., 2008). The loss of cortical cholinergic innervation in AD

can be attributed to the loss of BFCN present in the nbM (Whitehouse et al., 1981, 1982; McGeer et al., 1984; Rogers et al., 1985; Saper et al., 1985; Etienne et al., 1986; Vogels et al., 1990). The profound reductions in ChAT and AChE activities in cholinergic projecting areas of AD patients could result from impaired synthesis of these enzymes, from an abnormality in their axonal transport from BFCN bodies to terminals in the cortex or from degeneration or atrophy of BFCN. The primary source of cholinergic innervation to cortex and hippocampal formation is derived from large BFCN in the nbM and the complex MS-diagonal band of Broca respectively, and these cholinergic nuclei have been extensively examined in patients with AD. This is the case of a 74 year-old man who died after a period of progressive loss of memory and impairment of judgment. Notably, his father and paternal aunt and uncle suffered from a dementia beginning at approximately 60 years of age (Whitehouse et al., 1981). Histological analysis of the brain revealed the presence of neuritic plaques and neurofibrillary tangles diagnostic of AD. The histochemical studies carried out in serial slices, including the forebrain, were compared with slices from an age-matched control. The patient with AD exhibited a profound and selective loss of BFCN within the nbM (Figure 8), whereas the neurons in the adjacent structures were not affected by the degenerative process.

Several studies provided evidence of a significant decrease in ChAT and AChE activity in AD patients compared to non-demented control subjects, leading to a decrease in the synaptic availability of ACh in areas innervated by BFCN (Perry et al., 1977 and 1978a,b; Davies, 1979; Sims et al., 1981; McGeer et al., 1986). However, some immunohistochemical studies reported only changes in size, but not in the number of BFCN, and no significant loss of cortical ChAT was found in *postmortem* studies of mild AD patients (Pearson et al., 1983; DeKosky et al. 2002). Further quantitative analyses of ChAT-positive cells revealed a similar number of BFCN in the nbM in early AD patients and the healthy elderly (Gilmor et al. 1999). However, comparable numbers of BFCN do not necessarily reflect an intact and fully functional cholinergic system because shrinkage of BFCN has also been observed in AD patients, and this is likely to cause a significant loss of cortical synaptic contacts (Vogels et al. 1990). A comparison of the estimated BFCN density in the nbM with ChAT activity revealed that, when the enzyme activity was reduced by 90%, the BFCN density was decreased by 33% (Perry et al., 1982), 35% (Candy et al., 1983), 50% (Lehéricy et al., 1993) or 70% (Arendt et al., 1983), demonstrating both the loss of BFCN and atrophic BFCN processes (Cummings and Benson, 1987; Pearson et al., 1983). An *in situ* hybridization study demonstrated that there was a significant reduction in the expression of ChAT mRNA per remaining BFCN in AD patients,

supporting the hypothesis that the expression of the ChAT gene might be down-regulated in the surviving BFCN, suggesting the possibility of the functional restoration of ChAT synthesis (Strada et al., 1992).

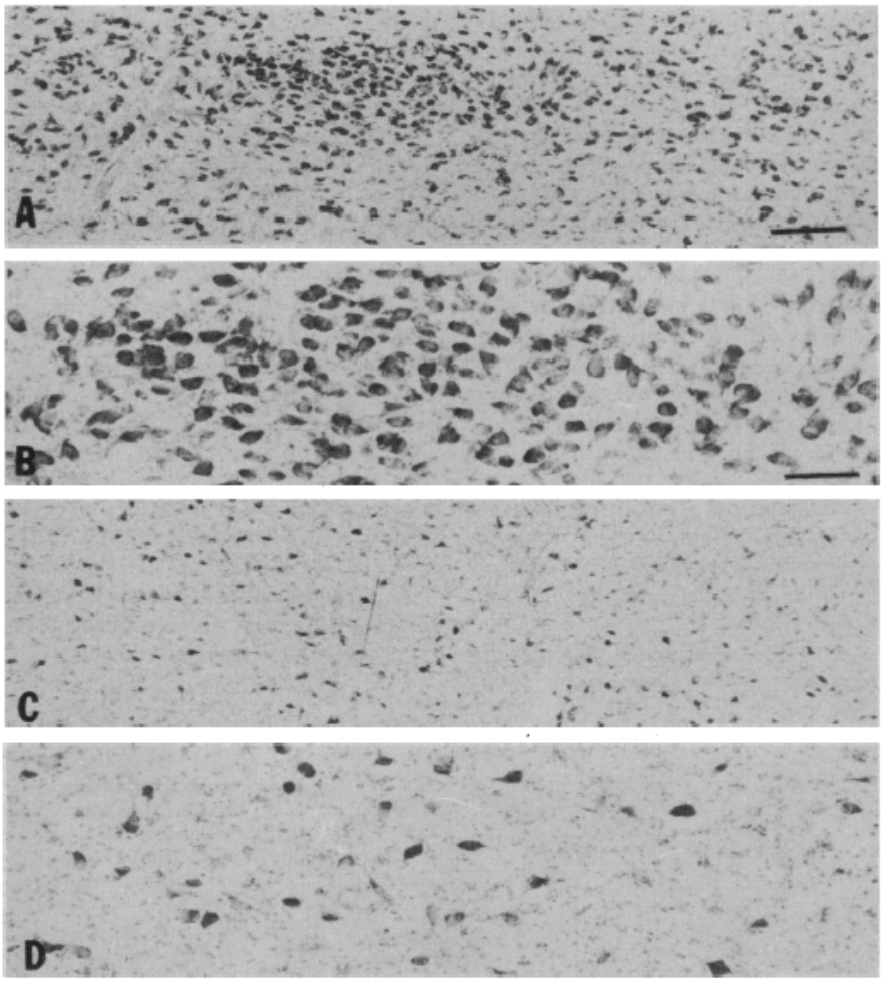

Figure 8. Photomicrographs from the midportion of the nbM of an age-matched control (A and B) and a patient with AD (C and D). (A and C) Normal density of BFCN in the control and the profound loss of neurons in the AD patient. At higher magnification, the BFCN in the control subject (B) appear as large cells with densely stained Nissl substance. Few neurons are present in the nbM of the patient with AD (D). Magnifications: (A and C) x 10; (B and D) x 25. Scale bar is 200 µm in (A) and 100 µm in (B). (Original figure extracted from Whitehouse et al., 1982).

Additional studies demonstrated that BFCN display hypertrophy in the early stages of AD, and gradually become atrophic in the advanced stages (Kobayashi et al., 1991). Interestingly, the relationship between the loss of BFCN in the nbM and the formation of neuritic plaques in the cortex of AD patients was examined and a correlation between the number of neuritic plaques in several neocortical areas and the loss of BFCN was found (Arendt et al. 1984), whilst others concluded that the dysfunction and death of BFCN was associated with extensive tangle formation

(Rasool et al., 1986). Thus, by using AChE-staining histochemical assay, a marked decrease in the density of stained BFCN, together with abundant neurofibrillary tangles were found in the nbM of AD patients (McGeer et al., 1986).

Due to the large number of neurochemical, neuropathological and functional observations which have been made in *postmortem* samples from AD patients, it is reasonable to think that the nbM is deeply involved in the manifestation and progression of AD. ChAT activity and AChE-positive fibers are markedly reduced in the frontal, parietal, temporal and visual cortices in AD. The depletion of cholinergic structures in the temporal lobe, including its limbic, paralimbic and associated components is similar to the distribution of the senile plaques (Mesulam and Geula, 1994). The different subdivisions of the BFCN also seem to be affected in a different way in AD which correlates with the cortical areas that are predominantly innervated by these BFCN subnuclei (reviewed in Kása et al., 1997).

The cholinergic innervation of the hippocampal formation is thought to play an important role in memory processes and there is a large body of evidence which supports that the basal forebrain cholinergic innervation of the hippocampus becomes reduced in the elderly as well as in AD patients. The distribution of AChE in AD hippocampal samples revealed reduced levels of both AChE activity and stained fiber densities (Henke and Lang, 1983; Green and Mesulam, 1988; Perry et al., 1992; De-Lacalle et al, 1994). However, the distribution and density of senile plaques is different from the density of AChE-positive fibers in the hippocampus from AD patients, despite some studies which demonstrate the presence of a large number of senile plaques intermingled with positively-stained fibers in the molecular layer of the dentate gyrus (Vágvölgyi et al., 1991). Regarding ChAT levels in AD hippocampal samples, different studies reported loss to an extent ranging from 25% up to 97%, depending on the area and layer examined (Perry et al., 1977; Davies, 1979; Rossor et al., 1982; Henke and Lang, 1983; Araujo et al., 1988; Sakurada et al., 1990).

The amygdaloid complex is relatively large and is composed of discrete neuronal nuclei located deeply within the temporal lobes of the brain. It is involved in the processing of memory, decision-making, and emotional reactions (Mishkin, 1978). The amygdala is considered part of the limbic system and a major locus of pathology associated with AD (Herzog and Kemper, 1980; Kromer-Vogt et al., 1990; Benzing et al., 1993; Emre et al., 1993). The cholinergic innervation of the amygdaloid complex from patients with AD has been studied by AChE histochemistry (Svendsen and Bird, 1985; Benzing et al., 1993), and ChAT immunohistochemistry (Benzing et al., 1993; Emre et al., 1993). In *postmortem* samples from AD patients, ChAT activity has been found to be significantly reduced in the amygdala (Rossor et al., 1982). The highest

reduction was found specifically in the basolateral nucleus (Emre et al. 1993). The density of senile plaques and the extent of neurofibrillary tangles in the amygdala do not apparently correlate with the loss of either the cholinergic innervation or BFCN density (Tago et al., 1987; Benzing et al., 1993; Emre et al., 1993).

Neuroimaging studies in AD

Neuroimaging techniques such as *in vivo* studies using PET markers of ChAT and AChE activity (Herholz et al., 2004), or cortical glucose metabolism (Peppard et al., 1990), demonstrated a significant reduction of cortical cholinergic function in AD patients. Additional functional imaging studies using PET revealed cortical cholinergic deficits in both AD and Parkinson´s disease patients, using a radioligand to label AChE (Bohnen et al., 2003). *In vivo* quantification of morphological changes in the nbM using magnetic resonance imaging (MRI), demonstrated that the thickness of the substantia innominata in the coronal plane provided a very close estimate of atrophy (Hanyu et al., 2002). These MRI measurements also proved to be predictive of response to treatments with AChE inhibitors (Tanaka et al., 2003). By using a volumetric pixel-based morphometry approach based on proton-diffusion-weighted images, Teipel et al. (2005) found a reduction of the signal intensity in the anterior lateral nbM (Ch4al) of AD patients, which may be related to the loss or degeneration of BFCN. Moreover, a positive correlation between decreased volumetric measurements in the nbM and reduced cortical gray matter density in several regions was observed, suggesting an anatomical degenerative link (Grothe et al., 2012 and 2013). Other studies have reported a reduced volume of specific nbM compartments associated with cognitive decline in MCI patients (Grothe et al., 2010). Additional volumetric neuroimaging studies confirmed that the degree of basal forebrain cholinergic degeneration in AD patients significantly correlated with cognitive decline by using the Mini-Mental State Examination (MMSE) (Choi et al., 2012). Moreover, atrophy of the nbM also predicted the development of dementia in Parkinson´s disease patients (Lee et al., 2013).

The development of neuroimaging techniques has led to the emergence of combined MRI and diffusion tensor imaging analyses which provide a powerful tool to identify neural tracts *in* vivo. Recent studies have used diffusion tensor MRI to identify the nbM and its projections in an attempt to relate the atrophy observed in MCI patients with either memory and/or attentional deficits, cognitive decline and conversion to AD (Brueggen et al. 2015; Grothe et al. 2016; van Dalen et al., 2016). These findings in neuroimaging, together with the neurochemical evidence found in *postmortem* samples from AD patients, support the hypothesis that damage to the integrity of the nbM may underlie the cognitive deficits associated with AD.

Regarding the areas innervated by the nbM, functional MRI in AD patients after a single dose of rivastigmine showed increased cortical activity which indicates a specific effect of cholinergic tone enhancement on cortical neuronal activity (Rombouts et al., 2002). Chronic administration of rivastigmine to early AD patients also increased cortical activation and increased MMSE scores (McGeown et al., 2008; Miettinen et al., 2011; 2015). Similar findings are observed in a functional MRI study carried out in MCI and AD patients following a chronic treatment with the AChE inhibitor donepezil (Saykin et al., 2004; Kircher et al., 2005).

Hippocampal volumetric measurement is recognized as one of the core *in vivo* neuroimaging biomarkers of AD as the hippocampus already undergoes neurodegenerative and atrophic processes during predementia stages of AD (Kaye et al., 1997). MRI volumetric studies have shown consistent patterns of hippocampal and basal forebrain cholinergic system atrophy in AD patients (Grothe et al., 2012; Teipel et al., 2005), and in those with amnestic (Grothe et al., 2010), or amyloid positive MCI (Teipel et al., 2014). Based on these findings, hippocampal volume has been analyzed as a biomarker of cognitive decline and response to cholinergic treatment in AD dementia and prodromal AD (Erten-Lyons et al., 2006; Jack et al., 1999; Macdonald et al., 2013). In addition, in a study conducted on patients with mild AD dementia, smaller hippocampal volume predicted cognitive decline during donepezil therapy (Csernansky et al., 2005). Additional evidence supporting the loss of hippocampal volume as a predictor of global cognitive decline in a prodromal AD cohort has recently been reported (Teipel et al., 2016). Nevertheless, the hippocampal volume does not seem to be a useful biomarker for predicting responses to AChE inhibitors.

Volumetric studies performed in the whole amygdala by using MRI techniques have consistently found reductions in patients with AD (Basso et al., 2006; Horínek et al., 2007). A more recent study reported significantly smaller amygdaloid volumes in both hemispheres in AD patients. Interestingly, structural differences were found when the different nuclei were individually mapped, highlighting a significant tissue loss in the central, medial, lateral and basolateral medial nuclei (Cavedo et al., 2011).

Cholinergic receptors in AD

When the supply of cortical ACh is interrupted as a consequence of BFCN degeneration and/or ChAT down-regulation, the cholinergic receptors located in projecting areas are devoid of the endogenous ligand and one should expect to observe a regulation to compensate for that loss of cholinergic input. The two classes of cholinergic receptors, the G protein-coupled mAChR and the ligand-gated ion channel nAChR, are not equally affected in AD. Nicotinic receptors are generally

decreased in AD, but both binding studies with non-selective muscarinic agonists and antagonists, and histochemical studies show either decreased levels, unchanged levels or even increased levels of mAChR in AD (reviewed in Kása et al., 1997; Ferreira-Vieira et al., 2016).

Muscarinic acetylcholine receptors in AD

The majority of the mAChR is located postsynaptically, and only a proportion of them are autoreceptors distributed in presynaptic membranes of BFCN (Mash et al., 1985; Gulya et al., 1989; Quirion et al., 1989a).

The studies performed in tissue homogenates using radioligands selective for mAChR have shown discrepancies in brain tissue samples from AD patients. [^{3}H]pirenzepine, a relatively selective M_1 mAChR radioligand, shows that binding parameters are generally unaltered in brain tissue samples from AD patients (Araujo et al., 1988; Giacobini, 1990). Since M_1 mAChR are mainly located in postsynaptic cholinoceptive neurons, they are probably conserved after the loss of BFCN. Regarding the M_2 mAChR subtype, different experimental designs make it possible to label these receptors by selectively blocking M_1 mAChR sites, such as [^{3}H]oxotremorine-M binding in the presence of pirenzepine (Vogt et al., 1992), or by using [^{3}H]AF-DX 116, a relatively selective M_2 mAChR antagonist (Quirion et al., 1989b). A significant loss of M_2 mAChR has been observed in specific brain areas of *postmortem* AD patients, including cortical areas and the hippocampal formation, and this is consistent with the idea that M_2 mAChR could be located on degenerating BFCN nerve terminals (Mash et al., 1985; Quirion et al., 1989a,b; Giacobini et al., 1990; Reinikainen et al., 1990; Nordberg, 1992). Due to the selective loss of M_2 mAChR in the brain regions of patients with AD which contain senile plaques, it has been suggested that presynaptic M_2-mediated signaling may be involved in the non-amyloidogenic processing pathway leading to maintain amyloid peptide homeostatic levels (Kása et al., 1997). However, the postsynaptic location of M_2 in cortical and hippocampal regions has also been described and this could mask the reductions in the presynaptic M_2 mAChR component (Levey et al., 1991 and 1995; Rossner et al., 1997).

Autoradiography represents a powerful pharmacological tool with which to analyze the radioligand binding in discrete and small brain areas or subfields in brain slices. Moreover, the density and distribution of receptors can readily be correlated with the density of neurons, neuritic plaques and neurofibrillary tangles, or with the degree of cholinergic dysfunction in the brain area of interest on slices consecutive to those processed for autoradiography. The first autoradiographic studies for mAChR in AD

patients showed that the densities and the proportions of the M_1 and M_2 mAChR subtypes in autopsied AD brain samples were not significantly different in slices of hippocampal tissue compared to those observed in non-demented controls (Griffiths et al., 1994; Probst et al., 1988). Conversely, further autoradiographic studies showed significant reductions of both [^{3}H]pirenzepine binding in the presence of cold oxotremorine (M_1 mAChR subtype) and [^{3}H]oxotremorine binding in the presence of an excess of cold pirenzepine (M_2 mAChR subtype) in entorhinal cortex and in most hippocampal strata in AD brain slices (Rodríguez-Puertas et al., 1997).

Immunohistochemical approaches have been used to anatomically describe the mAChR cellular distribution in *postmortem* brain samples from AD patients and have found a decrease in the M_1 protein in the cortex and hippocampus (Flynn et al., 1995). In neocortical and hippocampal regions, M_1 mAChR is mainly expressed in all pyramidal neurons where it displays a somatodendritic distribution (Levey et al., 1991; Levey, 1995). Behavioral studies have demonstrated deficits in learning and memory in mice lacking M_2 mAChR which suggests that the M_2 mAChR subtype plays a crucial role in cognitive processes (Tzavara et al., 2003b). In this sense, hippocampal muscarinic activation, through the high affinity M_2 mAChR subtype, promotes a rise in AMPA receptor sensitivity to glutamate which finally leads to the so-called 'muscarinic long term potentiation', essential to explain hippocampal neuronal plasticity (Segal and Auerbach, 1997). Regarding the distribution of the M_2 mAChR subtype, and consistent with radioligand binding assays, a decrease in protein levels was also found in AD patients that could probably be explained by the loss of BFCN during the disease. Cortical M_4 mAChR, which are expressed in the neuropil and in scattered perikarya, have been found to be significantly up-regulated in AD patients (Flynn et al., 1995). The M_4 loss in rodents leads to dysfunction in hippocampal synaptic transmission, suggesting that this subtype could be involved in neuronal plasticity-associated with memory formation (Mulugeta et al., 2006).

The expression of the genes for M_1 and M_2 mAChR were found to be unchanged in AD patients (Ohara et al., 1994). However, other authors reported increased mRNA levels of the M_1 mAChR subtype in the temporal and occipital cortices (Harrison et al., 1991).

In reference to the functionality of mAChR, the first studies analyzed radioligand binding in the presence of guanine nucleotides, in order to measure the "active receptors" (Warpman et al., 1993). A significant loss of high-affinity agonist binding to M_1 mAChR was described in the frontal cortex of patients with AD (Flynn et al., 1991). The decreased ability of the agonist carbachol to stimulate GTP-dependent [^{3}H]phosphatidylinositol-4,5-bisphosphate hydrolysis indicated defective mAChR-$G\alpha_{q/11}$

protein/PLCβ coupling in the disease (Ferrari-DiLeo and Flynn, 1993; Jope et al., 1997). The first evidence of the relationship between cholinergic muscarinic activation and amyloid precursor protein processing was demonstrated in carbachol-treated cell cultures which overexpressed M_1 and M_3 mAChR (Nitsch et al., 1992a). In fact, the activation of PKC and MAPK signal transduction pathways significantly decreased the generation of Aβ fragment in cultured human cells, and Aβ has been shown to induce the uncoupling of M_1 mAChR from G-protein, blocking the function of M_1 mAChR under the pathological conditions of AD (Kelly et al., 1996). More recent studies found that the attenuation of G-protein coupling to M_1 mAChR in the neocortex was associated with dementia severity, and indeed correlated with reductions in PKC activity and NMDA receptor density, suggesting a postsynaptic cholinergic dysfunction in AD (Tsang et al., 2007). [^{35}S]GTP gamma S binding to G proteins combined with immunoblot analysis of G protein subunits also revealed that the receptor-mediated activation of G proteins was reduced in brain cortex of AD patients (Wang and Friedman, 1994). Oxotremorine-M-mediated activation of the M_2 mAChR subtype did not trigger any change in the functional coupling of M_2 mAChR to G protein in the neocortex of patients with AD (Hernández-Hernández et al., 1995). Further studies have provided evidence of the loss of muscarinic receptor-G protein coupling in AD and support the hypothesis that muscarinic receptor-mediated cortical activation may be compromised in this disease (Ferrari-DiLeo et al., 1995).

Nicotinic acetylcholine receptors in AD

Different studies suggest that brains from AD patients present reduced densities of binding sites for nicotinic ligands such as [^{3}H]ACh, [^{3}H](-)nicotine, [^{3}H]methylcarbamylcholine and [125I]α-bungarotoxin, in comparison with brain samples from age-matched patients (reviewed in Kàsa et al., 1997).

The partial loss of nAChR in AD brains was confirmed by autoradiographic methods. For example, marked reductions in nicotinic binding (laminar binding distribution of [^{3}H]nicotine, [^{3}H]epibatidine, and [^{3}H]cytosine) throughout the cortical layers of the temporal cortex, the presubiculum and parahippocampal gyrus were observed in AD patients, which usually correlates with a decrease in ChAT activity (reviewed in Kása et al., 1997).

The detection of nicotinic receptor-specific mRNA sequences in brain slices by *in situ* hybridization showed a differential distribution of the mRNAs for the α3- and α4-subunits (Wevers et al., 1994). However, no alterations in the localization of the α4-subunit expressing neurons were detected in cortical regions of AD patients (Schröder et al., 1991).

The choline transporter (SDHACU) in AD

SDHACU is a classical presynaptic marker of the cholinergic terminals and pharmacological studies have reported contradictory results in the specific binding of [^{3}H]-HC-3, a highly specific competitive inhibitor, in *postmortem* samples from AD patients. Some authors described significantly decreased densities in tissue membrane homogenates by using binding methods which are very sensitive and precise, but poor in anatomical resolution (Pascual et al., 1991). Consistent with these results, a significant decrease in [^{3}H]-HC-3 binding sites was also found in the hippocampus, entorhinal cortex and layers I-III of the frontal cortex of AD brains (Rodríguez-Puertas et al., 1994). However, other authors have described an increase in [^{3}H]-HC-3 binding in membrane homogenates from AD frontal cortex (Slotking et al., 1994, Bissete et al., 1996). Choline uptake, rather than ChAT activity, is rate-limiting in ACh synthesis (Happe and Murrin, 1993), therefore, an increase in [^{3}H]-HC-3 binding together with a decline in the number of presynaptic terminals could represent a compensatory mechanism in the early stages of the disease, resulting in the maintenance of the total uptake capacity in order to increase both the synaptic ACh availability and finally the activity of the remaining BFCN. However, more recent studies have demonstrated differences in the distribution of the vesicular acetylcholine transporter by using single photon computed tomography. A significant decrease in [^{123}I]-IBVM binding (47-62%) was reported in AD subjects in cingulate cortex and parahippocampal-amygdaloid complex, suggesting that cholinergic degeneration occurs in the early stages of AD (Mazère et al., 2008).

Neurotrophic factors in AD

NGF and receptors

The nerve growth factor (NGF) and its high tyrosine kinase (TrkA) and low p75^{NTR} affinity receptors play a crucial role in BFCN function, and a deregulation of the levels of NGF and its receptors is an important factor underlying BFCN degeneration in AD (Mufson et al., 1999). NGF is synthesized as a precursor proNGF molecule that is proteolytically cleaved to a mature and biologically active neurotrophin peptide. TrkA receptor activation through mature NGF (mNGF) binding stimulates signal transduction pathways of NGF, thereby triggering the majority of its effects for survival and growth. However, p75^{NTR} has multiple additional functions, including apoptosis or cell death (Miller and Kaplan, 2001). The physiological effects of TrkA and p75^{NTR} signaling depend on their interactions with either proNGF or mNGF. In this context, immunoblotting studies demonstrated that proNGF is the predominant form of NGF

present in the cortex of elderly and cognitively healthy humans (Fahnestock et al., 2001). ProNGF levels are increased in the cortex of patients diagnosed with MCI or mild AD, compared to subjects who have no cognitive impairment (Peng et al., 2004). Interestingly, reduced TrkA levels in the cortex were positively associated with lower cognitive performance as assessed by MMSE scores (Counts et al., 2004), whereas increased cortical proNGF levels were negatively correlated with MMSE performance (Peng et al., 2004). Thus, the concomitant reduction of TrkA and the accumulation of proNGF in the cortex may be an early pathological marker of the onset of AD. Several studies indicate that increases in cortical proNGF may result in proapoptotic signaling through binding to the $p75^{NTR}$ receptor. Moreover, significantly increased levels of NGF are detectable in CSF of AD patients, demonstrating the potential utility of NGF as a diagnostic biomarker (Blasko et al., 2006).

Neurotrophin-based treatments in AD

A clinical trial with NGF was assayed by its intracerebroventricular (i.c.v.) administration to AD patients, but acute side effects such as pain, Schwann cell migration to the spinal cord and weight loss were reported and the trial finally had to be halted (Eriksdotter et al., 1998). In 2001, a new clinical trial based on using either *in vivo* or *ex vivo* NGF gene therapy was initiated to check for long-term effects on BFCN degeneration (Tuszynski et al., 2015). Trophic responses to NGF persisted up to ten years after gene transfer, revealing BFCN hypertrophy and CREB activation. Furthermore, no adverse pathological effects were observed over this period.

3.2. Rat model of basal forebrain cholinergic lesion

The first neurochemical deficit identified in AD was the observation that BFCN were selectively affected in AD patients, which has motivated the development of experimental animal models which imitate this impairment (Davies and Maloney, 1976; Perry et al., 1977). Further observations led to the “cholinergic hypothesis of geriatric memory dysfunction” (Bartus et al., 1982), and to the development of cholinergic enhacement therapies using AChE inhibitors. The effects of specific lesions of BFCN in learning and memory have been investigated in animal models of basal forebrain cholinergic dysfunction.

Excitotoxin-based approaches

Initially, the most common approach used in functional studies was the infusion of excitatory amino acid analogues. However, a few studies used non-specific electrolytic lesions (Motohashi et al., 1986; Pirch et al., 1986) or the infusion of ethylcholine aziridinium (AF64A) (Eva et al., 1987; Chrobak et al., 1988). The excitotoxic hypothesis of neurodegeneration that was predominant during the nineties led to the development of lesion models based on a stereotaxic injection of excitotoxins into the basal forebrain to produce a reduction in BFCN and cortico-hippocampal cholinergic neurotransmission dysfunction. The most commonly used excitotoxins were kainic acid (Stewart et al., 1985; Rigdon and Pirch, 1986; Reed et al., 1990), ibotenic acid (Flicker et al., 1983; Hepler et al., 1985; Whishaw et al., 1985) and quisqualic acid (Aaltonen et al., 1991; Riekkinen et al., 1991a,b; Zupan et al., 1993). One of the most important limitations of these lesion paradigms is the fact that, in the rodent, basal forebrain BFCN are surrounded by other different cell populations, especially GABA-containing neurons of the dorsal and ventral pallidum and non-cholinergic magnocellular corticopetal neurons (Zaborsky et al., 1999). The above-mentioned excitotoxins are far from selective for BFCN and trigger non-specific lesions, masking the specific neurochemical and behavioral effects of the basal forebrain cholinergic dysfunction. This is emphasized by studies which demonstrate that basal forebrain lesion-induced behavioral effects depend on the toxin used (Wenk et al., 1992). Therefore, additional methods are required to produce an efficient and selective BFCN lesion to mimic the specific basal forebrain cholinergic dysfunction extensively described in AD. Immunotoxins provide the opportunity to produce neurotoxic lesions of specific neurochemically-characterized neuronal populations by targeting cell-surface antigens that are exclusively expressed by the cells of interest.

192IgG-saporin

During the early nineties, 192IgG-saporin, a powerful tool for selective BFCN lesioning, was developed by Wiley et al. (1991) and revolutionized research on the cognitive functions of the basal forebrain cholinergic system. This compound consists of a monoclonal antibody (192IgG) which is armed with a ribosome inactivating protein (saporin) coupled to the antibody via a disulfide bond and specifically directed to the low-affinity nerve growth factor receptor $p75^{NTR}$. $P75^{NTR}$ is abundantly and specifically expressed in BFCN during the whole life of rodents (Springer et al., 1987; Woolf et al., 1989). The toxin follows receptor binding and internalization like the endogenous ligand of $p75^{NTR}$, and enzymatically inactivates the large ribosomal subunit, thereby blocking

protein synthesis and ultimately resulting in cell death by apoptosis; the neurodegenerative process can be considered complete in about 2 weeks (Wrenn and Wiley, 1998). Lesions of this selectivity and extent had proven impossible to produce using any other technique.

After an i.c.v. injection of 192IgG-saporin, the immunotoxin is taken up by cholinergic terminals and retrogradely transported to cell soma in the basal forebrain (Heckers et al., 1994). Thus, the i.c.v. administration of 192IgG-saporin results in massive BFCN loss, including those from the medial septum, vertical and horizontal limb of the diagonal band of Broca and nucleus basalis magnocellularis, whereas cholinergic cells in the adjacent ventral pallidum and cholinergic interneurons within the caudate putamen are not affected (Rossner et al., 1995a). The immunolesions keep loci of cholinergic degeneration free from mechanical damage and do not affect parvalbumin, calbindin or calretinin containing GABAergic neurons of the basal forebrain. The only additional non-cholinergic neurons known to be affected by the i.c.v. administration of 192IgG-saporin application are cerebellar Purkinje cells which also express $p75^{NTR}$ (Heckers et al., 1994; Waite et al., 1995). Lesions restricted to these cells can trigger substantial deficits in spatial learning in the Morris water maze (Waite et al., 1999). However, such damage results in impairments in a cued version of the water maze in which spatial learning is not required, suggesting that there is also a sensory or motor impairment associated with the loss of cerebellar Purkinje cells (Waite et al., 1995).

The basal forebrain cholinergic system is composed of different rostrocaudally distributed cholinergic nuclei (Ch1-Ch4) with particular innervating networks (Mesulam, 1983a). Intraparenchymal injections of 192IgG-saporin directly into specific nuclei of the basal forebrain allow us to understand the specific role of the different BFCN populations in behavioral and neurochemical aspects. The infusion of 192IgG-saporin in the distinct nuclei induces profound specific BFCN losses and cholinergic hypoactivity in the innervated areas and permits us to assess the contributions of single projection systems in a variety of learning and memory tests, thereby demonstrating the effectiveness of 192IgG-saporin (Wenk et al., 1994). It has been widely described that 192IgG-saporin, in a dose-dependent manner, induces dramatic and permanent decreases in the number of ChAT- and AChE-positive BFCN in the NBM (Torres et al., 1994; Wenk et al., 1994). Two weeks after an intraparenchymal injection into the NBM, significant, long-lasting decreases in the densities of AChE-positive fibers and ChAT activity in several cortical regions of adult rats are observed (Wenk et al., 1994; Szigeti et al., 2013).

Neurochemical effects of BFCN immunolesions in the NBM

Effects on cholinergic neurotransmission

The effects on cholinergic and non-cholinergic neurotransmission of 192IgG-saporin-induced BFCN depletion in the NBM have been extensively analyzed. Multiple neurotransmitter systems are affected in this lesion model, but cortical cholinergic neurotransmission becomes especially impaired. Profound alterations have been reported, such as reductions in several cortical cholinergic presynaptic markers including ChAT activity (up to 80%) and density (up to 50%), or AChE density (up to 90%) and SDHACU density ([^{3}H]HC-3 binding by up to 45%) (Waite et al., 1994; Wenk et al., 1994; Rossner et al., 1995a,b; Gil-Bea et al., 2005; Ljubojevic et al., 2014). As a consequence of interruption in the cortical ACh supply, specific adaptations related to neurotransmitter receptors are observed. Autoradiographic studies demonstrate that M_1 mAChR density is increased by up to 35% in the parietal cortex one week after the 192IgG-saporin infusion, whereas M_2 mAChR density is less affected (an increase of approximately 20%) which is in parallel with great reductions in AChE levels and choline uptake sites (Rossner et al., 1995a,b; Rossner et al., 1997). Cortical postsynaptic M_1 mAChR, which are mainly expressed in pyramidal cells in layers II/III and VI, have been found to be upregulated after the 192IgG-saporin lesion, and these receptors may be compensating for the loss of basal forebrain cholinergic input. Terminals located in cortical layer IV and at the border between layers V and VI exhibit strong M_2 mAChR labeling, in agreement with the dense cholinergic innervation of these cortical layers and the role of M_2 mAChR as an autoreceptor (Eckenstein et al., 1988; Mechawar et al. 2000). The fact that M_2 mAChR is increased after immunolesions (having lost up to 80% of BFCN terminals) supports the hypothesis that a significant population of M_2 mAChR could exist postsynaptically to cholinergic terminals in the cerebral cortex (Rossner et al., 1997; Mesulam, 1998). However, the expression of M_2 receptors in BFCN terminals still remains controversial. *Ex vivo* autoradiographic studies have confirmed significant and widespread decreases in cortical presynaptic terminals by using [^{123}I]BVM, a radioligand which targets the VAChT (Quinlivan et al., 2007). More recently, *in vivo* PET neuroimaging studies, carried out in rats with a 192IgG-saporin-induced lesion of the NBM, have demonstrated a significant decrease in fronto-cortical cholinergic terminals (Parent et al., 2012 and 2013), glucose metabolism (Mehlhorn et al., 1998; Jeong et al., 2016), and neuronal metabolic activity (Gelfo et al., 2013) by using [^{18}F]fluoroethoxybenzovesamicol to label the vesicular ACh transporter and [^{18}F]-2-fluoro-2-deoxyglucose and cytochrome oxidase activity assays.

Effects on other different neurotransmitter systems

As previously mentioned, specific basal forebrain cholinergic immunolesions also affect other neurotransmitter systems, including the glutamatergic, GABAergic, serotonergic and adrenergic systems. While NMDA receptors are reduced by approximately 20%, AMPA and kainate binding sites are increased by up to 30% in several cortical regions seven days after the 192IgG-saporin-induced lesion of the NBM. Moreover, when the BFCN from the medial septum, which innervate hippocampus, are eliminated, NMDA receptor binding sites are reduced by up to 35% in CA1, but with no significant changes in AMPA or kainate receptor binding, demonstrating that there are different effects depending on which of the basal forebrain cholinergic nuclei have been lesioned (Rossner et al., 1995c). Interestingly, upregulation of AMPA receptor expression after NBM lesion is prevented with the NMDA receptor antagonist MK-801 (Garrett et al., 2006). This effect is more pronounced in the frontal cortex of 192IgG-saporin-treated young adult rats than in middle-aged and aged rats, suggesting that cholinergic projections from the basal forebrain cholinergic system play a critical role in cortical plasticity and also that there are age-related differences in lesion-induced expression of AMPA receptors (Kim et al., 2005). Regarding GABAergic neurotransmission, the binding of [^{3}H]muscimol, but not [^{3}H]flunitrazepam, is increased by up to 20% after 192IgG-saporin administration in cortical regions, revealing a modulation of cortical inhibition (Rossner et al., 1995c). The selective BFCN damage in the NBM may be associated with a functional decline in cortical GABAergic neurotransmission and cognitive deficits (Jeong et al., 2011). Moreover, deep brain stimulation of the remaining BFCN after NBM lesion improves spatial memory performance and partially restores the two isoforms of glutamic acid decarboxylase, GAD65kDa and GAD67kDa and glutamate to control levels (Lee et al., 2016). These findings clearly demonstrate that basal forebrain cholinergic innervation has a pivotal role in cognitive processes by fine-tuning the cortical excitatory-inhibitory balance.

Basal forebrain cholinergic immunolesions do not alter α_1-adrenoceptor and $5HT_{1A}$ receptor binding in the neocortex, but α_2 and β-adrenoceptor and $5HT_{2A}$ display significant reductions in neocortical brain regions in parallel with the loss of BFCN terminals (Heider et al., 1997). More recent studies show that NBM cholinergic deafferentation triggers a significant down-regulation of $5HT_{2A}$ receptor levels in the frontal cortex, together with changes in serotonin and 5-hydroxytryptophan levels, suggesting a down-regulation of the rate-limiting enzyme for the synthesis of serotonin in combination with the cholinergic deficit (Severino et al., 2007). However, 5-HT_{1A} and

5-HT_{1B} receptors do not seem to mediate this process (Heider et al., 1997; Garcia-Alloza et al., 2006).

Effects on neurotrophin homeostasis

NGF plays a pivotal role in the development and maintenance of BFCN and neuronal plasticity (Conner et al. 1992). BFCN depletion in the NBM does not modify NGF protein levels in the basal forebrain but considering that much of this protein is located in BFCN cell bodies, the remaining BFCN probably compensate for the loss of cholinergic innervation (Rossner et al., 1997). Interestingly, when NGF is administered i.c.v. to 192IgG-saporin-lesioned rats, it displays a limited capacity to enhance the functioning of residual BFCN and increases fear-related behavior and adverse neuroproliferative changes (Winkler et al., 2000). However, a more recent study shows contradictory results as not only was BFCN rescued two weeks after 192IgG-saporin infusion, but learning and memory were also improved (Lee et al., 2013). The brain-derived neurotrophic factor (BDNF) has also been studied because of its role in survival, differentiation and the functioning of neurons (Huang and Reichardt, 2001; Mattson, 2008). Two weeks after a 192IgG-saporin-induced lesion of NBM, cortical BDNF protein levels are significantly reduced (Angelucci et al., 2011). The fact that NGF levels are increased, whereas BDNF is reduced after 192IgG-saporin lesioning of BFCN, suggests that there is a different regulation. Growth factors are very promising molecules, but neurotrophin-based therapeutic strategies should be handled cautiously until there is a complete understanding of their regulation in neurodegeneration since some clinical trials have had to be halted because of safety-issues (Eriksdotter et al., 1998).

Effects on neurogenesis and neuronal plasticity

Although the adult mammalian brain has limited capacity for structural repair after injury, adult neurogenesis has been demonstrated and promotes the proliferation of progenitor cells, migration to the target area and differentiation into mature neurons (Biebl et al., 2000; Winner, 2002). Adult neurogenesis is specifically restricted to the lateral ventricle wall and to the border between the hilus and the granule cell layer in the hippocampal dentate gyrus (Luskin, 1993; Kuhn et al., 1996). The i.c.v. administration of 192IgG-saporin in adult rats impairs adult neurogenic processes, increasing cell death in both the dentate gyrus and the olfactory bulb (Cooper-Kuhn et al., 2004). Impairment in spatial memory performance has also been observed in this lesion model, which is reverted by the systemic administration of physostigmine, presumably through M_1 and M_4 mAChR expressed in newly born cells (Mohapel et al.,

2005). Moreover, a 192IgG-saporin-induced lesion of BFCN in the NBM disrupts cortical map reorganization and impairs motor learning, supporting the hypothesis that cortical plasticity is a key substrate for enabling an animal to effectively learn a skilled motor behavior (Conner et al., 2003). Further studies have demonstrated that following focal cortical injury, the basal forebrain cholinergic system is required for the neccessary plasticity that behavioral recovery requires (Conner et al., 2005). These findings support the hypothesis that the basal forebrain cholinergic system is selectively required for modulating complex forms of cortical plasticity driven by behavioral experiences (Ramanathan et al., 2009).

Effects on gene regulation

Acquisition of new information is associated with changes in the cortical expression of several genes, some of which have been identified as playing a major role in learning and memory processes (Gusev and Gubin, 2010). The intraparenchymal administration of 192IgG-saporin directly in the NBM triggers profound regressive changes in dendritic morphology of frontal cortical neurons (Harmon and Wellman, 2003), and impairment of neuronal plasticity (Wellman and Sengelaub, 1991). When cDNA microarrays and qRT-PCR have been used to screen for the cortical gene expression profile in 192IgG-saporin-lesioned rats, specific changes in mRNA expression were reported in those behaviorally impaired animals, associated with the loss of BFCN in the NBM (Paban et al., 2011). It has been proposed that these genes are involved in biological processes such as intracellular signaling processes, transcription regulation (Gusev and Gubin, 2010), glial and vascular remodeling and cytoskeleton organization, dendritic proliferation and axon guidance (Maysami et al., 2006).

Behavioral effects of BFCN immunolesions in the NBM

It has been previously shown that a single intraparenchymal injection of 192IgG-saporin in the NBM results in an extensive and selective loss of BFCN, long-lasting cortical cholinergic hypoactivity and deficits in recognition memory capacity (nonmatching-to-position task, object recognition task and object location task), in delayed matching to position (T-maze task), configural association learning (operant conditioning task), spatial learning (Morris water maze) and aversive learning and memory (passive avoidance test) (Berger-Sweeney et al., 1994; Torres et al., 1994; Baxter et al., 1995; McGaughy et al., 1996; Butt et al., 2002; Pizzo et al., 2002; Bailey et al., 2003; Paban et al., 2005; Gibbs et al., 2007; Dashniani et al., 2009; Lee et al., 2013; Rastogi et al., 2014; Lee et al., 2016).

Further studies involving the lesioning of the NBM with 192IgG-saporin support the role of BFCN in an array of attentional functions including vigilance, reorienting of spatial attention and attentional resources directed at environmental stimuli (Bucci et al., 1998; Chiba et al., 1995 and 1999). All these previous results allow us to conclude that the NBM plays a major role in attention and that could have an influence on effects on learning and memory (Baxter and Chiba, 1999; McGaughy et al., 1996; Baxter et al., 2013).

Conversely, the results of other studies based on 192IgG-saporin-induced lesion of the NBM indicate that the role of the basal forebrain cholinergic system in cognitive functions is considerably more limited than was previously believed. Thus, impairments in spatial learning and memory, which are commonly observed after basal forebrain lesions produced with less selective methods (excitotoxins), are not observed following selective immunotoxic lesions of specific BFCN. Some authors report impairment in spatial learning and memory by lesions of the basal forebrain which are frequently attributed to BFCN loss, despite the lack of selectivity of the lesion method employed (reviewed in Baxter 2001 and Baxter et al., 2013). Several studies using the intraparenchymal infusion of 192IgG-saporin in the NBM have failed to show impairment in spatial learning tasks, or have produced only mild performance deficits (Wenk et al., 1994; Baxter et al, 1996). In contrast, when 192IgG-saporin is administered i.c.v., more consistent impairments in spatial learning and memory are reported (Berger-Sweeney et al., 1994; Waite et al., 1995; Walsh et al., 1995). Some authors have reported a higher depletion of cortical ChAT activity following i.c.v. 192IgG-saporin administration than with intraparenchymal injections, leading them to propose that a severe loss of cortical cholinergic input is required to induce deficits in learning and memory (Baxter et al., 2001).

In conclusion, the controversial behavioral findings suggest that the surgical procedures as well as the dose of immunotoxin used are critical variables when 192IgG-saporin is administered intraparenchymally. This model of basal forebrain cholinergic dysfunction, induced by the administration of 192IgG-saporin in the NBM, produces neurochemical perturbations related to ACh-related enzymatic machinery, neurotransmitter receptors, neurotrophin homeostasis and neuronal plasticity, leading to learning, memory and attentional deficits similar to the cognitive impairment observed in AD patients. Therefore, this model is useful to assay a wide range of pharmacological interventions aimed at modulating or partially restoring basal forebrain cholinergic neurotransmission.

3.3. Triple transgenic mice model (3xTg-AD mice)

As mentioned above, the basal forebrain cholinergic system which innervates the hippocampus and the entire cortical mantle plays a key role in cognitive processes and seems to be one of the most and one of the earliest atrophied brain areas in AD. However, there are identified familial mutations which contribute to the accumulation of the histopathologiocal markers of AD. Histopathologically, AD is characterized by the accumulation of senile plaques containing amyloid-β (Aβ), produced by the abnormal cleavage of the amyloid precursor protein (APP) due to β- and γ-secretases, and by the presence of hyperphosphorylated tau and neurofibrillary tangles. 3xTg-AD mice harboring βPP_{Swe}, $PS1_{M146V}$ and tau_{P301L} transgenes, have been extensively used as a model which shows some of the neuropathological markers of AD during the development of the familial type of the disease. These animals accumulate extracellular Aβ deposits prior to tangle formation and exhibit deficits in synaptic plasticity, including long-term potentiation, which coincides with intracellular accumulation of Aβ in brain areas related to the control of memory and emotional processing, such as cortex, hippocampus and amygdala (Oddo et al., 2003).

Cholinergic neurotransmission in 3xTg-AD mice also seems to be affected. Thus, hippocampal and cortical cholinergic neuritic dystrophy was first observed in middle-aged (8-10 month-old) mice with increasing levels in an age-dependent manner, together with a significant reduction (up to 23%) in the number of BFCN in the basal forebrain cholinergic system between young (2-4 month-old) and old (18-20 month-old) 3xTg-AD mice (Perez et al., 2011). Other authors report a decrease in the density of BFCN in the medial septum and deficits in the length of hippocampal cholinergic axons in 3xTg-AD mice which starts at 4 months of age (Girão da Cruz et al., 2012). Furthermore, the number of ChAT-immunoreactive neurons is decreased in the NBM, accompanied by a loss of cholinergic fibers in the frontal motor cortex and hippocampal CA1 area in 11-month-old 3xTg-AD-mice (Orta-Salazar et al., 2014). These results demonstrate a cholinergic dysfunction in the septo-hippocampal pathway and in cortical projections arising from the NBM. Interestingly, 192IgG-saporin-induced depletion of BFCN in 12-month-old transgenic mice leads to drastic increased levels of Aβ-plaques and hyperphosphorylated tau together with enhanced gliosis, which demonstrates that the basal forebrain cholinergic dysfunction contributes to worsen AD-like pathology in the 3xTg-AD mouse model, and, as Härtig et al. (2014) support, “drugs targeting the cholinergic neurotransmission remain justified as a potential treatment strategy of AD”.

The activation of M_1 mAChR with AF267B was enough to ameliorate spatial learning and memory impairment in 8 month-old transgenic mice. The cognitive impairment of 3xTg-AD mice was exacerbated by dicyclomine, a M_1 mAChR antagonist. Moreover, hippocampal plaque pathology was decreased by AF267B and increased after dicyclomine administration (Caccamo et al., 2006). An electrophysiological study reported a reduction in burst firing in response to carbachol application in 3xTg-AD mice. Thus, a moderate decrease was observed in 5 month-old transgenic mice whereas the difference was significantly higher in 10 month-old mice, suggesting a decline in cholinergic neurotransmission in an age-dependent manner (Akay et al., 2009). A more recent study analyzes the functional coupling of $G\alpha_{i/o}$ protein to M_2 and M_4 mAChR in 4-month-old (prodromal) and 15-month-old (advanced stages) 3xTg-AD mice (Manuel et al., 2016). A decrease in functional coupling was found in the posterior amygdala and an increase in the motor cortex in prodromal and advanced stages, respectively, suggesting that deregulated signaling in limbic areas in the prodromal stages underlie the anxious-like behaviour of these mice.

Several studies have evaluated cognition and emotional behavior by using passive avoidance or the novel object recognition tests, and have reported deficits in learning and memory (Caccamo et al., 2006; Clinton et al., 2007; Filali et al., 2012; Rasool et al., 2013). Modulation of anxiety, fear and phobias has also been reported in other types of tasks including the open field or the elevated plus maze (Nelson et al., 2007; Pietrapaolo et al., 2014).

As we have seen, 3xTg-AD mice progressively develop and manifest several features of AD, including senile plaque formation, intracellular tangle accumulation, cholinergic dysfunction, and cognitive impairment and, therefore, represent a useful model with which to evaluate therapeutic strategies for familial AD patients.

3.4. Endocannabinoid signaling in AD

Neuroanatomical and pharmacological evidence

The eCB system is made up of the eCB substances, the enzymatic machinery required for their synthesis and degradation, and the cannabinoid receptors that modulate the neuronal activity in different brain areas. CB_1 receptors are abundantly expressed in the CNS, including in areas related to learning and memory processes, such as the basal forebrain cholinergic system and innervation to cortex, amygdala and

hippocampus. Data obtained from human *postmortem* samples from AD patients suggest that the eCB system is modulated during the course of disease.

Westlake and colleagues analyzed both the mRNA expression for CB_1 receptors and [^{3}H]CP55,940 binding in *postmortem* brain samples from AD patients (Westlake et al., 1994). [^{3}H]CP55,940 binding was reduced in cortex, but no alterations in levels of CB_1 mRNA expression were observed in comparison with aged-matched controls. Although [^{3}H]CP55,940 binding was reduced, it was not selectively associated with AD-pathology and failed to dissociate changes in CB_1 receptor expression from normal aging. Other research groups found that both cortical and hippocampal CB_1 receptor levels remain unaltered in AD (Benito et al., 2003; Lee et al., 2010; Mulder et al., 2011; Ahmad et al., 2014). In contrast, other authors reported decreased levels of highly nitrosylated CB_1 receptor expression in cortical areas containing activated microglia (Ramirez et al., 2005), which did not correlate with any AD molecular marker or cognitive status (Solas et al., 2013). Receptor nitrosylation could indicate impaired coupling of CB_1 receptors to downstream effectors (Ramirez et al., 2005). Furthermore, autoradiographic studies using the selective CB_1 receptor radioligand [^{125}I]SD7015 revealed increased levels of CB_1 receptor expression in the frontal cortex in the early stages of AD (I-II), and a decline during the later stages (V-VI), which indicates that CB_1 receptor density inversely correlate with Braak tau pathology (Farkas et al., 2012). A recent detailed autoradiographic study showed increased levels of [^{3}H]CP55,940 binding in the frontal cortex during the middle stages of AD (III-IV), but no changes in the early stages (Manuel et al., 2014). Manuel et al. also reported a similar phenomenon within the hippocampus and in the caudate-putamen, showing that CB_1 receptor density inversely correlates with tau accumulation, according to the Braak classification. Moreover, the functional coupling of CB_1 receptors to $G\alpha_{i/o}$ protein was also analyzed by [^{35}S]GTPγS autoradiography in the same study. Data revealed a similar modulation of hippocampal CB_1 receptor activity to that observed in [^{3}H]CP55,940 binding and increased cortical CB_1 receptor activity during the initial stages of AD (I-II), preceding the increase in CB_1 receptor density (Manuel et al., 2014). Increased CB_1 receptor activity during the initial stages of AD might be an indication of neuroprotective mechanisms mediated by eCB signaling in response to initial neuronal damage.

With regards to CB_2 receptors, increased levels have been found in brain tissue samples from AD patients which seem to be associated with the activation of the microglia surrounding senile plaques (Ramirez et al., 2005). These results suggest a positive correlation with the density of both the glial fibrilar acidic protein (GFAP)

marker for astrocytes and senile plaques, but not with the cognitive status (Solas et al., 2013).

Moreover, FAAH density and activity is significantly increased and is associated with the overexpression of glial CB_2 receptors which probably contributes to inflammatory processes by increasing arachidonic acid as a consequence of the increased AEA metabolism in senile plaque enriched brain areas (Benito et al., 2003; Jung et al., 2012). Similarly to what has been observed in CB_1 receptor studies, the literature fails to report consistent results related to the regulation of eCB metabolism in AD. The increased levels of FAAH in AD brains support the idea that eCB and/or their precursors could be regulated in some way. Some studies reported decreased brain, but not plasmatic, levels of AEA and its precursor NArPE in cortical regions from AD patients, which positively correlated with cognitive deficiencies and, inversely, with senile plaque pathology, suggesting a possible involvement of AEA deregulated metabolism in cognitive dysfunction (Koppel et al., 2009; Jung et al., 2012). In these studies no alterations were observed in the levels of 2-AG in brain samples from AD patients. However, Mulder et al. (2011) reported that 2-AG-mediated signaling in the late stages of AD was deregulated in *postmortem* brain samples. The increased expression of DAGL-α, together with the decreased activity of MAGL and ABHD6, could contribute to 2-AG signaling-mediated synapse silencing. The absence of altered eCB plasmatic levels means that we cannot consider them as plasmatic biomarkers for AD.

Cannabinoids as therapeutic agents for AD

The effects of cannabinoid receptor agonists in reducing excitotoxicity, Ca^{2+} influx, neuroinflammatory processes, oxidative stress and apoptosis make the cannabinoid system a potential target for the treatment of neurodegenerative diseases. The eCB are modulators of other signaling pathways, and are involved in the activation of the phosphatidylinositol 3-kinase/protein kinase B pathway, the induction of phosphorylation of extracellularly regulated kinases and the expression of transcription factors and neurotrophins.

The synthesis of eCB is stimulated after neuronal damage, and their protective effects may be mediated by CB_1 receptors, as indicated by the increase of neuronal vulnerability when the CB_1 receptor is absent (Stella et al., 1997; Marsicano et al., 2003; van der Stelt et al., 2001a). The neuroprotective effects of cannabinoids (phyto and synthocannabinoids) have been demonstrated in *in vitro* models of excitotoxicity, in both neuronal (Skaper et al., 1996) and in organotypic brain cultures (Grabiec et al., 2012; Koch et al., 2011), as well as *in vivo* (van der Stelt et al., 2001b). The CB_1

receptor antagonists, SR141716A and AM251, but not the CB_2 antagonist, AM630, attenuate the neuroprotective effects of WIN55,212-2 and NADA on NMDA-mediated excitotoxicity models of cortical neurons (Kim et al., 2006) or organotypic brain cultures (Koch et al., 2011; Grabiec et al., 2012). Moreover, the negative excitotoxic effects are increased in CB_1 receptor knockout mice. The CB_1 receptor-mediated protection has been demonstrated to be sensitive to the pertussis toxin and PKA inhibition which leads to inhibition of presynaptic glutamate release or DSE (Marsicano et al., 2003), blockage of voltage-gated Ca^{2+} channels (Mackie and Hille et al., 1992; Twitchell et al., 1997; Koch et al., 2011) and inhibition of Ca^{2+} release from ryanodine sensitive stores (Zhuang et al., 2005). Excitotoxicity may be underlying or contributing to the neurodegenerative processes and memory impairment described in AD (Sonkusare et al., 2005). The reduction of glutamatergic neurotransmission through NMDA receptors or decreased levels of Ca^{2+} influx may confer neuroprotective effects. Thus, memantine, a noncompetitive antagonist of NMDA receptors, is used for the treatment of moderate-to-severe AD. The synthetic cannabinoid HU-210, in addition to acting as a full agonist of CB_1 receptors, also inhibits NMDA receptors and its beneficial effects against excitotoxicity have previously been described (Nadler at al., 1993). The activation of CB_1 receptors specifically located in glutamatergic networks by either the administration of exogenous cannabinoids or by the modulation of the eCB levels (e.g. through the inactivation of the degrading enzymes), may represent an alternative therapeutic approach to attenuate this neuropathological feature related to the excitatory imbalance described in AD.

Clinical evidence of therapeutic properties of cannabinoids in AD

Clinical data modestly support the beneficial effects of nabilone or dronabinol (cannabinoid agonist analog of Δ^9-THC) for some behavioral symptoms related to AD. One clinical trial including 15 AD patients resulted in a decrease in the severity of altered behavior after 6 weeks of dronabinol treatment, with its side effects limited to euphoria and somnolence (Volicer et al., 1997). Further clinical trials including eight patients with dementia reported a reduction in nighttime agitation and behavioral disturbances, without adverse effects during the trial periods with dronabinol (Walther et al., 2006, 2011). Moreover, the administration of nabilone to an advanced AD patient who was refractory to antipsychotic and anxiolytic medications, promptly and significantly improved the agitation and aggressiveness (Passmore, 2008). However, no evidence of cannabinoid-based improvement of dementia has yet been observed (Krishnan et al., 2009). Recently, a clinical trial with Δ^9-THC in 24 patients with dementia and relevant neuropsychiatric symptoms, revealed the absence of side

and/or beneficial effects after its daily oral administration for 3 weeks, suggesting that higher doses could be efficacious and equally well tolerated (van der Elsen et al., 2015). The number of patients included in these trials was limited and none of the trials evaluated cognitive or neurodegenerative markers, but the positive behavioral results are promising and provide us with valuable information, especially considering that no notable side effects were reported (Aso et al., 2014).

3.5. Lipids and AD

General considerations

There is increasing evidence that lipid metabolism alterations may underlie the onset or contribute to the progression of several neurodegenerative disorders, including AD, but the precise molecular mechanisms involved remain unclear. In addition, work is in progress to discover lipid-related prognostic markers with which to predict not only the risk of developing AD, but also the onset and progression of the disease. Thus, plasmatic (Mapstone et al., 2014; Fiandaca et al., 2015), cerebrospinal fluid (Koal et al., 2015; Fonteh et al., 2015) and brain (Mendis et al., 2016) lipid levels have been quantified in AD and compared with that of control subjects. Nevertheless, over the last few years, the development of matrix-assisted laser desorption/ionization imaging mass spectrometry (MALDI-IMS), has permitted the investigation of the anatomical distribution of small molecules, including lipids, within biological systems through the *in situ* analysis of tissue slices (Sugiura et al, 2009). Recently published studies have identified the distribution pattern of lipid species in hippocampal (Mendis et al., 2016) and frontal cortex slices from AD patients and age-matched control subjects by using MALDI-IMS (González de San Roman et al., 2017). However, it was Alois Alzheimer (1911) who firstly reported “the extraordinarily strong accumulation of lipoid material” or fatty deposits in his papers first describing the human brain of a demented patient (reviewed in Foley, 2010). In accordance with these original findings, subsequent studies have confirmed altered levels of brain and plasma lipid species thereby revealing a plausible link between aberrant lipid metabolism and neurodegeneration in AD (Ellison et al., 1987; Mulder et al., 2003; Mapstone et al., 2014; Mendis et al., 2016).

Structural lipid profile changes in AD

The different lipid species present in the brain can be grouped into three major categories: cholesterol, glycerophospholipids and sphingolipids (Jackson et al., 2005). The glycerophospholipids category includes the following classes of lipids: PC, PE, phosphatidylinositol mono, bis and trisphosphates and phosphatidylserines (PS) among others. Specifically, PC (Nitsch et al., 1992b; Martin et al., 2010), and PE (Ellison et al., 1987; Martin et al., 2010) species seem to be decreased in AD. Moreover, a modulation in the ratio between saturated and unsaturated fatty acids has been reported (Mulder et al 2003; Soderberg et al., 1991). Under normal physiological conditions, PS species are preferentially located in the inner leaflet of the plasma membrane, but the loss of asymmetry is an early indicator of apoptosis (Fadok et al., 1992), and/or glia-mediated synaptic pruning to remodel the neural circuit (reviewed in Bevers and Williamson, 2016). The loss of PS asymmetry with increased externalization to the outer leaflet of the lipid bilayer has been described in samples from AD patients probably indicating apoptosis rather than synaptic remodeling (Bader Lange et al., 2008). The sphingolipids category contains sphingomyelin (SM), cerebrosides, ceramides (Cer), sulfatides (SF) and gangliosides. Early studies reported an increase in levels of SF in AD (Majocha et al., 1989). There is now evidence of a significant SF depletion (up to 58% and 93% in gray and white matter, respectively), even at the onset of the clinical manifestations of the disease (Han et al., 2002). Moreover, a consequent elevation in ceramide (He et al., 2010) and GM levels was found in the entorhinal cortex and dentate gyrus of AD brain samples (Chan et al., 2012; Pernber et al., 2012). However, results are contradictory as a previous study reported decreased GM levels in the hippocampus of early-onset AD (Svennerholm and Gottfries, 1994).

As previously mentioned, the MALDI-IMS technique allows us to anatomically locate and further analyze many small molecules (e.g., lipids). The findings of Mendis et al. (2016) showed reduced levels of some PE species in regions of both gray and white matter in hippocampus, whereas the levels of some PC, PS, SM, Cer and SF are increased. Very recently, the depletion of different SF lipid species has been identified from the earliest stages of the disease in both white and gray matter areas of the frontal cortex (González de San Roman et al., 2017). The different classes of lipids mentioned above, which are deregulated in AD, constitute a large pool of Ch that can potentially be used for ACh synthesis when the demand for choline needed to sustain ACh release is enhanced (i.e. BFCN death in AD).

Choline metabolism and eCB in AD

BFCN do have a unique metabolic capability that might contribute to their selective vulnerability in AD, and perhaps in other cholinergic disorders (Blusztajn and Wurtman, 1983; Wurtman et al., 1985; Wurtman, 1992). BFCN, like any cell of the body use Ch to form phosphocholine after a process of phosphorylation, which is then further transformed into membrane PC, but additionally, these neurons acetylate it to form a compound designated for export; the neurotransmitter ACh (Wurtman, 1992). The biosynthesis of ACh is produced by the enzyme ChAT using Ch and acetyl-CoA (White and Wu, 1973).

As Wurtman noticed in 1992, the first element, Ch, is a metabolically, 'expensive' molecule due to the presence of three methyl groups. Ch is obtained from the diet and delivered to BFCN via the blood stream, whereas acetyl-CoA is a co-substrate involved in many metabolic pathways and, therefore, not specific for cholinergic neurotransmission (reviewed in Blusztajn and Wurtman, 1983). ACh hydrolysis provides approximately 50% of Ch, which is finally uptaken by the SDHACU. Interestingly, ChAT exhibits low affinity for its substrates (White and Wu, 1973). Consequently, the rates at which phosphocholine and ACh are formed in BFCN depend on the concentration of Ch (Millington and Wurtman, 1982). A secondary source of Ch derived from the hydrolysis of certain lipid species, such as membrane phospholipids has been described, and this led to the autocannibalism (autophagy) hypothesis as an adaptative response to stress provoked by the cholinergic dysfunction present in AD (Wurtman et al., 1985). In the synthetic pathway, PE from any specific membrane pool can be sequentially methylated to PC (Bremer et al., 1960a,b), which are then hydrolyzed to free Ch (Blusztajn et al., 1987), by membrane-associated phospholipase D (PLD) activation (Hattori and Kanfer, 1984; Exton, 1999). PIP_2, PKC and phorbol esters stimulate PLD activity (reviewed in Exton, 1999). Furthermore, PLD is reduced by up to 63% in homogenates of brain tissue samples from AD patients (Kanfer et al., 1986).

The relation between muscarinic neurotransmission and PC metabolism has previously been studied (Dolezal and Tucek, 1984; Qian et al., 1989). Thus, the stimulation of cortical synaptosomes with cholinergic agonists, including ACh, carbachol and muscarine, is able to increase PLD activity, which is also dependent on PKC activity involving PIP_2 and DAG, leading to the accumulation of free Ch (Qian et al., 1989). The effect of muscarinic-induced PLD activity is antagonized by atropine (Dolezal and Tucek, 1984). Consequently, $G\alpha_{q/11}$ protein-coupled muscarinic receptors such as M_1 and/or M_3 subtypes may be involved in these PC-related metabolic pathways. By using *postmortem* brain samples from AD patients, it was found that PC

turnover is accelerated and Ch availability decreased (Blusztajn et al., 1990; Nitsch et al., 1991, 1992). How changes in membrane phospholipid metabolism might relate to BFCN death, which is characteristic of AD, is a question that requires a more detailed research to be properly answered. In addition, abnormal Ch metabolism together with impaired muscarinic signaling might have a relevant role in the progression of AD.

As previously mentioned, cholinergic neurotransmission can be modulated by eCB signaling by the presynaptic activation of CB_1 receptors driven via the postsynaptic release of eCB. Both the synthesis of eCB and *de novo* synthesis of Ch share common membrane phospholipid precursors and metabolic pathways involving $G\alpha_{q/11}$-coupled mAChRs, different phospholipases and PIP_2-DAG metabolism. The BFCN which remain alive in AD patients probably increase their activity, and the membrane phospholipids may represent the only alternative pool to synthesize Ch *de novo* in an attempt to maintain the cholinergic tone in the brain areas innervated by the basal forebrain. If certain precursors for the synthesis of eCB in cholinergic synapses and in the basal forebrain are being exploited to maintain cortical cholinergic neurotransmission under neurodegenerative conditions the modulation of the eCB signaling may be useful in maintaining the homeostasis of both neurotransmitter systems. The analysis of the lipid profile in the basal forebrain cholinergic system and in the projection areas could not only provide new evidence of the relationship between the cholinergic and eCB systems, but also contribute to the discovery of innovative lipid-based therapeutic strategies for the treatment of neurodegenerative disorders.

Objectives

Objectives

The basal forebrain cholinergic pathways are progressively affected in Alzheimer´s disease, leading to a decline in cognitive functions and irreversible impairment of memory and thinking abilities. Neurolipidic systems, such as the endocannabinoid system, regulate different physiological processes including learning and memory. Endocannabinoid signaling becomes altered during the progression of AD, and there is increasing evidence that a deregulation of lipid metabolism may underlie the onset or contribute to the progression of several neurodegenerative disorders, including AD.

On the other hand, the synthesis of endocannabinoids is stimulated by muscarinic receptor activation and CB_1 cannabinoid receptor activation modulates the release of ACh. Furthermore, the synthesis of the endogenous ligands of both systems may share common metabolic pathways and membrane phospholipid precursors. Therefore, to further understand the relationship between the basal forebrain cholinergic neurotransmission and CB_1 receptor-mediated signaling in the pathways which arise in the basal forebrain, the objectives of the present study are:

I. To develop an *ex vivo* model of specific impairment of the basal forebrain cholinergic neurons (BFCN) by using the immunotoxin 192IgG-saporin in hemibrain organotypic cultures and to evaluate the effect of the cannabinoid agonist WIN55,212-2 by using immunohistochemistry.

II. To improve the *in vivo* model of specific BFCN lesion in the nucleus basalis magnocellularis in the adult rat by the intraparenchymal administration of 192IgG-saporin, to evaluate the behavioral outcomes related to learning and memory of an aversive stimulus by using the passive avoidance test, to verify the specificity and severity of the lesion and to analyze the cholinergic signaling mediated by M_2/M_4 muscarinic receptors.

III. To analyze CB_1 receptor-mediated endocannabinoid signaling in the *in vivo* model of BFCN lesion by using autoradiography and to analyze the cellular distribution of CB_1 receptors by using immunohistochemistry.

IV. To obtain the lipid profile by means of MALDI-IMS in the *in vivo* model of 192IgG-saporin-induced lesion, focusing on the analysis of membrane phospholipid precursors for both the *de novo* synthesis of choline and the synthesis of eCB.

V. To evaluate in a 7 month-old 3xTg-AD mice model of AD learning and memory of an aversive stimulus, to analyze CB_1 and M_2/M_4 receptor-mediated signaling by using autoradiography and to analyze the cellular distribution of these receptors by using immunohistochemistry.

VI. To evaluate the effects on the above mentioned behavioral and neurochemical parameters of the subchronic activation of the eCB system, following the administration of a direct (WIN55,212-2) and an indirect (JZL-184) cannabinoid agonist in 7 month-old 3xTg-AD mice.

Animals, Materials and Methods

1. Animals

1.1. Sprague-Dawley rats (Manuscript I)

We used male Sprague-Dawley rat pups at postnatal day 7 (P7) which weighed 14-20 g at the start of the experiments. Every effort was made to minimize animal suffering and to use the minimum number of animals. All procedures were performed in accordance with European animal research laws (Directive 2010/63/EU) and the Spanish National Guidelines for Animal Experimentation (RD 53/2013, Law 32/2007). Experimental protocols were approved by the Local Ethical Committee for Animal Research of the University of the Basque Country (CEEA 388/2014). The number of animals and organotypic cultures used is detailed in the manuscript.

These animals were used for the immunohistochemical detection of $p75^{NTR}$ in fixed tissue and the *ex vivo* experiments based on hemibrain organotypic cultures containing BFCN.

1.2. Sprague-Dawley rats (Manuscripts II and III)

Adult male Sprague-Dawley rats weighing 200-250 g and ranging from 8 to 10 weeks at the start of the experiment were used for the studies in manuscripts II and III. Rats were housed four per cage (50 cm length x 25 cm width x 15 cm height) at a temperature of 22ºC and in a humidity-controlled (65%) room with a 12:12 hours light/dark cycle, with access to food and water *ad libitum*. Every effort was made to minimize animal suffering and to use the minimum number of animals. All procedures were performed in accordance with European animal research laws (Directive 2010/63/EU) and the Spanish National Guidelines for Animal Experimentation (RD 53/2013, Law 32/2007). Experimental protocols were approved by the Local Ethical Committee for Animal Research of the University of the Basque Country (CEEA 388/2014).

These animals were used for the *in vivo* administration of 192IgG-saporin followed by behavioral tests and histochemical, immunohistochemical, autoradiographic or MALDI-IMS assays. The number of animals used for *in vivo* administration of 192IgG-saporin is detailed in manuscripts II and III.

1.3. CB_1 knockout mice (Manuscript III and IV)

CB_1 receptor knockout ($CB_1^{-/-}$) and wild-type ($CB_1^{+/+}$) mice were provided by Dr. C. Ledent. The generation of mice lacking the CB_1 receptor was previously described as follows (Ledent et al., 1999). Briefly, the CB_1 gene was cloned from the 129/Sv mouse genomic library, and the single coding exon was mapped and sequenced (EMBL/GenBank Y18374). A PGK-Neo cassette was inserted between Avr II and Sfi I sites located 1073 base pairs apart, replacing the first 233 codons of the gene. Homologous recombination in R1 cells and aggregation with CD1 eight-cell stage embryos were performed as described in Ledent et al (1997). A recombinant line was used to generate chimeras, allowing germ line transmission of the mutant gene. Heterozygous mice were bred for 30 generations on a CD1 background before generating the $CB_1^{-/-}$ and $CB_1^{+/+}$ varieties used in these studies.

For this study 9 week-old male $CB_1^{-/-}$ and $CB_1^{+/+}$ mice were used. Animals were housed and maintained under standard laboratory conditions (12:12 hours light/dark cycle, starting the light cycle at 8:00 am, with access to food and water *ad libitum*, 22 ± 2 ºC, 50-60% humidity). All procedures were performed in accordance with European animal research laws (Directive 2010/63/EU) and the Spanish National Guidelines for Animal Experimentation (RD 53/2013, Law 32/2007) and the Use of Genetically Modified Organisms (Law 32/2007 and 9/2003). Experimental protocols were approved by the Local Ethical Committee for Animal Research of the University of the Basque Country (CEIAB/21/2010/Rodríguez Puertas and CEEA 366-1 and 2). These animals were used for autoradiographic studies. The number of animals used is detailed in manuscript IV.

1.4. 3xTg-AD mice (Manuscript IV)

The triple transgenic mice (3xTg-AD), used as a model for familial AD , were obtained from the Department of Medical Psychology, Universitat Autonóma de Barcelona, Barcelona, Spain, in collaboration with Dr Lydia Giménez Llort. The 3xTg-AD mice harboring $PS1_{M146V}$, APP_{Swe} and Tau_{P301L} transgenes were genetically modified as described below, by LaFerla and colleagues at the Department of Neurobiology and Behavior, University of California, Irvine (Oddo et al., 2003). Briefly, two independent transgenes (encoding human APP_{Swe} and human tau_{P301L}, both under control of the mouse Thy1.2 regulatory element) were co-injected into single-cell embryos harvested from homozygous mutant $PS1_{M146V}$ knock-in (PS1KI) mice.

For the present study 7 month-old male 3xTg-AD mice and age-matched controls (Non-Tg mice) sharing the same background, but without genetic modifications, were used. All the animals were housed and maintained under standard

laboratory conditions (12:12 hours light/dark cycle, starting the light cycle at 8:00 am, with access to food and water *ad libitum*, 22 ± 2 ºC, 50-60% humidity). All procedures were performed in accordance with European animal research laws (Directive 2010/63/EU) and the Spanish National Guidelines for Animal Experimentation (RD 53/2013, Law 32/2007) and the Use of Genetically Modified Organisms (Law 32/2007 and 9/2003). Experimental protocols were approved by the Ethical Local Committee for Animal Research of the University of the Basque Country (CEIAB/21/2010/Rodríguez Puertas and CEEA 366-1 and 2).

These animals were used for behavioral tests, autoradiographic and immunofluorescence studies and synthocannabinoid-based pharmacological treatments. The number of animals used is detailed in manuscript IV as well as in Figure 11.

2. Materials

2.1. Reagents

192IgG-saporin (Batch 2441969) was acquired from Millipore (Temecula, CA, USA), [^{3}H]CP55,940 (131.8 Ci/mmol) and [^{35}S]GTPγS (1250 Ci/mmol) from PerkinElmer (Boston MA, USA). The [^{3}H]-microscales and [^{14}C]-microscales used as standards in the autoradiographic experiments were purchased from ARC (American Radiolabeled Chemicals, Saint Louis, MO, USA). The β-radiation sensitive films, Kodak Biomax MR, bovine serum albumin (BSA), DL-dithiothreitol (DTT), adenosine deaminase (ADA), guanosine 5´-diphosphate (GDP), guanosine5´-O-3-thiotriphosphate (GTPγS), ketamine, xylazine, acetylthiocholine iodide, 2-mercaptobenzothiazole (MBT), Hoechst 33258 and tetraisopropylpyrophosphoramide (iso-OMPA) were all acquired from Sigma-Aldrich (St Louis, MO, USA). The compounds necessary for the preparation of the different buffers, the fixation and the treatment of slides were of the highest commercially available quality for the purpose of our studies.

2.2. Drugs

R-(+)-[2,3-Dihydro-5-methyl-3-[(morpholinyl)methyl]pyrrolo[1,2,3-de]-1,4-benzoxazinyl]-(1-naphthalenyl)methanone mesylate (**WIN55,212-2**), *(-)-cis-3-[2-Hydroxy-4-(1,1-dimethylheptyl)phenyl]-trans-4-(3-hydroxypropyl) cyclohexanol* (**CP55,940**) and (2-Carbamoyloxyethyl) trimethylammonium chloride (**carbachol**) were acquired from Sigma-Aldrich; *4-Nitrophenyl 4-(dibenzo[d][1,3]dioxol-5-yl(hydroxy)methyl)piperidine-1-carboxylate* (**JZL184**) and *5-(4-chloro-3-methylphenyl)-1-[(4-methylphenyl)methyl]-N-[(1S,2S,4R)-1,3,3-trimethylbicyclo[2.2.1]hept-2-yl]-1pyrazole3-carboxamide* (**SR144528)** from Cayman-Chemicals (Ann Arbor, MI, USA); *N-(Piperidin-1-yl)-5-(4-chlorophenyl)-1-(2,4-dichlorophenyl)-4-methyl-1H-pyrazole-3-carboxamidehydrochloride* (**SR141716A**) and 1-(2,4-Dichlorophenyl)-5-(4-iodophenyl)-4-methyl-*N*-(piperidin-1-yl)-1*H*-pyrazole-3-carboxamide (**AM251**) from Tocris (Bristol, UK).

3. Methods

3.1. *Ex vivo* experiments (Manuscript I)

Tissue preparation for organotypic cultures

To prepare hemibrain organotypic cultures, P7 Sprague-Dawley rats were sacrificed by decapitation and their brains were quickly dissected under aseptic conditions inside a laminar flow cabinet (TELSTAR, BV-30/70) (Stoppini et al., 1991). After removal of the olfactory bulb and the most caudal part of the cerebellum, the brains were placed in minimal essential Dulbecco´s modified Eagle medium (DMEM, Sigma-Aldrich) supplemented with 0.1% (v/v) antibiotic/antimycotic (Gibco) at 4ºC.

The brains were vertically positioned resting on the cerebellum by means of cyanoacrylate. They were then cut, from the rostral to the caudal part, into coronal 300 µm-thick organotypic slices using a sliding vibratome (Leica VT 1.000 S, Leica Microsystems AG, Wetzlar, Germany). Approximately 6 slices containing the medial septum and another 6 slices containing the NBM were obtained from each brain and these were immediately transferred into cell culture inserts over membranes of 0.4 µm pore size (PIC50ORG, Millipore, MA, USA). The organotypic slices were then placed in 6-well culture dishes (Falcon, BD Biosciences Discovery Labware, Bedford, MA) that contained 1 ml culture medium per well (Figure 9). The culture medium consisted of 49% (v/v) Neurobasal Medium (NB, Sigma-Aldrich), 24% (v/v) Hanks' Balanced Salt Solution (HBSS, Gibco), 24% (v/v) Normal Horse Serum (NHS, Gibco), 1% (v/v) D-glucose, 0.5% glutamine (Sigma-Aldrich), 0.5% B27 supplement serum free (Gibco) and 1% antibiotic/antimycotic. The culture dishes were incubated at 37ºC in a fully humidified atmosphere supplemented with 5% CO_2 and the cell culture medium was replaced by fresh medium depending on each treatment protocol, but typically, on the second or third day.

Treatments

Drugs and vehicle. WIN55,212-2 and AM251 were dissolved in pure ethanol and stored at -20ºC until used. 192IgG-saporin was dissolved directly in the culture medium immediately prior to the treatment. The preparations were divided into different groups and treated according to different treatment schedules (Figure 9).

192IgG-saporin. At 2 DIV, at 5 DIV or at 2 and 5 DIV, organotypic cultures were incubated with the immunotoxin 192IgG-saporin (50-200 ng/ml).

Vehicle. Non-lesioned organotypic cultures were kept in the culture medium for 8 days without receiving any treatments and served as controls. At 2 and 5 DIV, organotypic cultures were treated with the vehicle ethanol. The maximal concentration of ethanol in the culture medium was set at 0.01% (v/v) based on the concentration used in previous studies (Koch et al., 2011).

Agonist. At 2 and 5 DIV, organotypic cultures were incubated with the cannabinoid agonist WIN55,212-2 (10 nM or 1 nM).

Agonist + 192IgG-saporin. At 2 and 5 DIV, organotypic cultures were treated with the cannabinoid agonist WIN55,212,2 (10 nM or 1 nM), 2h prior to adding the immunotoxin (100 ng/ml).

Antagonist + agonist + 192IgG-saporin. At 2 and 5 DIV, organotypic cultures were preincubated with the CB_1 receptor antagonist AM251 (1 µM) together with the cannabinoid agonist WIN55,212-2 (10 nM or 1 nM), 2h prior to adding the immunotoxin (100 ng/ml).

Cell death marker. After 8 DIV, organotypic cultures were incubated in the presence of 5 µg/ml of propidium iodide (PI) for 2 h prior to fixation. The uptake of PI stains the nuclei of degenerating cells bright red when observed by the appropriate immunofluorescence filters, identifying them in CNS organotypic cultures as previously described (Pozzo Miller et al., 1994; Dehghani et al., 2003; Koch et al., 2011a) (Figure 9).

Immunohistochemistry

After the different treatments, the organotypic cultures were gently and extensively rinsed with 0.9% saline solution (37ºC) followed by immersion in 4% paraformaldehyde and 3% picric acid in 0.1 M phosphate buffer (PB) (4ºC) for 1h. Then, the fixed organotypic slices were extensively rinsed in 0.1 M PB (pH 7.4) and simultaneously blocked and permeabilized with 4% normal goat serum (NGS) in 0.6% Triton X-100 in PBS (0.1 M, pH 7.4) for 2 h at 4ºC. All incubations were performed in free floating at 4ºC (48 h) with rabbit anti $p75^{NTR}$ primary antibody, diluted in 0.6% Triton X-100 in PBS with 5% BSA. The primary antibody was then revealed by incubation for 30 min at 37ºC with Alexa 488-labeled donkey anti-rabbit secondary antibody diluted in Triton X-100 (0.6%) in PBS. Then, organotypic slices were washed for 30 min by immersion in PBS and incubated for 15 min at room temperature with Hoechst 33258 for fluorescent counterstaining of the nuclei. Finally, slices were extensively rinsed with PBS and covered with p-phenylendiamine-glycerol (0.1%) in PBS for immunofluorescence observation.

Quantitative analyses of BFCN

200-fold magnification photomicrographs of the MS, VDB, HDB, NBM and cortex were acquired by means of an Axioskop 2 Plus microscope (Zeiss) equipped with a CCD imaging camera (SPOT Flex Shifting Pixel). All the images were acquired at similar brain coordinates, with as much accuracy as possible, under the same illumination and exposure time and contrasted to the same level. Both $p75^{NTR}$ immunoreactive BFCN and PI positive cells were manually counted by using the "manual cell counting and marking" tool of the ImageJ image processing program. The area of the images was then calculated based on the display resolution. Finally, the total number (N) in the whole image was obtained and the densities of BFCN or PI stained cells were expressed as N/mm^2.

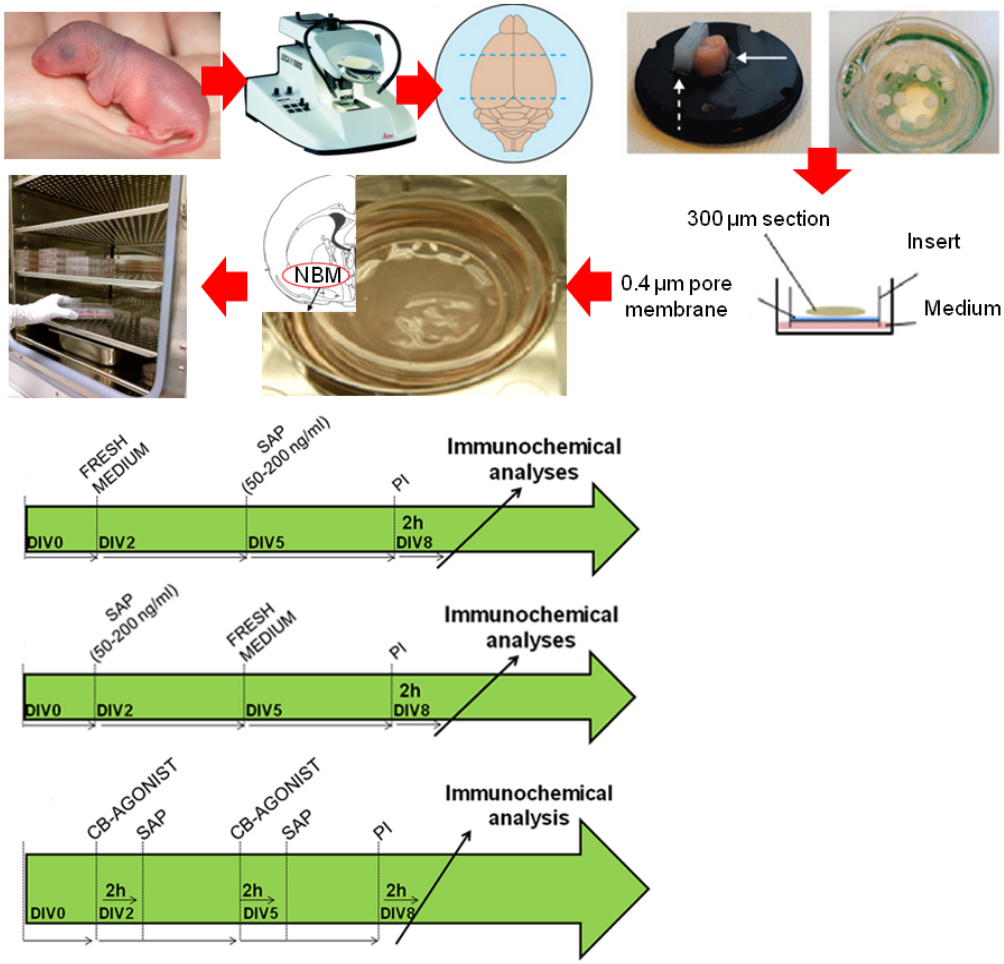

Figure 9. Synopsis of the experimental design including the generation and maintenance of the organotypic cultures and treatments schedule (below) (Modified from Ullrich et al., 2011).

3.2. *In vivo* experiments (Manuscript II, III and IV)

192IgG-saporin infusion (Manuscripts II and III)

All surgery was carried out under aseptic conditions. 192IgG-saporin was also used *in vivo* to selectively eliminate BFCN in the NBM. Rats were randomly assigned to one of three groups: sham-operated (SHAM), artificial cerebrospinal fluid as vehicle (aCSF) and lesion by 192IgG-saporin (SAP). The vehicle was prepared as follows: 0.15 M NaCl, 2.7 mM KCl, 0.85 mM $MgCl_2$, 1.2 mM $CaCl_2$ (pH 7.4) and sterilized by filtration with 0.4 µm-Ø filters (EMD Millipore, CA, USA). Rats were anesthetized with ketamine/xylazine (90/10 mg/kg; s.c.) and then placed in a stereotaxic instrument (Kopf, Tujunga, CA). After an incision was made in the skin along the midline of the skull, two holes were drilled. A 10-µl Hamilton syringe (Neuros^{TM} Syringe, 1701RN; Bonaduz, Switzerland) with a 0.008 inches (0.210 mm) diameter needle was carefully used to minimize brain damage. The intraparenchymal infusions were made into the NBM: - 1.5 mm anteroposterior from Bregma, ± 3 mm mediolateral from midline, + 8 mm dorsoventral from the cranial surface (Paxinos and Watson, 2005). 192IgG-saporin was dissolved in aCSF under aseptic conditions to a final concentration of 130 ng/µl. aCSF or 192IgG-saporin was bilaterally injected (1 µl/hemisphere) at a constant rate of 0.2 µl/min. The needle was kept in for 5 min before removal to avoid a possible backflow and to allow complete diffusion. During surgery, the body temperature was controlled and the eyes were kept hydrated with warm saline solution (0.9% NaCl). After the administration was completed, the wounds were closed with braided silk sutures and a broad-spectrum intramuscular antibiotic (2.25 mg/kg oxytetracycline) injection was given. The choice of coordinates, the infusion rate, volume and dose of immunotoxin were based on previous experiments performed in our laboratory.

The rats were allowed to recover from surgery for seven days. On day seven (acquisition) and day eight (retention) the learning and memory behavior of the animals was tested before the dissection of the brain for use in the neurochemical studies (Figure 10).

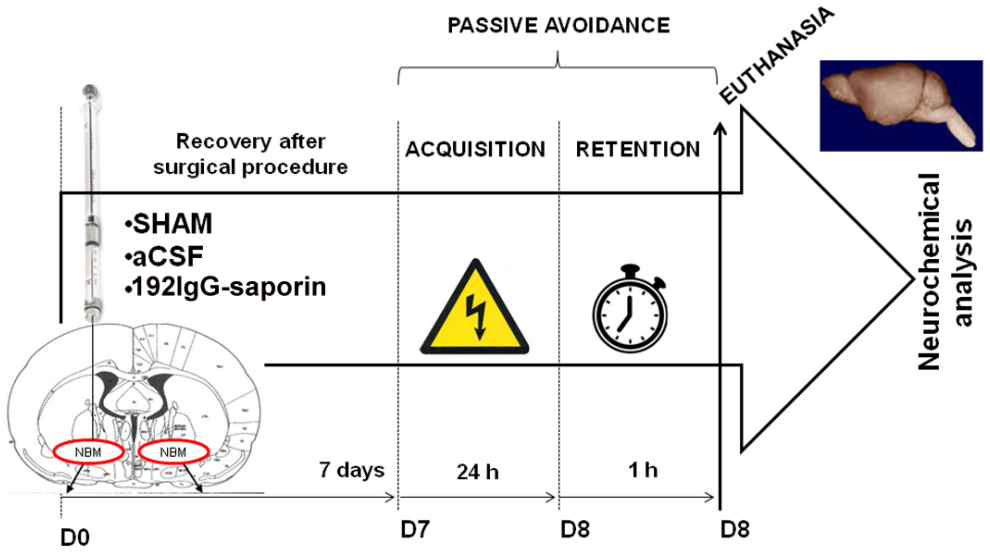

Figure 10. Synopsis of the experimental design including surgery schedule, behavioral assessment and euthanasia (manuscripts II and III).

Synthocannabinoid administration in 3xTg-AD mice (Manuscript IV)

Synthocannabinoids were administered intraperitoneally (5 ml/kg) once daily, for seven consecutive days. WIN55,212-2 and JZL184 were dissolved in pure DMSO and diluted with Kolliphor EL (Sigma-Aldrich) and 0.9% saline to a proportion of (1:1:18), respectively, as vehicle. Two independent sets of mice were randomly assigned to one of the following five groups (n = 10): [1] Non-Tg-vehicle, [2] 3xTg-AD-vehicle, [3] 3xTg-AD-WIN55,212-2 (0.1 mg/kg), [4] 3xTg-AD-WIN55,212-2 (1 mg/kg) and [5] 3xTg-AD-JZL184 (8 mg/kg). During the two days following the last administration, the different behavioral parameters were analyzed in the PA test (Figure 11).

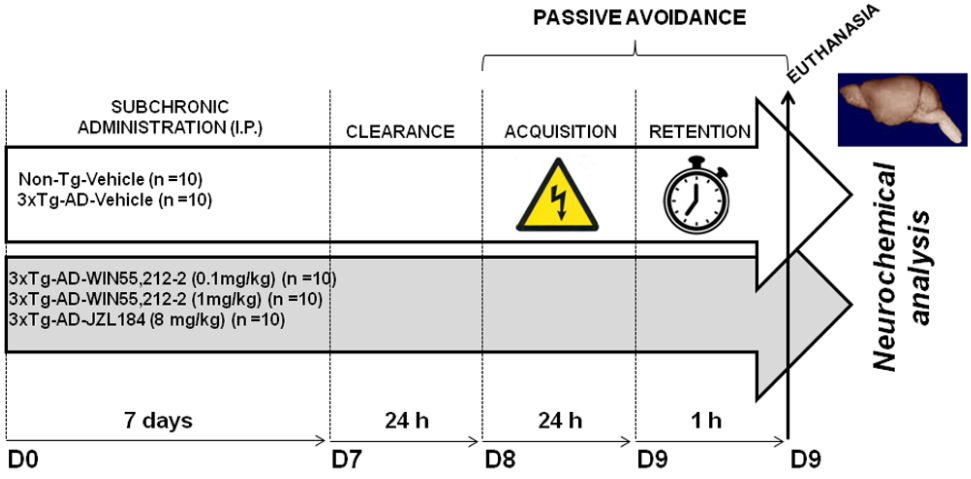

Figure 11. Synopsis of the experimental design showing the treatment schedule, behavioral assessment and euthanasia (manuscript IV).

Passive avoidance test (Manuscripts II, III and IV)

The passive avoidance apparatus for rats consists of two methacrylate compartments separated by a guillotine door. The first compartment is large, white illuminated and open-topped: 31 cm (W) x 31 cm (D) x 24 cm (H), and the other is small, dark and closed: 19.5 cm (W) x 10.8 cm (D) x 12 cm (H) (PanLab passive avoidance box LE870).

The dimensions of the compartments for mice are as follows. Large: 25 cm (W) x 25 cm (D) x 24 cm (H) and small: 19.5 cm (W) x 10.8 cm (D) x 12 cm (H) (PanLab passive avoidance box LE872).

The test consists of two sessions. The first one is called “the acquisition session”. Each animal was gently placed in the illuminated compartment with its head facing the closed door and allowed to explore it for 30 sec. Then, the guillotine door automatically opened and the animal was allowed to enter the dark compartment for 60 sec. When the animals cross the threshold, the guillotine door closed and the acquisition latency was measured, then a foot shock (0.4 mA/2 sec) was delivered. 10 sec after the foot shock, the animal was returned to its home cage. The animals which did not enter the dark compartment during the acquisition session were eliminated from the study. The second session, called the “retention session”, was performed 24 h later. The animals were again placed in the illuminated compartment and allowed to explore for 30 sec. Then the door opened and the step-through latency time to enter the dark compartment was measured up to a maximum cut-off time of 300 sec. No foot shock was delivered in the retention session.

Tissue preparation (Manuscripts I, II, III, IV)

P7 rats and the animals tested in the passive avoidance test were anesthetized with ketamine/xylazine (90/10 mg/kg; i.p.) and then sacrificed before the dissection of their brains.

Fixed tissue. Representative P7 rats, those rats from SHAM, aCSF and SAP groups and 3xTg-AD mice from the five treatment groups, were transcardially perfused via the ascending aorta with 50 ml warm (37ºC), calcium-free Tyrode’s solution (0.15 M NaCl, 5 mM KCl, 1.5 mM $MgCl_2$, 1 mM $MgSO_4$, 1.5 mM NaH_2PO_4, 5.5 mM Glucose, 25 mM $NaHCO_3$; pH 7.4) and 0.5% heparinized, followed by 4% paraformaldehyde and 3% picric acid in 0.1 M PB (4ºC) (100 ml/100 g b.w.). Their brains were subsequently removed and post-fixed in the same fixative solution for 90 min at 4ºC, and then were immersed in a cryoprotective solution of 20% sucrose in PB overnight at 4ºC. Then the tissue was frozen by immersion in isopentane and kept at -80ºC. The brains were cut into 10 µm coronal slices using a Microm HM550 cryostat (Thermo Scientific) equipped

with a freezing-sliding microtome at -25ºC and mounted onto gelatin-coated slides and finally stored at -25ºC until used.

Fresh tissue. The rest of the animals were sacrificed by decapitation after anesthesia. The brain samples from SHAM, aCSF and 192IgG-saporin treated rats, 3xTg-AD/Non-Tg and $CB_1^{-/-}/CB_1^{+/+}$ mice, as well as the spleens from $CB_1^{-/-}/CB_1^{+/+}$ mice, were quickly removed by dissection (4ºC), fresh frozen and kept at -80ºC. Later they were cut into 20 µm slices and mounted onto gelatin-coated slides and stored at -25ºC until used. Several brain areas including that of the basal forebrain cholinergic system, amygdaloid nuclei, cortical and hippocampal regions, basal ganglia and olfactory system were analyzed in these studies (Figure 12).

Histochemical methods (Manuscripts I, II, III and IV)

Histochemistry for AChE detection in fixed and fresh tissue (Manuscripts II and III)

For some histochemical procedures fresh slices from SHAM, aCSF and SAP groups were used. The slices were air dried for 20 min at room temperature, post-fixed in 4% paraformaldehyde in PBS for 30 min at 4ºC and washed in 0.1 M PBS, pH 7.4 (PBS) for 20 min.

BFCN in the NBM and cholinergic innervations were stained using the “direct coloring” thiocoline method for AChE (Karnovsky and Roots, 1964). The slices were rinsed twice in 0.1 M Tris-maleate buffer (pH 6.0) for 10 min and incubated in complete darkness, with constant and gentle agitation in the AChE reaction buffer: 0.1 M Tris-maleate; 5 mM sodium citrate; 3 mM $CuSO_4$; 0.1 mM iso-OMPA; 0.5 mM $K_3Fe(CN)_6$ and 2 mM acetylthiocholine iodide as reaction substrate. The incubation times were from 30 min for staining cholinergic somas in NBM or 100 min for staining cholinergic fibers. Finally, the enzymatic reaction was stopped by two consecutive washes (2x10 min) in 0.1 M Tris-maleate (pH 6.0). Slices were then dehydrated in increasing concentrations of ethanol and covered with di-n-butyl phthalate in xylene (DPX) as the mounting medium.

Immunohistochemistry (Manuscripts I, II, III and IV)

10 µm slices were simultaneously blocked and permeabilized with 4% NGS in 0.3% Triton X-100 in PBS (0.1 M, pH 7.4) for 2 h at room temperature (22 ± 2ºC). The slices were incubated at 4ºC overnight with primary antibodies, diluted in 0.3% Triton X-100 in PBS with 5% BSA. The primary antibodies were then revealed by incubation for 30 min at 37ºC in the darkness with fluorophore-labeled secondary antibodies diluted in Triton X-100 (0.3%) in PBS. Then, slices were washed for 30 min by immersion in PBS and incubated with Hoechst 33258 for 15 min at room temperature.

Finally, slices were extensively rinsed with PBS and mounted with p-phenylendiamine-glycerol (0.1%) in PBS for immunofluorescence. The list of primary and secondary antibodies as well as the supplier companies, the fluorophores, and the specific dilutions are shown in table 1.

Immunohistochemistry for CB_1 receptor with tyramide signal amplification (TSA) (Manuscripts III and IV)

To label CB_1 receptors, the primary rabbit antiserum against the CB_1 receptor, PA1-743, (Affinity BioReagents, CO, USA) was diluted [1:500] in TBS (Tris-buffered saline) (0.1 M Tris, 0.15 M NaCl, pH 7.4) containing 0.5% milk powder. Fixed 10 µm coronal slices were air dried for 20 min and washed by immersion in PBS for 15 min at room temperature. Then, the slices were blocked with 5% NGS in TBS buffer for 2 h at room temperature before being incubated with the primary antibody overnight at 4ºC. The tyramide signal amplification (TSA) method was used to amplify the signal associated with the CB_1 receptor antiserum. Briefly, slices were washed for 30 min in TNT buffer (0.05% Tween 20 in TBS, pH 7.4) and blocked in TNB solution (10 ml TNT buffer, 0.05 g blocking reagent, DuPont) for 1 h at room temperature. Later, the slices were incubated with horseradish peroxidase (HRP) goat anti-rabbit (1:150; Perkin Elmer, MA, USA) for 1 h followed by a tyramide-fluorescein-based amplification (1:100, Perkin Elmer, MA, USA) process in complete darkness for 10 min at room temperature. Slices were extensively rinsed in TBS and mounted with p-phenylendiamine-glycerol (0.1%) in PBS for immunofluorescence.

Colocalization studies

630-fold magnification images for colocalization were acquired on an Axioskop Observer A1 inverted microscope (Carl Zeiss) by optical sectioning (0.24 µm/X-Y-Z-resolution) using structured illumination (ApoTome, Carl Zeiss). Colocalization images were created by using ZEN2014 software (Carl Zeiss) and were defined as immuno-signals without physical signal separation.

Quantitative analyses of BFCN and AChE positive fibers (Manuscripts II and III)

200-fold magnification photomicrographs of the NBM were acquired by means of an Axioskop 2 Plus microscope (Carl Zeiss) equipped with a CCD imaging camera SPOT Flex Shifting Pixel. Both AChE stained and $p75^{NTR}$ immunoreactive BFCN were counted independently by two observers at three different stereotaxic levels (-1.08 mm, -1.56 mm and -2.04 mm from Bregma), and the total number of BFCN (N) in the whole image was obtained. The density of BFCN was expressed as N/mm^3.

The stained slices were scanned at 600 ppi of resolution, the images were converted to 8-bit gray-scale mode and AChE positive fiber density was quantified by using Image J software (NIH, Bethesda, MD, USA). This software defines the optical density (O.D.) of an anatomical area and the background from 0 (white) to 256 (black). The intensity values in arbitrary units (A.U.) were defined in the selected equivalent areas from both hemispheres of all the animals. Background or non-specific staining values were substracted from AChE positive signals to obtain the net AChE O.D. in each area. AChE staining values in the striatum served as control, and data were expressed as percentages of O.D. in striatum for each area.

Semiquantitative analyses of GAD65 immunoreactivity (Manuscript III)

200-fold magnification photomicrographs were acquired by using an Axioskop 2 Plus microscope (Carl Zeiss). All the images were acquired at the same brain coordinates with the same illumination and exposure time and contrasted to the same level. The immunoreactivity was measured as arbitrary units (AU) of optical density (O.D.) by using Image J software. We applied the same brightness and contrast to all images. Mean intensity values were defined by the software in the selected equivalent areas from both hemispheres of all the animals. The average value from both hemispheres was calculated for each animal.

Table 1. Details of primary and secondary antibodies used for immunohistochemistry.

Host	Primary ab	Source	Dilut	Host	Secondary ab	Fluorophore	Dilution	TSA
Rabbit	**$P75^{NTR}$**	Cell Signaling, MA, USA	[1:750]	Donkey	Anti-rabbit	**Alexa fluor-488**	[1:250]	NO
Goat	**ChAT**	Millipore, CA, USA	[1:200]	Donkey	Anti-goat	**Rhodamine**	[1:80]	NO
Mouse	**GAD65**	Millipore, CA, USA	[1:750]	Donkey	Anti-mouse	**Alexa fluor-555**	[1:250]	NO
Guinea pig	**VGLUT3**	Millipore, CA, USA	[1:750]	Donkey	Anti-guinea pig	**Alexa fluor-555**	[1:250]	NO
Rabbit	**M_2AChR**	Millipore, CA, USA	[1:400]	Donkey	Anti-rabbit	**Alexa fluor-488**	[1:250]	NO
Mouse	**M_4AChR**	Millipore, CA, USA	[1:250]	Donkey	Anti-mouse	**Alexa fluor-488**	[1:250]	NO
Rabbit	**CB_1**	Affinity BioReag, USA	[1:500]	Goat	Anti-rabbit (HRP)	**Tyramide-FITC**	[1:150]	YES

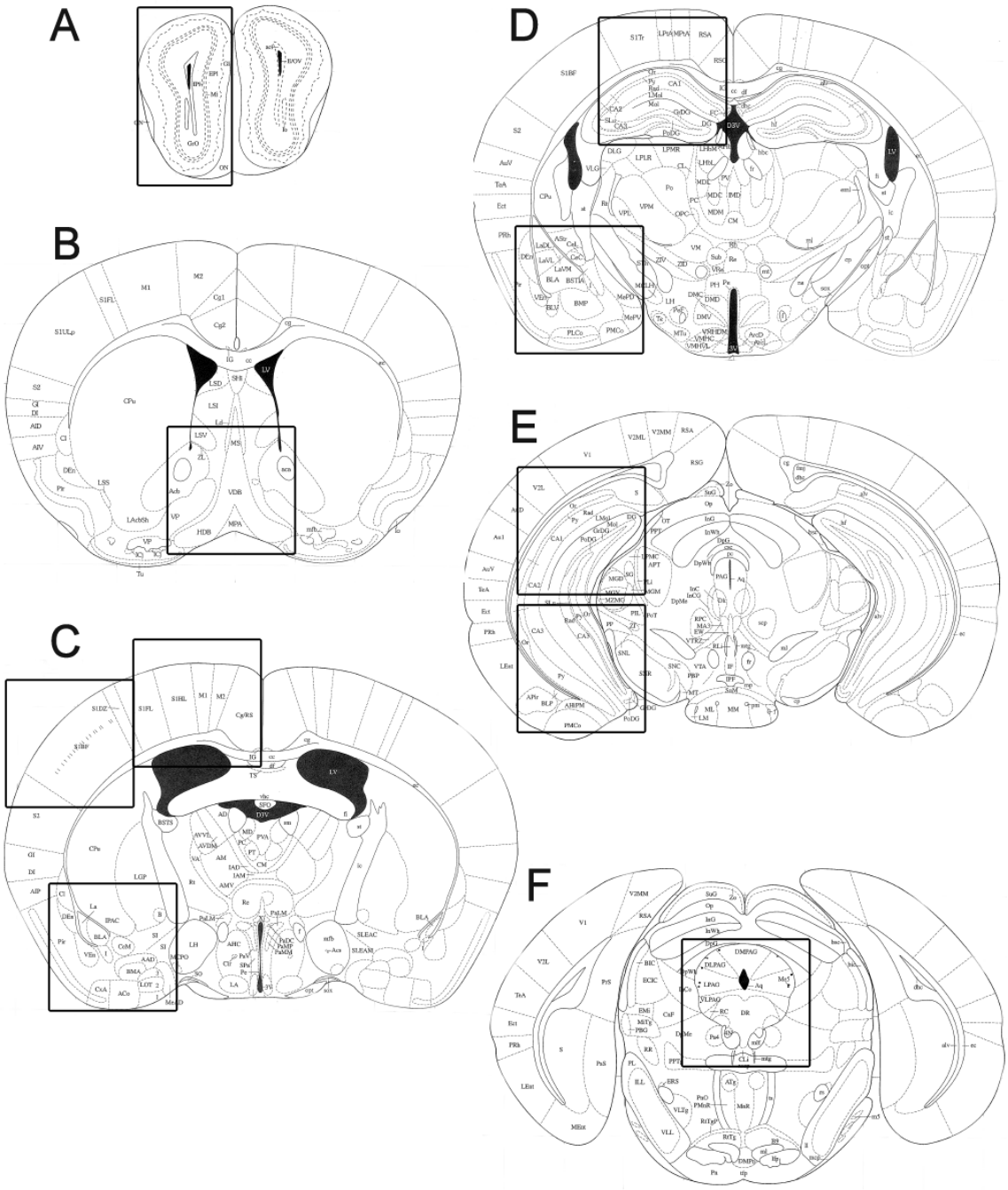

Figure 12. Different rodent brain sections in the coronal plane including the olfactory bulb structures (A), the basal forebrain cholinergic system and basal ganglia (B and C), cortical and dorsal hippocampal regions and amygdaloid nuclei (C and D), ventral hippocampal regions, subiculum, substantia nigra (E) and dorsal raphe and periaqueductal grey (F). Modified from Paxinos and Watson, 2005.

Autoradiographic studies (Manuscripts II, III and IV)

Cannabinoid receptor autoradiography (Manuscripts III and IV)

Fresh 20 µm brain slices from SHAM, aCSF and 192IgG-saporin treated rats, 3xTg-AD/Non-Tg and $CB_1^{-/-}/CB_1^{+/+}$ mice, as well as spleen slices from $CB_1^{-/-}/CB_1^{+/+}$ mice were air-dried and submerged in 50 mM Tris-HCl buffer containing 1% of BSA (pH 7.4) for 30 min at room temperature to remove the endogenous ligands. They were then incubated in the same buffer but in the presence of the CB_1/CB_2 receptor radioligand, [^{3}H]CP55,940 (3 nM) for 2 h at 37ºC. Nonspecific binding was measured by competition with non-labeled CP55,940 (10 µM) in another consecutive slice. The CB_1 receptor antagonist, SR141716A (0.1 µM) and the CB_2 receptor antagonist, SR144528 (0.1 µM), were used together with [^{3}H]CP55,940 in two consecutive slices to check for the CB_1 or CB_2 receptor binding specificity. Then, slices were washed in ice-cold (4ºC) 50 mM Tris-HCl buffer supplemented with 1% BSA (pH 7.4) to stop radioligand binding and were dipped in distilled cold water and cold dried (4ºC). Autoradiograms were generated by exposure of the tissues for 21 days at 4ºC to β-radiation sensitive films together with [^{3}H]-microscales used to calibrate the optical densities to fmol/mg tissue equivalent (fmol/mg t.e.).

Labeling of activated $G\alpha_{i/0}$ proteins by means of the [^{35}S]GTPγS binding assay (Manuscripts II, III and IV)

Fresh 20 µm slices from SHAM, aCSF and 192IgG-saporin-treated rats and 3xTg-AD mice (groups [1] to [5]) were dried, followed by two consecutive incubations in HEPES-based buffer (50 mM HEPES, 100 mM NaCl, 3 mM $MgCl_2$, 0.2 mM EGTA and 0.5% BSA, pH 7.4) for 30 min at 30ºC to remove the endogenous ligands. Briefly, slices were incubated for 2 h at 30ºC in the same buffer but supplemented with 2 mM GDP, 1 mM DTT, adenosine deaminase (3-Units/l) and 0.04 nM [^{35}S]GTPγS. The [^{35}S]GTPγS basal binding was determined in two consecutive slices in the absence of the agonist. The agonist-stimulated binding was determined in another consecutive slice with the same reaction buffer, but in the presence of the corresponding receptor agonists (e.g. WIN55,212-2 for CB_1/CB_2 receptors). The specific receptor antagonist, e.g. SR141716A (0.1 µM), was used together with WIN55,212-2 (10 µM) in one consecutive slice to check for the specific activation of the CB_1 receptor. Nonspecific binding was defined by competition with GTPγS (10 µM) in another section. Then, slices were washed twice in cold (4ºC) 50 mM HEPES buffer (pH 7.4), dried and exposed to β-radiation sensitive film with a set of [^{14}C] standards calibrated for ^{35}S calibration (Figure 13).

A similar procedure was followed for mAChR in the presence of the nonspecific agonist, carbachol (100 µM), but no BSA was used.

After 48 h, the films were developed, scanned and quantified by transforming optical densities into nCi/g tissue equivalence units using a calibration curve defined by the known values of the [^{14}C] standards (NIH-IMAGE, Bethesda, MD, USA). Nonspecific binding values were subtracted from all experimental conditions. The percentages of agonist-evoked stimulation were calculated from both the net basal and net agonist-stimulated [^{35}S]GTPγS binding densities according to the following formula: ([^{35}S]GTPγS agonist-stimulated binding x 100/[^{35}S]GTPγS basal binding)-100.

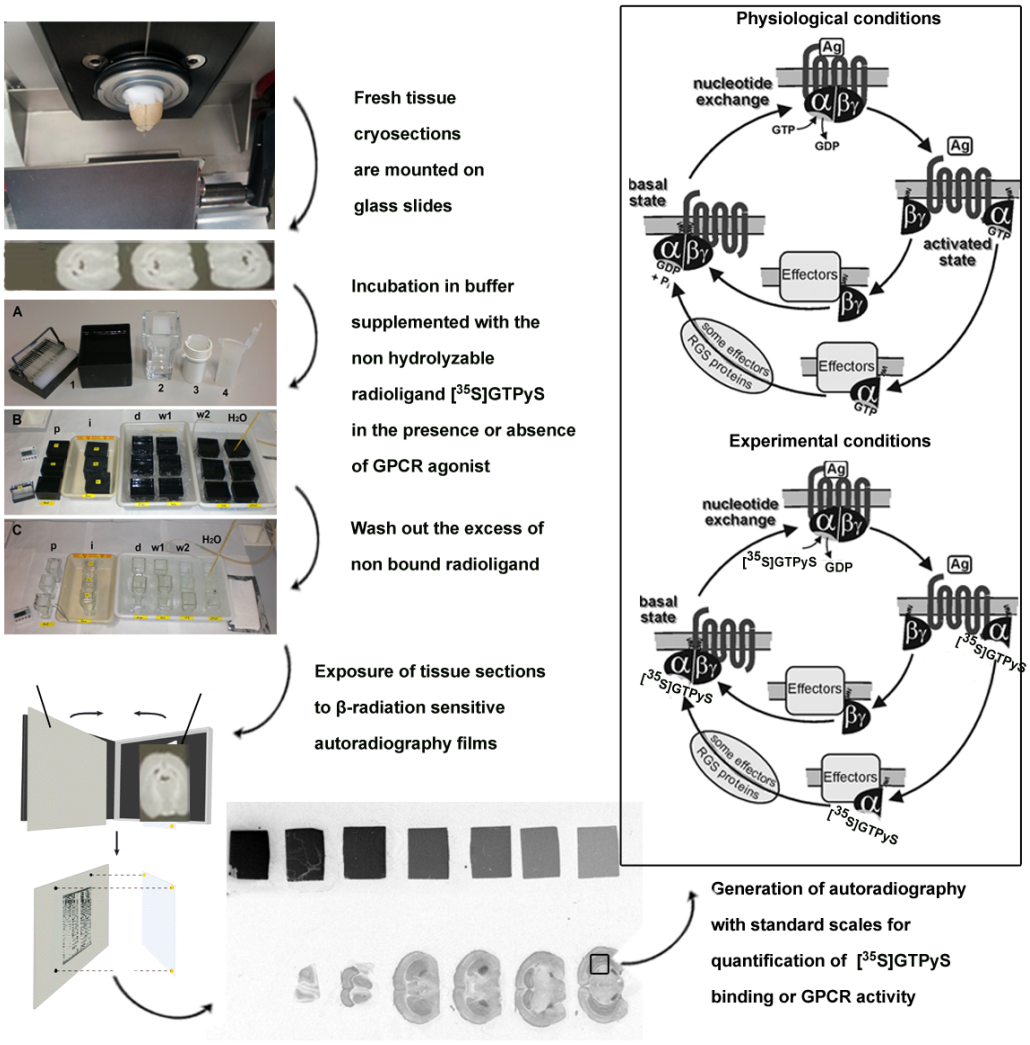

Figure 13. Schematic description of [^{35}S]GTPγS functional autoradiography. (Modified from Wettschureck and Offermanns, 2005 and Cortés et al., 2016).

Matrix-Assisted Laser Desorption Ionization-Imaging Mass Spectrometry (MALDI-IMS) (Manuscript II)

Sample preparation for MALDI-IMS. Matrix deposition

Both lipid species composition and their anatomical distribution were analyzed by using matrix-assisted laser desorption/ionization (MALDI)-imaging mass spectrometry (MALDI-IMS) in fresh 20 µm slices from aCSF and 192IgG-saporin-treated rats. Once the fresh tissue was sliced and mounted on gelatin-coated slides, the matrix 2-Mercaptobenzothiazole (MBT) was deposited on the tissue surface by a process of solvent-free sublimation, which allows the correct and homogenous deposition of the matrix and avoids lipid migration. MBT matrix reaches a good signal to noise ratio, both in extracts and in IMS experiments (Astigarraga et al., 2008). The sublimation was performed using 300 mg of MBT in a vacuum and the deposition time and temperature were controlled (30 min, 140ºC).

Matrix re-crystallization

For the re-crystallization of the matrix the sample was attached face-down to the bottom of a glass Petri plate which was placed on another Petri plate containing a methanol impregnated–piece of filter paper in its base. The Petri plates were then placed on a hot plate (1 min, 40ºC).

Mass spectrometer spectra and image analysis

A MALDI LTQ-XL-Orbitrap (Thermo Fisher, San Jose, CA) equipped with a nitrogen laser (λ = 337 nm, rep. rate = 60 Hz, spot size = 80 x 120 µm) was used for mass analysis. Thermo´s Imagequest and Xcalibur software were used for MALDI-IMS data and image acquisition in both positive and negative ion mode. The positive ion range was 500-1000 Da and the negative ion range was 400-1100 Da, with 10 laser shots per pixel at a laser fluence of 15 µJ. The target plate stepping distance was set at 150 µm for both x- and y-axes by the MSI image acquisition software. The data were normalized using the total ion current (TIC) values, as there may be potential displacement of the masses on the tissue due to experimental factors, e.g., the irregularities of the surface.

The MALDI images were generated by means of ImageQuest (Thermo Scientific). Each of the m/z values was plotted for signal intensity for each pixel (mass spectrum) across a given area (tissue section). The m/z range of interest was normalized using the ratio of the TIC for each mass spectrum. The intensity reached by each peak (m/z or molecule) was further calculated as a ratio of the peak with the

highest intensity, and the average was obtained using OriginPro8 (Northampton MA, USA) software. The most intense peak was considered to be 100%. The assignment of lipid species was facilitated by the use of the databases Lipid MAPS (http://www.lipidmaps.org/) and Madison Metabolomics (http://mmcd.nmrfam.wisc.edu), and 5 ppm mass accuracy was selected as the tolerance window for the assignment (Figure 14).

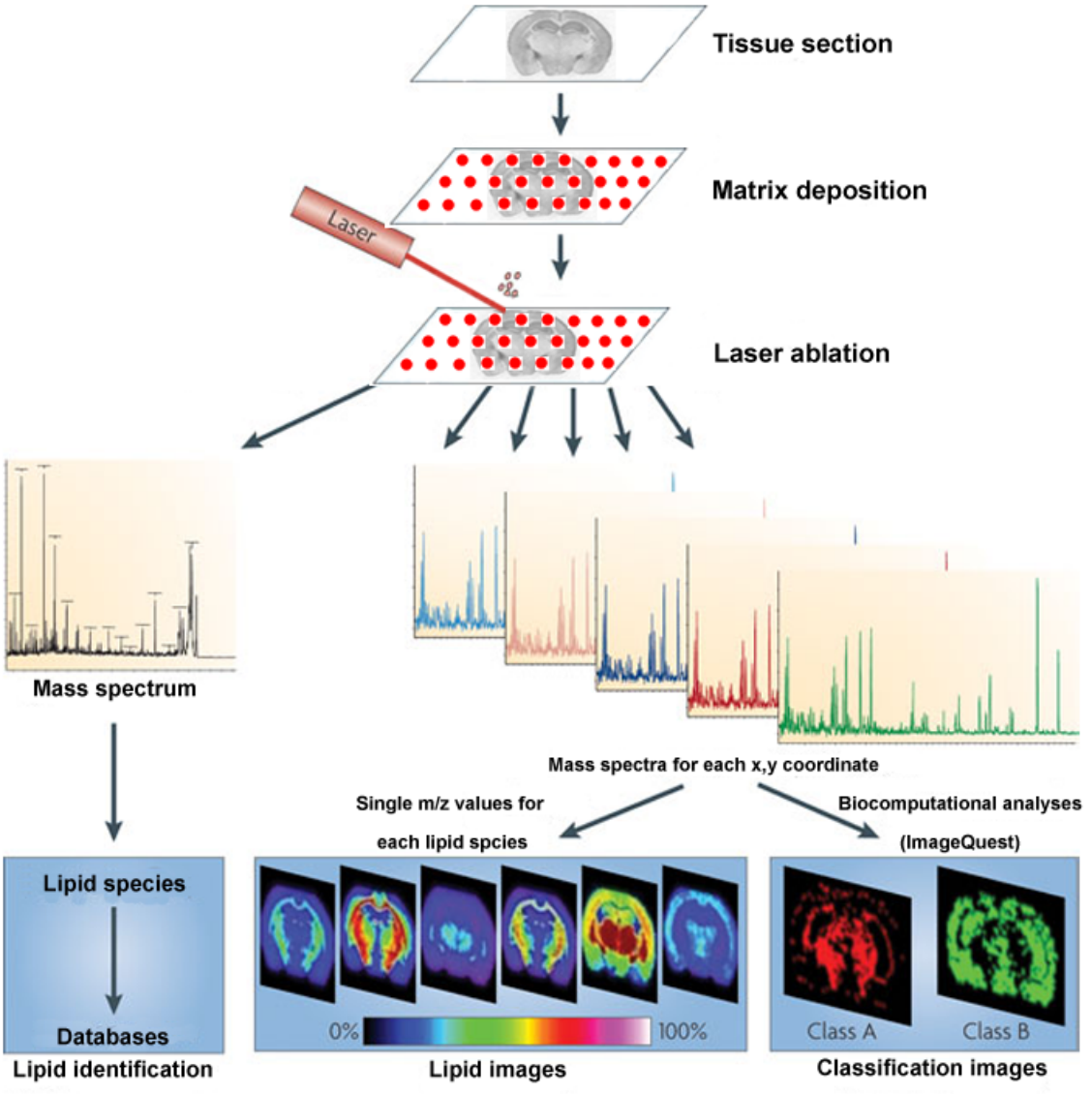

Figure 14. Schematic description of MALDI-IMS procedures. From the collection of the sample to the identification and quantification of the relative abundance of lipids and imaging acquisition (Modified from Schwamborn and Caprioli, 2010).

Statistical analyses

The two-tailed unpaired Student *t* test was used for comparisons between aCSF *vs* 192IgG-saporin-treated rats and Non-Tg *vs* 3xTg-AD mice treated with vehicle. The one-way analysis of variance (ANOVA) and Log-Rank analyses were used for multiple comparisons between treatments in organotypic cultures, treatments in 3xTg-AD mice and when SHAM, aCSF and 192IgG-saporin-treated groups were simultaneously compared. The statistical significance threshold was set at $p < 0.05$.

Passive avoidance test (Manuscripts II, III and IV). The acquisition latencies were statistically analyzed using the two-tailed unpaired Student *t* test, or by one-way analysis of variance (ANOVA) for multiple comparisons, followed by Bonferroni´s or Dunn's *post hoc* tests. The step-through latencies were represented as Kaplan-Meier survival curves, and for comparisons the nonparametric Log-rank/Mantel-Cox test was used which is appropriate when censored data must be analyzed. The existence of animals that reached the cut-off time of 300 s was the reason to choose this rigorous statistical analysis.

Histochemical data (Manuscripts I, II and III). Propidium iodide positive cells, BFCN density, AChE fiber density and GAD65 optical density were statistically analyzed using the two-tailed unpaired Student *t* test or one-way analysis of variance (ANOVA), followed by Bonferroni´s or Dunn's *post hoc* tests.

Autoradiographic data (Manuscripts II, III, IV). The percentages of agonist-evoked [^{35}S]GTPγS binding and the [^{3}H]CP55,940 densities were statistically analyzed using the two-tailed unpaired Student *t* test or one-way analysis of variance (ANOVA), followed by Bonferroni´s or Dunn's *post hoc* tests.

MALDI-IMS data (Manuscript III). The percentages of the relative intensity of lipids were statistically analyzed using the two-tailed unpaired Student *t* test.

Correlation analyses (Manuscript II, III and IV). Correlations between different neurochemical data were examined by linear regression analysis and the Pearson´s correlation coefficient was calculated.

Results

1. *Ex vivo* model of basal forebrain cholinergic lesion

(Manuscript I) WIN55,212-2-mediated protective effects of basal forebrain cholinergic system via CB_1 receptor activation in organotypic cultures treated with 192IgG-saporin

HIGHLIGHTS

- **P7 and adult rats show a similar anatomical distribution of basal forebrain cholinergic neurons (BFCN).**
- **The BFCN from P7 rats express somatodendritic $p75^{NTR}$ receptors.**
- **The BFCN are selectively eliminated by 192IgG-saporin in hemibrain organotypic cultures.**
- **WIN55,212-2, at nanomolar concentrations, protects basal forebrain cells from the damage induced by the elimination of BFCN.**

GRAPHICAL ABSTRACT

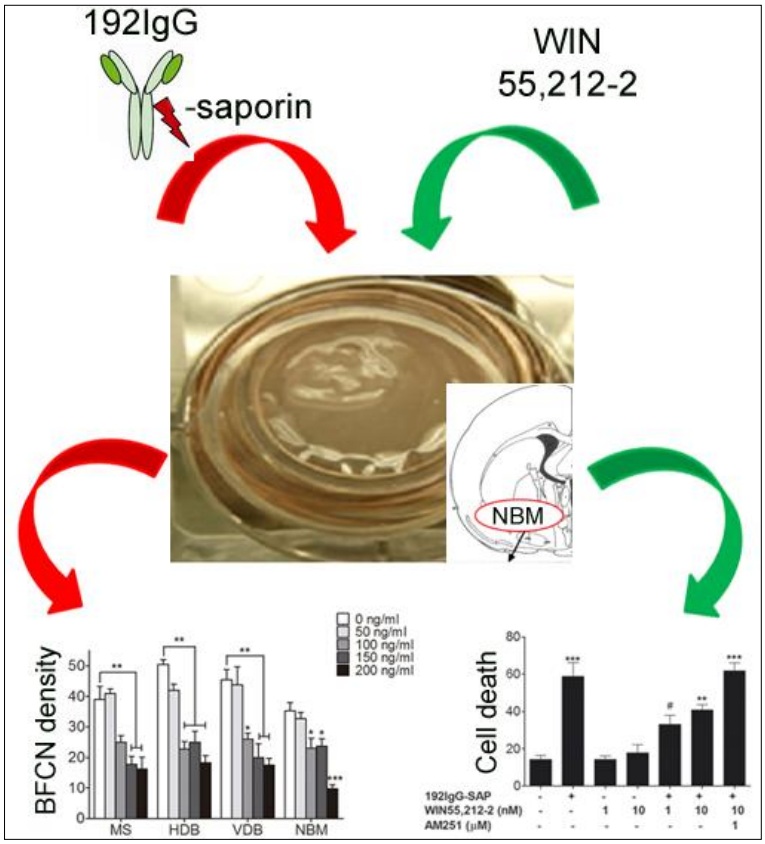

1.1. P75^{NTR} immunostaining in the basal forebrain of P7 rats

Prior to the use of the 192IgG-saporin to mimic an *ex vivo* model of basal forebrain cholinergic dysfunction, it was necessary to determine the presence of BFCN expressing the immunotoxin target p75^{NTR} in P7 rats. The immunofluorescence studies carried out in the basal forebrain cholinergic system from P7 rats revealed the presence of a high density of BFCN expressing p75^{NTR} in the different nuclei analyzed (Ch1-Ch4). The BFCN perikarya were intensely stained showing the typically somatodendritic distribution of p75^{NTR}. The BFCN are continuously distributed in partially discrete populations along the rostrocaudal axis in adult rodents as well as in human and non-human primates. According to this particular distribution of the BFCN, the Ch1 or the medial septum (MS) and the Ch2 or the vertical diagonal band of Broca (VDB) were first analyzed in P7 rats. The big immunoreactive BFCN from the MS and VDB were clearly distinguished from the smaller surrounding cells, showed a moderate Hoechst-staining and, moreover, were distributed along the midline (Figure 15 A) extending ventrally to the vertical limb of the VDB, (Figure 15 B), which revealed a continuum of p75^{NTR} positive BFCN located within Ch1 and Ch2. The BFCN from the horizontal diagonal band of Broca (HDB) or Ch3 (Figure 15 C), were distributed caudally to VDB and extended ventrally to the nucleus basalis magnocellularis (NBM) or Ch4 (Figure 15 D). The BFCN of these nuclei displayed similar staining patterns to those previously mentioned, including big but moderately stained nuclei, described for the MS and VDB. It should also be emphasized that the BFCN from the NBM showed the biggest size and the most extensive dendritic arborization among all BFCN.

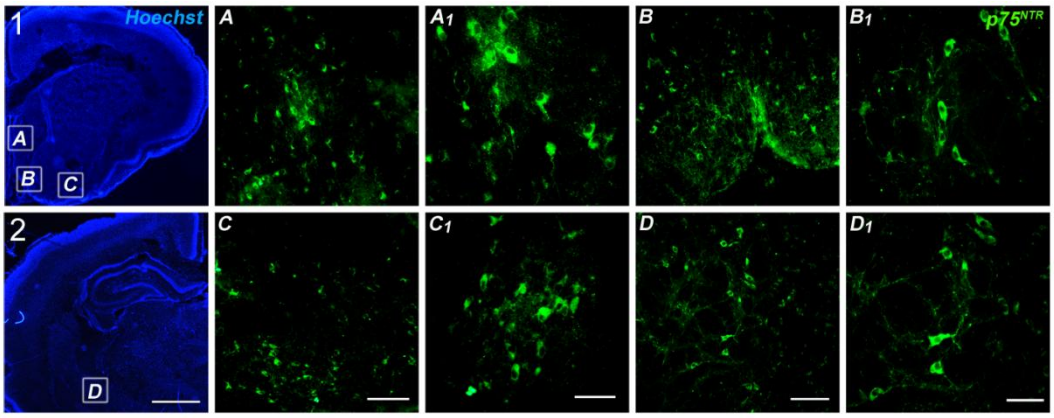

Figure 15. Low magnification (2.5X) photomicrographs of Hoechst staining in 10 µm tissue slices from P7 rats including the MS (1-A), both VDB (1-B) and HDB (1-C) and the NBM (2-D) (Scale bar = 1 mm). P75^{NTR} immunofluorescence in the MS (A-A1), VDB (B-B1), HDB (C-C1) and NBM (D-D1). (C-D scale bar = 100 µm and C1-D1 scale bar = 50 µm).

1.2. 192IgG-saporin-induced BFCN death in organotypic cultures

The application of different doses of 192IgG-saporin to hemibrain organotypic cultures containing the basal forebrain cholinergic system was able to induce specific reductions of BFCN, in a dose-dependent manner, according to the different assayed treatments (Figure 16). Increasing concentrations of 192IgG-saporin (50-200 ng/ml) were added at day five of culture *in vitro*, and let the toxin do its effect during another three days *in vitro* (DIV). The effective concentration of immunotoxin, which eliminated approximately 50% of BFCN was set around 100 ng/ml, leading to a reduction of BFCN density of up to 36% in the MS, 55% in HDB, 42% in VDB and 35% in the NBM. The highest concentrations of 192IgG-saporin (200 ng/ml) triggered a reduction of 58% in the number of $p75^{NTR}$ positive cells/mm^2 in the MS, 64% in the HDB, 61% in the VDB and 72% in the NBM (Figure 16 A). In another set of experiments the schedule was modified and the 192IgG-saporin was added at day two of culture which was let in the tissue acting during six additional DIV. The purpose was to evaluate more initial effects of the toxin for a longer period. It was observed a reduction of BFCN densities of up to 65% in the MS, 55% in HDB, 60% in VDB and 65% in the NBM (Figure 17 A). Interestingly, the BFCN reduction induced by 100 ng/ml of immunotoxin during six DIV was comparable to that observed with the highest dose (200 ng/ml) during three DIV, which demonstrated not only a 192IgG-saporin-induced BFCN death in a dose-dependent manner, but also in a time-dependent manner of exposure to the immunotoxin. The $p75^{NTR}$-immunoreactivity showed the presence of a great deal of debris and a significant atrophy related to smaller somatic size and a reduced dendritic arborization after the application of 192IgG-saporin (Figure 17 B). Furthermore, the PI uptake, indicative of compromised cell viability, showed dramatic levels of cell death in a dose-dependent manner including BFCN and non-cholinergic cells (Figure 18). Finally, the double application of 100 ng/ml of 192IgG-saporin at days two and five of culture *in vitro* during 6 DIV led to comparable levels of BFCN reduction to those observed with the single application at day two of culture *in vitro* (Figure 19). However, the double application of 200 ng/ml of immunotoxin led to an almost total elimination of BFCN as revealed by the nearly complete lack of $p75^{NTR}$ immunoreactivity and the intense PI staining recorded in the different cholinergic nuclei of the basal forebrain which further suggested non-specific damage.

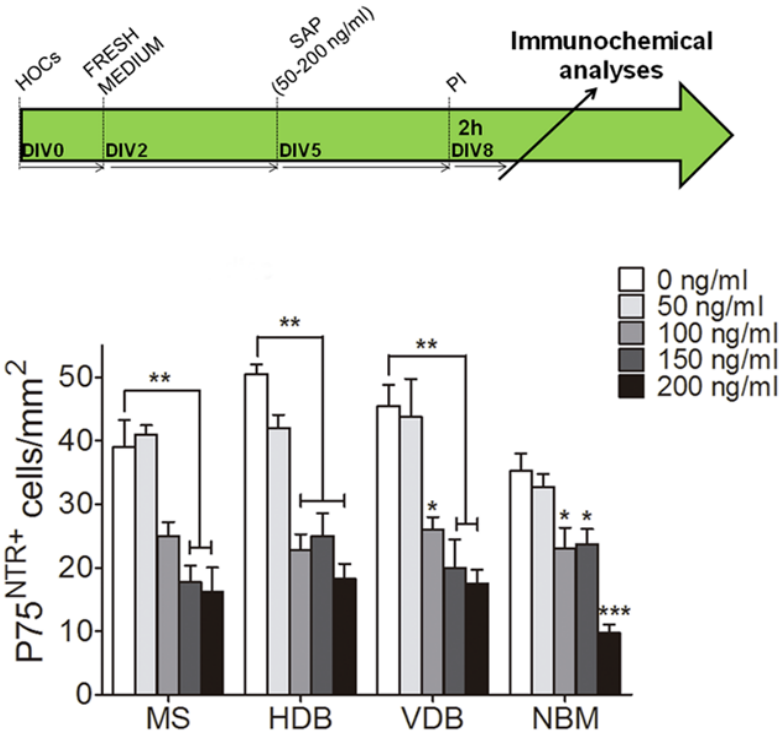

Figure 16. The 192IgG-saporin treatment during 3 days was able to induce a concentration dependent reduction in the densities of $p75^{NTR}$ positive cells in hemibrain organotypic cultures containing the MS, HDB, VDB and NBM basal forebrain cholinergic nucleus * $p < 0.05$; ** $p < 0.01$; *** $p < 0.001$ *vs* control (0 ng/ml).

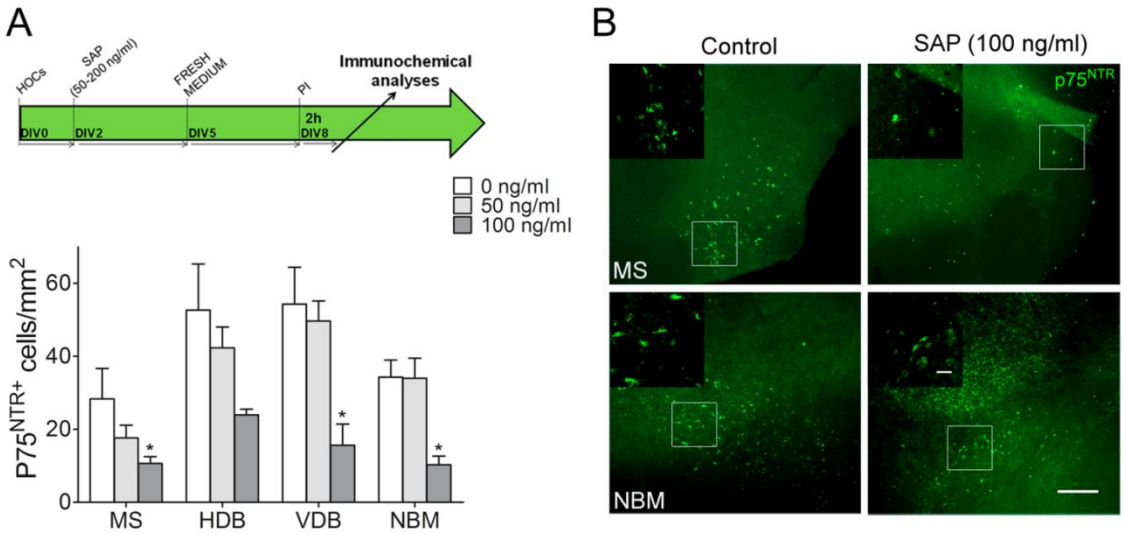

Figure 17. (A) Number of $p75^{NTR}$ immunoreactive BFCN in hemibrain organotypic cultures containing the different nucleus of the basal forebrain cholinergic system (MS, HDB, VDB and NBM) after the application of different concentrations of 192IgG-saporin according to the six days treatment schedule (A above). (B) $P75^{NTR}$ immunoreactive BFCN in the MS (top row) and the NBM (bottom row) in the absence (control) or in the presence of 100 ng/ml of the immunotoxin according to the treatment schedule described in (A). Low magnification scale bar = 200, and high magnification scale bar in the inset = 40 µm. * $p < 0.05$ *vs* control (0 ng/ml).

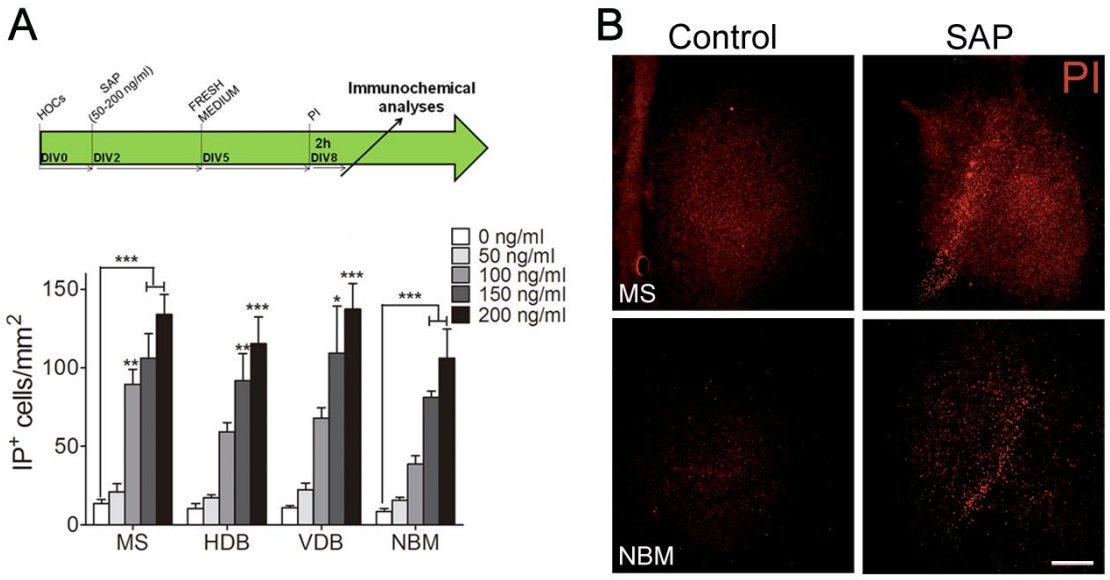

Figure 18. (A) Densities of PI positive cells in hemibrain organotypic cultures containing the basal forebrain cholinergic nuclei after the application of different concentrations of 192IgG-saporin according to the treatment schedule detailed in the green arrow graphic. (B) PI uptake in hemibrain organotypic cultures containing the MS (top row) and the NBM (bottom row) in the absence (control) or in the presence of 100 ng/ml of the immunotoxin (SAP) according to the treatment schedule described in (A above). Scale bar = 200 µm. * $p < 0.05$; ** $p < 0.01$; *** $p < 0.001$ *vs* control (0 ng/ml).

1.3. Effects of WIN55,212-2 in 192IgG-saporin-lesioned hemibrain organotypic cultures

P75^{NTR} immunoreactive BFCN

The pharmacological treatment of hemibrain organotypic cultures with the synthetic agonist for CB_1/CB_2 receptors, WIN55,212-2, or with the ethanol used as vehicle, did not exert any effect on the viability of the cultures nor on the density of BFCN (see treatment schedule in Figure 19 A). The application of 100 ng/ml of 192IgG-saporin at days two and five of culture *in vitro* during six DIV led to a statistically significant decrease in the density of BFCN (up to 60%), in both the MS (vehicle 64 ± 7.8 BFCN/mm^2 *vs* SAP 26 ± 4.2 BFCN/mm^2; $p < 0.01$) and NBM (vehicle 64 ± 3.8 BFCN/mm^2 *vs* SAP 26 ± 6.7 BFCN/mm^2; $p < 0.01$) (Figure 19). The pre-treatment of hemibrain organotypic cultures with either 1 nM or 10 nM of WIN55,212-2, 2h prior the application of 192IgG-saporin, did not trigger any relevant effect on the viability and density of BFCN but induced an attenuation of BFCN death in both, the MS (1 nM WIN55,212-2: 44 ± 4.2 BFCN/mm^2 and 10 nM WIN55,212-2: 43 ± 7.4 BFCN/mm^2) and NBM (1 nM WIN55,212-2: 31.56 ± 4.8 BFCN/mm^2 and 10 nM WIN55,212-2: 40 ± 2.9 BFCN/mm^2) (Figure 19 B-C). These effects were completely

abolished in the presence of the CB_1 receptor antagonist AM251 (1 µM) leading to BFCN levels similar or even lower to those observed in the cultures treated with the immunotoxin (Figure 19 B-C). The loss of BFCN was revealed by the absence of well-defined $p75^{NTR}$ immunostained magnocellular neuronal bodies (Figure 19 D).

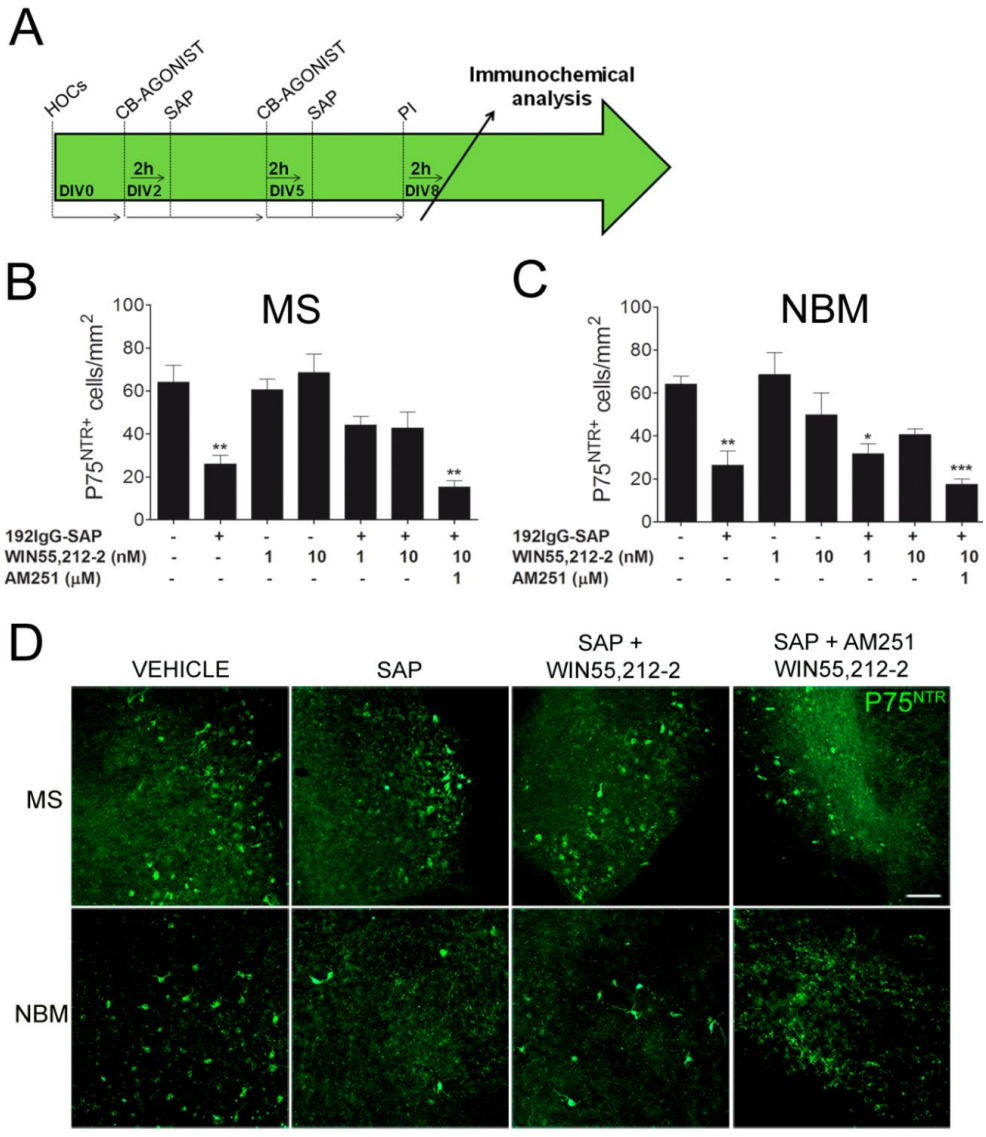

Figure 19. (B-C) Number of $p75^{NTR}$ immunoreactive BFCN in hemibrain organotypic cultures in the absence or presence of 100 ng/ml of 192IgG-saporin, the cannabinoid agonist WIN55,212-2 (1 or 10 nM) or the CB_1 receptor antagonist AM251 (1 µM) during 6 days according to the treatment schedule (A). (D) $P75^{NTR}$ immunoreactive BFCN in the MS (top row) and the NBM (bottom row) in the absence (vehicle) or presence of 100 ng/ml of the immunotoxin, treated with 1 nM WIN55,212-2 and 1 µM of AM251. Scale bar = 40 µm. * $p < 0.05$; ** $p < 0.01$; *** $p < 0.001$ *vs* control untreated tissues.

Cell death evaluated as PI positive cells

The PI uptake was also measured and the cell death quantified in the MS, NBM and cortex. The pharmacological treatment of the hemibrain organotypic cultures with the cannabinoid agonist for CB_1/CB_2 receptors, WIN55,212-2, or with the vehicle, did not exert any effect on the density of PI positive cells (Figure 20 A; see treatment schedule in figure 19 A). The application of 100 ng/ml of 192IgG-saporin during six DIV led to a statistically significant increase in the density of PI stained cells (approximately up to 300%) in the MS (vehicle 16.76 ± 2.3 cells/mm^2 *vs* SAP 70.26 ± 7.7 cells/mm^2; $p < 0.001$), NBM (14 ± 2.3 cells/mm^2 *vs* SAP 59 ± 7.5 cells/mm^2; $p < 0.001$) and cortex (18 ± 3.8 cells/mm^2 *vs* SAP 61.63 ± 8 cells/mm^2; $p < 0.001$) (Figure 20 A). The pre-treatment of hemibrain organotypic cultures with 1 nM or 10 nM of WIN55,212-2, prior to the application of 192IgG-saporin, induced protective effects on cell viability in the MS and in the NBM but no effects were observed in the cortex. A statistically significant decrease of cell death was observed as compared with 192IgG-saporin-treated hemibrain organotypic cultures in the MS (1 nM WIN55,212-2: 38 ± 4.2 PI cells/mm^2 and 10 nM WIN55,212-2: 39 ± 2.2 PI cells/mm^2; $p < 0.01$ *vs* SAP data above described), in the NBM (1 nM WIN55,212-2; 33 ± 4.9 PI cells/mm^2; $p < 0.05$ *vs* SAP data above described, and 10 nM: WIN55,212-2 41 ± 2.8 PI cells/mm^2; $p < 0.01$ *vs* SAP data above described) (Figure 20 A). The specific CB_1 receptor antagonist, AM251, was able to block the protective effects elicited by WIN55,212-2 leading to cell death levels similar to those observed in the cultures treated with the immunotoxin (Figure 20 A-C).

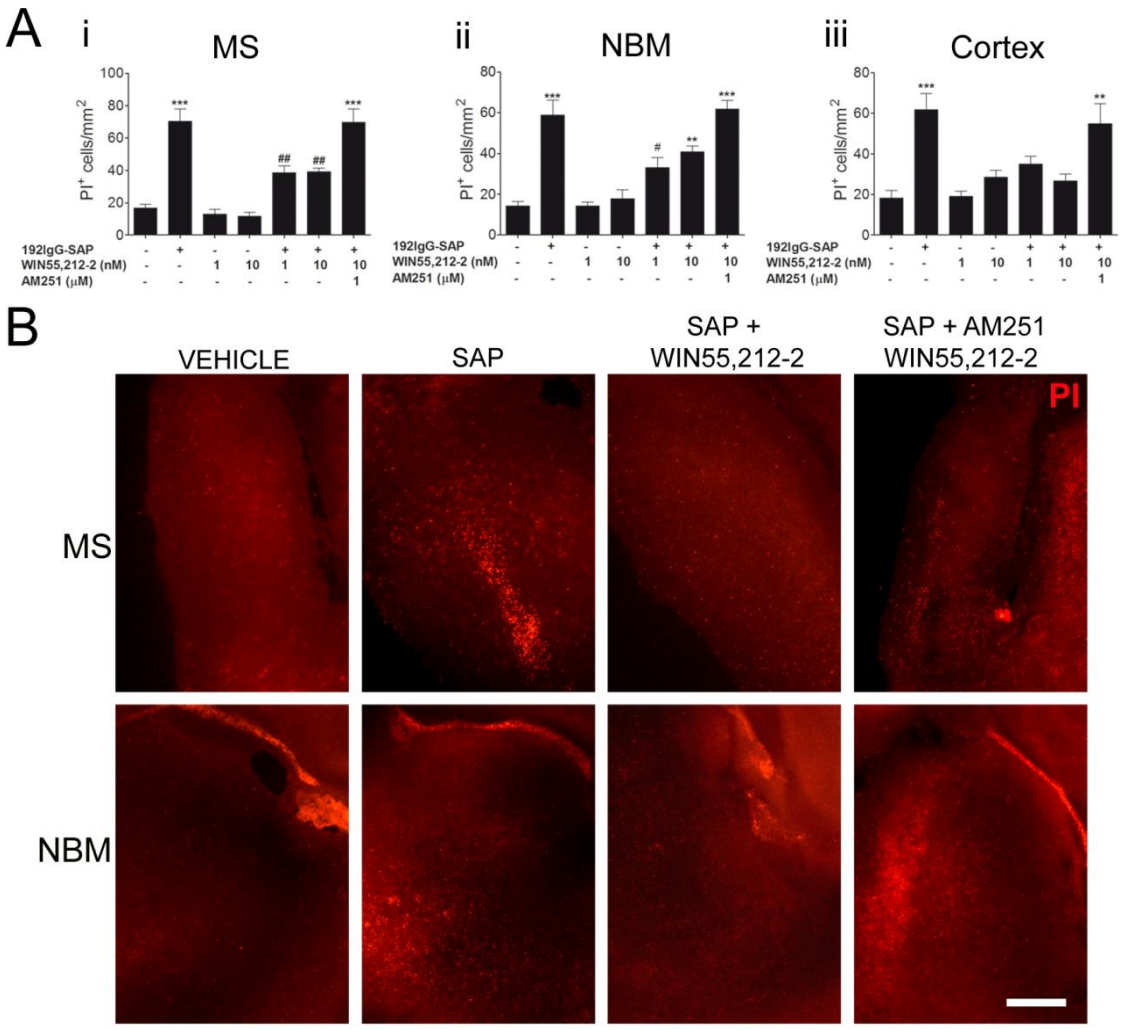

Figure 20. (A) Number of PI positive cells in hemibrain organotypic cultures containing the MS (i), the NBM (ii) and the cortex (iii) in the absence or presence of 100 ng/ml of 192IgG-saporin, the cannabinoid agonist WIN55,212-2 (1 or 10 nM) or the CB_1 receptor antagonist AM251 (1 µM) during 6 days according to the treatment schedule (see Figure 19 A). (B) PI uptake in the MS (top row) and the NBM (bottom row) in the absence (vehicle) or presence of 100 ng/ml of the immunotoxin, treated with WIN55,212-2 (1 nM) and of AM251 (1 µM). Scale bar = 200 µm. ** $p < 0.01$; *** $p < 0.001$ *vs* control and # $p < 0.05$; ## $p < 0.01$ *vs* 192IgG-saporin.

2. *In vivo* model of basal forebrain cholinergic lesion

(Manuscript II) Muscarinic neurotransmission and lipid profile changes in a rat model of cholinergic dysfunction

HIGHLIGHTS

- **The 192IgG-saporin lesion model of basal forebrain cholinergic damage has been improved minimizing artifactual impairment.**
- **The intraparenchymal infusion of 192IgG-saporin in the NBM specifically eliminates BFCN leading to a dramatic reduction of cortical cholinergic innervation and deficits in learning and memory.**
- **M_2/M_4 mAChR-mediated muscarinic cholinergic signaling is altered in the NBM and hippocampus where these receptors show specific distribution patterns.**
- **Changes in the phospholipid composition observed in this model contribute to understand their relation with the BFCN.**

GRAPHICAL ABSTRACT

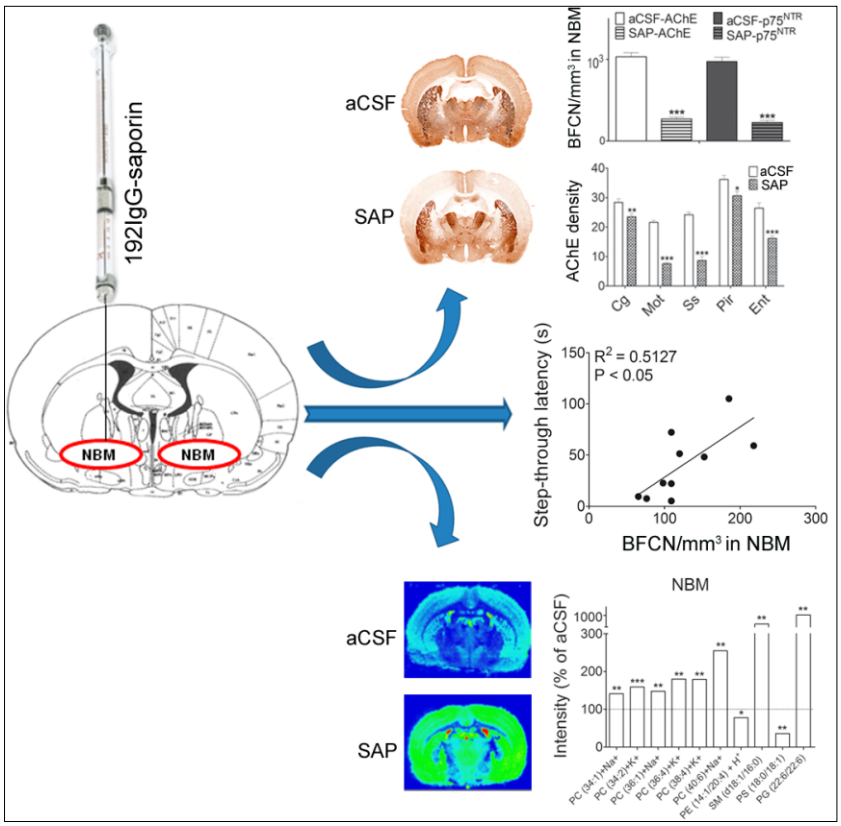

2.1. The specific loss of BFCN in the NBM leads to learning and memory impairment

To examine learning and memory behavior, the rats were trained and tested using the passive avoidance test. Seven days after the intraparenchymal infusion of 192IgG-saporin in the NBM we evaluated the acquisition latency parameter as the time that rats stayed in the open compartment before entering the dark and closed compartment where the aversive stimulus was then produced as an electrical foot-shock. No differences in acquisition latency were observed between the three groups (SHAM, aCSF and SAP: 10.2 ± 1 sec, 10.4 ± 0.9 sec and 11.14 ± 1.4 sec; respectively) (Figure 21 A). 24 h later, all trained animals were tested again to evaluate learning and memory. The step-through latency time was measured and represented as Kaplan-Meier survival curves to determine the estimated probability of a positive response; i.e., to reach the cut-off time. When the groups were compared, 100% of the SHAM, and 78% of the aCSF-treated rats, remembered the aversive stimulus and displayed a positive response. However, only the 40% of the 192IgG-saporin-treated rats remembered the aversive stimulus ($p = 0.0006$ vs aCSF; Log-Rank/Mantel-Cox test) (Figure 21 B). No statistically significant differences were observed between SHAM and aCSF-treated animals, which revealed the absence of a significant damage due to the needle or the vehicle used. The median latency was determined as the time where 50% of the animals cross the doorway. The median step-through latency could only be calculated for 192IgG-saporin-treated rats, which showed a median latency of 102 s.

On the other hand, the degree of the lesion was estimated by using the AChE enzymatic assay to stain BFCN somas and cholinergic fibers in the projecting areas. The $p75^{NTR}$ immunofluorescence assay was also used to stain the surviving target BFCN after the administration of 192IgG-saporin. The intraparenchymal infusion of 192IgG-saporin in the NBM resulted in an extensive reduction of both AChE stained (1032 ± 50 cells/mm^3 in aCSF group and 270 ± 23 cells/mm^3 in SAP group; $p < 0.0001$) and $p75^{NTR}$ immunoreactive BFCN (973 ± 53 cells/mm^3 in aCSF group and 226 ± 25 cells/mm^3 in 192IgG-saporin-treated rats, respectively; $p < 0.0001$) (Figure 21 C-D). Interestingly, correlation analysis between the step-through latencies and the number of BFCN in the NBM of those rats infused with the immunotoxin, revealed that the animals with higher reductions in BFCN density spent significantly less time to access the dark compartment; i.e., had a higher impairment in learning and memory behavior ($R^2 = 0.5127$; $p = 0.0199$) (Figure 21 E).

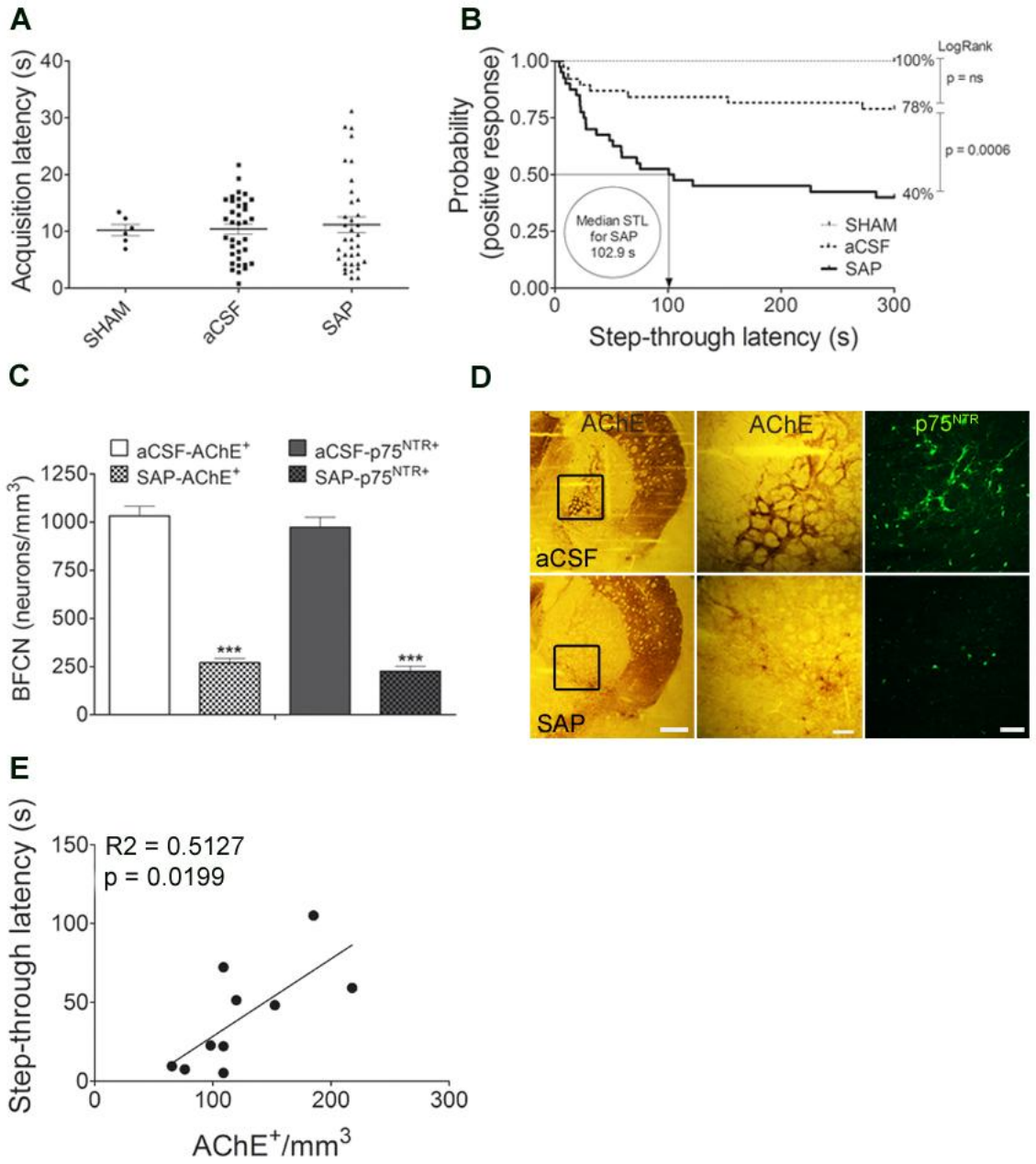

Figure 21. (A) Acquisition latency times in the learning trial of the passive avoidance test. (B) Step-through latency times of passive avoidance test represented as Kaplan-Meier survival curves ($p < 0.0001$ *vs* aCSF, Log-Rank/Mantel-Cox test). (C) Number of BFCN in the NBM of aCSF and 192IgG-saporin treated animals. (D) AChE enzymatic staining and $p75^{NTR}$ immunofluorescence in the NBM. (E) Correlation analysis between the step-through latencies and the density of BFCN in the NBM. Scale bars = 500 and 100 µm, respectively. Data are means ± SEM; ***$p < 0.001$ *vs* aCSF-AChE and *vs* aCSF-$p75^{NTR}$.

2.2. The specific loss of BFCN leads to a decrease of cholinergic innervations

The loss of BFCN in the NBM triggers a dramatic reduction in the AChE positive fibers in the brain areas innervated by the basal forebrain cholinergic system (Figure 22). The highest loss of cholinergic afferents was observed in the motor (60%), somatosensory (65%) and entorhinal (40%) cortices ($p < 0.001$ *vs* aCSF). A moderate loss of cholinergic fibers was recorded in other cortical areas such as the cingulate (20%) and piriform (15%) ($p < 0.05$ *vs* aCSF) (Figure 22 C-D). The AChE staining was also decreased in the amygdaloid complex, showing a significant reduction in the anterior (30%) ($p < 0.05$ *vs* aCSF), lateral (19%) ($p < 0.05$ *vs* aCSF) and medial (40%) ($p < 0.05$ *vs* aCSF) amygdaloid nuclei. In the hippocampus a significant cholinergic dennervation was also observed in CA3 (10%) and dentate gyrus (15%) ($p < 0.05$ *vs* aCSF) (Figure 22 D).

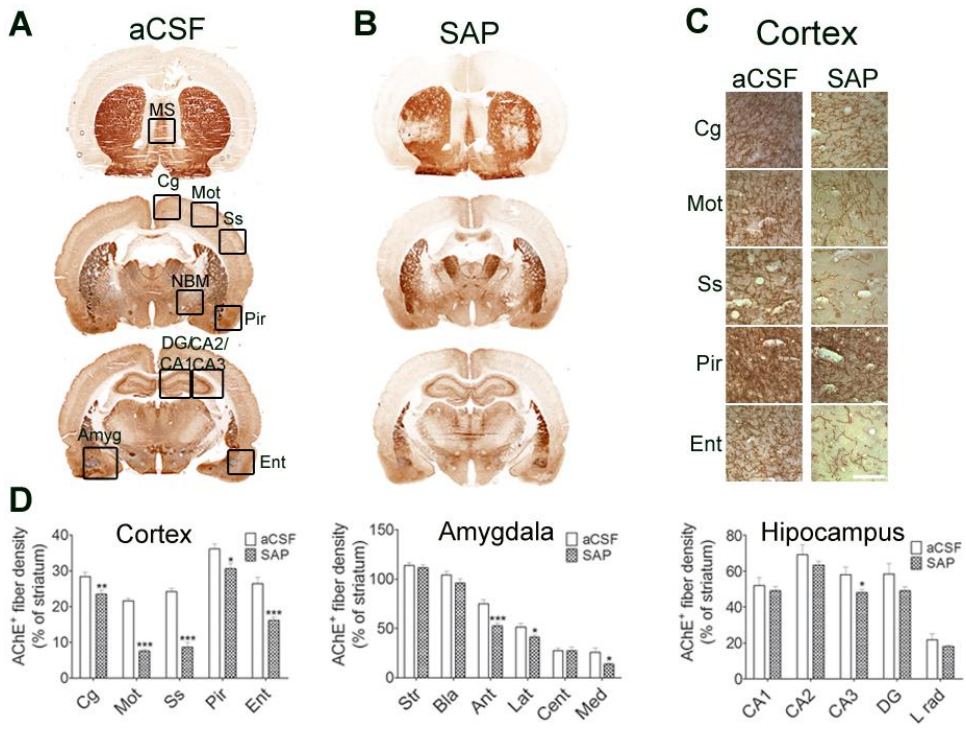

Figure 22. (A-B) AChE staining in brain slices at three different levels of aCSF and 192IgG-saporin-treated rats. (C) Microphotographs from different cortical regions of both groups at 400-fold magnification, revealing the decrease in AChE positive fibers induced by the immunotoxin (scale bar = 20 µm). (D) The histograms show the optical density of AChE expressed as percentages of the striatal levels (used as control area) in aCSF (n = 13) and SAP (n = 13) treated rats. *p < 0.05; **p < 0.01 and ***p < 0.001 *vs* aCSF-treated rats. MS: medial septum; Cg: cingular cortex; Mot: motor cortex; Ss: somatosensory cortex; Pir: piriform cortex; Ent: entorhinal cortex; Amyg: amygdala; DG: dentate gyrus.

2.3. The specific loss of BFCN positively correlates with reduced cholinergic innervation

As expected, the loss of BFCN in the NBM induced a significant decrease in AChE staining in projection areas. The linear regression analysis confirmed the relationship between the loss of BFCN and the reduction in AChE fiber densities in the cortex, including cingular (R^2 = 0.4886, $p < 0.001$), motor (R^2 = 0.8370; $p < 0.001$), piriform (R^2 = 0.3667, $p < 0.05$), somatosensory (R^2 = 0.8148, $p < 0.001$) and entorhinal (R^2 = 0.5536, $p < 0.001$) cortices. The same effect was measured in the amygdala, including the anterior (R^2 = 0.4245, $p < 0.01$), lateral (R^2 = 0.2296, $p < 0.05$) and medial (R^2 = 0.3134, $p < 0.05$) nuclei, and in the hippocampus, including the CA3 (R^2 = 0.4926, $p < 0.01$) and the dentate gyrus (R^2 = 0.3274, $p < 0.05$) regions (Figure 23).

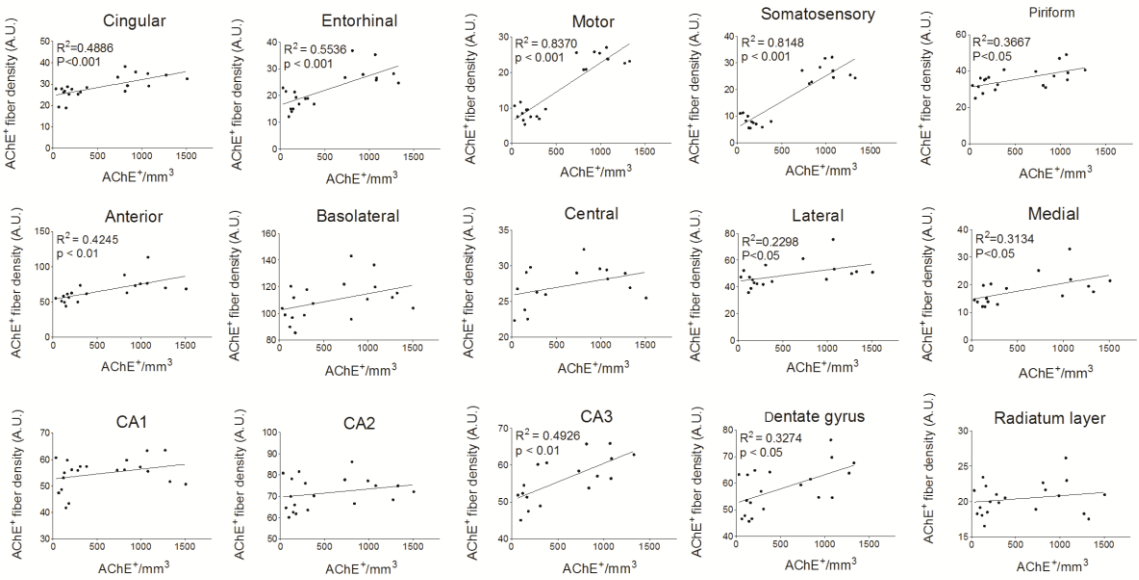

Figure 23. The plots show the number of AChE stained BFCN in the NBM (number of cells/mm^3) and the density of AChE stained fibers (arbitrary units) in different basal forebrain cholinergic projections including the cortex (top row), the amygdala (middle row) and the hippocampus (bottom row) from aCSF and 192IgG-saporin-treated rats. The regression analyses reveal a decrease in the density of AChE stained fibers directly related to the depletion of BFCN.

2.4. The specific loss of BFCN in the NBM leads to altered mAChR functionality

To examine M_2/M_4 mAChR-mediated signaling, the activity of $G_{i/o}$-coupled mAChR was analyzed by means of [^{35}S]GTPγS autoradiography assay. Basal binding values were similar in both groups (aCSF and SAP) in all the brain areas analyzed. The anatomical analysis of carbachol-induced [^{35}S]GTPγS binding stimulation revealed differences in the functional coupling of mAChR to $G_{i/o}$ proteins in several brain areas in 192IgG-saporin-treated animals (See tables 2-3). Thus, carbachol-induced stimulation of M_2/M_4 mAChR was decreased in the NBM (aCSF 45 ± 9.7% and SAP 15 ± 6.2%; $p < 0.05$) from 192IgG-saporin-treated rats. Despite the massive loss of the presynaptic cortical cholinergic innervation demonstrated in the previous section, no changes were found in any of the cortical areas (Figure 24 A). However, in the hippocampus, the lesion induced an enhancement of carbachol-induced [^{35}S]GTPγS binding in the pyramidal layer of the CA3 (aCSF 11 ± 5.6% and SAP 32 ± 4.2%; $p < 0.05$) and in the granular layer of the dentate gyrus (aCSF 27 ± 6% and SAP 62 ± 6.7%; $p < 0.05$) (Figure 24 B). On the contrary, a decrease of M_2/M_4 mAChR activity was recorded in the lateral nucleus of the amygdaloid complex (aCSF 41 ± 9.3% and SAP 36 ± 7.2%; $p < 0.05$) (Table 2).

Table 2. [^{35}S]GTPγS basal and carbachol-induced (100 μM) binding expressed as percentage of stimulation over the basal binding in the different amygdaloid nuclei and hippocampus from vehicle (aCSF) and 192IgG-saporin-treated rats (SAP).

	Basal binding (nCi/g t.e.)		**Carbachol stimulation (% over basal)**	
Brain region	aCSF	SAP	**aCSF**	**SAP**
Telencephalon				
Amygdaloid nuclei				
Anterior	421 ± 33	402 ± 29	**59 ± 9.1**	**47 ± 13.6**
Basolateral	487 ± 47	390 ± 44	**43 ± 6.6**	**48 ± 10.9**
Central	710 ± 91	525 ± 55	**27 ± 9.2**	**52 ± 7.8**
Lateral	483 ± 50	425 ± 43	**41 ± 9.3**	**36 ± 7.2***
Medial	720 ± 94	621 ± 69	**39 ± 8.5**	**34 ± 4.7**
Hippocampus				
CA1				
Oriens	320 ± 40	269 ± 32	**26 ± 9.4**	**40 ± 10.4**
Pyramidal	527 ± 64	457 ± 50	**40 ± 11.5**	**30 ± 6.2**
Radiatum	363 ± 33	323 ± 36	**45 ± 11.5**	**42 ± 9.0**
CA3				
Oriens	317 ± 26	303 ± 38	**26 ± 8.0**	**48 ± 6.6**
Pyramidal	477 ± 36	453 ± 42	**11 ± 5.6**	**32 ± 4.2***
Radiatum	328 ± 21	281 ± 32	**28 ± 9.5**	**40 ± 13.0**
Dentate gyrus				
Granular	467 ± 29	452 ± 50	**27 ± 6.0**	**62 ± 6.7***
Molecular	315 ± 49	278 ± 45	**34 ± 14.7**	**34 ± 9.5**
Polimorphic	314 ± 58	263 ± 39	**11 ± 18.2**	**25 ± 11.8**
Ventral subiculum	345 ± 29	294 ± 18	**37 ± 4.8**	**47 ± 6.7**

Data are mean ± S.E. M values from aCSF and SAP treated rats.
*$p < 0.05$, when compared to aCSF group.

Table 3. [^{35}S]GTPγS basal and carbachol-induced (100 μM) binding expressed as percentage of stimulation over the basal binding in several brain regions from vehicle (aCSF) and 192IgG-saporin-treated rats (SAP).

	Basal binding (nCi/g t.e.)		**Carbachol stimulation (% over basal)**	
Brain region	aCSF	SAP	**aCSF**	**SAP**
Cerebral cortex				
Cingulate	304 ± 26	306 ± 20	**52 ± 12.1**	**48 ± 6.7**
Ectorhinal	352 ± 34	290 ± 29	**66 ± 12.5**	**58 ± 8.0**
Entorhinal	342 ± 35	335 ± 36	**76 ± 10.5**	**93 ± 11.6**
Perirhinal	338 ± 49	309 ± 29	**35 ± 5.8**	**43 ± 3.5**
Piriform	292 ± 27	319 ± 29	**54 ± 15.2**	**33 ± 7.1**
Somatosensory	355 ± 28	333 ± 20	**31 ± 7.0**	**54 ± 10.6**
Motor	311 ± 33	319 ± 20	**21 ± 9.6**	**51 ± 8.2**
Basal ganglia				
Globus pallidus	335 ± 43	347 ± 36	**46 ± 13.2**	**49 ± 12.5**
Striatum	339 ± 26	345 ± 21	**74 ± 15.4**	**62 ± 11.1**
Diencephalon				
NBM	535 ± 49	398 ± 31	**45 ± 9.7**	**15 ± 6.6***
HDB	310 ± 25	327 ± 31	**121 ± 20.7**	**115 ± 17.6**
VDB	330 ± 25	399 ± 42	**135 ± 24.1**	**113 ± 23.2**
Medial septum	267 ± 24	284 ± 32	**152 ± 24.4**	**139 ± 23.7**
Rhinencephalon				
Lat olfactory tract	379 ± 45	324 ± 37	**82 ± 13.1**	**47 ± 11.5**
Rhomboencephalon				
Dorsal raphe	703 ± 103	590 ± 74	**19 ± 4.9**	**24 ± 4.7**
Locus coeruleus	220 ± 36	132 ± 16	**26 ± 11.9**	**78 ± 11.9**
Mesencephalon				
Periaqueductal gray	496 ± 44	469 ± 45	**51 ± 15.0**	**47 ± 8.5**
Substantia nigra	456 ± 52	399 ± 38	**31 ± 10.5**	**37 ± 5.4**

NBM: nucleus basalis magnocellularis, HDB: horizontal limb of the diagonal band, VDB: vertical limb of the diagonal band.
Data are mean ± S.E. M values from aCSF and SAP treated rats.
*$p < 0.05$, when compared to aCSF group.

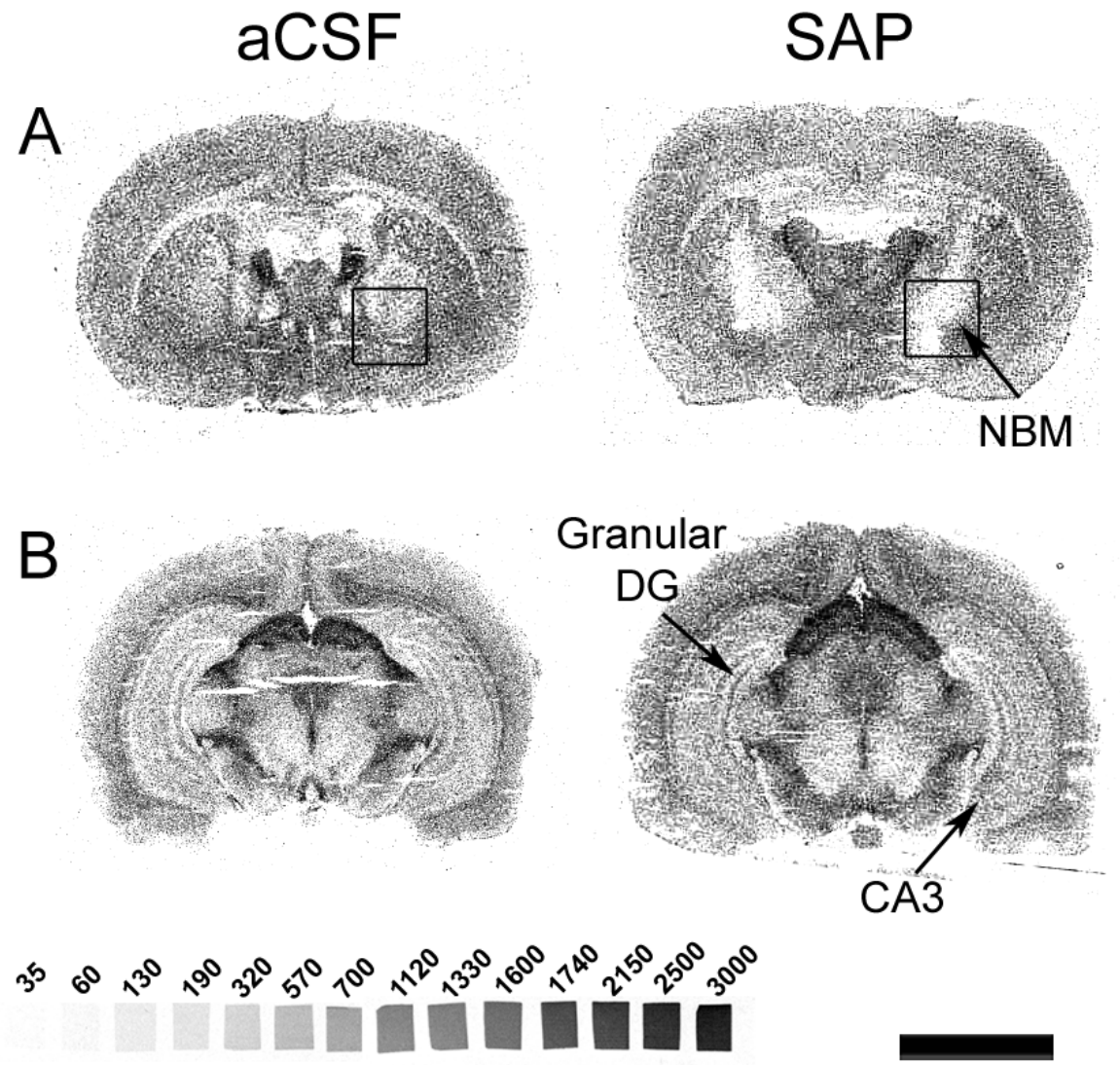

Figure 24. [^{35}S]GTPγS carbachol-evoked (100 µM) stimulation in representative brain coronal slices including the NBM (A) and the ventral hippocampus (B), obtained from aCSF and 192IgG-saporin-treated rats. NBM: nucleus basalis magnocellularis; Granular DG: granular dentate gyrus; CA3: CA3 region of hippocampus. [^{14}C]-microscales used as standards, values in nCi/g t.e. Scale bar: 5 mm.

2.5. Microscopic distribution of M_2 and M_4 mAChR

To examine the subcellular localization of M_2 and M_4 mAChR, immunofluorescence studies were performed in the basal forebrain cholinergic system, hippocampal dentate gyrus and CA3 and somatosensory cortex by using two different antibodies against i3 intercellular loop of human M_2 and M_4 mAChR. Taken together the distribution patterns obtained for M_2 and M_4 mAChR were similar to that observed for the M_2/M_4 mAChR activity. The highest level of M_2 mAChR expression was observed in the striatum, in the basal forebrain and in the pyramidal layers of different hippocampal subfields, and more moderate in the cortex (Figure 25). M_2 mAChR displayed a somatodendritic immunostaining in the NBM with the presence of a dense network of fibers surrounding the somas of ChAT positive cells, probably revealing presynaptic M_2 mAChR contacts (Figure 25 A-I-IV). ChAT enzyme is preferentially distributed in the somatodendritic compartment of BFCN which encloses the total area of these neurons. In the figure 25B, the surviving ChAT positive BFCN from 192IgG-saporin infused rats show somatic and nucleus shrinkage, together with reduced dendritic arborisation and almost a total absence of M_2 mAChR-immunoreactivity in the basal forebrain (Figure 25 B). On the other hand, M_4 mAChR immunoreactivity was distributed mainly in somatodendritic compartments in NBM which reveal a typically postsynaptic localization (Figure 26 A). 192IgG-saporin-treated rats showed a dramatic decrease in M_4 mAChR-immunoreactivity in the basal forebrain as a consequence of the loss of BFCN, as revealed by ChAT immunostaining (Figure 26 B).

In the hippocampal formation, M_2 mAChR-immunoreactivity was distributed throughout the large pyramidal neurons from CA1, CA3 and dentate gyrus as a dense network of fibers delineating the perikarya in basket-like formations, without immunoreactivity in the soma (Figure 27 A). In the somatosensory cortex, M_2 mAChR displayed a scattered distribution in presumably presynaptic compartments (Figure 27 C). The somatodendritic distribution of M_4 mAChR was also observed in the perikarya of hippocampal ChAT positive neurons (Figure 27 B) as well as in the cortex, where M_4 mAChR is distributed in a similar pattern to that observed in CA3 (Figure 27 D).

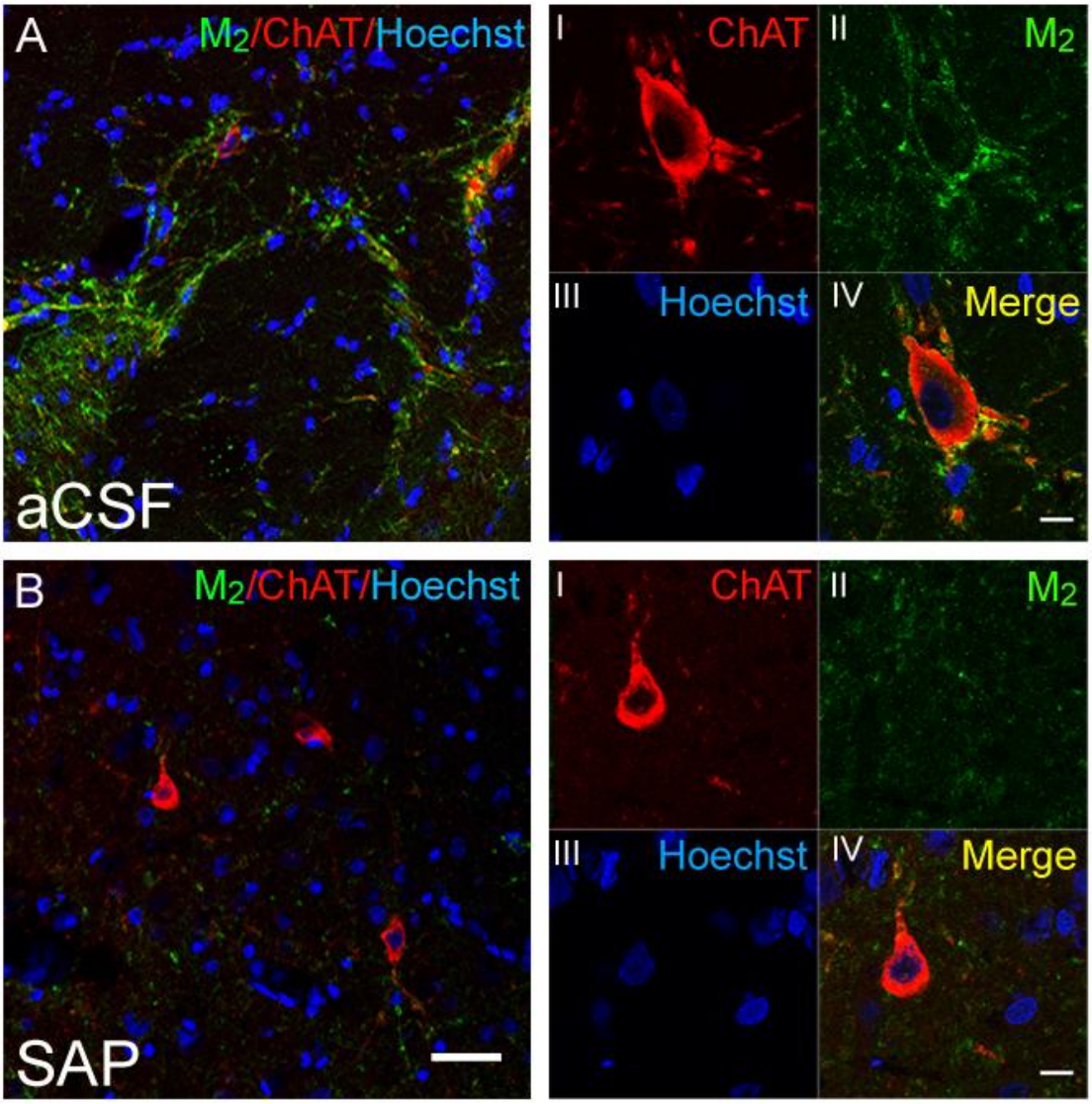

Figure 25. Confocal microscope images which show double immunofluorescence labeling in slices containing the NBM from representative aCSF (A) and 192IgG-saporin-treated (B) rats. ChAT (red) and M_2 mAChR (green) can be observed at 200-fold magnification (A, B). 192IgG-saporin induced a reduction in BFCN density and in M_2 mAChR immunoreactivity. Scale bar = 40 µm. High magnification images reveal a particular M_2 mAChR-immunostaining pattern surrounding the perikarya (A-II) of the large BFCN (A-I), which show a M_2 mAChR presumable presynaptic localization and a distribution in contact with plasmatic membrane, but with a modest degree of co-localization (A-IV). Interestingly, 192IgG-saporin-treated rats showed the presence of few shrunken ChAT-ir BFCN (B-I), whereas the loss of M_2 mAChR immunoreactivity is evident (B-II). Scale bar = 10 µm.

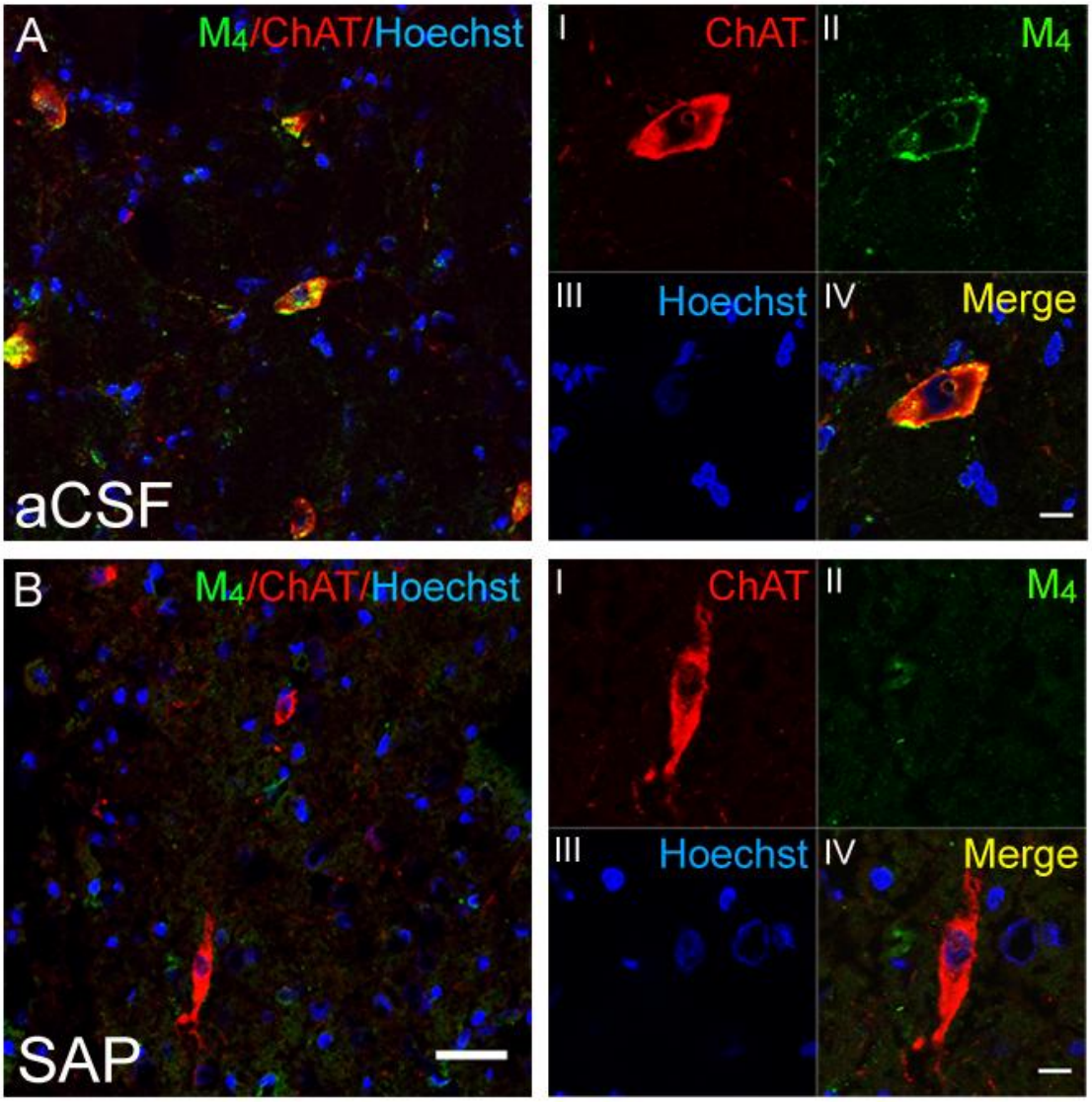

Figure 26. Double labeling in slices containing NBM from a representative aCSF (A) and 192IgG-saporin-treated rat (B). The immunofluorescence for ChAT (red) and M_4 mAChR (green) can be observed at the 200-fold magnification images obtained in a confocal microscope. 192IgG-saporin induced a reduction in BFCN density and in M_4 mAChR-immunoreactivity. Scale bar = 40 µm. High magnification images reveal a somatodendritic M_4 mAChR-immunostaining pattern surrounding the perikarya (A-II) of the large BFCN (A-I) with a high degree of co-localization. In 192IgG-saporin-treated rats there was a reduction of M_4 mAChR-immunoreactivity (B-II) but ChAT labeling still remained in surviving BFCN (B-I). Scale bar = 10 µm.

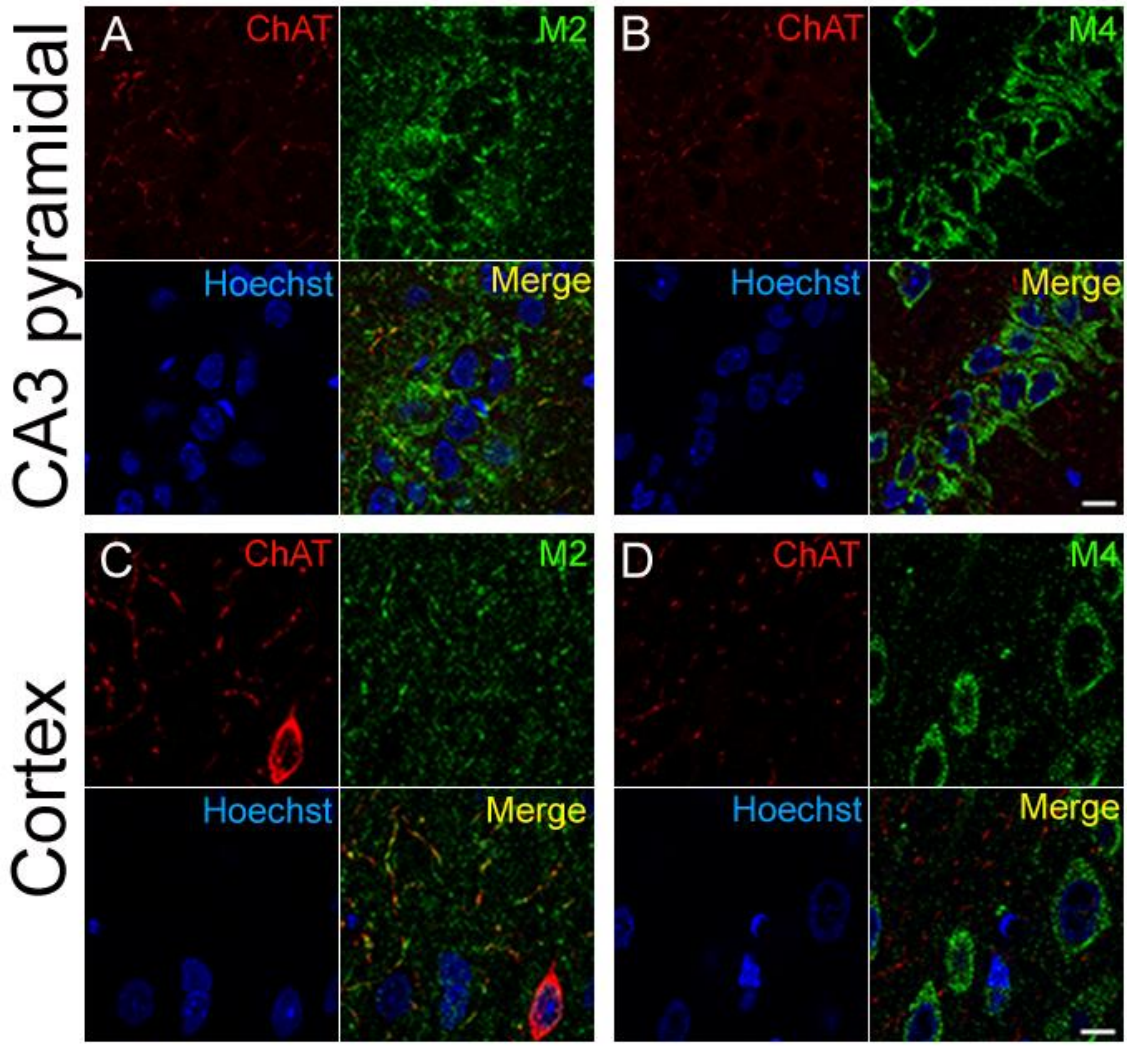

Figure 27. Confocal microscope images which show the double labeling of consecutive slices containing hippocampal CA3 pyramidal region (A and B) and somatosensory cortex (C and D) from a representative aCSF-treated rat, stained for ChAT (red), M_2 mAChR (A and C in green) and M_4 mAChR (B and D in green) at 630-fold magnification. The images show a presumable presynaptic distribution of M_2 mAChR, delineating the perikarya of the large CA3 pyramidal neurons in basket-like formations (A) and the somatodendritic distribution of M_4 mAChR in the perikarya of the same neurons (B). In the cortex, both M_2 (C) and M_4 (D) mAChR display a similar distribution pattern to that observed in CA3. Scale bar = 10 µm.

2.6. The specific loss of BFCN in the NBM leads to changes in lipid composition

The matrix-assisted laser desorption ionization-imaging mass spectrometry (MALDI-IMS) technique allows to anatomically localize lipid species in tissue slices. Furthermore, MALDI-IMS is a semiquantitative technique. In the present study we analyzed the complex lipid composition in both positive and negative ion detection modes of coronal slices from both aCSF and 192IgG-saporin-treated rat brains, including the NBM and cortical projections.

Firstly, MALDI-IMS was performed in positive ion detection mode and more than 300 peaks were obtained but the analyses were focused on those lipid species which may serve as precursors for the synthesis of choline in both the NBM and cortical innervation areas.

The relative intensities of different phosphatidylcholine (PC) species were found to be modified in the NBM and cortex of 192IgG-saporin-treated rats. Thus, increased levels of PC (36:1) + Na^+ (aCSF 14.62 ± 0,30% *vs* SAP 21.64 ± 1.53%, $p < 0.01$), PC (36:4) + K^+ (aCSF 10.32 ± 1.01% *vs* SAP 18.61 ± 2.71%, $p < 0.05$) and PC (40:6) + Na^+ (aCSF 0.88 ± 0.17% *vs* SAP 2.25 ± 0.40**%**, $p < 0.01$) were observed in the NBM of 192IgG-saporin-treated rats. However, in the cortex of 192IgG-saporin-treated rats, there was found a decrease in the level of PC (36:1) + Na^+ (aCSF 10.62 ± 0.48% *vs* SAP 8.95 ± 0.63%, $p < 0.05$) and increased levels of two species, the PC (36:4) + K^+ (aCSF 13.17 ± 0.99% *vs* SAP 15.63 ± 0.48%, $p < 0.05$) and PC (40:6) + Na^+ (aCSF 0,75 ± 0.11% *vs* SAP 1.14 ± 0.09**%**, $p < 0.05$). Furthermore, the levels of other clases of lipids were also found modified in the NBM of the injured rats, such as PE (14:1/20:4) + H^+ (aCSF 15.21 ± 0.70% *vs* SAP 11.87 ± 1.35%, $p < 0.05$), PE (40:4) (aCSF 0.82 ± 0.13 *vs* SAP 1.35 ± 0.17; $p < 0.05$) SM (d18:1/18:0) + H^+ (aCSF 7,11 ± 1,13% vs SAP 4,15 ± 0,80%, $p < 0.05$), SM (d18:1/16:0) + K^+ (aCSF 0.96 ± 0.14% *vs* SAP 10.53 ± 3.33%, $p < 0.01$) (Table 4 and Figure 28 A-B).

In negative ion detection mode, additional lipid species were found modified in the NBM including SM (d18:0/18:1) (aCSF 1.26 ± 0.24% *vs* SAP 6.44 ± 1.50%, $p < 0.01$) and PS (18:0/18:1) (aCSF 11.04 ± 2.16% *vs* SAP 3.95 ± 0.99%, $p < 0.01$). The intensity of PG (22:6/22:6) was also increased in 192IgG-saporin-treated rats (aCSF 0.06 ± 0.01% *vs* SAP 0.86 ± 0.24%; $p < 0.05$ and aCSF 0.04 ± 0.01% *vs* SAP 0.16 ± 0.05%; $p < 0.05$, in NBM and cortex, respectively) (Table 4 and Figure 28 A-B).

Table 4. Relative intensity of representative lipid species in the NBM and cortex from vehicle (aCSF) and 192IgG-saporin (SAP) treated rats, in both positive and negative ion mode.

			% Intensity[1]			
			NBM		Cortex	
Assignment	**Cal m/z**	**Exp m/z**	aCSF	**SAP**	aCSF	**SAP**
Positive ion mode						
PE (14:1/20:4)+H^+	710.4755	710.4893	15.21 ± 0.70	**11.87 ± 1.38***	9.97 ± 0.62	**10.67 ± 0.67**
SM (d18:1/18:0)+H^+	731.6061	731.6070	7.11 ± 1.13	**4.15 ± 0.80***	4.19 ± 0.44	**3.50 ± 0.53**
SM (d18:1/16:0)+K^+	741.5313	741.5311	0.96 ± 0.14	**10.63 ± 3.33****	0.55 ± 0.13	**0.78 ± 0.11**
PC (32:0)+Na^+/PC (34:3)+H^+	756.5514	756.5520	15.75 ± 1.23	**21.94 ± 2.46***	16.94 ± 1.02	**17.41 ± 1.31**
PC (34:2)+Na^+/PC (36:5)+H^+	780.5514	780.5521	0.85 ± 0.09	**2.02 ± 0.27****	1.10 ± 0.08	**1.07 ± 0.08**
PC (34:1)+Na^+/PC (36:4)+H^+	782.5670	782.5673	32.75 ± 1.65	**46.10 ± 3.86****	32.31 ± 1.64	**30.9 ± 1.29**
PC (34:2)+K^+	796.5253	796.5255	3.27 ± 0.17	**5.19 ± 0.30*****	4.20 ± 0.15	**4.16 ± 0.07**
PC (34:1)+K^+	798.5410	798.5405	100 ± 0	**100 ± 0**	100 ± 0	**100 ± 0**
PC (36:4)+Na^+/PC (38:7)+H^+	804.5514	804.5510	2.79 ± 0.31	**7.69 ± 1.52***	3.63 ± 0.31	**4.3 ± 0.24**
PC (36:1)+Na^+/PC (38:4)+H^+	810.5983	810.5984	14.62 ± 0.30	**21.64 ± 1.53****	10.62 ± 0.48	**8.95 ± 0.63***
PC (36:4)+K^+	820.5253	820.5249	10.32 ± 1.01	**18.61 ± 2.71***	13.17 ± 0.99	**15.63 ± 0.48***
PC (38:4)+Na^+/PC (40:7)+H^+	832.5827	832.5826	3.00 ± 0.30	**7.98 ± 1.40****	2.82 ± 0.25	**3.11 ± 0.21**
PC (38:4)+K^+/PC (42:9)+H^+	848.5566	848.5560	10.23 ± 0.93	**18.27 ± 2.15****	9.71 ± 0.80	**10.75 ± 0.38**
PC (40:6)+Na^+	856.5827	856.5820	0.88 ± 0.17	**2.25 ± 0.40****	0.75 ± 0.11	**1.14 ± 0.09***
Negative ion mode						
SM (d18:1/15:0)	687.5447	687.5443	1.26 ± 0.24	**6.44 ± 1.50****	0.94 ± 0.23	**1.52 ± 0.28**
PS (18:0/18:1)	788.5447	788.5447	11.04 ± 2.16	**3.95 ± 0.99****	8.54 ± 1.28	**6.30 ± 0.85**
PE (40:4)/PC (18:0/20:4)	794.5705	794.5705	0.82 ± 0.13	**1.35 ± 0.17***	0.83 ± 0.08	**0.98 ± 0.14**
PG (22:6/22:6)	865.5025	865.5033	0.06 ± 0.01	**0.86 ± 0.24****	0.04 ± 0.01	**0.16 ± 0.05***
PI (20:4/18:0)	885.5494	885.5496	100 ± 0	**100 ± 0**	100 ± 0	**100 ± 0**
ST (d18:1/h22:0)	878.6033	878.6037	23.18 ± 2.77	**13.13 ± 2.59***	16.37 ± 1.62	**14.87 ± 1.97**
ST (d18:1/24:1)	888.6240	888.6244	63.27 ± 5.08	**32.53 ± 7.37****	55.39 ± 6.16	**54.42 ± 4.64**
ST (d18:1/24:0)	890.6397	890.6388	38.39 ± 2.30	**19.92 ± 4.33****	36.40 ± 2.48	**34.75 ± 4.09**
ST (d18:1/h24:1)	904.6189	904.6191	45.35 ± 4.28	**22.93 ± 5.05****	29.09 ± 2.97	**26.15 ± 2.57**
ST (d18:1/h24:0)/(d18:1/h25:1)	906.6346	906.6439	54.16 ± 4.19	**27.50 ± 5.98****	45.20 ± 4.52	**40.12 ± 5.80**

[1] The maximal peak is the most intense peak of the lipid spectrum, in this case PC (34:1) in positive and PI (20:4/18:0) in negative ion modes, which are set at 100%. Data are mean ± S.E.M values from aCSF and 192IgG-saporin-treated rats. *p < 0.05, **p < 0.01 and ***p < 0.001 when compared to aCSF group. PC: phosphatidylcholine; SM: sphingomyelin; PS: phosphatidylserine; PE: phosphatidylethanolamine; PG: phosphoglycerol; ST: sulfatides; Cal: calculated; Exp: experimental.

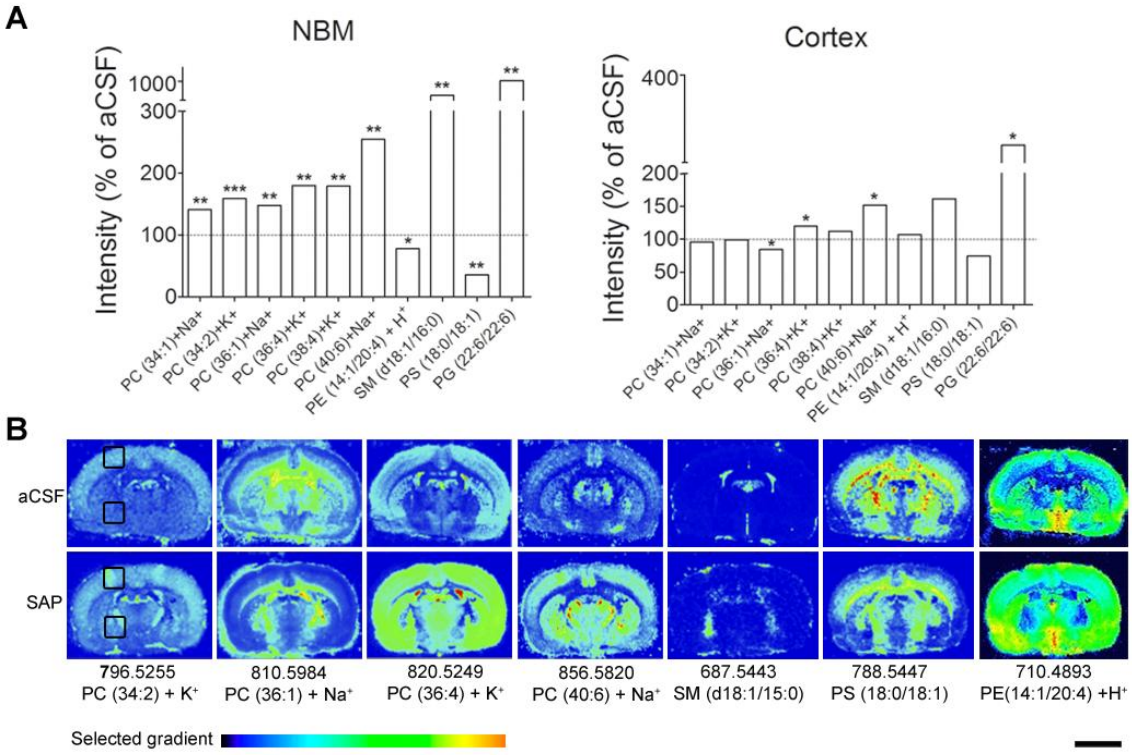

Figure 28. (A) The histograms show the relative abundance of different lipid species in the NBM (left) and cortex (right), expressed as percentages of the values obtained in the aCSF-treated group. (B) Matrix-assisted laser desorption ionization-imaging mass spectrometry (MALDI-IMS) of different lipids in brain slices containing the NBM and cortical projections from representative aCSF and 192IgG-saporin-treated rats. The intensities were measured in the areas marked with black squares of the somatosensory cortex and the NBM. *p < 0.05; **p < 0.01 and ***p < 0.001 *vs* aCSF-treated rats. PC: phosphatidylcholines; PE: phosphatidylethanolamines; PS: phosphatidylserines; SM: sphingomyelin; PG: phosphoglycerol. Scale bar = 5 mm.

(Manuscript III) Increase of cortical endocannabinoid signaling in a rat model of basal forebrain cholinergic dysfunction

HIGHLIGHTS

- **A crosstalk between cholinergic and cortical endocannabinoid signaling is proposed.**
- **The loss of basal forebrain cholinergic input decreases cortical GABAergic tone.**
- **CB_1 receptor-mediated signaling adaptation in response to cholinergic dysfunction.**
- **The activation of the endocannabinoid system may restore cholinergic deficits in Alzheimer's disease.**

GRAPHICAL ABSTRACT

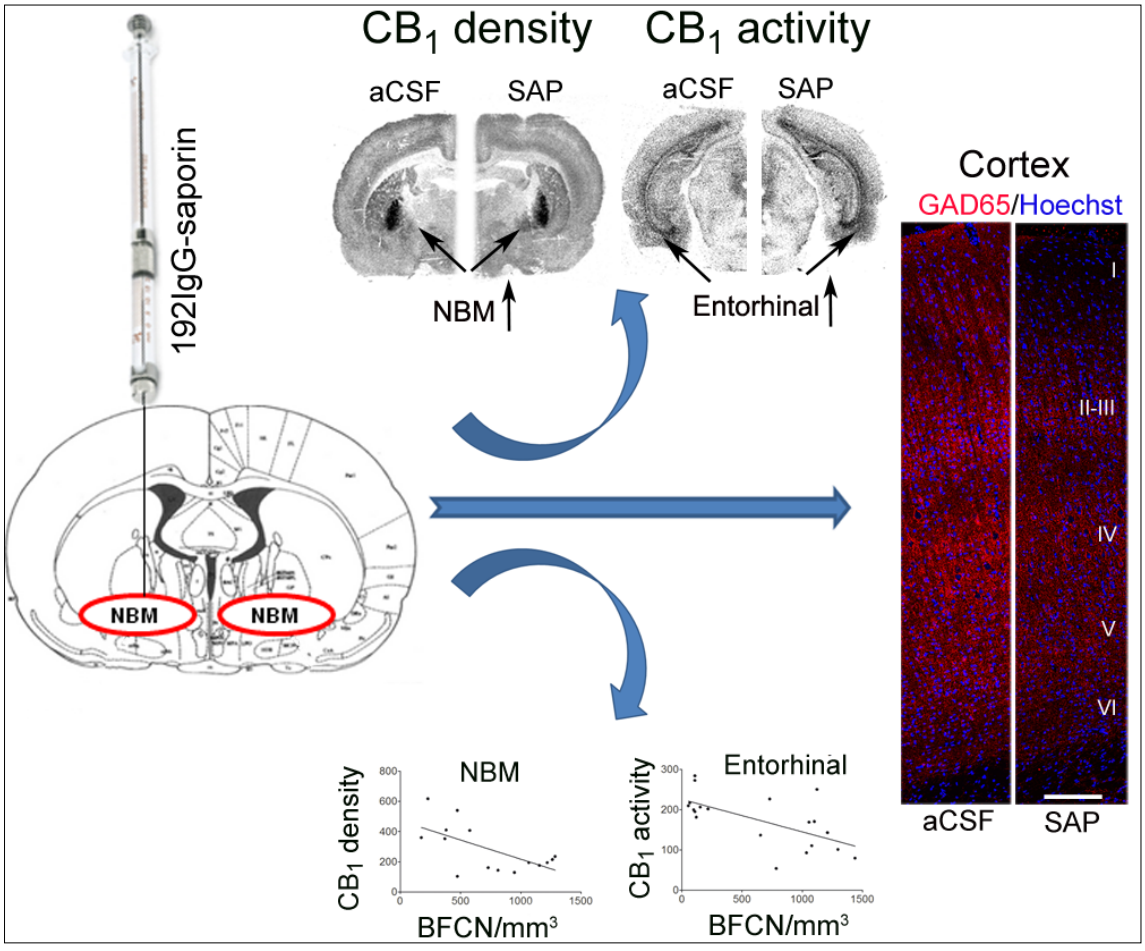

2.7. The specific loss of BFCN in the NBM leads to endocannabinoid signaling adaptation

CB_1 receptor density after basal forebrain cholinergic lesion

The density and activity of CB_1 receptors was analyzed by means of autoradiography. Despite of the massive loss of basal forebrain cholinergic terminals (up to 65%, as measured by AChE staining) arising from the NBM to cortical and subcortical brain areas, the 192IgG-saporin-treated rats showed no changes in [^{3}H]CP55,940 binding in the cortex (Table 5). However, [^{3}H]CP55,940 binding was increased in the NBM (180 ± 13 fmol/mg and 364 ± 63 fmol/mg, in aCSF and 192IgG-saporin-treated rats, respectively, $p < 0.05$). On the contrary, in some hippocampal subregions, we found a down regulation (oriens CA1: aCSF 1057 ± 67 fmol/mg, and SAP 721 ± 92 fmol/mg, $p < 0.05$; molecular dentate gyrus: aCSF 900 ± 63 fmol/mg, and SAP 603 ± 71 fmol/mg, $p < 0.01$) (Figure 29 B, tables 5-6). CP55,940 shows high affinity for both CB_1 and CB_2 receptors. Therefore, using two different cannabinoid antagonists we checked the specificity of the radioligand binding. SR141716A, a CB_1 antagonist, completely blocked the binding of [^{3}H]CP55,940 (Figure 29 C) while SR144528, a CB_2 antagonist, failed to do so (Figure 29 D), providing evidence that the changes in [^{3}H]CP55,940 binding are specifically related to CB_1 receptors. See also the Figure 37 for further details of the specificity of both antagonists.

Table 5. Autoradiographic densities of CB_1 receptors expressed in fmol/mg t.e., obtained as specific binding of [^{3}H]CP55.940 in different gray and white matter regions from vehicle (aCSF) and 192IgG-saporin (SAP) treated rats.

Specific binding of [^{3}H]CP55,940 (fmol/mg t.e.)		
Brain region	**aCSF**	**SAP**
Cerebral cortex		
Cingulate	223 ± 27	202 ± 21
Motor	211 ± 25	197 ± 20
Somatosensory	164 ± 21	149 ± 16
Piriform	87 ± 8	112 ± 13
Perirhinal	131 ± 22	104 ± 16
Ectorhinal	155 ± 15	128 ± 26
Entorhinal	114 ± 26	96 ± 12
Diencephalon		
NBM	180 ± 13	364 ± 63*
Rhinencephalon		
Lat.Olfact. Tract	190 ± 28	137 ± 18
Mesencephalon		
Substantia nigra	3068 ± 218	2633 ± 177
Basal ganglia		
Globus pallidus	2878 ± 264	2756 ± 303
Striatum	456 ± 33	518 ± 75
White matter tracts		
Corpus callosum	35 ± 7	33 ± 12
Fimbria fornix	55 ± 17	24 ± 9
Internal capsule	19 ± 8	30 ± 6
Optic tract	14 ± 9	5 ± 16

Data are mean ± S.E.M values from aCSF and SAP-treated rats.
*$p < 0.05$ when compared to aCSF.

Table 6. Autoradiographic densities of CB_1 receptors expressed in fmol/mg t.e., obtained as specific binding of [^{3}H]CP55.940 in different hippocampal regions and amygdaloid nuclei from vehicle (aCSF) and 192IgG-saporin (SAP) treated rats.

Specific binding of [^{3}H]CP55,940 (fmol/mg t.e.)		
Brain region	**aCSF**	**SAP**
Telencephalon		
Amygdaloid nuclei		
Anterior	126 ± 13	127 ± 6
Basolateral	102 ± 15	96 ± 19
Central	146 ± 18	138 ± 10
Lateral	109 ± 15	98 ± 23
Medial	62 ± 16	55 ± 14
Hippocampal formation		
CA1		
Oriens	1057 ± 67	721 ± 92*
Pyramidal	583 ± 56	340 ± 44
Radiatum	520 ± 26	384 ± 52
CA3		
Oriens	800 ± 64	550 ± 94
Pyramidal	408 ± 40	300 ± 56
Radiatum	537 ± 44	376 ± 67
Dentate gyrus		
Molecular	900 ± 63	603 ± 71**
Polimorphic	454 ± 49	305 ± 48
Granular	72 ± 18	96 ± 20
Lac. Moleculare	605 ± 42	436 ± 79
Ventral subiculum	300 ± 37	248 ± 26

Data are mean ± S.E.M values from aCSF and SAP-treated rats.
*$p < 0.05$, **$p < 0.01$ when compared to aCSF.

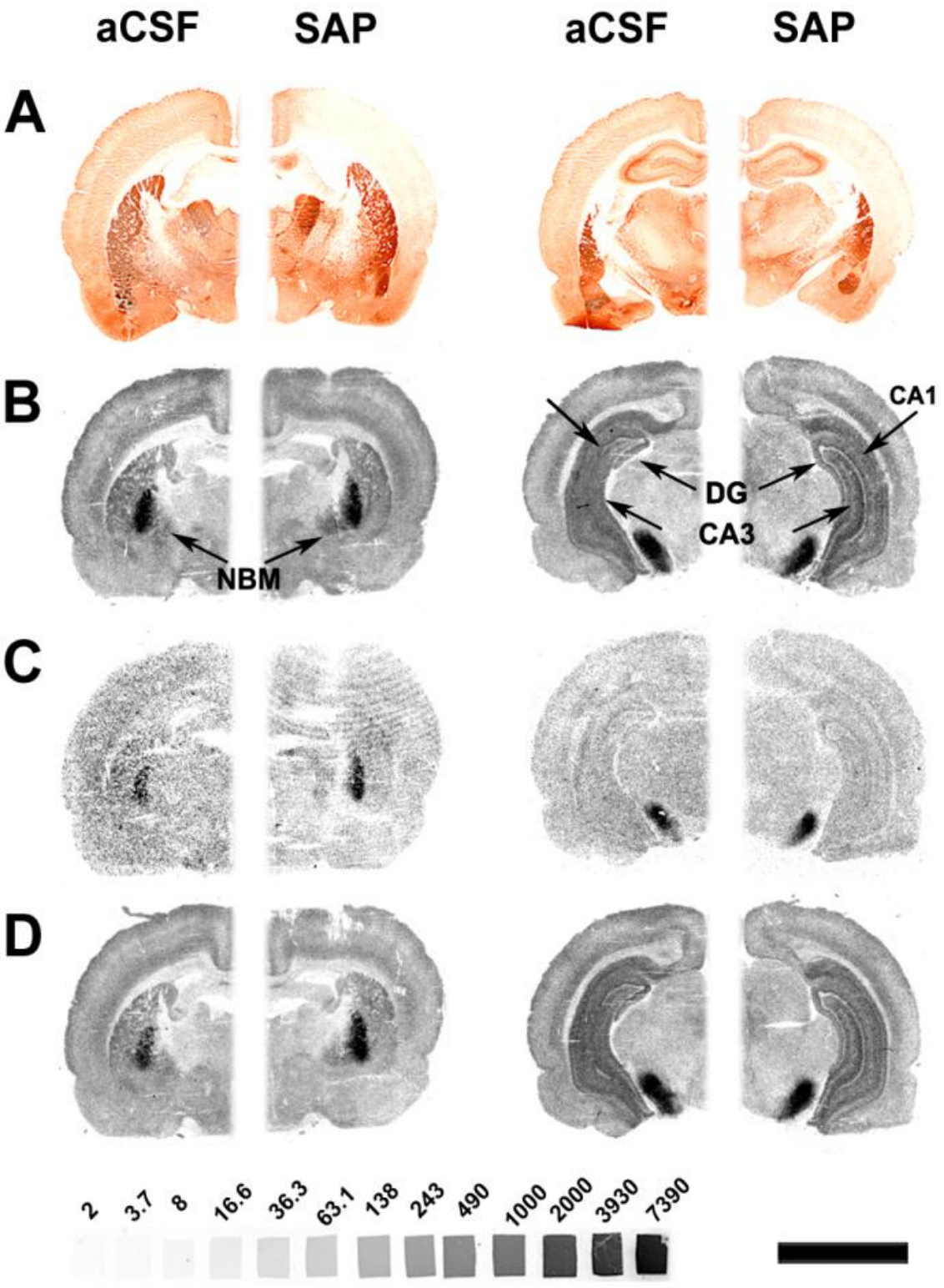

Figure 29. (A) AChE staining in representative fixed hemibrain slices at two different levels (right and left columns) from aCSF and 192IgG-saporin-treated rats. (B) [^{3}H]CP55,940 (3 nM) binding in hemibrain coronal slices from aCSF and 192IgG-saporin-treated rats. (C) The specificity of the binding was determined blocking the radioligand binding in the presence of the specific CB_1 receptor antagonist, SR141716A (0.1 µM) (D) The specific CB_2 antagonist SR144528 (0.1 µM) was not able to inhibit the [^{3}H]CP55,940 (3 nM) binding to rat brain slices (D) . DG: dentate gyrus; CA3: layer CA3 of hippocampus. Bottom, [^{3}H] standards (µCi/g tissue equivalent), tissue scale bar: 5 mm.

Endocannabinoid signaling deregulation in areas of cholinergic innervation

To study whether the changes in receptor density are reflected by CB_1 receptor activity mediated by $G_{i/o}$ protein signaling, we used the functional autoradiography technique analyzing the binding of [^{35}S]GTPγS. Basal binding values were similar in the both groups, aCSF and SAP, in all of the brain areas analyzed (Tables 7-9, Figures 30 A and C). The anatomical analysis of [^{35}S]GTPγS binding induced by the CB_1/CB_2 receptor agonist, WIN55,212-2 (10 µM), revealed changes in the functional coupling of cannabinoid receptors to $G_{i/o}$ proteins. Despite of the absence of changes in cortical CB_1 receptor density, agonist-induced stimulation of [^{35}S]GTPγS binding was enhanced in several cortical regions (entorhinal: aCSF 156 ± 17% vs SAP 277 ± 30%, $p < 0.01$; motor: aCSF 127 ± 20% vs SAP 203 ± 14%, $p < 0.05$; piriform: aCSF 72 ± 10% vs SAP 122 ± 9%, $p < 0.001$; somatosensory: aCSF 131 ± 29% vs SAP 218 ± 11%, $p < 0.05$), and was more evident in the internal layers, such as the layer VI of the entorhinal cortex (Table 7, Figures 30 B and D), which indicates a hyperactivity of cortical eCB signaling.

Also, in the striatum (aCSF 178 ± 28% vs SAP 252 ± 19%, $p < 0.05$) and in the NBM (aCSF 103 ± 18% vs SAP 142 ± 9%, $p<0.05$) there was an increase in WIN55,212-2-induced functional coupling of CB_1 receptors to $G_{i/o}$ proteins (Figure 31 B, tables 8-9). However, in the hippocampus and, in accordance with the results related to CB_1 receptor density, we found a decrease of the activity in the molecular layer of dentate gyrus (aCSF 299 ± 37% vs SAP 166 ± 25%, $p < 0.05$) (Figure 30 B, table 8). SR141716A almost completely blocked WIN55,212-2-evoked binding of [^{35}S]GTPγS, which indicates that the changes in eCB signaling were specifically through CB_1 receptors (Figure 31 C).

Table 7. [^{35}S]GTPγS basal binding and WIN55,212-2-induced (10 μM) binding expressed as percentage of stimulation over the basal binding in different cortical regions from vehicle (aCSF) and 192IgG-saporin (SAP) treated rats.

	Basal binding (nCi/g t.e.)		**WIN55.212-2 stimulation (% over basal)**	
Brain region	aCSF	SAP	**aCSF**	**SAP**
Cerebral cortex				
Cingulate				
I-III	351 ± 15	331 ± 20	**97 ± 22**	**120 ± 17**
IV-V	395 ± 22	399 ± 22	**104 ± 25**	**116 ± 19**
VI	548 ± 29	578 ± 37	**187 ± 30**	**176 ± 19**
Ectorhinal				
I-III	306 ± 16	316 ± 17	**122 ± 31**	**113 ± 14**
IV-V	352 ± 22	374 ± 22	**108 ± 25**	**157 ± 15**
VI	386 ± 29	455 ± 22	**209 ± 36**	**195 ± 19**
Entorhinal				
I-III	300 ± 25	337 ± 19	**174 ± 28**	**169 ± 20**
IV-V	394 ± 26	470 ± 32	**162 ± 24**	**164 ± 14**
VI	515 ± 35	531 ± 40	**156 ± 17**	**277 ± 30****
Motor				
I-III	399 ± 24	386 ± 33	**71 ± 14**	**122 ± 13***
IV-V	407 ± 17	420 ± 23	**110 ± 25**	**119 ± 7**
VI	535 ± 33	521 ± 27	**127 ± 20**	**203 ± 14***
Perirhinal				
I-III	276 ± 23	289 ± 16	**119 ± 23**	**189 ± 17**
IV-V	352 ± 21	357 ± 21	**155 ± 36**	**167 ± 25**
VI	388 ± 21	444 ± 25	**151 ± 24**	**218 ± 12***
Somatosensory				
I-III	380 ± 23	414 ± 34	**74 ± 20**	**68 ± 11**
IV-V	436 ± 30	460 ± 30	**118 ± 23**	**128 ± 7**
VI	495 ± 37	512 ± 34	**131 ± 29**	**218 ± 11***
Piriform	458 ± 29	457 ± 30	**72 ± 10**	**122 ± 9****

Data are mean ± S.E.M values from aCSF-treated and SAP-treated rats. *$p < 0.05$, **$p < 0.01$ when compared to aCSF.

Table 8. [^{35}S]GTPγS basal binding and WIN55,212-induced (10 μM) binding expressed as percentage of stimulation over the basal binding in different amygdaloid nuclei, hippocampal regions and basal ganglia from vehicle (aCSF) and 192IgG-saporin (SAP) treated rats.

	Basal binding (nCi/g t.e.)		**WIN55.212-2 stimulation (% over basal)**	
Brain region	aCSF	SAP	**aCSF**	**SAP**
Telencephalon				
Amygdaloid nuclei				
Anterior	416 ± 50	460 ± 30	**110 ± 18**	**99 ± 12**
Basolateral	395 ± 28	457 ± 36	**223 ± 24**	**150 ± 8**
Central	586 ± 52	649 ± 53	**100 ± 19**	**92 ± 4**
Lateral	359 ± 36	442 ± 30	**157 ± 24**	**150 ± 12**
Medial	512 ± 61	636 ± 69	**116 ± 20**	**50 ± 6***
Hippocampus				
CA1				
Oriens	308 ± 27	332 ± 26	**106 ± 19**	**99 ± 17**
Pyramidal	266 ± 29	264 ± 20	**155 ± 14**	**159 ± 22**
Radiatum	384 ± 36	418 ± 28	**150 ± 28**	**178 ± 30**
CA3				
Oriens	372 ± 45	377 ± 19	**223 ± 28**	**110 ± 20**
Pyramidal	272 ± 34	241 ± 23	**198 ± 52**	**233 ± 53**
Radiatum	254 ± 25	269 ± 21	**219 ± 38**	**181 ± 28**
Dentate gyrus				
Molecular	324 ± 42	387 ± 20	**299 ± 37**	**166 ± 25***
Polimorphic	194 ± 38	200 ± 20	**168 ± 29**	**211 ± 39**
Granular	216 ± 32	204 ± 20	**122 ± 30**	**116 ± 21**
Ventr. subiculum	264 ± 26	304 ± 14	**116 ± 13**	**161 ± 23**
Basal ganglia				
Globus pallidus	442 ± 31	456 ± 39	**986 ± 131**	**874 ± 126**
Striatum	368 ± 25	352 ± 16	**178 ± 28**	**252 ± 19***

Data are mean ± S.E.M values from aCSF-treated and SAP-treated rats. *$p < 0.05$ when compared to aCSF.

Table 9. [^{35}S]GTPγS basal binding and WIN55,212-induced (10 μM) binding expressed as percentage of stimulation over the basal binding in different gray and white matter regions from vehicle (aCSF) and 192IgG-saporin (SAP) treated rats.

	Basal binding (nCi/g t.e.)		**WIN55.212-2 stimulation (% over basal)**	
Brain region	aCSF	SAP	**aCSF**	**SAP**
Diencephalon				
NBM	496 ± 57	547 ± 34	**103 ± 18**	**142 ± 9***
Horiz. diagonal band	327 ± 36	320 ± 20	**91 ± 18**	**114 ± 21**
Vertic. diagonal band	341 ± 27	393 ± 24	**145 ± 27**	**119 ± 15**
Medial septum	309 ± 27	320 ± 21	**111 ± 23**	**114 ± 18**
Rhinencephalon				
Lat.Olfact. Tract nucleus	359 ± 40	364 ± 38	**55 ± 10**	**128 ± 13***
Rhomboencephalon				
Dorsal raphe	636 ± 72	665 ± 62	**59 ± 8**	**82 ± 6**
Locus coeruleus	254 ± 21	263 ± 40	**32 ± 7**	**44 ± 15**
Mesencephalon				
Periaqueductal gray	484 ± 44	503 ± 31	**69 ± 12**	**94 ± 11**
Substantia nigra	382 ± 31	463 ± 21	**835 ± 145**	**744 ± 97**
White matter tracts				
Corpus callosum	632 ± 64	691 ± 61	**86 ± 21**	**75 ± 9**
Cerebellum	169 ± 25	217 ± 26	**35 ± 9**	**42 ± 7**
Dorsal Hipp. Commisure	621 ± 70	733 ± 86	**52 ± 5**	**50 ± 6**
Fimbria fornix	450 ± 38	557 ± 41	**139 ± 15**	**63 ± 8****
Forceps major	550 ± 60	583 ± 55	**87 ± 11**	**93 ± 11**
Internal capsule	302 ± 30	278 ± 21	**42 ± 6**	**54 ± 8**
Lateral olfact. Tract	484 ± 49	567 ± 51	**65 ± 14**	**42 ± 9**

Data are mean ± S.E. M values from aCSF-treated and SAP-treated rats. *$p < 0.05$, **$p < 0.01$ when compared to aCSF.

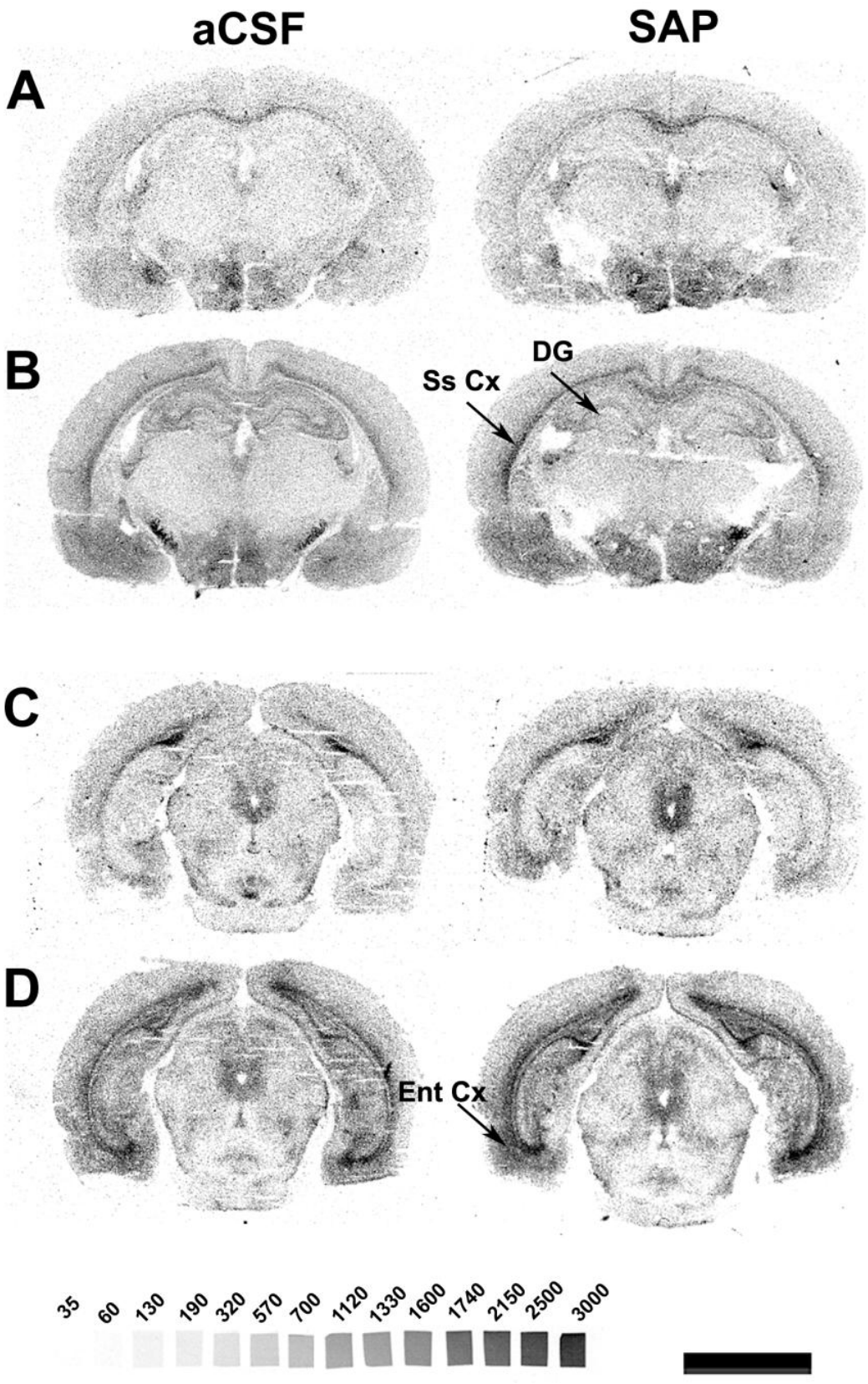

Figure 30. Representative autoradiograms including both dorsal (A, B) and ventral hippocampus (C, D) obtained from aCSF and SAP-treated rats that show [^{35}S]GTPγS basal binding (A and C) and WIN55,212-2 (10 µM) evoked activation of cannabinoid receptors (B and D). DG: dentate gyrus; Ss cx: somatosensory cortex; Ent cx: entorhinal cortex. Bottom, [^{14}C] standards (nCi/g tissue equivalent), tissue scale bar: 5 mm.

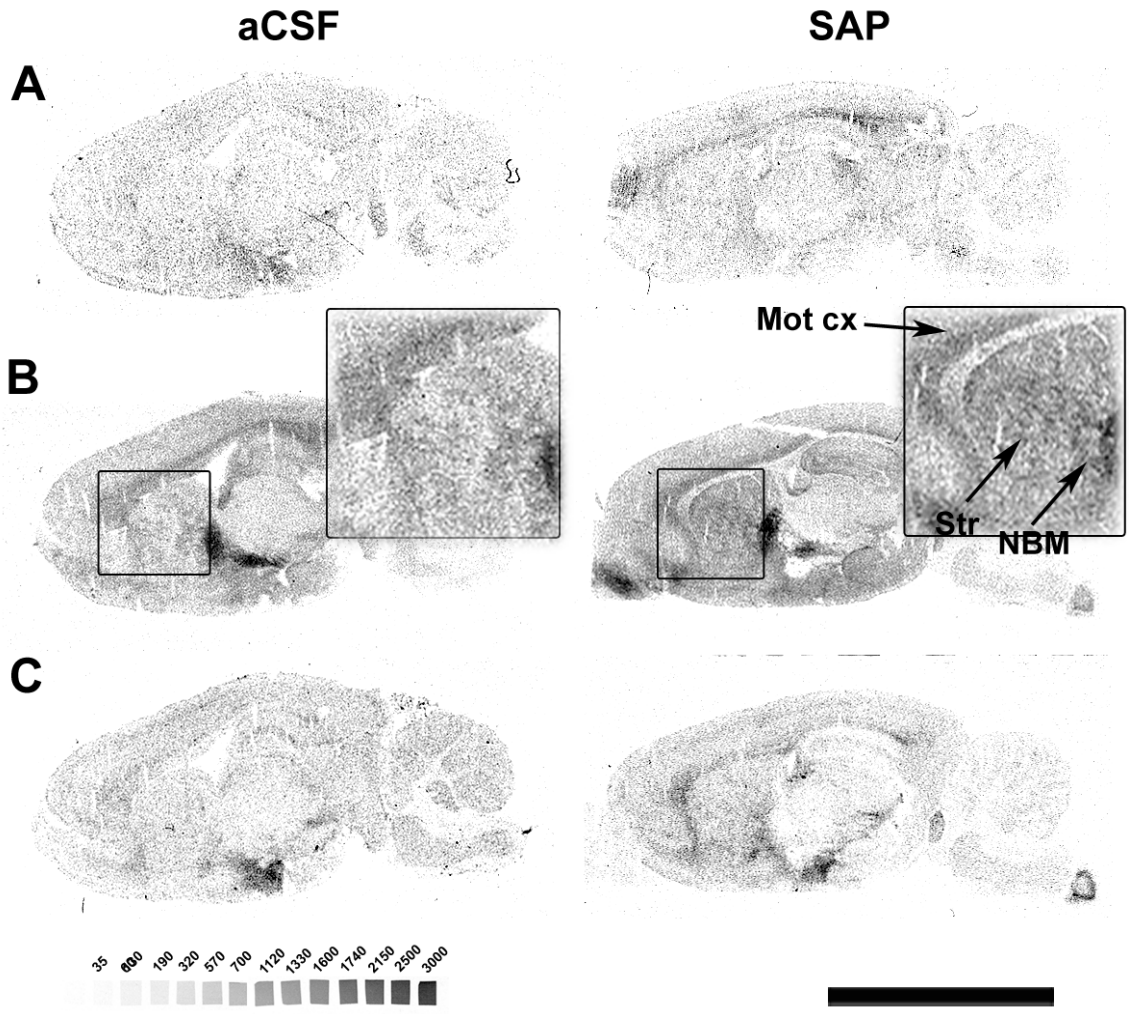

Figure 31. Autoradiographic images showing [^{35}S]GTPγS basal binding in sagittal slices from aCSF and 192IgG-saporin-treated rats (A), stimulated by WIN55,212-2 (10 µM) (B), and WIN55,212-2 (10 µM) stimulation antagonized by SR141716A (1 µM) (C). Mot cx: motor cortex; Str: striatum. Scale bar: 1 cm.

Linear regression analysis between CB_1 receptor changes and the number of surviving BFCN

To examine the relation between the results of the autoradiographic assays and the degree of lesion, firstly we correlated [^{3}H]CP55,940 binding (fmol/mg) with the number of basal forebrain cholinergic neurons in the NBM by using a regression analysis. These analyses showed that 40% in NBM ($p = 0.011$), 29% in the dentate gyrus ($p = 0.047$) and 36% in CA1 ($p = 0.018$) of the variation in the density of CB_1 receptors could be attributable to the loss of BFCN. The lower the BFCN density, the higher the CB_1 density in NBM and the lower in hippocampus, showing a different modulation depending on the brain area studied (Figure 32 A). Then, we correlated the number of BFCN with CB_1 receptor activity, and similar results were obtained. Thus,

the regression models showed that 39% in NBM (p = 0.007), 63% in striatum (p = 0.0002) and 40% in dentate gyrus (p = 0.009) of the variation in the functional coupling of cannabinoid receptors to $G_{i/o}$ proteins might be related to the loss of BFCN (Figure 32 B). When the entire cortical mantle was analyzed we found the lower the number of BFCN, the higher the CB_1 receptor activity. The regression models showed that 28% in motor (p = 0.02), 40% in somatosensory (p = 0.0025), 24% in entorhinal (p = 0.0349) and 43% in piriform cortices (p = 0.002), of the increase in the CB_1 activity could be related to the basal forebrain cholinergic lesion (Figure 32 C).

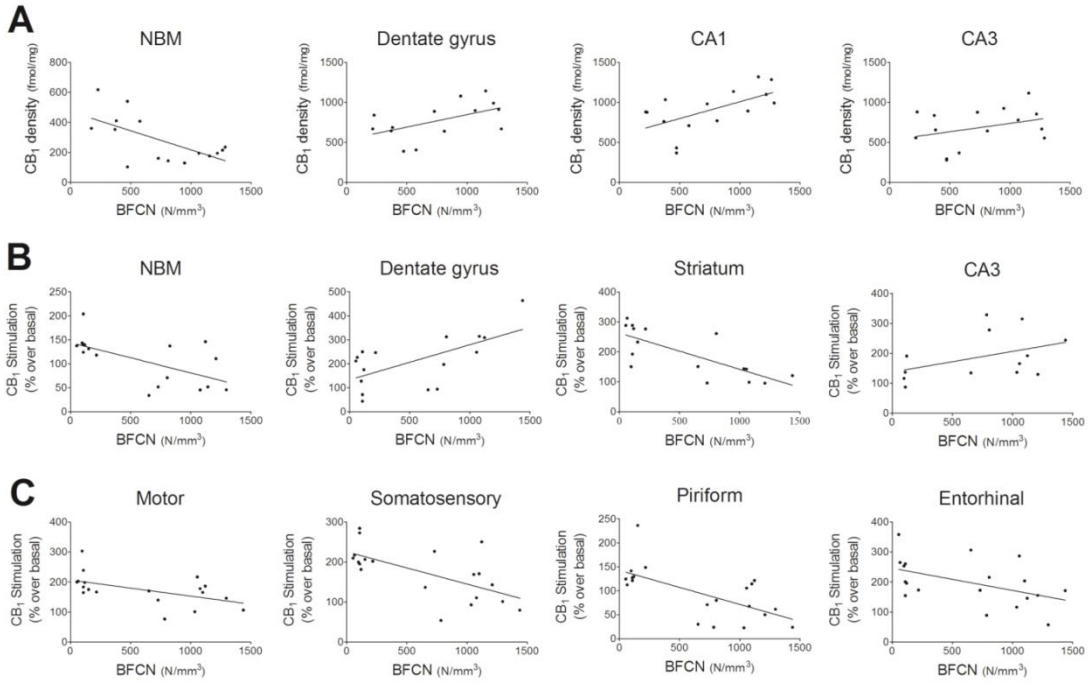

Figure 32. (A) The plots show the number of BFCN in the NBM (number of cells/mm^3) and the density of CB_1 receptors (fmol/mg) from aCSF and 192IgG-saporin-treated rats in different brain areas. The regression analyses reveal a decrease in the density of CB_1 receptor related to the depletion of BFCN in the dentate gyrus (R^2 = 0.29; p = 0.047) and CA1 (R^2 = 0.36; p = 0.018) and an increase in the NBM (R^2 = 0.40; p = 0.011). (B and C) The plots show the number of BFCN in the NBM and WIN55,212-2 (10 µM)-evoked stimulation of CB_1 receptors (% activity over basal) from aCSF and SAP treated rats in different brain areas. (B) The regression analyses reveal a hyperactivity of CB_1 receptors in the NBM (R^2 = 0.38; p = 0.007) and in the striatum (R^2 = 0.63; p = 0.0002), but a decrease in the dentate gyrus (R^2 = 0.4; p = 0.0089) related to the loss of BFCN. (C) The regression analyses reveal a hyperactivity of CB_1 receptors in cortical areas: motor (R^2 = 0.28; p = 0.0202), somatosensory (R^2 = 0.41; p = 0.0025), entorhinal (R^2 = 0.24; p = 0.0349) and piriform (R^2 = 0.43; p = 0.0018) cortices, related to the depletion of BFCN.

2.8. Anatomical distribution of CB_1 receptor

The subcellular localization of CB_1 receptors was determined by immunofluorescence studies using an antiserum against the C-terminus of the human CB_1 receptor. The regional distribution pattern of immunostaining was similar to that observed in the autoradiographic studies. Some areas exhibited very high CB_1 receptor expression, such as the olfactory bulb, globus pallidus, substantia nigra, amygdala and hippocampus. The different hippocampal layers exhibited differential CB_1 receptor-immunostaining patterns and were clearly defined. We studied the co-localization of CB_1 receptors with GAD65, the smaller isoform of the enzyme glutamate decarboxylase, which is mainly associated with nerve terminals (Kash et al., 1999), and with VGLUT3, the third subtype of glutamate vesicular transporter, which is mainly expressed in synaptic boutons, but also in somatodendritic compartments (Herzog et al., 2004). The abundant and dense CB_1 receptor immunoreactive puncta observed suggested a predominant localization of CB_1 receptors in presynaptic terminals with similar densities in both groups of animals. Immunofluorescence assays for GAD65 and VGLUT3 and the subsequent co-localization studies, allowed us to confirm the inhibitory nature of presynaptic boutons, which express CB_1 receptors in the hippocampus (Figure 33 A). Although, GAD65 and VGLUT3 had different patterns of distribution, no differences in the immunostaining pattern were observed between the two groups studied and therefore the immunofluorescence images shown in Figure 33 correspond to rats treated with 192IgG-saporin. Thus, GAD65 immunoreactivity was seen as a dense plexus of immunoreactive puncta around the pyramidal neurons and had a similar distribution to CB_1 receptors (Figure 33 Ai), while VGLUT3 displayed a postsynaptic somatodendritic immunostaining (Figure 33 Aii). The studies of co-localization that were performed in the Z-axis with a 0.24-µm resolution by using structured illumination, revealed an optimal penetration of the antibody in the tissue. The presence of CB_1 receptors in presynaptic GABAergic terminals, with a high degree of co-immunoreactivity with GAD65 was observed (Figure 33 Ai-YZ/XZ). CB_1 receptor immunostaining was found surrounding the VGLUT3-expressing somatodendritic compartment. A Z-stack analysis revealed the almost total absence of co-immunoreactivity with VGLUT3 (Figure 33 Aii-YZ/XZ).

However, in the cortex, CB_1 receptors were not clearly located in either presynaptic GABAergic or postsynaptic glutamatergic compartments (Figure 33 B). GAD65 was distributed presynaptically (Figure 33 Bi), while VGLUT3 displayed a somatodendritic distribution (Figure 33 Bii). The Z-stack analysis revealed a similar distribution of CB_1 receptors and GAD65 but with a very low degree of co-

immunoreactivity (Figure 33 Bi-YZ/XZ). However, a higher co-expression with VGLUT3 was observed, despite the different cellular distribution (Figure 33 Bii-YZ/XZ).

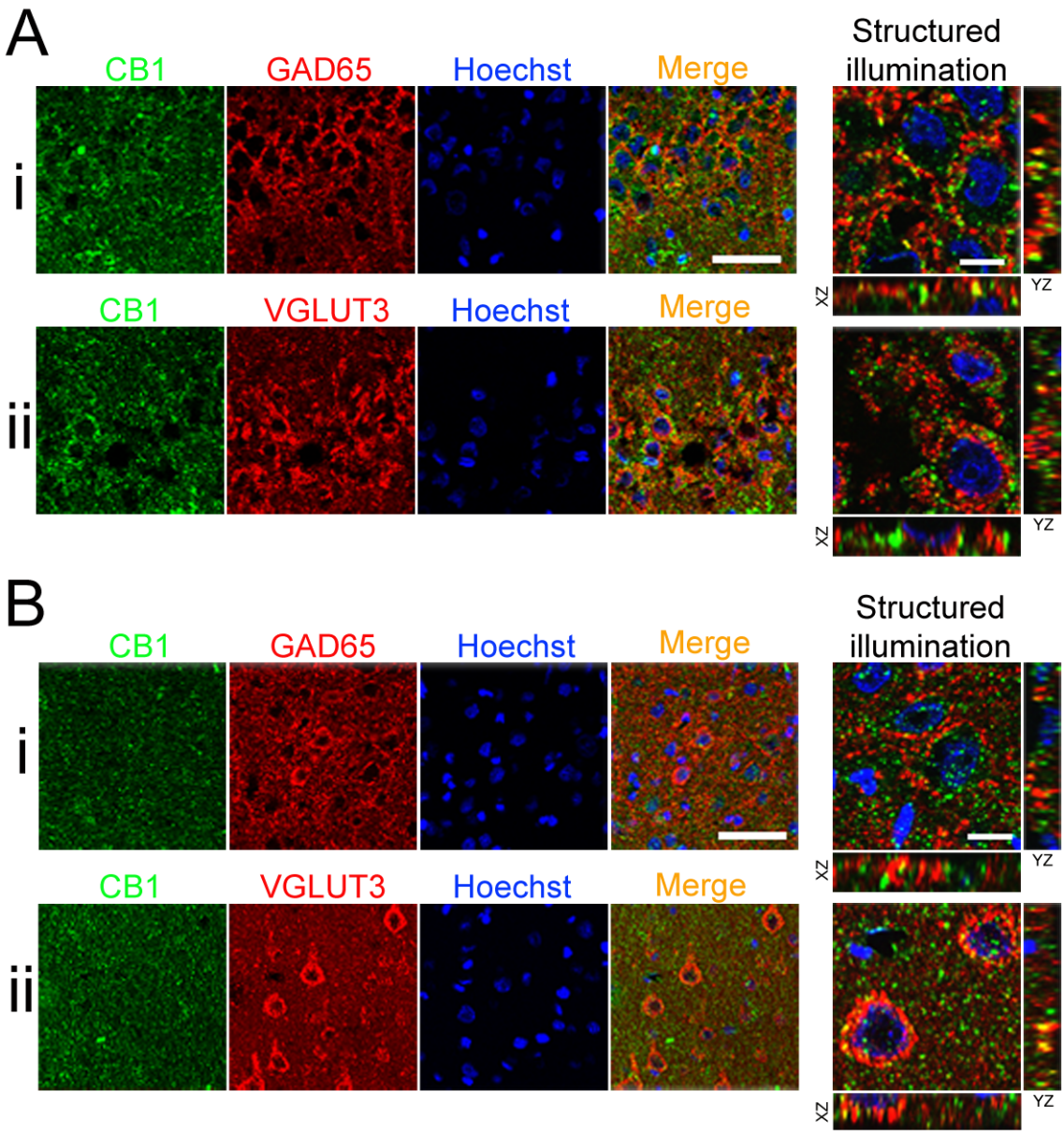

Figure 33. Immunostaining in a representative section from a rat treated with 192IgG-saporin. Immunoreactivity for CB_1 receptors in dentate gyrus (A) and in motor cortex (B), in combination with GAD65 (i) or VGLUT3 (ii). Nuclei were also stained with Hoechst. In merge images note the CB_1 co-localization in dentate gyrus with GAD65 and in cortex with VGLUT3. Triple labeling of tissue slices is shown at 200-fold magnification (merge) and at 630-fold magnification (structured illumination) in a single plane from the collecting Z-stacking. Scale bar = 50 µm and 10 µm, respectively.

2.9. The specific loss of BFCN in the NBM leads to a decrease of cortical presynaptic GABAergic tone

GAD65 immunofluorescence showed a different pattern of distribution in different cortical layers, with the highest density being in the layer IV, as shown for motor cortex (Figure 34 A). There was a large decrease in GAD65 positive cortical terminals in those animals lesioned with 192IgG-saporin, suggesting a down-regulation. Semiquantitative analysis in the motor cortex showed a reduction in motor cortex of 28%, 35% and 39% of GAD65-immunoreactivity in layers I, II-III and IV, respectively ($p < 0.05$) (Figure 34 B). The somatosensory and piriform cortices were also analyzed and a similar decrease of immunosignaling was found, 28%, 32% and 32% in layers I, II-III ($p < 0.01$) and IV ($p < 0.05$) in the somatosensory cortex and 25% in the piriform cortex ($p < 0.05$) (Figure 34 B). One of the most significant decreases of GAD65 immunoreactivity was registered in layer V of the entorhinal cortex (21% decrease, $p < 0.01$), but it was not modified in the dentate gyrus of the hippocampus (2% decrease).

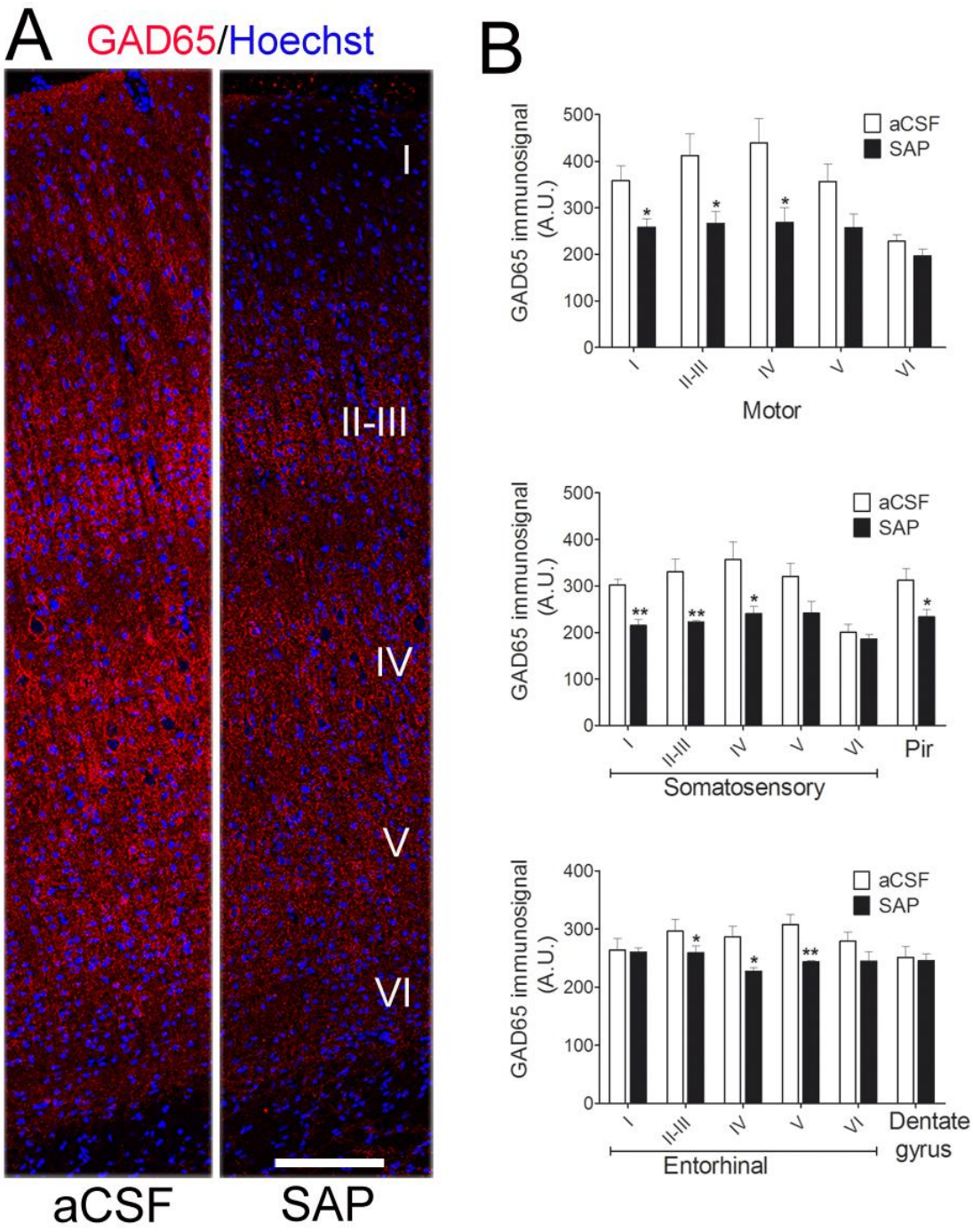

Figure 34. (A) Immunoreactivity for GAD65 in the motor cortex (layers I-VI) from representative rats, one treated with aCSF compared with other rat treated with 192IgG-saporin. (B) Note the differences in optical density of GAD65 positive presynaptic terminals in aCSF and SAP-treated rats, measured as arbitrary units (A.U.) of fluorescence, in motor, somatosensory and entorhinal cortical layers, and also in the total area of the piriform cortex and dentate gyrus. Data are means ± SEM; *p < 0.05; **p < 0.01. Scale bar = 150 µm.

3. Triple transgenic mice model of AD (3xTg-AD)

(Manuscript IV) Relationship of the Cannabinoid and Muscarinic Signaling with cognitive Impairments in 3xTg-AD Mice at the Onset of Alzheimer's Disease

HIGHLIGHTS

- **3xTg-AD mice exhibit anxiety-like symptoms and cognitive deficits at seven months of age as revealed in the passive avoidance test.**
- **CB_1 receptor-mediated hyperactivity in the BLA correlates with higher acquisition latency times which may be related with anxiety-like responses.**
- **Decreased muscarinic neurotransmission runs in parallel to the onset of cognitive decline in 3xTg-AD mice.**
- **Pharmacological desensitization of CB_1 receptors in 3xTg-AD mice restores behavioral responses.**
- **Subchronic activation of CB_1 receptors modulates muscarinic signaling in limbic areas.**

GRAPHICAL ABSTRACT

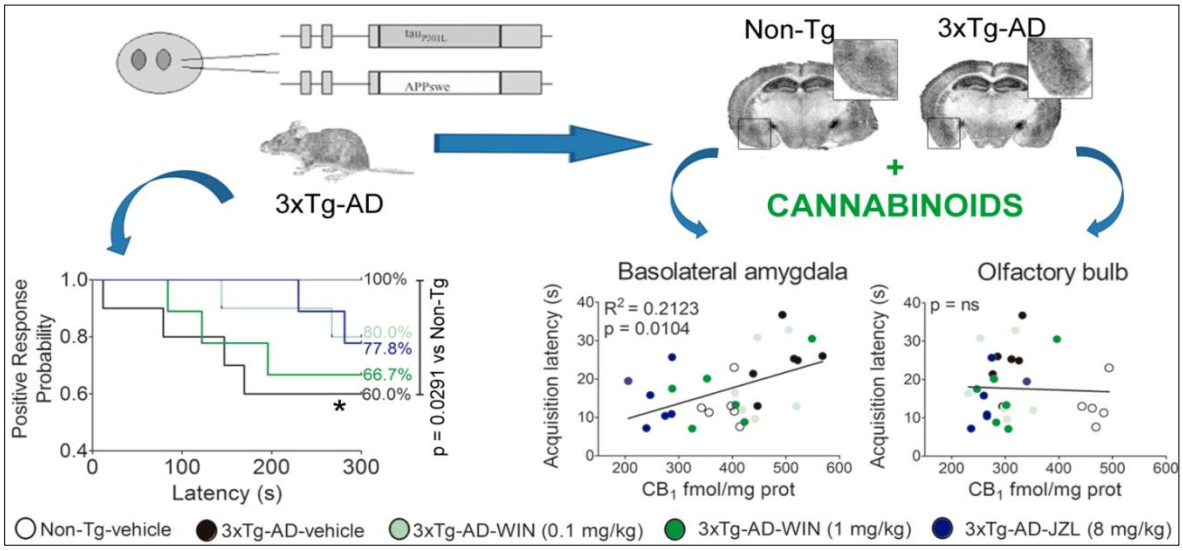

3.1. Learning and memory impairment in 3xTg-AD mice

To examine behavior, adult 3xTg-AD and matched Non-Tg mice at seven months of age were trained and tested on the passive avoidance test. We first examined the acquisition or transfer latency or the time that mice stayed under anxiogenic stimulus in the opened compartment, before receiving a foot-shock as an aversive stimulus when crossed to the closed-dark box. 24 h later, mice were tested evaluating the step-through latency in the retention phase and the step-through latencies were measured and represented as Kaplan-Meier survival curves to elucidate the estimated probability of showing a positive response (to reach the cut-off time). 3xTg-AD and Non-Tg mice clearly differed during the training and testing sessions on the passive avoidance test. Transgenic mice took significantly longer (26.24 ± 1.8 s) to enter the dark compartment than Non-Tg genotype (12.28 ± 1.9 s) ($p = 0.0002$, two-tailed unpaired student *t* test) (Figure 35 left). Not recorded observations showed higher periods of initial freezing in 3xTg-AD mice, immediately after placing in the illuminated compartment, in comparison to the control Non-Tg mice. Moreover, 40% of them failed to remember the foot shock as compared to the positive response shown in 100% of Non-Tg mice ($p = 0.029$, Log-Rank/Mantel-Cox test) (Figure 35 right).

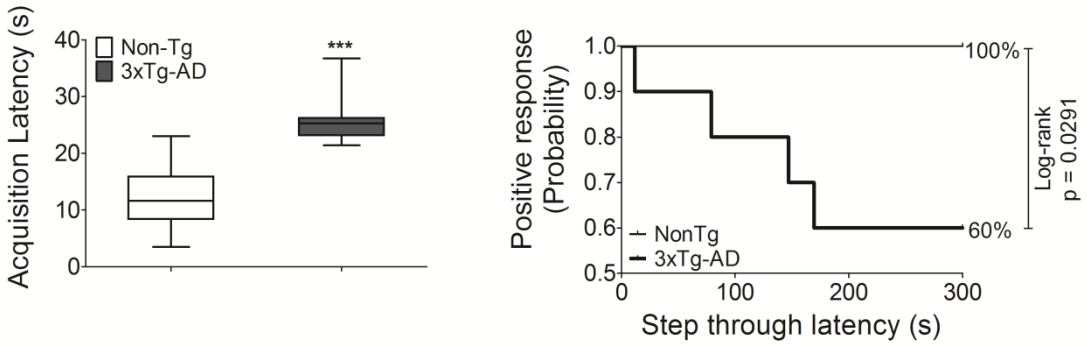

Figure 35. Acquisition latency during the learning trial (left) represented as box plot and step-through latency (right) represented as Kaplan-Meier survival curves in both genotypes and in the absence of treatment. *** $p < 0.001$ *vs* Non-Tg mice.

3.2. Deregulated endocannabinoid signaling in 3xTg-AD mice

CB_1 receptor density

To examine CB_1 receptor density in 3xTg-AD mice and matched Non-Tg mice, cannabinoid receptor autoradiography was performed. Quantitative densitometry showed an increase in the BLA of transgenic mice (Non-Tg 386 ± 12 fmol/mg t.e.; 3xTg-AD 497 ± 19 fmol/mg t.e.; p = 0.0008) and in the lateral olfactory tract nucleus (Non-Tg 281 ± 40 fmol/mg t.e.; 3xTg-AD 424 ± 38 fmol/mg t.e.; p = 0.0274), but a decrease in the glomerular olfactory bulb (Non-Tg 470 ± 8 fmol/mg t.e.; 3xTg-AD 304 ± 9 fmol/mg t.e.; p < 0.0001) (two-tailed unpaired student *t* test) (Student *t*-test, table 10; Figures 36 and 41 A).

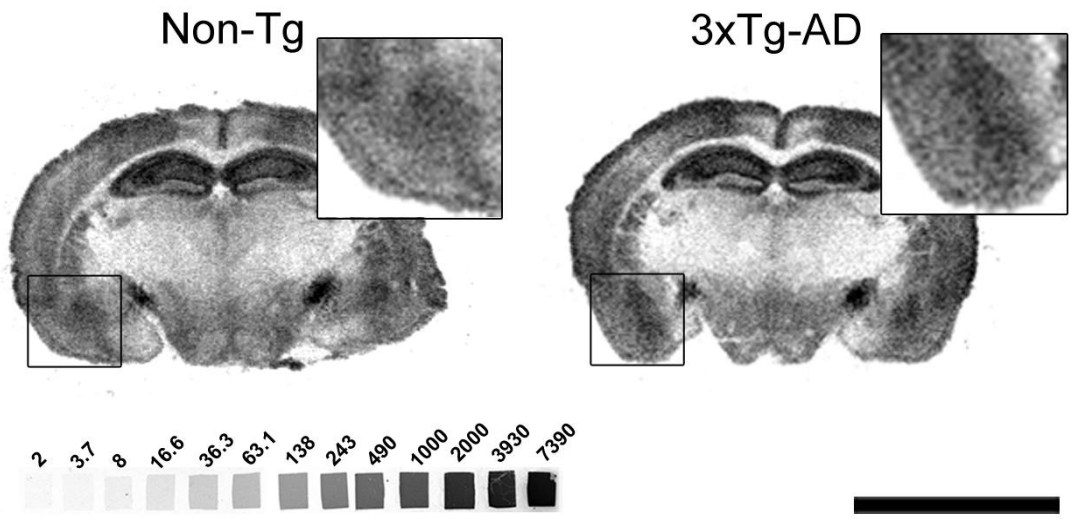

Figure 36. [^{3}H]CP55,940 binding autoradiography showed the cannabinoid receptor distribution in representative brain coronal slices from Non-Tg and 3xTg-AD mice. Note the increase in the density of cannabinoid receptors in the basolateral amygdala (BLA) of 3xTgAD mice. [^{3}H]-microscales used as standards in µCi/g t.e.

Specificity of [^{3}H]CP55,940 binding

SR141716A and SR144528, well known selective antagonists for CB_1 and CB_2 receptors respectively, were used in combination with brain and spleen samples from $CB_1^{+/+}$ and $CB_1^{-/-}$ mice to check the specific subtype of cannabinoid receptor involved in the observed changes. SR141716A blocked [^{3}H]CP55,940 binding in brain slices from 3xTg-AD and $CB_1^{+/+}$ mice, but failed in spleen. SR144528 completely blocked [^{3}H]CP55,940 binding in spleen slices but failed in brain samples. $CB_1^{-/-}$ mice displayed similar binding levels in the spleen to those obtained in $CB_1^{+/+}$ mice, demonstrating the selectivity of both antagonists and the specific deregulation of the CB_1 receptor subtype in 3xTg-AD mice (Figure 37).

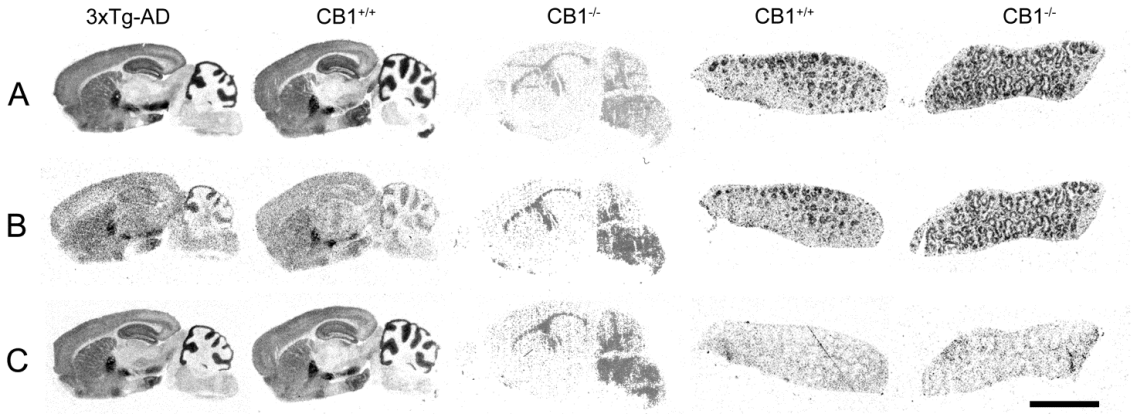

Figure 37. [^{3}H]CP55,940 binding autoradiography showing the cannabinoid receptor distribution in brain and spleen samples from 3xTg-AD, CB_1 receptor knockout ($CB_1^{-/-}$) and wild type ($CB_1^{+/+}$) mice. The total binding is shown in the top row (A), displaying the characteristic and well-described distribution of cannabinoid receptors in the brain, and surrounding the lymphatic nodules (white pulp) in the spleen. In the presence of SR141716A (0.1 µM) (rimonabant), a CB_1 specific antagonist, binding is almost completely blocked in the brain but not in the spleen (B). SR144528 (0.1 µM), a CB_2 specific antagonist, completely displaced the [^{3}H]CP55,940 binding in the spleen without affecting the binding in the brain (C). Note the absence of binding in the brain from $CB_1^{-/-}$ and the identical distribution in the spleen from both Non-Tg and knockout mice, revealing the preponderance of CB_1 receptors in the brain and CB_2 receptors in spleen tissue, and the specificity of the cannabinoid antagonists. Scale bar = 5 mm.

3.3. Subchronic cannabinoid administration restores acquisition latency to control Non-Tg levels

The subchronic administration of direct or indirect cannabinoid agonists in 3xTg-AD mice reduced the increase in acquisition latencies observed in the vehicle-treated 3xTg-AD group (one-way ANOVA, Dunn's multiple comparison test), restoring the latencies to Non-Tg levels (Figure 38). Thus, WIN55,212-2 elicited a behavioral dose-response with slight (0.1 mg/kg, reduction 35%) and marked (1 mg/kg, reduction 50%, $p < 0.05$) reductions in the acquisition latency as compared with those observed in the vehicle-treated 3xTg-AD animals. JZL184 (8 mg/kg), a monoacylglycerol lipase (MAGL) inhibitor, also induced such an effect (reduction 42%, $p < 0.05$) (Figure 38 left). The treatments elicited subtle variations in learning and memory (step-through latency) in 3xTg-AD mice, as shown in the Kaplan-Meier representation, although they did not reach statistical significance (Figure 38 right).

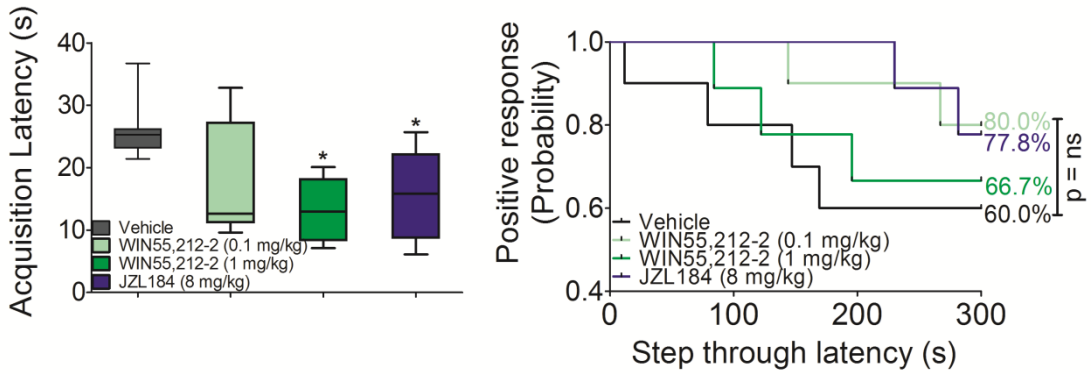

Figure 38. The subchronic administration of WIN55,212-2 (1 mg/kg) and JZL184 (8 mg/kg) for seven consecutive days triggered a statistically significant decrease in the acquisition latency (left) compared to that obtained in the Non-Tg group (as previously shown in Figure 34). Step-through latency in 3xTg-AD mice represented as Kaplan-Meier survival curves (right). The probability is plotted over the step-through latencies in 3xTg-AD mice after different cannabinoid-based treatments.

3.4. CB_1 receptor desensitization induced by direct and indirect cannabinoids

[^{3}H]CP55,940 autoradiography revealed specific modifications in cerebral CB_1 receptor density following the subchronic eCB system activation. WIN55,212-2 (0.1 mg/kg) did not modify CB_1 receptor density, but WIN55,212-2 (1 mg/kg) induced a significant decrease in BLA (22%) (Figures 39 and 41 C). Furthermore, the administration of JZL184 dramatically down-regulated CB_1 receptor, including cortical, hippocampal and amygdaloid regions (Tables 10-11, Figure 39 and 41 C). Functional [^{35}S]GTPγS autoradiography of CB_1 receptor activation showed a decrease of 24% and 32% in the BLA following treatment with WIN55,212-2 (1 mg/kg) and JZL184 (8 mg/kg), respectively (Table 12, Figure 40 C-D and 42 C). The basal binding of [^{35}S]GTPγS was not modified by the different cannabinoid compounds, which probably indicates the absence of changes in the constitutive activity of G-protein coupled receptors (GPCR).

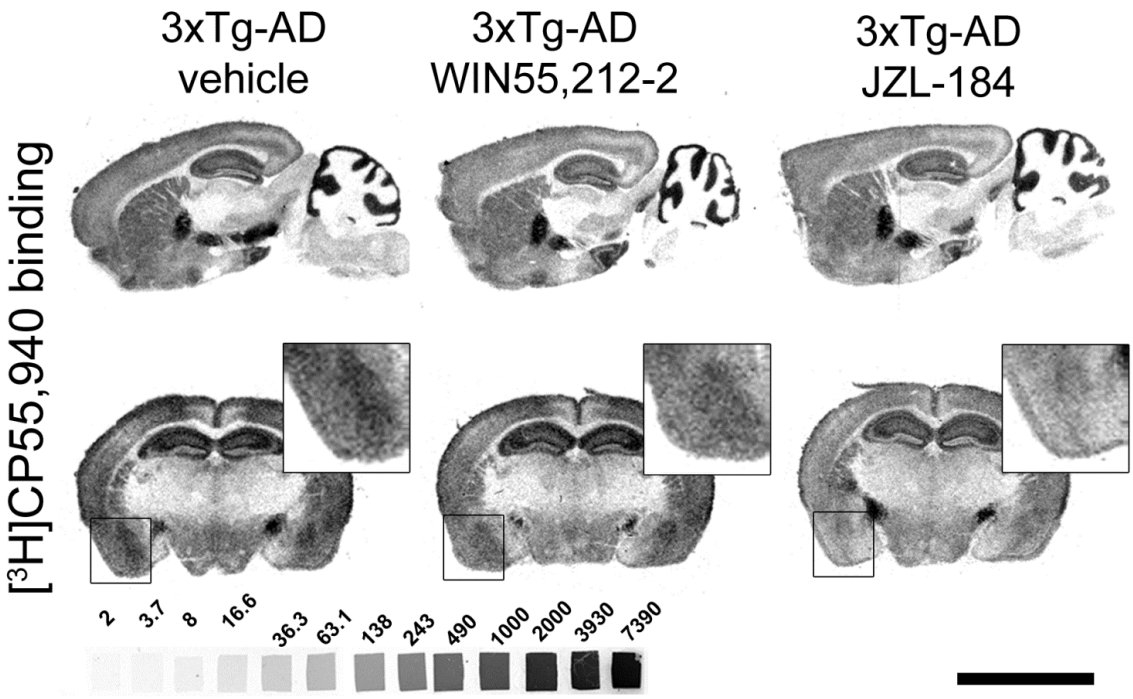

Figure 39. (A) 3xTg-AD mice treated with different cannabinoid agonists. [^{3}H]CP55,940 binding autoradiography in representative brain sagittal (top images) and coronal (bottom images) slices from 3xTg-AD mice administered with vehicle (A), WIN55,212-2 (1 mg/kg) (B), and JZL184 (8 mg/kg) (C). Note that both pharmacological treatments decreased the density of receptors in the whole grey matter including the BLA (boxed area). [^{3}H]-microscales used as standards in µCi/g t.e. Scale bar: 5 mm.

Table 10. [^{3}H]CP55,940 binding in different brain areas of seven month-old Non-Tg and 3xTg-AD mice expressed in fmol/mg t.e. of CB_1 receptors.

	Non-Tg Vehicle	3xTg-AD Vehicle	3xTg-AD WIN55,212-2 [0.1 mg/kg]	3xTg-AD WIN55,212-2 [1 mg/kg]	3xTg-AD JZL184 [8 mg/kg]
Brain region					
Grey matter					
Telencephalon					
Amygdala					
Anterior	209 ± 16	269 ± 16	240 ± 20	244 ± 19	209 ± 11
Basolateral	386 ± 12	497 ± 19***	469 ± 20	385 ± 32$^{\$}$	247 ± 14$^{\#\#\#a,b,c,d}$
Central	169 ± 6	216 ± 17	190 ± 27	211 ± 24	172 ± 12
Lateral	230 ± 10	253 ± 10	272 ± 29	246 ± 23	182 ± 16$^{\#c}$
Medial	121 ± 8	174 ± 16	155 ± 23	178 ± 24	122 ± 14
Globus pallidus	1950 ± 137	1708 ± 123	1805 ± 83	1425 ± 102	1756 ± 142
Striatum	461 ± 44	376 ± 36	384 ± 18	359 ± 17	282 ± 29
Diencephalon					
Nucleus basalis	246 ± 14	251 ± 19	276 ± 23	291 ± 15	196 ± 14$^{\#a,b,c,d}$
Rhinencephalon					
Lat. Olf. Tract N	281 ± 40	424 ± 38*	389 ± 32	327 ± 22	239 ± 17$^{\#\#b,\#c}$
Glom olf. bulb	470 ± 8	304 ± 9***	293 ± 15***	308 ± 19***	276 ± 12***
Mesencephalon					
Sustantia nigra	2034 ± 145	1830 ± 109	1761 ± 51	1692 ± 83	1631 ± 49
White matter					
Corpus callosum	55 ± 13	76 ± 15	75 ± 14	116 ± 18	84 ± 12
Fimbria fornix	56 ± 7	98 ± 12	103 ± 15	140 ± 12	79 ± 7
Internal capsule	-5 ± 12	17 ± 10	24 ± 16	38 ± 10	11 ± 5
Lateral olf tract	195 ± 28	237 ± 27	227 ± 20	255 ± 20	184 ± 15
Optic tract	12 ± 13	33 ± 27	60 ± 25	60 ± 17	31 ± 10

Data are expressed as mean ± S.E.M. *p<0.05, ***p<0.001 vs Non-Tg (vehicle).
$^{\#}$p<0.05, $^{\#\#}$p<0.01, $^{\#\#\#}$p<0.001 vs Non-Tg (vehicle) (**a**); 3xTg-AD (vehicle) (**b**); 3xTg-AD (WIN-0.1 mg/kg) (**c**); 3xTg-AD (WIN-1 mg/kg) (**d**). $^{\$}$p<0.05 vs 3xTg-AD (vehicle).

Table 11. [^{3}H]CP55,940 binding in different brain areas of seven month-old Non-Tg and 3xTg-AD mice expressed in fmol/mg t.e. of CB_1 receptors.

	Non-Tg Vehicle	3xTg-AD Vehicle	3xTg-AD WIN55,212-2 [0.1 mg/kg]	3xTg-AD WIN55,212-2 [1 mg/kg]	3xTg-AD JZL184 [8 mg/kg]
Brain region					
Grey matter					
Telencephalon					
Hippocampus					
CA1	593 ± 38	607 ± 28	542 ± 30	473 ± 32	410 ± 25
Oriens	541 ± 36	592 ± 37	584 ± 30	486 ± 18	366 ± 28**^{b,c}
Pyramidal	924 ± 75	909 ± 69	878 ± 42	679 ± 47$^{\$}$	529 ± 56**^{b,c}
Radiatum	603 ± 56	613 ± 51	559 ± 29	482 ± 34	434 ± 44
CA3	591 ± 40	599 ± 19	543 ± 36	496 ± 24	396 ± 27
Oriens	545 ± 51	481 ± 39	499 ± 59	378 ± 32	394 ± 27
Pyramidal	885 ± 70	818 ± 65	763 ± 80	618 ± 67	599 ± 26*^{a,b}
Radiatum	630 ± 89	596 ± 43	591 ± 58	487 ± 59	419 ± 45
Dentate gyrus	473 ± 37	487 ± 17	454 ± 26	434 ± 40	348 ± 22
Granular	922 ± 75	855 ± 49	836 ± 50	711 ± 27	574 ± 35**^{a,b,c}
Molecular	569 ± 55	544 ± 48	489 ± 32	404 ± 30	371 ± 32
Polimorphic	272 ± 25	267 ± 33	224 ± 25	233 ± 19	189 ± 11
Subiculum	861 ± 86	909 ± 38	866 ± 53	712 ± 48	449 ± 56***$^{a,b,c;*d}$
Lac moleculare	678 ± 83	637 ± 70	592 ± 50	472 ± 66	394 ± 54
Cerebral cortex					
Cingular	286 ± 17	316 ± 15	332 ± 25	308 ± 15	247 ± 10*^{c}
Ectorhinal	291 ± 28	321 ± 17	331 ± 32	308 ± 31	220 ± 16*$^{b,\ c}$
Entorhinal	254 ± 21	276 ± 18	271 ± 17	254 ± 19	164 ± 12*$^{b,\ c}$
Frontal	499 ± 17	427 ± 16	501 ± 22	415 ± 17	310 ± 10**$^{a,\ c}$
Motor	340 ± 8	314 ± 13	347 ± 24	317 ± 20	241 ± 11**$^{a,\ c;\ *b,\ d}$
Perirhinal	278 ± 32	302 ± 9	280 ± 23	271 ± 32	195 ± 13*^{b}
Piriform	229 ± 9	216 ± 22	235 ± 20	248 ± 25	193 ± 10
Somatosensory	204 ± 21	220 ± 18	241 ± 23	254 ± 23	211 ± 10

Data are expressed as mean ± S.E.M. *p<0.05, **p<0.01, ***p<0.001 compared with Non-Tg (vehicle) (**a**); 3xTg-AD (vehicle) (**b**); 3xTg-AD (WIN-0.1 mg/kg) (**c**); 3xTg-AD (WIN-1 mg/kg) (**d**).

3.5. CB_1 receptor functionality

To check for a presumed modification of eCB signaling, [^{35}S]GTPγS autoradiography assay was performed. This technique represents a powerful functional approach to anatomically localize and quantify the receptor-dependent $G_{i/o}$ protein activity directly in tissue slices. Basal $G_{i/o}$ protein activity was firstly examined and no differences between genotypes were observed. The activity of CB_1 receptors evoked by WIN55,212-2 (10 µM), was higher in the BLA of 3xTg-AD ($p = 0.0303$) but lower in several areas such as the striatum ($p = 0.0285$), the glomerular olfactory bulb ($p = 0.0043$), and the molecular layer of hippocampal dentate gyrus ($p = 0.0040$; Student *t*-test) (Tables 12-13; Figures 40 and 42 A).

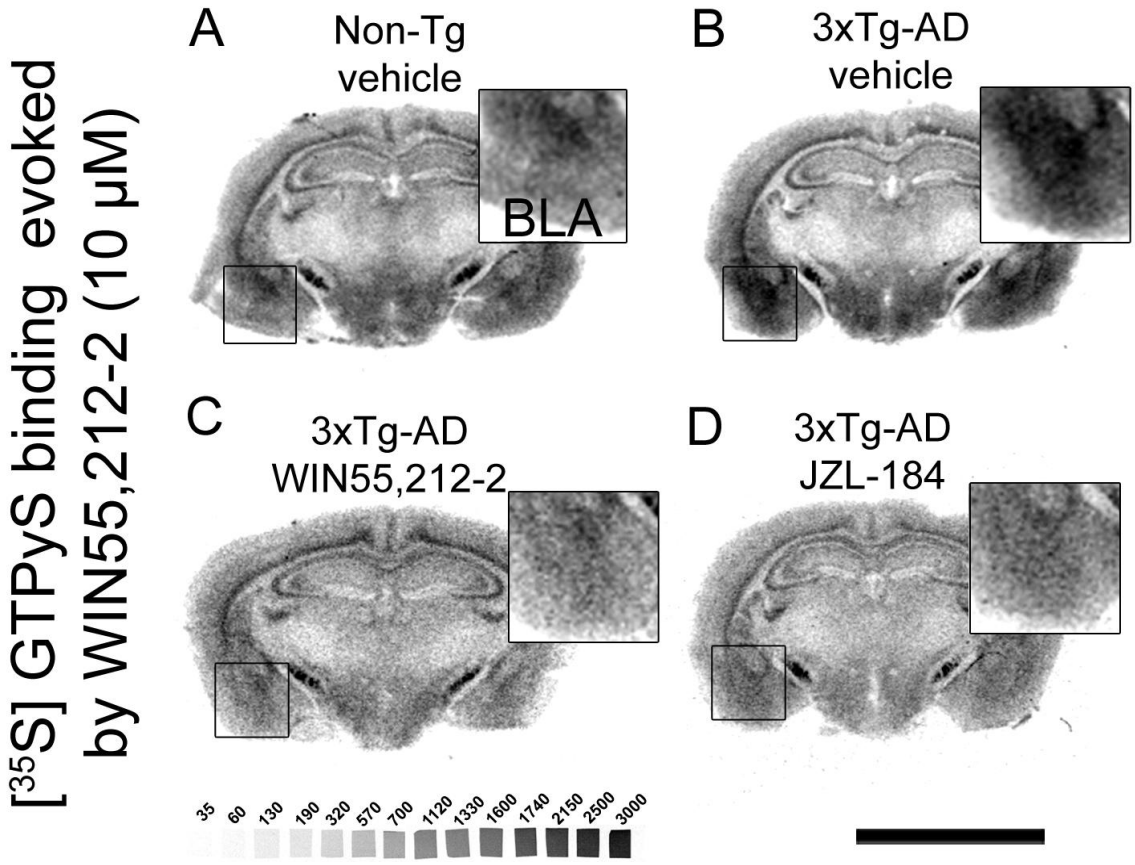

Figure 40. [^{35}S]GTPγS autoradiography evoked by WIN55,212-2 (10 µM) for cannabinoid receptors in representative coronal brain slices from Non-Tg (A) and 3xTg-AD mice treated with vehicle (B) and cannabinoid agonists (C-D). The highest CB_1 receptor stimulation was found in the hippocampus, the most caudal portion of the globus pallidus, the deeper layers of the cortex, and the amygdaloid complex. Thus, in the amygdala, the latero-basolateral region (boxed area) seems to be the most activated, displaying a hyperactivation in 3xTg-AD mice (B) which is attenuated with both cannabinoids (C-D). [^{14}C]-microscales used as standards in µCi/g t.e. Scale bar: 5 mm.

Table 12. [^{35}S]GTPγS binding in different brain areas of seven-month-old Non-Tg and 3xTg-AD mice evoked by WIN55,212-2 (10 μM) expressed as percentage of stimulation over the basal binding.

	NonTg Vehicle	3xTg-AD Vehicle	3xTg-AD WIN55.212-2 [0.1 mg/kg]	3xTg-AD WIN55.212-2 [1 mg/kg]	3xTg-AD JZL-184 [8 mg/kg]
Brain region					
Telencephalon					
Amygdala					
Anterior	82 ± 16	79 ± 16	68 ± 14	98 ± 16	89 ± 24
Basolateral	168 ± 24	281 ± 41*	311 ± 42	213 ± 25	191 ± 31
Central	76 ± 28	61 ± 14	66 ± 17	58 ± 19	63 ± 21
Lateral	156 ± 26	197 ± 36	167 ± 45	159 ± 26	123 ± 23
Medial	35 ± 13	56 ± 9	100 ± 15	77 ± 20	89 ± 20
Globus pallidus	1188 ± 157	1161 ± 116	1026 ± 73	1114 ± 56	1057 ± 85
Striatum	134 ± 19	81 ± 8*	80 ± 6	102 ± 10	73 ± 13
Diencephalon					
Nucleus basalis	130 ± 26	112 ± 18	104 ± 9	121 ± 15	97 ± 12
Rhinencephalon					
Lat. Olf. Tract N	221 ± 58	232 ± 71	230 ± 44	325 ± 61	326 ± 60
Glom olf. bulb	580 ± 61	343 ± 18**	317 ± 41	391 ± 50	331 ± 22
Mesencephalon					
Sustantia nigra	1974 ± 181	1781 ± 166	1541 ± 111	1595 ± 97	1356 ± 91
White matter					
Corpus callosum	5 ± 9	11 ± 5	11 ± 7	12 ± 14	23 ± 5
Fimbria fornix	96 ± 8	40 ± 12	42 ± 5	48 ± 16	52 ± 12
Internal capsule	50 ± 17	1 ± 7	20 ± 14	19 ± 9	21 ± 7
Lateral olfactory tract	90 ± 32	63 ± 26	76 ± 25	70 ± 13	86 ± 6
Optic tract	28 ± 27	24 ± 11	57 ± 21	31 ± 12	34 ± 8

Data are expressed as mean ± S.E.M.

*****$p < 0.05$; ******$p < 0.01$ *vs* Non-Tg (vehicle)

Table 13. [^{35}S]GTPγS binding in different brain areas of seven-month-old Non-Tg and 3xTg-AD mice evoked by WIN55,212-2 (10 μM) expressed as percentage of stimulation over the basal binding.

	NonTg Vehicle	3xTg-AD Vehicle	3xTg-AD WIN55.212-2 [0.1 mg/kg]	3xTg-AD WIN55.212-2 [1 mg/kg]	3xTg-AD JZL-184 [8 mg/kg]
Brain region					
Telencephalon					
Hippocampus					
CA1	114 ± 17	63 ± 13	64 ± 6	61 ± 9.9	59 ± 8
Oriens	183 ± 40	164 ± 14	132 ± 11	178 ± 16	110 ± 19
Pyramidal	142 ± 23	165 ± 49	157 ± 15	151 ± 20	112 ± 22
Radiatum	144 ± 32	141 ± 34	105 ± 16	109 ± 16	53 ± 7$^{\#}$
CA3	154 ± 14	104 ± 19	105 ± 11	96 ± 15	116 ± 25
Oriens	143 ± 18	161 ± 17	134 ± 21	143 ± 16	121 ± 21
Pyramidal	94 ± 21	117 ± 22	135 ± 25	141 ± 23	82 ± 13
Radiatum	189 ± 51	123 ± 35	94 ± 19	89 ± 13	93 ± 13
Dentate gyrus	119 ± 17	70 ± 8	65 ± 8	62 ± 10	68 ± 12
Granular	293 ± 71	143 ± 20	193 ± 12	186 ± 36	152 ± 25
Molecular	199 ± 34	108 ± 18*	99 ± 13	113 ± 8	112 ± 20
Polimorphic	261 ± 24	146 ± 20	104 ± 14	134 ± 13	112 ± 13
Ventral subiculum	162 ± 37	130 ± 21	106 ± 15	125 ± 18	127 ± 19
Lacunosum moleculare	132 ± 27	135 ± 34	88 ± 15	108 ± 15	92 ± 19
Cerebral cortex					
Cingular	90 ± 10	110 ± 14	102 ± 14	98 ± 10	69 ± 7
Ectorhinal	159 ± 37	131 ± 12	141 ± 21	115 ± 25	93 ± 19
Entorhinal	154 ± 27	165 ± 36	135 ± 22	180 ± 17	149 ± 20
Frontal	101 ± 14	114 ± 20	99 ± 13	115 ± 17	107 ± 15
Motor	108 ± 10	127 ± 18	93 ± 17	88 ± 6	87 ± 5
Perirhinal	168 ± 41	146 ± 29	127 ± 21	107 ± 21	85 ± 12
Piriform	89 ± 18	71 ± 9	74 ± 9	91 ± 21	70 ± 6
Somatosensory	62 ± 9	68 ± 8	51 ± 13	59 ± 9	66 ± 9

Data are expressed as mean ± S.E.M.

*****p < 0.05 *vs* Non-Tg (vehicle)

# p < 0.05 *vs* 3xTg-AD (vehicle)

3.6. CB_1 receptor up-regulation positively correlates with the acquisition latencies

The regression analyses showed that the greater the density of CB_1 receptors the higher the acquisition latencies estimating that 50% and 33% of the variation in the acquisition latencies was related to changes in CB_1 receptors density at BLA (Figure 41 A) (r^2 = 0.5096, p = 0.0091; Figure 41 C) and/or to changes in CB_1 receptor activity (evoked by WIN55,212-2) (Figure 42 A) (r^2 = 0.3299, p = 0.0508; Figure 42 C). No statistically significant correlations were found when other brain areas were compared such as the lateral olfactory tract nucleus and glomerular olfactory bulb (p = ns). Both treatments, JZL184 (8 mg/kg) and WIN55,212-2 (1 mg/kg), decreased the acquisition latencies of 3xTg-AD mice to Non-Tg mice control values due to the pharmacological down-regulation of CB_1 receptors to levels even lower than those observed in Non-Tg mice (Figure 41 B). When the groups were compared all together, a positive and statistically significant correlation between CB_1 receptor density in the BLA (Figure 41 B) and acquisition latencies was found, showing that 25% of the acquisition latencies variation was explained by changes in CB_1 density (r^2 = 0.2499, p = 0.013; Figure 41 D), but not by changes in CB_1 activity (Figure 42 D).

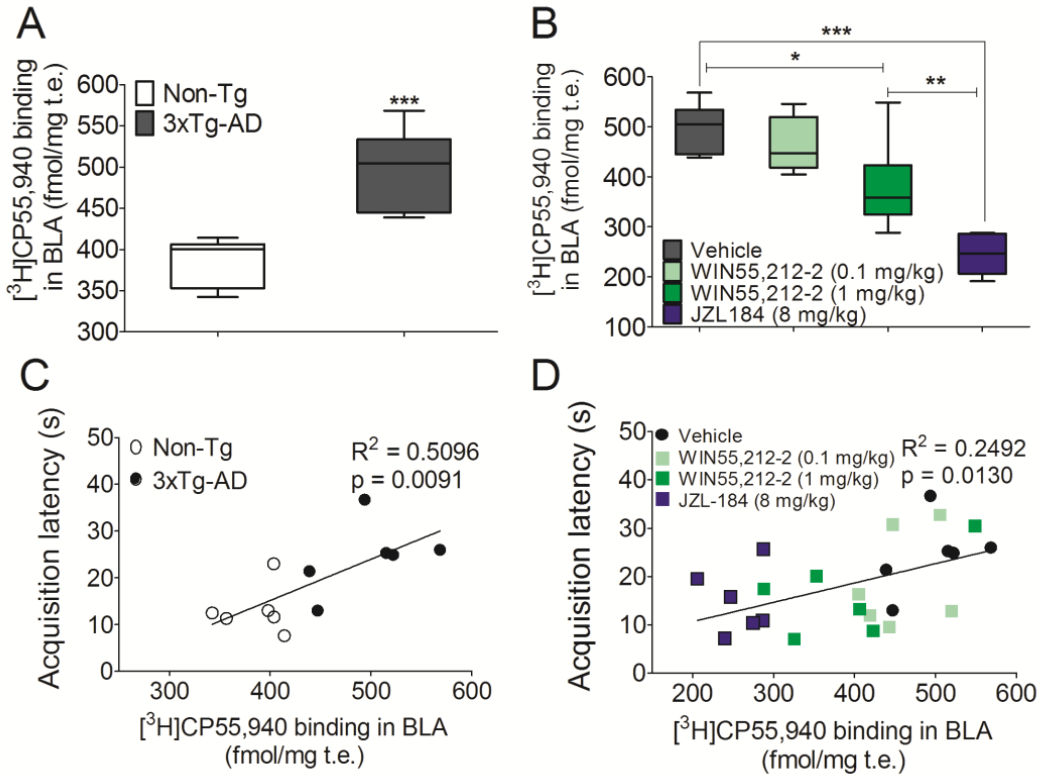

Figure 41. (A) CB_1 receptor density in the BLA in both genotypes (3xTg-AD *vs* Non-Tg) without any pharmacological treatment and (B) in 3xTg-AD mice seven days after the administration of WIN55,212-2 (0.1 and 1 mg/kg) or JZL184 (8 mg/kg). (C) Correlation analyses between the CB_1 density in the BLA and the acquisition latencies between both genotypes and (D) in 3xTg-AD mice after cannabinoid administration. Note that data are grouped according to both genotype and cannabinoid-based treatment *$p < 0.05$; **$p < 0.01$ and *** $p < 0.001$.

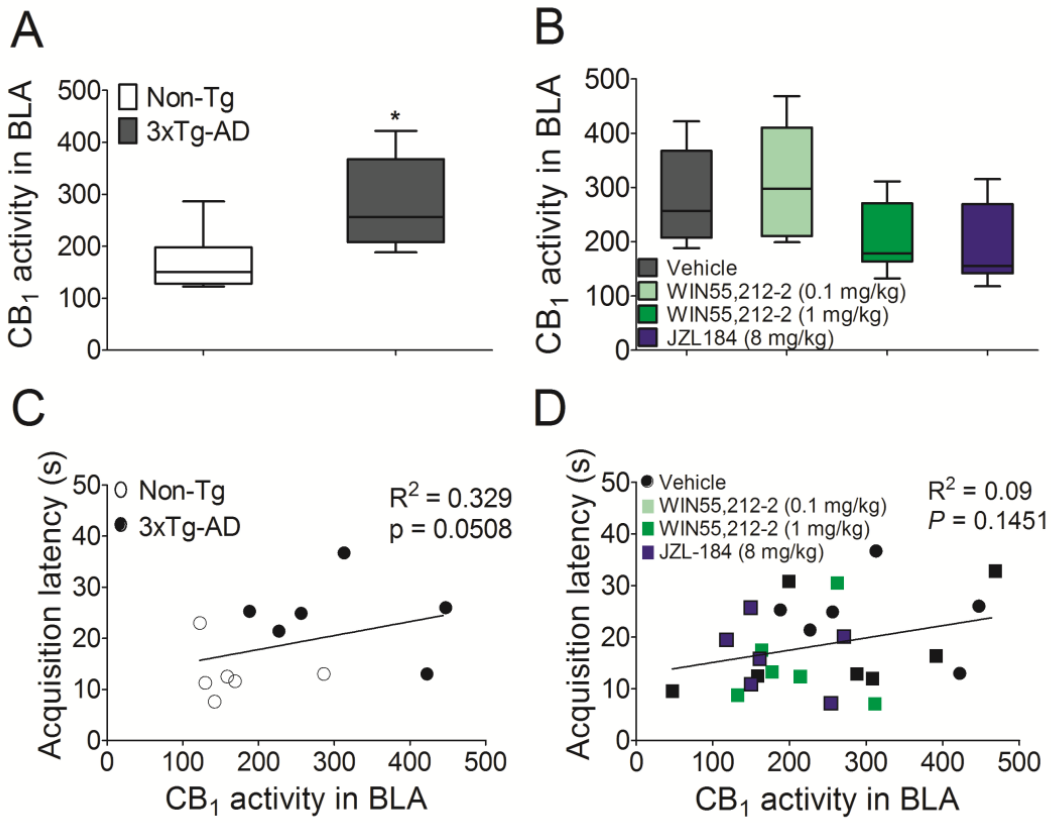

Figure 42. (A) Quantification of CB_1 receptor stimulation (% over basal activity) evoked by WIN55,212-2 (10 μM) in the BLA in both genotypes (Non-Tg *vs* 3xTg-AD) and (B) in 3xTg-AD mice seven days after the administration of different doses of WIN55,212-2 (0.1 mg/kg and 1 mg/kg) or JZL184 (8 mg/kg). (C) Correlation analysis between the eCB signaling in the BLA and the acquisition latencies in both genotypes and (D) in 3xTg-AD mice after cannabinoid administration. Note that data are grouped according to genotype but not to treatment *p < 0.05 *vs* Non-Tg; two-tailed unpaired Student *t* test.

3.7. Decreased M_2/M_4 mAChR-mediated activity in 3xTg-AD is modulated by cannabinoid administration

We analyzed the functional coupling of mAChR to $G_{i/o}$ proteins evoked by carbachol (100 µM) in both genotypes and in cannabinoid treated 3xTg-AD mice. Transgenic mice showed decreased functional coupling in the BLA (Non-Tg 102 ± 13.7% and 3xTg-AD 55 ± 10.5%; $p = 0.0258$), in the lateral amygdala (Non-Tg 96 ± 18.3% and 3xTg-AD 41 ± 11.3%; $p = 0.0303$) and hippocampal pyramidal CA1 (Non-Tg 30 ± 6% and 3xTg-AD 16 ± 6.8%; $p = 0.0227$). Moreover, increased M_2/M_4 mAChR receptor activity was found in the glomerular olfactory bulb (Non-Tg 193 ± 25.9% and 3xTg-AD 295 ± 14.9%; $p = 0.0095$). The administration of 1 mg/kg of WIN55,212-2 was able to increase the M_2/M_4 mAChR-mediated activity to similar values of Non-Tg mice; up to 60% in the BLA (97 ± 12.6%; $p < 0.05$) and up to 100% in the lateral amygdala (84 ± 9.1%; $p < 0.01$). No modulation of M_2/M_4 mAChR-mediated activity was observed in other brain areas (Tables 14-15; Figure 43 C-D).

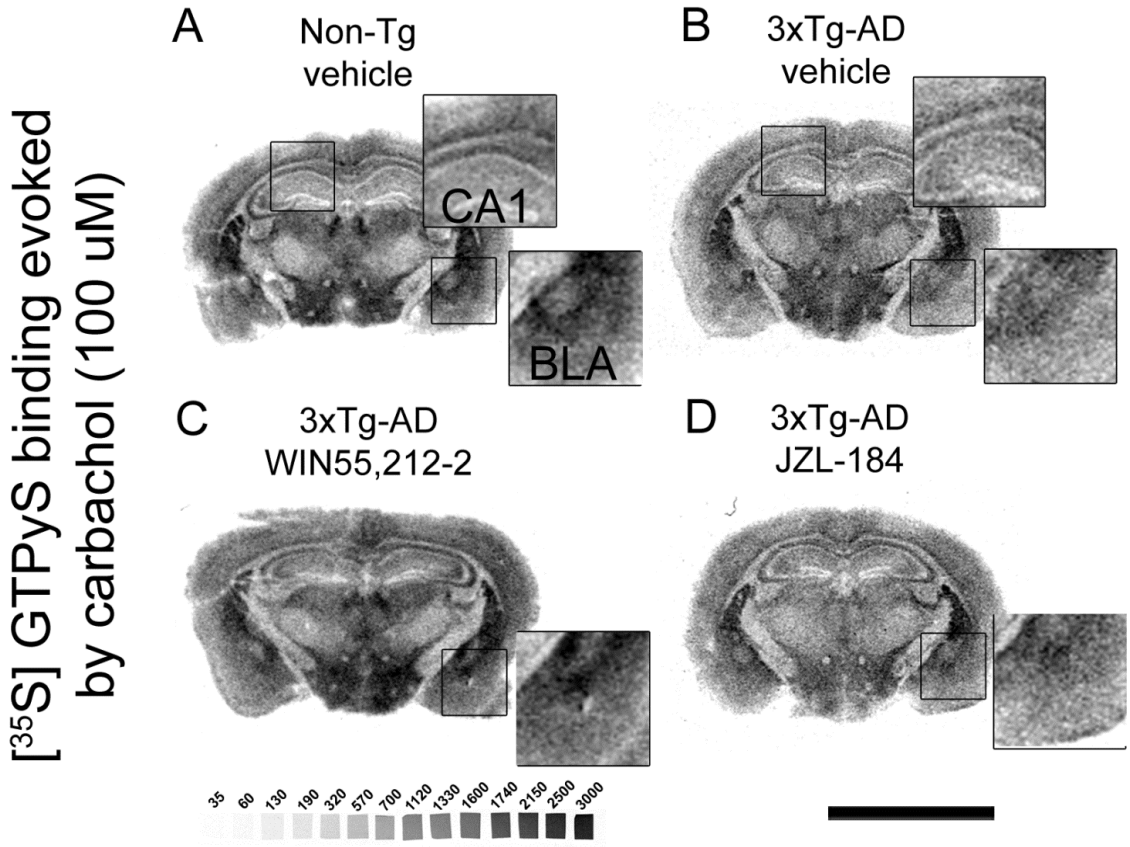

Figure 43. [^{35}S]GTPγS autoradiography evoked by carbachol (100 µM) for M_2/M_4 mAChR, in representative coronal brain slices from Non-Tg (A) and 3xTg-AD mice treated with vehicle (B) and cannabinoid agonists (C-D). A deregulation of mAChR functionality in 3xTg-AD mice was found. Note the decrease in the latero-basolateral region and in the pyramidal layer of the hippocampal CA1 region (boxed areas) (B) and the potentiation of muscarinic signaling in the amygdala following the subchronic administration of 1 mg/kg of WIN55,212-2 (C). [^{14}C]-microscales used as standards in µCi/g t.e. Scale bar: 5 mm.

Table 14. [^{35}S]GTPγS binding in different brain areas of seven-month-old Non-Tg and 3xTg-AD mice evoked by carbachol (100 μM) expressed as percentage of stimulation over the basal binding.

	NonTg Vehicle	3xTg-AD Vehicle	3xTg-AD WIN55.212-2 [0.1 mg/kg]	3xTg-AD WIN55.212-2 [1 mg/kg]	3xTg-AD JZL-184 [8 mg/kg]
Brain region					
Telencephalon					
Amygdala					
Anterior	89 ± 18.0	92 ± 21.1	128 ± 19.9	116 ± 9.7	82 ± 17.4
Basolateral	102 ± 13.7	55 ± 10.5*	68 ± 16.0	97 ± 12.6#	71 ± 11.0
Central	43 ± 7.6	31 ± 9.5	40 ± 8.5	43 ± 5.9	53 ± 15.1
Lateral	96 ± 18.3	41 ± 11.3*	43 ± 11.9	84 ± 9.1##	55 ± 8.1
Medial	66 ± 5.8	49 ± 14.6	31 ± 6.7	54 ± 10.0	46 ± 11.2
Hippocampus					
CA1	42 ± 6.6	21 ± 3.0*	38 ± 8.5	39 ± 12.0	28 ± 7.6
Oriens	33 ± 6.9	29 ± 9.2	36 ± 7.6	59 ± 11.0	26 ± 8.7
Pyramidal	30 ± 6.0	16 ± 6.8*	23 ± 6.1	34 ± 7.0	14 ± 4.8
CA3	43 ± 9.1	33 ± 6.4	43 ± 5.4	47 ± 15.1	46 ± 9.3
Oriens	30 ± 11.9	24 ± 9.9	27 ± 8.0	49 ± 11.7	27 ± 4.6
Pyramidal	34 ± 14.4	29 ± 5.2	28 ± 10.2	53 ± 15.0	33 ± 7.3
Dentate gyrus	34 ± 7.6	21 ± 4.7	28 ± 6.4	21 ± 5.2	21 ± 4.1
Granular	23 ± 8.8	26 ± 9.4	32 ± 10.5	19 ± 5.6	21 ± 6.4
Molecular	21 ± 6.2	19 ± 4.4	16 ± 13.2	17 ± 4.2	8 ± 3.1
Polimorphic	16 ± 15.1	24 ± 5.2	3 ± 12.3	23 ± 13.2	11 ± 5.7
Cerebral cortex					
Cingular	62 ± 12.2	64 ± 13.0	54 ± 9.6	68 ± 10.9	58 ± 9.5
Ectorhinal	39 ± 14.8	42 ± 11.7	38 ± 12.8	46 ± 8.7	37 ± 5.2
Entorhinal	41 ± 12.9	30 ± 13.6	27 ± 9.2	37 ± 11.3	34 ± 8.8
Frontal	54 ± 17.9	57 ± 11.8	42 ± 8.9	68 ± 11.9	57 ± 9.6
Motor	59 ± 10.9	56 ± 12.1	50 ± 10.7	59 ± 11.5	46 ± 8.5
Perirhinal	46 ± 6.7	40 ± 4.7	43 ± 9.8	45 ± 5.4	51 ± 12.5
Rhinencephalon					
Lat. Olfact. Tract N	173 ± 22.3	107 ± 15.9*	125 ± 14.3	140 ± 19.9	112 ± 8.2
Glom Olfact bulb	193 ± 25.9	295 ± 14.9*	312 ± 45.0	279 ± 53.7	266 ± 37.6

Data are expressed as mean ± S.E.M.

*****p < 0.05 *vs* Non-Tg (vehicle)

#p < 0.05; ##p < 0.01 *vs* 3xTg-AD (vehicle)

Table 15. [^{35}S]GTPγS binding in different brain areas of seven-month-old Non-Tg and 3xTg-AD mice evoked by carbachol (100 μM) expressed as percentage of stimulation over the basal binding.

	NonTg Vehicle	3xTg-AD Vehicle	3xTg-AD WIN55.212-2 [0.1 mg/kg]	3xTg-AD WIN55.212-2 [1 mg/kg]	3xTg-AD JZL-184 [8 mg/kg]
Brain region					
Telencephalon					
Hippocampus					
CA1	42 ± 6.6	21 ± 3.0*	38 ± 8.5	39 ± 12.0	28 ± 7.6
Oriens	33 ± 6.9	29 ± 9.2	36 ± 7.6	59 ± 11.0	26 ± 8.7
Pyramidal	30 ± 6.0	16 ± 6.8*	23 ± 6.1	34 ± 7.0	14 ± 4.8
CA3	43 ± 9.1	33 ± 6.4	43 ± 5.4	47 ± 15.1	46 ± 9.3
Oriens	30 ± 11.9	24 ± 9.9	27 ± 8.0	49 ± 11.7	27 ± 4.6
Pyramidal	34 ± 14.4	29 ± 5.2	28 ± 10.2	53 ± 15.0	33 ± 7.3
Dentate gyrus	34 ± 7.6	21 ± 4.7	28 ± 6.4	21 ± 5.2	21 ± 4.1
Granular	23 ± 8.8	26 ± 9.4	32 ± 10.5	19 ± 5.6	21 ± 6.4
Molecular	21 ± 6.2	19 ± 4.4	16 ± 13.2	17 ± 4.2	8 ± 3.1
Polimorphic	16 ± 15.1	24 ± 5.2	3 ± 12.3	23 ± 13.2	11 ± 5.7
Cerebral cortex					
Cingular	62 ± 12.2	64 ± 13.0	54 ± 9.6	68 ± 10.9	58 ± 9.5
Ectorhinal	39 ± 14.8	42 ± 11.7	38 ± 12.8	46 ± 8.7	37 ± 5.2
Entorhinal	41 ± 12.9	30 ± 13.6	27 ± 9.2	37 ± 11.3	34 ± 8.8
Frontal	54 ± 17.9	57 ± 11.8	42 ± 8.9	68 ± 11.9	57 ± 9.6
Motor	59 ± 10.9	56 ± 12.1	50 ± 10.7	59 ± 11.5	46 ± 8.5
Perirhinal	46 ± 6.7	40 ± 4.7	43 ± 9.8	45 ± 5.4	51 ± 12.5
Piriform	45 ± 10.8	77 ± 23.6	73 ± 14.4	41 ± 4.8	28 ± 8.5
Somatosensory	69 ± 16.4	54 ± 9.7	60 ± 12.5	55 ± 12.1	43 ± 7.6

Data are expressed as mean ± S.E.M.

*****$p < 0.05$ *vs* Non-Tg (vehicle)

3.8. CB_1 receptors in BLA and M_2 mAChR in hippocampus colocalize with GABAergic terminals

The different nuclei of the amygdala exhibited distinct CB_1-immunostaining patterns and were clearly defined (Figure 44 B). The dense CB_1 immunoreactive puncta observed in the BLA (Figures 44 A1 and B1), suggested a presynaptic localization of CB_1. Immunofluorescence assays for VGLUT3 (Figure 44 A2) and GAD65 (Figure 44 B2), and the subsequent colocalization studies, allowed us to confirm the inhibitory nature of CB_1 receptor containing presynaptic boutons (Figure 44 B-merge and D4).

M_2 immunoreactivity was differentially localized in the hippocampus (Figure 45 A-B). The pyramidal neurons of CA1-CA3 displayed a dense network of fibers delineating the perikarya in basket-like formations (Figure 45 A2 and B2). VGLUT3 (Figure 45 A1) displayed a somato-dendritic immunostaining, whereas GAD65 (Figure 45 B1) was present as a dense plexus of fibers around pyramidal neurons with a similar distribution to M_2 mAChR. Colocalization studies showed the presence of M_2 mAChR (Figure 45 B-merge) in presynaptic GABAergic terminals with a high degree of co-immunoreactivity with GAD65 (Figure 45 D4), and an almost total absence of expression on VGLUT3 positive cells (Figure 45 C4).

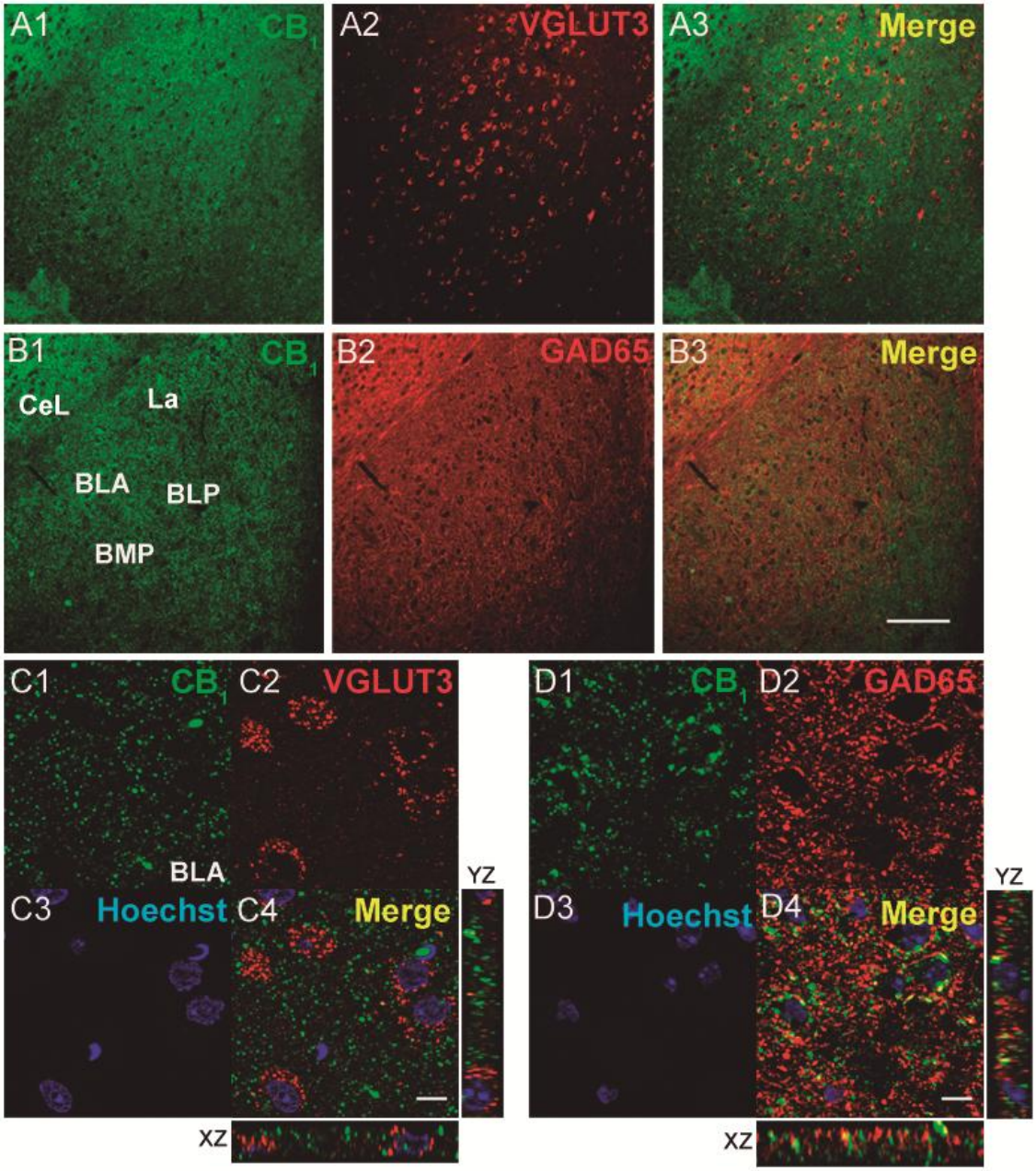

Figure 44. Double labeling of tissue slices including the amygdaloid complex from seven month-old 3xTg-AD mice processed for CB_1 receptor (in green) and VGLUT3 (A2 and C2 in red) as a glutamatergic marker, and GAD65 (B2 and D2 in red) as a GABAergic presynaptic marker. The different amygdaloid nuclei exhibited specific CB_1-immunostaining patterns. VGLUT3 was distributed presumably in post-synaptic somatodendritic compartment (A2 and C2) while GAD65 immunostaining was clearly delineated presynaptic inhibitory boutons (B2 and D2). In low magnification images, note the distribution of CB_1 receptors surrounding positive glutamatergic neurons (A3) and sharing localization with GAD65 (B3); scale bar: 150 µm. High magnification images showed the intracellular localization of VGLUT3 (C2) closely surrounding the nuclei stained with Hoechst (C3 in blue) revealing the almost complete lack of colocalization with CB_1 (C4). Conversely, CB_1 was located on GAD65-positive terminals (D4), revealing its presynaptic localization on inhibitory synaptic boutons. Scale bar = 10 µm. Bregma -1.82 mm. CeL: central amygdaloid nucleus, lateral division; La: lateral amygdaloid nucleus; BLA: basolateral amygdaloid nucleus, anterior part; BLP: basolateral amygdaloid nucleus, posterior part; BMP: basomedial amygdaloid nucleus, posterior part.

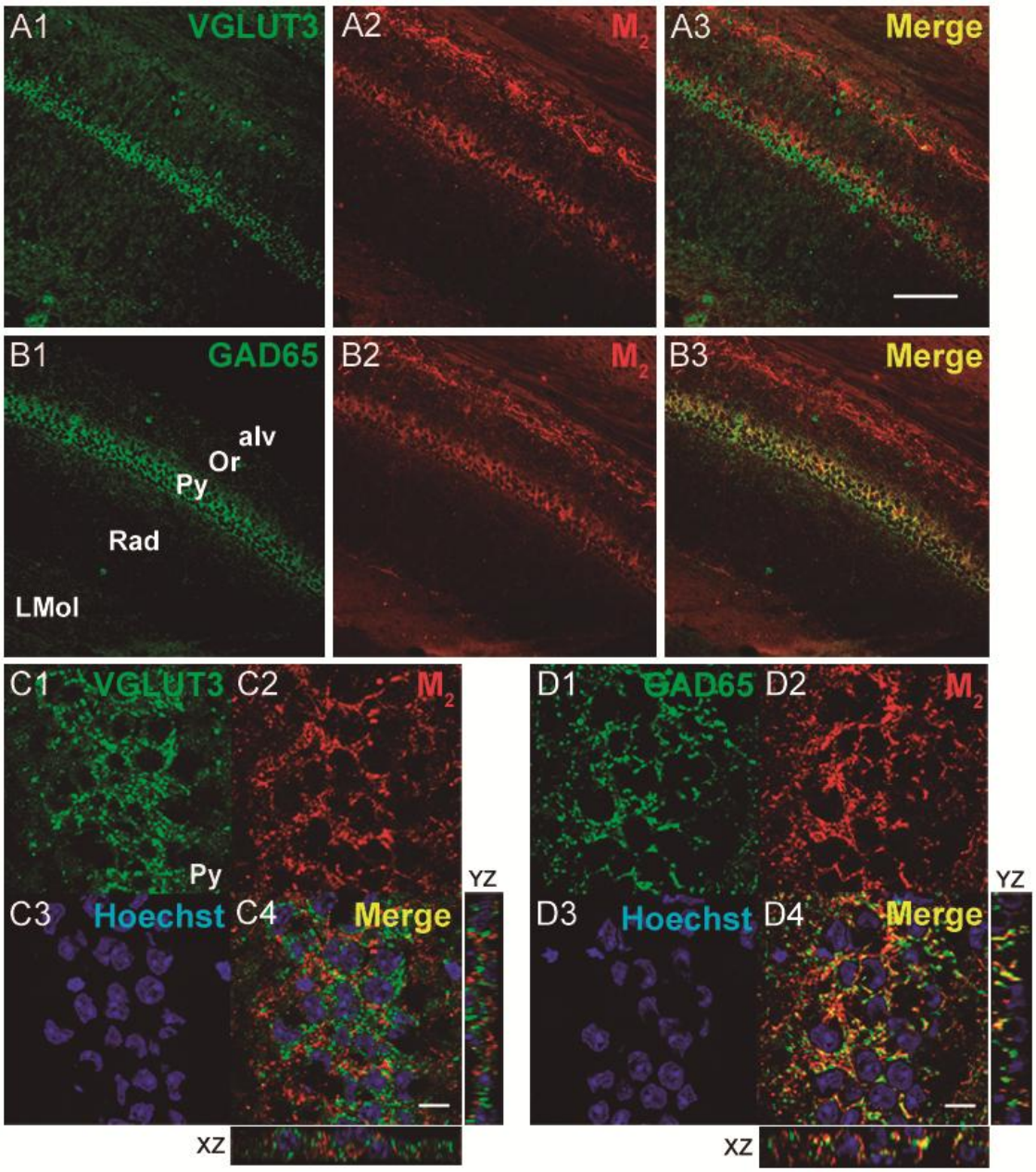

Figure 45. Double labeling of tissue slices including the CA1 field of the hippocampus from a representative 7-month-old 3xTg-AD mouse processed for M_2 (in red) and VGLUT3 (A1 and C1 in green) as a glutamatergic marker, and GAD65 (B1 and D1 in green) as a GABAergic presynaptic marker (B). The different hippocampal subfields exhibited specific M_2-immunostaining patterns delineating the perikarya of the large pyramidal neurons in basket-like formations. VGLUT3 was distributed near the nucleus (A1 and C1), presumably in the somatodendritic compartment of pyramidal neurons, while GAD65 immunostaining (B1 and D1) clearly delineated presynaptic inhibitory boutons. In low magnification images, note that M_2-immunoreactivity showed a complementary distribution to VGLUT3, surrounding the pyramidal neurons (A3), and was localized in GAD65-positive presynaptic terminals (B3); scale bar: 150 µm. High magnification images revealed the intracellular localization of VGLUT3 (C1) closely surrounding the nuclei stained with Hoechst (C3 in blue) and the almost complete lack of colocalization with M_2 (C4). Conversely, M_2 was distributed in GAD65-positive terminals, revealing the presynaptic localization on inhibitory synaptic boutons (C4). Scale bar = 10 µm. Bregma -3.08 mm. Alv: alveus of the hippocampus; Or: oriens layer of the hippocampus; Py: pyramidal cell layer of the hippocampus; Rad: radiatum layer of the hippocampus; LMol: lacunosum molecular layer of the hippocampus.

Discussion

The cholinergic hypothesis of AD was postulated in the early 1980s due to a big deal of evidence supporting the role of central cholinergic neurotransmission in learning and memory processes, as well as the specific vulnerability of this neurotransmitter system during the progression, but probably also at the onset, of AD (Bartus et al., 1982). From the first reports in the mid 1970s, which described degenerative processes of the basal forebrain cholinergic system by means of histochemical analyses in *postmortem* samples, up to the present, with the *in vivo* neuroimaging studies in AD patients, a large quantity of data has been acquired which points to the cholinergic neurotransmission arising from the basal forebrain as a key neuromodulatory element involved in the pathophysiology of AD.

Potentiation of cholinergic neurotransmission in the CNS has been a consistent challenge which has been addressed by using different therapeutic strategies. Since tacrine was approved by the FDA as the first AChE inhibitor for the treatment of symptoms of AD in 1997, the cholinergic drugs that inhibit the breakdown of ACh, donepezil, galantamine and rivastigmine, are considered to be the first choice in drug therapy for mild to moderate AD. On the other hand, several attempts to reduce the deficit of ACh by the administration of cholinergic enhancers or precursors such as Ch or lecithin have failed, whereas treatments based on phospholipids including PC and PS, or based on Ch alphoscerate and citicholine, provided slight, but noticeable benefits (Carotenuto et al., 2017).

Furthermore, lipid-based signaling molecules or neurolipids, which include eCB, contribute to cellular communication usually involving GPCR-mediated signaling. The synthesis of eCB can be stimulated by cholinergic neurotransmission through muscarinic receptor activation, and cholinergic neurotransmission is modulated by the eCB signaling through the activation of CB_1 receptors in several brain areas that control learning and memory processes. Specific membrane phospholipids may serve as lipid precursors for the synthesis of eCB as well as for the *de novo* synthesis of Ch. The described impairment of cholinergic neurotransmission observed in AD, together with altered eCB signaling and profound changes in the lipid profile, provide the clinical evidence in support of the general objective of this study, i.e., to analyze the relationship between both systems under neurodegenerative conditions by using different experimental models of basal forebrain cholinergic dysfunction.

Brain organotypic cultures lesioned with 192IgG-saporin as an *ex vivo* model of AD

Firstly, an ex vivo model of basal forebrain cholinergic lesion based on brain organotypic cultures was characterized and used to evaluate the effects of the activation of the eCB system by the synthetic cannabinoid agonist WIN55,212-2. Organotypic cultures of brain slices have become a useful tool with which to study the physiological and pharmacological properties of tissues. Brain organotypic slices can be maintained in culture for several weeks and represent a versatile, reproducible and rapid method to evaluate cellular interactions and mechanisms. Cultured brain slices can be treated with specific toxins to develop *ex vivo* models that mimic some neuropathological features of several neurological disorders. They can be considered an intermediate stage between *in vitro* cell cultures and *in vivo* models, maintaining a well-preserved three dimensional structure and the cytoarchitecture and the microenvironment of the original tissue, and they represent a powerful tool for the evaluation of the neuroprotective effects of different compounds (Daviaud et al., 2013).

Individual immunotoxins are designed in neuroscience research to eliminate specific cells or neuronal populations after binding to specific surface antigens. We have used 192IgG-saporin to specifically eliminate BFCN expressing $p75^{NTR}$ in hemibrain organotypic cultures from P7 rats. The immunotoxin-mediated depletion of BFCN in adult rats has been extensively described, but was first reported in the early 90s (Wiley et al., 1991). When 192IgG-saporin is administered to adult rats it induces a massive and specific loss of BFCN. However, the levels of expression of $p75^{NTR}$, as well as the cells expressing this receptor, vary during brain development and increase following neural injury (Ibañez and Simi, 2012). We first checked the anatomical distribution of the $p75^{NTR}$ receptor in the basal forebrain cholinergic system of formalin-fixed P7 rats, prior to the application of the immunotoxin to hemibrain organotypic cultures obtained from animals of exactly the same age. The immunofluorescence studies clearly demonstrated the presence of $p75^{NTR}$ in the different nuclei of the basal forebrain cholinergic system, including the MS, VDB, HDB and NBM, which expressed the highest levels of $p75^{NTR}$ immunoreactivity, consistent with the patterns of expression in the adult brain (Kiss et al., 1988; Woolf et al., 1989). The process itself for obtaining and further culturing brain organotypic cultures causes a massive lesion and damages to the integrity of the brain tissue, which could modulate the expression of $p75^{NTR}$, as suggested by Ibañez and Simi (2012), as well as the proliferation of glial cells surrounding the whole slice culture (del Rio et al., 1991). The application of

different concentrations of 192IgG-saporin to hemibrain organotypic cultures resulted in a significant loss of BFCN in a dose and time-dependent manner. It is well known that $p75^{NTR}$ mediates the retrograde transport of neurotrophins, and in a similar way contributes to the movement of the monoclonal antibody coupled to saporin from axon terminals. This process explains the loss of BFCN following the uptake of 192IgG-saporin when it is administered by intracerebroventricular (i.c.v.) infusion *in vivo* (Schweitzer, 1987; Heckers et al., 1994). As the hemibrain organotypic cultures were obtained in the coronal plane and BFCN display a rostrocaudal distribution pattern of axonal branching travelling in the sagittal plate, it is reasonable to assume that the anterior, the medial and the lateral basal forebrain cholinergic pathways described for rodents (Kristt et al., 1985), and conserved in human brain (Selden et al., 1998), are transected. Therefore, the only way for the internalization of 192IgG-saporin in hemibrain organotypic cultures is through $p75^{NTR}$ located in the somatodendritic compartment. This process also explains how 192IgG-saporin is uptaken when the immunotoxin is directly infused *in* vivo into the basal forebrain (intraparenchymal).

A secondary neuronal or cellular damage critically mediates the future fate of the neurons and cells which survive the initial lesion (Koch et al., 2011b). The present results suggest that a single daily *in vitro* application of increasing concentrations of 192IgG-saporin for three DIV begining on day five of *in vitro* culture triggers a partial loss of BFCN, which leads to secondary cellular damage. This secondary cell damage is further demonstrated by the increased levels of propidium iodide (PI) uptake when hemibrain organotypic cultures are treated on day two of the *in vitro* culture for 6 DIV. PI has previously been established as a marker that identifies degenerating cells in hemibrain organotypic cultures (Pozzo Miller et al., 1994**;** Dehghani et al., 2003). The density of PI positive cells is significantly higher than the values of $p75^{NTR}$ immunoreactive BFCN in organotypic cultures treated with 192IgG-saporin, providing further support of secondary neuronal or glial cell damage as a consequence of the initial BFCN lesion. A double application of the immunotoxin on days two and five of the *in vitro* culture was assayed to avoid the washout of the toxin when the culture medium was replaced, and showed more reproducible effects. The concentration of immunotoxin that was able to eliminate approximately 50%-60% of BFCN (EC50) was selected for further assays aimed at evaluating the effects of endocannabinoid system activation in this *ex vivo* model of AD.

The *in vivo* administration of 192IgG-saporin to adult rats triggers secondary alterations in different neurotransmitter systems such as a deregulation of the "on/off" glutamatergic/GABAergic signaling. Excitotoxicity could be one of the consequences together with cortical and hippocampal reorganization in an attempt to compensate for

the reduced cholinergic presynaptic input (Rossner et al., 1995a; reviewed in Rossner, 1997; Conner et al., 2003; Lee et al., 2016; Jeong da et al., 2016). More evidence of secondary neuronal or cellular damage is provided by the activation of microglia (Rossner et al., 1995d). Furthermore, different authors have reported findings which range from changes in dendritic morphology (Harmon and Wellman, 2003), to impairment of neuronal plasticity (Wellman and Sengelaub, 1991) and a negative impact on the adult neurogenic processes (Cooper-Kuhn et al., 2004). The consequences of the partial removal of BFCN in hemibrain organotypic cultures treated with the immunotoxin need to be evaluated and compared with *in vivo* administration. However, this model allows us to initiate the pharmacological evaluation of compounds that could ameliorate the subsequent effects on cell viability.

WIN55,212-2-mediated protective effects in the *ex vivo* model of basal forebrain cholinergic dysfunction

In the present study we observed that CB_1 receptors are involved in the WIN55,212-2-mediated reduction of PI uptake after 192IgG-saporin application because the protective effect of the synthetic cannabinoid agonist was blocked by the application of the specific CB_1 receptor antagonist AM251. The density of $p75^{NTR}$ immunoreactive neurons in the presence of WIN55,212-2 was not clearly enhanced, which may indicate that there is, a modest and probably indirect protective effect on the surviving BFCN. Therefore, the decrease in cell death observed in the presence of WIN55,212-2 is presumably related to secondary neuroprotective effects, and not to a direct protection from the toxic effects of 192IgG-saporin. On the other hand, WIN55,212-2 has a similar affinity for both CB_1 and CB_2 receptors. As mentioned above, the CB_1 receptor antagonist, AM251, blocked neuroprotection at a micromolar concentration, therefore, the contribution of microglial CB_2 receptors cannot be totally excluded.

The precise mechanism by which direct BFCN death induced by 192IgG-saporin spreads out to additional BFCN or non-cholinergic cells in hemibrain organotypic cultures remains elusive. The deleterious effects described in the *in vivo* model of 192IgG-saporin administration suggest that the protective effects mediated by CB_1 receptor activation in the present model could be related to the attenuation of excitotoxicity or to the modulation of aberrant synaptic transmission after BFCN degeneration, very probably involving the activation of glial cells. Excitotoxic brain lesions contribute to microglial activation and migration towards the sites of injury,

thereby increasing secondary damage (Kim and Ko, 1998; Kreutz et al., 2007). Neuroprotective effects of cannabinoid compounds have been previously described in models of excitotoxicity in organotypic cultures. Thus, 2-AG, through microglial CB_2 receptor activation or microglial abnormal-cannabidiol-sensitive receptor activation, triggers neuroprotective effects in hippocampal organotypic cultures, whereas Δ^9-THC or anandamide failed to provide neuroprotection, despite the fact that there was a reduction in microglial cell density (Kreutz et al., 2007; Kreutz et al., 2009). On the other hand, palmitoylethanolamide, through the peroxisome proliferator-activated receptor-alpha, together with WIN55,212-2 and N-arachidonoyldopamine, through CB_1 receptor activation, were able to induce neuroprotection in the same model of excitotoxicity. However, these effects were blocked by specific CB_1 receptor antagonists and were absent in mutant knockout mice (Koch et al., 2011a; Koch et al., 2011b; Grabiec et al., 2012). Interestingly, opposite effects of the phytocannabinoid Δ^9-THC and the synthetic agonist WIN55,212-2 have been described depending on the dose, but probably also on the time of exposure (Acquas et al., 2001, Tzavara et al., 2003a). The complexity of eCB signaling can be explained by the phenomenon of functional selectivity or biased agonism, i.e., the ability of ligands to activate a subset of the full repertoire of signaling cascades available to individual GPCR (Urban et al., 2007). Thus, the binding of WIN55,212-2 to CB_1 receptors significantly differs from that of other cannabinoids, such as 2-AG (Howlett et al., 2002). Different alternative signaling pathways could be activated by WIN55,212-2 in addition to classical eCB-mediated signaling cascades. Nevertheless, neuroprotective effects have been described for both cannabinoids, WIN55,212-2 and 2-AG, in different brain areas such as the hippocampal dentate gyrus (Koch et al., 2011b). Moreover, prolonged activation of the CB_1 receptor results in a rapid attenuation of signaling due to desensitization and/or CB_1 receptor internalization (Howlett et al., 2004). The internalized complex of phosphorylated CB_1 receptors and β-arrestins mediates intracellular signaling pathways that control the activation of several cascades, including ERK1/2, JNK1/2/3, CREB and P38a, and leads to the regulation of gene expression and protein synthesis which most likely contribute to the protective effects of chronic activation of CB_1 receptors by WIN55,212-2 (Delgado-Peraza et al., 2016).

The synthesis of eCB can be stimulated by neuronal damage, and their protective effects are exerted through CB_1 receptors, since the lack of this receptor increases neuronal vulnerability (Stella et al., 1997; van der Stelt et al., 2001a; Marsicano et al., 2003; Kallendrusch et al., 2012). The imbalance of the excitatory/inhibitory input described in the *in vivo* model of 192IgG-saporin administration could also contribute to an excessive glutamatergic neurotransmission

(Rossner et al., 1995a). A hyper-activation of glutamatergic receptors triggers an intracellular increase of Ca^{2+} levels, leading to excitotoxicity by which neurons can be damaged or killed (Manev et al., 1989). Interestingly, increasing levels of glutamatergic transmission after a 192IgG-saporin-induced lesion is prevented by the NMDA receptor antagonist, MK-801 (Garrett et al., 2006), and this effect is more pronounced in 192IgG-saporin-treated young adult rats than in middle-aged and aged rats (Kim et al., 2005), suggesting that cholinergic projections from the basal forebrain play a critical role in cortical plasticity, and also revealing age-related differences in the lesion-induced expression of glutamate receptors. The fact that a reduction in glutamatergic neurotransmission through NMDA receptors or decreased levels of Ca^{2+} influx may confer neuroprotective effects, led to the use of memantine, a noncompetitive antagonist of NMDA receptors, as a therapeutic drug for AD. Pharmacological enhancement of CB_1 receptor activity could elicit comparable effects and modulate excessive excitatory neurotransmission. Koch et al. (2011b) reported the neuroprotective effects of WIN55,212-2 in excitotoxically lesioned organotypic cultures, depending on the concentration of the agonist. Thus, low concentrations for three DIV elicited neuroprotection by directly activating CB_1 receptors. We observed decreased levels of cell death in the MS and in the NBM with low doses of WIN55,212-2 during 6 DIV in 192IgG-saporin-treated hemibrain organotypic cultures, and it is reasonable to assume that the neuroprotective effects may be related to a possible tissue or neurotransmission restoration by CB_1 receptor activation in cells which are still undefined, since the localization of CB_1 receptors in BFCN remains unclear. Data suggest that rodent BFCN in the NBM are devoid of CB_1 receptors but interestingly, all of them contain eCB degrading enzymes and display a fine CB_1 receptor fiber meshwork surrounding the perikarya, which suggests that BFCN may utilize eCB for retrograde control of cholinergic neurotransmission (Harkany et al., 2003). However, microscopy studies reported the existence of differentiated BFCN in the MS of the rat, some of which express CB_1 receptors (Nyíri et al., 2005). Additional studies are necessary to further understand the precise mechanisms underlying 192IgG-saporin-induced secondary cell damage, as well as the levels of expression, the precise location and the functionality of cannabinoid receptors under conditions of BFCN degeneration.

As mentioned above, brain organotypic cultures represent an intermediate stage between *in vitro* studies and *in vivo* models. The administration of 192IgG-saporin *in vivo* allows us to further understand the role of BFCN in learning and memory processes, in several histological and biochemical parameters and in the crosstalk with other neurotransmitter systems.

Learning and memory impairment following the administration of 192IgG-saporin in adult rats

The NBM is a neuronal nucleus which is located deeply within the brain, close to the border of the ventral limit. Firstly, we analyzed the mechanical lesion produced by the needle crossing from the dorsal cranial surface to almost the ventral border, and the intraparenchymal infusion of the vehicle. Previous studies from our laboratory demonstrated that the administration of the vehicle by using a common Hamilton syringe was sufficient to produce brain damage which led to learning and memory deficits in the control group, as observed in the passive avoidance test. Therefore, a new model of Hamilton neurosyringe, equipped with an ultra thin gauge needle, was used in order to minimize the mechanical lesion.

Eight days after the intraparenchymal infusion of 192IgG-saporin, 75% of BFCN in the NBM had disappeared leading to learning and memory impairment, as demonstrated by the results of the passive avoidance test. In the retention trial, 100% of SHAM-operated rats remembered the foot-shock and no statistically significant differences were observed between SHAM-operated and aCSF-treated groups. Moreover, the histochemical (AChE staining) and immunohistochemical ($p75^{NTR}$-immunoreactivity) studies revealed similar densities of BFCN in SHAM-operated rats and in those which had received aCSF used as the vehicle, thereby demonstrating that the intraparenchymal infusion of the vehicle by itself had no effect on the survival rate of BFCN. The extent of the specific basal forebrain cholinergic lesion was also demonstrated by the dramatic loss of AChE-positive fibers in cortical regions. The infusion of 192IgG-saporin had no effects on acquisition latency, suggesting that the motivation to explore, the level of anxiety and/or the motor functions of the rats were apparently unaffected. In this context, longer acquisition latency times in the passive avoidance test induced by BFCN depletion in the medial septum have been reported, showing that there are different effects on aversive learning, depending on the specific cholinergic nucleus lesioned (Babalola et al., 2012). As already mentioned, 192IgG-saporin is directed against $p75^{NTR}$, which is predominantly expressed in BFCN from the MS, VDB, HDB and NBM (Wiley et al., 1991). The specificity of the lesion in the NBM is demonstrated by the absence of damage in the complex MS-VDB (Ch1-Ch2) which mainly innervates the hippocampus, as observed by AChE staining. The evaluation of learning and memory behavior in the present study does not discriminate other parameters such as acquisition, consolidation, extinction or retrieval of new aversive information, but previous studies using the olfactory discrimination learning test have

demonstrated that 192IgG-saporin-induced lesions of the NBM impair attention capacity and early acquisition during a learning process (Bailey et al., 2003).

Kaplan-Meier survival curves were used to graphically represent the estimated probability of reaching the cut-off time (300 s) for each group. Then, data were analyzed by using the Log-rank/Mantel-Cox test to compare the survival distributions or the estimated probability of each group to reach the cut off time. Doing so was regarded as a positive response. It was found that a statistically significant higher percentage of immunotoxin-treated animals showed a negative behavioral response in comparison with those which had received aCSF.

The present results provide evidence that cortical cholinergic innervation arising from the NBM plays a pivotal role in learning and memory processes. In previous studies, step-through latency times were represented as histograms, evaluating censored latency times (cut-off time of 300 s) as threshold values, but the above-mentioned statistical analysis is more appropriate to test the probability of reaching the cut-off time and eliminates the threshold bias. Based on a previous report, the statistical handling of data in the present study improves the analysis of the results and represents an alternative way to interpret behavioral responses when using the passive avoidance paradigm (Barreda et al., 2015).

The effects of cholinergic lesions on learning and memory have been extensively studied, but controversial data have been reported depending on the severity of the lesion, the dose, schedule and route of 192IgG-saporin administration, the specific cholinergic nucleus affected or the passive avoidance test conditions (reviewed in Myhrer, 2003). A previous study demonstrated that a 50% reduction of BFCN in the NBM produced a 25-30% decrease in ChAT activity, but was not sufficient to impair memory five weeks after lesioning (Wenk et al., 1994). The experimental design differed from ours in several aspects: lower doses of the immunotoxin, repeated learning trials and footshock deliveries, the post-operatory recovery period and the statistical analysis used. Our results are consistent with other studies which have demonstrated that avoidance testing is impaired after a specific lesion in the NBM with the excitotoxins ibotenic acid (Flicker et al., 1983; Hepler et al., 1985; Whishaw et al., 1985), or quisqualic acid (Aaltonen et al., 1991; Riekkinen et al., 1991a,b, 1993; Zupan et al., 1993). In the studies using non-specific excitotoxins, the effects of the lesions are not restricted to BFCN, but also affect to non-cholinergic neurons in the same structures (Kosaka et al., 1988). However, when the lesion was induced with 192IgG-saporin, other authors reported small, but significant deficits associated with the BFCN lesion in the NBM in a single learning trial of the passive avoidance test (Torres et al., 1994). Moreover, and consistent with the present results, the relationship between the

severity of passive avoidance behavioral deficits and the degree of BFCN loss was demonstrated (Zhang et al., 1996; Martinez-Gardeazabal et al., 2017). The present findings unequivocally support the pivotal role of NBM-cortical cholinergic neurotransmission in learning and memory processes in rats.

The loss of BFCN induces alterations in density and functionality of M_2/M_4 mAChR

Different alterations related to the cholinergic neurotransmission have been reported in *postmortem* samples from AD patients (Davies and Maloney, 1976; Davies, 1979; Whitehouse et al., 1982; Rodríguez-Puertas et al., 1994 and 1997; Flynn et al., 1995). In the present study, functional autoradiography showed a decrease in carbachol-induced stimulation of [^{35}S]GTPγS binding in the NBM and an increase in hippocampus, but no significant change in this parameter was observed in the entire cortical mantle of 192IgG-saporin-treated rats. Although the cholinergic connectivity between these three brain areas is not fully understood, they are all areas involved in learning and memory.

BFCN from the NBM are thought to express M_2 and/or M_4 mAChR as autoreceptors in the synaptic terminals. Therefore, in the lesion model the decrease in M_2/M_4 mAChR activity recorded at the NBM may be a direct consequence of the lesion and indicates a loss of cholinergic interconnections within the nucleus that constitutes the cholinergic basal forebrain. However, despite the elimination of up to 70% of presynaptic basal forebrain cholinergic terminals in some cortical regions of 192IgG-saporin-treated rats, the [^{35}S]GTPγS autoradiographic study showed no differences in the functional coupling of M_2/M_4 mAChR to $G_{i/o}$ proteins in the cortical areas analyzed. M_2 and M_4 mAChR are differentially distributed in the cortex. Thus, M_2 mAChR-immunoreactivity is dense in the deeper layers of the cortex, is located in cell bodies, and is associated with fibers and presumably terminals, and occasionally with perikarya. Using the NBM-lesioned rat model, previous studies reported a decrease in M_2 mAChR density in frontal and parietal cortices seven days after ibotenic acid administration or mechanical lesioning of the NBM, by means of autoradiography and *in situ* hybridization techniques, which is in consistent with the presynaptic localization of M_2 mAChR in BFCN terminals (Bogdanovic et al., 1993; Schliebs et al., 1994). As previously mentioned, mechanical or excitotoxin-based lesioning of the BFCN may trigger non-specific damage to non-cholinergic neurons, and this could result in contradictory results. Therefore, when the lesion was produced by 192IgG-saporin, as

observed in the study of Rossner et al. (1995b), an increase of up to 20% in M_2 mAChR density in the parietal cortex was reported, suggesting the existence of a significant population of M_2 mAChR located postsynaptically (reviewed in Rossner, 1997). In AD, the severe loss of cortical cholinergic innervation is accompanied by a depletion of M_2 mAChR, but M_1 mAChR density remains relatively stable (Mash et al., 1985). It has been assumed that the M_2 mAChR is a presynaptic autoreceptor located in all cholinergic axons which arise in the NBM and innervate the cerebral cortex, the NBM being the main source of cortical M_2 mAChR. The depletion of M_2 mAChR was therefore thought to be the consequence of the cholinergic axonal loss in AD. However, the expression of M_2 mAChR in BFCN terminals still remains controversial. The interpretation of some authors was that the cholinergic axons coming from the NBM do not substantially contribute to the overall pool of cortical M_2 mAChR, and M_2 mAChR-expressing postsynaptic neurons could be partially responsible for the decrease of these receptors observed in AD (Mesulam, 1998). The existence of cortical postsynaptic M_2 mAChR and/or the possibility that they are located in non-cholinergic terminals of either intrinsic or extrinsic origin, makes it plausible that the degeneration of cortical M_2 mAChR-immunoreactive neurons could also be contributing to the described loss of M_2 mAChR in AD (Mrzljak et al., 1998; Raevsky et al., 1998). Interestingly, electron microscopic analysis failed to reveal changes in M_2 mAChR distribution following the intraparenchymal administration of 192IgG-saporin in the NBM of rhesus monkeys, and moreover, clearly showed that membrane-linked receptors were also located in dendritic spines of pyramidal neurons and associated with membranes in all cellular compartments of nonpyramidal neurons (Mrzljak et al., 1998). Furthermore, M_2 mAChR which modulate ACh release are not located in NBM cholinergic terminals, but are predominantly found in the membranes of postsynaptic sites in the NBM (Meyer et al., 1987; Pascual-Alonso and Gonzalez-Zarate, 1992; Decossas et al., 2003). However, the co-expression of M_2 mAChR at presynaptic sites and VAChT has been observed by using both light and electron microscopy (Decossas et al., 2003).

On the other hand, the cortical pool of M_4 mAChR is relatively small and this subtype is mainly located in the neuropil and in scattered perikarya (Levey et al., 1991). The reported localization of M_4 mAChR binding sites and mRNA is comparable in all layers of the neocortex (Buckley et al., 1988; Sugaya et al., 1997; Vilaró et al., 1994). The present immunofluorescence assays revealed a higher density of M_4 mAChR located in somas and plasma membrane, in comparison with M_2 mAChR, which seem to be located presynaptically, clearly showing that there is a different pattern of distribution. Although we did not observe changes in the activity mediated by

M_2/M_4 mAChR in cortical areas, the role of cortical M_4 mAChR in this lesion model and their precise distribution remains unclear. Further research into the role of these receptors, carried out by using this model of basal forebrain cholinergic dysfunction, could provide valuable physiological information.

The immunosignal associated with both M_2 and M_4 mAChR was dramatically reduced in the basal forebrain after the lesion, thereby providing evidence of the contribution of both receptors to the cholinergic neurotransmission impairment in the NBM. As previously described, the precise anatomical distribution of M_2 and M_4 mAChR in the basal forebrain still remains controversial, but present immunohistochemical findings suggest a mainly presynaptic localization of M_2 mAChR and a somatodendritic distribution of M_4 mAChR in the BFCN of the NBM. However, the expression of M_2 mAChR and M_4 mAChR in BFCN, including those from the MS, VDB, HDB and NBM, has previously been studied by using *in situ* hybridization, [^{3}H]-oxotremorine autoradiography and immunohistochemical assays (Harata et al., 1991; Vilaró et al., 1992 and 1994; Sugaya et al., 1997). The co-expression of these receptors and ChAT has also been detected in approximately 80% of BFCN by using light and electron microscopy (Decossas et al., 2003**)**. In addition, dissociated NBM neurons are stimulated with carbachol and antagonized with the M_2 mAChR antagonist, AF-DX-116 (Harata et al., 1991**)**.

In summary, the present findings show a significant decrease in $G_{i/o}$-mediated muscarinic signaling in the NBM, mediated by the pool of presynaptic M_2 and somatodendritic M_4 mAChR, and the absence of changes in pre- and postsynaptic M_2/M_4 mAChR-mediated signaling in the cortex of immunotoxin-treated rats. Eight days after the administration of 192IgG-saporin, the loss of both the cortical source of ACh and the M_2/M_4 mAChR-mediated signaling associated with the loss of BFCN in the NBM could contribute to the deregulation of cortical neurotransmission responsible for the cognitive impairment observed in the passive avoidance test.

Conversely, the increased M_2/M_4 mAChR-mediated signaling in the dentate gyrus and CA3 regions of the hippocampus, cannot be directly attributed to cholinergic denervation from NBM because the major source of cholinergic innervation to the hippocampus proceeds from the MS and the VDB. In fact, the results of the autoradiographic assays and the AChE staining in these nuclei were similar to those obtained in the aCSF group, suggesting the absence of non-specific damage to other basal forebrain cholinergic nuclei, except that generated in the NBM. Nevertheless, lesions directed at the septohippocampal cholinergic projections have been used to evaluate the involvement of this pathway in cognition (Baxter et al., 2013; Köppen et al., 2016), and to explore the distribution of mAChR in the hippocampus at different

postsurgical times, demonstrating dynamic changes in densities of pre- and postsynaptic pools of M_2 and M_4 mAChR (Bauer et al., 1992; Wall et al., 1994; Levey et al., 1995).

Our immunofluorescence studies in the hippocampus suggest that the M_2 mAChR in the granular dentate gyrus and pyramidal CA1-CA3 are located presynaptically, whereas the M_4 mAChR are postsynaptically distributed in the somatodendritic compartment of pyramidal neurons. Furthermore, presynaptic M_2/M_4 mAChR inhibit ACh release (Raiteri et al., 1984; Levey et al., 1995). In this context, the observed increase in hippocampal cholinergic neurotransmission through M_2 mAChR may contribute to the so-called “muscarinic long term potentiation” mediated by the potentiation of glutamatergic NMDA receptors, essential to explain hippocampal neuronal plasticity (Segal and Auerbach, 1997). Interestingly, mice lacking M_2 mAChR, but not mice lacking M_4 mAChR, showed deficits in learning and memory, as demonstrated by means of the passive avoidance test, together with profound alterations in ACh homeostasis in the hippocampus, suggesting that the M_2 mAChR subtype plays a crucial role in cognitive processes (Tzavara et al., 2003b). Additional studies in M_2 mAChR knockout mice reported significant deficits in the Barnes circular maze. In addition, this was associated with impairment in both short- and long-term potentiation and was completely reversed with the $GABA_A$ receptor antagonist, bicuculline (Seeger et al., 2004). M_2 mAChR are also expressed in diverse hippocampal interneurons and control GABA release from presynaptic inhibitory terminals which leads to an increase in activity in the dendritic region of pyramidal neurons (Hajos et al., 1998). The increase in hippocampal muscarinic functionality mediated by M_2 mAChR may modulate the GABAergic tone to compensate for excitatory-inhibitory imbalance. The M_4 mAChR subtype might also be involved in neuronal plasticity-associated learning and memory formation, as has been reported in adrenalectomized rats, whereas the loss of M_4 mAChR leads to dysfunction in hippocampal synaptic transmission (Mulugeta et al., 2006).

However, the influence of other neurotransmitter systems in learning and memory processes has been studied using the passive avoidance paradigm. Dopaminergic antagonists either impair (Lazarova et al., 1991; Doyle and Regan, 1993), or improve (Chugh et al., 1991), passive avoidance performance, while glutamatergic and GABAergic antagonists usually impair it (Venable and Kelly, 1990; Anglade et al., 1994). To fully understand learning and memory processes, it is necessary to clarify the interaction among the different neurotransmitter systems and each one´s contribution to the cognitive deficits associated with aging and AD. In this context, the eCB system modulates the release of the above-mentioned

neurotransmitters (Katona et al., 2001), regulates diverse physiological processes including learning and memory (Busquets-García et al., 2011), and is deregulated under neurodegenerative conditions such as AD (Manuel et al., 2014, Mulder et al., 2011).

Endocannabinoid signaling is modulated in the *in vivo* model of BFCN depletion

Once the model of BFCN depletion in the NBM was validated and cholinergic neurotransmission and cognitive impairment were demonstrated, we further explored a possible interaction between cholinergic neurotransmission and CB_1 receptor-mediated eCB signaling. Some authors propose that rodent BFCN are devoid of CB_1 receptors, but all BFCN contain eCB degrading enzymes and exhibit a fine CB_1 receptor immunoreactive fiber meshwork surrounding the perikarya, which suggests that BFCN may use eCB for retrograde control of neurotransmission (Harkany et al., 2003). Similar results were obtained in the gray mouse lemur, revealing evolutionarily conserved networks (Harkany et al., 2005). However, other studies reported a dense labeling of CB_1 receptor in ChAT positive neurons in monkey basal forebrain (Lu et al., 1999), and the existence of BFCN expressing CB_1 receptors in rat (Nyíri et al., 2005). The eCB compounds act as retrograde synaptic messengers on presynaptic CB_1 receptors, fine-tuning neurotransmitter release (Katona et al., 2001; Ohno-Shosaku et al., 2001). To further understand the role of CB_1 receptors, it is important to study which elements of the brain's excitatory-inhibitory networks, i.e., GABAergic or glutamatergic, express this receptor. GAD65, the smaller isoform of the enzyme, glutamic acid decarboxylase, is associated with nerve terminals (Kash et al., 1999), while VGLUT3 is expressed in synaptic buttons, but mainly in somatodendritic compartments (Herzog et al., 2004).

CB_1 receptor-mediated signaling in the NBM and hippocampus of 192IgG-saporin treated rats

The present findings show the loss of three quarters of BFCN in the NBM following the intraparenchymal infusion of 192IgG-saporin, but the autoradiographic studies revealed an increase in both density and activity of CB_1 receptors in the NBM of lesioned rats. The CB_1 up-regulation could indicate an activation of the system in order to counteract the effects of the lesion, but the precise anatomical distribution of

CB_1 receptors and the neurophysiological relevance of this modulation still remain unclear. Nevertheless, our results are consistent with those obtained by Harkany et al. (2003), which suggests the absence of a somatodendritic distribution of CB_1 receptors in BFCN.

Conversely, the decreased eCB signaling in the hippocampus cannot be explained as a direct consequence of cholinergic denervation since the NBM mainly projects to the cortex. It could be a secondary neuroadaptive process, which somehow either compensates for or even worsens the loss of cortical cholinergic inputs. Previous immunochemical studies indicated the inhibitory role of hippocampal CB_1 receptor-positive terminals which had before been described as GABAergic interneurons (Katona et al., 1999; Tsou et al., 1999). However, further studies demonstrated that CB_1 receptors are also present in hippocampal glutamatergic synapses, albeit at much lower levels (Katona et al., 2006; Kawamura et al., 2006). In this context, despite the reported negative effects of cannabimimetics on memory in humans, the literature fails to provide strong evidence for hippocampal CB_1 receptor-mediated action (reviewed in Davies et al., 2002) although, a recent study associates hippocampal mitochondrial CB_1 receptors with learning and memory impairment (Hebert-Chatelain et al., 2016). The present study shows a moderate decrease in CB_1 receptor density and activity in the hippocampus of BFCN-lesioned rats and the immunofluorescence images clearly indicate that CB_1 receptors are mainly located in GABAergic presynaptic terminals. Transgenic mice with enhanced GABAergic inhibition exhibit impairment in both hippocampal long-term potentiation (LTP) and Morris water maze performance (Gong et al., 2009) and, moreover, learning and memory deficits in these mice or in wild-type mice treated with Δ^9-THC are reversed by $GABA_A$ receptor antagonists (Varvel et al., 2005; Cui et al., 2008). In this sense, a decrease in the eCB signaling in certain hippocampal regions may induce an increase in the GABAergic tone and probably contributes to the cognitive impairment observed in the passive avoidance test. CB_1 receptor-mediated signaling is also affected in the hippocampus of patients diagnosed with severe AD (Manuel et al., 2014). The present animal model shows a considerable reduction in BFCN, which partially mimics the serious degeneration of the basal forebrain cholinergic pathway which innervates the hippocampus through the entorhinal cortex described in AD patients in the final Braak's stages (V-VI) of the disease (Ikonomovic et al., 2003).

CB_1 receptor-mediated signaling in the cortex of 192IgG-saporin treated rats

The dramatic reduction in cortical cholinergic projections following the infusion of the immunotoxin, as observed by AChE staining, was not accompanied by a similar

decrease in [^{3}H]CP55,940 binding in any of the different regions of brain cortex which suggests the absence of synthesis of CB_1 receptors in the BFCN. These results are in agreement with previous immunochemical studies which reported that cortical cholinergic terminals lack any detectable CB_1 receptors (Harkany et al., 2003). Interestingly, the hyperactivity of cortical CB_1 receptor-mediated eCB signaling that we found in BFCN lesioned-animals was similar to that described in human brain during the early stages of AD (Manuel et al., 2014). Therefore, we further explored the different regulation of receptors in the cortex at the subcellular level by carrying out immunofluorescence studies (see next section).

CB_1 receptor activation is involved in the regulation of cortical glutamatergic input; CB_1 receptor agonists inhibit, while the antagonist, SR141716A, enhances cortical glutamatergic synaptic transmission and favors LTP (Auclair et al., 2000). CB_1 receptor–dependent activation is thought to be an early step in a protective cascade against kainic acid-induced excitotoxicity (Marsicano et al., 2003). A CB_1 receptor-mediated decrease in TNFα-induced expression of AMPA receptors protects against excitotoxic neuroinflammation (Zhao et al., 2010). As mentioned above, Garrett et al. (2006) reported increased levels of cortical glutamatergic transmission induced by the infusion of 192IgG-saporin in the NBM. In addition, previous studies using a similar lesion in basal forebrain showed a marked reduction in NMDA, α_2-and β-adrenoceptors and 5-HT_{2A} receptors, an increase in AMPA, kainate and $GABA_A$ receptors and a decrease in high-affinity choline uptake sites in cortical regions (Rossner et al., 1994, 1995c; Schliebs et al., 1994; Heider et al., 1997). On the basis of such compelling data, the 192IgG-saporin-induced lesion in the NBM clearly leads to an irreversible loss of cholinergic innervation in almost the entire cortical mantle, sufficient to lead to an excess of excitatory neurotransmission that may be controlled by the activation of CB_1 receptors present in cortical areas.

Decreased cortical presynaptic GABAergic inputs after the BFCN lesion

Previous studies have reported that almost all CB_1 receptor-positive cortical cells also express cholecystokinin and GAD65, confirming the existence of an inhibitory phenotype of CB_1 receptor containing terminals (Marsicano and Lutz, 1999). By using optical and electron microscopy, other authors described a presynaptic localization of CB_1 receptors in GABAergic nerve terminals, as well as a compartmental distribution of these receptors in cell bodies of two distinct subpopulations of cholecystokinin or calbindin positive interneurons in rat somatosensory cortex and in calbindin positive

interneurons in rat prefrontal cortex (Bodor et al., 2005; Wedzony and Chocyk, 2009). These studies demonstrated that, independently of the precise anatomical location, CB_1 receptor-mediated signaling promotes specific inhibitory functions**.** The present immunofluorescence studies did not help us to determine its precise location, but a marked decrease of GAD65-immunoreactivity was found, suggesting either a down-regulation of GAD65 density or a loss of inhibitory cortical inputs. The results confirm that the BFCN terminals are essentially devoid of CB_1 receptor expression and this model exhibits a selective down-regulation of the presynaptic cortical GABA-synthesizing enzyme. In this context, a reduction in brain cholinergic metabolism, accompanied by decreased GAD levels, was found in samples from AD patients (Perry et al., 1977). A recent study demonstrated that 192IgG-saporin-induced BFCN loss was sufficient to decrease GAD65/67 levels in the prefrontal cortex, promoting the overexpression of the glutamate transporter. Moreover, deep brain stimulation of the remaining BFCN in the NBM improved spatial memory and partially restored GAD65/67 to control levels (Lee et al., 2016). The excessive excitatory neurotransmission described in this model is prevented by NMDA receptor antagonists and BFCN are essential for enabling plasticity mechanisms required for functional recovery after cortical brain injury (Conner et al., 2005; Kim et al., 2005; Garrett et al., 2006).

The present findings demonstrate that a BFCN lesion in the NBM impairs memory and triggers changes in cortical eCB signaling together with a decrease in cortical GABAergic immunoreactivity. BFCN represent the main source of cortical ACh and contribute to the inhibitory tone in cortical projections. The depletion of BFCN also contributes to a deregulation of excitatory neurotransmission, which probably explains the hyperactivation of CB_1 receptors. We propose that a CB_1 receptor-mediated regulation of the cortical eCB tone is a compensatory mechanism to regulate a possible BFCN death-evoked glutamatergic-GABAergic imbalance. Further studies should be focused on discovering wether the eCB system is being regulated in response to excessive glutamatergic neurotransmission or, conversely, contributes to its worsening. Understanding the underlying mechanisms of this regulation could lead to the discovery of innovative cannabinoid-based pharmacological approaches towards the treatment of common pathological features of different neurological disorders.

In summary, the results from studies using the *in vivo* model of basal forebrain cholinergic dysfunction show that the intraparenchymal administration of 192IgG-saporin into the NBM of adult rats selectively eliminates BFCN and leads to a dramatic loss of cortical cholinergic innervation, accompanied by changes in the activity of M_2/M_4 mAChR and CB_1 receptors in the NBM-cortico-hippocampal circuitry. During the progression of AD, basal forebrain cholinergic pathways degenerate causing disrupted

supply of ACh and irreversible impairment of memory and thinking abilities, together with changes in lipid homeostasis and neurolipid neurotransmission, such as eCB signaling (Whitehouse et al., 1982; Wymann and Schneiter, 2008; Mulder et al., 2011; Manuel et al., 2014). The regulation of lipid composition is especially relevant in brain processes which require a modification of cell membranes, including the formation of new memories for which the genesis of dendritic spines and new synapses are necessary. Therefore, all deregulated levels or changes in the distribution of certain lipid species could be indicating adaptations, but may also be underlying mechanisms associated with neurodegeneration. There follows a description of the lipid profile of 192IgG-saporin-treated rats which focuses on the analysis of the phospholipid species that are suspected of being used as precursors for the synthesis of both ACh or eCB when there is specific basal forebrain cholinergic neurodegeneration.

Lipid profile in NBM and cortex in the rat model of BFCN lesion

MALDI-IMS analysis showed changes in the brain lipid profile of 192IgG-saporin-treated rats. The relative intensities of different lipid species, including PC, SM, PE and PS were modified in the basal forebrain and in areas of cortical projection.

ChAT enzyme has low affinities for Ch and acetyl-CoA, and the rate of synthesis of ACh mainly depends on the levels of Ch (Millington and Wurtman, 1982; reviewed in Blusztajnn and Wurtman, 1983). As previously mentioned, the 192IgG-saporin-induced lesion model causes a considerable reduction in the level of ACh. Moreover, the loss of approximately 50% of BFCN has been associated with 40-60% reductions in ChAT and SDHACU activities throughout the basal forebrain cholinergic system (Rossner et al., 1996). In this context, the membrane phospholipids become an important source from which Ch can be synthesized *de novo*. This *de novo* synthesis requires PE from any membrane pool as a substrate to be sequentially methylated to PC (Bremer et al., 1960a,b). PC can be hydrolyzed to free Ch by membrane-associated phospholipase D (PLD) activation (Hattori and Kanfer, 1984; Blusztajn et al., 1987a; Exton, 1999). Phosphatidylinositol 4,5-bisphosphate (PIP_2), protein kinase C (PKC) and phorbol esters stimulate PLD activity which, furthermore, has been found to be reduced by up to 63% in homogenates of brain tissue samples from AD patients (Kanfer et al., 1986; reviewed in Exton, 1999). Then, Ch can be acetylated to form ACh in order to sustain neurotransmission at the expense of membrane formation which may finally impair synaptic plasticity or compromise membrane viability (Maire and

Wurtman, 1985; Ulus et al., 1989). Wurtman et al. (1985) described this process as autocannibalism of the cholinergic cells.

On the other hand, the synthesis of eCB is comparable to the described alternative source of Ch. The eCB are not stored in intracellular compartments or vesicles, as are other classical neurotransmitters; they are synthesized on demand by receptor-stimulated cleavage of membrane lipid precursors. The pathways leading to the synthesis and release of AEA and 2-AG from neuronal and non-neuronal cells are still somewhat unclear. In this context, different authors have found a relationship between cannabinoid and cholinergic neurotransmission (Gifford et al., 1996; Kathman et al., 2001; Fukudome et al., 2004). Therefore, it is tempting to interpret the modifications of lipid composition in the *in vivo* model of basal forebrain cholinergic dysfunction as potential precursors for both eCB and Ch synthesis.

If the hydrolysis of phospholipids from membranes of presynaptic terminals (cortical area) and/or the somatodendritic compartment (NBM area) served for the *de novo* synthesis of Ch, one would expect a regulation of certain lipid species in both anatomical regions due to the loss of approximately 80% of BFCN in the NBM and 60% of cortical cholinergic innervations.

Phosphatidylcholines and phosphatidylserines

We found an increase in PC (36:1) + Na^+ in NBM and a reduction in cortical regions, while PS (18:0/18:1) was found to be decreased in the NBM after the infusion of 192IgG-saporin. The physiological role of PC (36:1) + Na^+ still remains unclear, but its presence in both rat and human brain, mainly in regions of white matter has been previously described (Jackson et al., 2005a,b; Astigarraga et al., 2008; Veloso et al., 2011). The proliferation of glial cells and the loss of both BFCN in the NBM and in the cortical cholinergic axons could explain either the increase or the decrease in the levels of this particular species in the NBM and cortex, respectively. The characterization of the lipid profile of the different types of cells present in the CNS could verify this interpretation. Moreover, these changes may also be an indication of an adaptive process with which to reconstruct the axonal branching following lesioning of the BFCN, rather than an alternative source for *de novo* synthesis of Ch. On the other hand, under normal physiological conditions, PS (18:0/18:1) is preferentially located in the inner leaflet of the plasma membrane, but the loss of asymmetry is an early indicator of apoptosis and/or glia-mediated synaptic pruning to remodel the neural circuit (Fadok et al., 1992; reviewed in Bevers and Williamson, 2016). The loss of PS asymmetry with increased externalization to the outer leaflet of the lipid bilayer has been described in samples from AD patients (Bader Lange et al., 2008). 18 h after the

internalization of saporin, apoptosis is induced, and apoptotic activity is enhanced when the toxin is bound to immunoglobulins such as 192IgG (Bergamaschi et al., 1996). These findings suggest that the loss of PS (18:0/18:1) in the NBM may be a consequence of the immunotoxin-induced depletion of BFCN and, therefore, is probably not related to phospholipid hydrolysis for eCB or Ch synthesis.

In addition, PC (40:6) + Na^+ and PC (36:4) + K^+, which are mainly present in the gray matter of rat CNS, were also found to be increased in the NBM and in the cortex. PC (40:6) + Na^+ is probably composed of stearic acid (18:0) and docosahexaenoic acid (DHA; 22:6), the latter being a polyunsaturated fatty acid (PUFA) which, when added to the diet of hypertensive rats, restores both their cerebral Ch and ACh levels and their performance in the passive avoidance test (Minami et al., 1997). Furthermore, there is a large body of evidence which indicates that DHA has important biological functions in neuronal homeostasis, mostly linked to its role in neurogenesis, synaptogenesis, neuronal differentiation, neurite outgrowth and maintenance of membrane fluidity, and this could be consistent with the need to repair the structural brain damage induced by 192IgG-saporin (Belkouch et al., 2016). The most probable acyl chain composition of PC (36:4) + K^+, is palmitic acid (16:0) and AA (20:4). Interestingly, AA is a well-known pro-inflammatory precursor but, indeed, phospholipids containing AA are the most suitable candidates as precursors for the synthesis of the eCB, AEA and 2-AG (Di Marzo et al., 1994; Sugiura et al., 1995). Moreover, the synthesis of eCB can be stimulated not only by neuronal damage (Stella et al., 1997; Marsicano et al., 2003; van der Stelt et al., 2001a) but also by the activation of $G\alpha_{q/11}$-coupled mAChR (Kim et al., 2002), and the suppression of CB_1 receptors increases neuronal vulnerability (Marsicano et al., 2003). By using genetically modified mice lacking any of the subtypes of mAChR, it was demonstrated that $G\alpha_{q/11}$-coupled mAChR activation is responsible for the PLCβ-mediated stimulation of 2-AG synthesis which finally induces short-term plasticity at cholinergic synapses (Fukudome et al., 2004).

The study of lipids in samples from AD patients reveals an enhancement of plasmatic levels of PC (40:6) which has been found to positively correlate with CSF tau concentrations in AD patients carrying the *presenilin1* mutation (Chatterjee et al., 2015). In contrast, plasmatic levels of PC (36:4) and PC (40:6) have been found to be decreased in AD and have been proposed as biomarkers of phenoconversion to either amnestic mild cognitive impairment or late-onset AD (Mapstone et al., 2014; Fiandaca et al., 2015). Reduced relative densities of PC species have been found in AD brains and attributed to a pathological hyperactivation of phospholipase A2 (PLA2) (Nitsch et al., 1992; Klein, 2000). The result of this is an increase in the breakdown of certain phospholipids and a variation in the ratio of saturated and unsaturated fatty acids in PC

and PE (Mulder et al., 2003). These findings suggest a different regulation in the biosynthesis, turnover, and acyl chain remodeling of phospholipids in AD. Essential PUFA, such as AA and DHA, provide the structural functionality of the membranes, but lipid catabolism (e.g., during neurodegeneration, neuroinflammation or autophagy) generates intermediate metabolites that are not usually recycled, and increased demands are made on the bloodstream (Fiandaca el al., 2015). This could explain the decreased levels of PC (36:4) and PC (40:6) recorded in plasma from AD patients, in contrast with the increase observed in 192IgG-saporin-treated rat brains. Additional lipidomic studies of brain samples from AD patients are necessary to further elucidate if the plasmatic levels of certain lipid-based biomarkers correlate in some way with those levels observed directly in the brain tissue by means of imaging techniques such as MALDI-IMS.

Sphingomyelins

There was a significant increase in the levels of SM (d18:1/16:0) + K^+ in the NBM, but the SM (d18:0/18:1) + H^+ was found to be significantly decreased in the same region. Sphingolipid metabolism is essential for tissue homeostasis and regulates the synthesis of several bioactive lipids and second messengers that are critical in cellular signaling (Wymann and Schneiter, 2008). The sphingomyelinase–driven catabolism of sphingolipids triggers the release and accumulation of Cer which are directly involved in neurodegenerative disorders and contribute to AD pathology (Han et al., 2011). Interestingly, the CB_1 receptor-driven breakdown of SM with ceramide production has been previously described in glial cells independently of $G_{i/o}$ protein activation, which indeed, was blocked by using the CB_1 receptor antagonist SR141716A (reviewed in Guzmán et al., 2001b; Sanchez et al., 2001; Velasco et al., 2005). Cer participate in cell differentiation, proliferation or apoptosis. The intracellular accumulation of Cer has been described in neurodegenerative disorders including AD, Parkinson's disease, epilepsy and ischemia. Thus, the upregulated levels of SM (d18:1/16:0) + K^+ observed may be a consequence of the necessary basal forebrain remodeling following the immunotoxin-induced apoptosis of BFCN rather than being related to Ch metabolism or eCB signaling. Recent studies have found a depletion of SM (d18:1/16:0) in CSF and a reduction in acid sphingomyelinase activity together with reduced levels of amyloid β_{42} in AD patients (Fonteh et al., 2015). However, SM (d18:0/18:1) was found to be decreased in the NBM following the immunotoxin-induced lesion. The fact that CB_1 receptor-mediated endocannabinoid signaling increases following the lesion allows us to speculate that CB_1 receptor activation in the NBM could be stimulating the hydrolysis of this specific SM species. In samples from AD

patients, SM (d18:0/18:1) levels are increased in both the hippocampal gray matter and CSF, and positively correlate with the total CSF tau level, but negatively with the CSF amyloid β_{42} level (Mendis et al., 2016; Koal et al., 2015). The relationship between the observed regulation in SM species with previous findings which indicate a CB_1-receptor-mediated regulation of hippocampal endocannabinoid signaling in AD patients must be further explored (Manuel et al., 2014). Moreover, additional studies focused on the quantification of Cer in this lesion model will contribute to a better understanding of the link between BFCN degeneration, CB_1 receptor-mediated endocannabinoid signaling and deregulation of specific SM species. In the meantime, the significance of the specific regulation of lipid species and their physiological role in the CNS remain elusive, but their lipid mapping by IMS in both normal and diseased human brain and in models of disease would help to clarify these questions (Martínez-Gardeazabal et al., 2017; González de San Román et al., 2017).

Phosphatidylethanolamines

Interestingly, PE (14:1/20:4) and PE (40:4), both of which may be composed of a molecule of arachidonic acid (AA; 20:4), were found to be deregulated in the NBM, revealing a possible membrane phospholipid source for the synthesis of Ch since PE are considered as precursors for PC synthesis in the ACh synthetic pathway, as explained above (Blusztajn et al., 1987a). Moreover, PE have diverse cellular functions and are involved in autophagy (reviewed in Calzada et al., 2016). PE are also the main substrate for the synthesis of eCB. The AEA precursor, NAPE, which is produced from the transfer of an acyl group (e.g. AA) from membrane phospholipids (e.g. PC) to the N-position of a PE, is catalyzed by a Ca^{2+}-dependent trans-acylase, which correlates with the biosynthesis of AEA in the CNS after depolarization (Di Marzo et al., 1994). Thus, PE (14:1/20:4) is decreased, whereas there is an increase in PE (40:4) in the NBM, and it is reasonable to hypothesize that these particular phospholipids could be used for the synthesis of eCB since the CB_1 receptor-mediated signaling in this brain area is up-regulated, as demonstrated by autoradiographic studies, which may increase the demand for their membrane lipid precursors. Since eCB are not apparently stored in vesicles, the generation of pools of lipids for further synthesis of eCB is difficult to understand and one would expect to observe a reduction in any possible PE precursors for eCB synthetic processing, pointing to PE (14:1/20:4) as a plausible candidate. However, the increase in the relative density of a specific lipid such as PE (40:4) allows us to hypothesize that a reservoir is created by an unknown storing mechanism from which to further synthesize eCB.

Sulfatides

Finally, the changes observed in certain species of sulfatides following the loss of BFCN indicate a pathological link similar to that found in the brains of AD patients. Certainly, one of the most consistent lipid changes described in these patient´s brains is the decrease in sulfatides during the early stages of disease (Han et al., 2002; Cheng et al., 2013).

Summary of findings in the *in vivo* model of NBM lesion

The M_2/M_4 mAChR-mediated muscarinic neurotransmission coupled to Gi/o proteins is not modified in cortical projection areas from the lesioned NBM. However other authors using a similar animal model have described that M_1 and M_2 mAChR density was increased (Rossner et al., 1995b). The relationship between muscarinic neurotransmission and phospholipid metabolism has also previously been studied, showing that the stimulation of cortical synaptosomes by cholinergic agonists was able to increase PLD activity, which was also dependent on PKC activity involving PIP_2 and DAG, which led to the accumulation of free Ch (Qian et al., 1989). The muscarinic signaling-induced PLD activity was antagonized by atropine (Dolezal and Tucek, 1984). Furthermore, eCB signaling is enhanced in cortical regions and in the NBM of 192IgG-saporin-infused rats, areas with a marked reduction in cholinergic innervation. The relative intensities of phospholipid species containing AA, such as PE (14:1/20:4), PE (40:4) and PC (36:4) + K^+, are also modulated in these same areas, suggesting a metabolic link between cholinergic neurotransmission and the eCB system. In summary, it would appear that $G_{q\text{-}11}$ protein-coupled mAChR such as M_1 and/or M_3 subtypes, may be key modulatory elements of the phospholipid-related regulation observed in this model. Detailed analysis of the different phospholipases activities mediated by mAChR (mainly M_1 and/or M_3 subtypes) in this lesion model will contribute to a better understanding of the underlying processes that could link the changes in lipid profile to the cholinergic-cannabinoid crosstalk. The 192IgG-saporin-induced modulation could be related to a compensatory mechanism for the loss of cortical ACh supply, or conversely, represent a pathological consequence of the massive death of BFCN in the NBM, regardless of muscarinic signaling. Several attempts to reduce the deficit of ACh in AD patients by the administration of cholinergic enhancers or precursors such as Ch or lecithin have failed, while treatments based on AChE inhibitors, phosphatidylserine, Ch alphoscerate and CDP-Ch have provided slight, but

noticeable benefits (reviewed in Amenta et al., 2001). Perhaps future treatments aimed at potentiating cholinergic neurotransmission should be based on the modulation of the complex enzymatic machinery, which so finely regulates lipid metabolism through mAChR-mediated signaling. In this context, the mAChR-driven eCB-mediated modulation of cholinergic neurotransmission at excitatory (Straiker and Mackie, 2007) and inhibitory synapses through the activation of CB_1 receptors (Narushima et al., 2007) is well known. Further research focused on muscarinic-eCB crosstalk may be useful for the discovery of innovative therapeutic treatments for neurodegenerative disorders.

3xTg-AD mice

The study of AD requires the use of well established models which include transgenic mice of AD (e.g., 3xTg-AD). Regarding the cholinergic neurotransmission, hippocampal and cortical cholinergic neuritic dystrophy, a decrease in the density of BFCN in the medial septum and deficits in the length of hippocampal cholinergic axons starting at 4 months, as well as a significant reduction in the number of ChAT-immunoreactive neurons in the NBM together with a loss of cholinergic fibers in cortical and hippocampal areas have been previously described in 3xTg-AD mice (Perez et al., 2011; Girão da Cruz et al., 2012; Orta-Salazar et al., 2014). This model recapitulates some classical histopathological markers of AD, leading to deficits in synaptic plasticity and impaired learning and memory (Oddo et al., 2003). Similarly to the changes found in AD patients, changes in CB_1 receptors have recently been described in several brain areas of 3xTg-AD mice rendering this model a suitable tool for the study of the relationship between both cholinergic and eCB systems (Bedse et al., 2014; Manuel et al., 2016).

Altered cannabinoid and muscarinic signaling is correlative to emotional learning and memory impairment in seven month-old 3xTg-AD mice

Changes in CB_1 receptors have recently been described in several brain areas of 3xTg-AD mice which are similar to the changes found in the brains of AD patients, rendering this model suitable for the study of the neuronal correlates (Bedse et al., 2014; Manuel et al., 2016). In the present study, we provide evidence of neuroanatomical and neurochemical modifications related to the eCB neuromodulatory system and muscarinic cholinergic signaling in the 3xTg-AD mice model, and of

behavioral modifications at the onset of disease (7 months of age), when cognitive impairment is clearly established and is concurrent with limbic system mediated symptoms. The results point to the eCB system as a key element controlling neuronal homeostasis as well as the limbic component of cognition.

The results of behavioral assessment during the passive avoidance test, one typically used to evaluate learning and memory under anxiogenic conditions, may also indicate the presence of fear and diminished motivation to explore as shown in a lesion rat model of AD (Babalola et al., 2012). 3xTg-AD mice had higher acquisition latency times than did controls. This is in agreement with the reduced exploratory activity and increased freezing behavior shown in the contextual fear-conditioning test, in the open field and in the passive avoidance test in this same transgenic mouse model of AD at 6 months of age (Gimenez-Llort et al., 2007; España et al., 2010; Filali et al., 2012). In addition, anxiety, fear, agitation and phobias may help to create a state of confusion which contributes to other behavioral disorders observed in AD patients, including learning and memory impairment (Ferretti et al., 2001; Aso and Ferrer, 2014).

The eCB system has emerged as a promising target for the treatment of several neurodegenerative disorders and has received a good deal of attention in AD. In this study, we report specific changes in density and in activity of CB_1 receptors, indicative of a potentiation of cannabinoid signaling in the BLA and an attenuation in the olfactory bulb and hippocampal dentate gyrus of transgenic mice. The specificity for CB_1 receptors was demonstrated by the anatomical pattern of distribution of [^{3}H]CP55,940 binding sites in brain, in comparison with that of spleen. [^{3}H]CP55,940 binding in 3xTg-AD and $CB_1^{+/+}$ mice was blocked by SR141716A and totally absent in $CB_1^{-/-}$ mouse brain. Indeed, SR144528, a specific CB_2 receptor antagonist, failed to block the binding in the brain but completely inhibited it in the spleen (where the CB_2 subtype is predominant) of both $CB_1^{+/+}$ and $CB_1^{-/-}$ mice. On the other hand, up-regulation of CB_2 receptors is reported to occur during neuroinflammation associated with neurodegenerative processes (Benito et al., 2003; Tolón et al., 2009; Schmöle et al., 2015). Therefore, the absence of a CB_2 receptor-mediated signal in the CNS of seven month-old 3xTg-AD mice, is in agreement with the lack of neuritic plaque-associated neuroinflammation at the onset of disease. Our results coincide with those of studies which report a significant increase in CB_1 receptor density in BLA when only intracellular Aβ accumulation can be detected, and which may be related to the symptoms of fear and anxiety observed in these mice (España et al., 2010; Bedse et al., 2014).

Behavioral outcomes of 3xTg-AD mice after the subchronic administration of synthetic cannabinoids. Possible functional interplay with muscarinic cholinergic signaling

The present study examines for the first time the neurochemical effects of cannabinoid agonism in 3xTg-AD mice and their behavioral correlates in a learning and memory task, which may be relevant in terms of clinical interventions in humans at the onset of disease. The results provide evidence that CB_1 receptor activation, following repeated cannabinoid administration, was able to decrease the acquisition latency times in 3xTg-AD mice to Non-Tg levels during the learning trial, which may be related to the CB_1 receptor density desensitization recorded in the BLA. Stressing factors can result in a modulation of the endocannabinoid levels in the amygdala, and can also induce a subsequent CB_1 receptor-mediated suppression of GABA release in the BLA (Jenniches et al., 2015; Di et al., 2016; Morena et al., 2016). Interestingly, we observed both a down-regulation of CB_1 receptors and an attenuation of their functional coupling to $G_{i/o}$ proteins induced by the subchronic administration of JZL-184, comparable to the results obtained in a previous study, but at different doses (Kinsey et al., 2013). Moreover, the administration of WIN55,212-2 (1 mg/kg), decreases the acquisition latency times without significantly changing CB_1 receptor functionality in the BLA. Our results confirm previous findings which showed that JZL184 selectively increased brain 2-AG and also indicated that the inhibition of MAGL could be promising as a way to indirectly potentiate the activation of CB_1 or CB_2 receptors (Busquets-Garcia et al., 2011; Kinsey et al., 2011). In this context, the pharmacological blockade or genetic deletion of MAGL dramatically raises brain 2-AG levels, down-regulates CB_1 receptor, and modulates synaptic plasticity, learning, memory and anxiety-like behavior (Pan et al., 2011). Accordingly, URB597, an AEA degrading enzyme inhibitor, induced CB_1 receptor-mediated anxiolytic effects in the elevated plus maze (Moise et al., 2008). Moreover, a recent study shows that the intra-BLA administration of both AEA and 2-AG hydrolysis inhibitors is able to attenuate anxiety-like responses, which are dependent on deregulated levels of eCB in the amygdala (Morena et al., 2016). Conversely, chronic CB_1 receptor blockade induced up-regulation of CB_1 receptor expression, down-regulation in hippocampus, and modified anxiety-like behavior (Tambaro et al., 2013).

Depending on the specific location of CB_1 receptors in inhibitory or excitatory neurons, the functional and physiological outcomes of this deregulated endocannabinoid signaling may be useful to understand the present results. In order to address this issue, immunochemical studies were performed and we found that in the

BLA, CB_1 receptor are more frequently located in GABAergic than in glutamatergic compartments, even though they have previously been detected in both of them (Kodirov et al., 2009; Ruehle et al., 2013; Shonesy et al., 2014; Robinson et al., 2016). The CB_1 receptors in BLA were located in the proximity of GAD65 (the enzyme glutamate decarboxylase; GAD, associated with inhibitory nerve termini) (Kash et al., 1999). In addition, the detection of VGLUT3 (the third subtype of glutamate vesicular transporter) has been used to identify both excitatory presynaptic boutons and glutamatergic somatodendritic compartments (Herzog et al., 2004). Although CB_1 receptors are present in both GABAergic and glutamatergic cellular compartments in areas such as the hippocampus, their activity could be lower in the inhibitory terminals (Steindel et al., 2013). However, in the BLA, CB_1 receptors are highly expressed in axon terminals of GABAergic neurons which modulate GABA release via a presynaptic mechanism (Katona et al., 2001). Some authors have related a long-lasting increase in anxiety-like behavior with a hyperactivity of BLA, as a consequence of a decrease in the inhibitory synaptic transmission (Almeida-Suhett et al., 2014). Thus, eCB-mediated suppression of inhibitory inputs to BLA neurons is involved in the cellular mechanism for stress-induced increases in anxiety-like behavior (Roozendaal et al., 2009). The genetic deletion of MAGL or GAD65 triggers an excitatory-inhibitory imbalance leading to increased anxiety-like responses (Imperatore et al., 2015; Müller et al., 2015). The glucocorticoid-induced suppression of inhibitory synaptic inputs to BLA principal neurons has recently been proposed as playing a pivotal role in the regulation of emotional disorders (Di et al., 2016). Globally, the present findings suggest that an up-regulation of the eCB tone in areas such as the BLA alters the local excitatory–inhibitory balance, and may be an underlying mechanism involved in the observed differences in cognitive behavior. Furthermore, a reversion to Non-Tg mice behavioral parameters was recorded after the attenuation of eCB signaling mediated by a pharmacological desensitization of CB_1 receptors. We propose that there is a CB_1 receptor-induced enhancement of the excitatory drive in brain areas such as the BLA due to the suppression of inhibition mediated by up-regulated CB_1 receptor signaling, which, by decreasing GABAergic neurotransmission, is an important component of the neurobiological mechanisms that control some cognitive deficits observed in 3xTg-AD mice (acquisition latency).

Moreover, the administration of WIN55,212-2 (1 mg/kg), but not JZL-184, was able to induce a significant increase in the activity mediated by mAChR in the BLA, revealing a possible interaction between both systems in limbic areas. This specific CB_1 receptor-driven modulation of cholinergic neurotransmission in the amygdala could also be involved in the behavioral outcomes recorded with the passive avoidance test.

In addition, these results support those of previous studies in which the role of the BLA cholinergic system, via mAChR, in memory retrieval during fear-induced learning was described (Malin et al., 2006; Nazarinia et al., 2017). Further behavioral studies are necessary in order to understand the meaning of CB_1 receptor-induced modulation of muscarinic control and its influence on acquisition latency, and to verify its validity as a possible indicator of anxiety, attention, agitation or states of confusion.

Regarding memory, step-through latency clearly distinguished the cognitively impaired AD-phenotype of 3xTg-AD mice, in accordance with previous studies (Clinton et al., 2007; Filali et al., 2012). Thus, 40% of 3xTg-AD mice did not remember the aversive stimulus received, while all the Non-Tg control mice did. However, under the present experimental conditions, we cannot rule out the possibility that the differences found in acquisition, or even putatively in consolidation, may also contribute to the performance of step-through latency. The desensitization of CB_1 receptors by means of subchronic administration of direct and indirect agonists failed to induce significant modifications in this variable. On the other hand, the analgesic effects of CB_1 receptor activation are well known (Meng et al., 1998). Subsequently, the pain threshold of the foot-shock in the passive avoidance test may be increased (Abush and Akirav, 2010). Therefore, the subtle variations in step-through latencies recorded after cannabinoid administration could be biased by the cannabinoid-induced analgesia. Further behavioral analyses by means of non-aversive stimulus-based learning and memory tests will help to clarify this question since 3xTg-AD mice do not seem to differ from Non-Tg in terms of pain thresholds (Filali et al., 2012; Baeta-Corral et al., 2015). However, the limbic system which is involved in cholinergic neurotransmission may be controlling specifically the consolidation and extinction of aversive or traumatic memories (Vazdarjanova and McGaugh, 1999).

3xTg-AD mice present deficits in cognition and synaptic plasticity associated with intraneuronal Aβ accumulation (Oddo et al., 2003). Muscarinic activation, through the M_2 mAChR subtype, promotes a rise in AMPA receptor sensitivity to glutamate, which finally leads to the so-called ‘muscarinic long term potentiation’ essential to explain hippocampal neuronal plasticity (Segal and Auerbach, 1997). Behavioral and neurochemical studies in M_2 mAChR knockout mice showed that the lack of receptors was accompanied by cognitive impairment in the passive avoidance test (Tzavara et al., 2003). The present immunofluorescence studies revealed the presynaptic localization of M_2 mAChR in GABAergic terminals, presumably making contact with postsynaptic VGLUT3 immunoreactive pyramidal neurons in CA1-CA3. The present findings in 3xTg-AD mice are similar to those reported in rat brain, suggesting that ACh via M_2 mAChR may reduce GABA release from presynaptic inhibitory terminals,

leading to increased activity in the dendritic region of pyramidal neurons (Levey et al., 1995; Hájos et al., 1998). The significant reduction in choline acetyltransferase activity described in hippocampus from middle-aged 3xTg-AD mice, but not associated with the loss of cholinergic neurons, may be related to the observed decrease in mAChR functionality (Perez et al., 2011). We suggest that intraneuronal accumulation of Aβ, beginning at 4 months of age, may trigger an early deregulation of the hippocampal muscarinic neurotransmission at the onset of disease, as observed in seven month-old 3xTg-AD mice, thereby contributing to the cognitive impairment observed in this model (Billings et al., 2005). Moreover, an excitatory/inhibitory imbalance mediated by a deregulated presynaptic muscarinic neurotransmission in the hippocampus may underlie the impaired synaptic plasticity, i.e., the neurobiological substrate for creating and maintaining new memories.

In summary, we provide evidence that muscarinic and cannabinoid signaling is altered in seven month-old 3xTg-AD mice, showing a specific regional and neuronal distribution in vulnerable limbic areas at the onset of disease. CB_1 receptor-mediated hyperactivity in some specific brain areas may have behavioral correlates that correspond with the restoration to control levels after direct and indirect pharmacological desensitization of CB_1 receptors. Finally, decreased muscarinic neurotransmission may be involved in memory-related impairment in 3xTg-AD mice. We propose that CB_1 receptor desensitization is a plausible strategy to palliate specific behavioral impairment associated with genetic variants of AD.

Conclusions

I. The specific removal of basal forebrain cholinergic neurons in organotypic cultures by the immunotoxin 192IgG-saporin leads to secondary cell damage in non-cholinergic cells. The same immunotoxin causes a dramatic loss of cortical cholinergic innervation in adult rats which is associated with deficits in learning and memory. Both *ex vivo* and *in vivo* models of basal forebrain cholinergic dysfunction are valid to identify therapeutic targets for the development of new pharmacological treatments aimed at restoring cholinergic neurotransmission.

II. The loss of basal forebrain cholinergic neurons in the nucleus basalis magnocellularis of adult rats causes a reduction in both the density and activity of muscarinic receptors coupled to $G_{i/o}$ proteins in the basal forebrain, but does not modify either of these parameters in cortical projections. M_2 and M_4 muscarinic receptors are not located in cortical presynaptic terminals which arise from basal forebrain cholinergic neurons. However, the increase in muscarinic neurotransmission recorded in the hippocampus could be interpreted as a compensatory mechanism.

III. Basal forebrain cholinergic dysfunction does not modify CB_1 receptor density which indicates the lack of CB_1 receptors in cortical terminals arising from basal forebrain, but increases the endocannabinoid signaling together with a reduction of GABAergic terminals in cortical projections. The activation of cortical endocannabinoid signaling could be regulating the glutamatergic-GABAergic imbalance induced by the dramatic loss of cortical cholinergic input.

IV. Different phosphatidylethanolamines and phosphatidylcholines containing arachidonic acid which, after the lesion, are regulated in the baso-cortical cholinergic pathway, might be precursors for *de novo* synthesis of both choline and endocannabinoids and may indicate the existence of a metabolic link between both systems in the CNS when there is basal forebrain cholinergic neurodegeneration.

V. The triple transgenic mice model of AD (3xTg-AD) shows altered CB_1 receptor and M_2/M_4 muscarinic receptor-mediated signaling associated with learning and memory deficits. The increased endocannabinoid tone recorded in 3xTg-AD mice mediates the hyperactivation of principal neurons in the basolateral amygdala which correlates with anxiety-like behavioral response.

VI. The subchronic administration of direct or indirect synthetic cannabinoids to 3xTg-AD mice leads to CB_1 receptor desensitization, which normalizes anxiety-like behavior and restores local endocannabinoid signaling. These effects together with the potentiation of muscarinic cholinergic signaling in limbic areas may contribute to improve learning and memory.

VII. In summary, the different experimental models used show that basal forebrain cholinergic dysfunction modulates the endocannabinoid system. Understanding the signaling mechanisms could lead to the discovery of innovative cannabinoid-based pharmacological approaches for the treatment of neurodegenerative disorders such as AD.

Acronyms and abbreviations

2-AG	2-Arachidonoylglycerol
[^{3}H] NMS	[^{3}H]-N-methylscopolamine
[^{3}H] QNB	[^{3}H]-quinuclidinyl benzilate
3xTg-AD	Triple transgenic mice model
5-HT	5-hydroxytryptamine receptor/serotonin receptor
Δ^9-THC	(--)-Δ^9-tetrahydrocannabinol
AA	Arachidonic acid
ABHD12	Alpha/beta-hydrolase domain containing 12
ABHD6	Alpha/beta-hydrolase domain containing 6
Acetyl-CoA	Acetyl coenzyme A
ACh	Acetylcholine
AChE	Acetylcholinesterase
aCSF	Artificial cerebrospinal fluid
AD	Alzheimer´s disease
AEA	Anandamide
AMPA	α-amino-3-hydroxy-5-methyl-4-isoxazolepropionic acid receptor
APP	Amyloid precursor protein
APP_{Swe}	Swedish mutation in amyloid precursor protein
AU	Arbitrary units
Aβ	Amyloid-beta
BDNF	Brain-derived neurotrophic factor
BFCN	Basal forebrain cholinergic neurons
BSA	Bovine serum albumin
cAMP	Cyclic adenosine monophosphate
CB_1 receptor	Subtype one of cannabinoid receptors
$CB_1^{-/-}$	CB_1 receptor knockout mice
$CB_1^{+/+}$	CB_1 receptor wild type mice
CB_2 receptor	Subtype two of cannabinoid receptors
CCD	Charge-coupled device
Cer	Ceramides
Ch	Choline
ChAT	Choline acetyltransferase
CNS	Central nervous system
CREB	cAMP response element-binding
CSF	Cerebrospinal fluid
DAG	Diacylglycerol
DAGL	Diacylglycerol lipase

DIV	Days in vitro
DSE	Depolarization-Induced suppression of excitation
DSI	Depolarization-Induced suppression of Inhibition
DTT	DL-dithiothreitol
eCB	Endocannabinoid
FAAH	Fatty acid amide hydrolase
FITC	Fluorescein
GABA	Gamma aminobutyric acid
GAD65	Glutamic acid decarboxylase 65kDa
GAD67	Glutamic acid decarboxylase 67kDa
GDP	Guanosine 5′-diphosphate
GFAP	Glial fibrilar acidic protein
GPCR	G protein-coupled receptor
GPR55	G Protein-coupled receptor 55
GTPγS	Guanosine 5'-O-(3-thiotriphosphate)
HBSS	Hanks' balanced salt solution
HC-3	Hemicholinium-3
HDB	Horizontal diagonal band of Broca
HOC	Hemibrain organotypic cultures
HRP	Horseradish peroxidase
I.c.v.	Intracerebroventricular
IMS	Imaging mass spectrometry
IP_3	Inositol trisphosphate
Iso-OMPA	Tetraisopropylpyrophosphoramide
LDTg	Laterodorsal tegmental area
LTD	Long-term depression
mAChR	Muscarinic acetylcholine receptor
MAGL	Monoacylglycerol lipase
MALDI	Matrix assisted laser desorption ionization
MAPK	Mitogen-activated protein kinase
MBT	2-mercaptobenzothiazole
MCI	Mild cognitive impairment
mGluR	Metabotropic glutamate receptors
MMSE	Mini-mental state examination
mNGF	Mature nerve growth factor
MRI	Magnetic resonance imaging
MS	Medial septal nucleus/medial septum

nAChR	Nicotinic acetylcholine receptors
NAPE	N-acyl-phosphatidylethanolamines
NArPE	N-arachidonoyl-phosphatidylethanolamine
NB	Neurobasal medium
NBM	Nucleus basalis magnocellularis
nbM	Nucleus basalis of Meynert
NGF	Nerve growth factor
NGS	Normal goat serum
NHS	Normal horse serum
NMDA	N-methyl D-aspartate
Non-Tg	Non transgenic mice
O.D.	Optical density
P7	7-day-old postnatal rats
$P75^{NTR}$	Low affinity nerve-growth factor receptor
PB	Phosphate buffer
PBS	Phosphate-buffered saline
PC	Phosphatidylcholine
PE	Phosphatidylethanolamine
PET	Positron emission tomography
PI	Propidium iodide
PI3K	Phosphatidylinositol-4,5-bisphosphate 3-kinase
PIP_2	Phosphatidylinositol 4,5-bisphosphate
PKA	Protein kinase A
PKC	Protein kinase C
PLA1	Phospholipase A1
PLA2	Phospholipase A2
PLC	Phospholipase C
PLD	Phospholipase D
Ppi	Pixels per inch
PPTg	Pedunculopontine tegmental area
ProNGF	Precursor nerve growth factor
PSIM146VM	146V mutation in presenilin1
RT-PCR	Reverse transcription polymerase chain reaction
SAP	192IgG-saporin-treated group
S.c.	Subcutaneous
SDHACU	Sodium dependent-high affinity choline uptake
ST	Sulfatides

SM	Sphingomyelins
STD	Short-term depression
Tau_{P301L}	P301L mutation in tau protein
TBS	Tris-buffered saline
T.E.	Tissue equivalent
TIC	Total ion current
TM	Transmembrane
TNB	Tris-NaCl-Tween blocking buffer
TNT	Tris-NaCl-Tween buffer
TrkA	Tyrosine kinase
VAChT	Vesicular Acetylcholine transporter
VDB	Vertical diagonal band of Broca
VGLUT3	Vesicular glutamate transporter subtype 3

References

Aaltonen M, Riekkinen P, Sirviö J, Riekkinen P Jr (1991). Effects of THA on passive avoidance and spatial performance in quisqualic acid nucleus basalis-lesioned rats. Pharmacol Biochem Behav. 39(3):563-567.

Abush, H, Akirav, I (2010). Cannabinoids modulate hippocampal memory and plasticity. Hippocampus 20(10),1126-1138.

Acquas E, Pisanu A, Marrocu P, Di Chiara G (2000). Cannabinoid CB(1) receptor agonists increase rat cortical and hippocampal acetylcholine release in vivo. Eur J Pharmacol. 401(2):179-185.

Acquas E, Pisanu A, Marrocu P, Goldberg SR, Di Chiara G (2001). Delta9-tetrahydrocannabinol enhances cortical and hippocampal acetylcholine release in vivo: a microdialysis study. Eur J Pharmacol. 419(2-3):155-161.

Ahmad R, Goffin K, Van den Stock J, De Winter FL, Cleeren E, Bormans G, Tournoy J, Persoons P, Van Laere K, Vandenbulcke M (2014). In vivo type 1 cannabinoid receptor availability in Alzheimer's disease. Eur Neuropsychopharmacol. 24(2):242-250.

Akay M, Wang K, Akay YM, Dragomir A, Wu J (2009). Nonlinear dynamical analysis of carbachol induced hippocampal oscillations in mice. Acta Pharmacol Sin. 30(6):859-867.

Albuquerque EX, Pereira EF, Alkondon M, Rogers SW (2009). Mammalian nicotinic acetylcholine receptors: from structure to function. Physiol Rev. 89(1):73-120.

Almeida-Suhett CP, Prager EM, Pidoplichko V, Figueiredo TH, Marini AM, Li Z, Eiden LE, Braga MF (2014). Reduced GABAergic inhibition in the basolateral amygdala and the development of anxiety-like behaviors after mild traumatic brain injury. PLoS One 9(7).

Alzheimer A (1911). Über eigenartige Krankheitsfälle des späteren Alters : (On certain peculiar diseases of old age). History of Psychiatry 1991; 2: 74.

Amara SG, Kuhar MJ (1993). Neurotransmitter transporters: recent progress. Annu Rev Neurosci. 16:73-93.

Amenta F, Parnetti L, Gallai V, Wallin A (2001). Treatment of cognitive dysfunction associated with Alzheimer's disease with cholinergic precursors. Ineffective treatments or inappropriate approaches? Mech Ageing Dev. 122(16):2025-2040. Review.

Angelucci F, Gelfo F, De Bartolo P, Caltagirone C, Petrosini L (2011). BDNF concentrations are decreased in serum and parietal cortex in immunotoxin 192 IgG-Saporin rat model of cholinergic degeneration. Neurochem Int. 59(1):1-4.

Anglade F, Bizot JC, Dodd RH, Baudoin C, Chapouthier G. (1994). Opposite effects of cholinergic agents and benzodiazepine receptor ligands in a passive avoidance task in rats. Neurosci Lett. 182(2):247-250.

Araujo DM, Lapchak PA, Robitaille Y, Gauthier S, Quirion R (1988). Differential alteration of various cholinergic markers in cortical and subcortical regions of human brain in Alzheimer's disease. J Neurochem. (6):1914-1923.

Arendt T, Bigl V, Arendt A, Tennstedt A (1983). Loss of neurons in the nucleus basalis of Meynert in Alzheimer's disease, paralysis agitans and Korsakoff's Disease. Acta Neuropathol. 61(2):101-108.

Arendt T, Bigl V, Tennstedt A, Arendt A (1984). Correlation between cortical plaque count and neuronal loss in the nucleus basalis in Alzheimer's disease. Neurosci Lett. 48(1):81-85.

Ashton JC, Glass M (2007). The cannabinoid CB2 receptor as a target for inflammation-dependent neurodegeneration. Curr Neuropharmacol. 5(2):73-80.

Aso E, Ferrer I (2014). Cannabinoids for treatment of Alzheimer's disease: moving toward the clinic. Front Pharmacol. 5:37. Review.

Astigarraga E, Barreda-Gómez G, Lombardero L, Fresnedo O, Castaño F, Giralt MT, Ochoa B, Rodríguez-Puertas R, Fernández JA (2008). Profiling and imaging of lipids on brain and liver tissue by matrix-assisted laser desorption/ ionization mass spectrometry using 2-mercaptobenzothiazole as a matrix. Anal Chem. 80(23):9105-9114.

Atwood BK, Mackie K (2010). CB2: a cannabinoid receptor with an identity crisis. Br J Pharmacol. 160(3):467-79. Review.

Auclair N, Otani S, Soubrie P, Crepel F (2000). Cannabinoids modulate synaptic strength and plasticity at glutamatergic synapses of rat prefrontal cortex pyramidal neurons. J Neurophysiol. 83(6):3287-3293.

Babalola PA, Fitz NF, Gibbs RB, Flaherty PT, Li PK, Johnson DA (2012). The effect of the steroid sulfatase inhibitor (p-O-sulfamoyl)-tetradecanoyl tyramine (DU-14) on learning and memory in rats with selective lesion of septal-hippocampal cholinergic tract. Neurobiol Learn Mem. 98(3):303-310.

Bader Lange ML, Cenini G, Piroddi M, Abdul HM, Sultana R, Galli F, Memo M, Butterfield DA (2008). Loss of phospholipid asymmetry and elevated brain apoptotic protein levels in subjects with amnestic mild cognitive impairment and Alzheimer disease. Neurobiol Dis. 29(3):456-464.

Baeta-Corral R, Defrin R, Pick CG, Giménez-Llort L (2015) Tail-flick test response in 3×Tg-AD mice at early and advanced stages of disease. Neurosci Lett. 600:158-163.

Bailey AM, Rudisill ML, Hoof EJ, Loving ML (2003). 192 IgG-saporin lesions to the nucleus basalis magnocellularis (nBM) disrupt acquisition of learning set formation. Brain Res. 969(1-2):147-159.

Barker L, A Dowdall MJ, Whittaker VP (1972). Choline metabolism in the cerebral cortex of guinea pig. Biochem. J. 130:1063–1075.

Barreda-Gómez G, Lombardero L, Giralt MT, Manuel I, Rodríguez-Puertas R (2015). Effects of galanin subchronic treatment on memory and muscarinic receptors. Neuroscience 293:23-34.

Bartus RT, Dean RL 3rd, Beer B, Lippa AS (1982). The cholinergic hypothesis of geriatric memory dysfunction. Science 217(4558):408-414.

Basso M, Yang J, Warren L, MacAvoy MG, Varma P, Bronen RA, van Dyck CH (2006). Volumetry of amygdala and hippocampus and memory performance in Alzheimer's disease. Psychiatry Res. 146(3):251-261.

Bauer A, Schulz JB, Zilles K (1992). Muscarinic desensitization after septal lesions in rat hippocampus: evidence for the involvement of G-proteins. Neuroscience 47(1):95-103.

Baxter MG, Bucci DJ, Gorman LK, Wiley RG, Gallagher M (1995). Selective immunotoxic lesions of basal forebrain cholinergic cells: effects on learning and memory in rats. Behav Neurosci. 109(4):714-722.

Baxter MG, Bucci DJ, Sobel TJ, Williams MJ, Gorman LK, Gallagher M (1996). Intact spatial learning following lesions of basal forebrain cholinergic neurons. Neuroreport. 7(8):1417-1420.

Baxter MG, Chiba AA (1999). Cognitive functions of the basal forebrain. Curr Opin Neurobiol. 9(2):178-183. Review.

Baxter MG (2001). Effects of selective immunotoxic lesions on learning and memory. Methods Mol Biol. 166:249-265. Review.

Baxter MG, Bucci DJ, Gorman LK, Wiley RG, Gallagher M (2013). Selective immunotoxic lesions of basal forebrain cholinergic cells: effects on learning and memory in rats. Behav Neurosci. 127(5):619-627.

Bayewitch M, Avidor-Reiss T, Levy R, Barg J, Mechoulam R, Vogel Z (1995). The peripheral cannabinoid receptor: adenylate cyclase inhibition and G protein coupling. FEBS Lett. 375(1-2):143-147.

Bedse G, Romano A, Cianci S, Lavecchia AM, Lorenzo P, Elphick MR, Laferla FM, Vendemiale G, Grillo C, Altieri F, Cassano T, Gaetani S (2014) Altered expression of the CB1 cannabinoid receptor in the triple transgenic mouse model of Alzheimer's disease. J Alzheimers Dis. 40(3):701-712.

Belkouch M, Hachem M, Elgot A, Lo Van A, Picq M, Guichardant M, Lagarde M, Bernoud-Hubac N (2016). The pleiotropic effects of omega-3 docosahexaenoic acid on the hallmarks of Alzheimer's disease. J Nutr Biochem. 38:1-11.

Bellocchio L, Lafenêtre P, Cannich A, Cota D, Puente N, Grandes P, Chaouloff F, Piazza PV, Marsicano G (2010). Bimodal control of stimulated food intake by the endocannabinoid system. Nat Neurosci. 13(3):281-283.

Beltramo M, Stella N, Calignano A, Lin SY, Makriyannis A, Piomelli D (1997). Functional role of high-affinity anandamide transport, as revealed by selective inhibition. Science 277(5329):1094-1097.

Beltramo M, Bernardini N, Bertorelli R, Campanella M, Nicolussi E, Fredduzzi S, Reggiani A (2006). CB2 receptor-mediated antihyperalgesia: possible direct involvement of neural mechanisms. Eur J Neurosci. 23(6):1530-1538.

Benagiano V, Virgintino D, Flace P, Girolamo F, Errede M, Roncali L, Ambrosi G (2003). Choline acetyltransferase-containing neurons in the human parietal neocortex. Eur J Histochem. 47(3):253-256.

Benito C, Núñez E, Tolón RM, Carrier EJ, Rábano A, Hillard CJ, Romero J (2003). Cannabinoid CB2 receptors and fatty acid amide hydrolase are selectively overexpressed in neuritic plaque-associated glia in Alzheimer's disease brains. J Neurosci. 23(35):11136-11141.

Benzing WC, Mufson EJ, Armstrong DM (1993). Immunocytochemical distribution of peptidergic and cholinergic fibers in the human amygdala: their depletion in Alzheimer's disease and morphologic alteration in non-demented elderly with numerous senile plaques. Brain Res. 625(1):125-138.

Bergamaschi G, Perfetti V, Tonon L, Novella A, Lucotti C, Danova M, Glennie MJ, Merlini G, Cazzola M (1996). Saporin, a ribosome-inactivating protein used to prepare immunotoxins, induces cell death via apoptosis. Br J Haematol. 93(4):789-794.

Berger-Sweeney J, Heckers S, Mesulam MM, Wiley RG, Lappi DA, Sharma M (1994). Differential effects on spatial navigation of immunotoxin-induced cholinergic lesions of the medial septal area and nucleus basalis magnocellularis. J Neurosci. 14(7):4507-4519.

Berrendero F, Sepe N, Ramos JA, Di Marzo V, Fernández-Ruiz JJ (1999). Analysis of cannabinoid receptor binding and mRNA expression and endogenous cannabinoid contents in the developing rat brain during late gestation and early postnatal period. Synapse 33(3):181-191.

Best AR, Regehr WG (2008). Serotonin evokes endocannabinoid release and retrogradely suppresses excitatory synapses. J Neurosci. 28(25):6508-6515.

Bevers EM, Williamson PL (2016). Getting to the Outer Leaflet: Physiology of Phosphatidylserine Exposure at the Plasma Membrane. Physiol Rev. 96(2):605-645.

Biebl M, Cooper CM, Winkler J, Kuhn HG (2000). Analysis of neurogenesis and programmed cell death reveals a self-renewing capacity in the adult rat brain. Neurosci Lett. 291(1):17-20.

Billings LM, Oddo S, Green KN, McGaugh JL, LaFerla FM (2005) Intraneuronal Abeta causes the onset of early Alzheimer's disease-related cognitive deficits in transgenic mice. Neuron 45:675-688.

Bisogno T, Delton-Vandenbroucke I, Milone A, Lagarde M, Di Marzo V (1999). Biosynthesis and inactivation of N-arachidonoylethanolamine (anandamide) and N-docosahexaenoylethanolamine in bovine retina. Arch Biochem Biophys. 370(2):300-307.

Bisogno T, Melck D, Bobrov MYu, Gretskaya NM, Bezuglov VV, De Petrocellis L, Di Marzo V (2000). N-acyl-dopamines: novel synthetic CB(1) cannabinoid-receptor ligands and inhibitors of anandamide inactivation with cannabimimetic activity in vitro and in vivo. Biochem J. 351 Pt 3:817-824.

Bisogno T, Maccarrone M, De Petrocellis L, Jarrahian A, Finazzi-Agrò A, Hillard C, Di Marzo V (2001). The uptake by cells of 2-arachidonoylglycerol, an endogenous agonist of cannabinoid receptors. Eur J Biochem. 268(7):1982-1989.

Bissette G, Seidler FJ, Nemeroff CB, Slotkin TA (1996). High affinity choline transporter status in Alzheimer's disease tissue from rapid autopsy. Ann N Y Acad Sci. 777:197-204.

Blankman JL, Simon GM, Cravatt BF (2007). A comprehensive profile of brain enzymes that hydrolyze the endocannabinoid 2-arachidonoylglycerol. Chem Biol.14(12):1347-1356.

Blankman JL, Cravatt BF (2013). Chemical probes of endocannabinoid metabolism. Pharmacol Rev. 65(2):849-871.

Blasko I, Lederer W, Oberbauer H, Walch T, Kemmler G, Hinterhuber H, Marksteiner J, Humpel C (2006). Measurement of thirteen biological markers in CSF of patients with Alzheimer's disease and other dementias. Dement Geriatr Cogn Disord. 21(1):9-15.

Blusztajn JK, Wurtman RJ (1983). Choline and cholinergic neurons. Science 221(4611):614-620.

Blusztajn JK, Liscovitch M, Richardson UI (1987). Synthesis of acetylcholine from choline derived from phosphatidylcholine in a human neuronal cell line. Proc Natl Acad Sci U S A 84(15):5474-5477.

Blusztajn JK, Lopez Gonzalez-Coviella I, Logue M, Growdon JH, Wurtman RJ (1990). Levels of phospholipid catabolic intermediates, glycerophosphocholine and glycerophosphoethanolamine,

are elevated in brains of Alzheimer's disease but not of Down's syndrome patients. Brain Res. 536(1-2):240-244.

Bodor AL, Katona I, Nyíri G, Mackie K, Ledent C, Hájos N, Freund TF (2005). Endocannabinoid signaling in rat somatosensory cortex: laminar differences and involvement of specific interneuron types. J Neurosci. 25(29):6845-6856.

Bogdanovic N, Islam A, Nilsson L, Bergström L, Winblad B, Adem A (1993). Effects of nucleus basalis lesion on muscarinic receptor subtypes. Exp Brain Res. 97 (2):225-232.

Bohnen NI, Kaufer DI, Ivanco LS, Lopresti B, Koeppe RA, Davis JG, Mathis CA, Moore RY, DeKosky ST (2003). Cortical cholinergic function is more severely affected in parkinsonian dementia than in Alzheimer disease: an in vivo positron emission tomographic study. Arch Neurol. 60(12):1745-1748.

Bonner TI, Buckley NJ, Young AC, Brann MR (1987). Identification of a family of muscarinic acetylcholine receptor genes. Science 237: 527–532.

Bonner TI, Youn A C, Brann MR and Buckley N J (1988). Cloning and expression of the human and rat m5 acetylcholine receptor genes. Neuron 1: 403–410.

Bonner TI (1989). The molecular basis of muscarinic receptor diversity. Trends Neurosci. 12: 148–151.

Bonner TI, Modi WS, Seuanez HN and O'Brien SJ (1991). Chromosomal mapping of the fi ve human genes encoding the muscarinic acetylcholine receptors. Cytogenet. Cell. Genet. 58: 1850–1851.

Bouaboula M, Poinot-Chazel C, Bourrié B, Canat X, Calandra B, Rinaldi-Carmona M, Le Fur G, Casellas P (1995). Activation of mitogen-activated protein kinases by stimulation of the central cannabinoid receptor CB1. Biochem J. 312 (Pt 2):637-641.

Bouaboula M, Poinot-Chazel C, Marchand J, Canat X, Bourrié B, Rinaldi-Carmona M, Calandra B, Le Fur G, Casellas P (1996). Signaling pathway associated with stimulation of CB2 peripheral cannabinoid receptor. Involvement of both mitogen-activated protein kinase and induction of Krox-24 expression. Eur J Biochem. 237(3):704-711.

Bouaboula M, Perrachon S, Milligan L, Canat X, Rinaldi-Carmona M, Portier M, Barth F, Calandra B, Pecceu F, Lupker J, Maffrand JP, Le Fur G, Casellas P (1997). A selective inverse agonist for central cannabinoid receptor inhibits mitogen-activated protein kinase activation stimulated by insulin or insulin-like growth factor 1. Evidence for a new model of receptor/ligand interactions. J Biol Chem. 272(35):22330-22339.

Bremer J, Figard PH, Greenberg DM (1960a). The biosynthesis of choline and its relation to phospholipid metabolism. Biochim Biophys Acta 43: 477-488.

Bremer J, Greenberg DM (1960b). Biosynthesis of choline in vitro. Biochim Biophys Acta 37:173-175.

Brimijoin S (1983). Molecular forms of acetylcholinesterase in brain, nerve and muscle: nature, localization and dynamics. Prog Neurobiol. 21(4):291-322. Review.

Brown DA, Adams P R (1980). Muscarinic suppression of a novel voltage-sensitive K+ current in a vertebrate neurone. Nature 283: 673–676.

Brown SM, Wager-Miller J, Mackie K (2002). Cloning and molecular characterization of the rat CB2 cannabinoid receptor. Biochim Biophys Acta 1576(3):255-264.

Brueggen K, Dyrba M, Barkhof F, Hausner L, Filippi M, Nestor PJ, Hauenstein K, Klöppel S, Grothe MJ, Kasper E, Teipel SJ (2015). Basal Forebrain and Hippocampus as Predictors of Conversion to Alzheimer's Disease in Patients with Mild Cognitive Impairment - A Multicenter DTI and Volumetry Study. J Alzheimers Dis. 48(1):197-204.

Bucci DJ, Holland PC, Gallagher M (1998). Removal of cholinergic input to rat posterior parietal cortex disrupts incremental processing of conditioned stimuli. J Neurosci. (19):8038-8046.

Buckley NJ, Bonner TI, Brann MR (1988). Localization of a family of muscarinic receptor mRNAs in rat brain. J Neurosci. 8: 4646–4652.

Busquets-Garcia A, Puighermanal E, Pastor A, de la Torre R, Maldonado R, Ozaita A (2011). Differential role of anandamide and 2-arachidonoylglycerol in memory and anxiety-like responses. Biological Psychiatry 70(5):479-486.

Butt AE, Noble MM, Rogers JL, Rea TE (2002). Impairments in negative patterning, but not simple discrimination learning, in rats with 192 IgG-saporin lesions of the nucleus basalis magnocellularis. Behav Neurosci. 116(2):241-255.

Caccamo A, Oddo S, Billings LM, Green KN, Martinez-Coria H, Fisher A, LaFerla FM (2006). M1 receptors play a central role in modulating AD-like pathology in transgenic mice. Neuron 49(5):671-682.

Calignano A, La Rana G, Giuffrida A, Piomelli D (1998). Control of pain initiation by endogenous cannabinoids. Nature 394(6690):277-281.

Calzada E, Onguka O, Claypool SM (2016). Phosphatidylethanolamine Metabolism in Health and Disease. Int Rev Cell Mol Biol. 321:29-88.

Candy JM, Perry RH, Perry EK, Irving D, Blessed G, Fairbairn AF, Tomlinson BE (1983). Pathological changes in the nucleus of Meynert in Alzheimer's and Parkinson's diseases. J Neurol Sci. 59(2):277-289.

Carlson G, Wang Y, Alger BE (2002). Endocannabinoids facilitate the induction of LTP in the hippocampus. Nat Neurosci. 5(8):723-724.

Carotenuto A, Rea R, Traini E, Fasanaro AM, Ricci G, Manzo V, Amenta F (2017). The Effect of the Association between Donepezil and Choline Alphoscerate on Behavioral Disturbances in Alzheimer's Disease: Interim Results of the ASCOMALVA Trial. J Alzheimers Dis. 56(2):805-815.

Carta G, Nava F, Gessa GL (1998). Inhibition of hippocampal acetylcholine release after acute and repeated Delta9-tetrahydrocannabinol in rats. Brain Res. 809(1):1-4.

Caulfield MP (1993). Muscarinic receptors--characterization, coupling and function. Pharmacol Ther. 58(3):319-379. Review

Caulfield MP, Birdsall NJ (1998). International Union of Pharmacology. XVII. Classification of muscarinic acetylcholine receptors. Pharmacol Rev. 50(2):279-290.

Cavedo E, Boccardi M, Ganzola R, Canu E, Beltramello A, Caltagirone C, Thompson PM, Frisoni GB (2011). Local amygdala structural differences with 3T MRI in patients with Alzheimer disease. Neurology 76(8):727-733.

Chakrabarti A, Onaivi ES, Chaudhuri G (1995). Cloning and sequencing of a cDNA encoding the mouse brain-type cannabinoid receptor protein. DNA Seq. 5(6):385-388.

Chan RB, Oliveira TG, Cortes EP, Honig LS, Duff KE, Small SA, Wenk MR, Shui G, Di Paolo G (2012). Comparative lipidomic analysis of mouse and human brain with Alzheimer disease. J Biol Chem. 287(4):2678-2688.

Chatterjee P, Lim WL, Shui G, Gupta VB, James I, Fagan AM, Xiong C, Sohrabi HR, Taddei K, Brown BM, Benzinger T, Masters C, Snowden SG, Wenk MR, Bateman RJ, Morris JC, Martins RN (2015). Plasma Phospholipid and Sphingolipid Alterations in Presenilin1 Mutation Carriers: A Pilot Study. J Alzheimers Dis. 50(3):887-894.

Cheng H, Wang M, Li JL, Cairns NJ, Han X (2013). Specific changes of sulfatide levels in individuals with preclinical Alzheimer's disease: an early event in disease pathogenesis. J. Neurochem. 127 (6) (2013) 733–738.

Chiba AA, Bucci DJ, Holland PC, Gallagher M (1995). Basal forebrain cholinergic lesions disrupt increments but not decrements in conditioned stimulus processing. J Neurosci. 15(11):7315-7322.

Chiba AA, Bushnell PJ, Oshiro WM, Gallagher M (1999). Selective removal of cholinergic neurons in the basal forebrain alters cued target detection. Neuroreport 10(14):3119-3123.

Choi SH, Olabarrieta M, Lopez OL, Maruca V, Dekosky ST, Hamilton RL, Becker JT. Gray matter atrophy associated with extrapyramidal signs in the Lewy body variant of Alzheimer's disease (2012). J Alzheimers Dis. 32(4):1043-1049.

Chrobak JJ, Hanin I, Schmechel DE, Walsh TJ (1988). AF64A-induced working memory impairment: behavioral, neurochemical and histological correlates. Brain Res. 463(1):107-117.

Chugh Y, Saha N, Sankaranarayanan A, Sharma PL (1991). Possible mechanism of haloperidol-induced enhancement of memory retrieval. Methods Find Exp Clin Pharmacol. 13(3):161-164.

Clinton LK, Billings LM, Green KN, Caccamo A, Ngo J, Oddo S, McGaugh JL, LaFerla FM (2007). Age-dependent sexual dimorphism in cognition and stress response in the 3xTg-AD mice. Neurobiol Dis. 28(1):76-82.

Collerton D (1986). Cholinergic function and intellectual decline in Alzheimer's disease. Neuroscience 19(1):1-28.

Conner JM, Muir D, Varon S, Hagg T, Manthorpe M (1992). The localization of nerve growth factor-like immunoreactivity in the adult rat basal forebrain and hippocampal formation. J Comp Neurol. 319(3):454-462.

Conner JM, Culberson A, Packowski C, Chiba AA, Tuszynski MH (2003). Lesions of the Basal forebrain cholinergic system impair task acquisition and abolish cortical plasticity associated with motor skill learning. Neuron 38(5):819-829.

Conner JM, Chiba AA, Tuszynski MH (2005). The basal forebrain cholinergic system is essential for cortical plasticity and functional recovery following brain injury. Neuron 46(2):173-179.

Cooper-Kuhn CM, Winkler J, Kuhn HG (2004). Decreased neurogenesis after cholinergic forebrain lesion in the adult rat. J Neurosci Res. 77(2):155-165.

Cortés R, Vilaró MT, Mengod G (2016). Visualization of 5-HT Receptors Using Radioligand-Binding Autoradiography. Curr Protoc Pharmacol. 75:78.

Counts SE, Nadeem M, Wuu J, Ginsberg SD, Saragovi HU, Mufson EJ (2004). Reduction of cortical TrkA but not p75(NTR) protein in early-stage Alzheimer's disease. Ann Neurol. 56(4):520-531.

Cravatt BF, Giang DK, Mayfield SP, Boger DL, Lerner RA, Gilula NB (1996). Molecular characterization of an enzyme that degrades neuromodulatory fatty-acid amides. Nature 384(6604):83-87.

Cravatt BF, Demarest K, Patricelli MP, Bracey MH, Giang DK, Martin BR, Lichtman AH (2001). Supersensitivity to anandamide and enhanced endogenous cannabinoid signaling in mice lacking fatty acid amide hydrolase. Proc Natl Acad Sci U S A 98(16):9371-9376.

Csernansky JG, Wang L, Swank J, Miller JP, Gado M, McKeel D, Miller MI, Morris JC (2005). Preclinical detection of Alzheimer's disease: hippocampal shape and volume predict dementia onset in the elderly. Neuroimage 25(3):783-792.

Cui Y, Costa RM, Murphy GG, Elgersma Y, Zhu Y, Gutmann DH, Parada LF, Mody I, Silva AJ (2008). Neurofibromin regulation of ERK signaling modulates GABA release and learning. Cell 135(3):549-560.

Cullen KM, Halliday GM (1998). Neurofibrillary degeneration and cell loss in the nucleus basalis in comparison to cortical Alzheimer pathology. Neurobiol Aging. 19(4):297-306.

Cummings JL, Benson DF (1987). The role of the nucleus basalis of Meynert in dementia: review and reconsideration. Alzheimer Dis Assoc Disord. 1(3):128-155. Review.

Cummings JL, Back C (1998) The cholinergic hypothesis of neuropsychiatric symptoms in Alzheimer's disease. Am J Geriatr Psychiatry 6(2 Suppl 1):S64-78. Review.

Cummings J, Lai TJ, Hemrungrojn S, Mohandas E, Yun Kim S, Nair G, Dash A (2016). Role of Donepezil in the Management of Neuropsychiatric Symptoms in Alzheimer's Disease and Dementia with Lewy Bodies. CNS Neurosci Ther.1-8.

Dale HH (1937). Transmission of nervous effects by acetylcholine. Harvey Lect. 32: 229–245.

Dashniani M, Burjanadze M, Beselia G, Maglakelidze G, Naneishvili T (2009). Spatial memory following selective cholinergic lesion of the nucleus basalis magnocellularis. Georgian Med News (174):77-81.

Daviaud N, Garbayo E, Schiller PC, Perez-Pinzon M, Montero-Menei CN (2013). Organotypic cultures as tools for optimizing central nervous system cell therapies. Exp Neurol. 248:429-440. Review.

Davies P, Maloney AJ (1976). Selective loss of central cholinergic neurons in Alzheimer's disease. Lancet 2(8000):1403.

Davies P (1979). Neurotransmitter-related enzymes in senile dementia of the Alzheimer type. Brain Res. 171(2):319-327.

Davies SN, Pertwee RG, Riedel G (2002). Functions of cannabinoid receptors in the hippocampus. Neuropharmacology 42(8):993-1007.

De Lacalle S, Lim C, Sobreviela T, Mufson EJ, Hersh LB, Saper CB (1994). Cholinergic innervation in the human hippocampal formation including the entorhinal cortex. J Comp Neurol. 345(3):321-344.

Decossas M, Bloch B, Bernard V (2003). Trafficking of the muscarinic m2 autoreceptor in cholinergic basalocortical neurons in vivo: differential regulation of plasma membrane receptor availability and intraneuronal localization in acetylcholinesterase-deficient and -inhibited mice. J Comp Neurol. 462(3):302-314.

Dehghani F, Hischebeth GT, Wirjatijasa F, Kohl A, Korf HW, Hailer NP. The immunosuppressant mycophenolate mofetil attenuates neuronal damage after excitotoxic injury in hippocampal slice cultures. Eur J Neurosci. 18(5):1061-1072.

DeKosky ST, Ikonomovic MD, Styren SD, Beckett L, Wisniewski S, Bennett DA, Cochran EJ, Kordower JH, Mufson EJ (2002). Upregulation of choline acetyltransferase activity in hippocampus and frontal cortex of elderly subjects with mild cognitive impairment. Ann Neurol. 51(2):145-155.

del Rio JA, Heimrich B, Soriano E, Schwegler H, Frotscher M (1991). Proliferation and differentiation of glial fibrillary acidic protein-immunoreactive glial cells in organotypic slice cultures of rat hippocampus. Neuroscience 43(2-3):335-347.

Delgado-Peraza F, Ahn KH, Nogueras-Ortiz C, Mungrue IN, Mackie K, Kendall DA, Yudowski GA (2016). Mechanisms of Biased β-Arrestin-Mediated Signaling Downstream from the Cannabinoid 1 Receptor. Mol Pharmacol. 89(6):618-629.

Derkinderen P, Toutant M, Burgaya F, Le Bert M, Siciliano JC, de Franciscis V, Gelman M, Girault JA (1996). Regulation of a neuronal form of focal adhesion kinase by anandamide. Science 273(5282):1719-1722.

Deutsch DG, Chin SA (1993). Enzymatic synthesis and degradation of anandamide, a cannabinoid receptor agonist. Biochem Pharmacol. 46(5):791-796.

Devane WA, Dysarz FA 3rd, Johnson MR, Melvin LS, Howlett AC (1988). Determination and characterization of a cannabinoid receptor in rat brain. Mol Pharmacol. 34(5):605-613.

Devane WA, Hanus L, Breuer A, Pertwee RG, Stevenson LA, Griffin G, Gibson D, Mandelbaum A, Etinger A, Mechoulam R (1992). Isolation and structure of a brain constituent that binds to the cannabinoid receptor. Science 258(5090):1946-1949.

Di, S, Itoga, CA, Fisher, MO, Solomonow, J, Roltsch, EA, Gilpin, NW, Tasker, JG, (2016). Acute Stress Suppresses Synaptic Inhibition and Increases Anxiety via Endocannabinoid Release in the Basolateral Amygdala. J. Neurosci. 36(32), 8461-8470.

Di Marzo V, Gianfrani C, De Petrocellis L, Milone A, Cimino A (1994). Polyunsaturated-fatty-acid oxidation in Hydra: regioselectivity, substrate-dependent enantioselectivity and possible biological role. Biochem J. 300(Pt 2): 501–507.

Di Marzo V, De Petrocellis L, Sugiura T, Waku K (1996). Potential biosynthetic connections between the two cannabimimetic eicosanoids, anandamide and 2-arachidonoyl-glycerol, in mouse neuroblastoma cells. Biochem Biophys Res Commun. 227(1):281-288.

Di Marzo V (2006). A brief history of cannabinoid and endocannabinoid pharmacology as inspired by the work of British scientists. Trends Pharmacol Sci. 27(3):134-140.

Di Marzo V (2008). Endocannabinoids: synthesis and degradation. Rev Physiol Biochem Pharmacol. 160:1-24.

Dinh TP, Freund TF, Piomelli D (2002). A role for monoglyceride lipase in 2-arachidonoylglycerol inactivation. Chem Phys Lipids 121(1-2):149-158. Review.

Dolezal V, Tucek S (1984). Activation of muscarinic receptors stimulates the release of choline from brain slices. Biochem Biophys Res Commun. 120(3):1002-1007.

Doyle E, Regan CM (1993). Cholinergic and dopaminergic agents which inhibit a passive avoidance response attenuate the paradigm-specific increases in NCAM sialylation state. J Neural Transm Gen Sect.. General section 92(1):33-49.

Drachman DA, Leavitt J (1974). Human memory and the cholinergic system. A relationship to aging? Arch Neurol. 30(2):113-121.

Eckenstein FP, Baughman RW, Quinn J (1988). An anatomical study of cholinergic innervation in rat cerebral cortex. Neuroscience 25(2):457-474.

Egertová M, Elphick MR (2000). Localisation of cannabinoid receptors in the rat brain using antibodies to the intracellular C-terminal tail of CB. J Comp Neurol. 422(2):159-171.

Ehlert FJ, Roeske WR, Yamamura HI (1994). Muscarinic receptors and novel strategies for the treatment of age-related brain disorders. Life Sci. 55(25-26):2135-2145. Review.

Eldeeb K, Leone-Kabler S, Howlett AC (2016). CB1 cannabinoid receptor-mediated increases in cyclic AMP accumulation are correlated with reduced Gi/o function. J Basic Clin Physiol Pharmacol. 27(3):311-322.

Ellis J, Pediani JD, Canals M, Milasta S, Milligan G (2006). Orexin-1 receptor-cannabinoid CB1 receptor heterodimerization results in both ligand-dependent and -independent coordinated alterations of receptor localization and function. J Biol Chem. 281(50):38812-38824.

Ellison DW, Beal MF, Martin JB (1987). Phosphoethanolamine and ethanolamine are decreased in Alzheimer's disease and Huntington's disease. Brain Res. 417(2):389-392.

Elsohly MA, Slade D (2005). Chemical constituents of marijuana: the complex mixture of natural cannabinoids. Life Sci. 78(5):539-548.

Emre M, Heckers S, Mash DC, Geula C, Mesulam MM (1993). Cholinergic innervation of the amygdaloid complex in the human brain and its alterations in old age and Alzheimer's disease. J Comp Neurol. 336(1):117-134.

Eriksdotter Jönhagen M, Nordberg A, Amberla K, Bäckman L, Ebendal T, Meyerson B, Olson L, Seiger, Shigeta M, Theodorsson E, Viitanen M, Winblad B, Wahlund LO (1998). Intracerebroventricular infusion of nerve growth factor in three patients with Alzheimer's disease. Dement Geriatr Cogn Disord. 9(5):246-257.

Erten-Lyons D, Howieson D, Moore MM, Quinn J, Sexton G, Silbert L, Kaye J (2006). Brain volume loss in MCI predicts dementia. Neurology 66(2):233-235.

España J, Giménez-Llort L, Valero J, Miñano A, Rábano A, Rodriguez-Alvarez J, LaFerla FM, and Saura C (2010) Intraneuronal beta-amyloid accumulation in the amygdala enhances fear and anxiety in Alzheimer’s disease transgenic mice. Biol Psychiatry 67:513-521.

Etienne P, Robitaille Y, Wood P, Gauthier S, Nair NP, Quirion R (1986). Nucleus basalis neuronal loss, neuritic plaques and choline acetyltransferase activity in advanced Alzheimer's disease. Neuroscience 19(4):1279-1291.

Eva C, Fabrazzo M, Costa E (1987). Changes of cholinergic, noradrenergic and serotonergic synaptic transmission indices elicited by ethylcholine aziridinium ion (AF64A) infused intraventricularly. J Pharmacol Exp Ther. 241(1):181-186.

Evans DM, Johnson MR, Howlett AC (1992). Ca(2+)-dependent release from rat brain of cannabinoid receptor binding activity. J Neurochem. 58(2):780-792.

Evans DM, Lake JT, Johnson MR, Howlett AC (1994). Endogenous cannabinoid receptor binding activity released from rat brain slices by depolarization. J Pharmacol Exp Ther. 268(3):1271-1277.

Exton JH (1999). Regulation of phospholipase D. Biochim Biophys Acta 1439(2):121-133. Review.

Fadok VA, Voelker DR, Campbell PA, Cohen JJ, Bratton DL, Henson PM (1992). Exposure of phosphatidylserine on the surface of apoptotic lymphocytes triggers specific recognition and removal by macrophages. J Immunol. 148(7):2207-2216.

Fahnestock M, Michalski B, Xu B, Coughlin MD (2001). The precursor pro-nerve growth factor is the predominant form of nerve growth factor in brain and is increased in Alzheimer's disease. Mol Cell Neurosci. 18(2):210-220.

Farkas S, Nagy K, Palkovits M, Kovács GG, Jia Z, Donohue S, Pike V, Halldin C, Máthé D, Harkany T, Gulyás B, Csiba L (2012). [^{125} I]SD-7015 reveals fine modalities of CB_1 cannabinoid receptor density in the prefrontal cortex during progression of Alzheimer's disease. Neurochem Int. 60(3):286-291.

Feldberg W (1945). Present views on the mode of action of acetylcholine in the central nervous system. Physiol Rev. 25: 596–642.

Felder CC, Joyce KE, Briley EM, Mansouri J, Mackie K, Blond O, Lai Y, Ma AL, Mitchell RL (1995). Comparison of the pharmacology and signal transduction of the human cannabinoid CB1 and CB2 receptors. Mol Pharmacol. 48(3):443-450.

Ferrari-DiLeo G, Flynn DD (1993). Diminished muscarinic receptor-stimulated [3H]-PIP2 hydrolysis in Alzheimer's disease. Life Sci. 53(25):PL439-44.

Ferreira-Vieira TH, Guimaraes IM, Silva FR, Ribeiro FM (2016). Alzheimer's disease: Targeting the Cholinergic System. Curr Neuropharmacol. 14(1):101-115.

Ferretti L, McCurry SM, Logsdon R, Gibbons L, Teri L (2001) Anxiety and Alzheimer's disease. J Geriatr Psychiatry Neurol. 14:52–58.

Fiandaca MS, Zhong X, Cheema AK, Orquiza MH, Chidambaram S, Tan MT, Gresenz CR, FitzGerald KT, Nalls MA, Singleton AB, Mapstone M, Federoff HJ (2015). Plasma 24-metabolite Panel Predicts Preclinical Transition to Clinical Stages of Alzheimer's Disease. Front Neurol. 6:237.

Filali M, Lalonde R, Theriault P, Julien C, Calon F, and Planel E (2012). Cognitive and non-cognitive behaviors in the triple transgenic mouse model of Alzheimer's disease expressing mutated APP, PS1, and Mapt (3xTg-AD). Behav Brain Res. 234:334–342.

Fisar Z (2009). Phytocannabinoids and endocannabinoids. Curr Drug Abuse Rev. 2(1):51-75.

Flicker C, Dean RL, Watkins DL, Fisher SK, Bartus RT (1983). Behavioral and neurochemical effects following neurotoxic lesions of a major cholinergic input to the cerebral cortex in the rat. Pharmacol Biochem Behav. 18(6):973-981.

Flynn DD, Ferrari-DiLeo G, Levey AI, Mash DC (1995). Differential alterations in muscarinic receptor subtypes in Alzheimer's disease: implications for cholinergic-based therapies. Life Sci. 56(11-12):869-876.

Flynn DD, Reever CM, Ferrari-DiLeo G (1997). Pharmacological strategies to selectively label and localize muscarinic receptor subtypes. Drug Dev Res. 40: 104–116, 1997.

Foley P (2010). Lipids in Alzheimer's disease: A century-old story. Biochim Biophys Acta 1801(8):750-753.

Fonteh AN, Ormseth C, Chiang J, Cipolla M, Arakaki X, Harrington MG (2015). Sphingolipid metabolism correlates with cerebrospinal fluid Beta amyloid levels in Alzheimer's disease. PLoS One 10(5):e0125597.

Freund TF, Katona I, Piomelli D (2003). Role of endogenous cannabinoids in synaptic signaling. Physiol Rev. 83(3):1017-1066.

Fride E, Mechoulam R (1993). Pharmacological activity of the cannabinoid receptor agonist, anandamide, a brain constituent. Eur J Pharmacol. 231(2):313-324.

Fukudome Y, Ohno-Shosaku T, Matsui M, Omori Y, Fukaya M, Tsubokawa H, Taketo MM, Watanabe M, Manabe T, Kano M (2004).Two distinct classes of muscarinic action on hippocampal inhibitory synapses: M2-mediated direct suppression and M1/M3-mediated indirect suppression through endocannabinoid signalling. Eur J Neurosci. 19(10):2682-92.

Galiègue S, Mary S, Marchand J, Dussossoy D, Carrière D, Carayon P, Bouaboula M, Shire D, Le Fur G, Casellas P (1995). Expression of central and peripheral cannabinoid receptors in human immune tissues and leukocyte subpopulations. Eur J Biochem. 232(1):54-61.

Galve-Roperh I, Rueda D, Gómez del Pulgar T, Velasco G, Guzmán M (2002). Mechanism of extracellular signal-regulated kinase activation by the CB(1) cannabinoid receptor. Mol Pharmacol. 62(6):1385-1392.

Gao Y, Vasilyev DV, Goncalves MB, Howell FV, Hobbs C, Reisenberg M, Shen R, Zhang MY, Strassle BW, Lu P, Mark L, Piesla MJ, Deng K, Kouranova EV, Ring RH, Whiteside GT, Bates B, Walsh FS, Williams G, Pangalos MN, Samad TA, Doherty P (2010). Loss of retrograde endocannabinoid signaling and reduced adult neurogenesis in diacylglycerol lipase knock-out mice. J Neurosci. 30(6):2017-2024.

Gaoni Y, Mechoulam R (1964). Isolation, structure and partial synthesis of an active constituent of hashish. J Am Chem Soc. 86: 1646–1647.

Garcia-Alloza M, Zaldua N, Diez-Ariza M, Marcos B, Lasheras B, Javier Gil-Bea F, Ramirez MJ (2006). Effect of selective cholinergic denervation on the serotonergic system: implications for learning and memory. J Neuropathol Exp Neurol. 65(11):1074-1081.

Garrett JE, Kim I, Wilson RE, Wellman CL (2006). Effect of N-methyl-D-aspartate receptor blockade on plasticity of frontal cortex after cholinergic deafferentation in rat. Neuroscience 140(1):57-66.

Gelfo F, Petrosini L, Graziano A, De Bartolo P, Burello L, Vitale E, Polverino A, Iuliano A, Sorrentino G, Mandolesi L (2013). Cortical metabolic deficits in a rat model of cholinergic basal forebrain degeneration. Neurochem Res. 38(10):2114-2123.

Gérard C, Mollereau C, Vassart G, Parmentier M (1990). Nucleotide sequence of a human cannabinoid receptor cDNA. Nucleic Acids Res. 18(23):7142.

Gérard CM, Mollereau C, Vassart G, Parmentier M (1991). Molecular cloning of a human cannabinoid receptor which is also expressed in testis. Biochem J. 279 (Pt 1):129-134.

Gessa GL, Mascia MS, Casu MA, Carta G (1997). Inhibition of hippocampal acetylcholine release by cannabinoids: reversal by SR 141716A. Eur J Pharmacol. 327(1):R1-2.

Geula C, Nagykery N, Nicholas A, Wu CK (2008). Cholinergic neuronal and axonal abnormalities are present early in aging and in Alzheimer disease. J Neuropathol Exp Neurol. 67(4):309-318.

Giacobini E (1990). The cholinergic system in Alzheimer disease. Prog Brain Res. 84:321-332. Review.

Gibbs RB, Johnson DA (2007). Cholinergic lesions produce task-selective effects on delayed matching to position and configural association learning related to response pattern and strategy. Neurobiol Learn Mem. 88(1):19-32.

Gifford AN, Ashby CR Jr (1996). Electrically evoked acetylcholine release from hippocampal slices is inhibited by the cannabinoid receptor agonist, WIN 55212-2, and is potentiated by the cannabinoid antagonist, SR 141716A. J Pharmacol Exp Ther. 277(3):1431-1436.

Gifford AN, Bruneus M, Gatley SJ, Volkow ND (2000). Cannabinoid receptor-mediated inhibition of acetylcholine release from hippocampal and cortical synaptosomes. Br J Pharmacol. 131(3):645-650.

Gil-Bea FJ, García-Alloza M, Domínguez J, Marcos B, Ramírez MJ (2005). Evaluation of cholinergic markers in Alzheimer's disease and in a model of cholinergic deficit. Neurosci Lett. 375(1):37-41.

Gilmor ML, Erickson JD, Varoqui H, Hersh LB, Bennett DA, Cochran EJ, Mufson EJ, Levey AI (1999). Preservation of nucleus basalis neurons containing choline acetyltransferase and the vesicular acetylcholine transporter in the elderly with mild cognitive impairment and early Alzheimer's disease. J Comp Neurol. 411(4):693-704.

Giménez-Llort L, Blázquez G, Cañete T, Johansson B, Oddo S, Tobeña A, LaFerla FM, Fernández-Teruel A (2007) Modeling behavioral and neuronal symptoms of Alzheimer's disease in mice: a role for intraneuronal amyloid. Neurosci Biobehav Rev. 31:125-147.

Girão da Cruz MT, Jordão J, Dasilva KA, Ayala-Grosso CA, Ypsilanti A, Weng YQ, Laferla FM, McLaurin J, Aubert I (2012). Early increases in soluble amyloid-β levels coincide with cholinergic degeneration in 3xTg-AD mice. J Alzheimers Dis. 32(2):267-272.

Giuffrida A, Parsons LH, Kerr TM, Rodríguez de Fonseca F, Navarro M, Piomelli D (1999). Dopamine activation of endogenous cannabinoid signaling in dorsal striatum. Nat Neurosci. 2(4):358-363.

Giuffrida A, Beltramo M, Piomelli D (2001). Mechanisms of endocannabinoid inactivation: biochemistry and pharmacology. J Pharmacol Exp Ther. 298(1):7-14. Review.

Glass M, Felder CC (1997). Concurrent stimulation of cannabinoid CB1 and dopamine D2 receptors augments cAMP accumulation in striatal neurons: evidence for a Gs linkage to the CB1 receptor. J Neurosci. 17(14):5327-5333.

Gong, N., Li, Y., Cai, G.Q., Niu, R.F., Fang, Q., Wu, K., Chen, Z., Lin, L.N., Xu, L., Fei, J., & Xu, T.L. (2009). GABA transporter-1 activity modulates hippocampal theta oscillation and theta burst stimulation-induced long-term potentiation. J Neurosci. 29(50):15836-15845.

Gonsiorek W, Lunn C, Fan X, Narula S, Lundell D, Hipkin RW (2000). Endocannabinoid 2-arachidonyl glycerol is a full agonist through human type 2 cannabinoid receptor: antagonism by anandamide. Mol Pharmacol. 57(5):1045-1050.

Gorry JD (1963). Studies on the comparative anatomy of the ganglion basale of Meynert. Acta Anat. 55, 51–104.

Gotti C, Fornasari D, Clementi F (1997). Human neuronal nicotinic receptors. Prog Neurobiol. 53(2):199-237. Review.

Gotti C, Clementi F (2004). Neuronal nicotinic receptors: from structure to pathology. Prog Neurobiol. 74(6):363-396. Review.

Grabiec U, Koch M, Kallendrusch S, Kraft R, Hill K, Merkwitz C, Ghadban C, Lutz B, Straiker A, Dehghani F (2012). The endocannabinoid N-arachidonoyldopamine (NADA) exerts neuroprotective effects after excitotoxic neuronal damage via cannabinoid receptor 1 (CB(1)). Neuropharmacology 62(4):1797-1807.

Gratwicke J, Kahan J, Zrinzo L, Hariz M, Limousin P, Foltynie T, Jahanshahi M (2013). The nucleus basalis of Meynert: a new target for deep brain stimulation in dementia?. Neurosci Biobehav Rev. 37(10 Pt 2):2676-2688.

Green RC, Mesulam MM (1988). Acetylcholinesterase fiber staining in the human hippocampus and parahippocampal gyrus. J Comp Neurol. 273(4):488-499.

Griffin G, Wray EJ, Tao Q, McAllister SD, Rorrer WK, Aung MM, Martin BR, Abood ME (1999). Evaluation of the cannabinoid CB2 receptor-selective antagonist, SR144528: further evidence for cannabinoid CB2 receptor absence in the rat central nervous system. Eur J Pharmacol. 377(1):117-125.

Griffiths PD, Perry RH, Crossman AR (1994). A detailed anatomical analysis of neurotransmitter receptors in the putamen and caudate in Parkinson's disease and Alzheimer's disease. Neurosci Lett. 169(1-2):68-72.

Gritti, I, Mainville, L, Jones BE (1993). Codistribution of GABA− with acetylcholine synthesizing neurons in the basal forebrain of the rat. J. Comp. Neurol. 329, 438–457.

Grothe M, Zaborszky L, Atienza M, Gil-Neciga E, Rodriguez-Romero R, Teipel SJ, Amunts K, Suarez-Gonzalez A, Cantero JL (2010). Reduction of basal forebrain cholinergic system parallels cognitive impairment in patients at high risk of developing Alzheimer's disease. Cereb Cortex 20(7):1685-1695.

Grothe M, Heinsen H, Teipel SJ (2012). Atrophy of the cholinergic Basal forebrain over the adult age range and in early stages of Alzheimer's disease. Biol Psychiatry 2012 71(9):805-813.

Grothe M, Heinsen H, Teipel S (2013). Longitudinal measures of cholinergic forebrain atrophy in the transition from healthy aging to Alzheimer's disease. Neurobiol Aging 34(4):1210-1220.

Grothe MJ, Heinsen H, Amaro E Jr, Grinberg LT, Teipel SJ (2016). Alzheimer's Disease Neuroimaging Initiative (2016). Cognitive Correlates of Basal Forebrain Atrophy and Associated Cortical Hypometabolism in Mild Cognitive Impairment. Cereb Cortex 26(6):2411-2426.

Gulya K, Budai D, Kása P (1989). Muscarinic autoreceptors are differentially affected by selective muscarinic antagonists in rat hippocampus. Neurochem Int. 15(2):153-156.

Gusev PA, Gubin AN (2010). Arc/Arg3.1 mRNA global expression patterns elicited by memory recall in cerebral cortex differ for remote versus recent spatial memories. Front Integr Neurosci 4:15.

Guzmán M, Sánchez C (1999). Effects of cannabinoids on energy metabolism. Life Sci. 65(6-7):657-664. Review.

Guzmán M, Sánchez C, Galve-Roperh I (2001a). Control of the cell survival/death decision by cannabinoids. J Mol Med (Berl). 78(11):613-625. Review.

Guzmán M, Galve-Roperh I, Sánchez C (2001b). Ceramide: a new second messenger of cannabinoid action. Trends Pharmacol Sci. 22(1):19-22. Review.

Haga T (1971). Synthesis and release of (14 C)acetylcholine in synaptosomes. J Neurochem. 18(6):781-798.

Haga T, Noda H (1973). Choline uptake systems of rat brain synaptosomes. Biochim. Biophys. Acta. 291: 564–575.

Haj-Dahmane S, Shen RY (2005). The wake-promoting peptide orexin-B inhibits glutamatergic transmission to dorsal raphe nucleus serotonin neurons through retrograde endocannabinoid signaling. J Neurosci. 25(4):896-905.

Hájos N, Papp EC, Acsády L, Levey AI, Freund TF (1998). Distinct interneuron types express m2 muscarinic receptor immunoreactivity on their dendrites or axon terminals in the hippocampus. Neuroscience 82(2):355-376.

Hájos N, Ledent C, Freund TF (2001). Novel cannabinoid-sensitive receptor mediates inhibition of glutamatergic synaptic transmission in the hippocampus. Neuroscience 106(1):1-4.

Happe HK, Murrin LC (1993). High-affinity choline transport sites: use of [3H]hemicholinium-3 as a quantitative marker. J Neurochem. 60(4):1191-1201.

Hammer R, Berrie CP, Birdsall, NJM, Burgen, ASV and Hulme EC (1980). Pirenzepine distinguishes between different subclasses of muscarinic receptors. Nature 283: 90–92.

Hammer R and Giachetti A (1982). Muscarinic receptor subtypes: M1 and M2 biochemical and functional characterization. Life Sci. 31: 2991–2998.

Han X, M Holtzman D, McKeel DW Jr, Kelley J, Morris JC (2002). Substantial sulfatide deficiency and ceramide elevation in very early Alzheimer's disease: potential role in disease pathogenesis. J Neurochem. 82(4):809-818.

Han X, Rozen S, Boyle SH, Hellegers C, Cheng H, Burke JR, Welsh-Bohmer KA, Doraiswamy PM, Kaddurah-Daouk R (2011). Metabolomics in early Alzheimer's disease: identification of altered plasma sphingolipidome using shotgun lipidomics. PLoS One 6(7):e21643.

Hansen HS, Lauritzen L, Moesgaard B, Strand AM, Hansen HH (1998). Formation of N-acyl-phosphatidylethanolamines and N-acetylethanolamines: proposed role in neurotoxicity. Biochem Pharmacol. 55(6):719-725. Review.

Hanus L, Breuer A, Tchilibon S, Shiloah S, Goldenberg D, Horowitz M, Pertwee RG, Ross RA, Mechoulam R, Fride E (1999). HU-308: a specific agonist for CB(2), a peripheral cannabinoid receptor. Proc Natl Acad Sci U S A 96(25):14228-14233.

Hanus L, Abu-Lafi S, Fride E, Breuer A, Vogel Z, Shalev DE, Kustanovich I, Mechoulam R (2001). 2-arachidonyl glyceryl ether, an endogenous agonist of the cannabinoid CB1 receptor. Proc Natl Acad Sci U S A 98(7):3662-3665.

Hanyu H, Tanaka Y, Sakurai H, Takasaki M, Abe K (2002). Atrophy of the substantia innominata on magnetic resonance imaging and response to donepezil treatment in Alzheimer's disease. Neurosci Lett. 319(1):33-36.

Harata N, Tateishi N, Akaike N (1991). Acetylcholine receptors in dissociated nucleus basalis of Meynert neurons of the rat. Neurosci Lett. 130(2):153-156.

Häring M, Kaiser N, Monory K, Lutz B (2011). Circuit specific functions of cannabinoid CB1 receptor in the balance of investigatory drive and exploration. PLoS One 6(11):e26617.

Harkany T, Härtig W, Berghuis P, Dobszay MB, Zilberter Y, Edwards RH, Mackie K, Ernfors P (2003). Complementary distribution of type 1 cannabinoid receptors and vesicular glutamate transporter 3 in basal forebrain suggests input-specific retrograde signalling by cholinergic neurons. Eur J Neurosci. 18(7):1979-1992.

Harkany T, Dobszay MB, Cayetanot F, Härtig W, Siegemund T, Aujard F, Mackie K (2005). Redistribution of CB1 cannabinoid receptors during evolution of cholinergic basal forebrain territories and their cortical projection areas: a comparison between the gray mouse lemur (Microcebus murinus, primates) and rat. Neuroscience 135(2):595-609.

Harmon KM, Wellman CL (2003). Differential effects of cholinergic lesions on dendritic spines in frontal cortex of young adult and aging rats. Brain Res. 992(1):60-68.

Harrison PJ, Barton AJ, Najlerahim A, McDonald B, Pearson RC (1991). Increased muscarinic receptor messenger RNA in Alzheimer's disease temporal cortex demonstrated by in situ hybridization histochemistry. Brain Res Mol Brain Res. 9(1-2):15-21.

Härtig W, Saul A, Kacza J, Grosche J, Goldhammer S, Michalski D, Wirths O (2014). Immunolesion-induced loss of cholinergic projection neurones promotes β-amyloidosis and tau hyperphosphorylation in the hippocampus of triple-transgenic mice. Neuropathol Appl Neurobiol. 40(2):106-120.

Hashimotodani Y, Ohno-Shosaku T, Tsubokawa H, Ogata H, Emoto K, Maejima T, Araishi K, Shin HS, Kano M (2005). Phospholipase Cbeta serves as a coincidence detector through its Ca2+ dependency for triggering retrograde endocannabinoid signal. Neuron 45(2):257-268.

Hattori H, Kanfer JN (1984). Synaptosomal phospholipase D: potential role in providing choline for acetylcholine synthesis. Biochem Biophys Res Commun. 124(3):945-949.

He X, Huang Y, Li B, Gong CX, Schuchman EH (2010). Deregulation of sphingolipid metabolism in Alzheimer's disease. Neurobiol Aging 31(3):398-408.

Hebert-Chatelain E, et al., (2016). A cannabinoid link between mitochondria and memory. Nature. 539(7630):555-559.

Heckers S, Ohtake T, Wiley RG, Lappi DA, Geula C, Mesulam MM (1994). Complete and selective cholinergic denervation of rat neocortex and hippocampus but not amygdala by an immunotoxin against the p75 NGF receptor. J Neurosci. 14(3 Pt 1):1271-1289.

Hedreen JC, Struble RG, Whitehouse PJ, Price DL (1984). Topography of the magnocellular basal forebrain system in human brain. J Neuropathol Exp Neurol. 43(1):1-21.

Heider M, Schliebs R, Rossner S, Bigl V (1997). Basal forebrain cholinergic immunolesion by 192IgG-saporin: evidence for a presynaptic location of subpopulations of alpha 2- and beta-adrenergic as well as 5-HT2A receptors on cortical cholinergic terminals. Neurochem Res. 22(8):957-966.

Heifets BD and Castillo PE (2009). Endocannabinoid signaling and long-term synaptic plasticity. Annu Rev Physiol. 71:283-306.

Henke H, Lang W (1983). Cholinergic enzymes in neocortex, hippocampus and basal forebrain of non-neurological and senile dementia of Alzheimer-type patients. Brain Res. 267(2):281-291.

Hepler DJ, Olton DS, Wenk GL, Coyle JT (1985). Lesions in nucleus basalis magnocellularis and medial septal area of rats produce qualitatively similar memory impairments. J Neurosci. 5(4):866-873.

Hepler DJ, Wenk GL, Cribbs BL, Olton DS, Coyle JT (1985). Memory impairments following basal forebrain lesions. Brain Res. 346(1):8-14.

Herholz K, Weisenbach S, Zündorf G, Lenz O, Schröder H, Bauer B, Kalbe E, Heiss WD (2004). In vivo study of acetylcholine esterase in basal forebrain, amygdala, and cortex in mild to moderate Alzheimer disease. Neuroimage 21(1):136-143.

Herkenham M, Lynn AB, Little MD, Johnson MR, Melvin LS, de Costa BR, Rice KC (1990). Cannabinoid receptor localization in brain. Proc Natl Acad Sci U S A 87(5):1932-1936.

Herkenham M, Lynn AB, de Costa BR, Richfield EK (1991). Neuronal localization of cannabinoid receptors in the basal ganglia of the rat. Brain Res. 547(2):267-274.

Hérnandez-Hérnandez A, Adem A, Ravid R, Cowburn RF (1995). Preservation of acetylcholine muscarinic M2 receptor G-protein interactions in the neocortex of patients with Alzheimer's disease. Neurosci Lett. 186(1):57-60.

Herrera B, Carracedo A, Diez-Zaera M, Guzmán M, Velasco G (2005). p38 MAPK is involved in CB2 receptor-induced apoptosis of human leukaemia cells. FEBS Lett. 579(22):5084-5088.

Herzog AG, Kemper TL (1980). Amygdaloid changes in aging and dementia. Arch Neurol. 37(10):625-629.

Herzog E, Gilchrist J, Gras C, Muzerelle, A, Ravassard P, Giros B, Gaspar P and El Mestikawy S. (2004). Localization of VGLUT3, the vesicular glutamate transporter type 3, in the rat brain. Neuroscience 123(4):983-1002.

Hirasawa M, Schwab Y, Natah S, Hillard CJ, Mackie K, Sharkey KA, Pittman QJ (2004). Dendritically released transmitters cooperate via autocrine and retrograde actions to inhibit afferent excitation in rat brain. J Physiol. 559(Pt 2):611-624.

Hohmann AG, Briley EM, Herkenham M (1999a). Pre- and postsynaptic distribution of cannabinoid and mu opioid receptors in rat spinal cord. Brain Res. 822(1-2):17-25.

Hohmann AG and Herkenham M (1999b). Localization of central cannabinoid CB1 receptor messenger RNA in neuronal subpopulations of rat dorsal root ganglia: a double-label in situ hybridization study. Neuroscience 90(3):923-931.

Hong JH, Jang SH (2010). Neural pathway from nucleus basalis of Meynert passing through the cingulum in the human brain. Brain Res. 1346:190-194.

Horínek D, Varjassyová A, Hort J (2007). Magnetic resonance analysis of amygdalar volume in Alzheimer's disease. Curr Opin Psychiatry 20(3):273-277.

Horn F, van der Wenden EM, Oliveira L, Ijzerman AP, Vriend G (2000). Receptors coupling to G proteins: is there a signal behind the sequence? Proteins 41: 448–459.

Howlett AC (1984). Inhibition of neuroblastoma adenylate cyclase by cannabinoid and nantradol compounds. Life Sci. 35(17):1803-1810.

Howlett AC, Fleming RM (1984). Cannabinoid inhibition of adenylate cyclase. Pharmacology of the response in neuroblastoma cell membranes. Mol Pharmacol. 26(3):532-538.

Howlett AC (1985). Cannabinoid inhibition of adenylate cyclase. Biochemistry of the response in neuroblastoma cell membranes. Mol Pharmacol. 27(4):429-436.

Howlett AC, Qualy JM, Khachatrian LL (1986). Involvement of Gi in the inhibition of adenylate cyclase by cannabimimetic drugs. Mol Pharmacol. 29(3):307-313.

Howlett AC, Bidaut-Russell M, Devane WA, Melvin LS, Johnson MR, Herkenham M (1990). The cannabinoid receptor: biochemical, anatomical and behavioral characterization. Trends Neurosci. 13(10):420-423.

Howlett AC, Barth F, Bonner TI, Cabral G, Casellas P, Devane WA, Felder CC, Herkenham M, Mackie K, Martin BR, Mechoulam R, Pertwee RG (2002). International Union of Pharmacology. XXVII. Classification of cannabinoid receptors. Pharmacol Rev. 54(2):161-202.

Howlett AC, Breivogel CS, Childers SR, Deadwyler SA, Hampson RE, Porrino LJ (2004). Cannabinoid physiology and pharmacology: 30 years of progress. Neuropharmacology 47 Suppl 1:345-58. Review.

Hua T, Vemuri K, Pu M, Qu L, Han GW, Wu Y, Zhao S, Shui W, Li S, Korde A, Laprairie RB, Stahl EL, Ho JH, Zvonok N, Zhou H, Kufareva I, Wu B, Zhao Q, Hanson MA, Bohn LM, Makriyannis A, Stevens RC, Liu ZJ (2016). Crystal Structure of the Human Cannabinoid Receptor CB1. Cell 167(3):750-762.

Huang EJ, Reichardt LF (2001). Neurotrophins: roles in neuronal development and function. Annu Rev Neurosci. 24:677-736. Review.

Hudson BD, Hébert TE, Kelly ME (2010). Ligand- and heterodimer-directed signaling of the CB(1) cannabinoid receptor. Mol Pharmacol. 77(1):1-9. Review.

Huffman JW, Yu S, Showalter V, Abood ME, Wiley JL, Compton DR, Martin BR, Bramblett RD, Reggio PH (1996). Synthesis and pharmacology of a very potent cannabinoid lacking a phenolic hydroxyl with high affinity for the CB2 receptor. J Med Chem. 39(20):3875-3877.

Hulme EC, Birdsall N JM, Buckley NJ (1990). Muscarinic receptor subtypes. Ann. Rev. Pharmacol. Toxicol. 30: 633–673.

Ibáñez CF, Simi A (2012). p75 neurotrophin receptor signaling in nervous system injury and degeneration: paradox and opportunity. Trends Neurosci. 35(7):431-440.

Ikonomovic MD, Mufson EJ, Wuu J, Cochran EJ, Bennett DA, DeKosky ST (2003). Cholinergic plasticity in hippocampus of individuals with mild cognitive impairment: correlation with Alzheimer's neuropathology. J Alzheimers Dis. 1:39-48

Imperatore R, Morello G, Luongo L, Ulrike T, Romano R, De Gregorio D, Belardo C, Maione S, Di Marzo V, Cristino L (2015) Genetic deletion of monoacylglycerol lipase leads to impaired cannabinid receptor CB_1R signaling and anxiety-like behavior. J Neurochem. 135:77-813.

Jack CR Jr, Petersen RC, Xu YC, O'Brien PC, Smith GE, Ivnik RJ, Boeve BF, Waring SC, Tangalos EG, Kokmen E (1999). Prediction of AD with MRI-based hippocampal volume in mild cognitive impairment. Neurology 52(7):1397-1403.

Jackson SN, Wang HY, Woods AS (2005a). Direct profiling of lipid distribution in brain tissue using MALDI-TOFMS. Anal Chem. 77(14):4523-4527.

Jackson SN, Wang HY, Woods AS, Ugarov M, Egan T, Schultz JA (2005b). Direct tissue analysis of phospholipids in rat brain using MALDI-TOFMS and MALDI-ion mobility-TOFMS. J Am Soc Mass Spectrom. 16(2):133-138.

Jacob A, Todd AR (1940). Cannabidiol and Cannabol, Constituents of *Cannabis indica* Resin. Nature 145, 350-350.

Jenniches, I, Ternes, S, Albayram, O, Otte, DM, Bach, K, Bindila, L. Michel, K, Lutz, B, Bilkei-Gorzo, A, Zimmer, A, (2015). Anxiety, stress, and fear response in mice with reduced endocannabinoid levels. Biol. Psychiatry 79, 858-868.

Jeong DU, Chang WS, Hwang YS, Lee D, Chang JW (2011). Decrease of GABAergic markers and arc protein expression in the frontal cortex by intraventricular 192 IgG-saporin. Dement Geriatr Cogn Disord. 32(1):70-78.

Jeong da U, Oh JH, Lee JE, Lee J, Cho ZH, Chang JW, Chang WS (2016). Basal Forebrain Cholinergic Deficits Reduce Glucose Metabolism and Function of Cholinergic and GABAergic Systems in the Cingulate Cortex. Yonsei Med J. 57(1):165-172.

Jin W, Brown S, Roche JP, Hsieh C, Celver JP, Kovoor A, Chavkin C, Mackie K (1999). Distinct domains of the CB1 cannabinoid receptor mediate desensitization and internalization. J Neurosci. 19(10):3773-3780.

Johnson MR, Melvin LS (1986). The discovery of nonclassical cannabinoid analgetics. In: Mechoulam, R., ed. Cannabinoids as Therapeutic Agents. New York: CRC Press, pp. 121-145.

Jones B.E, Cuello AC (1989). Afferents to the basal forebrain cholinergic cell area from pontomesencephalic–catecholamine, serotonin, and acetylcholine–neurons. Neuroscience 31, 37–61.

Jones CK, Byun N, Bubser M (2012). Muscarinic and nicotinic acetylcholine receptor agonists and allosteric modulators for the treatment of schizophrenia. Neuropsychopharmacology 37(1):16-42.

Jones EG, Burton H, Saper CB, Swanson LW (1976). Midbrain, diencephalic and cortical relationships of the basal nucleus of Meynert and associated structures in primates. J. Comp. Neurol. 167, 385–419.

Jope RS, Song L, Powers RE (1997). Cholinergic activation of phosphoinositide signaling is impaired in Alzheimer's disease brain. Neurobiol Aging 18(1):111-120.

Jung KM, Astarita G, Yasar S, Vasilevko V, Cribbs DH, Head E, Cotman CW, Piomelli D (2012). An amyloid β42-dependent deficit in anandamide mobilization is associated with cognitive dysfunction in Alzheimer's disease. Neurobiol Aging 33(8):1522-1532.

Kallendrusch S, Hobusch C, Ehrlich A, Nowicki M, Ziebell S, Bechmann I, Geisslinger G, Koch M, Dehghani F (2012). Intrinsic up-regulation of 2-AG favors an area specific neuronal survival in different in vitro models of neuronal damage. PLoS One 7(12):e51208.

Kalmbach A, Hedrick T, Waters J (2012). Selective optogenetic stimulation of cholinergic axons in neocortex. J. Neurophysiol. 107, 2008–2019.

Kanfer JN, Hattori H, Orihel D (1986). Reduced phospholipase D activity in brain tissue samples from Alzheimer's disease patients. Ann Neurol. 20(2):265-257.

Kano M, Ohno-Shosaku T, Hashimotodani Y, Uchigashima M, Watanabe M (2009). Endocannabinoid-mediated control of synaptic transmission. Physiol Rev. 89(1):309-380.

Kano M (2014). Control of synaptic function by endocannabinoid-mediated retrograde signaling. Proc Jpn Acad Ser B Phys Biol Sci. 90(7):235-250. Review.

Karczmar AG (1967). Pharmacologic, toxicologic and therapeutic properties of anticholinesterase agents. In: “Physiological Pharmacology,” W. S. Root and F. G. Hofman, Eds., 3:163–322, Academic Press, New York.

Karlsson M, Contreras JA, Hellman U, Tornqvist H, Holm C (1997). cDNA cloning, tissue distribution, and identification of the catalytic triad of monoglyceride lipase. Evolutionary relationship to esterases, lysophospholipases, and haloperoxidases. J Biol Chem. 272(43):27218-27223.

Kása P (1986). The cholinergic systems in brain and spinal cord. Prog Neurobiol. 26(3):211-272.

Kása P, Rakonczay Z, Gulya K (1997). The cholinergic system in Alzheimer's disease. Prog Neurobiol. 52(6):511-535.

Kash SF, Tecott LH, Hodge C, Baekkeskov S (1999). Increased anxiety and altered responses to anxiolytics in mice deficient in the 65-kDa isoform of glutamic acid decarboxylase. Proc Natl Acad Sci U S A 96:1698–1703.

Kathmann M, Flau K, Redmer A, Tränkle C, Schlicker E (2006). Cannabidiol is an allosteric modulator at mu- and delta-opioid receptors. Naunyn Schmiedebergs Arch Pharmacol. 372(5):354-361.

Kathmann M, Weber B, Zimmer A, Schlicker E (2001). Enhanced acetylcholine release in the hippocampus of cannabinoid CB(1) receptor-deficient mice. Br J Pharmacol. 132(6):1169-1173.

Katona I, Sperlágh B, Sík A, Käfalvi A, Vizi ES, Mackie K, Freund TF (1999). Presynaptically located CB1 cannabinoid receptors regulate GABA release from axon terminals of specific hippocampal interneurons. J Neurosci. 19(11):4544-4558.

Katona I, Sperlágh B, Maglóczky Z, Sántha E, Köfalvi A, Czirják S, Mackie K, Vizi ES, Freund TF (2000). GABAergic interneurons are the targets of cannabinoid actions in the human hippocampus. Neuroscience 100(4):797-804.

Katona I, Rancz EA, Acsady L, Ledent C, Mackie K, Hajos N, Freund TF (2001). Distribution of CB1 cannabinoid receptors in the amygdala and their role in the control of GABAergic transmission. J Neurosci. 21(23):9506-9518.

Katona I, Urbán GM, Wallace M, Ledent C, Jung KM, Piomelli D, Mackie K, Freund TF (2006). Molecular composition of the endocannabinoid system at glutamatergic synapses. J Neurosci. 26(21):5628-5637.

Katona I, Freund TF (2012). Multiple functions of endocannabinoid signaling in the brain. Annu Rev Neurosci. 35:529-558.

Kawamura Y, Fukaya M, Maejima T, Yoshida T, Miura E, Watanabe M, Ohno-Shosaku T, Kano M (2006). The CB1 cannabinoid receptor is the major cannabinoid receptor at excitatory presynaptic sites in the hippocampus and cerebellum. J Neurosci. 26(11):2991-3001.

Kaye JA, Swihart T, Howieson D, Dame A, Moore MM, Karnos T, Camicioli R, Ball M, Oken B, Sexton G (1997). Volume loss of the hippocampus and temporal lobe in healthy elderly persons destined to develop dementia. Neurology 48(5):1297-1304.

Kearn CS, Blake-Palmer K, Daniel E, Mackie K, Glass M (2005). Concurrent stimulation of cannabinoid CB1 and dopamine D2 receptors enhances heterodimer formation: a mechanism for receptor cross-talk? Mol Pharmacol. 67(5):1697-1670.

Kelly JF, Furukawa K, Barger SW, Rengen MR, Mark RJ, Blanc EM, Roth GS, Mattson MP (1996). Amyloid beta-peptide disrupts carbachol-induced muscarinic cholinergic signal transduction in cortical neurons. Proc Natl Acad Sci U S A 93(13):6753-6758.

Kendall DA, Yudowski GA (2017). Cannabinoid Receptors in the Central Nervous System: Their Signaling and Roles in Disease . Front Cell Neurosci. 10:294

Kim I, Wilson RE, Wellman CL (2005). Aging and cholinergic deafferentation alter GluR1 expression in rat frontal cortex. Neurobiol Aging 26(7):1073-1081.

Kim J, Isokawa M, Ledent C, Alger BE (2002). Activation of muscarinic acetylcholine receptors enhances the release of endogenous cannabinoids in the hippocampus. J Neurosci. 22(23):10182-10191.

Kim J, Alger BE (2004). Inhibition of cyclooxygenase-2 potentiates retrograde endocannabinoid effects in hippocampus. Nat Neurosci. 7(7):697-708.

Kim SH, Won SJ, Mao XO, Jin K, Greenberg DA (2006). Molecular mechanisms of cannabinoid protection from neuronal excitotoxicity. Mol Pharmacol. 69(3):691-696.

Kim WK, Ko KH (1998). Potentiation of N-methyl-D-aspartate-mediated neurotoxicity by immunostimulated murine microglia. J Neurosci Res. 54(1):17-26.

Kinsey SG, O'Neal ST, Long JZ, Cravatt BF, Lichtman AH (2011) Inhibition of endocannabinoid catabolic enzymes elicits anxiolytic-like effects in the marble burying assay. Pharmacol Biochem Behav. 98(1):21-27.

Kinsey SG, Wise LE, Ramesh D, Abdullah R, Selley DE, Cravatt BF, Lichtman AH (2013) Repeated low-dose administration of the monoacylglycerol lipase inhibitor JZL184 retains cannabinoid receptor type 1-mediated antinociceptive and gastroprotective effects. J Pharmacol Exp Ther. 345(3):492-501.

Kircher TT, Erb M, Grodd W, Leube DT (2005). Cortical activation during cholinesterase-inhibitor treatment in Alzheimer disease: preliminary findings from a pharmaco-fMRI study. Am J Geriatr Psychiatry 13(11):1006-1013.

Kiss J, McGovern J, Patel AJ (1988). Immunohistochemical localization of cells containing nerve growth factor receptors in the different regions of the adult rat forebrain. Neuroscience 27(3):731-748.

Klein J (2000). Membrane breakdown in acute and chronic neurodegeneration: focus on choline-containing phospholipids. J Neural Transm (Vienna) 107(8-9):1027-1063.

Koal T, Klavins K, Seppi D, Kemmler G, Humpel C (2015). Sphingomyelin SM(d18:1/18:0) is significantly enhanced in cerebrospinal fluid samples dichotomized by pathological amyloid-β42, tau, and phospho-tau-181 levels. J Alzheimers Dis. 44(4):1193-1201.

Kobayashi K, Miyazu K, Fukutani Y, Nakamura I, Yamaguchi N (1991). Morphometric study on the CH4 of the nucleus basalis of Meynert in Alzheimer's disease. Mol Chem Neuropathol. 15(3):193-206.

Kobayashi Y, Okuda T, Fujioka Y, Matsumura G, Nishimura Y, Haga T (2002). Distribution of the high-affinity choline transporter in the human and macaque monkey spinal cord. Neurosci Lett. 317(1):25-28.

Koch M, Kreutz S, Böttger C, Benz A, Maronde E, Ghadban C, Korf HW, Dehghani F (2011a). Palmitoylethanolamide protects dentate gyrus granule cells via peroxisome proliferator-activated receptor-α. Neurotox Res. 19(2):330-340.

Koch M, Kreutz S, Böttger C, Grabiec U, Ghadban C, Korf HW, Dehghani F (2011b). The cannabinoid WIN 55,212-2-mediated protection of dentate gyrus granule cells is driven by CB1 receptors and modulated by TRPA1 and Cav 2.2 channels. Hippocampus 21(5):554-564.

Kodirov SA, Jasiewicz J, Amirmahani P, Psyrakis D, Bonni K, Wehrmeister M, Lutz B (2009) Endogenous cannabinoids trigger the depolarization-induced suppression of excitation in the lateral amygdala. Learn Mem. 17(1):43-49.

Kölliker A (1896). Handbuch der Gewebelehre des Menschen. Vol. 2. Nervensystem. Engelmann, Leipzig.

Koppel J, Bradshaw H, Goldberg TE, Khalili H, Marambaud P, Walker MJ, Pazos M, Gordon ML, Christen E, Davies P (2009). Endocannabinoids in Alzheimer's disease and their impact on normative cognitive performance: a case-control and cohort study. Lipids Health Dis. 8:2.

Köppen JR, Stuebing SL, Sieg ML, Blackwell AA, Blankenship PA, Cheatwood JL, Wallace DG (2016). Cholinergic deafferentation of the hippocampus causes non-temporally graded retrograde amnesia in an odor discrimination task. Behav Brain Res. 299:97-104.

Kosaka T, Tauchi M, Dahl JL (1988). Cholinergic neurons containing GABA-like and/or glutamic acid decarboxylase-like immunoreactivities in various brain regions of the rat. Exp Brain Res. 70(3):605-617.

Kreitzer AC, Regehr WG (2001). Retrograde inhibition of presynaptic calcium influx by endogenous cannabinoids at excitatory synapses onto Purkinje cells. Neuron 29(3):717-727.

Kreutz S, Koch M, Ghadban C, Korf HW, Dehghani F (2007). Glia. 57(3):286-294. Cannabinoids and neuronal damage: differential effects of THC, AEA and 2-AG on activated microglial cells and degenerating neurons in excitotoxically lesioned rat organotypic hippocampal slice cultures. Exp Neurol. 203(1):246-257.

Kreutz S, Koch M, Böttger C, Ghadban C, Korf HW, Dehghani F (2009). 2-Arachidonoylglycerol elicits neuroprotective effects on excitotoxically lesioned dentate gyrus granule cells via abnormal-cannabidiol-sensitive receptors on microglial cells. Glia 57(3):286-294.

Krishnan S, Cairns R, Howard R (2009). Cannabinoids for the treatment of dementia. Cochrane Database Syst Rev. 2):CD007204.

Kristt DA, McGowan RA Jr, Martin-MacKinnon N, Solomon J (1985). Basal forebrain innervation of rodent neocortex: studies using acetylcholinesterase histochemistry, Golgi and lesion strategies. Brain Res. 337(1):19-39.

Kromer Vogt LJ, Hyman BT, Van Hoesen GW, Damasio AR (1990). Pathological alterations in the amygdala in Alzheimer's disease. Neuroscience 37(2):377-385.

Kubo T, Fukuda K, Mikami A, Maeda A, Takahashi H, Mishina M, Haga T, Haga K, Ichiyama A, Kangawa K, et al. (1986). Cloning, sequencing and expression of complementary DNA encoding the muscarinic acetylcholine receptor. Nature 323: 411–416.

Kuhn HG, Dickinson-Anson H, Gage FH (1996). Neurogenesis in the dentate gyrus of the adult rat: age-related decrease of neuronal progenitor proliferation. J Neurosci. 16(6):2027-2033.

Kurosawa M, Sato A, Sato Y (1989). Stimulation of the nucleus basalis of Meynert increases acetylcholine release in the cerebral cortex in rats. Neurosci. Lett. 98, 45–50.

Lafenêtre P, Chaouloff F, Marsicano G (2009). Bidirectional regulation of novelty-induced behavioral inhibition by the endocannabinoid system. Neuropharmacology 57(7-8):715-721.

Lauckner JE, Hille B, Mackie K (2005). The cannabinoid agonist WIN55,212-2 increases intracellular calcium via CB1 receptor coupling to Gq/11 G proteins. Proc Natl Acad Sci U S A 102(52):19144-19149.

Lawrence DK, Gill EW (1975). The effects of delta1-tetrahydrocannabinol and other cannabinoids on spin-labeled liposomes and their relationship to mechanisms of general anesthesia. Mol Pharmacol. 11(5):595-602.

Lazarova-Bakarova MB, Petkova BP, Todorov IK, Petkov VD (1991). Memory impairment induced by combined disturbance of noradrenergic and dopaminergic neurotransmissions: effects of nootropic drugs. Acta Physiol Pharmacol Bulg. 17(1):29-34.

Ledent C, Vaugeois JM, Schiffmann SN, Pedrazzini T, El Yacoubi M, Vanderhaeghen JJ, Costentin J, Heath JK, Vassart G, Parmentier M (1997). Aggressiveness, hypoalgesia and high blood pressure in mice lacking the adenosine A2a receptor. Nature. 388(6643):674-678.

Ledent C, Valverde O, Cossu G, Petitet F, Aubert JF, Beslot F, Böhme GA, Imperato A, Pedrazzini T, Roques BP, Vassart G, Fratta W, Parmentier M (1999). Unresponsiveness to cannabinoids and reduced addictive effects of opiates in CB1 receptor knockout mice. Science. 283(5400):401-404.

Lee JE, Han PL (2013). An update of animal models of Alzheimer disease with a reevaluation of plaque depositions. Exp Neurobiol. 22(2):84-95.

Lee JE, Jeong da U, Lee J, Chang WS, Chang JW (2016). The effect of nucleus basalis magnocellularis deep brain stimulation on memory function in a rat model of dementia. BMC Neurol.16:6.

Lee JH, Agacinski G, Williams JH, Wilcock GK, Esiri MM, Francis PT, Wong PT, Chen CP, Lai MK (2010). Intact cannabinoid CB1 receptors in the Alzheimer's disease cortex. Neurochem Int. 57(8):985-989.

Lehéricy S, Hirsch EC, Cervera-Piérot P, Hersh LB, Bakchine S, Piette F, Duyckaerts C, Hauw JJ, Javoy-Agid F, Agid Y (1993). Heterogeneity and selectivity of the degeneration of cholinergic neurons in the basal forebrain of patients with Alzheimer's disease. J Comp Neurol. 330(1):15-31.

Levey AI, Kitt CA, Simonds WF, Price DL, Brann MR (1991). Identification and localization of muscarinic acetylcholine receptor proteins in brain with subtype-specific antibodies. J Neurosci. 11(10):3218-3226.

Levey AI, Edmunds SM, Heilman CJ, Desmond TJ and Frey KA (1994). Localization of muscarinic m3 receptor protein and M3 receptor binding in rat brain. Neuroscience 63: 207–221.

Levey AI, Edmunds SM, Hersch SM, Wiley RG, Heilman CJ (1995). Light and electron microscopic study of m2 muscarinic acetylcholine receptor in the basal forebrain of the rat. J Comp Neurol. 351(3):339-356

Little PJ, Compton DR, Johnson MR, Melvin LS, Martin BR (1988). Pharmacology and stereoselectivity of structurally novel cannabinoids in mice. J Pharmacol Exp Ther. 247(3):1046-1051.

Ljubojevic V, Luu P, De Rosa E (2014). Cholinergic contributions to supramodal attentional processes in rats. J Neurosci. 34(6):2264-2275.

Llano I, Leresche N, Marty A (1991). Calcium entry increases the sensitivity of cerebellar Purkinje cells to applied GABA and decreases inhibitory synaptic currents. Neuron 6(4):565-574.

Long JZ, Li W, Booker L, Burston JJ, Kinsey SG, Schlosburg JE, Pavón FJ, Serrano AM, Selley DE, Parsons LH, Lichtman AH, Cravatt BF (2009). Selective blockade of 2-arachidonoylglycerol hydrolysis produces cannabinoid behavioral effects. Nat Chem Biol. 5(1):37-44.

Lu XR, Ong WY, Mackie K (1999). A light and electron microscopic study of the CB1 cannabinoid receptor in monkey basal forebrain. J Neurocytol. 28(12):1045-1051.

Lukas RJ, Changeux JP, Le Novère N, Albuquerque EX, Balfour DJ, Berg DK, Bertrand D, Chiappinelli VA, Clarke PB, Collins AC, Dani JA, Grady SR, Kellar KJ, Lindstrom JM, Marks MJ, Quik M, Taylor PW, Wonnacott S (1999). International Union of Pharmacology. XX. Current status of the nomenclature for nicotinic acetylcholine receptors and their subunits. Pharmacol Rev. 51(2):397-401.

Luskin MB (1993). Restricted proliferation and migration of postnatally generated neurons derived from the forebrain subventricular zone. Neuron 11(1):173-189.

Macdonald KE, Bartlett JW, Leung KK, Ourselin S, Barnes J; ADNI investigators (2013). The value of hippocampal and temporal horn volumes and rates of change in predicting future conversion to AD. Alzheimer Dis Assoc Disord. 27(2):168-173.

Mackie K, Hille B (1992). Cannabinoids inhibit N-type calcium channels in neuroblastoma-glioma cells. Proc Natl Acad Sci U S A 89(9):3825-3829.

Mackie K, Lai Y, Westenbroek R, Mitchell R (1995). Cannabinoids activate an inwardly rectifying potassium conductance and inhibit Q-type calcium currents in AtT20 cells transfected with rat brain cannabinoid receptor. J Neurosci. 15(10):6552-6561.

Maejima T, Hashimoto K, Yoshida T, Aiba A, Kano M (2001). Presynaptic inhibition caused by retrograde signal from metabotropic glutamate to cannabinoid receptors. Neuron 31(3):463-475.

Maejima T, Oka S, Hashimotodani Y, Ohno-Shosaku T, Aiba A, Wu D, Waku K, Sugiura T, Kano M (2005). Synaptically driven endocannabinoid release requires Ca2+-assisted metabotropic glutamate receptor subtype 1 to phospholipase Cbeta4 signaling cascade in the cerebellum. J Neurosci. 25(29):6826-6835.

Mailleux P, Vanderhaeghen JJ (1992). Distribution of neuronal cannabinoid receptor in the adult rat brain: a comparative receptor binding radioautography and in situ hybridization histochemistry. Neuroscience 48(3):655-668.

Maire JC, Wurtman RJ (1985). Effects of electrical stimulation and choline availability on the release and contents of acetylcholine and choline in superfused slices from rat striatum. J Physiol (Paris) 80(3):189-195.

Majocha RE, Jungalwala FB, Rodenrys A, Marotta CA (1989). Monoclonal antibody to embryonic CNS antigen A2B5 provides evidence for the involvement of membrane components at sites of Alzheimer degeneration and detects sulfatides as well as gangliosides. J Neurochem. 53(3):953-961.

Makara JK, Katona I, Nyíri G, Németh B, Ledent C, Watanabe M, de Vente J, Freund TF, Hájos N (2007). Involvement of nitric oxide in depolarization-induced suppression of inhibition in hippocampal pyramidal cells during activation of cholinergic receptors. J Neurosci. 27(38):10211-10222.

Malin EL, McGaugh JL (2006) Differential involvement of the hippocampus, anterior cingulate cortex, and basolateral amygdala in memory for context and footshock. Proc Natl Acad Sci U S A 103(6):1959-1963.

Maneuf YP, Brotchie JM (1997). Paradoxical action of the cannabinoid WIN 55,212-2 in stimulated and basal cyclic AMP accumulation in rat globus pallidus slices. Br J Pharmacol. 120(8):1397-1408.

Manev H, Favaron M, Guidotti A, Costa E (1989). Delayed increase of Ca2+ influx elicited by glutamate: role in neuronal death. Mol Pharmacol. 36(1):106-112.

Manuel I, González de San Román E, Giralt MT, Ferrer I, Rodríguez-Puertas R (2014). Type-1 cannabinoid receptor activity during Alzheimer's disease progression. J Alzheimers Dis. 42(3):761-766.

Manuel I, Lombardero L, LaFerla FM, Giménez-Llort L, Rodríguez-Puertas R (2016). Activity of muscarinic, galanin and cannabinoid receptors in the prodromal and advanced stages in the triple transgenic mice model of Alzheimer's disease. Neuroscience 329:284-293.

Mapstone M, Cheema AK, Fiandaca MS, Zhong X, Mhyre TR, MacArthur LH, Hall WJ, Fisher SG, Peterson DR, Haley JM, Nazar MD, Rich SA, Berlau DJ, Peltz CB, Tan MT, Kawas CH, Federoff HJ (2014). Plasma phospholipids identify antecedent memory impairment in older adults. Nat Med. 20(4):415-418.

Margulies JE, Hammer RP Jr (1991). Delta 9-tetrahydrocannabinol alters cerebral metabolism in a biphasic, dose-dependent manner in rat brain. Eur J Pharmacol. 202(3):373-378.

Marsicano, G, Lutz, B (1999). Expression of the cannabinoid receptor CB1 in distinct neuronal subpopulations in the adult mouse forebrain. European Journal of Neuroscience 11(12):4213-4225.

Marsicano G, Wotjak CT, Azad SC, Bisogno T, Rammes G, Cascio MG, Hermann H, Tang J, Hofmann C, Zieglgänsberger W, Di Marzo V, Lutz B (2002). The endogenous cannabinoid system controls extinction of aversive memories. Nature 418(6897):530-534.

Marsicano G, Goodenough S, Monory K, Hermann H, Eder M, Cannich A, Azad SC, Cascio MG, Gutiérrez SO, van der Stelt M, López-Rodriguez ML, Casanova E, Schütz G, Zieglgänsberger W, Di Marzo V, Behl C, Lutz B (2003). CB1 cannabinoid receptors and on-demand defense against excitotoxicity. Science 302(5642):84-88.

Martin HG, Bernabeu A, Lassalle O, Bouille C, Beurrier C, Pelissier-Alicot AL, Manzoni OJ (2015). Endocannabinoids Mediate Muscarinic Acetylcholine Receptor-Dependent Long-Term Depression in the Adult Medial Prefrontal Cortex. Front Cell Neurosci. 9:457.

Martín V, Fabelo N, Santpere G, Puig B, Marín R, Ferrer I, Díaz M (2010). Lipid alterations in lipid rafts from Alzheimer's disease human brain cortex. J Alzheimers Dis. 19(2):489-502.

Martínez-Gardeazabal J, González de San Román E, Moreno M, Llorente-Ovejero A, Manuel I, Rodriguez-Puertas R (2017). Lipid mapping of the rat brain for models of disease. Biochim Biophys Acta.

Mash DC, Flynn DD, Potter LT (1985). Loss of M2 muscarine receptors in the cerebral cortex in Alzheimer's disease and experimental cholinergic denervation. Science 228(4703):1115-1117.

Mash DC, Potter LT (1986). Autoradiographic localization of M1 and M2 muscarine receptors in the rat brain. Neuroscience 19: 551–564.

Matsuda LA, Lolait SJ, Brownstein MJ, Young AC, Bonner TI (1990). Structure of a cannabinoid receptor and functional expression of the cloned cDNA. Nature 346(6284):561-564.

Mattson MP (2008). Glutamate and neurotrophic factors in neuronal plasticity and disease. Ann N Y Acad Sci. 1144:97-112. Review.

Maysami S, Nguyen D, Zobel F, Heine S, Höpfner M, Stangel M (2006). Oligodendrocyte precursor cells express a functional chemokine receptor CCR3: implications for myelination. J Neuroimmunol. 178(1-2):17-23.

Mazère J, Prunier C, Barret O, Guyot M, Hommet C, Guilloteau D, Dartigues JF, Auriacombe S, Fabrigoule C, Allard M (2008). In vivo SPECT imaging of vesicular acetylcholine transporter using [(123)I]-IBVM in early Alzheimer's disease. Neuroimage 40(1):280-288.

McCoy KL, Matveyeva M, Carlisle SJ, Cabral GA (1999). Cannabinoid inhibition of the processing of intact lysozyme by macrophages: evidence for CB2 receptor participation. J Pharmacol Exp Ther. 289(3):1620-1625.

McGaughy J, Kaiser T, Sarter M (1996). Behavioral vigilance following infusions of 192 IgG-saporin into the basal forebrain: selectivity of the behavioral impairment and relation to cortical AChE-positive fiber density. Behav Neurosci. 110(2):247-265.

McGeer EG, McGeer PL, Kamo H, Tago H, Harrop R (1986). Cortical metabolism, acetylcholinesterase staining and pathological changes in Alzheimer's disease. Can J Neurol Sci. 13(4 Suppl):511-516.

McGeer PL, McGeer EG, Suzuki J, Dolman CE, Nagai T (1984). Aging, Alzheimer's disease, and the cholinergic system of the basal forebrain. Neurology 34(6):741-745.

McGeown WJ, Shanks MF, Venneri A (2008). Prolonged cholinergic enrichment influences regional cortical activation in early Alzheimer's disease. Neuropsychiatr Dis Treat. 4(2):465-476.

Mechawar N, Cozzari C, Descarries L (2000). Cholinergic innervation in adult rat cerebral cortex: a quantitative immunocytochemical description. J Comp Neurol. 428(2):305-318.

Mechoulam R, Shani A, Edery H, Grunfeld Y (1970). Chemical basis of hashish activity. Science 169(3945):611-612.

Mechoulam R (1986). The Pharmacohistory of Cannabis sativa. Boca Raton, FL: CRC.

Mechoulam R, Ben-Shabat S, Hanus L, Ligumsky M, Kaminski NE, Schatz AR, Gopher A, Almog S, Martin BR, Compton DR, et al (1995). Identification of an endogenous 2-monoglyceride, present in canine gut, that binds to cannabinoid receptors. Biochem Pharmacol. 50(1):83-90.

Mehlhorn G, Löffler T, Apelt J, Rossner S, Urabe T, Hattori N, Nagamatsu S, Bigl V, Schliebs R (1998). Glucose metabolism in cholinoceptive cortical rat brain regions after basal forebrain cholinergic lesion. Int J Dev Neurosci.16(7-8):675-690.

Melvin LS, Milne GM, Johnson MR, Subramaniam B, Wilken GH, Howlett AC (1993). Structure-activity relationships for cannabinoid receptor-binding and analgesic activity: studies of bicyclic cannabinoid analogs. Mol Pharmacol. 44(5):1008-1015.

Mendis LH, Grey AC, Faull RL, Curtis MA (2016). Hippocampal lipid differences in Alzheimer's disease: a human brain study using matrix-assisted laser desorption/ionization-imaging mass spectrometry. Brain Behav. 6(10):e00517.

Meng ID, Manning BH, Martin WJ, Fields HL (1998) An analgesia circuit activated by cannabinoids. Nature 395(6700):381-383.

Mesulam MM, Mufson EJ, Wainer BH, Levey AI (1983a). Central cholinergic pathways in the rat: an overview based on an alternative nomenclature (Ch1-Ch6). Neuroscience 10(4):1185-1201.

Mesulam MM, Mufson E.J, Levey AI, Wainer B.H (1983b). Cholinergic innervation of cortex by the basal forebrain: cytochemistry and cortical connections of the septal area, diagonal band nuclei, nucleus basalis (substantia innominata), and hypothalamus in the rhesus monkey. J. Comp. Neurol. 214, 170–197.

Mesulam MM, Mufson EJ (1984). Neural inputs into the nucleus basalis of the substantia innominata (Ch4) in the rhesus monkey. Brain 107 (Pt 1), 253–274.

Mesulam MM, Mufson EJ, Levey AI, Wainer BH (1984). Atlas of cholinergic neurons in the forebrain and upper brainstem of the macaque based on monoclonal choline acetyltransferase immunohistochemistry and acetylcholinesterase histochemistry. Neuroscience 12(3):669-686.

Mesulam MM (1987). Asymmetry of neural feedback in the organization of behavioral states. Science 237, 537–538.

Mesulam MM and Geula C (1988). Nucleus basalis (Ch4) and cortical cholinergic innervation in the human brain: observations based on the distribution of acetylcholinesterase and choline acetyltransferase. J Comp Neurol. 275(2):216-240.

Mesulam MM, Geula C, Bothwell MA, Hersh LB (1989). Human reticular formation: cholinergic neurons of the pedunculopontine and laterodorsal tegmental nuclei and some cytochemical comparisons to forebrain cholinergic neurons. J Comp Neurol. 283(4):611-633.

Mesulam MM (1990). Human brain cholinergic pathways. Prog Brain Res. 84:231-241.

Mesulam MM and Geula C (1994). Chemoarchitectonics of axonal and perikaryal acetylcholinesterase along information processing systems of the human cerebral cortex. Brain Res Bull. 33(2):137-153.

Mesulam MM (1995). Cholinergic pathways and the ascending reticular activating system of the human brain. Ann N Y Acad Sci. 757:169-179.

Mesulam MM (1998). Some cholinergic themes related to Alzheimer's disease: synaptology of the nucleus basalis, location of m2 receptors, interactions with amyloid metabolism, and perturbations of cortical plasticity. J Physiol Paris 92(3-4):293-298. Review.

Mesulam MM (2004). The cholinergic innervation of the human cerebral cortex. Prog Brain Res. 145:67-78.

Mesulam MM (2013). Cholinergic circuitry of the human nucleus basalis and its fate in Alzheimer's disease. J Comp Neurol. 521(18):4124-4144.

Metna-Laurent M, Soria-Gómez E, Verrier D, Conforzi M, Jégo P, Lafenêtre P, Marsicano G (2012). Bimodal control of fear-coping strategies by CB_1 cannabinoid receptors. J Neurosci. 32(21):7109-7118.

Meyer EM, Arendash GW, Judkins JH, Ying L, Wade C, Kem WR (1987). Effects of nucleus basalis lesions on the muscarinic and nicotinic modulation of [3H]acetylcholine release in the rat cerebral cortex. J Neurochem. 49(6):1758-1762.

Meynert, T. (J.J. Putnam, Trans.) (1872). The brain of mammals. In: Stricker, S. (Ed.), A Manual of Histology. William Wood, New York, pp. 650–766.

Miettinen PS, Pihlajamäki M, Jauhiainen AM, Tarkka IM, Gröhn H, Niskanen E, Hänninen T, Vanninen R, Soininen H (2011). Effect of cholinergic stimulation in early Alzheimer's disease - functional imaging during a recognition memory task. Curr Alzheimer Res. 8(7):753-764.

Miettinen PS, Jauhiainen AM, Tarkka IM, Pihlajamäki M, Gröhn H, Niskanen E, Hänninen T, Vanninen R, Soininen H (2015). Long-Term Response to Cholinesterase Inhibitor Treatment Is Related to Functional MRI Response in Alzheimer's Disease. Dement Geriatr Cogn Disord. 40(5-6):243-255.

Miller FD, Kaplan DR (2001). Neurotrophin signalling pathways regulating neuronal apoptosis. Cell Mol Life Sci. 58(8):1045-1053.

Millington WR, Wurtman RJ (1982). Choline administration elevates brain phosphorylcholine concentrations. J Neurochem. 38(6):1748-1752.

Minami M, Kimura S, Endo T, Hamaue N, Hirafuji M, Togashi H, Matsumoto M, Yoshioka M, Saito H, Watanabe S, Kobayashi T, Okuyama H (1997). Dietary docosahexaenoic acid increases cerebral acetylcholine levels and improves passive avoidance performance in stroke-prone spontaneously hypertensive rats. Pharmacol Biochem Behav. 58(4):1123-1129.

Misawa H, Nakata K, Matsuura J, Nagao M, Okuda T, Haga T (2001). Distribution of the high-affinity choline transporter in the central nervous system of the rat. Neuroscience 105(1):87-98.

Mishkin M (1978). Memory in monkeys severely impaired by combined but not by separate removal of amygdala and hippocampus. Nature 273(5660):297-308.

Mohapel P, Leanza G, Kokaia M, Lindvall O (2005). Forebrain acetylcholine regulates adult hippocampal neurogenesis and learning. Neurobiol Aging 26(6):939-946.

Moise AM, Eisenstein SA, Astarita G, Piomelli D, Hohmann AG (2008) An endocannabinoid signaling system modulates anxiety-like behavior in male Syrian hamsters. Psychopharmacology (Berl) 200(3):333-346.

Monory K, Polack M, Remus A, Lutz B, Korte M (2015). Cannabinoid CB1 receptor calibrates excitatory synaptic balance in the mouse hippocampus. J Neurosci. 35(9):3842-3850.

Morena M, Leitl KD, Vecchiarelli HA, Gray JM, Campolongo P, Hill MN (2016) Emotional arousal state influences the ability of amygdalar endocannabinoid signaling to modulate anxiety. Neuropharmacology 111:59-69.

Motohashi N, Dubois A, Scatton B (1986). Lesion of nucleus basalis magnocellularis decreases [3H]hemicholinium-3 binding (as measured by autoradiography) in the amygdala and frontal cortex of the rat. Neurosci Lett. 71(1):7-12.

Mrzljak L, Levey AI, Belcher S, Goldman-Rakic PS (1998). Localization of the m2 muscarinic acetylcholine receptor protein and mRNA in cortical neurons of the normal and cholinergically deafferented rhesus monkey. J Comp Neurol. 390(1):112-132.

Muccioli GG, Xu C, Odah E, Cudaback E, Cisneros JA, Lambert DM, López Rodríguez ML, Bajjalieh S, Stella N (2007). Identification of a novel endocannabinoid-hydrolyzing enzyme expressed by microglial cells. J Neurosci. 27(11):2883-2889.

Mufson EJ, Kroin JS, Sendera TJ, Sobreviela T (1999). Distribution and retrograde transport of trophic factors in the central nervous system: functional implications for the treatment of neurodegenerative diseases. Prog Neurobiol. 57(4):451-484. Review.

Mufson EJ, Ginsberg SD, Ikonomovic MD, DeKosky ST (2003). Human cholinergic basal forebrain: chemoanatomy and neurologic dysfunction. J. Chem. Neuroanat. 26, 233–242.

Mulder C, Wahlund LO, Teerlink T, Blomberg M, Veerhuis R, van Kamp GJ, Scheltens P, Scheffer PG (2003). Decreased lysophosphatidylcholine/phosphatidylcholine ratio in cerebrospinal fluid in Alzheimer's disease. J Neural Transm (Vienna). 110(8):949-955.

Mulder J, Zilberter M, Pasquaré SJ, Alpár A, Schulte G, Ferreira SG, Köfalvi A, Martín-Moreno AM, Keimpema E, Tanila H, Watanabe M, Mackie K, Hortobágyi T, de Ceballos ML, Harkany T (2011). Molecular reorganization of endocannabinoid signalling in Alzheimer's disease. Brain 134(Pt 4):1041-1060.

Müller I, Çalışkan G, Stork O (2015) The GAD65 knock out mouse – a model for GABAergic processes in fear- and stress-induced psychopathology. Genes Brain Behav 14(1):37-45.

Mulugeta E, Chandranath I, Karlsson E, Winblad B, Adem A (2006). Temporal and region-dependent changes in muscarinic M4 receptors in the hippocampus and entorhinal cortex of adrenalectomized rats. Exp Brain Res. 173(2):309-317.

Munro S, Thomas KL, Abu-Shaar M (1993). Molecular characterization of a peripheral receptor for cannabinoids. Nature 365(6441):61-65.

Myhrer, T. (2003). Neurotransmitter systems involved in learning and memory in the rat: a meta-analysis based on studies of four behavioral tasks. Brain Research Reviews 41(2-3):268-287.

Nadler V, Mechoulam R, Sokolovsky M (1993). Blockade of 45Ca2+ influx through the N-methyl-D-aspartate receptor ion channel by the non-psychoactive cannabinoid HU-211. Brain Res. 622(1-2):79-85.

Narushima M, Uchigashima M, Fukaya M, Matsui M, Manabe T, Hashimoto K, Watanabe M, Kano M (2007). Tonic enhancement of endocannabinoid-mediated retrograde suppression of inhibition by cholinergic interneuron activity in the striatum. J Neurosci. 27(3):496-506.

Navarrete M, Araque A (2008). Endocannabinoids mediate neuron-astrocyte communication. Neuron 57(6):883-893.

Nazarinia, E, Rezayof, A, Sardari, M, Yazdanbakhsh, N (2017). Contribution of the basolateral amygdala NMDA and muscarinic receptors in rat's memory retrieval. Neurobiol. Learn. Mem. 139, 28-36.

Neary D, Snowden JS, Mann DM, Bowen DM, Sims NR, Northen B, Yates PO, Davison AN. Alzheimer's disease: a correlative study (1986). J Neurol Neurosurg Psychiatry. 49(3):229-237.

Nelson RL, Guo Z, Halagappa VM, Pearson M, Gray AJ, Matsuoka Y, Brown M, Martin B, Iyun T, Maudsley S, Clark RF, Mattson MP (2007). Prophylactic treatment with paroxetine ameliorates behavioral deficits and retards the development of amyloid and tau pathologies in 3xTgAD mice. Exp Neurol. 205(1):166-176.

Nie J, Lewis DL (2001). Structural domains of the CB1 cannabinoid receptor that contribute to constitutive activity and G-protein sequestration. J Neurosci. 21(22):8758-8764.

Nitsch R, Pittas A, Blusztajn JK, Slack BE, Growdon JH, Wurtman RJ (1991). Alterations of phospholipid metabolites in postmortem brain from patients with Alzheimer's disease. Ann N Y Acad Sci. 640:110-113.

Nitsch RM, Slack BE, Wurtman RJ, Growdon JH (1992a). Release of Alzheimer amyloid precursor derivatives stimulated by activation of muscarinic acetylcholine receptors. Science 258(5080):304-307.

Nitsch RM, Blusztajn JK, Pittas AG, Slack BE, Growdon JH, Wurtman RJ (1992b). Evidence for a membrane defect in Alzheimer disease brain. Proc Natl Acad Sci U S A 89(5):1671-1675.

Nordberg A (1992). Neuroreceptor changes in Alzheimer disease. Cerebrovasc Brain Metab Rev. 4(4):303-328. Review.

Nordberg A, Alafuzoff I, Winblad B (1992). Nicotinic and muscarinic subtypes in the human brain: changes with aging and dementia. J Neurosci Res. 31(1):103-111.

Nordberg A, Lundqvist H, Hartvig P, Lilja A, Långström B (1995). Kinetic analysis of regional (S)(-)11C-nicotine binding in normal and Alzheimer brains--in vivo assessment using positron emission tomography. Alzheimer Dis Assoc Disord. Spring 9(1):21-27.

Nyíri G, Szabadits E, Cserép C, Mackie K, Shigemoto R, Freund TF (2005). GABAB and CB1 cannabinoid receptor expression identifies two types of septal cholinergic neurons. Eur J Neurosci. 21(11):3034-3042.

Oddo S, Caccamo A, Shepherd JD, Murphy MP, Golde TE, Kayed R, Metherate R, Mattson MP, Akbari Y, LaFerla FM (2003). Triple-transgenic model of Alzheimer's disease with plaques and tangles: intracellular Abeta and synaptic dysfunction. Neuron 39(3):409-421.

Ohara K, Kondo N, Xie D, Tanabe K, Yamamoto T, Kosaka K, Miyasato K, Ohara K (1994). Normal sequences of muscarinic acetylcholine receptors (m1 and m2) in patients with Alzheimer's disease and vascular dementia. Neurosci Lett. 178(1):23-26.

Ohno-Shosaku, T., Maejima, T., & Kano, M. (2001). Endogenous cannabinoids mediate retrograde signals from depolarized postsynaptic neurons to presynaptic terminals. Neuron 29(3):729-738.

Ohno-Shosaku T, Shosaku J, Tsubokawa H, Kano M (2002). Cooperative endocannabinoid production by neuronal depolarization and group I metabotropic glutamate receptor activation. Eur J Neurosci. 15(6):953-961.

Ohno-Shosaku T, Matsui M, Fukudome Y, Shosaku J, Tsubokawa H, Taketo MM, Manabe T, Kano M (2003). Postsynaptic M1 and M3 receptors are responsible for the muscarinic enhancement of retrograde endocannabinoid signalling in the hippocampus. Eur J Neurosci. 18(1):109-116.

Ohno-Shosaku T, Hashimotodani Y, Ano M, Takeda S, Tsubokawa H, Kano M (2007). Endocannabinoid signalling triggered by NMDA receptor-mediated calcium entry into rat hippocampal neurons. J Physiol. 584(Pt 2):407-418.

Okuda, T. and Haga, T (2003). High-affinity choline transporter. Neurochem Res. 28: 483–488.

Orta-Salazar E, Aguilar-Vázquez A, Martínez-Coria H, Luquín-De Anda S, Rivera-Cervantes M, Beas-Zarate C, Feria-Velasco A, Díaz-Cintra S (2014). REST/NRSF-induced changes of ChAT protein expression in the neocortex and hippocampus of the 3xTg-AD mouse model for Alzheimer's disease. Life Sci. 116(2):83-89.

Paban V, Chambon C, Farioli F, Alescio-Lautier B (2011). Gene regulation in the rat prefrontal cortex after learning with or without cholinergic insult. Neurobiol Learn. 95(4):441-452.

Paban V, Chambon C, Jaffard M, Alescio-Lautier B (2005). Behavioral effects of basal forebrain cholinergic lesions in young adult and aging rats. Behav Neurosci. 119(4):933-945.

Pacheco MA, Ward SJ, Childers SR (1993). Identification of cannabinoid receptors in cultures of rat cerebellar granule cells. Brain Res. 603(1):102-110.

Palazuelos J, Aguado T, Egia A, Mechoulam R, Guzmán M, Galve-Roperh I (2006). Non-psychoactive CB2 cannabinoid agonists stimulate neural progenitor proliferation. FASEB J. 20(13):2405-2407.

Pan B, Wang W, Blankman JL, Cravatt BF, Liu QS (2011) Alterations of endocannabinoid signaling, synaptic plasticity, learning, and memory in monoacylglycerol lipase knock-out mice. J Neurosci. 31(38):13420-13430.

Pan X, Ikeda SR, Lewis DL (1998). SR 141716A acts as an inverse agonist to increase neuronal voltage-dependent Ca2+ currents by reversal of tonic CB1 cannabinoid receptor activity. Mol Pharmacol. 54(6):1064-1072.

Parent M, Bedard MA, Aliaga A, Soucy JP, Landry St-Pierre E, Cyr M, Kostikov A, Schirrmacher E, Massarweh G, Rosa-Neto P (2012). PET imaging of cholinergic deficits in rats using [18F]fluoroethoxybenzovesamicol ([18F]FEOBV). Neuroimage 1;62(1):555-561.

Parent MJ, Cyr M, Aliaga A, Kostikov A, Schirrmacher E, Soucy JP, Mechawar N, Rosa-Neto P, Bedard MA (2013). Concordance between in vivo and postmortem measurements of cholinergic denervation in rats using PET with [18F]FEOBV and choline acetyltransferase immunochemistry. EJNMMI Res. 3(1):70.

Pascual J, Fontán A, Zarranz JJ, Berciano J, Flórez J, Pazos A (1991). High-affinity choline uptake carrier in Alzheimer's disease: implications for the cholinergic hypothesis of dementia. Brain Res. 552(1):170-174.

Pascual-Alonso T, González-Zárate JL (1992). Subtypes of muscarinic acetylcholine receptor following the experimental denervation of the cholinergic pathway ascending to the neocortex. Arch Neurobiol (Madr). 55(3):116-123.

Passmore MJ (2008). The cannabinoid receptor agonist nabilone for the treatment of dementia-related agitation. Int J Geriatr Psychiatry 23(1):116-117.

Pearson RC, Sofroniew MV, Cuello AC, Powell TP, Eckenstein F, Esiri MM, Wilcock GK (1983). Persistence of cholinergic neurons in the basal nucleus in a brain with senile dementia of the Alzheimer's type demonstrated by immunohistochemical staining for choline acetyltransferase. Brain Res. 289(1-2):375-379.

Peng S, Wuu J, Mufson EJ, Fahnestock M (2004). Increased proNGF levels in subjects with mild cognitive impairment and mild Alzheimer disease. J Neuropathol Exp Neurol. 63(6):641-649.

Peppard RF, Martin WR, Clark CM, Carr GD, McGeer PL, Calne DB (1990). Cortical glucose metabolism in Parkinson's and Alzheimer's disease. J Neurosci Res. 1990 Dec;27(4):561-568.

Perez SE, He B, Muhammad N, Oh KJ, Fahnestock M, Ikonomovic MD, Mufson EJ (2011). Cholinotrophic basal forebrain system alterations in 3xTg-AD transgenic mice. Neurobiol Dis. 41(2):338-352.

Pernber Z, Blennow K, Bogdanovic N, Månsson JE, Blomqvist M (2012). Altered distribution of the gangliosides GM1 and GM2 in Alzheimer's disease. Dement Geriatr Cogn Disord. 33(2-3):174-188.

Perry EK, Gibson PH, Blessed G, Perry RH, Tomlinson BE (1977). Neurotransmitter enzyme abnormalities in senile dementia. Choline acetyltransferase and glutamic acid decarboxylase activities in necropsy brain tissue. J Neurol Sci. 34(2):247-265.

Perry EK, Perry RH, Blessed G, Tomlinson BE (1978a). Changes in brain cholinesterases in senile dementia of Alzheimer type. Neuropathol Appl Neurobiol. 4(4):273-277.

Perry EK, Tomlinson BE, Blessed G, Bergmann K, Gibson PH, Perry RH (1978b). Correlation of cholinergic abnormalities with senile plaques and mental test scores in senile dementia. Br Med J. 2(6150):1457-1459.

Perry EK, Johnson M, Kerwin JM, Piggott MA, Court JA, Shaw PJ, Ince PG, Brown A, Perry RH (1992). Convergent cholinergic activities in aging and Alzheimer's disease. Neurobiol Aging 13(3):393-400.

Perry E, Walker M, Grace J, Perry R (1999). Acetylcholine in mind: a neurotransmitter correlate of consciousness? Trends Neurosci. 22(6):273-280. Review.

Perry RH, Candy JM, Perry EK, Irving D, Blessed G, Fairbairn AF, Tomlinson BE (1982). Extensive loss of choline acetyltransferase activity is not reflected by neuronal loss in the nucleus of Meynert in Alzheimer's disease. Neurosci Lett. 33(3):311-315.

Pertwee RG (1999). Pharmacology of cannabinoid receptor ligands. Curr Med Chem. 6(8):635-664. Review.

Pertwee RG (2005). Pharmacological actions of cannabinoids Handb Exp Pharmacol. (168):1-51. Review.

Pertwee RG (2008). Ligands that target cannabinoid receptors in the brain: from THC to anandamide and beyond. Addict Biol. 13(2):147-159. Review.

Pertwee RG, Howlett AC, Abood ME, Alexander SP, Di Marzo V, Elphick MR, Greasley PJ, Hansen HS, Kunos G, Mackie K, Mechoulam R, Ross RA (2010). International Union of Basic and Clinical Pharmacology. LXXIX. Cannabinoid receptors and their ligands: beyond CB_1 and CB_2 . Pharmacol Rev. 62(4):588-631. Review.

Pietropaolo S, Feldon J, Yee BK (2014). Environmental enrichment eliminates the anxiety phenotypes in a triple transgenic mouse model of Alzheimer's disease. Cogn Affect Behav Neurosci. 14(3):996-1008.

Piomelli D, Beltramo M, Glasnapp S, Lin SY, Goutopoulos A, Xie XQ, Makriyannis A (1999). Structural determinants for recognition and translocation by the anandamide transporter. Proc Natl Acad Sci U S A 96(10):5802-5827.

Pirch JH, Corbus MJ, Rigdon GC, Lyness WH (1986). Generation of cortical event-related slow potentials in the rat involves nucleus basalis cholinergic innervation. Electroencephalogr Clin Neurophysiol. (5):464-475.

Pitler TA, Alger BE (1992). Postsynaptic spike firing reduces synaptic GABAA responses in hippocampal pyramidal cells. J Neurosci. 12(10):4122-4132.

Pizzo DP, Thal LJ, Winkler J (2002). Mnemonic deficits in animals depend upon the degree of cholinergic deficit and task complexity. Exp Neurol. 177(1):292-305.

Porter AC, Sauer JM, Knierman MD, Becker GW, Berna MJ, Bao J, Nomikos GG, Carter P, Bymaster FP, Leese AB, Felder CC (2002). Characterization of a novel endocannabinoid, virodhamine, with antagonist activity at the CB1 receptor. J Pharmacol Exp Ther. 301(3):1020-1024.

Pozzo Miller LD, Mahanty NK, Connor JA, Landis DM (1994). Spontaneous pyramidal cell death in organotypic slice cultures from rat hippocampus is prevented by glutamate receptor antagonists. Neuroscience 63(2):471-487.

Probst A, Cortés R, Ulrich J, Palacios JM (1988). Differential modification of muscarinic cholinergic receptors in the hippocampus of patients with Alzheimer's disease: an autoradiographic study. Brain Res. 450(1-2):190-201.

Qian Z, Drewes LR (1989). Muscarinic acetylcholine receptor regulates phosphatidylcholine phospholipase D in canine brain. J Biol Chem. 264(36):21720-21724.

Quinlivan M, Chalon S, Vergote J, Henderson J, Katsifis A, Kassiou M, Guilloteau D (2007). Decreased vesicular acetylcholine transporter and alpha(4)beta(2) nicotinic receptor density in the rat brain following 192 IgG-saporin immunolesioning. Neurosci Lett. 415(2):97-101.

Quirion R, Aubert I, Lapchak PA, Schaum RP, Teolis S, Gauthier S, Araujo DM (1989a). Muscarinic receptor subtypes in human neurodegenerative disorders: focus on Alzheimer's disease. Trends Pharmacol Sci. Suppl:80-84. Review.

Quirion R, Araujo D, Regenold W, Boksa P (1989b). Characterization and quantitative autoradiographic distribution of [3H]acetylcholine muscarinic receptors in mammalian brain. Apparent labelling of an M2-like receptor sub-type. Neuroscience 29(2):271-289.

Raevsky VV, Dawe GS, Sinden JD, Stephenson JD (1998). Lesions of the nucleus basalis magnocellularis do not alter the proportions of pirenzepine- and gallamine-sensitive responses of somatosensory cortical neurones to acetylcholine in the rat. Brain Res. 782(1-2):324-328.

Raiteri M, Leardi R, Marchi M (1984). Heterogeneity of presynaptic muscarinic receptors regulating neurotransmitter release in the rat brain. J Pharmacol Exp Ther. 228(1):209-214.

Ramanathan D, Tuszynski MH, Conner JM (2009). The basal forebrain cholinergic system is required specifically for behaviorally mediated cortical map plasticity. J Neurosci. 29(18):5992-6000.

Ramírez BG, Blázquez C, Gómez del Pulgar T, Guzmán M, de Ceballos ML (2005). Prevention of Alzheimer's disease pathology by cannabinoids: neuroprotection mediated by blockade of microglial activation. J Neurosci. 25(8):1904-1913.

Rasool CG, Svendsen CN, Selkoe DJ (1986). Neurofibrillary degeneration of cholinergic and non-cholinergic neurons of the basal forebrain in Alzheimer's disease. Ann Neurol. 20(4):482-488.

Rasool S, Martinez-Coria H, Wu JW, LaFerla F, Glabe CG (2013). Systemic vaccination with anti-oligomeric monoclonal antibodies improves cognitive function by reducing Aβ deposition and tau pathology in 3xTg-AD mice. J Neurochem. 126(4):473-482.

Rastogi S, Unni S, Sharma S, Laxmi TR, Kutty BM (2014). Cholinergic immunotoxin 192 IgG-SAPORIN alters subicular theta-gamma activity and impairs spatial learning in rats. Neurobiol Learn Mem. 114:117-126.

Reed LJ, de Belleroche J (1990). Induction of ornithine decarboxylase in cerebral cortex by excitotoxin lesion of nucleus basalis: association with postsynaptic responsiveness and N-methyl-D-aspartate receptor activation. J Neurochem. 55(3):780-787.

Reever CM, Ferrari-DiLeo G, Flynn DD (1997). The M5 (m5) receptor subtype: fact or fiction? Life Sci. 60: 1105–1112.

Reinikainen KJ, Soininen H, Riekkinen PJ (1990). Neurotransmitter changes in Alzheimer's disease: implications to diagnostics and therapy. J Neurosci Res. 27(4):576-586.

Ren J, Qin C, Hu F, Tan J, Qiu L, Zhao S, Feng G, Luo M (2011). Habenula "cholinergic" neurons co-release glutamate and acetylcholine and activate postsynaptic neurons via distinct transmission modes. Neuron 69(3):445-452.

Rhee MH, Bayewitch M, Avidor-Reiss T, Levy R, Vogel Z (1998). Cannabinoid receptor activation differentially regulates the various adenylyl cyclase isozymes. J Neurochem. 71(4):1525-1534.

Riekkinen M, Riekkinen P, Riekkinen P Jr (1991a). Comparison of quisqualic and ibotenic acid nucleus basalis magnocellularis lesions on water-maze and passive avoidance performance. Brain Res Bull. 27(1):119-123.

Riekkinen P Jr, Riekkinen M, Sirviö J, Miettinen R, Riekkinen P (1991b). Comparison of the effects of acute and chronic ibotenic and quisqualic acid nucleus basalis lesioning. Brain Res Bull. 27(2):199-206.

Riekkinen P Jr, Riekkinen M, Sirviö J (1993). Cholinergic drugs regulate passive avoidance performance via the amygdala. J Pharmacol Exp Ther. 267(3):1484-1492.

Rigdon GC, Pirch JH (1986). Nucleus basalis involvement in conditioned neuronal responses in the rat frontal cortex. J Neurosci. 6(9):2535-2542.

Riker W F and Wescoe WC (1951). The pharmacology of flaxedil with observations on certain analogs. Ann. N.Y. Acad. Sci. 54: 373–394.

Rinaldi-Carmona M, Barth F, Héaulme M, Shire D, Calandra B, Congy C, Martinez S, Maruani J, Néliat G, Caput D, et al., (1994). SR141716A, a potent and selective antagonist of the brain cannabinoid receptor. FEBS Lett. 350(2-3):240-244.

Rinaldi-Carmona M, Barth F, Millan J, Derocq JM, Casellas P, Congy C, Oustric D, Sarran M, Bouaboula M, Calandra B, Portier M, Shire D, Brelière JC, Le Fur GL (1998). SR 144528, the first potent and selective antagonist of the CB2 cannabinoid receptor. J Pharmacol Exp Ther. 284(2):644-650.

Rios C, Gomes I, Devi LA (2006). mu opioid and CB1 cannabinoid receptor interactions: reciprocal inhibition of receptor signaling and neuritogenesis. Br J Pharmacol. 148(4):387-395.

Robinson SL, Alexander NJ, Bluett RJ, Patel S, McCool BA (2016) Acute and chronic ethanol exposure differentially regulate CB1 receptor function at glutamatergic synapses in the rat basolateral amygdala. Neuropharmacology 108:474-484.

Rodríguez-Puertas R, Pazos A, Zarranz JJ, Pascual J (1994). Selective cortical decrease of high-affinity choline uptake carrier in Alzheimer's disease: an autoradiographic study using 3H-hemicholinium-3. J Neural Transm Park Dis Dement Sect. 8(3):161-169.

Rodríguez-Puertas R, Pascual J, Vilaró T, Pazos A (1997). Autoradiographic distribution of M1, M2, M3, and M4 muscarinic receptor subtypes in Alzheimer's disease. Synapse 26(4):341-350.

Rogers JD, Brogan D, Mirra SS (1985). The nucleus basalis of Meynert in neurological disease: a quantitative morphological study. Ann Neurol. 17(2):163-170.

Rombouts SA, Barkhof F, Van Meel CS, Scheltens P (2002). Alterations in brain activation during cholinergic enhancement with rivastigmine in Alzheimer's disease. J Neurol Neurosurg Psychiatry 73(6):665-671.

Romero-Sandoval EA, Horvath R, Landry RP, DeLeo JA (2009). Cannabinoid receptor type 2 activation induces a microglial anti-inflammatory phenotype and reduces migration via MKP induction and ERK dephosphorylation. Mol Pain 5:25.

Roozendaal, B, McReynolds, JR, Van der Zee, EA, Lee, S, McGaugh, JL, McIntyre, CK, 2009. Glucocorticoid effects on memory consolidation depend on functional interactions between the medial prefrontal cortex and basolateral amygdala. J. Neurosci. 29, 14299 –14308.

Rossner S, Schliebs R and Bigl V (1994). Ibotenic acid lesions of nucleus basalis magnocellularis differentially affects cholinergic, glutamatergic and GABAergic markers in cortical rat brain regions. Brain Res. 668:85-99.

Rossner S, Schliebs R, Perez-Polo JR, Wiley RG, Bigl V (1995a). Differential changes in cholinergic markers from selected brain regions after specific immunolesion of the rat cholinergic basal forebrain system. J Neurosci Res. 40(1):31-43.

Rossner S, Schliebs R, Härtig W, Bigl V (1995b). 192IGG-saporin-induced selective lesion of cholinergic basal forebrain system: neurochemical effects on cholinergic neurotransmission in rat cerebral cortex and hippocampus. Brain Res Bull. 38(4):371-381.

Rossner S, Schliebs R, Bigl V (1995c). 192IgG-saporin-induced immunotoxic lesions of cholinergic basal forebrain system differentially affect glutamatergic and GABAergic markers in cortical rat brain regions. Brain Res. 696(1-2):165-176.

Rossner S, Härtig W, Schliebs R, Brückner G, Brauer K, Perez-Polo JR, Wiley RG, Bigl V (1995d). 192IgG-saporin immunotoxin-induced loss of cholinergic cells differentially activates microglia in rat basal forebrain nuclei. J Neurosci Res. 41(3):335-346.

Rossner S, Yu J, Pizzo D, Werrbach-Perez K, Schliebs R, Bigl V, Perez-Polo JR (1996). Effects of intraventricular transplantation of NGF-secreting cells on cholinergic basal forebrain neurons after partial immunolesion. J Neurosci Res. 45(1):40-56.

Rossner S (1997). Cholinergic immunolesions by 192IgG-saporin--useful tool to simulate pathogenic aspects of Alzheimer's disease. Int J Dev Neurosci. 15(7):835-850. Review.

Rossor MN, Garrett NJ, Johnson AL, Mountjoy CQ, Roth M, Iversen LL (1982). A post-mortem study of the cholinergic and GABA systems in senile dementia. Brain 105(Pt 2):313-330.

Roszkowski AP (1961). An unusual type of sympathetic ganglionic stimulant. J. Pharmacol. Exp. Ther. 132:156–170.

Rubboli F, Court JA, Sala C, Morris C, Perry E, Clementi F (1994). Distribution of neuronal nicotinic receptor subunits in human brain. Neurochem Int. 25(1):69-71.

Ruehle S, Remmers F, Romo-Parra H, Massa F, Wickert M, Wörtge S, Häring M, Kaiser N, Marsicano G, Pape HC, Lutz B (2013) Cannabinoid CB1 receptor in dorsal telencephalic glutamatergic neurons: distinctive sufficiency for hippocampus-dependent and amygdala-dependent synaptic and behavioral functions. J Neurosci. 33(25):10264-10277.

Rush DK (1988) Scopolamine amnesia of passive avoidance: a deficit of information acquisition. Behav Neural Biol. 50(3):255-274.

Russchen FT, Amaral DG, Price JL, (1985). The afferent connections of the substantia innominata in the monkey, Macaca fascicularis. J. Comp. Neurol. 242, 1–27.

Russo EB, Burnett A, Hall B, Parker KK (2005). Agonistic properties of cannabidiol at 5-HT1a receptors. Neurochem Res. 30(8):1037-1043.

Ryberg E, Larsson N, Sjögren S, Hjorth S, Hermansson NO, Leonova J, Elebring T, Nilsson K, Drmota T, Greasley PJ (2007). The orphan receptor GPR55 is a novel cannabinoid receptor. Br J Pharmacol. 152(7):1092-1101.

Sakurada T, Alufuzoff I, Winblad B, Nordberg A (1990). Substance P-like immunoreactivity, choline acetyltransferase activity and cholinergic muscarinic receptors in Alzheimer's disease and multi-infarct dementia. Brain Res. 521(1-2):329-332.

Sánchez C, de Ceballos ML, Gomez del Pulgar T, Rueda D, Corbacho C, Velasco G, Galve-Roperh I, Huffman JW, Ramón y Cajal S, Guzmán M (2001). Inhibition of glioma growth in vivo by selective activation of the CB(2) cannabinoid receptor. Cancer Res. 61(15):5784-5789.

Sánchez C, Rueda D, Ségui B, Galve-Roperh I, Levade T, Guzmán M (2001). The CB(1) cannabinoid receptor of astrocytes is coupled to sphingomyelin hydrolysis through the adaptor protein fan. Mol Pharmacol. 59(5):955-959.

Saper CB, German DC, White CL 3rd (1985). Neuronal pathology in the nucleus basalis and associated cell groups in senile dementia of the Alzheimer's type: possible role in cell loss. Neurology 35(8):1089-1095.

Saykin AJ, Wishart HA, Rabin LA, Flashman LA, McHugh TL, Mamourian AC, Santulli RB (2004). Cholinergic enhancement of frontal lobe activity in mild cognitive impairment. Brain 127(Pt 7):1574-1583.

Schatz AR, Lee M, Condie RB, Pulaski JT, Kaminski NE (1997). Cannabinoid receptors CB1 and CB2: a characterization of expression and adenylate cyclase modulation within the immune system. Toxicol Appl Pharmacol. 142(2):278-287.

Schliebs R, Feist T, Rossner S, Bigl V (1994). Receptor function in cortical rat brain regions after lesion of nucleus basalis. J Neural Transm Suppl. 44:195-208.

Schmid HH, Schmid PC, Natarajan V (1996). The N-acylation-phosphodiesterase pathway and cell signalling. Chem Phys Lipids. 80(1-2):133-142.

Schmöle AC, Lundt R, Ternes S, Albayram Ö, Ulas T, Schultze JL, Bano D, Nicotera P, Alferink J, Zimmer A (2015) Cannabinoid receptor 2 deficiency results in reduced neuroinflammation in an Alzheimer's disease mouse model. Neurobiol Aging 36(2):710-719.

Schröder H, Giacobini E, Struble RG, Zilles K, Maelicke A, Luiten PG, Strosberg AD (1991). Cellular distribution and expression of cortical acetylcholine receptors in aging and Alzheimer's disease. Ann N Y Acad Sci. 640:189-192.

Schweitzer JB (1987). Nerve growth factor receptor-mediated transport from cerebrospinal fluid to basal forebrain neurons. Brain Res. 423(1-2):309-317.

Seeger T, Fedorova I, Zheng F, Miyakawa T, Koustova E, Gomeza J, Basile AS, Alzheimer C, Wess J (2004). M2 muscarinic acetylcholine receptor knock-out mice show deficits in behavioral flexibility, working memory, and hippocampal plasticity. J Neurosci. 24(45):10117-10127.

Segal M, Auerbach JM (1997). Muscarinic receptors involved in hippocampal plasticity. Life Sci. 60(13-14):1085-1091. Review.

Selden NR, Gitelman DR, Salamon-Murayama N, Parrish TB, Mesulam MM (1998). Trajectories of cholinergic pathways within the cerebral hemispheres of the human brain. Brain 121 (Pt 12):2249-2257.

Severino M, Pedersen AF, Trajkovska V, Christensen E, Lohals R, Veng LM, Knudsen GM, Aznar S (2007). Selective immunolesion of cholinergic neurons leads to long-term changes in 5-HT2A receptor levels in hippocampus and frontal cortex. Neurosci Lett. 428(1):47-51.

Shen M, Piser TM, Seybold VS, Thayer SA (1996). Cannabinoid receptor agonists inhibit glutamatergic synaptic transmission in rat hippocampal cultures. J Neurosci. 16(14):4322-4334.

Shire D, Calandra B, Rinaldi-Carmona M, Oustric D, Pessègue B, Bonnin-Cabanne O, Le Fur G, Caput D, Ferrara P (1996). Molecular cloning, expression and function of the murine CB2 peripheral cannabinoid receptor. Biochim Biophys Acta 1307(2):132-136.

Shonesy BC, Bluett RJ, Ramikie TS, Báldi R, Hermanson DJ, Kingsley PJ, Marnett LJ, Winder DG, Colbran RJ, Patel S (2014) Genetic disruption of 2-arachidonoylglycerol synthesis reveals a key role for endocannabinoid signaling in anxiety modulation. Cell Rep. 9(5):1644-1653

Showalter VM, Compton DR, Martin BR, Abood ME (1996). Evaluation of binding in a transfected cell line expressing a peripheral cannabinoid receptor (CB2): identification of cannabinoid receptor subtype selective ligands. J Pharmacol Exp Ther. 278(3):989-999.

Sims NR, Bowen DM, Davison AN (1981). [14C]acetylcholine synthesis and [14C]carbon dioxide production from [U-14C]glucose by tissue prisms from human neocortex. Biochem J. 196(3):867-876.

Skaper SD, Buriani A, Dal Toso R, Petrelli L, Romanello S, Facci L, Leon A (1996). The ALIAmide palmitoylethanolamide and cannabinoids, but not anandamide, are protective in a delayed postglutamate paradigm of excitotoxic death in cerebellar granule neurons. Proc Natl Acad Sci U S A 93(9):3984-3989.

Slipetz DM, O'Neill GP, Favreau L, Dufresne C, Gallant M, Gareau Y, Guay D, Labelle M, Metters KM (1995). Activation of the human peripheral cannabinoid receptor results in inhibition of adenylyl cyclase. Mol Pharmacol. 48(2):352-361.

Slotkin TA, Nemeroff CB, Bissette G, Seidler FJ (1994). Overexpression of the high affinity choline transporter in cortical regions affected by Alzheimer's disease. Evidence from rapid autopsy studies. J Clin Invest. 94(2):696-702.

Smiley JF, Mesulam MM (1999). Cholinergic neurons of the nucleus basalis of Meynert receive cholinergic, catecholaminergic and GABAergic synapses: an electron microscopic investigation in the monkey. Neuroscience 88(1):241-255.

Smith TD, Annis SJ, Ehlert FJ and Leslie FM (1991). N-[3H]methylscopolamine labeling of non-M1, non- M2 muscarinic receptor binding sites in rat brain. J. Pharmacol. Exp. Ther. 256: 1173–1181.

Snyder SH, Chang KJ, Kuhar MJ, Yamamura HI (1975). Biochemical identification of the mammalian muscarinic cholinergic receptor. Fed. Proc. 34: 1915–1921.

Söderberg M, Edlund C, Kristensson K, Dallner G (1991). Fatty acid composition of brain phospholipids in aging and in Alzheimer's disease. Lipids 26(6):421-425.

Solas M, Francis PT, Franco R, Ramirez MJ (2013). CB2 receptor and amyloid pathology in frontal cortex of Alzheimer's disease patients. Neurobiol Aging 34(3):805-808.

Soltesz I, Alger BE, Kano M, Lee SH, Lovinger DM, Ohno-Shosaku T, Watanabe M (2015). Weeding out bad waves: towards selective cannabinoid circuit control in epilepsy. Nat Rev Neurosci. 16(5):264-277. Review. Erratum in: Nat Rev Neurosci. 16(6):372.

Sonkusare SK, Kaul CL, Ramarao P (2005). Dementia of Alzheimer's disease and other neurodegenerative disorders--memantine, a new hope. Pharmacol Res. 51(1):1-17. Review.

Sparks DL, Hunsaker JC 3rd, Slevin JT, DeKosky ST, Kryscio RJ, Markesbery WR (1992). Monoaminergic and cholinergic synaptic markers in the nucleus basalis of Meynert (nbM): normal age-related changes and the effect of heart disease and Alzheimer's disease. Ann Neurol. 31(6):611-620.

Springer JE, Koh S, Tayrien MW, Loy R (1987). Basal forebrain magnocellular neurons stain for nerve growth factor receptor: correlation with cholinergic cell bodies and effects of axotomy. J Neurosci Res. 17(2):111-118.

Stedman E, Stedman E (1937). The mechanism of biological synthesis of acetylcholine. The isolation of acetylcholine produced by brain tissue in vitro. Biochem. J. 31: 817–827.

Steindel F, Lerner R, Häring M, Ruehle S, Marsicano G, Lutz B, Monory K (2013). Neuron-type specific cannabinoid-mediated G protein signalling in mouse hippocampus. J Neurochem. 124(6):795-807.

Stella N (2004). Cannabinoid signaling in glial cells. Glia 48(4):267-277. Review.

Stella N, Schweitzer P, Piomelli D (1997). A second endogenous cannabinoid that modulates long-term potentiation. Nature 388(6644):773-778.

Stempel AV, Stumpf A, Zhang HY, Özdoğan T, Pannasch U, Theis AK, Otte DM, Wojtalla A, Rácz I, Ponomarenko A, Xi ZX, Zimmer A, Schmitz D (2016). Cannabinoid Type 2 Receptors Mediate a Cell Type-Specific Plasticity in the Hippocampus. Neuron 90(4):795-809.

Stewart DJ, MacFabe DF, Leung LW (1985). Topographical projection of cholinergic neurons in the basal forebrain to the cingulate cortex in the rat. Brain Res. 358(1-2):404-407.

Stoppini L, Buchs PA, Muller D (1991). A simple method for organotypic cultures of nervous tissue. J Neurosci. Methods 37(2):173-82.

Strada O, Vyas S, Hirsch EC, Ruberg M, Brice A, Agid Y, Javoy-Agid F (1992). Decreased choline acetyltransferase mRNA expression in the nucleus basalis of Meynert in Alzheimer disease: an in situ hybridization study. Proc Natl Acad Sci U S A 89(20):9549-9553.

Straiker A, Mackie K (2007). Metabotropic suppression of excitation in murine autaptic hippocampal neurons. J Physiol. 578(Pt 3):773-785.

Sugaya K, Clamp C, Bryan D, McKinney M (1997). mRNA for the m4 muscarinic receptor subtype is expressed in adult rat brain cholinergic neurons. Brain Res Mol Brain Res. 50(1-2):305-313.

Sugiura T, Kondo S, Sukagawa A, Nakane S, Shinoda A, Itoh K, Yamashita A, Waku K (1995). 2-Arachidonoylglycerol: a possible endogenous cannabinoid receptor ligand in brain. Biochem Biophys Res Commun. 215(1):89-97..

Sugiura T, Kodaka T, Kondo S, Nakane S, Kondo H, Waku K, Ishima Y, Watanabe K, Yamamoto I (1997). Is the cannabinoid CB1 receptor a 2-arachidonoylglycerol receptor? Structural requirements for triggering a Ca2+ transient in NG108-15 cells.J Biochem. 1997 Oct;122(4):890-895

Sugiura T, Kondo S, Kishimoto S, Miyashita T, Nakane S, Kodaka T, Suhara Y, Takayama H, Waku K (2000). Evidence that 2-arachidonoylglycerol but not N-palmitoylethanolamine or anandamide is the physiological ligand for the cannabinoid CB2 receptor. Comparison of the agonistic activities of various cannabinoid receptor ligands in HL-60 cells. J Biol Chem. 275(1):605-612.

Sugiura T, Waku K (2002). Cannabinoid receptors and their endogenous ligands. J Biochem. 132(1):7-12. Review.

Sugiura Y, Konishi Y, Zaima N, Kajihara S, Nakanishi H, Taguchi R, Setou M (2009). Visualization of the cell-selective distribution of PUFA-containing phosphatidylcholines in mouse brain by imaging mass spectrometry. J Lipid Res. 50(9):1776-1788.

Sulcova E, Mechoulam R, Fride E (1998). Biphasic effects of anandamide. Pharmacol Biochem Behav. 59(2):347-352.

Sun YX, Tsuboi K, Okamoto Y, Tonai T, Murakami M, Kudo I, Ueda N (2004). Biosynthesis of anandamide and N-palmitoylethanolamine by sequential actions of phospholipase A2 and lysophospholipase D. Biochem J. 380(Pt 3):749-756.

Svendsen CN, Bird ED (1985). Acetylcholinesterase staining of the human amygdala. Neurosci Lett. 54(2-3):313-318.

Svennerholm L, Gottfries CG (1994). Membrane lipids, selectively diminished in Alzheimer brains, suggest synapse loss as a primary event in early-onset form (type I) and demyelination in late-onset form (type II). J Neurochem. 62(3):1039-1047.

Szigeti C, Bencsik N, Simonka AJ, Legradi A, Kasa P, Gulya K (2013). Long-term effects of selective immunolesions of cholinergic neurons of the nucleus basalis magnocellularis on the ascending cholinergic pathways in the rat: a model for Alzheimer's disease. Brain Res Bull. 94:9-16.

Tago H, McGeer PL, McGeer EG (1987). Acetylcholinesterase fibers and the development of senile plaques. Brain Res. 406(1-2):363-369.

Tambaro S, Tomasi ML, Bortolato M (2013). Long-term CB_1 receptor blockade enhances vulnerability to anxiogenic-like effects of cannabinoids. Neuropharmacology 70:268-277.

Tanaka Y, Hanyu H, Sakurai H, Takasaki M, Abe K (2003). Atrophy of the substantia innominata on magnetic resonance imaging predicts response to donepezil treatment in Alzheimer's disease patients. Dement Geriatr Cogn Disord. 16(3):119-125.

Tanimura A, Yamazaki M, Hashimotodani Y, Uchigashima M, Kawata S, Abe M, Kita Y, Hashimoto K, Shimizu T, Watanabe M, Sakimura K, Kano M (2010). The endocannabinoid 2-arachidonoylglycerol produced by diacylglycerol lipase alpha mediates retrograde suppression of synaptic transmission. Neuron 65(3):320-327.

Teipel SJ, Flatz WH, Heinsen H, Bokde AL, Schoenberg SO, Stöckel S, Dietrich O, Reiser MF, Möller HJ, Hampel H (2005). Measurement of basal forebrain atrophy in Alzheimer's disease using MRI. Brain 128(Pt 11):2626-2644.

Teipel S, Heinsen H, Amaro E Jr, Grinberg LT, Krause B, Grothe M (2014). Alzheimer's Disease Neuroimaging Initiative. Cholinergic basal forebrain atrophy predicts amyloid burden in Alzheimer's disease. Neurobiol Aging 35(3):482-491.

Teipel SJ, Cavedo E, Grothe MJ, Lista S, Galluzzi S, Colliot O, Chupin M, Bakardjian H, Dormont D, Dubois B, Hampel H; Hippocampus Study Group (2016). Predictors of cognitive decline and treatment response in a clinical trial on suspected prodromal Alzheimer's disease. Neuropharmacology 108:128-135.

Tolón RM, Núñez E, Pazos MR, Benito C, Castillo AI, Martínez-Orgado JA, Romero J (2009) The activation of cannabinoid CB2 receptors stimulates in situ and in vitro beta-amyloid removal by human macrophages. Brain Res. 1283:148-154.

Tornqvist H, Belfrage P (1976). Purification and some properties of a monoacylglycerol-hydrolyzing enzyme of rat adipose tissue. J Biol Chem. 251(3):813-819.

Torres EM, Perry TA, Blockland A, Wilkinson LS, Wiley RG, Lappi DA, Dunnet SB (1994). Behavioural, histochemical and biochemical consequences of selective immunolesions in discrete regions of the basal forebrain cholinergic system. Neuroscience 63(1):95-122.

Touboul D, Piednoël H, Voisin V, De La Porte S, Brunelle A, Halgand F, Laprévote O (2004). Changes of phospholipid composition within the dystrophic muscle by matrix-assisted laser desorption/ionization mass spectrometry and mass spectrometry imaging. Eur J Mass Spectrom (Chichester). 10(5):657-664.

Tsang SW, Pomakian J, Marshall GA, Vinters HV, Cummings JL, Chen CP, Wong PT, Lai MK (2007). Disrupted muscarinic M1 receptor signaling correlates with loss of protein kinase C activity and glutamatergic deficit in Alzheimer's disease. Neurobiol Aging 28(9):1381-1387.

Tsou K, Mackie K, Sañudo-Peña MC, Walker JM (1999). Cannabinoid CB1 receptors are localized primarily on cholecystokinin-containing GABAergic interneurons in the rat hippocampal formation. Neuroscience 93(3):969-975.

Tucek S (1984). Problems in the organization and control of acetylcholine synthesis in brain neurons. Progr. Biophys. Molec. Biol. 44:1–46.

Turkanis SA, Karler R (1981). Excitatory and depressant effects of delta 9-tetrahydrocannabinol and cannabidiol on cortical evoked responses in the conscious rat. Psychopharmacology (Berl). 75(3):294-298.

Tuszynski MH, Yang JH, Barba D, U HS, Bakay RA, Pay MM, Masliah E, Conner JM, Kobalka P, Roy S, Nagahara AH (2015). Nerve Growth Factor Gene Therapy: Activation of Neuronal Responses in Alzheimer Disease. JAMA Neurol. 72(10):1139-1147.

Twitchell W, Brown S, Mackie K (1997). Cannabinoids inhibit N- and P/Q-type calcium channels in cultured rat hippocampal neurons. J Neurophysiol. 78(1):43-50.

Tzavara ET, Wade M, Nomikos GG (2003a). Biphasic effects of cannabinoids on acetylcholine release in the hippocampus: site and mechanism of action. J Neurosci. 23(28):9374-9384.

Tzavara ET, Bymaster FP, Felder CC, Wade M, Gomeza J, Wess J, McKinzie DL, Nomikos GG (2003b). Dysregulated hippocampal acetylcholine neurotransmission and impaired cognition in M2, M4 and M2/M4 muscarinic receptor knockout mice. Mol Psychiatry 8(7):673-679.

Ullrich C, Daschil N, Humpel C (2011). Organotypic vibroslices: novel whole sagittal brain cultures. J Neurosci Methods 201(1):131-141.

Ulus IH, Wurtman RJ, Mauron C, Blusztajn JK (1989). Choline increases acetylcholine release and protects against the stimulation-induced decrease in phosphatide levels within membranes of rat corpus striatum. Brain Res. 484(1-2):217-227.

Urban JD, Clarke WP, von Zastrow M, Nichols DE, Kobilka B, Weinstein H, Javitch JA, Roth BL, Christopoulos A, Sexton PM (2007). Functional selectivity and classical concepts of quantitative pharmacology. J Pharmacol Exp Ther. 320: 1–13.

Vágvölgyi J, Bodosi M, Hlavati I, Karcsfl S, Kfisa P (1991). Lack of correlation between plaque numbers and acetylcholinesterase- positive axons in the temporal cortex and hippocampus of the Alzheimer's disease brain. First Hungarian Conference on Alzheimer's Disease Abstr. 50.

van Dalen JW, Caan MW, van Gool WA, Richard E (2016). Neuropsychiatric symptoms of cholinergic deficiency occur with degradation of the projections from the nucleus basalis of Meynert. Brain Imaging Behav. DOI: 10.1007/s11682-016-9631-5.

van den Elsen GA, Ahmed AI, Verkes RJ, Kramers C, Feuth T, Rosenberg PB, van der Marck MA, Olde Rikkert MG (2015). Tetrahydrocannabinol for neuropsychiatric symptoms in dementia: A randomized controlled trial. Neurology 84(23):2338-2346.

van der Stelt M, Veldhuis WB, van Haaften GW, Fezza F, Bisogno T, Bar PR, Veldink GA, Vliegenthart JF, Di Marzo V, Nicolay K (2001a). Exogenous anandamide protects rat brain against acute neuronal injury in vivo. J Neurosci. 21(22):8765-8771.

van der Stelt M, Veldhuis WB, Bär PR, Veldink GA, Vliegenthart JF, Nicolay K (2001b). Neuroprotection by Delta9-tetrahydrocannabinol, the main active compound in marijuana, against ouabain-induced in vivo excitotoxicity. J Neurosci. 21(17):6475-6479.

Van Sickle MD, Duncan M, Kingsley PJ, Mouihate A, Urbani P, Mackie K, Stella N, Makriyannis A, Piomelli D, Davison JS, Marnett LJ, Di Marzo V, Pittman QJ, Patel KD, Sharkey KA (2005). Identification and functional characterization of brainstem cannabinoid CB2 receptors. Science 310(5746):329-332.

Varvel, S.A., Anum, E., Niyuhire, F., Wise, L.E., & Lichtman, A.H. (2005). Delta(9)-THC-induced cognitive deficits in mice are reversed by the GABA(A) antagonist bicuculline. Psychopharmacology (Berl) 178(2-3):317-327.

Vásquez C, Lewis DL (1999). The CB1 cannabinoid receptor can sequester G-proteins, making them unavailable to couple to other receptors. J Neurosci. 19(21):9271-9280.

Vazdarjanova A, McGaugh JL (1999) Basolateral amygdala is involved in modulating consolidation of memory for classical fear conditioning. J Neurosci. 19(15):6615-6622.

Veloso A, Astigarraga E, Barreda-Gómez G, Manuel I, Ferrer I, Giralt MT, Ochoa B, Fresnedo O, Rodríguez-Puertas R, Fernández JA (2011). Anatomical distribution of lipids in human brain cortex by imaging mass spectrometry. J Am Soc Mass Spectrom. 22(2):329-338.

Velasco G, Galve-Roperh I, Sánchez C, Blázquez C, Haro A, Guzmán M (2005). Cannabinoids and ceramide: two lipids acting hand-by-hand. Life Sci. 77(14):1723-1731.

Venable N, Kelly PH (1990). Effects of NMDA receptor antagonists on passive avoidance learning and retrieval in rats and mice. Psychopharmacology (Berl), 100(2):215-221.

Vilaró MT, Wiederhold KH, Palacios JM, Mengod G (1992). Muscarinic M2 receptor mRNA expression and receptor binding in cholinergic and non-cholinergic cells in the rat brain: a correlative study using in situ hybridization histochemistry and receptor autoradiography. Neuroscience 47(2):367-393.

Vilaró MT, Palacios JM, Mengod G (1994). Multiplicity of muscarinic autoreceptor subtypes? Comparison of the distribution of cholinergic cells and cells containing mRNA for five subtypes of muscarinic receptors in the rat brain. Brain Res Mol Brain Res. 21(1-2):30-46.

Vogels OJ, Broere CA, ter Laak HJ, ten Donkelaar HJ, Nieuwenhuys R, Schulte BP (1990). Cell loss and shrinkage in the nucleus basalis Meynert complex in Alzheimer's disease. Neurobiol Aging 1990 11(1):3-13.

Vogt BA, Crino PB, Vogt LJ (1992). Reorganization of cingulate cortex in Alzheimer's disease: neuron loss, neuritic plaques, and muscarinic receptor binding. Cereb Cortex. 2(6):526-535.

Volicer L, Stelly M, Morris J, McLaughlin J, Volicer BJ (1997). Effects of dronabinol on anorexia and disturbed behavior in patients with Alzheimer's disease. Int J Geriatr Psychiatry 12(9):913-919.

von Engelhardt J, Eliava M, Meyer AH, Rozov A, Monyer H (2007). Functional characterization of intrinsic cholinergic interneurons in the cortex. J Neurosci 27(21):5633-5642.

Wainer BH, Mesulam MM (1990). Ascending cholinergic pathways in the rat brain. In: Steriade, M., Biesold, D. (Eds.), Brain Cholinergic Systems. Oxford University Press, Oxford, pp. 65–119.

Waite JJ, Wardlow ML, Chen AC, Lappi DA, Wiley RG, Thal LJ (1994). Time course of cholinergic and monoaminergic changes in rat brain after immunolesioning with 192 IgG-saporin. Neurosci Lett. 169(1-2):154-158.

Waite JJ, Chen AD, Wardlow ML, Wiley RG, Lappi DA, Thal LJ (1995). 192 immunoglobulin G-saporin produces graded behavioral and biochemical changes accompanying the loss of cholinergic neurons of the basal forebrain and cerebellar Purkinje cells. Neuroscience 65(2):463-476.

Waite JJ, Wardlow ML, Power AE (1999). Deficit in selective and divided attention associated with cholinergic basal forebrain immunotoxic lesion produced by 192-saporin; motoric/sensory deficit associated with Purkinje cell immunotoxic lesion produced by OX7-saporin. Neurobiol Learn Mem. 71(3):325-352.

Wall SJ, Wolfe BB, Kromer LF (1994). Cholinergic deafferentation of dorsal hippocampus by fimbria-fornix lesioning differentially regulates subtypes (m1-m5) of muscarinic receptors. J Neurochem. 62(4):1345-1351.

Walsh TJ, Kelly RM, Dougherty KD, Stackman RW, Wiley RG, Kutscher CL (1995). Behavioral and neurobiological alterations induced by the immunotoxin 192-IgG-saporin: cholinergic and non-cholinergic effects following i.c.v. injection. Brain Res. 702(1-2):233-245.

Walter L, Franklin A, Witting A, Wade C, Xie Y, Kunos G, Mackie K, Stella N (2003). Nonpsychotropic cannabinoid receptors regulate microglial cell migration. J Neurosci. 23(4):1398-1405.

Walther S, Mahlberg R, Eichmann U, Kunz D (2006). Delta-9-tetrahydrocannabinol for nighttime agitation in severe dementia. Psychopharmacology (Berl) 185(4):524-528.

Walther S, Schüpbach B, Seifritz E, Homan P, Strik W (2011). Randomized, controlled crossover trial of dronabinol, 2.5 mg, for agitation in 2 patients with dementia. J Clin Psychopharmacol. 31(2):256-258.

Wang HY, Friedman E (1994). Receptor-mediated activation of G proteins is reduced in postmortem brains from Alzheimer's disease patients. Neurosci Lett. 173(1-2):37-39.

Warpman U, Alafuzoff I, Nordberg A (1993). Coupling of muscarinic receptors to GTP proteins in postmortem human brain--alterations in Alzheimer's disease. Neurosci Lett. 150(1):39-43.

O'Shaughnessy WB (1843). On the Preparations of the Indian Hemp, or Gunjah* Cannabis Indica Their Effects on the Animal System in Health, and their Utility in the Treatment of Tetanus and other Convulsive Diseases. Prov Med J Retrosp Med Sci. 5(123): 363–369.

Wedzony K, Chocyk A (2009). Cannabinoid CB1 receptors in rat medial prefrontal cortex are colocalized with calbindin- but not parvalbumin- and calretinin-positive GABA-ergic neurons. Pharmacol Rep. 61(6):1000-1007.

Weiner DM, Levey AI and Brann MR (1990). Expression of muscarinic acetylcholine and dopamine receptor mRNAs in rat basal ganglia. Proc Natl Acad Sci USA 87: 7050–7054.

Wellman CL, Sengelaub DR (1991). Cortical neuroanatomical correlates of behavioral deficits produced by lesion of the basal forebrain in rats. Behav Neural Biol. 56(1):1-24.

Wenk GL, Harrington CA, Tucker DA, Rance NE, Walker LC (1992). Basal forebrain neurons and memory: a biochemical, histological, and behavioral study of differential vulnerability to ibotenate and quisqualate. Behav Neurosci. 106(6):909-923.

Wenk GL, Stoehr JD, Quintana G, Mobley S, Wiley RG (1994). Behavioral, biochemical, histological, and electrophysiological effects of 192 IgG-saporin injections into the basal forebrain of rats. J Neurosci. 14(10):5986-5995.

Wess J (1993). Molecular basis of muscarinic acetylcholine function. Trends Pharmacol Sci. 14: 308–313.

Westlake TM, Howlett AC, Bonner TI, Matsuda LA, Herkenham M (1994). Cannabinoid receptor binding and messenger RNA expression in human brain: an in vitro receptor autoradiography and in situ hybridization histochemistry study of normal aged and Alzheimer's brains. Neuroscience 63(3):637-652.

Wettschureck N, Offermanns S (2005). Mammalian G proteins and their cell type specific functions. Physiol Rev. 85(4):1159-1204.

Wevers A, Jeske A, Lobron C, Birtsch C, Heinemann S, Maelicke A, Schröder R, Schröder H (1994). Cellular distribution of nicotinic acetylcholine receptor subunit mRNAs in the human cerebral cortex as revealed by non-isotopic in situ hybridization. Brain Res Mol Brain Res. 25(1-2):122-128.

Whishaw IQ, O'Connor WT, Dunnett SB (1985). Disruption of central cholinergic systems in the rat by basal forebrain lesions or atropine: effects on feeding, sensorimotor behaviour, locomotor activity and spatial navigation. Behav Brain Res. 17(2):103-115.

White HL, Wu JC (1973). Kinetics of choline acetyltransferases (EC 2.3.1.6) from human and other mammalian central and peripheral nervous tissues. J Neurochem. 20(2):297-307.

Whitehouse PJ, Price DL, Clark AW, Coyle JT, DeLong MR (1981). Alzheimer disease: evidence for selective loss of cholinergic neurons in the nucleus basalis. Ann Neurol. 10(2):122-126.

Whitehouse PJ, Price DL, Struble RG, Clark AW, Coyle JT, Delon MR (1982). Alzheimer's disease and senile dementia: loss of neurons in the basal forebrain.Science. 215(4537):1237-1239.

Wiley RG, Oeltmann TN, Lappi DA (1991). Immunolesioning: selective destruction of neurons using immunotoxin to rat NGF receptor. Brain Res. 562(1):149-153.

Wilson RI, Nicoll RA (2001). Endogenous cannabinoids mediate retrograde signalling at hippocampal synapses. Nature. 410(6828):588-592. Erratum in: Nature (2001) 411(6840):974.

Wilson RI, Kunos G, Nicoll RA (2001). Presynaptic specificity of endocannabinoid signaling in the hippocampus. Neuron 31(3):453-462.

Winkler J, Ramirez GA, Thal LJ, Waite JJ (2000). Nerve growth factor (NGF) augments cortical and hippocampal cholinergic functioning after p75NGF receptor-mediated deafferentation but impairs inhibitory avoidance and induces fear-related behaviors. J Neurosci. (2):834-844.

Winner B, Cooper-Kuhn CM, Aigner R, Winkler J, Kuhn HG (2002). Long-term survival and cell death of newly generated neurons in the adult rat olfactory bulb. Eur J Neurosci. 16(9):1681-1689.

Wood T (1899) Cannabinol, part I. J Chem Soc. 75: 20–36.

Woolf NJ, Gould E, Butcher LL (1989). Nerve growth factor receptor is associated with cholinergic neurons of the basal forebrain but not the pontomesencephalon. Neuroscience 30(1):143-152.

Woolf NJ (1991). Cholinergic systems in mammalian brain and spinal cord. Prog Neurobiol. 37(6):475-524.

Woolf NJ (1997). A possible role for cholinergic neurons of the basal forebrain and pontomesencephalon in consciousness. Conscious Cogn. 6(4):574-596. Review.

Wrenn CC and Wiley RG (1998). The behavioral functions of the cholinergic basal forebrain: lessons from 192 IgG-saporin. Int J Dev Neurosci. 16(7-8):595-602. Review.

Wurtman RJ, Blusztajn JK, Maire JC (1985). "Autocannibalism" of choline-containing membrane phospholipids in the pathogenesis of Alzheimer's disease-A hypothesis. Neurochem Int. 7(2):369-372.

Wurtman RJ. Nutrients affecting brain composition and behavior (1987). Integr Psychiatry. (4):226-38; discussion 238-257. Review.

Wurtman RJ (1992). Choline metabolism as a basis for the selective vulnerability of cholinergic neurons. Trends Neurosci. 15(4):117-122. Review.

Wymann MP, Schneiter R (2008). Lipid signalling in disease. Nat Rev Mol Cell Biol. 9(2):162-176.

Xi ZX, Peng XQ, Li X, Song R, Zhang HY, Liu QR, Yang HJ, Bi GH, Li J, Gardner EL (2011). Brain cannabinoid CB_2 receptors modulate cocaine's actions in mice. Nat Neurosci. 14(9):1160-1166.

Yamamura HJ, Snyder SH (1973). High affi nity transport of choline into synaptosomes of rat Brain J. Neurochem. 21: 1355–1374.

Yoshino H, Miyamae T, Hansen G, Zambrowicz B, Flynn M, Pedicord D, Blat Y, Westphal RS, Zaczek R, Lewis DA, Gonzalez-Burgos G (2011). Postsynaptic diacylglycerol lipase mediates retrograde endocannabinoid suppression of inhibition in mouse prefrontal cortex. J Physiol. 589(Pt 20):4857-4884.

Younts TJ, Chevaleyre V, Castillo PE (2013). CA1 pyramidal cell theta-burst firing triggers endocannabinoid-mediated long-term depression at both somatic and dendritic inhibitory synapses. J Neurosci. 33(34):13743-13757.

Zaborszky L, Duque A (2000). Local synaptic connections of basal forebrain neurons. Behav Brain Res 115:143–158.

Zhang ZJ, Berbos TG, Wrenn CC, Wiley RG (1996). Loss of nucleus basalis magnocellularis, but not septal, cholinergic neurons correlates with passive avoidance impairment in rats treated with 192-saporin. Neurosci Lett. 203(3):214-218.

Zhao Y, Tzounopoulos T (2011). Physiological activation of cholinergic inputs controls associative synaptic plasticity via modulation of endocannabinoid signaling. J Neurosci. 31(9):3158-3168.

Zhao P, Leonoudakis D, Abood ME, Beattie EC (2010). Cannabinoid receptor activation reduces TNFalpha-induced surface localization of AMPAR-type glutamate receptors and excitotoxicity. Neuropharmacology 58(2):551-558.

Zhuang SY, Bridges D, Grigorenko E, McCloud S, Boon A, Hampson RE, Deadwyler SA (2005). Cannabinoids produce neuroprotection by reducing intracellular calcium release from ryanodine-sensitive stores. Neuropharmacology 48(8):1086-1096.

Zupan G, Casamenti F, Scali C, Pepeu G (1993). Lesions of the nucleus basalis magnocellularis in immature rats: short- and long-term biochemical and behavioral changes. Pharmacol Biochem Behav. 45(1):19-25.

Manuscripts

I

WIN55,212-2-mediated protective effects of basal forebrain cholinergic system via CB_1 receptor activation in organotypic cultures treated with 192IgG-saporin

Alberto Llorente-Ovejero[1] (MSc), Laura Lombardero[1] (PhD), Iván Manuel[1] (PhD), Maria Teresa Giralt[1] (PhD), Rafael Rodríguez-Puertas[1] (PhD).

[1]Department of Pharmacology, Faculty of Medicine and Nursing, University of the Basque Country (UPV/EHU), Bº Sarriena s/n, 48940 Leioa, Spain.

*Corresponding author

Rafael Rodríguez-Puertas

Department of Pharmacology, Faculty of Medicine and Nursing

University of the Basque Country

E-48940 Leioa, Vizcaya, Spain.

Tel.: +34-94-6012739; fax: +34-94-6013220.

E-mail address: rafael.rodriguez@ehu.es

Glossary

2-AG: 2-arachidonoylglycerol; AD: Alzheimer´s disease; BFCN: Basal forebrain cholinergic neurons; CB_1 receptor: Subtype 1 of cannabinoid receptors; CB_2 receptor: Subtype 2 of cannabinoid receptors; DIV: Days *in vitro;* HDB: Horizontal diagonal band of Broca; MS: Medial septum; NBM: Nucleus basalis magnocellularis; P7: 7-day-old postnatal rats; $P75^{NTR}$: Low-affinity nerve growth factor receptor $p75^{NTR}$; PI: Propidium iodide; SAP: 192IgG-saporin treated cultures; VDB: Vertical diagonal band of Broca.

Abstract

In the present study hemibrain organotypic cultures containing basal forebrain cholinergic nuclei were treated with the immunotoxin 192IgG-saporin, which specifically eliminates basal forebrain cholinergic neurons expressing the low-affinity nerve growth factor receptor $p75^{NTR}$ in a dose and time of exposure-dependent manner. The most effective dose of immunotoxin, which eliminated approximately 50% (EC50) of basal forebrain cholinergic neurons, was set to 100 ng/ml. The effects of CB_1 receptor activation in the *ex vivo* model of basal forebrain cholinergic dysfunction were evaluated by using the synthetic cannabinoid agonist WIN55,212-2, that at nanomolar concentrations was able to induce protective effects on secondary cells in the medial septum and the nucleus basalis magnocellularis. The CB_1 receptor antagonist AM251 blocked the protective effects mediated by the cannabinoid agonist. Present findings support the protective role of cannabinoid system through the specific activation of CB_1 receptors during specific cholinergic damage.
Keywords: 192IgG-saporin, cholinergic, cannabinoid, organotypic.

Introduction

One of the main common pathological features underlying the course of neurodegenerative diseases is the neuronal damage and glial proliferation. In Alzheimer´s disease (AD), a specific vulnerability of basal forebrain cholinergic neurons (BFCN) has been described (Davies and Maloney, 1976). This vulnerability contributes to the progressive loss of memory and thinking abilities which led to the "cholinergic hypothesis of geriatric memory dysfunction" proposed by Bartus et al. (1982). The loss of basal forebrain cholinergic innervation may indirectly trigger an excitatory/inhibitory imbalance further contributing to secondary neuronal or cell damage. This phenomenon is the result of neurotoxic and neuroprotective events which involves complex interactions between neurons and activated glial cells (Kreutz et al., 2007).

192IgG-saporin consists of a monoclonal antibody (192IgG), which is armed with a ribosome inactivating protein (saporin) and specifically directed to the low-affinity nerve growth factor receptor ($p75^{NTR}$). $P75^{NTR}$ is abundantly and specifically expressed on BFCN in the basal forebrain during the whole life of the rodents (Springer et al., 1987; Woolf et al., 1989). Following receptor binding and internalization, saporin enzymatically inactivates the large ribosomal subunit, thereby blocking protein synthesis and ultimately resulting in BFCN death by apoptosis (Wrenn and Wiley, 1998).The basal forebrain cholinergic degeneration partially mimics the cholinergic dysfunction described in AD. The loss of BFCN in rodents has been associated with deregulated levels of cortical and hippocampal glutamate and GABA receptors as well as a reduction in the GABA synthesizing enzyme levels, probably leading to an excess of glutamatergic neurotransmission and revealing secondary alterations due to the loss of basal forebrain cholinergic inputs. (Rossner et al.,1995a; reviewed in Rossner, 1997; Lee et al., 2016)

The endocannabinoid signaling, which is altered in AD (Manuel et al., 2014; Mulder et al., 2011), fine tunes the neuronal transmission at both excitatory (Kreitzer and Regehr, 2001), and inhibitory synapses (Wilson and Nicoll, 2001) leading to a transient suppression of excitatory or inhibitory transmission by a presynaptic mechanism mediated by the subtype 1 of cannabinoid receptors (CB_1 receptor). Moreover, pharmacological and histological evidences support the endocannabinoid-driven modulation of cholinergic neurotransmission through CB_1 receptor activation (Gifford et al., 1996). The activation of the endocannabinoid system has also been associated with neuroprotective effects *in vitro* (Skaper et al., 1996), *in vivo* (van der Stelt et al., 2001a, b) and *ex vivo* (Kreutz et al., 2007; Koch et al., 2011a, b). The neurochemical mechanisms involve the activation of CB_1 but also CB_2 receptors mainly

in glial cells. The *ex vivo* model of organotypic culture comprises functional cellular networks involving neurons and glial cells (Hailer et al., 2001). This type of tissue culture allows to induce specific neuronal damage with toxins but also to evaluate the effects of pharmacological treatments. In the present study, the role of CB_1 receptor activation has been analyzed in the *ex vivo* model of 192IgG-saporin-induced BFCN dysfunctionin hemibrain organotypic cultures of 7-day-old postnatal male Sprague-Dawley rats (P7). The aim is to further understand the crosstalk between the endocannabinoid and cholinergic systems in the Alzheimer's disease.

Experimental procedures

Animals

P7 (n = 25) weighing 14-20 g at the onset of the experiments were used. Every effort was made to minimize animal suffering and to use the minimum number of animals. All procedures were performed in accordance with European animal research laws (Directive 2010/63/EU) and the Spanish National Guidelines for Animal Experimentation (RD 53/2013, Law 32/2007). Experimental protocols were approved by the Local Ethical Committee for Animal Research of the University of the Basque Country (CEEA 388/2014).

Fixed tissue preparation

Two representative P7 rats, were anesthetized with ketamine/xylazine (90/10 mg/kg; i.p.) and transcardially perfused with 0.1 M phosphate buffer (PB), 0.5% heparinized (37ºC, pH 7.4) followed by 4% paraformaldehyde and 3% picric acid in 0.1M PB (4ºC) (10 ml/10 g b.w.). Their brains were subsequently removed and post-fixed in the same fixative solution for 90 min at 4ºC, followed by immersion in a cryoprotective solution of 20% sucrose in PB during 8h at 4ºC. Then the tissue was frozen by immersion in isopentane and kept at -80ºC. The brains were coronally cut into 10 µm slices containing the basal forebrain cholinergic neurons (BFCN) from the different nuclei of the basal forebrain cholinergic system; Ch1 or medial septum (MS); Ch2 or vertical diagonal band of Broca (VDB); Ch3 or horizontal diagonal band of Broca (HDB) and Ch4 or nucleus basalis magnocellularis (NBM) according to the classification proposed by Mesulam et al. (1983) using a Microm HM550 cryostat (Thermo Scientific) equipped with a freezing-sliding microtome at -25ºC and mounted onto gelatin-coated slides and finally stored at -25ºC until used.

Hemibrain organotypic cultures

To prepare hemibrain organotypic cultures, P7 rats were sacrificed by decapitation and their brains were quickly dissected under aseptic conditions inside a laminar flow cabinet (TELSTAR, BV-30/70). After removal of the olfactory bulbs and the most caudal part of the cerebellum, the brains were placed in minimal essential Dulbecco´s Modified Eagle Medium (DMEM, Sigma-Aldrich) supplemented with 0.1% (v/v) antibiotic/antimycotic (Gibco) at 4ºC and incubated according to the method proposed by Stoppini et al. (1991). Briefly, the brains were vertically positioned resting on the cerebellum by means of cyanocrylate on a teflon stage. These preparations were rostro-caudally cut into coronal 300 µm-thick vibrosections using a sliding vibratome (Leica VT 1,000 S, Leica Microsystems AG, Wetzlar, Germany). Approximately, 10 hemibrain vibrosections containing the MS-VDB subregions and additional 10 vibrosections containing the HDB-NBM were obtained from each brain, which were immediately transferred into cell culture inserts (3 vibrosections per insert) (PIC50ORG, Millipore), fitted with a membrane of 0.4 µm pore size. The hemibrain organotypic cultures were then placed in 6-well culture dishes (Falcon, BD Biosciences Discovery Labware, Bedford, MA) that contained 1 ml culture medium per well. The culture medium consisted of 49% (v/v) Neurobasal Medium (NB, Sigma-Aldrich), 24% (v/v) Hanks' Balanced Salt Solution (HBSS, Gibco), 24% (v/v) Normal Horse Serum (NHS, Gibco), 1% (v/v) D-glucose, 0.5% glutamine (Sigma-Aldrich), 0.5% B27 supplement serum free (Gibco) and 1% antibiotic/antimycotic. The culture dishes were incubated at 37ºC in a fully humidified atmosphere supplemented with 5% CO_2 and the cell culture medium was replaced by fresh medium depending on the treatment protocol but typically, the second or third day.

Immunotoxin, drugs and vehicle

192IgG-saporin (batch 2441969) was acquired from Millipore (Temecula, CA, USA) and dissolved directly in culture medium immediately prior to the treatment. *R-(+)-[2,3-Dihydro-5-methyl-3-[(morpholinyl) methyl]pyrrolo [1,2,3-de]-1,4-benzoxazinyl]-(1-naphthalenyl)methanone mesylate* (WIN55,212-2, from Sigma-Aldrich, St Louis, MO, USA) and 1-(2,4-Dichlorophenyl)-5-(4-iodophenyl)-4-methyl-*N*-(piperidin-1-yl)-1*H*-pyrazole-3-carboxamide (AM251, from Tocris, Bristol, UK) were dissolved in pure ethanol and stored at -20ºC until use.

192IgG-saporin (SAP) treatment schedules

[1] Nonlesioned hemibrain organotypic cultures (n = 6) were kept in culture medium for eight days *in vitro* (DIV) without any treatment and served as controls.

[2] At day five of culture *in vitro*, the hemibrain organotypic cultures (n = 4-5 per condition) were incubated with 192IgG-saporin (50-200 ng/ml) during three DIV.

[3] At day two of culture *in vitro*, the hemibrain organotypic cultures (n = 4-5 per condition) were incubated with 192IgG-saporin (50-200 ng/ml) during six DIV.

[**4]** At day two and five of culture *in vitro*, the hemibrain organotypic cultures (n = 4-5 per condition) were incubated with 192IgG-saporin (100 or 200 ng/ml) during six DIV.

Cannabinoid treatment schedules

Vehicle. Nonlesioned hemibrain organotypic cultures (n = 6 including the SM + 6 including the NBM) were kept in culture medium for eight DIV without any treatment and served as controls. At 2 and 5 DIV, the organotypic cultures were treated with the vehicle ethanol. The maximal final solvent ethanol concentration in culture medium was set at 0.01% (v/v), according to previous reports (Koch et al., 2011a).

Agonist. At day two and five of culture *in vitro*, hemibrain organotypic cultures (n = 5 including the SM + 5 including the NBM) were incubated with the cannabinoid agonist WIN55,212,2 (10 nM or 1 nM) during six DIV.

192IgG-saporin. At day two and five of culture *in vitro*, hemibrain organotypic cultures (n = 7 including the SM + 7 including the NBM) were incubated with the immunotoxin 192IgG-saporin (100 ng/ml) during six DIV.

Agonist + 192IgG-saporin. At day two and five of culture *in vitro*, hemibrain organotypic cultures (n = 6 including the SM + 6 including the NBM) were treated with the cannabinoid agonist WIN55,212,2 (10 nM or 1 nM) during six DIV, 2h prior the addition of the immunotoxin 192IgG-saporin (100 ng/ml).

Antagonist + agonist + 192IgG-saporin. At day two and five of culture *in vitro*, hemibrain organotypic cultures (n = 5 including the SM + 5 including the NBM) were preincubated with the CB_1 receptor antagonist AM251 (1 µM) immediately prior to the treatment with the cannabinoid agonist WIN55,212,2 (10 nM or 1 nM). 2h later the immunotoxin 192IgG-saporin was added (100 ng/ml) to the culture medium during six DIV.

Cell death marker. At day eight of culture *in vitro*, hemibrain organotypic cultures were incubated in the presence of 5 µg/ml of propidium iodide (PI) for 2 h prior to fixation. Uptake of PI stains the nuclei of degenerating cells intensely red and its use for identifying degenerating cells in CNS organotypic cultures has been previously established (Pozzo Miller et al., 1994; Dehghani et al., 2003; Koch et al., 2011a).

Immunohistochemical studies

After the different treatments, the hemibrain organotypic cultures were processed for the immunohistochemical localization of BFCN. Briefly, they were gently and extensively rinsed with 0.9% saline solution (37ºC) followed by immersion in 4% paraformaldehyde and 3% picric acid in 0.1M PB (4ºC) for 1h. Then, the fixed vibroslices were extensively rinsed in 0.1M PB (pH 7.4) and simultaneously blocked and permeabilized with 4% normal goat serum (NGS) in 0.6% Triton X-100 in PBS (0.1 M, pH 7.4) for 2 h at 4ºC. The incubation was performed in free floating at 4ºC (48 h) with rabbit anti $p75^{NTR}$ primary antibody, diluted to [1:500] in 0.6% Triton X-100 in PBS with 5% BSA. The primary antibody was then revealed by incubation for 30 min at 37ºC in the darkness with Alexa488-labeled donkey anti-rabbit secondary antibody diluted to [1:250] in Triton X-100 (0.6%) in PBS. Then, were washed for 30 min by immersion in PBS and incubated with Hoechst 33258 for 15 min at room temperature. Finally, slices were extensively rinsed with PBS and mounted with p-phenylendiamine-glycerol (0.1%) in PBS for immunofluorescence.

Fixed 10 µm slices were extensively rinsed in 0.1M PB (pH 7.4), simultaneously blocked and permeabilized with 4% NGS in 0.3% Triton X-100 in PBS (0.1 M, pH 7.4) for 2 h at 4ºC in PBS with 5% BSA and incubated with rabbit anti $p75^{NTR}$ primary overnight diluted as previously mentioned. The rest of the process was carried out in a similar way as for the hemibrain organotypic cultures.

Quantification

200-fold magnification photomicrographs of the Ch1-Ch4 nuclei were acquired by means of an Axioskop 2 Plus microscope (Zeiss) equipped with a CCD imaging camera (SPOT Flex Shifting Pixel). Both $p75^{NTR}$ immunoreactive BFCN and PI positive cells were counted and the total number (N) in the whole image was obtained. The population of $p75^{NTR}$ immunoreactive BFCN or PI stained cells was expressed as N/mm^2.

Statistical analyses

The average number of BFCN density and PI positive stained cells was calculated for each experimental group. Then, data were statistically analyzed by means of one-way analysis of variance (ANOVA) to determine whether the effect of the different concentrations of 192IgG-saporin in each area or the effect of the cannabinoid treatment on the density of $p75^{NTR}$ immunoreactive BFCN or PI stained cells. If significant differences were detected, the one-way ANOVA test was followed by

Bonferroni´s *post hoc* test for multiple comparisons. Data are means ± SEM and the statistical significance threshold was set at $p < 0.05$.

Results

$P75^{NTR}$ immunostaining of BFCN in the basal forebrain cholinergic system of P7 rats

Prior to the use of the 192IgG-saporin to mimic an *ex vivo* model of cholinergic dysfunction, it was important to determine the presence of BFCN expressing the immunotoxin target $p75^{NTR}$, in P7 rats. The immunofluorescence studies carried out in the basal forebrain cholinergic system from P7 rats revealed the presence of a high density of BFCN expressing $p75^{NTR}$ in the different nuclei analyzed (Ch1-Ch4). The BFCN perikarya were intensely stained showing the typically somatodendritic distribution of $p75^{NTR}$. The BFCN are continuously distributed in partially discrete populations along the rostrocaudal axis in adult rodents as well as in human and non-human primates. According to this particular distribution of the BFCN, the Ch1 or the MS and the Ch2 or the VDB were first analyzed in P7 rats. The immunoreactive BFCN from the MS and VDB were clearly distinguished from the surrounding cells by showing big-size but moderate Hoechst-staining nuclei and were distributed along the midline (Figure 1A) extending ventrally to the vertical limb of the VDB, (Figure 1B), which revealed a continuum of $p75^{NTR}$ positive BFCN located within Ch1 and Ch2. The BFCN from the HDB or Ch3 (Figure 1C) were distributed caudally to VDB and extended ventrally to the NBM or Ch4 (Figure 1D). The BFCN of these nuclei displayed similar staining patterns to those previously mentioned, including big but moderately stained nuclei, described for the MS and VDB. It should also be emphasized that those BFCN from the NBM showed the biggest size and the most extensive dendritic arborization among all BFCN.

192IgG-saporin-induced BFCN death in hemibrain organotypic cultures

The application of different doses of 192IgG-saporin to hemibrain organotypic cultures containing the basal forebrain cholinergic system was able to induce specific reductions of BFCN in a dose-dependent manner according to the different assayed treatments (Figure 2). Increasing concentrations of 192IgG-saporin (50-200 ng/ml) were administered at day five of culture *in vitro*, and let the toxin do its effect during another three days *in vitro* (DIV). The effective concentration of immunotoxin, which eliminated approximately 50% of BFCN, was set around 100 ng/ml, leading to a

reduction of BFCN densities of up to 36% in the MS, 55% in HDB, 42% in VDB and 35% in the NBM. The highest concentrations of 192IgG-saporin (200 ng/ml) triggered a reduction of 58% in the number of $p75^{NTR}$ positive cells/mm^2 in the MS, 64% in the HDB, 61% in the VDB and 72% in the NBM (Figure 2 A). In another set of experiments the schedule was modified and the 192IgG-saporin was administered at day two of culture, and let it act in the tissue during six additional DIV. The purpose was to evaluate more initial effects of the toxin for a longer period. It was observed a reduction of BFCN densities of up to 65% in the MS, 55% in HDB, 60% in VDB and 65% in the NBM (Figure 3 A). Interestingly, the BFCN reduction induced by 100 ng/ml of immunotoxin during 6 DIV was comparable to that observed with the highest dose (200 ng/ml) during three DIV which demonstrated not only a 192IgG-saporin-induced BFCN death in a dose-dependent manner, but also a dependence on the time of exposure to the immunotoxin. The $p75^{NTR}$-immunoreactivity showed the presence of a great deal of debris and a significant atrophy related to smaller somatic size and reduced dendritic arborisation after the application of 192IgG-saporin (Figure 3 B). Furthermore, the PI uptake, indicative of compromised cell viability, led to dramatic levels of cell death (Figure 4) in a dose dependent manner including BFCN and non-cholinergic cells. Finally, the double application of 100 ng/ml of 192IgG-saporin at days two and five of culture *in vitro* during 6 DIV led to comparable levels of BFCN reduction to those observed with the single application at day two of culture *in vitro*. However, the double application of 200 ng/ml of immunotoxin led to an almost total reduction of BFCN density accompanied by a massive cell death as revealed by the almost lack of $p75^{NTR}$ immunoreactivity and the intensely PI staining recorded in the different cholinergic nuclei of the basal forebrain.

WIN55,212-2 treatment in 192IgG-saporin-lesioned hemibrain organotypic cultures

$P75^{NTR}$ immunoreactive BFCN quantification

The pharmacological treatment of hemibrain organotypic cultures with the CB_1/CB_2 receptor cannabinoid synthetic agonist WIN55,212-2 or ethanol used as vehicle did not exert any effect on the viability of the cultures as well as on the density of BFCN (Figure 5 A).The application of 100 ng/ml of 192IgG-saporin at days two and five of culture *in vitro* during six DIV led to a statistically significant decrease in the density of BFCN (approximately up to 60%) in both the MS (vehicle 64 ± 7.8 BFCN/mm^2 vs SAP 26 ± 4.2 BFCN/mm^2; $p < 0.01$) and NBM (vehicle 64 ± 3.8 BFCN/mm^2 vs SAP 26 ± 6.7 BFCN/mm^2; $p < 0.01$) (Figure 5 A). The pre-treatment of hemibrain organotypic cultures with either 1 nM or 10 nM of WIN55,212-2, 2h prior the

application of 192IgG-saporin, did not trigger any relevant effect on the viability and density of BFCN but induced a modest although not statistically significant attenuation of BFCN death in the MS (1 nM WIN55,212-2 44 ± 4.2 BFCN/mm^2 and 10 nM WIN55,212-2 43 ± 7.4 BFCN/mm^2) and NBM (1 nM WIN55,212-2 31.56 ± 4.8 BFCN/mm^2 and 10 nM WIN55,212-2 40 ± 2.9 BFCN/mm^2) (Figure 5 A). This effect was specifically driven through the activation of CB_1 receptors since it was completely abolished by the specific blocking of CB_1 receptors by means of the receptor antagonist AM251, leading to immunotoxin-induced levels of BFCN (Figure 5 A-C). The loss of BFCN was revealed by the absence of well-defined magnocellular neuronal bodies as well as by the presence of a great deal of p75^{NTR}-immunoreactive neuronal debris (Figure 5 D).

PI positive cells quantification

The PI uptake was also measured and the cell death quantified in the MS, NBM and cortex. The pharmacological treatment of the hemibrain organotypic cultures with the CB_1/CB_2 receptor synthetic cannabinoid agonist WIN55,212-2 or ethanol did not exert any effect on the viability of the cultures as well as on the density of PI positive cells (Figure 6 A). The application of 100 ng/ml of 192IgG-saporin at days two and five of culture *in vitro* during six DIV led to a statistically significant increase in the density of PI stained cells (approximately up to 300%) in the MS (vehicle 16.76 ± 2.3 cells/mm^2 vs SAP 70.26 ± 7.7 cells/mm^2; $p < 0.001$), NBM (14 ± 2.3 cells/mm^2 vs SAP 59 ± 7.5 cells/mm^2; $p < 0.001$) and cortex (18 ± 3.8 cells/mm^2 vs SAP 61.63 ± 8 cells/mm^2; $p < 0.001$) (Figure 6 A). The pre-treatment of hemibrain organotypic cultures with either 1 nM or 10 nM of WIN55,212-2, 2h prior the application of 192IgG-saporin, induced protective effects on cell viability in the MS and in the NBM but no effects were observed in the cortex. A statistically significant decrease of cell death was observed as compared with 192IgG-saporin-treated hemibrain organotypic cultures in the MS (1 nM WIN55,212-2 38 ± 4.2 PI cells/mm^2 and 10 nM WIN55,212-2 39 ± 2.2 PI cells/mm^2; $p < 0.01$ vs SAP), in the NBM (1 nM WIN55,212-2 33 ± 4.9 PI cells/mm^2; $p < 0.05$ vs SAP and 10 nM WIN55,212-2 41 ± 2.8 PI cells/mm^2; $p < 0.01$ vs SAP) (Figure 6 A). The specific CB_1 receptor antagonist AM251 was able to block the protective effects elicited by WIN55,212-2 leading to cell death levels similar to those observed in those hemibrain organotypic cultures treated with the immunotoxin (Figure 6 A-C).

Discussion

Individual immunotoxins are designed in neuroscience research to eliminate specific cells or neuronal populations after binding to specific surface antigens. We have used 192IgG-saporin to specifically eliminate BFCN expressing $p75^{NTR}$ in hemibrain organotypic cultures from P7 rats. The immunotoxin-mediated depletion of BFCN in adult rats has been extensively described, but was first reported in the early 90s (Wiley et al., 1991). When 192IgG-saporin is administered to adult rats it induces a massive and specific loss of BFCN. However, the levels of expression of $p75^{NTR}$, as well as the cells expressing this receptor, vary during brain development and increase following neural injury (Ibañez and Simi, 2012). We first checked the anatomical distribution of this $p75^{NTR}$ receptor in the basal forebrain cholinergic system of formalin-fixed P7 rats, prior to the application of the immunotoxin to hemibrain organotypic cultures obtained from animals of exactly the same age. The immunofluorescence studies clearly demonstrated the presence of $p75^{NTR}$ in the different nuclei of the basal forebrain cholinergic system, including the MS, VDB, HDB and NBM, which expressed the highest levels of $p75^{NTR}$ immunoreactivity, consistent with the patterns of expression in the adult brain (Kiss et al., 1988; Woolf et al., 1989). The process for obtaining and further culturing brain organotypic cultures causes a massive lesion and damages to the integrity of the brain tissue, which could modulate the expression of $p75^{NTR}$, as suggested by Ibañez and Simi (2012), as well as the proliferation of glial cells surrounding the whole slice culture (del Rio et al., 1991). The application of different concentrations of 192IgG-saporin to hemibrain organotypic cultures resulted in a significant loss of BFCN in a dose and time-dependent manner. It is well known that $p75^{NTR}$ mediates the retrograde transport of neurotrophins, and in a similar way contributes to the movement of the monoclonal antibody coupled to saporin from axon terminals. This process explains the loss of BFCN following the uptake of 192IgG-saporin when it is administered by intracerebroventricular (i.c.v.) infusion *in vivo* (Schweitzer, 1987; Heckers et al., 1994). As the hemibrain organotypic cultures were obtained in the coronal plane and BFCN display a rostrocaudal distribution pattern of axonal branching travelling in the sagittal plate, it is reasonable to assume that the anterior, the medial and the lateral basal forebrain cholinergic pathways described in rodent (Kristt et al., 1985) and conserved in human brain (Selden et al., 1998), are transected. Therefore, the only way for the internalization of 192IgG-saporin in hemibrain organotypic cultures is through $p75^{NTR}$ located in the somatodendritic compartment. This process also explains how 192IgG-saporin is uptaken when the immunotoxin is directly infused *in* vivo into the basal forebrain (intraparenchymal).

A secondary neuronal or cellular damage critically mediates the future fate of the neurons and cells which survive the initial lesion (Koch et al., 2011b). The present results suggest that a single daily *in vitro* application of increasing concentrations of 192IgG-saporin for three DIV begining on day five of *in vitro* culture triggers a partial loss of BFCN, which leads to secondary cellular damage. This secondary cell damage is further demonstrated by the increased levels of propidium iodide (PI) uptake when hemibrain organotypic cultures are treated on day two of the *in vitro* culture for 6 DIV. PI has previously been established as a marker that identifies degenerating cells in hemibrain organotypic cultures (Pozzo Miller et al., 1994**;** Dehghani et al., 2003). The density of PI positive cells is significantly higher than the values of $p75^{NTR}$ immunoreactive BFCN in organotypic cultures treated with 192IgG-saporin, providing further support of secondary neuronal or glial cell damage as a consequence of the initial BFCN lesion. A double application of the immunotoxin on days two and five of the *in vitro* culture was assayed to avoid the washout of the toxin when the culture medium was replaced, and showed more reproducible effects. The concentration of immunotoxin that was able to eliminate approximately 50%-60% of BFCN (EC50) was selected for further assays aimed at evaluating the effects of endocannabinoid system activation in this *ex vivo* model of AD.

The *in vivo* administration of 192IgG-saporin to adult rats triggers secondary alterations in different neurotransmitter systems such as a deregulation of the "on/off" glutamatergic/GABAergic signaling. Excitotoxicity could be one of the consequences together with cortical and hippocampal reorganization in an attempt to compensate for the reduced cholinergic presynaptic input (Rossner et al., 1995a; reviewed in Rossner, 1997; Conner et al., 2003; Lee et al., 2016; Jeong da et al., 2016). More evidence of secondary neuronal or cellular damage is provided by the activation of microglia (Rossner et al., 1995d). Furthermore, different authors have reported findings which range from changes in dendritic morphology (Harmon and Wellman, 2003) to impairment of neuronal plasticity (Wellman and Sengelaub, 1991) and a negative impact on the adult neurogenic processes (Cooper-Kuhn et al., 2004). The consequences of the partial removal of BFCN in hemibrain organotypic cultures treated with the immunotoxin need to be evaluated and compared with *in vivo* administration. However, this model allows us to initiate the pharmacological evaluation of compounds that could ameliorate the subsequent effects on cell viability.

In the present study we observed that CB_1 receptors are involved in the WIN55,212-2-mediated reduction of PI uptake after 192IgG-saporin application because the protective effect of the synthetic cannabinoid agonist was blocked by the

application of the specific CB_1 receptor antagonist AM251. The density of $p75^{NTR}$ immunoreactive neurons in the presence of WIN55,212-2 was not clearly enhanced, which may indicate that there is, a modest and probably indirect protective effect on the surviving BFCN. Therefore, the decrease in cell death observed in the presence of WIN55,212-2 is presumably related to secondary neuroprotective effects, and not to a direct protection from the toxic effects of 192IgG-saporin. On the other hand, WIN55,212-2 has a similar affinity for both CB_1 and CB_2 receptors. As mentioned above, the CB_1 antagonist, AM251, blocked neuroprotection at a micromolar concentration, therefore, the contribution of microglial CB_2 receptors cannot be totally excluded

The precise mechanism by which direct BFCN death induced by 192IgG-saporin spreads out to additional BFCN or non-cholinergic cells in hemibrain organotypic cultures remains elusive. The deleterious effects described in the *in vivo* model of 192IgG-saporin administration suggest that the protective effects mediated by CB_1 receptor activation in the present model could be related to the attenuation of excitotoxicity or to the modulation of aberrant synaptic transmission after BFCN degeneration, very probably involving the activation of glial cells. Excitotoxic brain lesions contribute to microglial activation and migration towards the sites of injury, thereby increasing secondary damage (Kim and Ko, 1998; Kreutz et al., 2007). Neuroprotective effects of cannabinoid compounds have been previously described in models of excitotoxicity in organotypic cultures. Thus, 2-Arachidonoylglycerol (2-AG), through microglial CB_2 receptor activation or microglial abnormal-cannabidiol-sensitive receptor activation, triggers neuroprotective effects in hippocampal organotypic cultures, whereas Δ^9-THC or anandamide failed to provide neuroprotection, despite the fact that there was a reduction in microglial cell density (Kreutz et al., 2007; Kreutz et al., 2009). On the other hand, palmitoylethanolamide, through the peroxisome proliferator-activated receptor-alpha, together with WIN55,212-2 and N-arachidonoyldopamine, through CB_1 receptor activation, were able to induce neuroprotection in the same model of excitotoxicity. However, these effects were blocked by specific CB_1 receptor antagonists and were absent in mutant knockout mice (Koch et al., 2011a; Koch et al., 2011b; Grabiec et al., 2012). Interestingly, opposite effects of the phytocannabinoid Δ^9-THC and the synthetic agonist WIN55,212-2 have been described depending on the dose, but probably also on the time of exposure (Acquas et al., 2001, Tzavara et al., 2003a). The complexity of eCB signaling can be explained by the phenomenon of functional selectivity or biased agonism, i.e., the ability of ligands to activate a subset of the full repertoire of signaling cascades available to individual GPCR (Urban et al., 2007). Thus, the binding of WIN55,212-2 to

CB_1 receptors significantly differs from that of other cannabinoids, such as 2-AG (Howlett et al., 2002). Different alternative signaling pathways could be activated by WIN55,212-2 in addition to classical eCB-mediated signaling cascades. Nevertheless, neuroprotective effects have been described for both cannabinoids, WIN55,212-2 and 2-AG, in different brain areas such as the hippocampal dentate gyrus (Koch et al., 2011b). Moreover, prolonged activation of the CB_1 receptor results in a rapid attenuation of signaling due to desensitization and/or CB_1 receptor internalization (Howlett et al., 2004). The internalized complex of phosphorylated CB_1 receptors and β-arrestins mediates intracellular signaling pathways that control the activation of several cascades, including ERK1/2, JNK1/2/3, CREB and P38a,and leads to the regulation of gene expression and protein synthesis which most likely contribute to the protective effects of chronic activation of CB_1 receptors by WIN55,212-2 (Delgado-Peraza et al., 2016).

The synthesis of eCB can be stimulated by neuronal damage, and their protective effects are exerted through CB_1 receptors, since the lack of this receptor increases neuronal vulnerability (Stella et al., 1997; van der Stelt et al., 2001a; Marsicano et al., 2003; Kallendrusch et al., 2012). The imbalance of the excitatory/inhibitory input described in the *in vivo* model of 192IgG-saporin administration may also be contributing to an excessive glutamatergic neurotransmission (Rossner et al., 1995a). A hyper-activation activation of glutamatergic receptors triggers an intracellular increase of Ca^{2+} levels, leading to excitotoxicity by which neurons can be damaged or killed (Manev et al., 1989). Interestingly, increasing levels of glutamatergic transmission after a 192IgG-saporin-induced lesion is prevented by the NMDA receptor antagonist, MK-801 (Garrett et al., 2006), and this effect is more pronounced in 192IgG-saporin-treated young adult rats than in middle-aged and aged rats (Kim et al., 2005), suggesting that cholinergic projections from the basal forebrain play a critical role in cortical plasticity, and also revealing age-related differences in the lesion-induced expression of glutamate receptors. The fact that a reduction in glutamatergic neurotransmission through NMDA receptors or decreased levels of Ca^{2+} influx may confer neuroprotective effects led to the use of memantine, a noncompetitive antagonist of NMDA receptors, as a therapeutic drug for AD. Pharmacological enhancement of CB_1 receptor activity could elicit comparable effects and modulate excessive excitatory neurotransmission. Koch et al. (2011b) reported the neuroprotective effects of WIN55,212-2 in excitotoxically lesioned organotypic cultures, depending on the concentration of the agonist. Thus, low concentrations for three DIV elicited neuroprotection by directly activating CB_1 receptors. We observed decreased levels of cell death in the MS and in the NBM with

low doses of WIN55,212-2 during 6 DIV in 192IgG-saporin-treated hemibrain organotypic cultures, and it is reasonable to assume that the neuroprotective effects may be related to a possible tissue or neurotransmission restoration by CB_1 receptor activation in cells which are still undefined, since the localization of CB_1 receptors in BFCN remains unclear. Data suggest that rodent BFCN in the NBM are devoid of CB_1 receptors but interestingly, all of them contain eCB degrading enzymes and display a fine CB_1 receptor fiber meshwork surrounding the perikarya, which suggests that BFCN may utilize eCB for retrograde control of cholinergic neurotransmission (Harkany et al., 2003). However, microscopy studies reported the existence of differentiated BFCN in the MS of the rat, some of which express CB_1 receptors (Nyíri et al., 2005). Additional studies are necessary to further understand the precise mechanisms underlying 192IgG-saporin-induced secondary cell damage, as well as the levels of expression, the precise location and the functionality of cannabinoid receptors under conditions of BFCN degeneration.

In summary, brain organotypic cultures represent an intermediate stage between *in vitro* studies and *in vivo* models and represent a suitable scenario to create *ex vivo* models of neurodegeneration with which to further evaluate pharmacological interventions. The present work shows that 192IgG-saporin eliminates basal forebrain cholinergic neurons in an attempt to create an *ex vivo* model of AD. The initial immunotoxin-induced cholinergic lesion led to secondary cell damage which was partially reversed by the cannabinoid agonist WIN55,212-2 at nanomolar concentration. The agonist-mediated effects were blocked by the antagonist AM251, demonstrating the specific CB_1 receptor–induced protective effects.

References

Acquas E, Pisanu A, Marrocu P, Di Chiara G (2000), Cannabinoid CB(1) receptor agonists increase rat cortical and hippocampal acetylcholine release in vivo. Eur J Pharmacol 401(2):179-185.

Bartus RT, Dean RL 3rd, Beer B, Lippa AS (1982), The cholinergic hypothesis of geriatric memory dysfunction. Science 217(4558):408-414.

Conner JM, Culberson A, Packowski C, Chiba AA, Tuszynski MH (2003), Lesions of the Basal forebrain cholinergic system impair task acquisition and abolish cortical plasticity associated with motor skill learning. Neuron 38(5):819-829.

Cooper-Kuhn CM, Winkler J, Kuhn HG (2004), Decreased neurogenesis after cholinergic forebrain lesion in the adult rat. J Neurosci Res 77(2):155-165.

Davies P, Maloney AJ (1976), Selective loss of central cholinergic neurons in Alzheimer's disease. Lancet 2(8000):1403.

Dehghani F, Hischebeth GT, Wirjatijasa F, Kohl A, Korf HW, Hailer NP (2003), The immunosuppressant mycophenolate mofetil attenuates neuronal damage after excitotoxic injury in hippocampal slice cultures. Eur J Neurosci 18(5):1061-1072.

del Rio JA, Heimrich B, Soriano E, Schwegler H, Frotscher M (1991), Proliferation and differentiation of glial fibrillary acidic protein-immunoreactive glial cells in organotypic slice cultures of rat hippocampus. Neuroscience 43(2-3):335-347.

Delgado-Peraza F, Ahn KH, Nogueras-Ortiz C, Mungrue IN, Mackie K, Kendall DA, Yudowski GA (2016), Mechanisms of Biased β-Arrestin-Mediated Signaling Downstream from the Cannabinoid 1 Receptor. Mol Pharmacol 89(6):618-629.

Garrett JE, Kim I, Wilson RE, Wellman CL (2006), Effect of N-methyl-d-aspartate receptor blockade on plasticity of frontal cortex after cholinergic deafferentation in rat. Neuroscience 140(1):57-66.

Gifford AN, Ashby CR Jr (1996), Electrically evoked acetylcholine release from hippocampal slices is inhibited by the cannabinoid receptor agonist, WIN 55212-2, and is potentiated by the cannabinoid antagonist, SR 141716A. J Pharmacol Exp Ther 277(3):1431-1436.

Grabiec U, Koch M, Kallendrusch S, Kraft R, Hill K, Merkwitz C, Ghadban C, Lutz B, Straiker A, Dehghani F (2012), The endocannabinoid N-arachidonoyldopamine (NADA) exerts neuroprotective effects after excitotoxic neuronal damage via cannabinoid receptor 1 (CB(1)). Neuropharmacology 62(4):1797-807.

Hailer NP, Wirjatijasa F, Roser N, Hischebeth GT, Korf HW, Dehghani F (2001), Astrocytic factors protect neuronal integrity and reduce microglial activation in an in vitro model of N-methyl-D-aspartate-induced excitotoxic injury in organotypic hippocampal slice cultures. Eur J Neurosci 14(2):315-326.

Harkany T, Härtig W, Berghuis P, Dobszay MB, Zilberter Y, Edwards RH, Mackie K, Ernfors P (2003), Complementary distribution of type 1 cannabinoid receptors and vesicular glutamate transporter 3 in basal forebrain suggests input-specific retrograde signalling by cholinergic neurons. Eur J Neurosci 18(7):1979-1992.

Harmon KM, Wellman CL (2003), Differential effects of cholinergic lesions on dendritic spines in frontal cortex of young adult and aging rats. Brain Res 992(1):60-68.

Heckers S, Ohtake T, Wiley RG, Lappi DA, Geula C, Mesulam MM (1994), Complete and selective cholinergic denervation of rat neocortex and hippocampus but not amygdala by an immunotoxin against the p75 NGF receptor. J Neurosci 14(3 Pt 1):1271-1289.

Howlett AC, Barth F, Bonner TI, Cabral G, Casellas P, Devane WA, Felder CC, Herkenham M, Mackie K, Martin BR, Mechoulam R, Pertwee RG (2002), International Union of Pharmacology. XXVII. Classification of cannabinoid receptors. Pharmacol Rev 54(2):161-202.

Howlett AC, Breivogel CS, Childers SR, Deadwyler SA, Hampson RE, Porrino LJ (2004), Cannabinoid physiology and pharmacology: 30 years of progress. Neuropharmacology 47 Suppl 1:345-58.

Ibáñez CF, Simi A (2012), p75 neurotrophin receptor signaling in nervous system injury and degeneration: paradox and opportunity. Trends Neurosci 35(7):431-440.

Jeong da U, Oh JH, Lee JE, Lee J, Cho ZH, Chang JW, Chang WS (2016), Basal Forebrain Cholinergic Deficits Reduce Glucose Metabolism and Function of Cholinergic and GABAergic Systems in the Cingulate Cortex. Yonsei Med J 57(1):165-172.

Kallendrusch S, Hobusch C, Ehrlich A, Nowicki M, Ziebell S, Bechmann I, Geisslinger G, Koch M, Dehghani F (2012), Intrinsic up-regulation of 2-AG favors an area specific neuronal survival in different in vitro models of neuronal damage. PLoS One 2012;7(12):e51208.

Kim WK, Ko KH (1998), Potentiation of N-methyl-D-aspartate-mediated neurotoxicity by immunostimulated murine microglia. J Neurosci Res 54(1):17-26.

Kim I, Wilson RE, Wellman CL (2005), Aging and cholinergic deafferentation alter GluR1 expression in rat frontal cortex. Neurobiol Aging (7):1073-1081.

Kiss J, McGovern J, Patel AJ (1988), Immunohistochemical localization of cells containing nerve growth factor receptors in the different regions of the adult rat forebrain. Neuroscience 27(3):731-748.

Koch M, Kreutz S, Böttger C, Grabiec U, Ghadban C, Korf HW, Dehghani F (2011), The cannabinoid WIN 55,212-2-mediated protection of dentate gyrus granule cells is driven by CB1 receptors and modulated by TRPA1 and Cav 2.2 channels. Hippocampus 21(5):554-564.

Koch M, Kreutz S, Böttger C, Benz A, Maronde E, Ghadban C, Korf HW, Dehghani F (2011), Palmitoylethanolamide protects dentate gyrus granule cells via peroxisome proliferator-activated receptor-α. Neurotox Res 19(2):330-340.

Kreitzer AC, Regehr WG (2001), Retrograde inhibition of presynaptic calcium influx by endogenous cannabinoids at excitatory synapses onto Purkinje cells. Neuron 29(3):717-727.

Kreutz S, Koch M, Ghadban C, Korf HW, Dehghani F (2007), Cannabinoids and neuronal damage: differential effects of THC, AEA and 2-AG on activated microglial cells and degenerating neurons in excitotoxically lesioned rat organotypic hippocampal slice cultures. Exp Neurol. 203(1):246-257.

Kreutz S, Koch M, Böttger C, Ghadban C, Korf HW, Dehghani F (2009), 2-Arachidonoylglycerol elicits neuroprotective effects on excitotoxically lesioned dentate gyrus granule cells via abnormal-cannabidiol-sensitive receptors on microglial cells. Glia 57(3):286-294.

Kristt DA, McGowan RA Jr, Martin-MacKinnon N, Solomon J (1985), Basal forebrain innervation of rodent neocortex: studies using acetylcholinesterase histochemistry, Golgi and lesion strategies. Brain Res 337(1):19-39.

Lee JE, Jeong da U, Lee J, Chang WS, Chang JW (2016), The effect of nucleus basalis magnocellularis deep brain stimulation on memory function in a rat model of dementia. BMC Neurol16:6.

Manev H, Favaron M, Guidotti A, Costa E (1989), Delayed increase of Ca2+ influx elicited by glutamate: role in neuronal death. Mol Pharmacol 36(1):106-112.

Manuel I, González de San Román E, Giralt MT, Ferrer I, Rodríguez-Puertas R (2014), Type-1 cannabinoid receptor activity during Alzheimer's disease progression. J Alzheimers Dis 42(3):761-766.

Marsicano G, Goodenough S, Monory K, Hermann H, Eder M, Cannich A, Azad SC, Cascio MG, Gutiérrez SO, van der Stelt M, López-Rodriguez ML, Casanova E, Schütz G,

Zieglgänsberger W, Di Marzo V, Behl C, Lutz B (2003), CB1 cannabinoid receptors and on-demand defense against excitotoxicity. Science 302(5642):84-88.

Mesulam MM, Mufson EJ, Wainer BH, Levey AI (1983), Central cholinergic pathways in the rat: an overview based on an alternative nomenclature (Ch1-Ch6). Neuroscience 10(4):1185-1201.

Mulder J, Zilberter M, Pasquaré SJ, Alpár A, Schulte G, Ferreira SG, Köfalvi A, Martín-Moreno AM, Keimpema E, Tanila H, Watanabe M, Mackie K, Hortobágyi T, de Ceballos ML, Harkany T (2011), Molecular reorganization of endocannabinoid signalling in Alzheimer's disease. Brain 134(Pt 4):1041-1060.

Nyíri G, Szabadits E, Cserép C, Mackie K, Shigemoto R, Freund TF (2005), GABAB and CB1 cannabinoid receptor expression identifies two types of septal cholinergic neurons. Eur J Neurosci 21(11):3034-3042.

Pozzo Miller LD, Mahanty NK, Connor JA, Landis DM (1994), Spontaneous pyramidal cell death in organotypic slice cultures from rat hippocampus is prevented by glutamate receptor antagonists. Neuroscience 63(2):471-487.

Rossner S, Schliebs R, Bigl V (1995a), 192IgG-saporin-induced immunotoxic lesions of cholinergic basal forebrain system differentially affect glutamatergic and GABAergic markers in cortical rat brain regions. Brain Res 696(1-2):165-176.

Rossner S, Härtig W, Schliebs R, Brückner G, Brauer K, Perez-Polo JR, Wiley RG, Bigl V (1995b), 192IgG-saporin immunotoxin-induced loss of cholinergic cells differentially activates microglia in rat basal forebrain nuclei. J Neurosci Res 41(3):335-346.

Rossner S (1997), Cholinergic immunolesions by 192IgG-saporin--useful tool to simulate pathogenic aspects of Alzheimer's disease. Int J Dev Neurosci 15(7):835-850.

Schweitzer JB (1987), Nerve growth factor receptor-mediated transport from cerebrospinal fluid to basal forebrain neurons. Brain Res 423(1-2):309-317.

Selden NR, Gitelman DR, Salamon-Murayama N, Parrish TB, Mesulam MM (1998), Trajectories of cholinergic pathways within the cerebral hemispheres of the human brain. Brain 121 (Pt 12):2249-2257.

Skaper SD, Buriani A, Dal Toso R, Petrelli L, Romanello S, Facci L, Leon A (1996), The ALIAmide palmitoylethanolamide and cannabinoids, but not anandamide, are protective in a delayed postglutamate paradigm of excitotoxic death in cerebellar granule neurons. Proc Natl Acad Sci U S A 93(9):3984-3989.

Springer JE, Koh S, Tayrien MW, Loy R (1987), Basal forebrain magnocellular neurons stain for nerve growth factor receptor: correlation with cholinergic cell bodies and effects of axotomy. J Neurosci Res 17(2):111-118.

Stella N, Schweitzer P, Piomelli D (1997), A second endogenous cannabinoid that modulates long-term potentiation. Nature 388(6644):773-778.

Stoppini L, Buchs PA, Muller D (1991), A simple method for organotypic cultures of nervous tissue. J Neurosci Methods 37(2):173-182.

Tzavara ET, Bymaster FP, Felder CC, Wade M, Gomeza J, Wess J, McKinzie DL, Nomikos GG (2003), Dysregulated hippocampal acetylcholine neurotransmission and impaired cognition in M2, M4 and M2/M4 muscarinic receptor knockout mice. Mol Psychiatry 8(7):673-679.

Urban JD, Clarke WP, von Zastrow M, Nichols DE, Kobilka B, Weinstein H, Javitch JA, Roth BL, Christopoulos A, Sexton PM, Miller KJ, Spedding M, Mailman RB (2007), Functional selectivity and classical concepts of quantitative pharmacology. J Pharmacol Exp Ther 320: 1–13.

van der Stelt M, Veldhuis WB, van Haaften GW, Fezza F, Bisogno T, Bar PR, Veldink GA, Vliegenthart JF, Di Marzo V, Nicolay K (2001a), Exogenous anandamide protects rat brain against acute neuronal injury in vivo. J Neurosci 21(22):8765-8771.

van der Stelt M, Veldhuis WB, Bär PR, Veldink GA, Vliegenthart JF, Nicolay K (2001b), Neuroprotection by Delta9-tetrahydrocannabinol, the main active compound in marijuana, against ouabain-induced in vivo excitotoxicity. J Neurosci 21(17):6475-6479.

Wellman CL, Sengelaub DR (1991), Cortical neuroanatomical correlates of behavioral deficits produced by lesion of the basal forebrain in rats. Behav Neural Biol 56(1):1-24.

Wiley RG, Oeltmann TN, Lappi DA (1991), Immunolesioning: selective destruction of neurons using immunotoxin to rat NGF receptor. Brain Res 562(1):149-153.

Wilson RI, Nicoll RA (2001), Endogenous cannabinoids mediate retrograde signalling at hippocampal synapses. Nature. 410(6828):588-592. Erratum in: Nature 2001 Jun 21; 411(6840):974.

Woolf NJ, Gould E, Butcher LL (1989), Nerve growth factor receptor is associated with cholinergic neurons of the basal forebrain but not the pontomesencephalon. Neuroscience 30(1):143-152.

Wrenn CC, Wiley RG (1998), The behavioral functions of the cholinergic basal forebrain: lessons from 192 IgG-saporin. Int J Dev Neurosci 16(7-8):595-602.

Acknowledgements:

This work was supported by the Departments of Economic Development (Elkartek KK-2016/00045) and Education (IT975-16) of the Basque Government. Technical and human support was provided by General Research Services SGIker from The University of the Basque Country (UPV/EHU), co-financed by the Ministry of Economy and Competitiveness (MINECO) of the Spanish Government, European Regional Development Fund (ERDF) and the European Social Fund (ESF). A. LL. is the recipient of a fellowship from the Basque Government (BFI 2012-119). The authors declare no conflict of interest.

Figures

Figure 1

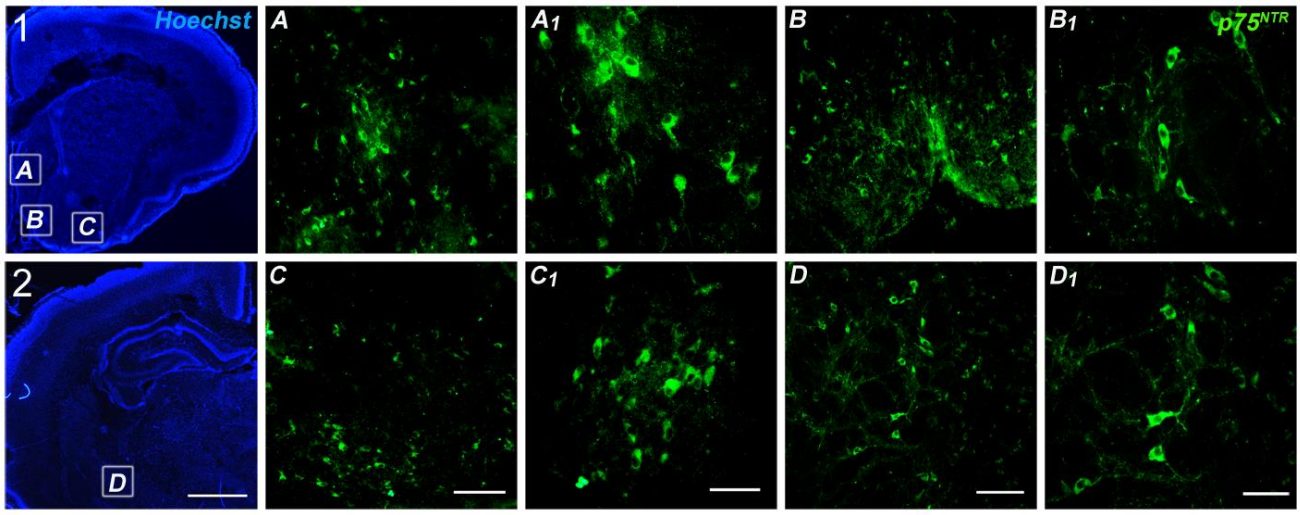

Figure 2

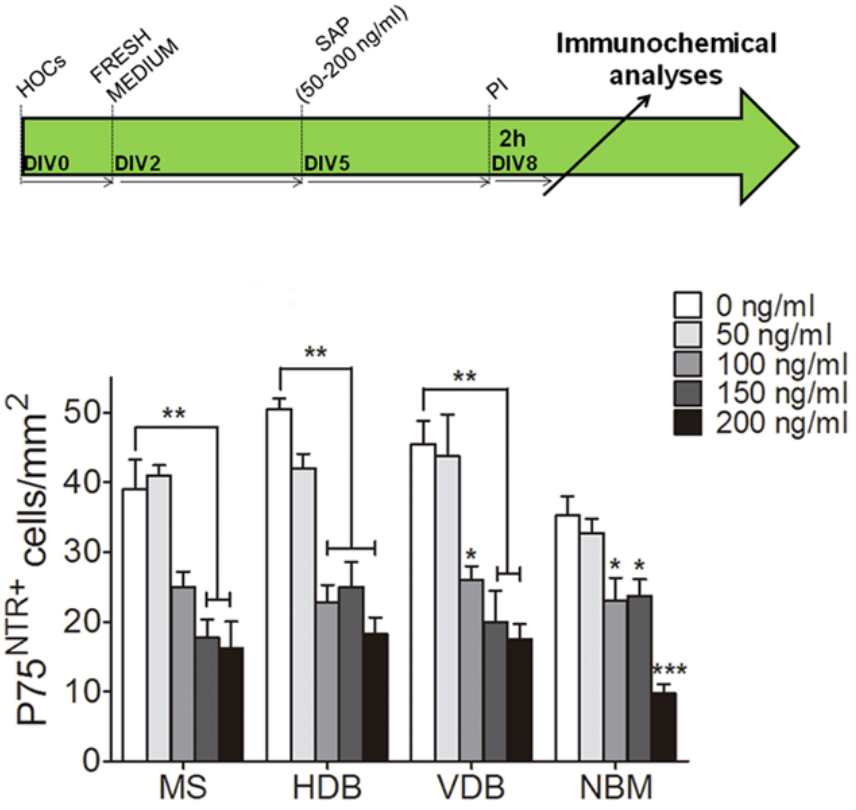
HOCs
FRESH MEDIUM
SAP (50-200 ng/ml)
PI
Immunochemical analyses
DIV0
DIV2
DIV5
2h DIV8
0 ng/ml
50 ng/ml
100 ng/ml
150 ng/ml
200 ng/ml
P75NTR+ cells/mm2
0
10
20
30
40
50
**
**
**
*
*
*
***
MS
HDB
VDB
NBM

Figure 3

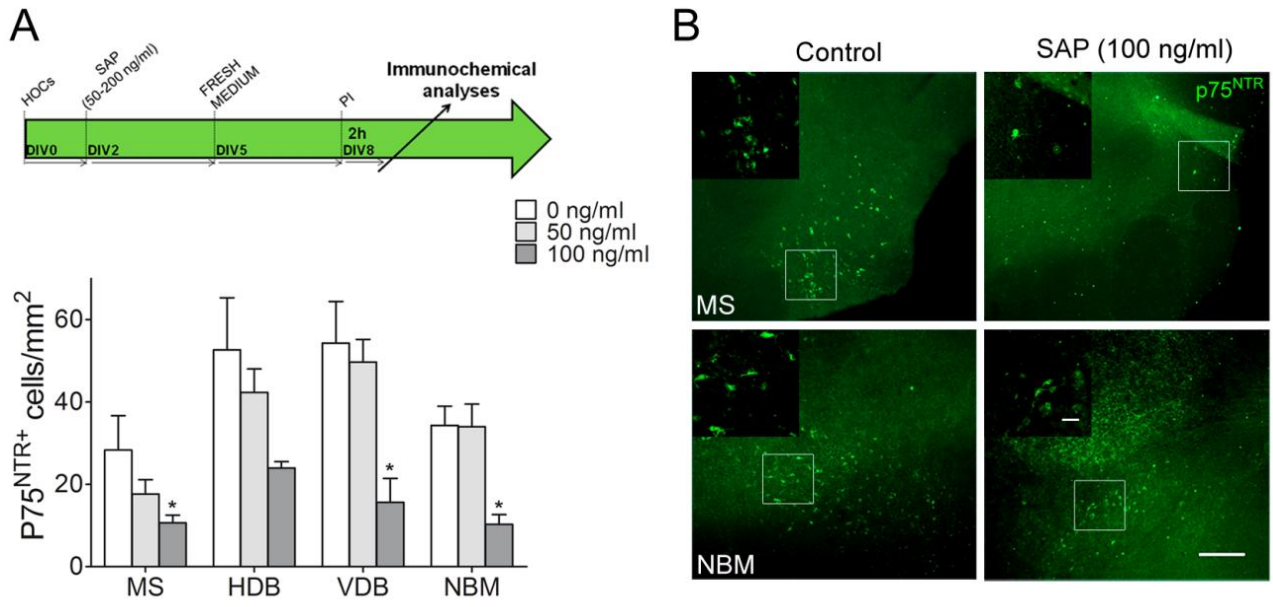
A
HOCs
SAP (50-200 ng/ml)
FRESH MEDIUM
PI
Immunochemical analyses
DIV0
DIV2
DIV5
2h DIV8
0 ng/ml
50 ng/ml
100 ng/ml
P75NTR+ cells/mm2
60
40
20
0
MS
HDB
VDB
NBM
B
Control
SAP (100 ng/ml)
p75NTR
MS
NBM

Figure 4

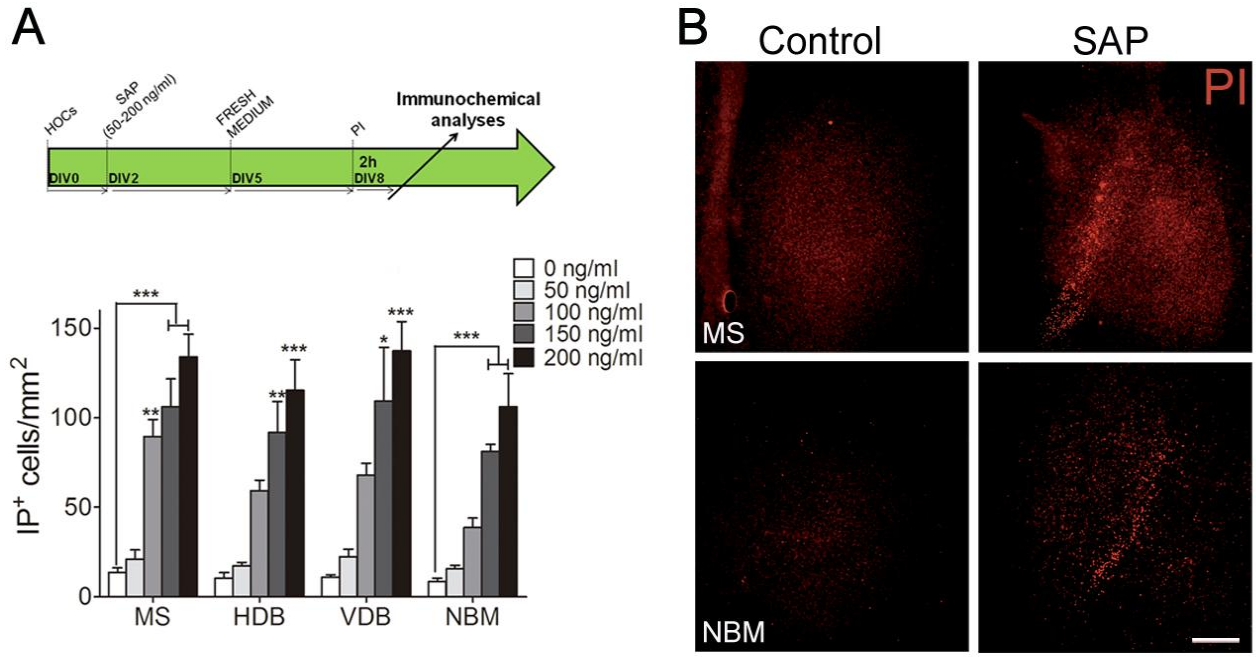
A
HOCs
SAP (50-200 ng/ml)
FRESH MEDIUM
PI
Immunochemical analyses
DIV0
DIV2
DIV5
DIV8
2h
0 ng/ml
50 ng/ml
100 ng/ml
150 ng/ml
200 ng/ml
IP+ cells/mm2
150
100
50
0
MS
HDB
VDB
NBM
B
Control
SAP
PI
MS
NBM

Figure 5

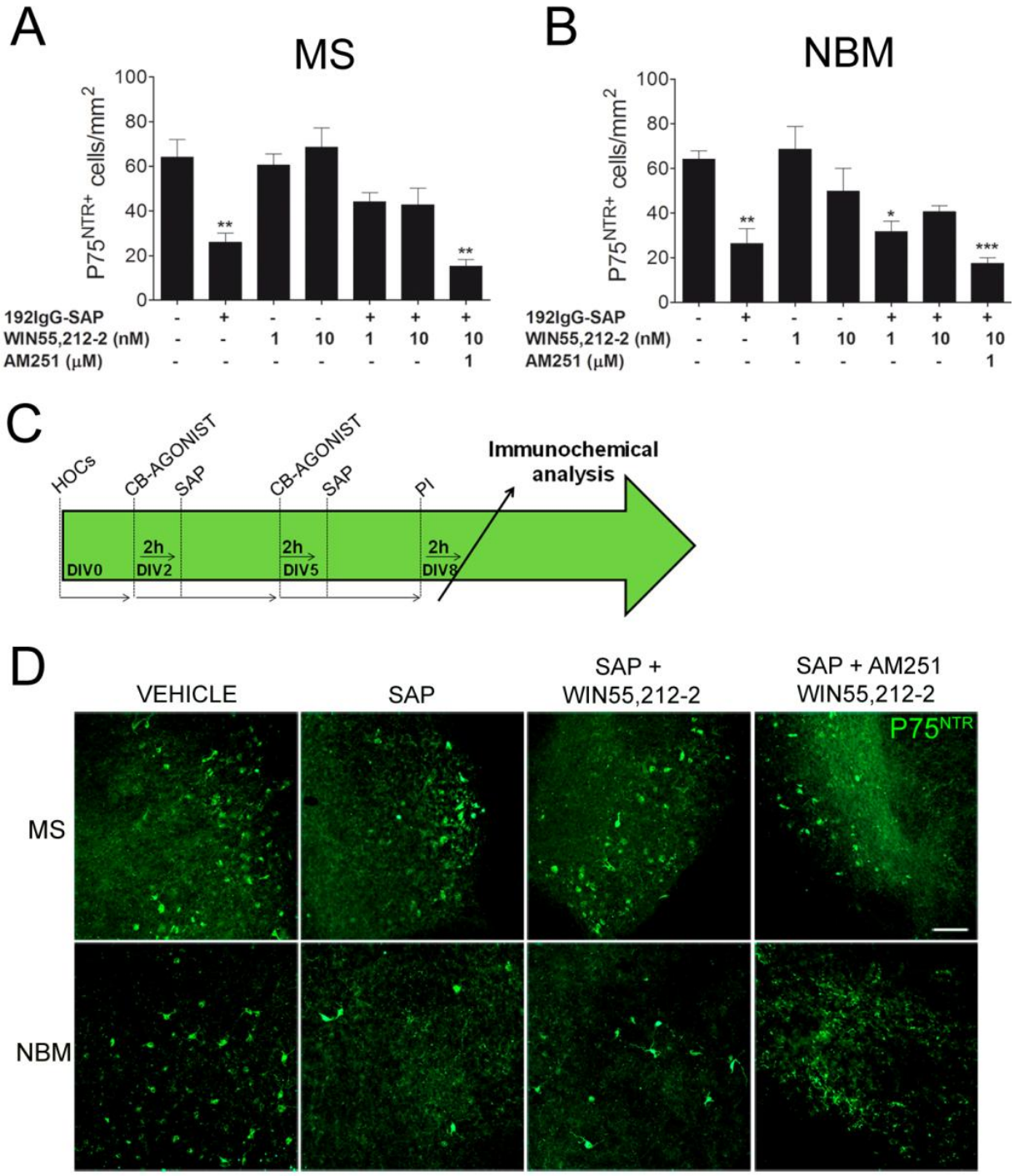
A
MS
P75NTR+ cells/mm2
100
80
60
40
20
0
**
**
192IgG-SAP - + - - + + +
WIN55,212-2 (nM) - - 1 10 1 10 10
AM251 (μM) - - - - - - 1
B
NBM
P75NTR+ cells/mm2
100
80
60
40
20
0
**
*
***
192IgG-SAP - + - - + + +
WIN55,212-2 (nM) - - 1 10 1 10 10
AM251 (μM) - - - - - - 1
C
HOCs
CB-AGONIST
SAP
CB-AGONIST
SAP
PI
Immunochemical analysis
2h
2h
2h
DIV0
DIV2
DIV5
DIV8
D
VEHICLE
SAP
SAP + WIN55,212-2
SAP + AM251 WIN55,212-2
P75NTR
MS
NBM

Figure 6

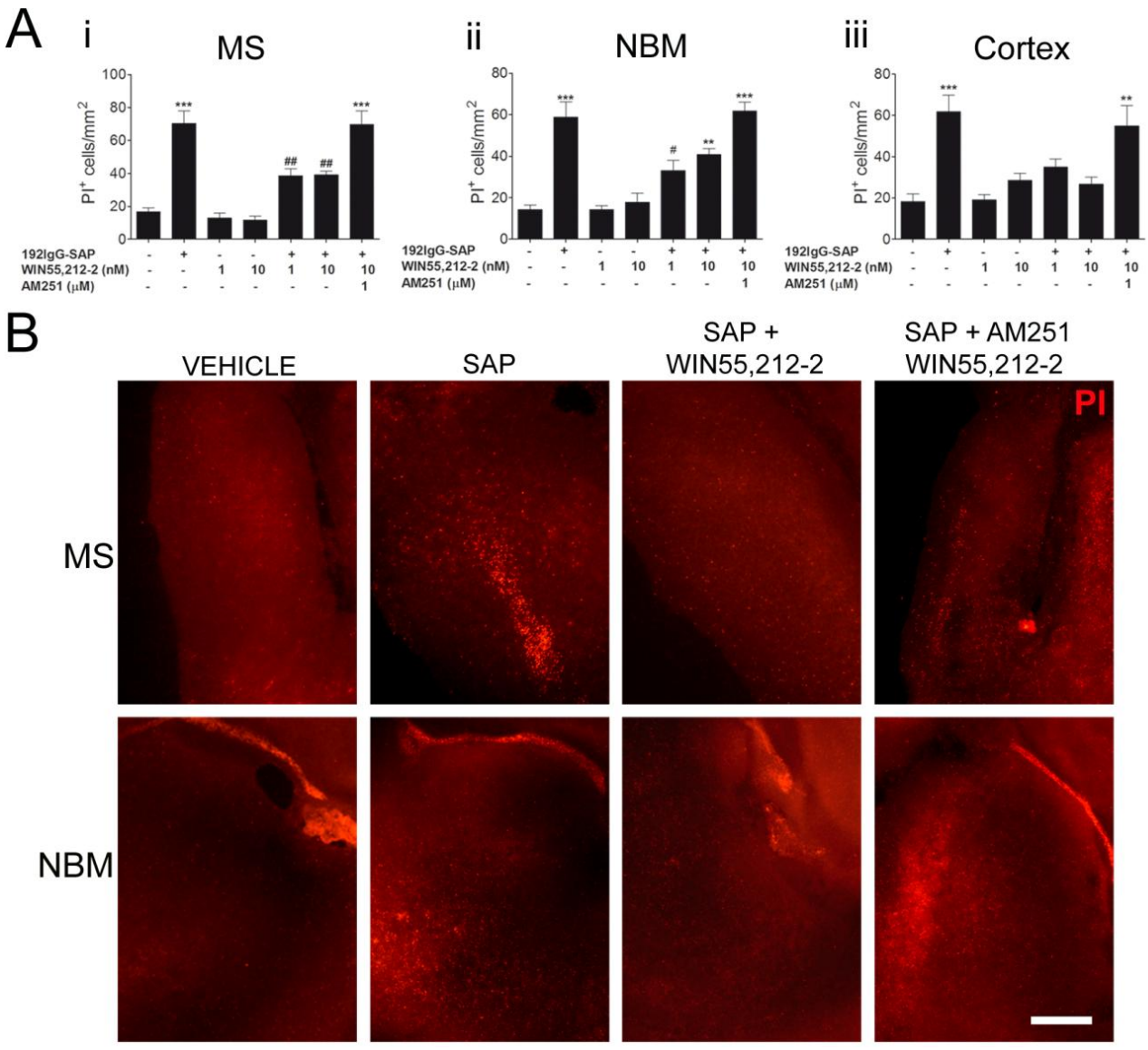
A
i
MS
ii
NBM
iii
Cortex
PI+ cells/mm2
192IgG-SAP
WIN55,212-2 (nM)
AM251 (μM)
B
VEHICLE
SAP
SAP + WIN55,212-2
SAP + AM251 WIN55,212-2
PI
MS
NBM

Figure legends

Figure 1. Low magnification (2.5X) photomicrographs of Hoechst staining in 10 µm tissue slices from P7 rats including the medial septum (MS) (1-A) and both the vertical (VDB) (1-B) and horizontal diagonal band of Broca (HDB) (1-C) and the nucleus basalis magnocellularis (NBM) (2-D) (Scale bar = 1 mm). $P75^{NTR}$ immunofluorescence in the MS (A-A1), VDB (B-B1), HDB (C-C1) and NBM (D-D1). (C-D scale bar = 100 µm and C1-D1 scale bar = 50 µm).

Figure 2. Number of $p75^{NTR}$ positive cells in hemibrain organotypic cultures containing the basal forebrain cholinergic system after the application of different concentrations of 192IgG-saporin according to the treatment schedule. (A) * $p < 0.05$; ** $p < 0.01$; *** $p < 0.001$ vs control (0 ng/ml).

Figure 3. (A) Number of $p75^{NTR}$ immunoreactive BFCN in hemibrain organotypic cultures containing the basal forebrain cholinergic system after the application of different concentrations of 192IgG-saporin according to the treatment schedule. (B) $P75^{NTR}$ immunoreactive BFCN in the MS (top row) and the NBM (bottom row) in the absence (control) or in the presence of 100 ng/ml of the immunotoxin according to the treatment schedule described in (A). Low magnification and high magnification images scale bar = 200 and 40 µm, respectively. (A-B) * $p < 0.05$ vs control (0 ng/ml).

Figure 4. (A) Number of PI positive cells in hemibrain organotypic cultures containing the basal forebrain cholinergic system after the application of different concentrations of 192IgG-saporin according to the treatment schedule. (B) PI uptake in hemibrain organotypic cultures containing the MS (top row) and the NBM (bottom row) in the absence (control) or in the presence of 100 ng/ml of the immunotoxin according to the treatment schedule described in (A). Scale bar = 200 µm. (A) * $p < 0.05$; ** $p < 0.01$; *** $p < 0.001$ vs control (0 ng/ml) and (B) *** $p < 0.001$ vs 200 ng/ml.

Figure 5. (A-B) Number of $p75^{NTR}$ immunoreactive BFCN in hemibrain organotypic cultures in the absence or presence of 100 ng/ml of 192IgG-saporin, the cannabinoid agonist WIN55,212-2 (1 or 10 nM) or the CB_1 receptor antagonist AM251 (1 µM) during 6 DIV according to the treatment schedule (C). (D) $P75^{NTR}$ immunoreactive BFCN in the MS (top row) and the NBM (bottom row) in the absence (vehicle) or presence of 100 ng/ml of the immunotoxin, treated with 1 nM WIN55,212-2 and 1 µM of AM251. Scale bar = 40 µm. * $p < 0.05$; ** $p < 0.01$; *** $p < 0.001$ vs control.

Figure 6. (A) Number of PI positive cells in hemibrain organotypic cultures containing the MS (i), the NBM (ii) and the cortex (iii) in the absence or presence of 100 ng/ml of 192IgG-saporin, the cannabinoid agonist WIN55,212-2 (1 or 10 nM) or the CB_1 receptor antagonist AM251 (1 µM) during 6 DIV according to the treatment schedule (see Figure 5 C). (B) PI uptake in the MS (top row) and the NBM (bottom row) in the absence (vehicle) or presence of 100 ng/ml of the immunotoxin, treated with 1 nM WIN55,212-2 and 1 µM of AM251. Scale bar = 200 µm. ** $p < 0.01$; *** $p < 0.001$ vs control and # $p < 0.05$; ## $p < 0.01$ vs 192IgG-saporin.

Highlights

- P7 and adult rats show a similar anatomical distribution of basal forebrain cholinergic neurons.
- The basal forebrain cholinergic neurons from P7 rats express somatodendritic $p75^{NTR}$ receptors.
- Basal forebrain cholinergic neurons are selectively eliminated by 192IgG-saporin in hemibrain organotypic cultures.
- WIN55,212-2, at nanomolar concentrations, protects basal forebrain cells from damage induced by the elimination of BFCN.

Graphical abstract

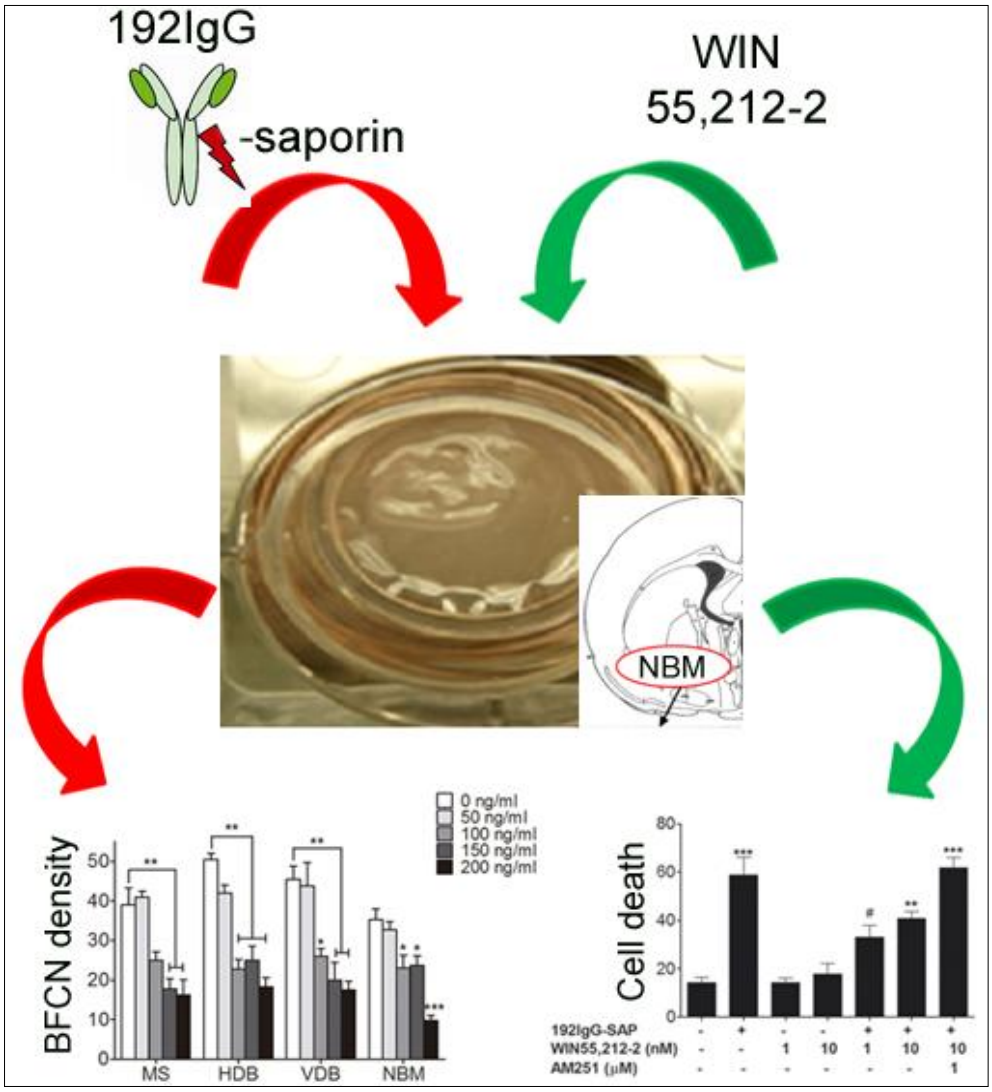

II

Muscarinic neurotransmission and lipid profile changes in a rat model of cholinergic dysfunction

Alberto Llorente-Ovejero[1], Jonatan Martínez-Gardeazabal[1], Estíbaliz González de San Román[1], Marta Moreno-Rodríguez[1], Iván Manuel[1], Maria Teresa Giralt[1], Rafael Rodríguez-Puertas[1]

[1]Department of Pharmacology, Faculty of Medicine and Nursing. University of the Basque Country (UPV/EHU), Bº Sarriena s/n, 48940 Leioa, Spain.

*Corresponding author

Rafael Rodríguez-Puertas

Department of Pharmacology, Faculty of Medicine and Nursing.

University of the Basque Country. E-48940 Leioa, Vizcaya, Spain.

Tel.: +34-94-6012739; fax: +34-94-6013220.

E-mail address: rafael.rodriguez@ehu.es

Running title: **Muscarinic and lipids in cholinergic degeneration**

Keywords: cholinergic, 192IgG-saporin, autoradiography, muscarinic, lipids, MALDI

Abbreviations: AA: arachidonic acid; ACh: Acetylcholine; AChE: Acetylcholinesterase; aCSF: artificial cerebrospinal fluid; BFCN: Basal forebrain cholinergic neurons; Ch: Choline; ChAT: Choline acetyltransferase; DHA: Docosahexaenoic acid. GTPγS: Guanosine5´-O-3-thiotriphosphate; M_2/M_4 mAChR: subtype-2/4 of muscarinic acetylcholine receptor; mAChR: Muscarinic acetylcholine receptor; Maldi-IMS: Matrix-assisted laser desorption ionization-imaging mass spectrometry; NBM: Nucleus basalis magnocellularis; PC: Phosphatidylcholines; PE: Phosphatidylethanolamines; PG: Phosphoglycerol; PI: Phosphatidylinositol; PS: Phosphatidylserines; PUFA: Polyunsaturated fatty acid; SAP: 192IgG-saporin treated rats; SM: Sphingomyelins.

Abstract

Alzheimer's disease (AD) is associated with a selective vulnerability of cholinergic neurotransmission. The loss of basal forebrain cholinergic neurons (BFCN) described in AD leads to decreased levels of acetylcholine associated to pathological changes of muscarinic signaling. Under neuropathological conditions autophagy or autocannibalism is considered as an adaptive response to maintain cellular homeostasis. When choline is in short supply and the surviving BFCN are physiologically more active, membrane phospholipids represent a source for the synthesis of choline *de novo,* a process that can be regulated by muscarinic receptors. Several lipid species involved in the metabolism of choline are deregulated and serve as possible biomarkers of phenoconversion to AD. In the present study we used a rat model with basal forebrain cholinergic dysfunction, induced by the intraparenchymal infusion of 192IgG-saporin in the nucleus basalis magnocellularis (NBM), to evaluate the effects on learning and memory under the passive avoidance paradigm. In addition,both muscarinic signaling and lipid composition are measured by using autoradiography and matrix-assisted laser desorption ionization-imaging mass spectrometry (MALDI-IMS), respectively. The findings show that depletion of BFCN in the NBM leads to a dramatic loss of cortical cholinergic innervation which runs in parallel to learning and memory impairment. TheA decrease in muscarinic neurotransmission in the NBM was found, while no changes were observed in cortical muscarinic signaling. Finally, marked changes in the lipid profile were found in NBM and the innervated cortical areas, including species related to choline metabolism, which supports the hypothesis that the modulation of lipid metabolism could represent an alternative therapeutic strategy to potentiate cholinergic neurotransmission.

Introduction

Alzheimer's disease (AD), the most common cause of dementia in the elderly, is clinically characterized by a progressive and irreversible impairment of memory and thinking abilities. During the progression of AD a specific vulnerability of the cholinergic neurotransmission system has been extensively described. Thus, the loss of basal forebrain cholinergic neurons (BFCN) (Davis and Maloney, 1976; Whitehouse et al., 1982), decreased levels of choline acetyltransferase (ChAT) activity (Davis and Maloney, 1976; Davis, 1979), which lead to cholinergic hypoactivity (Perry et al., 1977), decreased levels of high-affinity choline uptake carriers (Rodríguez-Puertas et al., 1994) and altered distribution and impaired functionality of both muscarinic (mAChR) (Nordberg, 1992; Rodríguez-Puertas et al., 1997) and nicotinic receptors. (Hellstrom-Lindahl et al., 1999) have been reported. These findings and the observation that muscarinic antagonists induced amnesia and cognitive impairment in healthy young subjects (Drachman and Leavitt, 1974), contributed to the development of the cholinergic hypothesis of geriatric memory dysfunction (Bartus et al., 1982). Furthermore, changes in cholinergic neurotransmission are involved in the short-term learning deficits and memory loss described at the onset of adult dementia disorders (Avery et al., 1997).

The BFCN from the nucleus basalis magnocellularis (NBM) innervate almost the entire cerebral cortex, provide the main source of cortical acetylcholine (ACh) and control learning and memory processes. 192IgG-saporin is an immunotoxin directed at the low affinity neurotrophin receptor $p75^{NTR}$, which is abundantly expressed in BFCN, and represents a powerful tool with which to specifically eliminate BFCN in order to mimic the cholinergic degeneration described in AD patients (Wiley et al., 1991).

The biosynthesis of ACh is carried out by the enzyme ChAT using choline (Ch), which cannot be synthesized *de novo* in neurons, is obtained from the diet and delivered to the neurons via the blood stream (reviewed in Blusztajnn and Wurtman, 1983). ACh hydrolysis provides approximately 50% of Ch and the high affinity carrier is responsible for its uptake. A secondary source for Ch derived from the hydrolysis of certain lipid species, such as membrane phospholipids, has been described leading to the *autocannibalism* (autophagy) hypothesis as an adaptative response to stress provoked by the cholinergic dysfunction described in AD (Wurtman et al., 1985), which probably involves cholinergic muscarinic neurotransmission (Qian et al., 1989; Dolezal and Tucek, 1984). The intraparenchymal infusion of 192IgG-saporin in the NBM decreases ChAT and acetylcholinesterase (AChE) levels, reduces high-affinity choline carrier and neurotrophins levels and contributes to alter the activity and distribution of

muscarinic (see review from Rossner, 1997) and nicotinic receptors (Bednar et al., 1998; Quinlivan et al., 2007).

Due to the fact that lipids are the main structural components of membranes involved in multiple signaling pathways and in energy metabolism, one would expect to observe a regulation of certain species after the immunotoxin-induced death of BFCN in the NBM. Moreover, both the structural lipids of BFCN and those involved in the metabolism of ACh, including species of phosphatidylcholines (PC), phosphatidylethanolamines (PE), phosphatidylserines (PS) and sphingomyelins (SM) should be modulated in some way. Many studies have detailed dyshomeostatic levels of different lipid species in AD, including PC (Martın et al., 2010; Nitsch et al., 1992), PE (Martın et al., 2010) and PS (Pettegrew et al., 2001). Many efforts to reduce the deficit of ACh in AD patients following the administration of precursors such as Ch have failed in clinical trials (Amenta et al., 2001). The use of immunotoxins to selective eliminate specific neuronal populations represents a suitable scenario with which to mimic certain pathological features of neurodegenerative disorders.

The aims of the present study were to analyze learning and memory by using the passive avoidance test, the muscarinic-mediated cholinergic signaling and the distribution of muscarinic receptors by means of [^{35}S]GTPγS autoradiography and immunofluorescence and the lipid profile by using matrix-assisted laser desorption ionization-imaging mass spectrometry (MALDI-IMS) after the specific depletion of BFCN in the NBM as an appropriate *in vivo* model of AD.

Materials and methods

Chemicals

192IgG-saporin (Batch 2441969) was acquired from Millipore (Temecula, CA, USA) and [^{35}S]GTPγS (1250 Ci/mmol) from PerkinElmer (Boston MA, USA). The [^{14}C]-microscales used as standards in the autoradiographic experiments were purchased from ARC (American Radiolabelled Chemicals, Saint Louis, MI, USA). The β-radiation sensitive films Kodak Biomax MR, bovine serum albumine (BSA), DL-dithiothreitol (DTT), adenosine deaminase (ADA), guanosine 5´-diphosphate (GDP), guanosine5´-O-3-thiotriphosphate (GTPγS), ketamine, xylazine, acetylthiocholine iodide, 2-mercaptobenzothiazole (MBT) and tetraisopropylpyrophosphoramide (iso-OMPA) were all acquired from Sigma-Aldrich (St Louis, MO, USA). The compounds necessary for the preparation of the different buffers, the fixation and the treatment of slides were of the highest commercially available quality.

Animals

Seventy adult male Sprague-Dawley rats, weighing 225-275 g and ranging in age from 8 to 10 weeks at the onset of the experiment, were used in this study. Rats were housed four per cage in 50 cm (length) x 25 cm (width) x 15 cm (height) cages at a temperature of 22ºC and in a humidity-controlled (65%) room with a 12:12 hour light/dark cycle, with access to food and water *ad libitum*. All procedures were performed in accordance with European animal research laws (Directive 2010/63/EU) and the Spanish National Guidelines for Animal Experimentation (RD 53/2013, Law 32/2007). Experimental protocols were approved by the Local Ethical Committee for Animal Research of the University of the Basque Country (CEEA 388/2014).

Basal forebrain cholinergic lesion

All surgery was carried out under aseptic conditions. 192IgG-saporin was used to selectively eliminate basal forebrain cholinergic neurons (BFCN) in the nucleus basalis magnocellularis (NBM). Rats were randomly assigned to one of three groups: sham-operated (SHAM; n = 6), artificial cerebrospinal fluid, used as vehicle, (aCSF; n = 32) and 192IgG-saporin (SAP; n = 32). The vehicle was prepared as follows: 0.15 M NaCl, 2.7 mM KCl, 0.85 mM $MgCl_2$, 1.2 mM $CaCl_2$ (pH = 7.4) and sterilized by filtration with 0.4 µm-Ø filters (EMD Millipore, CA, USA). Rats were anesthetized with ketamine/xylazine (90/10 mg/kg; s.c.) and then placed in a stereotaxic instrument (Kopf, Tujunga, CA). After an incision was made in the skin along the midline of the skull, two holes were drilled and by using a 10-µl Hamilton syringe (Neuros^{TM} Syringe, 7000 series; Bonaduz, Switzerland) with a 26-gauge needle, the intraparenchymal infusions were made into the NBM: - 1.5 mm anteroposterior from Bregma, ± 3 mm mediolateral from midline, + 8 mm dorsoventral from cranial surface (Paxinos and Watson, 2005). 192IgG-saporin was dissolved in aCSF to a final concentration of 130 ng/µl. The aCSF or the immunotoxin were bilaterally injected (1 µl/hemisphere) at a constant rate of 0.2 µl/min. The needle was kept in for an additional 5 min before removal, to avoid a possible backflow and to allow complete diffusion. The SHAM group was treated in the same way as the aCSF group but without vehicle infusion. During surgery, the body temperature was controlled and the eyes were kept hydrated with warm saline solution (0.9% NaCl). After completing the administration, the wounds were closed with braided silk sutures and a broad-spectrum antibiotic injection was given (2.25 mg/kg oxytetracicline; i.m.). The choice of coordinates, infusion rate, volume and dose of the immunotoxin were based on previous experiments performed in our laboratory.

Passive avoidance test

The rats were allowed seven days to recover from surgery and were then subjected to the passive avoidance test (PanLab passive avoidance box LE870/872). The apparatus for the test consists of two methacrylate compartments separated by a guillotine door. The first compartment is large, white, illuminated and open-topped: (31 cm x 31 cm x 24 cm) and the other is small, dark and closed (19.5 cm x 10.8 cm x 12 cm. The position of the animal is detected by the use of highly sensitive weight transducers. The passive avoidance test involves two sessions. The first, which is called "the learning trial", was performed on day 7 after surgery. Each animal was gently placed in the illuminated compartment and allowed to explore it for 30 sec. Then, the guillotine door was automatically opened and the rat was given a maximum of 60 sec to enter the dark compartment. When the rat crossed the door-way the door closed, the acquisition latency time (i.e. the time that rats remained in the open-topped compartment) was measured, and a foot shock (0.4 mA/2 sec) was delivered. 10 sec after the foot shock, the rat was returned to its home cage. The rats, which did not enter the dark compartment, were eliminated from the study. 24 h later, for the second session called "the retention trial", the rats were again placed in the illuminated compartment and allowed to explore for 30 sec. Then the door opened and the time taken to enter the dark compartment, the step-through latency time, was measured, with a cut-off of 300 sec.

Tissue preparation

Following the passive avoidance test, all the animals were anaesthetized with ketamine/xylazine (90/10 mg/ kg; i.p.) and sacrificed by decapitation.

Fresh tissue. The brains from aCSF (n = 31) and SAP (n = 32) groups were quickly removed by dissection, fresh frozen and kept at -80ºC. Later, they were cut into 20 µm slices and mounted onto gelatin-coated slides and *stored at -25ºC until used.*

Fixed tissue. Representative animals from aCSF (n = 2) and SAP (n = 2) groups were transcardially perfused via the ascending aorta with 50 ml warm (37ºC), calcium-free Tyrode's solution (0.15 M NaCl, 5 mM KCl, 1.5 mM $MgCl_2$, 1 mM $MgSO_4$, 1.5 mM NaH_2PO_4, 5.5 mM Glucose, 25 mM $NaHCO_3$; pH 7.4), 0.5% heparinized, followed by 4% paraformaldehyde and 3% picric acid in 0.1M PB (4ºC) (100 ml/100 g b.w.) (37ºC, pH = 7.4). Their brains were subsequently removed and post-fixed in the same fixative solution for 90 min at 4ºC, followed by immersion in a cryoprotective solution of 20% sucrose in PB overnight at 4ºC, and then frozen by immersion in isopentane and kept at -80ºC. At a later date the brains were coronally cut into10 µm slices using a Microm HM550 cryostat (Thermo Scientific) equipped with a freezing-sliding microtome at -

25ºC and mounted onto gelatin-coated slides and finally stored at -25ºC until used for the immunofluorescence assays.

AChE staining and quantitative analysis

Prior to staining procedures, fresh tissue slices containing basal forebrain and hippocampus from aCSF (n = 13) and SAP (n = 13) treated rats were fixed in 4% paraformaldehyde in PB (0.1M) for 30 min at 4ºC and washed in 0.1 M PBS, pH 7.4 for 20 min. Cholinergic innervations were stained using the "direct coloring" thiocoline method for AChE (Karnovsky and Roots, 1964) as follows: the slices were rinsed twice in 0.1 M Tris-Maleate buffer (pH = 6.0) for 10 min and incubated for 100 min in complete darkness in the AChE reaction buffer (0.1 M Tris-Maleate, 5 mM sodium citrate, 3 mM $CuSO_4$, 0.1 mM iso-OMPA, 0.5 mM $K_3Fe(CN)_6$) and 2 mM acetylthiocholine iodide, as a reaction substrate), whilst being constantly and gently agitated.The enzymatic reaction was finally stopped by carrying out two consecutive washes (2 x 10 min) in 0.1 M Tris-maleate (pH = 6.0). Slices were dehydrated in increasing concentrations of ethanol and covered with the mounting medium, DPX.

The stained slices were scanned at 600 ppi and AChE positive fiber density was quantified by using Image J software (NIH, Bethesda, MD, USA), and the images were converted to 8-bit grey-scale mode. This software defines the optical density of an anatomical area and the background from 0 (white) to 256 (black). The intensity values in arbitrary units were defined in the selected equivalent areas from both hemispheres in all the animals. Background or non-specific staining values were substracted from AChE positive signals to obtain the net AChE optical density in each area. AChE staining values in the striatum served as control and data were expressed as percentages of striatum in each area.

[^{35}S]GTPγS autoradiography and quantitative analysis of autoradiograms

The functional coupling of muscarinic receptors to $G_{i/o}$ proteins was performed in fresh frozen 20 µm slices from each rat, aCSF (n = 10) and SAP (n = 11) groups, which were air dried for 30 min, followed by two consecutive pre-incubations in HEPES-based buffer (50 mM HEPES, 100 mM NaCl, 3 mM $MgCl_2$ and 0.2 mM EGTA, pH = 7.4) for 30 min at 30ºC in a thermostatic bath in order to eliminate the endogenous ACh. Then, the slices were incubated for 2 h at 30ºC in the reaction buffer, which was similar to the pre-incubation buffer, but supplemented with 2 mM GDP, 1 mM DTT, ADA (3U l^{-1}) and 0.04 nM [^{35}S]GTPγS. The [^{35}S]GTPγS basal binding was determined in two consecutive slices in the absence of the agonist. The agonist stimulated binding was also determined in two consecutive slices in the same reaction

buffer, but in the presence of 100 µM carbachol, a non-specific muscarinic receptor agonist. Non-specific binding was defined by competition with 10 µM of non-labelled cold GTPγS in another consecutive section. Later, the slices were washed twice in a cold (4ºC) 50 mM HEPES buffer (pH = 7.4) to stop the binding reaction and were then gently dipped in cold (4ºC) distilled water and dried with cold air. Finally, the slides were exposed to β radiation-sensitive autoradiographic films with a set of [^{14}C] standards to calibrate the images (gray densities) in hermetically closed cassettes.

The films were developed after 48 h, scanned and quantified by transforming optical densities into nCi/g tissue equivalent (nCi/g t.e.) using a calibration curve defined by the known values of the [^{14}C] standards (NIH-IMAGE, Bethesda, MA, USA) and freely available on internet at http://rsb.info.nih.gov/nih-image/). This software defines the optical density of an anatomical area from 0 (white) to 256 (black). The specific binding for each area in consecutive slices, was calculated as follows: non-specific binding values were substracted from the values obtained in both agonist-stimulated and basal-stimulated conditions. Then, the net basal stimulation values were substracted from agonist-stimulated values to obtain net agonist-stimulation ([agonist-stimulated - nonspecific] - [basal - nonspecific]). The percentages of carbachol-evoked stimulation were calculated from both the net basal and net carbachol-stimulated [^{35}S]GTPγS binding densities according to the following formula: ([^{35}S]GTPγS agonist-stimulated binding x 100/[^{35}S]GTPγS basal binding) - 100.

Double immunofluorescence studies

In order to perform the immunofluorescence assays, the frozen tissue slices were dried at room temperature for 20 min.

BFCN were located by using goat anti choline acetyltransferase (ChAT) [1:200] as primary antiserum. To study the cellular localization of M_2 and M_4 mAChR, primary rabbit anti M_2 mAChR [1:400] and mouse anti M_4 mAChR [1:250] (EMD Millipore, CA, USA) were used. Primary antibodies were diluted in PBS (0.1 M, pH 7.4) containing 0.5% BSA and the tissue samples were incubated overnight at 4ºC. They were then washed for 30 min in PBS and incubated for 30 min at 37ºC with the appropriate secondary antibodies; rhodamine donkey anti-goat for ChAT [1:80], Alexa-fluor 488 donkey anti-rabbit [1:250] for M_2 mAChR and Alexa-fluor 488 donkey anti-mouse [1:250] for M_4 mAChR. Then, the slices were washed for 30 min at room temperature by immersion in PBS and incubated with Hoechst 33258 [1:10^6] for 15 min at room temperature. Finally, slices were washed for 15 min by immersion in PBS and mounted with p-phenylendiamine-glicerol (0.1%) for immunofluorescence. 630-fold magnification images for colocalization (M_2 mAChR-ChAT or M_4 mAChR-ChAT) were acquired on an

Axioskop Obsever A1 inverted microscope (Carl Zeiss) by optical sectioning (0.24 µm/X-Y-Z-resolution) using structured illumination (ApoTome, Carl Zeiss). Colocalization images were created by using ZEN2014 software (Carl Zeiss) and were defined as immunosignals without physical signal separation.

Sample preparation for MALDI-IMS

Lipid composition and anatomical distribution were analyzed by using MALDI-IMS in fresh 20 µm slices from each rat in the aCSF (n = 8) and SAP (n = 8) groups, following the recommendations of Schwartz et al (2003). Once the tissue was sliced and mounted on slides, the matrix (MBT) was deposited on the tissue surface by a process of sublimation. The sublimation was performed using 300 mg of MBT and the deposition time and temperature were controlled (30 min, 140ºC). For the re-crystallization of the matrix, the sample was attached to the bottom of a glass Petri plate face-down, which was placed on another Petri plate containing a methanol impregnated-piece of filter paper in its base. The Petri plates were then placed on a hot plate (1 min, 40ºC).

Mass spectrometer and image and spectra analysis

A MALDI LTQ-XL-Orbitrap (Thermo Fisher, San Jose, CA) equipped with a nitrogen laser (λ = 337 nm, rep. rate = 60 Hz, spot size = 80 x 120 µm) was used for mass analysis. Thermo´s Imagequest and Xcalibur software were used for MALDI-IMS data and image acquisition in both positive and negative ion mode. The positive ion range was 500-1000 Da, and the negative ion range was 400-1100 Da, with 10 laser shots per pixel at a laser fluence of 15 µJ. The target plate stepping distance was set at 150 µm for both x- and y-axes by the MSI image acquisition software. The data were normalized using the total ion current values, as there may be potential displacement of the masses on the tissue due to experimental factors e.g., the irregularities of the surface.

The MALDI images were generated using ImageQuest (Thermo Scientific). Each of the m/z values was plotted for signal intensity for each pixel (mass spectrum) across a given area (tissue section). The m/z range of interest was normalized using the ratio of the total ion current for each mass spectrum. The intensity reached by each spectrum (m/z or molecule) was further calculated as a ratio of the peak with the highest intensity, and the average was obtained using OriginPro8 (Northampton MA, USA) software. The most intense peak was considered to be 100%. The assignment of lipid species was facilitated by the use of the databases Lipid MAPS

(http://www.lipidmaps.org/) and Madison Metabolomics (http://mmcd.nmrfam.wisc.edu) and 5 ppm mass accuracy was selected as the tolerance window for the assignment.

Statistical analyses

Step through latencies were represented as Kaplan-Meier survival curves, and for comparisons between groups, the Log-rank/Mantel-Cox test was used. Acquisition latencies, AChE densities, the percentages of agonist-evoked [^{35}S]GTPγS stimulation, and the percentages of the relative intensity of lipids were statistically analyzed using the two-tailed unpaired Student *t* test. The statistical significance threshold was set at $p < 0.05$

Results

Learning and memory evaluation after basal forebrain cholinergic lesion

To examine learning and memory, the animals from the three groups were trained and tested using the passive avoidance test. One week after administration of the immunotoxin, the acquisition latency was measured. No differences were observed between the three groups (10.20 ± 0.98 s, 10.76 ± 1.2 s and 10.88 ± 1.54 s in SHAM, aCSF and SAP, respectively) (Figure 1A). 24 h later, rats were again tested to evaluate the step-through latency. This was measured and represented as Kaplan-Meier survival curves to determine the estimated probability of a positive response (i.e. to reach the cut-off time). When the three groups were compared, 100% and 78% of the SHAM and aCSF-treated rats, respectively (p = n.s.), remembered the aversive stimulus and displayed a positive response, while only 40% of the immunotoxin-treated rats did (p = 0.0001 vs SHAM and p = 0.0006 vs aCSF). The median latency time was 102.9 s for 192IgG-saporin-treated rats (Figure 1B).

AChE staining

AChE enzymatic assay was used to stain cholinergic fibers both in the projecting areas from the NBM, and in the somatodendritic compartment of BFCN. SHAM-operated rats showed equivalent levels of AChE staining to those measured in the aCSF-treated group (data not shown). The intraparenchymal infusion of 192IgG-saporin in the NBM did not modify the $AChE^+$ fiber density in the striatum (aCSF 113 ± 3.26 vs SAP 111 ± 3.08), but resulted in a great reduction of AChE staining in the entire cortical mantle, ranging from 20% in cingular (aCSF 28.3 ± 1.2% vs SAP 23.5 ± 1%, $p < 0.01$) and piriform (aCSF 36.1 ±1.5% vs SAP 30.6 ± 1,5%, $p < 0.05$) cortices to

60-70% in motor (aCSF 21.6 ± 0.8% vs SAP 7.6 ± 0.5%, $p < 0.001$), somatosensory (aCSF 24.1 ± 0.9% vs SAP 8.6 ± 1.4%, $p < 0.001$) and entorhinal (aCSF 26.4 ± 1,7% vs SAP 16.2 ± 0.9%, $p < 0.001$) cortices. In the amygdaloid complex of 192IgG-saporin-treated animals a more moderate decrease was observed in some nuclei, such as in the anterior (aCSF 74.7 ± 4.4% vs SAP 52.7 ± 2.9%, $p < 0.001$), the lateral (aCSF 51.4 ± 3.8% vs SAP 41.3 ± 2.3%, $p < 0.05$) and the medial (aCSF 25.6 ± 4.5% vs SAP 13.8 ± 0.93% $p < 0.05$). No differences were observed in the medial septum, revealing the absence of non-specific damage in other basal forebrain cholinergic nuclei, although the CA3 field of hippocampus showed a moderate decrease in AChE staining (aCSF 51.9 ± 4.4% vs SAP 49.1 ± 2.3%, $p < 0.05$) (Fig 2).

[^{35}S]GTPγS autoradiography

To examine M_2/M_4 mAChR-mediated signaling, the activity of $G_{i/o}$-coupled muscarinic receptors was measured by using [^{35}S]GTPγS autoradiography assay. Basal binding values were similar in both groups (aCSF and SAP) in all the brain areas analyzed. The anatomical analysis of carbachol-induced [^{35}S]GTPγS binding stimulation revealed differences in the functional coupling of muscarinic receptors to $G_{i/o}$ proteins in some brain areas in immunotoxin-treated animals (See tables 1-2). Thus, carbachol-induced stimulation of M_2/M_4 mAChR was decreased in the NBM ($p < 0.05$ vs SAP) from 192IgG-saporin-treated rats, but no changes were found in any of the cortical areas (Fig 3B). In the hippocampus an enhancement of carbachol-induced [^{35}S]GTPγS binding in the pyramidal layer of the CA3 ($p < 0.05$ vs SAP) and in the granular layer of the dentate gyrus ($p < 0.05$ vs SAP) was found (Fig 3D). However, there was a hypoactivity in the lateral nucleus of the amygdaloid complex ($p < 0.05$ vs SAP) (Table 1).

Immunofluorescence

To examine the localization of the receptors, immunofluorescence studies were performed using an antiserum against i3 intercellular loop of human M_2 and M_4 mAChR. The pattern of distribution of M_2/M_4 mAChR was very similar to that observed in the [^{35}S]GTPγS autoradiographic study, clearly delineating certain brain subregions. There was a high expression of M_2 mAChR in the striatum, the basal forebrain (Figure 4) and in the pyramidal layers of different hippocampal subfields, while it was more moderate in the cortex (Figure 6). BFCN of NBM displayed a modest somatodendritic immunostaining, but the presence of a dense network of fibers surrounding the somas revealed presynaptic contacts from M_2 mAChR-positive axon terminals (Figure 4A-I-IV). 192IgG-saporin-treated rats showed an almost total absence of M_2 mAChR-

immunoreactivity in the basal forebrain due to the disappearance of BFCN, as revealed by ChAT immunostaining (Figure 4B-I-IV). M_2 mAChR-immunoreactivity was differentially distributed throughout the hippocampal formation. The large pyramidal neurons from CA1-CA3 and dentate gyrus displayed a dense network of fibers which delineate the perikarya in basket-like formations, without there being immunoreactivity in the soma (Figure 6A). In the somatosensory cortex, M_2 mAChR presented a scattered distribution in presumably presynaptic compartments (Figure 6C). On the other hand, M_4 mAChR-immunoreactivity was distributed mainly in somatodendritic compartments in NBM (Figure 5), hippocampus and cortex (Figure 6), and displayed a typically somatodendritic localization (Figure 5A-I-IV). Immunotoxin-treated rats showed a dramatic decrease in M_4 mAChR-immunoreactivity in the basal forebrain, accompanied by the disappearance of BFCN, as revealed by ChAT immunostaining (Figure 5B-I-IV).

Lipid species analysis by MALDI-IMS

The matrix-assisted laser desorption ionization-imaging mass spectrometry (MALDI-IMS) technique allows us to anatomically localize and semiquantify several lipid species in tissue slices. In this study we carried out a lipid analysis in coronal brain slices, which include the NBM, from aCSF or SAP-groups in both positive and negative ion detection modes. Firstly, IMS was performed in positive ion detection mode and more than 300 peaks were obtained. There were changes in the relative levels of several PC species in the NBM, but only the levels of three of them were also different in the cortex of the rats treated with the immunotoxin (Table 3 and Figure 7). Thus, in the NBM increased levels of PC (36:1) + Na^+ (aCSF 14.62 ± 0,30% vs SAP 21.64 ± 1.53%, $p < 0.01$), PC (36:4) + K^+ (aCSF 10.32 ± 1.01% vs SAP 18.61 ± 2.71%, $p < 0.05$) and PC (40:6) + Na^+ (aCSF 0.88 ± 0.17% vs SAP 2.25 ± 0.40**%**, $p < 0.01$) were observed in 192IgG-saporin-treated rats. However, in the cortex there was a decrease in the level of a single species PC (36:1) + Na^+ (aCSF 10.62 ± 0.48% vs SAP 8.95 ± 0.63%, $p < 0.05$), while increased levels of two species PC (36:4) + K^+ (aCSF 13.17 ± 0.99% vs SAP 15.63 ± 0.48%, $p < 0.05$) and PC (40:6) + Na^+ (aCSF 0,75 ± 0.11% vs SAP 1.14 ± 0.09**%**, $p < 0.05$) were found in 192IgG-saporin-treated rats. The levels of other lipids were also modified in the NBM of the lesioned rats, such as PE (14:1/20:4) + H^+ (aCSF 15.21 ± 0.70% vs SAP 11.87 ± 1.35%, $p < 0.05$), SM (d18:1/18:0) + H^+ (aCSF 7,11 ± 1,135% vs SAP 4,15 ± 0,799%, $p < 0.05$) and SM (d18:1/16:0) + K^+ (aCSF 0.96 ± 0.14% vs SAP 10.53 ± 3.33%, $p < 0.01$). Secondly, the negative ion detection mode was used and the levels of several lipid species were found to be modified in the NBM, such as SM (d18:0/18:1) (aCSF 1.26 ± 0.24% vs SAP 6.44 ±

1.50%, $p < 0.01$) and PS (18:0/18:1) (aCSF 11.04 ± 2.16% vs SAP 3.95 ± 0.99%, $p < 0.01$). However, the level of only one species of phosphoglycerol, PG (22:6/22:6), was also changed in the cortex of 192IgG-saporin-treated rats (aCSF 0.06 ± 0.01% vs SAP 0.86 ± 0.24%; $p < 0.05$ and aCSF 0.04 ± 0.01% vs SAP 0.16 ± 0.05%, in NBM and cortex, respectively; $p < 0.05$) (Table 3 and Figure 7).

Discussion

Learning and memory impairment after BFCN depletion

The NBM is a neuronal nucleus which is located deeply within the brain, close to the border of the ventral limit. Firstly, we analyzed the mechanical lesion produced by the needle crossing from the dorsal cranial surface to almost the ventral border, and the intraparenchymal infusion of the vehicle. Previous studies from our laboratory demonstrated that the administration of the vehicle by using a common Hamilton syringe was sufficient to produce brain damage which led to learning and memory deficits in the control group, as observed in the passive avoidance test. Therefore, a new model of Hamilton neurosyringe, equipped with an ultra thin gauge needle, was used in order to minimize the mechanical lesion.

Eight days after the intraparenchymal infusion of 192IgG-saporin, 75% of BFCN in the NBM had disappeared leading to learning and memory impairment, as demonstrated by the results of the passive avoidance test. In the retention trial, 100% of SHAM-operated rats remembered the foot-shock and no statistically significant differences were observed between SHAM-operated and aCSF-treated groups. Moreover, the histochemical (AChE staining) and immunohistochemical ($p75^{NTR}$-immunoreactivity) studies revealed similar densities of BFCN in SHAM-operated rats and in those which had received aCSF used as the vehicle, thereby demonstrating that the intraparenchymal infusion of the vehicle by itself had no effect on the survival rate of BFCN. The extent of the specific basal forebrain cholinergic lesion was also demonstrated by the dramatic loss of AChE-positive fibers in cortical regions. The infusion of 192IgG-saporin had no effects on acquisition latency, suggesting that the motivation to explore, the level of anxiety and/or the motor functions of the rats were apparently unaffected. In this context, longer acquisition latency times in the passive avoidance test induced by BFCN depletion in the medial septum have been reported, showing that there are different effects on aversive learning, depending on the specific cholinergic nucleus lesioned (Babalola et al., 2012). As already mentioned, 192IgG-

saporin is directed against $p75^{NTR}$, which is predominantly expressed in BFCN from the MS, VDB, HDB and NBM (Wiley et al., 1991). The specificity of the lesion in the NBM is demonstrated by the absence of damage in the complex MS-VDB (Ch1-Ch2) which mainly innervates the hippocampus, as observed by AChE staining. The evaluation of learning and memory behavior in the present study does not discriminate other parameters such as acquisition, consolidation, extinction or retrieval of new aversive information, but previous studies using the olfactory discrimination learning test have demonstrated that 192IgG-saporin-induced lesions of the NBM impair attention capacity and early acquisition during a learning process (Bailey et al., 2003).

Kaplan-Meier survival curves were used to graphically represent the estimated probability of reaching the cut-off time (300 s) for each group. Then, data were analyzed by using the Log-rank/Mantel-Cox test to compare the survival distributions or the estimated probability of each group to reach the cut off time. Doing so was regarded as a positive response. It was found that a statistically significant higher percentage of immunotoxin-treated animals showed a negative behavioral response in comparison with those which had received aCSF. The present results provide evidence that cortical cholinergic innervation arising from the NBM plays a pivotal role in learning and memory processes. In previous studies, step-through latency times were represented as histograms, evaluating censored latency times (cut-off time of 300 s) as threshold values, but the above-mentioned statistical analysis is more appropriate to test the probability of reaching the cut-off time and eliminates the threshold bias. Based on a previous report, the statistical handling of data in the present study improves the analysis of the results and represents an alternative way to interpret behavioral responses when using the passive avoidance paradigm (Barreda et al., 2015). The effects of cholinergic lesions on learning and memory have been extensively studied, but controversial data have been reported depending on the severity of the lesion, the dose, schedule and route of 192IgG-saporin administration, the specific cholinergic nucleus or the passive avoidance test conditions (reviewed in Myhrer, 2003). A previous study demonstrated that a 50% reduction of BFCN in the NBM produced a 25-30% decrease in ChAT activity, but was not sufficient to impair memory five weeks after lesioning (Wenk et al., 1994). The experimental design differed from ours in several aspects: lower doses of the immunotoxin, repeated learning trials and footshock deliveries, the post-operatory recovery period and the statistical analysis used. Our results are consistent with other studies which have demonstrated that avoidance testing is impaired after a specific lesion in the NBM with the excitotoxins ibotenic acid (Flicker et al., 1983; Hepler et al., 1985; Whishaw et al., 1985) or quisqualic acid (Aaltonen et al., 1991; Riekkinen et al., 1991a,b, 1993; Zupan et al.,

1993). In the studies using non-specific excitotoxins, the effects of the lesions are not restricted to BFCN, but also affect to non-cholinergic neurons in the same structures (Kosaka et al., 1988). However, when the lesion was induced with 192IgG-saporin, other authors reported small, but significant deficits associated with the BFCN lesion in the NBM in a single learning trial of the passive avoidance test (Torres et al., 1994). Moreover, and consistent with the present results, the relationship between the severity of passive avoidance behavioral deficits and the degree of BFCN loss was demonstrated (Zhang et al., 1996; Martinez-Gardeazabal et al., 2017). The present findings unequivocally support the pivotal role of NBM-cortical cholinergic neurotransmission in learning and memory processes in rats.

BFCN lesion-induced alteration in functionality and distribution of M_2/M_4 mAChR

Different alterations to the cholinergic neurotransmission have been reported in *postmortem* samples from AD patients (Davies and Maloney, 1976; Davies, 1979; Whitehouse et al., 1982; Rodríguez-Puertas et al., 1994 and 1997; Flynn et al., 1995). In the present study, functional autoradiography showed a decrease in carbachol-induced stimulation of [^{35}S]GTPγS binding in the NBM and an increase in hippocampus, but no significant change in this parameter was observed in the entire cortical mantle of 192IgG-saporin-treated rats. Although the cholinergic connectivity between these three brain areas is not fully understood, they are all areas involved in learning and memory.

BFCN from the NBM are thought to express M_2 and/or M_4 mAChR as autoreceptors in the synaptic terminals, therefore, in the lesion model the decrease in M_2/M_4 mAChR activity recorded at the NBM may be a direct consequence of the lesion and indicates a loss of cholinergic interconnections within the nucleus that constitutes the cholinergic basal forebrain. However, despite the elimination of up to 70% of presynaptic basal forebrain cholinergic terminals in some cortical regions of 192IgG-saporin-treated rats, the [^{35}S]GTPγS autoradiographic study showed no differences in the functional coupling of M_2/M_4 mAChR to $G_{i/o}$ proteins in the cortical areas analyzed. M_2 and M_4 mAChR are differentially distributed in the cortex. Thus, M_2 mAChR-immunoreactivity is dense in the deeper layers of the cortex, is located in cell bodies, and is associated with fibers and presumably terminals, and occasionally with perikarya. Using the NBM-lesioned rat model, previous studies reported a decrease in M_2 mAChR density in frontal and parietal cortices seven days after ibotenic acid administration or mechanical lesioning of the NBM, by means of autoradiography and *in situ* hybridization techniques, which is in consistent with the presynaptic localization of M_2 mAChR in BFCN terminals (Bogdanovic et al., 1993; Schliebs et al., 1994). As

previously mentioned, mechanical or excitotoxin-based lesioning of the BFCN may trigger non-specific damage to non-cholinergic neurons, and this could result in contradictory results. Therefore, when the lesion was produced by 192IgG-saporin, as observed in the study of Rossner et al. (1995b), an increase of up to 20% in M_2 mAChR density in the parietal cortex was reported, suggesting the existence of a significant population of M_2 mAChR located postsynaptically (reviewed in Rossner, 1997). In AD, the severe loss of cortical cholinergic innervation is accompanied by a depletion of M_2 mAChR, but M_1 mAChR density remains relatively stable (Mash et al., 1985). It has been assumed that the M_2 mAChR is a presynaptic autoreceptor located in all cholinergic axons which arise in the NBM and innervate the cerebral cortex, the NBM being the main source of cortical M_2 mAChR. The depletion of M_2 mAChR was therefore thought to be the consequence of the cholinergic axonal loss in AD. However, the expression of M_2 mAChR in BFCN terminals still remains controversial. The interpretation of some authors was that the cholinergic axons coming from the NBM do not substantially contribute to the overall pool of cortical M_2 mAChR, and M_2 mAChR-expressing postsynaptic neurons could be partially responsible for the decrease of these receptors observed in AD (Mesulam, 1998). The existence of cortical postsynaptic M_2 mAChR and/or the possibility that thet are located in non-cholinergic terminals of either intrinsic or extrinsic origin, makes it plausible that the degeneration of cortical M_2 mAChR-immunoreactive neurons could also be contributing to the described loss of M_2 mAChR in AD (Mrzljak et al., 1998; Raevsky et al., 1998). Interestingly, electron microscopic analysis failed to reveal changes in M_2 mAChR distribution following the intraparenchymal administration of 192IgG-saporin in the NBM of rhesus monkeys and moreover, clearly showed that membrane-linked receptors were also located in dendritic spines of pyramidal neurons and associated with membranes in all cellular compartments of nonpyramidal neurons (Mrzljak et al., 1998). Furthermore, M_2 mAChR which modulate ACh release are not located in NBM cholinergic terminals, but are predominantly found in the membranes of postsynaptic sites in the NBM (Meyer et al., 1987; Pascual-Alonso and Gonzalez-Zarate, 1992; Decossas et al., 2003). However, the co-expression of M_2 mAChR at presynaptic sites and VAChT has been observed by using both light and electron microscopy (Decossas et al., 2003).

On the other hand, the cortical pool of M_4 mAChR is relatively small and this subtype is mainly located in the neuropil and in scattered perikarya (Levey et al., 1991). The reported localization of M_4 mAChR binding sites and mRNA is comparable in all layers of the neocortex (Buckley et al., 1988; Sugaya et al., 1997; Vilaró et al., 1994). The present immunofluorescence assays revealed a higher density of M_4

mAChR located in somas and plasma membrane, in comparison with M_2 mAChR, which seem to be located presynaptically, clearly showing that there is a different pattern of distribution. Although we did not observe changes in the activity mediated by M_2/M_4 mAChR in cortical areas, the role of cortical M_4 mAChR in this lesion model and their precise distribution remains unclear. Further research into the role of these receptors, carried out by using this model of basal forebrain cholinergic dysfunction, could provide valuable physiological information.

The immunosignal associated with both M_2 and M_4 mAChR was dramatically reduced in the basal forebrain after the lesion, thereby providing evidence of the contribution of both receptors to the cholinergic neurotransmission impairment in the NBM. As previously described, the precise anatomical distribution of M_2 and M_4 mAChR in the basal forebrain still remains controversial, but present immunohistochemical findings suggest a mainly presynaptic localization of M_2 mAChR and a somatodendritic distribution of M_4 mAChR in the BFCN of the NBM. However, the expression of M_2 mAChR and M_4 mAChR in BFCN, including those from the MS, VDB, HDB and NBM, has previously been studied by using *in situ* hybridization, [^{3}H]-oxotremorine autoradiography and immunohystochemical assays (Harata et al., 1991; Vilaró et al., 1992 and 1994; Sugaya et al., 1997). The co-expression of these receptors and ChAT has also been detected in approximately 80% of BFCN by using light and electron microscopy (Decossas et al., 2003**)**. In addition, dissociated NBM neurons are stimulated with carbachol and antagonized with the M_2 mAChR antagonist, AF-DX-116 (Harata et al., 1991**)**.

In summary, the present findings show a significant decrease in $G_{i/o}$-mediated muscarinic signaling in the NBM, mediated by the pool of presynaptic M_2 and somatodendritic M_4 mAChR, and the absence of changes in pre and postsynaptic M_2/M_4 mAChR-mediated signaling in the cortex of immunotoxin-treated rats. Eight days after the administration of 192IgG-saporin, the loss of both the cortical source of ACh and the M_2/M_4 mAChR-mediated signaling associated with the loss of BFCN in the NBM may be contributing to the deregulation of cortical neurotransmission responsible for the cognitive impairment observed in the passive avoidance test.

Conversely, the increased M_2/M_4 mAChR-mediated signaling in the dentate gyrus and CA3 regions of the hippocampus, cannot be directly attributed to cholinergic denervation from NBM because the major source of cholinergic innervation to the hippocampus proceeds from the MS and the VDB. In fact, the results of the autoradiographic assays and the AChE staining in these nuclei were similar to those obtained in the aCSF group, suggesting the absence of non-specific damage to other basal forebrain cholinergic nuclei, except that generated in the NBM. Nevertheless,

lesions directed at the septohippocampal cholinergic projections have been used to evaluate the involvement of this pathway in cognition (Baxter et al., 2013; Köppen et al., 2016), and to explore the distribution of mAChR in the hippocampus at different postsurgical times, demonstrating dynamic changes in densities of pre and postsynaptic pools of M_2 and M_4 mAChR (Bauer et al., 1992; Wall et al., 1994; Levey et al., 1995).

Our immunofluorescence studies in the hippocampus suggest that the M_2 mAChR in the granular dentate gyrus and pyramidal CA1-CA3 are located presynaptically, whereas the M_4 mAChR are postsynaptically distributed in the somatodendritic compartment of pyramidal neurons. Furthermore, presynaptic M_2/M_4 mAChR inhibit ACh release (Raiteri et al., 1984; Levey et al., 1995). In this context, the observed increase in hippocampal cholinergic neurotransmission through M_2 mAChR may contribute to the so-called "muscarinic long term potentiation" mediated by the potentiation of glutamatergic NMDA receptors, essential to explain hippocampal neuronal plasticity (Segal and Auerbach, 1997). Interestingly, mice lacking M_2 mAChR but not mice lacking M_4 mAChR, showed deficits in learning and memory, as demonstrated by means of the passive avoidance test, together with profound alterations in ACh homeostasis in the hippocampus, suggesting that the M_2 mAChR subtype plays a crucial role in cognitive processes (Tzavara et al., 2003b). Additional studies in M_2 mAChR knockout mice reported significant deficits in the Barnes circular maze. In addition, this was associated with impairment in both short and long-term potentiation and was completely reversed with the $GABA_A$ receptor antagonist, bicuculline (Seeger et al., 2004). M_2 mAChR are also expressed in diverse hippocampal interneurons and control GABA release from presynaptic inhibitory terminals which leads to an increase in activity in the dendritic region of pyramidal neurons (Hajos et al., 1998). The increase in hippocampal muscarinic functionality mediated by M_2 mAChR may modulate the GABAergic tone to compensate for excitatory-inhibitory imbalance. The M_4 mAChR subtype might also be involved in neuronal plasticity-associated learning and memory formation, as has been reported in adrenalectomized rats, whereas the loss of M_4 mAChR leads to dysfunction in hippocampal synaptic transmission (Mulugeta et al., 2006).

NBM and cortical lipid profile changes after 192IgG-saporin-induced BFCN lesion

MALDI-IMS analysis showed changes in the brain lipid profile of 192IgG-saporin-treated rats. The relative intensities of different lipid species, including PC (phosphatidylcholines), SM (sphingomyelins), PE (phosphatidylethanolamines) and PS

(phosphatidylserines) were regulated in the basal forebrain and in areas of cortical projection.

ChAT enzyme has low affinities for Ch and acetyl coenzyme A, and the rate of synthesis of ACh mainly depends on the levels of Ch (Millington and Wurtman, 1982; reviewed in Blusztajnn and Wurtman, 1983). As previously mentioned, the 192IgG-saporin-induced lesion model causes a considerable reduction in the level of ACh. Moreover, the loss of approximately 50% of BFCN has been associated with 40-60% reductions in ChAT and SDHACU activities throughout the basal forebrain cholinergic system (Rossner et al., 1996). In this context, the membrane phospholipids become an important source from which Ch can be synthesized *de novo*. This *de novo* synthesis requires PE from any membrane pool as a substrate to be sequentially methylated to PC (Bremer et al., 1960a,b). PC can be hydrolyzed to free Ch by membrane-associated phospholypase D (PLD) activation (Hattori and Kanfer, 1984; Blusztajn et al., 1987a; Exton, 1999). Phosphatidylinositol 4,5-bisphosphate (PIP_2), protein kinase C (PKC) and phorbol esters stimulate PLD activity which, furthermore, has been found to be reduced by up to 63% in homogenates of brain tissue samples from AD patients (Kanfer et al., 1986; reviewed in Exton, 1999). Then, Ch can be acetylated to form ACh in order to sustain neurotransmission at the expense of membrane formation which may finally impair synaptic plasticity or compromise membrane viability (Maire and Wurtman, 1985; Ulus et al., 1989). Wurtman et al. (1985) described this process as autocannibalism of the cholinergic cells.

On the other hand, the synthesis of eCB is comparable to the described alternative source of Ch. ECB are not stored in intracellular compartments or vesicles, as are other classical neurotransmitters; they are synthesized on demand by receptor-stimulated cleavage of membrane lipid precursors. The pathways leading to the synthesis and release of AEA and 2-AG from neuronal and non-neuronal cells are still somewhat unclear. In this context, different authors have found a relationship between cannabinoid and cholinergic neurotransmission (Gifford et al., 1996; Kathman et al., 2001; Fukudome et al., 2004). Therefore, it is tempting to interpret the modifications of lipid composition in the *in vivo* model of basal forebrain cholinergic dysfunction as potential precursors for both eCB and Ch synthesis.

If the hydrolysis of phospholipids from membranes of presynaptic terminals (cortical area) and/or the somatodendritic compartment (NBM area) served for the *de novo* synthesis of Ch, one would expect a regulation of certain lipid species in both anatomical regions due to the loss of approximately 80% of BFCN in the NBM and 60% of cortical cholinergic innervations.

Phosphatidylcholines and phosphatidylserines

We found an increase in PC (36:1) + Na^+ in NBM and a reduction in cortical regions, while PS (18:0/18:1) was found to be decreased in the NBM after the infusion of 192IgG-saporin. The physiological role of PC (36:1) + Na^+ still remains unclear, but its presence in both rat and human brain, mainly in regions of white matter has been previously described (Jackson et al., 2005a,b; Astigarraga et al., 2008; Veloso et al., 2011). The proliferation of glial cells and the loss of both BFCN in the NBM and in the cortical cholinergic axons could explain either the increase or the decrease in the levels of this particular species in the NBM and cortex, respectively. The characterization of the lipid profile of the different types of cells present in the CNS could verify this interpretation. Moreover, these changes may also be an indication of an adaptive process with which to reconstruct the axonal branching following lesioning of the BFCN, rather than an alternative source for *de novo* synthesis of Ch.

On the other hand, under normal physiological conditions, PS (18:0/18:1) is preferentially located in the inner leaflet of the plasma membrane, but the loss of asymmetry is an early indicator of apoptosis and/or glia-mediated synaptic pruning to remodel the neural circuit (Fadok et al., 1992; reviewed in Bevers and Williamson, 2016). The loss of PS asymmetry with increased externalization to the outer leaflet of the lipid bilayer has been described in samples from AD patients (Bader Lange et al., 2008). 18 h after the internalization of saporin, apoptosis is induced, and apoptotic activity is enhanced when the toxin is bound to immunoglobulins such as 192IgG (Bergamaschi et al., 1996). These findings suggest that the loss of PS (18:0/18:1) in the NBM may be a consequence of the immunotoxin-induced depletion of BFCN and, therefore, is probably not related to phospholipid hydrolysis for eCB or Ch synthesis.

In addition, PC (40:6) + Na^+ and PC (36:4) + K^+, which are mainly present in the gray matter of rat CNS, were also found to be increased in the NBM and in the cortex. PC (40:6) + Na^+ is probably composed of stearic acid (18:0), docosahexaenoic acid (DHA; 22:6), the latter being a polyunsaturated fatty acid (PUFA) which, when added to the diet of hypertensive rats, restores both their cerebral Ch and ACh levels and their performance in the passive avoidance test (Minami et al., 1997). Furthermore, there is a large body of evidence which indicates that DHA has important biological functions in neuronal homeostasis, mostly linked to its role in neurogenesis, synaptogenesis, neuronal differentiation, neurite outgrowth and maintenance of membrane fluidity, and this could be consistent with the need to repair the structural brain damage induced by 192IgG-saporin (Belkouch et al., 2016). The most probable acyl chain composition of PC (36:4) + K^+, is palmitic acid (16:0) and AA (20:4). Interestingly, AA is a well-known pro-inflammatory precursor but, indeed, phospholipids containing AA are the most

suitable candidates as precursors for the synthesis of the eCB, AEA and 2-AG (**Di** Marzo et al., 1994; Sugiura et al., 1995). Moreover, the synthesis of eCB can be stimulated not only by neuronal damage (Stella et al., 1997; Marsicano et al., 2003; van der Stelt et al., 2001a) but also by the activation of $G\alpha_{q/11}$-coupled mAChR (Kim et al., 2002), and the suppression of CB_1 receptors increases neuronal vulnerability (Marsicano et al., 2003). By using genetically modified mice lacking any of the subtypes of mAChR, it was demonstrated that $G\alpha_{q/11}$-coupled mAChR activation is responsible for the PLCβ-mediated stimulation of 2-AG synthesis which finally induces short-term plasticity at cholinergic synapses (Fukudome et al., 2004).

The study of lipids in samples from AD patients reveals an enhancement of plasmatic levels of PC (40:6) which has been found to positively correlate with CSF tau concentrations in AD patients carrying the *presenilin1* mutation (Chatterjee et al., 2015). In contrast, plasmatic levels of PC (36:4) and PC (40:6) have been found to be decreased in AD and have been proposed as biomarkers of phenoconversion to either amnestic mild cognitive impairment or late-onset AD (Mapstone et al., 2014; Fiandaca et al., 2015). Reduced relative densities of PC species have been found in AD brains and attributed to a pathological hyperactivation of phospholipase A2 (PLA2) (Nitsch et al., 1992; Klein, 2000). The result of this is an increase in the breakdown of certain phospholipids and a variation in the ratio of saturated and unsaturated fatty acids in PC and PE (Mulder et al., 2003). These findings suggest a different regulation in the biosynthesis, turnover, and acyl chain remodeling of phospholipids in AD. Essential PUFA, such as AA and DHA, provide the structural functionality of the membranes, but lipid catabolism (e.g., during neurodegeneration, neuroinflammation or autophagy) generates intermediate metabolites that are not usually recycled, and increased demands are made on the bloodstream (Fiandaca el al., 2015). This could explain the decreased levels of PC (36:4) and PC (40:6) recorded in plasma from AD patients, in contrast with the increase observed in 192IgG-saporin-treated rat brains. Additional lipidomic studies of brain samples from AD patients are necessary to further elucidate if the plasmatic levels of certain lipid-based biomarkers correlate in some way with those levels observed directly in the brain tissue by means of imaging techniques such as MALDI-IMS.

Sphingomyelins

There was a significant increase in the levels of SM (d18:1/16:0) + K^+ in the NBM, but the SM (d18:0/18:1) + H^+ was found to be significantly decreased in the same region. Sphingolipid metabolism is essential for tissue homeostasis and regulates the synthesis of several bioactive lipids and second messengers that are

critical in cellular signaling (Wymann and Schneiter, 2008). The sphingomyelinase–driven catabolism of sphingolipids triggers the release and accumulation of ceramides which are directly involved in neurodegenerative disorders and contribute to AD pathology (Han et al., 2011). Interestingly, the CB_1 receptor-driven breakdown of sphingomyelins with ceramide production has been previously described in glial cells (reviewed in Guzmán et al., 2001b; Velasco et al., 2005). Ceramides participate in cell differentiation, proliferation or apoptosis. The intracellular accumulation of ceramides has been described in neurodegenerative disorders including AD, Parkinson's disease, epilepsy and ischemia. Thus, the upregulated levels of SM (d18:1/16:0) + K^+ observed may be a consequence of the necessary basal forebrain remodeling following the immunotoxin-induced apoptosis of BFCN rather than being related to Ch metabolism or eCB signaling. Recent studies have found a depletion of SM (d18:1/16:0) in CSF and a reduction in acid sphingomyelinase activity together with reduced levels of amyloid β_{42} in AD patients (Fonteh et al., 2015). However, SM (d18:0/18:1) was found to be decreased in the NBM following the immunotoxin-induced lesion. The fact that CB_1-mediated endocannabinoid signaling increases following the lesion allows us to speculate that CB_1 receptor activation in the NBM could be stimulating the hydrolysis of this specific SM species. In samples from AD patients, SM (d18:0/18:1) levels are increased in both the hippocampal gray matter and CSF, and positively correlate with the total CSF tau level, but negatively with the CSF amyloid β_{42} level (Mendis et al., 2016; Koal et al., 2015). The relationship between the observed regulation in SM species with previous findings which indicate a CB_1-receptor-mediated regulation of hippocampal endocannabinoid signaling in AD patients must be further explored (Manuel et al., 2014). Moreover, additional studies focused on the quantification of ceramides in this lesion model will contribute to a better understanding of the link between BFCN degeneration, CB_1-mediated endocannabinoid signaling and deregulation of specific SM species. In the meantime, the significance of the specific regulation of lipid species and their physiological role in the CNS remain elusive, but their lipid mapping by IMS in both normal and diseased human brain and in models of disease would help to clarify these questions (Martínez-Gardeazabal et al., 2017; González de San Román et al., 2017).

Phosphatidylethanolamines

Interestingly, PE (14:1/20:4) and PE (40:4), both of which may be composed of a molecule of arachidonic acid (AA; 20:4), were found to be deregulated in the NBM, revealing a possible membrane phospholipid source for the synthesis of Ch since PE are considered as precursors for PC synthesis in the ACh synthetic pathway, as

explained above (Blusztajn et al., 1987a). Moreover, PE have diverse cellular functions and are involved in autophagy (reviewed in Calzada et al., 2016). PE are also the main precursor for the synthesis of eCB. The AEA precursor, NAPE, which is produced from the transfer of an acyl group (e.g. AA) from membrane phospholipids (e.g. PC) to the N-position of a PE, is catalyzed by a Ca^{2+}-dependent trans-acylase, which correlates with the biosynthesis of AEA in the CNS after depolarization (Di Marzo et al., 1994). Thus, the relative levels of PE (14:1/20:4) are decreased, whereas PE (40:4) are increased in the NBM, and it is reasonable to hypothesize that these particular phospholipids could be being used for the synthesis of eCB since the CB_1 receptor-mediated signaling in this brain area is up-regulated, as previously demonstrated by autoradiographic studies, which may increase the demand for their membrane lipid precursors (Llorente-Ovejero et al; unpublished results). Since eCB are not apparently stored in vesicles, the generation of pools of lipids for further synthesis of eCB is difficult to understand and one would expect to observe a reduction in any possible PE precursors for eCB synthetic processing, pointing to PE (14:1/20:4) as a plausible candidate. However, the increase in the relative density of a specific lipid such as PE (40:4) allows us to hypothesize that a reservoir is created by an unknown storing mechanism from which to further synthesize eCB.

The muscarinic neurotransmission through M_2/M_4 receptors coupled to Gi/o proteins is not modified in cortical projection areas from the lesioned NBM. However other authors using a similar animal model have described that M_1 and M_2 mAChR density was increased (Rossner et al., 1995b). The relationship between muscarinic neurotransmission and phospholipid metabolism has also been studied previously, showing that the stimulation of cortical synaptosomes with cholinergic agonists was able to increase PLD activity, which was also dependent on PKC activity involving PIP_2 and DAG leading to the accumulation of free Ch (Qian et al., 1989). The muscarinic signaling-induced PLD activity was antagonized by atropine (Dolezal and Tucek, 1984).

Furthermore, the eCB signaling is enhanced in cortical regions and NBM of 192IgG-saporin-infused rats, areas with a marked decrease of cholinergic innervation. The relative intensities of phospholipid species containing AA, such as PE (14:1/20:4), PE (40:4) and PC (36:4) + K^+, are also modulated in these same areas, suggesting a metabolic link between cholinergic neurotransmission and the eCB system.

In summary, it would appear that G_{q-11} protein-coupled mAChR such as M_1 and/or M_3 subtypes may be key modulatory elements of the phospholipid-related

regulation observed in this model and detailed analysis of the different phospholipases activities mediated by mAChR (mainly M_1 and/or M_3 subtypes) in this lesion model will contribute to further understand the underlying processes, that could link the changes in lipid profile with the cholinergic-cannabinoid cross-talk to compensate for the loss of cortical ACh supply, or conversely, represent a pathological consequence of the 192IgG-saporin-induced massive death of BFCN in the NBM regardless of muscarinic signaling.

Several attempts to reduce the deficit of ACh in AD patients by the administration of cholinergic enhancers or precursors such as Ch or lecithin have failed, while treatments based on AChE inhibitors, phosphatidylserine, Ch alphoscerate and CDP-Ch provided slight, but noticeable benefits (reviewed in Amenta et al., 2001). Perhaps, future treatments based on potentiating cholinergic neurotransmission should be based on the modulation of the complex enzymatic machinery, which so finely regulates lipid metabolism through the mAChR-mediated signaling. In this sense, it is well known the mAChR-driven eCB-mediated modulation of cholinergic neurotransmission at excitatory synapses (Straiker and Mackie, 2007) and inhibitory synapses through the activation of CB_1 receptors (Narushima et al., 2007). Further research focused on muscarinic-eCB crosstalk may be useful in the discovery of innovative therapeutic targets for neurodegenerative disorders.

References

Aaltonen M., Riekkinen P., Sirviö J. and Riekkinen P. Jr (1991) Effects of THA on passive avoidance and spatial performance in quisqualic acid nucleus basalis-lesioned rats. Pharmacol Biochem Behav. 39(3), 563-567.

Amenta F., Parnetti L., Gallai V. and Wallin A. (2001) Treatment of cognitive dysfunction associated with Alzheimer's disease with cholinergic precursors. Ineffective treatments or inappropriate approaches? Mech Ageing Dev. 122(16), 2025-2040. Review.

Astigarraga E., Barreda-Gómez G., Lombardero L., Fresnedo O., Castaño F., Giralt M.T., Ochoa B., Rodríguez-Puertas R. and Fernández J.A. (2008) Profiling and imaging of lipids on brain and liver tissue by matrix-assisted laser desorption/ionization mass spectrometry using 2-mercaptobenzothiazole as a matrix. Anal Chem. 80(23), 9105-9114.

Avery E.E., Baker L.D. and Asthana S. (1997) Potential role of muscarinic agonists in Alzheimer's disease. Drugs Aging. 11(6), 450-459.

Babalola P.A., Fitz N.F., Gibbs R.B., Flaherty P.T., Li P.K. and Johnson D.A. (2012) The effect of the steroid sulfatase inhibitor (p-O-sulfamoyl)-tetradecanoyl tyramine (DU-14) on learning and memory in rats with selective lesion of septal-hippocampal cholinergic tract. Neurobiol. Learn. Mem. 98(3), 303-310.

Bader Lange M.L., Cenini G., Piroddi M., Abdul H.M., Sultana R., Galli F., Memo M. and Butterfield D.A. (2008) Loss of phospholipid asymmetry and elevated brain apoptotic protein levels in subjects with amnestic mild cognitive impairment and Alzheimer disease. Neurobiology of Disease 29, 456–464.

Bailey A.M., Rudisill M.L., Hoof E.J. and Loving M.L. (2003) 192 IgG-saporin lesions to the nucleus basalis magnocellularis (nBM) disrupt acquisition of learning set formation. Brain Res. 969(1-2), 147-159.

Barreda-Gómez G., Lombardero L., Giralt M.T., Manuel I. and Rodríguez-Puertas R. (2015) Effects of galanin subchronic treatment on memory and muscarinic receptors. Neuroscience 293, 23-34.

Bartus R.T., Dean R.L., Beer B., Lippa A.S. (1982) The cholinergic hypothesis of geriatric memory dysfunction. Science 217(4558), 408-414.

Bauer A., Schulz J.B. and Zilles K. (1992) Muscarinic desensitization after septal lesions in rat hippocampus: evidence for the involvement of G-proteins. Neuroscience 47(1), 95-103.

Baxter M.G., Bucci D.J., Gorman L.K., Wiley R.G. and Gallagher M. (2013) Selective immunotoxic lesions of basal forebrain cholinergic cells: effects on learning and memory in rats. Behav Neurosci. 127(5), 619-627.

Bednar I., Zhang X., Dastranj-Sedghi R. and Nordberg A. (1998) Differential changes of nicotinic receptors in the rat brain following ibotenic acid and 192-IgG saporin lesions of the nucleus basalis magnocellularis. Int J Dev Neurosci. 16(7-8), 661-668.

Bergamaschi G., Perfetti V., Tonon L., Novella A., Lucotti C., Danova M., Glennie M.J., Merlini G. and Cazzola M. (1996) Saporin, a ribosome-inactivating protein used to prepare immunotoxins, induces cell death via apoptosis. Br J Haematol. 93(4), 789-794.

Bevers E.M. and Williamson P.L. (2016) Getting to the Outer Leaflet: Physiology of Phosphatidylserine Exposure at the Plasma Membrane. Physiol Rev. 96(2), 605-645.

Blusztajn J.K., Liscovitch M. and Richardson U.I. (1987) Synthesis of acetylcholine from choline derived from phosphatidylcholine in a human neuronal cell line. Proc Natl Acad Sci U S A. 84(15), 5474-5477.

Blusztajn J.K. and Wurtman R.J. (1983) Choline and cholinergic neurons. Science 221(4611), 614-620.

Bogdanovic N., Islam A., Nilsson L., Bergström L., Winblad B. and Adem A. (1993) Effects of nucleus basalis lesion on muscarinic receptor subtypes. Exp Brain Res. 97 (2), 225-232.

Bremer J., Figard P.H. and Greenberg D.M. (1960) The biosynthesis of choline and its relation to phospholipid metabolism. Biochim. Biophys. Acta 43, 477-488.

Buckley N.J., Bonner T.I. and Brann M.R. (1988) Localization of a family of muscarinic receptor mRNAs in rat brain. J Neurosci. 8(12), 4646-4652.

Calzada E., Onguka O. and Claypool S.M. (2016) Phosphatidylethanolamine Metabolism in Health and Disease. Int Rev Cell Mol Biol. 321, 29-88.

Chatterjee P., Lim W.L., Shui G., Gupta V.B., James I., Fagan A.M., Xiong C., Sohrabi H.R., Taddei K., Brown B.M., Benzinger T., Masters C., Snowden S.G., Wenk M.R., Bateman R.J., Morris J.C. and Martins R.N. (2015) Plasma Phospholipid and Sphingolipid Alterations in Presenilin1 Mutation Carriers: A Pilot Study. J Alzheimers Dis. 50(3), 887-894.

Davies P. (1979) Neurotransmitter-related enzymes in senile dementia of the Alzheimer type. Brain Res 171(2), 319-327.

Davies P. and Maloney A.J. (1976) Selective loss of central cholinergic neurons in Alzheimer's disease. Lancet 2(8000), 1403.

Decossas M., Bloch B. and Bernard V. (2003) Trafficking of the muscarinic m2 autoreceptor in cholinergic basalocortical neurons in vivo: differential regulation of plasma membrane receptor availability and intraneuronal localization in acetylcholinesterase-deficient and -inhibited mice. J Comp Neurol. 462(3), 302-314.

Dolezal V. and Tucek S. (1984) Activation of muscarinic receptors stimulates the release of choline from brain slices. Biochem Biophys Res Commun. 120(3), 1002-1007.

Drachman D.A. and Leavitt J. (1974) Human memory and the cholinergic system. A relationship to aging? Arch Neurol. 30(2), 113-121.

Exton J.H. (1999) Regulation of phospholipase D. Biochim Biophys Acta. 1439(2), 121-33. Review.

Fadok V.A., Voelker D.R., Campbell P.A., Cohen J.J., Bratton D.L. and Henson P.M. 1992. Exposure of phosphatidylserine on the surface of apoptotic lymphocytes triggers specific recognition and removal by macrophages. J. Immunol. 148, 2207–2216.

Fiandaca M.S., Zhong X., Cheema A.K., Orquiza M.H., Chidambaram S., Tan M.T., Gresenz C.R., FitzGerald K.T., Nalls M.A., Singleton A.B., Mapstone M. and Federoff H.J. (2015) Plasma 24-metabolite Panel Predicts Preclinical Transition to Clinical Stages of Alzheimer's Disease. Front Neurol. 6, 237.

Flicker C., Dean R.L., Watkins D.L., Fisher S.K. and Bartus R.T. (1983) Behavioral and neurochemical effects following neurotoxic lesions of a major cholinergic input to the cerebral cortex in the rat. Pharmacol Biochem Behav. 18(6), 973-981.

Flynn D.D., Ferrari-DiLeo G., Levey A.I. and Mash D.C. (1995). Differential alterations in muscarinic receptor subtypes in Alzheimer's disease: implications for cholinergic-based therapies. Life Sci. 56(11-12), 869-876.

Fonteh A.N., Ormseth C., Chiang J., Cipolla M., Arakaki X. and Harrington M.G. (2015) Sphingolipid metabolism correlates with cerebrospinal fluid Beta amyloid levels in Alzheimer's disease. PLoS One 10(5), e0125597.

Hájos N., Papp E.C., Acsády L., Levey A.I. and Freund T.F. (1998) Distinct interneuron types express m2 muscarinic receptor immunoreactivity on their dendrites or axon terminals in the hippocampus. Neuroscience 82(2), 355-376.

Han X., Rozen S., Boyle S.H., Hellegers C., Cheng H., Burke J.R., Welsh-Bohmer K.A., Doraiswamy P.M. and Kaddurah-Daouk R. (2011) Metabolomics in early Alzheimer's disease: identification of altered plasma sphingolipidome using shotgun lipidomics. PLoS One. 6(7), e21643.

Harata N., Tateishi N. and Akaike N. (1991) Acetylcholine receptors in dissociated nucleus basalis of Meynert neurons of the rat. Neurosci Lett. 130(2), 153-156.

Hattori H. and Kanfer J.N. (1984) Synaptosomal phospholipase D: potential role in providing choline for acetylcholine synthesis. Biochem Biophys Res Commun. 124(3), 945-949.

Hellström-Lindahl E., Mousavi M., Zhang X., Ravid R. and Nordberg A. (1999) Regional distribution of nicotinic receptor subunit mRNAs in human brain: comparison between Alzheimer and normal brain. Brain Res Mol Brain Res. 66(1-2), 94-103.

Hepler D.J., Wenk G.L., Cribbs B.L., Olton D.S. and Coyle J.T. (1985) Memory impairments following basal forebrain lesions. Brain Res. 346(1), 8-14.

Jackson S.N., Wang H.Y., Woods A.S., Ugarov M., Egan T. and Schultz J.A. (2005) Direct tissue analysis of phospholipids in rat brain using MALDI-TOFMS and MALDI-ion mobility-TOFMS. J Am Soc Mass Spectrom. 16(2), 133-138.

Kanfer J.N., Hattori H. and Orihel D. (1986) Reduced phospholipase D activity in brain tissue samples from Alzheimer's disease patients. Ann Neurol. 20(2), 265-257.

Karnovsky M.J. and Roots L. (1964) A "direct-coloring" thiocholine method for cholinesterases. J Histochem Cytochem. 12, 219-221.

Klein J. (2000) Membrane breakdown in acute and chronic neurodegeneration: focus on choline-containing phospholipids. J Neural Transm (Vienna). 107(8-9), 1027-1063.

Koal T., Klavins K., Seppi D., Kemmler G. and Humpel C. (2015) Sphingomyelin SM(d18:1/18:0) is significantly enhanced in cerebrospinal fluid samples dichotomized by pathological amyloid-β42, tau, and phospho-tau-181 levels. J Alzheimers Dis. 44(4), 1193-1201.
Köppen J.R., Stuebing S.L., Sieg M.L., Blackwell A.A., Blankenship P.A., Cheatwood J.L. and Wallace D.G. (2016) Cholinergic deafferentation of the hippocampus causes non-temporally graded retrograde amnesia in an odor discrimination task. Behav Brain Res. 299, 97-104.
Kosaka T., Tauchi M. and Dahl J.L. (1988) Cholinergic neurons containing GABA-like and/or glutamic acid decarboxylase-like immunoreactivities in various brain regions of the rat. Exp Brain Res. 70(3), 605-617.
Levey A.I., Kitt C.A., Simonds W.F., Price D.L. and Brann M.R. (1991) Identification and localization of muscarinic acetylcholine receptor proteins in brain with subtype-specific antibodies. The Journal of Neuroscience. 11(10), 3218-3226.
Levey A.I., Edmunds S.M., Koliatsos V., Wiley R.G. and Heilman C.J. (1995) Expression of m1-m4 muscarinic acetylcholine receptor proteins in rat hippocampus and regulation by cholinergic innervation. J Neurosci. 15(5 Pt 2), 4077-4092.
Maire J.C. and Wurtman R.J. (1985) Effects of electrical stimulation and choline availability on the release and contents of acetylcholine and choline in superfused slices from rat striatum. J Physiol (Paris). 80(3), 189-195.
Mapstone M., Cheema A.K., Fiandaca M.S., Zhong X., Mhyre T.R., MacArthur L.H., Hall W.J., Fisher S.G., Peterson D.R., Haley J.M., Nazar M.D., Rich S.A., Berlau D.J., Peltz C.B., Tan M.T., Kawas C.H. and Federoff H.J. (2014). Plasma phospholipids identify antecedent memory impairment in older adults. Nat Med. 20(4), 415-418.
Martın, V., Fabelo, N., Santpere, G., Puig, B., Marın, R., Ferrer, I. and Dıaz, M. (2010) Lipid alterations in lipid rafts from Alzheimer's disease human brain cortex. J Alzheimers Dis 19, 489–502.
Mash D.C., Flynn D.D. and Potter L.T. (1985) Loss of M2 muscarine receptors in the cerebral cortex in Alzheimer's disease and experimental cholinergic denervation. Science 228(4703), 1115-1117.
Mendis L.H., Grey A.C., Faull R.L. and Curtis M.A. (2016) Hippocampal lipid differences in Alzheimer's disease: a human brain study using matrix-assisted laser desorption/ionization-imaging mass spectrometry. Brain Behav. 6(10), e00517.
Mesulam M.M. (1998) Some cholinergic themes related to Alzheimer's disease: synaptology of the nucleus basalis, location of m2 receptors, interactions with amyloid metabolism, and perturbations of cortical plasticity. J Physiol Paris. 92(3-4), 293-308. Review.
Meyer E.M., Arendash G.W., Judkins J.H., Ying L., Wade C. and Kem W.R. (1987) Effects of nucleus basalis lesions on the muscarinic and nicotinic modulation of [3H]acetylcholine release in the rat cerebral cortex. J Neurochem. 49(6), 1758-1762.
Millington W.R. and Wurtman R.J. (1982) Choline administration elevates brain phosphorylcholine concentrations. J Neurochem. 38(6), 1748-1752.

Minami M., Kimura S., Endo T., Hamaue N., Hirafuji M., Togashi H., Matsumoto M., Yoshioka M., Saito H., Watanabe S., Kobayashi T. and Okuyama H. (1997) Dietary docosahexaenoic acid increases cerebral acetylcholine levels and improves passive avoidance performance in stroke-prone spontaneously hypertensive rats. Pharmacol Biochem Behav. 58(4), 1123-1129.

Mulder C., Wahlund L.O., Teerlink T., Blomberg M., Veerhuis R., van Kamp G.J., Scheltens P. and Scheffer P.G. (2003) Decreased lysophosphatidylcholine/ phosphatidylcholine ratio in cerebrospinal fluid in Alzheimer's disease. Journal of Neural Transmission 110, 949–955.

Mulugeta E., Chandranath I., Karlsson E., Winblad B. and Adem A. (2006) Temporal and region-dependent changes in muscarinic M4 receptors in the hippocampus and entorhinal cortex of adrenalectomized rats. Exp Brain Res. 173(2), 309-317.

Myhrer T. (2003) Neurotransmitter systems involved in learning and memory in the rat: a meta-analysis based on studies of four behavioral tasks. Brain Res Brain Res Rev. 41(2-3), 268-287. Review.

Nitsch R.M., Blusztajn J.K., Pittas A.G., Slack B.E., Growdon J.H. and Wurtman R.J. (1992) Evidence for a membrane defect in Alzheimer disease brain. Proc Natl Acad Sci U S A. 89, 1671–1675.

Nordberg A. (1992) Neuroreceptor changes in Alzheimer's disease. Cerebrovasc. Brain Met. Rev. 4, 303-328.

Pascual-Alonso T. and González-Zárate J.L. (1992) Subtypes of muscarinic acetylcholine receptor following the experimental denervation of the cholinergic pathway ascending to the neocortex. Arch Neurobiol (Madr). 55(3), 116-123.

Perry E.K., Gibson P.H., Blessed G., Perry R.H. and Tomlinson B.E. (1977) Neurotransmitter enzyme abnormalities in senile dementia. Choline acetyltransferase and glutamic acid decarboxylase activities in necropsy brain tissue. J Neurol Sci. 34(2), 247-265.

Pettegrew J.W., Panchalingam K., Hamilton R.L. and McClure R.J. (2001) Brain membrane phospholipid alterations in Alzheimer's disease. Neurochemical Research 26, 771–782.

Qian Z. and Drewes L.R. (1989) Muscarinic acetylcholine receptor regulates phosphatidylcholine phospholipase D in canine brain. J Biol Chem. 264(36), 21720-21724.

Quinlivan M., Chalon S., Vergote J., Henderson J., Katsifis A., Kassiou M. and Guilloteau D. (2007) Decreased vesicular acetylcholine transporter and alpha(4)beta(2) nicotinic receptor density in the rat brain following 192 IgG-saporin immunolesioning. Neurosci Lett. 415(2), 97-101.

Raevsky V.V., Dawe G.S., Sinden J.D. and Stephenson J.D. (1998) Lesions of the nucleus basalis magnocellularis do not alter the proportions of pirenzepine- and gallamine-sensitive responses of somatosensory cortical neurones to acetylcholine in the rat. Brain Res. 782(1-2), 324-328.

Raiteri M., Leardi R. and Marchi M. (1984) Heterogeneity of presynaptic muscarinic receptors regulating neurotransmitter release in the rat brain. J Pharmacol Exp Ther. 228(1), 209-214.

Riekkinen M., Riekkinen P. and Riekkinen P. Jr (1991) Comparison of quisqualic and ibotenic acid nucleus basalis magnocellularis lesions on water-maze and passive avoidance performance. Brain Res Bull. 27(1), 119-123.

Riekkinen P. Jr, Riekkinen M. and Sirviö J. (1993) Cholinergic drugs regulate passive avoidance performance via the amygdala. J Pharmacol Exp Ther. 267(3), 1484-1492.

Rodríguez-Puertas R., Pascual J., Vilaró T. and Pazos A. (1997) Autoradiographic distribution of M1, M2, M3, and M4 muscarinic receptor subtypes in Alzheimer's disease. Synapse 26(4), 341-350.

Rodríguez-Puertas R., Pazos A., Zarranz J.J. and Pascual J. (1994) Selective cortical decrease of high-affinity choline uptake carrier in Alzheimer's disease: an autoradiographic study using 3H-hemicholinium-3. J Neural Transm Park Dis Dement Sect. 8(3), 161-169.

Rossner S., Schliebs R., Perez-Polo J.R., Wiley R.G. and Bigl V. (1995) Differential changes in cholinergic markers from selected brain regions after specific immunolesion of the rat cholinergic basal forebrain system. J Neurosci Res. 40(1), 31-43.

Rossner S. (1997) Cholinergic immunolesions by 192IgG-saporin--useful tool to simulate pathogenic aspects of Alzheimer's disease. Int J Dev Neurosci. 15(7), 835-50. Review.

Schliebs R., Feist T., Rossner S. and Bigl V. (1994) Receptor function in cortical rat brain regions after lesion of nucleus basalis. J Neural Transm Suppl. 44, 195-208.

Schwartz S.A., Reyzer M.L. and Caprioli R.M. (2003) Direct tissue analysis using matrix-assisted laser desorption/ionization mass spectrometry: practical aspects of sample preparation. J Mass Spectrom. 38(7), 699-708.

Seeger T., Fedorova I., Zheng F., Miyakawa T., Koustova E., Gomeza J., Basile A.S., Alzheimer C. and Wess J. (2004) M2 muscarinic acetylcholine receptor knock-out mice show deficits in behavioral flexibility, working memory, and hippocampal plasticity. J Neurosci. 24(45), 10117-10127.

Segal M. and Auerbach J.M. (1997) Muscarinic receptors involved in hippocampal plasticity. Life Sci. 60(13-14), 1085-1091.

Sugaya K., Clamp C., Bryan D. and McKinney M. (1997) mRNA for the m4 muscarinic receptor subtype is expressed in adult rat brain cholinergic neurons. Brain Res Mol Brain Res. 50(1-2), 305-313.

Torres E.M., Perry T.A., Blockland A., Wilkinson L.S., Wiley R.G., Lappi D.A. and Dunnet S.B. (1994) Behavioural, histochemical and biochemical consequences of selective immunolesions in discrete regions of the basal forebrain cholinergic system. Neuroscience 63(1), 95-122.

Tzavara E.T., Bymaster F.P., Felder C.C., Wade M., Gomeza J., Wess J., McKinzie D.L. and Nomikos G.G. (2003) Dysregulated hippocampal acetylcholine neurotransmission and impaired cognition in M2, M4 and M2/M4 muscarinic receptor knockout mice. Mol Psychiatry 8(7), 673-679.

Ulus I.H., Wurtman R.J., Mauron C. and Blusztajn J.K. (1989) Choline increases acetylcholine release and protects against the stimulation-induced decrease in phosphatide levels within membranes of rat corpus striatum. Brain Res. 484(1-2), 217-227.

Veloso A., Astigarraga E., Barreda-Gómez G., Manuel I., Ferrer I., Giralt M.T., Ochoa B., Fresnedo O., Rodríguez-Puertas R. and Fernández J.A. (2011) Anatomical distribution of lipids in human brain cortex by imaging mass spectrometry. J Am Soc Mass Spectrom. 22(2), 329-338.

Vilaró M.T., Wiederhold K.H., Palacios J.M. and Mengod G. (1992) Muscarinic M2 receptor mRNA expression and receptor binding in cholinergic and non-cholinergic cells in the rat brain: a correlative study using in situ hybridization histochemistry and receptor autoradiography. Neuroscience 47(2), 367-393.

Vilaró M.T., Palacios J.M. and Mengod G. (1994) Multiplicity of muscarinic autoreceptor subtypes? Comparison of the distribution of cholinergic cells and cells containing mRNA for five subtypes of muscarinic receptors in the rat brain. Brain Res Mol Brain Res. 21(1-2), 30-46.

Wall S.J., Wolfe B.B. and Kromer L.F. (1994) Cholinergic deafferentation of dorsal hippocampus by fimbria-fornix lesioning differentially regulates subtypes (m1-m5) of muscarinic receptors. J Neurochem. 62(4), 1345-1351.

Wenk G.L., Stoehr J.D., Quintana G., Mobley S. and Wiley R.G. (1994) Behavioral, biochemical, histological, and electrophysiological effects of 192 IgG-saporin injections into the basal forebrain of rats. J Neurosci. 14(10), 5986-5995.

Whishaw I.Q., O'Connor W.T. and Dunnett S.B. (1985) Disruption of central cholinergic systems in the rat by basal forebrain lesions or atropine: effects on feeding, sensorimotor behaviour, locomotor activity and spatial navigation. Behav Brain Res. 17(2), 103-115.

Whitehouse P.J., Price D.L., Struble R.G., Clark A.W., Coyle J.T. and Delon M.R. (1982) Alzheimer's disease and senile dementia: loss of neurons in the basal forebrain. Science 215(4537):1237-1239.

Wiley RG, Oeltmann TN, Lappi DA (1991). Immunolesioning: selective destruction of neurons using immunotoxin to rat NGF receptor. Brain Res. 562(1), 149-153.

Wurtman R.J., Blusztajn J.K. and Maire J.C. (1985) "Autocannibalism" of choline-containing membrane phospholipids in the pathogenesis of Alzheimer's disease-A hypothesis. Neurochem Int. 7(2), 369-372.

Wymann M.P. and Schneiter R. (2008) Lipid signalling in disease. Nat Rev Mol Cell Biol. 9(2), 162-176.

Zhang Z.J., Berbos T.G., Wrenn C.C. and Wiley R.G. (1996) Loss of nucleus basalis magnocellularis, but not septal, cholinergic neurons correlates with passive avoidance impairment in rats treated with 192-saporin. Neurosci Lett. 203(3), 214-218.

Zupan G., Casamenti F., Scali C. and Pepeu G. (1993) Lesions of the nucleus basalis magnocellularis in immature rats: short- and long-term biochemical and behavioral changes. Pharmacol Biochem Behav. 45(1), 19-25.

Table 1. [^{35}S]GTPγS basal and carbachol-induced (100 µM) binding in the different amygdaloid nuclei and hippocampus from vehicle (aCSF) and 192IgG-saporin-treated rats.

	Basal binding (nCi/g t.e.)		**Carbachol stimulation (% Over basal)**	
Brain region	aCSF	SAP	**aCSF**	**SAP**
Telencephalon				
Amygdaloid nuclei				
Anterior	421 ± 33	402 ± 29	**59 ± 9.1**	**47 ± 13.6**
Basolateral	487 ± 47	390 ± 44	**43 ± 6.6**	**48 ± 10.9**
Central	710 ± 91	525 ± 55	**27 ± 9.2**	**52 ± 7.8**
Lateral	483 ± 50	425 ± 43	**41 ± 9.3**	**36 ± 7.2**
Medial	720 ± 94	621 ± 69	**39 ± 8.5**	**34 ± 4.7**
Hippocampus				
CA1				
Oriens	320 ± 40	269 ± 32	**26 ± 9.4**	**40 ± 10.4**
Pyramidal	527 ± 64	457 ± 50	**40 ± 11.5**	**30 ± 6.2**
Radiatum	363 ± 33	323 ± 36	**45 ± 11.5**	**42 ± 9.0**
CA3				
Oriens	317 ± 26	303 ± 38	**26 ± 8.0**	**48 ± 6.6**
Pyramidal	477 ± 36	453 ± 42	**11 ± 5.6**	**32 ± 4.2***
Radiatum	328 ± 21	281 ± 32	**28 ± 9.5**	**40 ± 13.0**
Dentate gyrus				
Granular	467 ± 29	452 ± 50	**27 ± 6.0**	**62 ± 6.7***
Molecular	315 ± 49	278 ± 45	**34 ± 14.7**	**34 ± 9.5**
Polymorphic	314 ± 58	263 ± 39	**11 ± 18.2**	**25 ± 11.8**
Ventral subiculum	345 ± 29	294 ± 18	**37 ± 4.8**	**47 ± 6.7**

Data are mean ± S.E. M values from aCSF (n = 10) and SAP (n = 11) treated rats. ***** $p < 0.05$, when compared to aCSF group.

Table 2. [^{35}S]GTPγS basal and carbachol-induced (100 µM) binding in several brain regions from vehicle (aCSF) and 192IgG-saporin-treated rats.

	Basal binding (nCi/g t.e.)		**Carbachol stimulation (% Over basal)**	
Brain region	aCSF	SAP	**aCSF**	**SAP**
Cerebral cortex				
Cingulate	304 ± 26	306 ± 20	**52 ± 12.1**	**48 ± 6.7**
Ectorhinal	352 ± 34	290 ± 29	**66 ± 12.5**	**58 ± 8.0**
Entorhinal	342 ± 35	335 ± 36	**76 ± 10.5**	**93 ± 11.6**
Perirhinal	338 ± 49	309 ± 29	**35 ± 5.8**	**43 ± 3.5**
Piriform	292 ± 27	319 ± 29	**54 ± 15.2**	**33 ± 7.1**
Somatosensory	355 ± 28	333 ± 20	**31 ± 7.0**	**54 ± 10.6**
Motor	311 ± 33	319 ± 20	**21 ± 9.6**	**51 ± 8.2**
Basal ganglia				
Globus pallidus	335 ± 43	347 ± 36	**46 ± 13.2**	**49 ± 12.5**
Striatum	339 ± 26	345 ± 21	**74 ± 15.4**	**62 ± 11.1**
Diencephalon				
NBM	535 ± 49	398 ± 31	**45 ± 9.7**	**15 ± 6.6***
Horizontal diag band	310 ± 25	327 ± 31	**121 ± 20.7**	**115 ± 17.6**
Vertical diag band	330 ± 25	399 ± 42	**135 ± 24.1**	**113 ± 23.2**
Medial septum	267 ± 24	284 ± 32	**152 ± 24.4**	**139 ± 23.7**
Rhinencephalon				
Lat olfactory tract	379 ± 45	324 ± 37	**82 ± 13.1**	**47 ± 11.5**
Rhomboencephalon				
Dorsal raphe	703 ± 103	590 ± 74	**19 ± 4.9**	**24 ± 4.7**
Locus coeruleus	220 ± 36	132 ± 16	**26 ± 11.9**	**78 ± 11.9**
Mesencephalon				
Periaqueductal gray	496 ± 44	469 ± 45	**51 ± 15.0**	**47 ± 8.5**
Substantia nigra	456 ± 52	399 ± 38	**31 ± 10.5**	**37 ± 5.4**

Data are mean ± S.E. M values from aCSF (n = 10) and SAP (n = 8) treated rats. ***** $p < 0.05$, when compared to aCSF group.

Table 3. Relative intensity of representative lipid species in the NBM and cortex from vehicle (aCSF) and 192IgG-saporin treated rats, in both positive and negative ion mode.

			% Intensity[1]			
			NBM		Cortex	
Assignment	**Cal m/z**	**Exp m/z**	aCSF	**SAP**	aCSF	**SAP**
Positive ion mode						
PE (14:1/20:4)+H^+	710.4755	710.4893	15.21 ± 0.70	**11.87 ± 1.38***	9.97 ± 0.62	**10.67 ± 0.67**
SM (d18:1/18:0)+H^+	731.6061	731.6070	7.11 ± 1.13	**4.15 ± 0.80***	4.19 ± 0.44	**3.50 ± 0.53**
SM (d18:1/16:0)+K^+	741.5313	741.5311	0.96 ± 0.14	**10.63 ± 3.33****	0.55 ± 0.13	**0.78 ± 0.11**
PC (32:0)+Na^+/PC (34:3)+H^+	756.5514	756.5520	15.75 ± 1.23	**21.94 ± 2.46***	16.94 ± 1.02	**17.41 ± 1.31**
PC (34:2)+Na^+/PC (36:5)+H^+	780.5514	780.5521	0.85 ± 0.09	**2.02 ± 0.27****	1.10 ± 0.08	**1.07 ± 0.08**
PC (34:1)+Na^+/PC (36:4)+H^+	782.5670	782.5673	32.75 ± 1.65	**46.10 ± 3.86****	32.31 ± 1.64	**30.9 ± 1.29**
PC (34:2)+K^+	796.5253	796.5255	3.27 ± 0.17	**5.19 ± 0.30*****	4.20 ± 0.15	**4.16 ± 0.07**
PC (34:1)+K^+	798.5410	798.5405	100 ± 0	**100 ± 0**	100 ± 0	**100 ± 0**
PC (36:4)+Na^+/PC (38:7)+H^+	804.5514	804.5510	2.79 ± 0.31	**7.69 ± 1.52***	3.63 ± 0.31	**4.3 ± 0.24**
PC (36:1)+Na^+/PC (38:4)+H^+	810.5983	810.5984	14.62 ± 0.30	**21.64 ± 1.53****	10.62 ± 0.48	**8.95 ± 0.63***
PC (36:4)+K^+	820.5253	820.5249	10.32 ± 1.01	**18.61 ± 2.71***	13.17 ± 0.99	**15.63 ± 0.48***
PC (38:4)+Na^+/PC (40:7)+H^+	832.5827	832.5826	3.00 ± 0.30	**7.98 ± 1.40****	2.82 ± 0.25	**3.11 ± 0.21**
PC (38:4)+K^+/PC (42:9)+H^+	848.5566	848.5560	10.23 ± 0.93	**18.27 ± 2.15****	9.71 ± 0.80	**10.75 ± 0.38**
PC (40:6)+Na^+	856.5827	856.5820	0.88 ± 0.17	**2.25 ± 0.40****	0.75 ± 0.11	**1.14 ± 0.09***
Negative ion mode						
SM (d18:1/15:0)	687.5447	687.5443	1.26 ± 0.24	**6.44 ± 1.50****	0.94 ± 0.23	**1.52 ± 0.28**
PS (18:0/18:1)	788.5447	788.5447	11.04 ± 2.16	**3.95 ± 0.99****	8.54 ± 1.28	**6.30 ± 0.85**
PE (40:4)/PC (18:0/20:4)	794.5705	794.5705	0.82 ± 0.13	**1.35 ± 0.17***	0.83 ± 0.08	**0.98 ± 0.14**
PG (22:6/22:6)	865.5025	865.5033	0.06 ± 0.01	**0.86 ± 0.24****	0.04 ± 0.01	**0.16 ± 0.05***
PI (20:4/18:0)	885.5494	885.5496	100 ± 0	**100 ± 0**	100 ± 0	**100 ± 0**

[1] The maximal peak is the most intense peak of the lipid spectrum, in this case PC (34:1) in positive and PI (20:4/18:0) in negative ion modes, which are set at 100%. Data are mean ± S.E.M values from aCSF and 192IgG-saporin-treated rats. *$p < 0.05$, **$p < 0.01$ and ***$p < 0.001$ when compared to aCSF group. PC: phosphatidylcholine; SM: sphingomyelin; PS: phosphatidylserine; PE: phosphatidylethanolamine; PG: phosphoglycerol; PI: phosphatidylinositol; Cal: calculated; Exp: experimental.

Figure 1

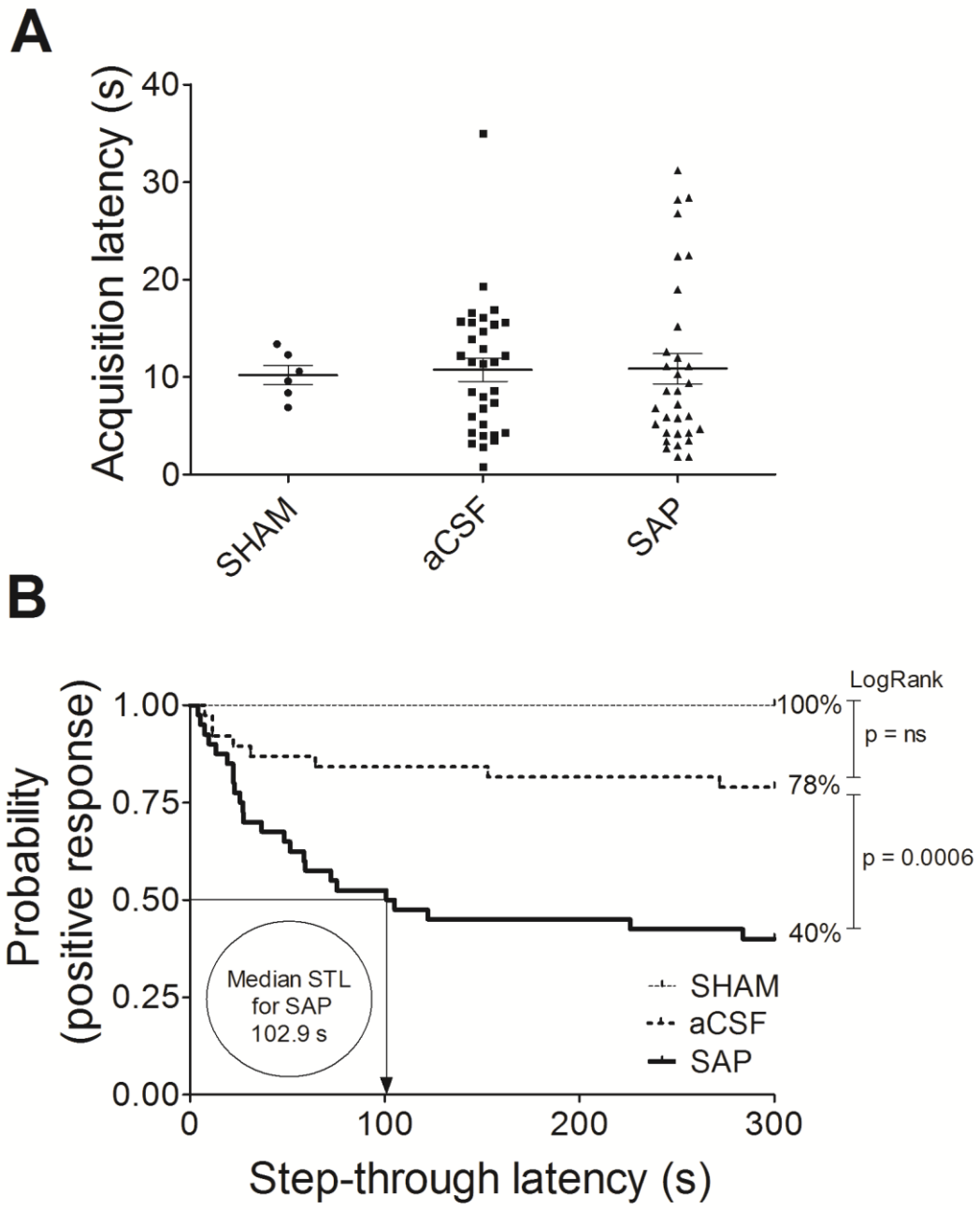
A
Acquisition latency (s)
40
30
20
10
0
SHAM
aCSF
SAP
B
Probability (positive response)
1.00
0.75
0.50
0.25
0.00
0
100
200
300
Step-through latency (s)
LogRank
100%
78%
40%
p = ns
p = 0.0006
Median STL for SAP 102.9 s
SHAM
aCSF
SAP

Figure 2

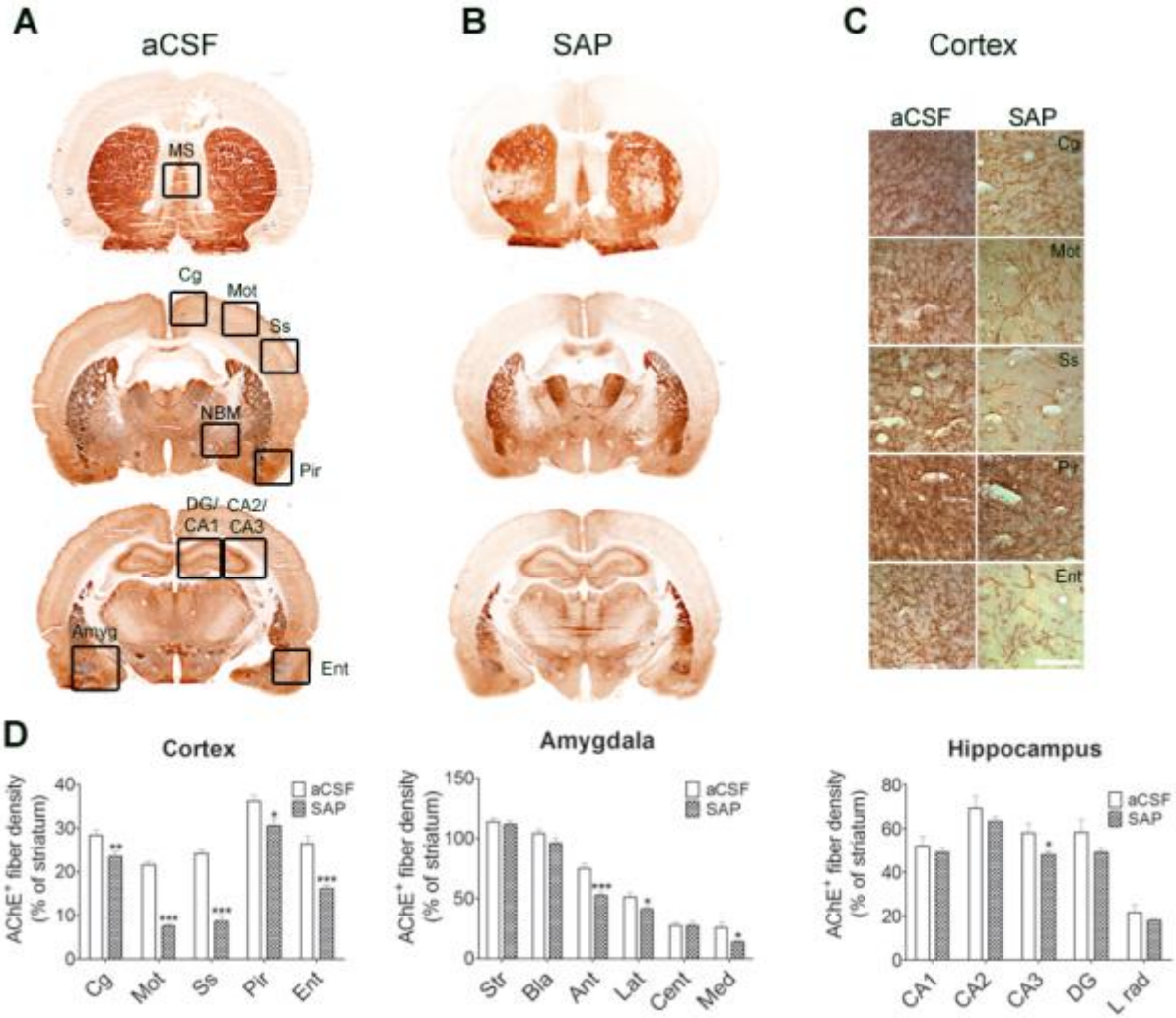
A
aCSF
MS
Cg
Mot
Ss
NBM
Pir
DG/ CA1
CA2/ CA3
Amyg
Ent
B
SAP
C
Cortex
aCSF
SAP
Cg
Mot
Ss
Pir
Ent
D
Cortex
AChE+ fiber density (% of striatum)
aCSF
SAP
Cg
Mot
Ss
Pir
Ent
Amygdala
Str
Bla
Ant
Lat
Cent
Med
Hippocampus
CA1
CA2
CA3
DG
L rad

Figure 3

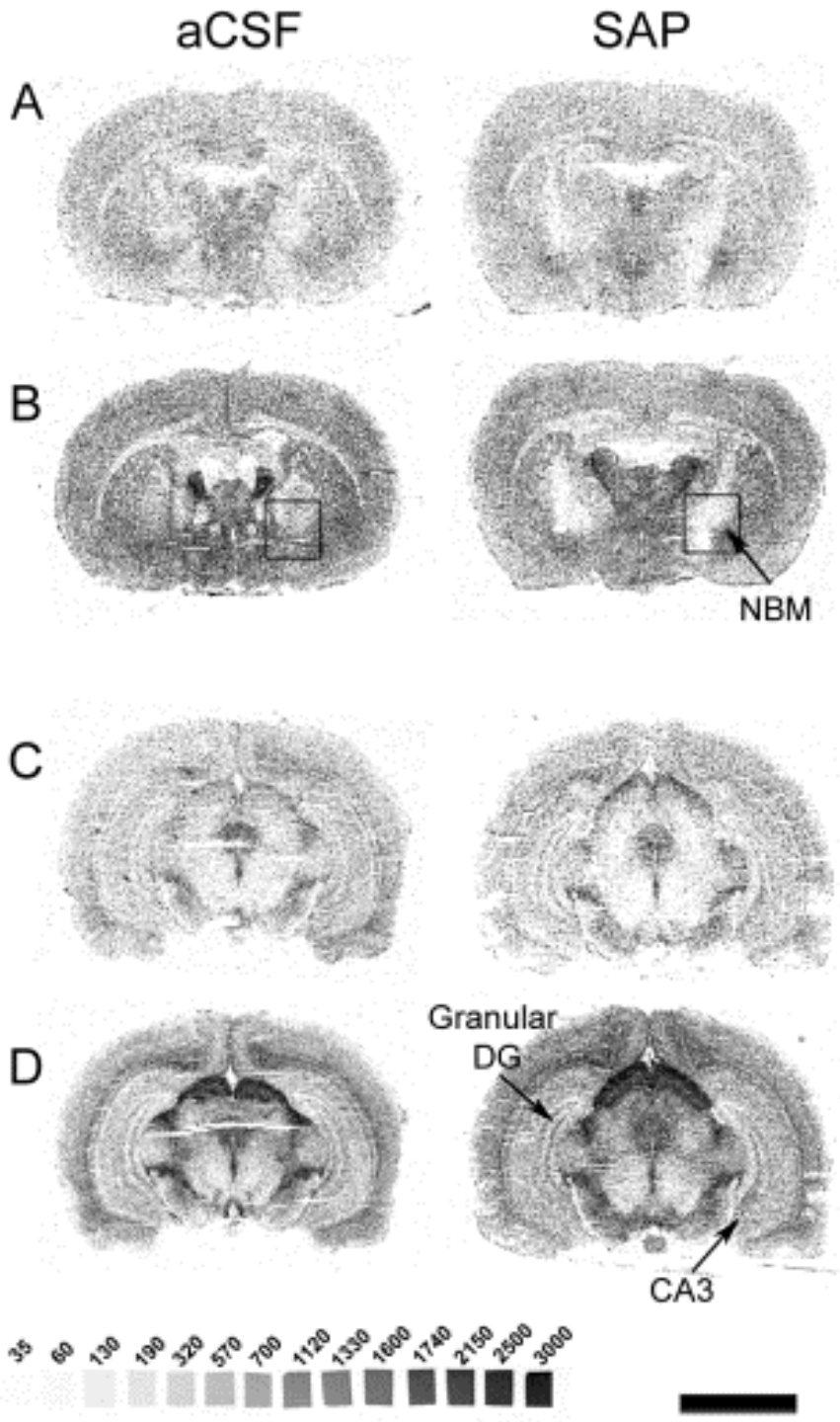
aCSF
SAP
A
B
NBM
C
D
Granular
DG
CA3
35
60
130
190
320
570
700
1120
1330
1600
1740
2150
2500
3000

Figure 4

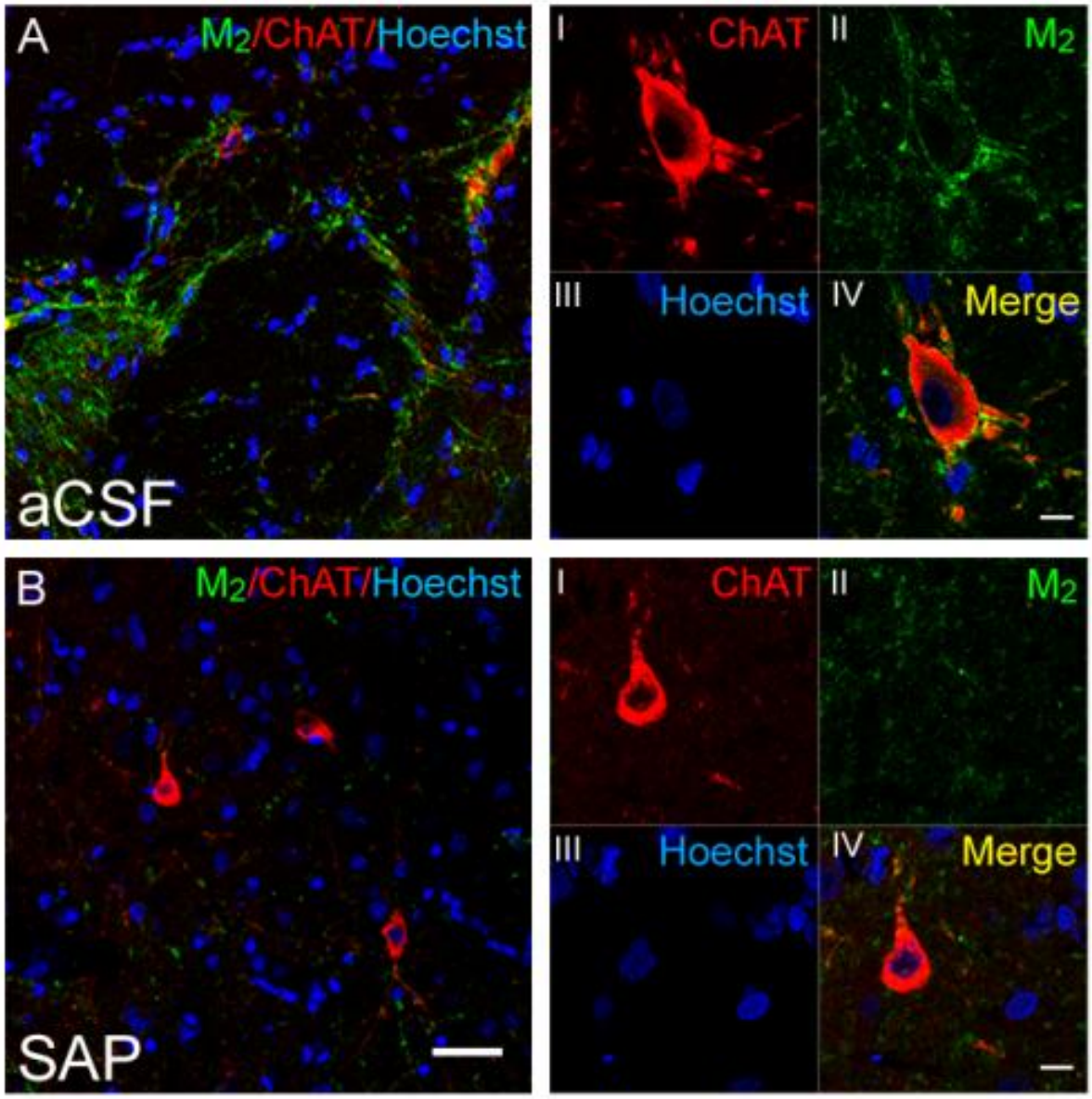
A
M2/ChAT/Hoechst
aCSF
I
ChAT
II
M2
III
Hoechst
IV
Merge
B
M2/ChAT/Hoechst
SAP
I
ChAT
II
M2
III
Hoechst
IV
Merge

Figure 5

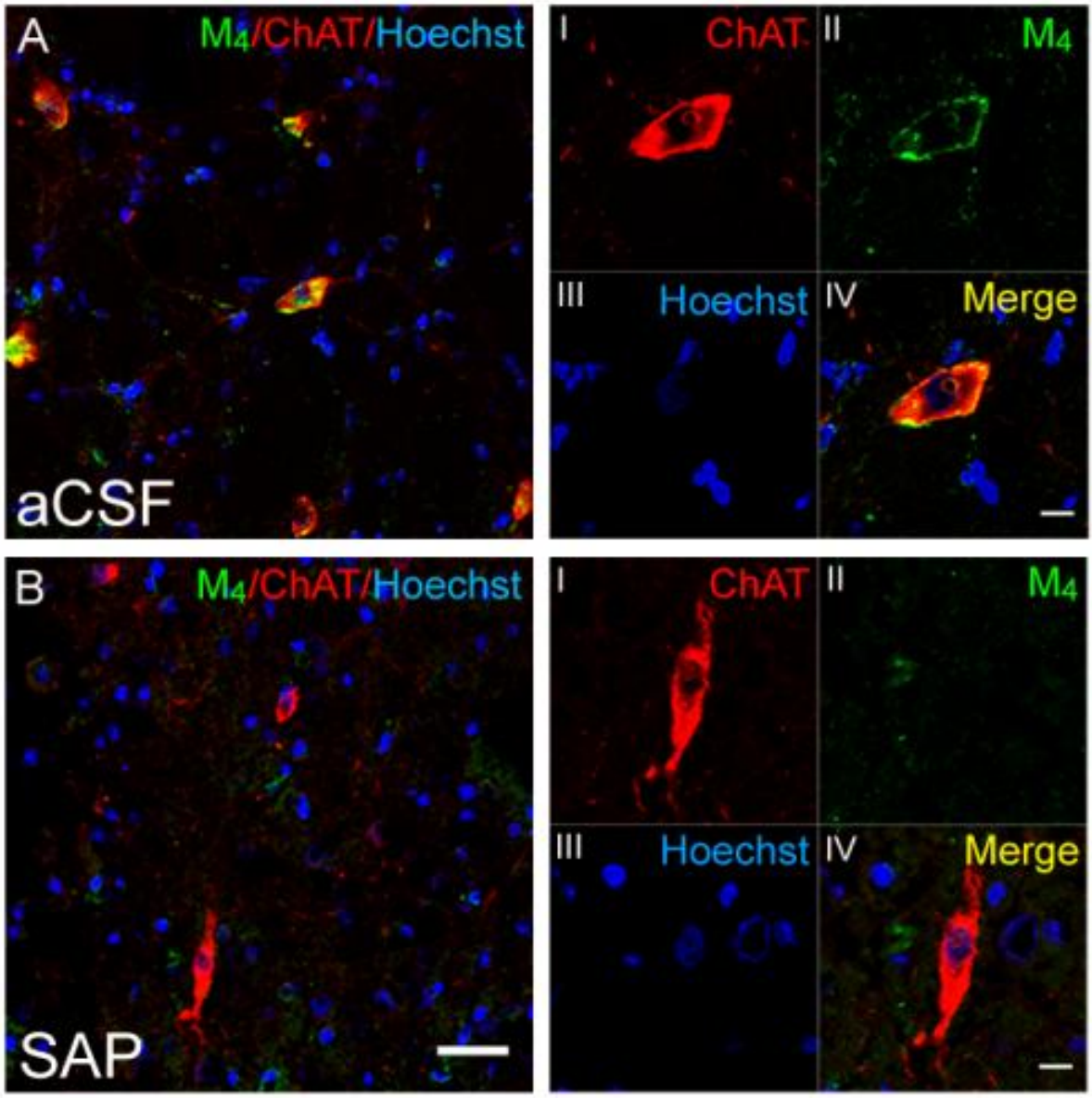
A
M4/ChAT/Hoechst
aCSF
I
ChAT
II
M4
III
Hoechst
IV
Merge
B
M4/ChAT/Hoechst
SAP
I
ChAT
II
M4
III
Hoechst
IV
Merge

Figure 6

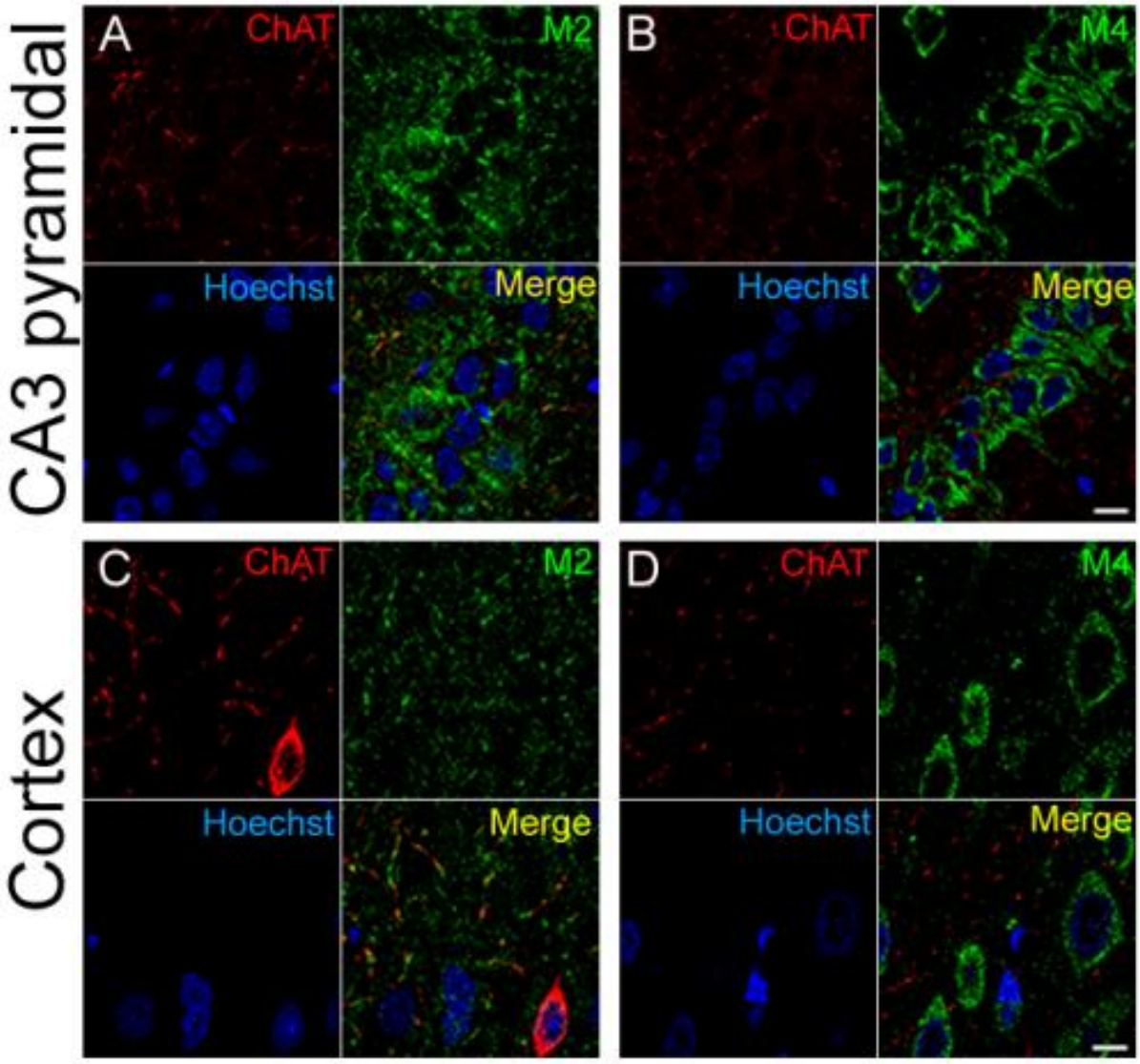
CA3 pyramidal
Cortex
A
ChAT
M2
Hoechst
Merge
B
ChAT
M4
Hoechst
Merge
C
ChAT
M2
Hoechst
Merge
D
ChAT
M4
Hoechst
Merge

Figure 7

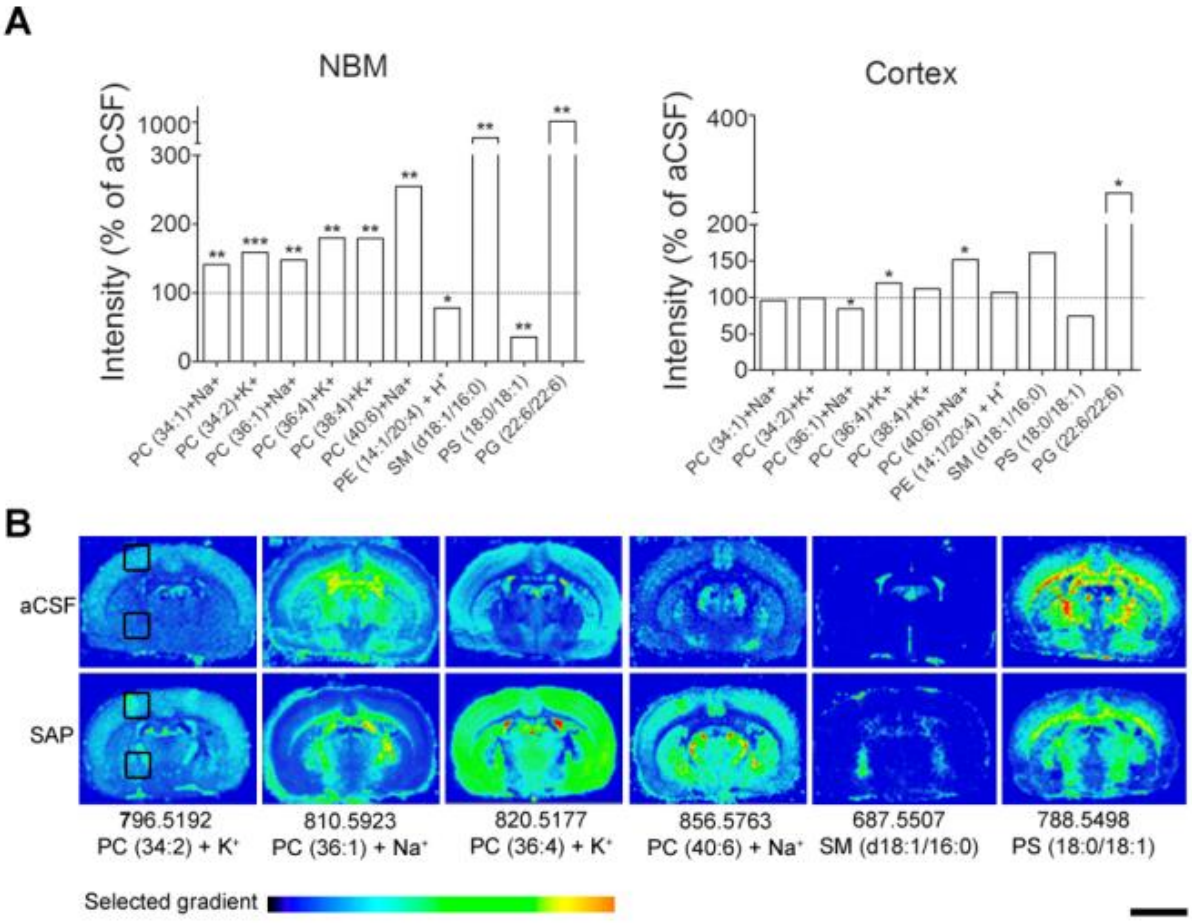
A
NBM
Cortex
Intensity (% of aCSF)
PC (34:1)+Na+
PC (34:2)+K+
PC (36:1)+Na+
PC (36:4)+K+
PC (38:4)+K+
PC (40:6)+Na+
PE (14:1/20:4) + H+
SM (d18:1/16:0)
PS (18:0/18:1)
PG (22:6/22:6)
B
aCSF
SAP
796.5192
PC (34:2) + K+
810.5923
PC (36:1) + Na+
820.5177
PC (36:4) + K+
856.5763
PC (40:6) + Na+
687.5507
SM (d18:1/16:0)
788.5498
PS (18:0/18:1)
Selected gradient

Figure legends

Figure 1. (A) Acquisition latency times in the learning trial of the passive avoidance test of SHAM (n = 6), aCSF (n = 32) and SAP (n = 32) rats. The figure shows the mean ± SEM of each group. (B) Step-through latency times in the retention trial of the passive avoidance test, represented as Kaplan-Meier survival curves. The median step-through latency or the time spent to enter the dark compartment by 50% of the immunotoxin-treated population should be 102,9 seconds (aCSF vs SHAM p = n.s.; SAP vs aCSF p < 0.001, Log-rank test).

Figure 2. (A and B) AChE staining in representative brain slices at three different levels of aCSF and 192IgG-saporin-treated rats. (C) Microphotographs from different cortical regions of aCSF and 192IgG-saporin-treated rats at 400-fold magnification, revealing the decrease in AChE positive fibers in immunotoxin-treated rats (scale bar = 20 µm). (D) The histograms show the optical density of AChE expressed as percentages of the striatum (used as control area) in aCSF (n = 13) and SAP (n = 13) treated rats. *p < 0.05; **p < 0.01 and ***p < 0.001 vs aCSF-treated rats. MS: medial septum; Cg: cingular cortex; Mot: motor cortex; Ss: somatosensory cortex; Pir: piriform cortex; Ent: entorhinal cortex; Amyg: amygdala; DG: dentate gyrus.

Figure 3. [^{35}S]GTPγS autoradiography in representative brain coronal slices at two different levels (A and B) and (C and D) obtained from aCSF and 192IgG-saporin-treated rats that show [^{35}S]GTPγS basal binding (A and C) and carbachol-evoked (100 µM) stimulation of muscarinic M_2/M_4 mAChR (B and D). NBM: nucleus basalis magncellularis; Granular DG: granular dentate gyrus; CA3: CA3 region of hippocampus. [^{14}C]-microscales used as standards in nCi/g t.e. Scale bar: 5 mm.

Figure 4. Double labeling in slices containing NBM from representative aCSF (A) and 192IgG-saporin-treated (B) rats, stained for ChAT (red) and M_2 mAChR (green) at 200-fold magnification. 192IgG-saporin induced a reduction in BFCN density and in M_2 mAChR-immunoreactivity. Scale bar = 40 µm. High magnification images reveal a particular M_2 mAChR-immunostaining pattern surrounding the perikarya (A-II) of the large BFCN (A-I) which show a presynaptic localization and a presumable distribution in plasmatic membrane, but with a modest degree of co-localization (A-IV). Interestingly, 192IgG-saporin-treated rats showed the presence of ChAT (B-I), whereas the loss of mAChR immunoreactivity is evident (B-II). Scale bar = 10 µm.

Figure 5. Double labeling in slices containing NBM from a representative aCSF (A) and 192IgG-saporin-treated rat (B), stained for ChAT (red) and M_4 mAChR (green) at 200-fold magnification. 192IgG-saporin induced a reduction in BFCN density and in M_4 mAChR-immunoreactivity. Scale bar = 40 µm. High magnification images reveal a somatodendritic M_4 mAChR-immunostaining pattern surrounding the perikarya (A-II) of the large BFCN (A-I) with a high degree of co-localization. There was a reduction of M_4 mAChR-immunoreactivity (B-II) but ChAT still remained in BFCN (B-I) in 192IgG-saporin-treated rats. Scale bar = 10 µm.

Figure 6. Double labeling of consecutive slices containing hippocampal CA3 pyramidal region (A and B) and somatosensory cortex (C and D) from a representative aCSF-treated rat, stained for ChAT (red), M_2 mAChR (A and C in green) and M_4 mAChR (B and D in green) at 630-fold magnification. The images show a presumable presynaptic distribution of M_2 mAChR, delineating the perikarya of the large CA3 pyramidal neurons in basket-like formations (A) and the somatodendritic distribution of M_4 mAChR in the perikarya of the same neurons (B). In the cortex, both M_2 (C) and M_4 (D) mAChR distribution displays a similar pattern to that observed in CA3. Scale bar = 10 µm.

Figure 7. (A) The histograms show the relative abundance of different lipid species in NBM (left) and cortex (right), expressed as percentages of the values obtained in the aCSF-treated group. (B) Matrix-assisted laser desorption ionization-imaging mass spectrometry (MALDI-IMS) of different lipids in brain slices containing the NBM and cortical projections from representative aCSF and 192IgG-saporin-treated rats. The intensities were measured in the black squares of the somatosensory cortex and the NBM. *$p < 0.05$; **$p < 0.01$ and ***$p < 0.001$ vs aCSF-treated rats. PC (phosphatidylcholines); PE (phosphatidylethanolamines); PS (phosphatidylserines); SM (sphingomyelin); PG (phosphoglycerol). Scale bar = 5 mm.

Supplementary material

Table S1. [^{35}S]GTPγS basal and carbachol-induced (100 μM) binding in different regions of grey matter from SHAM-operated rats.

	Basal binding (nCi/g t.e.)	**Carbachol stimulation (% Over basal)**		Basal binding (nCi/g t.e.)	**Carbachol stimulation (% Over basal)**
Brain region			**Brain region**		
Telencephalon			**Cerebral cortex**		
Amygdala			Cingulate	354 ± 30	**43 ± 12.7**
Anterior	403 ± 33	**37 ± 14.4**	Ectorhinal	337 ± 56	**36 ± 6.5**
Basolateral	387 ± 41	**53 ± 10.5**	Entorhinal	308 ± 30	**47 ± 7.1**
Central	536 ± 53	**32 ± 8.39**	Perirhinal	309 ± 43	**36 ± 13.5**
Lateral	373 ± 53	**78 ± 16.9**	Piriform	270 ± 31	**61 ± 9.8**
Medial	672 ± 84	**34 ± 11.7**	Somatosensory	368 ± 28	**34 ± 4.9**
Hippocampus			Motor	353 ± 37	**34 ± 14.8**
CA1			**Basal ganglia**		
Oriens	252 ± 25	**27 ± 12.0**	Globus pallidus	275 ± 25	**54 ± 12.2**
Pyramidal	366 ± 44	**55 ± 15.6**	Striatum	330 ± 37	**85 ± 14.0**
Radiatum	279 ± 19	**42 ± 9.8**	*Diencephalon*		
CA3			NBM	492 ± 51	**47 ± 12.3**
Oriens	280 ± 44	**21 ± 6.8**	Horiz diag band	356 ± 29	**115 ± 19.5**
Pyramidal	419 ± 52	**9 ± 6.2**	Vertical diag band	366 ± 28	**112 ± 25.6**
Radiatum	264 ± 38	**40 ± 19.8**	Medial septum	280 ± 50	**150 ± 41.2**
Dentate gyrus			*Rhinencephalon*		
Granular	437 ± 32	**25 ± 1.2**	Lat olfactory tract	356 ± 27	**41 ± 9.8**
Molecular	263 ± 45	**44 ± 9.2**	*Rhomboencephalon*		
Polimorphic	290 ± 39	**28 ± 15.7**	Dorsal raphe	533 ± 102	**42 ± 9.4**
Vent subic	301 ± 35	**49 ± 11.4**	Locus coeruleus	197 ± 30	**52 ± 6.0**
			Mesencephalon		
Brainstem			Periaqueduc gray	450 ± 82	**47 ± 10.3**
Spinal trig N	178 ± 25	**87 ± 19.8**	Substantia nigra	361 ± 56	**32 ± 14.9**

III

Increase of cortical endocannabinoid signaling in a rat model of basal forebrain cholinergic dysfunction

ALBERTO LLORENTE-OVEJERO[1], IVÁN MANUEL[1], MARIA TERESA GIRALT[1], RAFAEL RODRÍGUEZ-PUERTAS[1]

[1]Department of Pharmacology, Faculty of Medicine and Nursing. University of the Basque Country (UPV/EHU), Bº Sarriena s/n, 48940 Leioa, Spain.

*Corresponding author

Rafael Rodríguez-Puertas

Department of Pharmacology, Faculty of Medicine and Nursing.

University of the Basque Country. E-48940 Leioa, Vizcaya, Spain.

Tel.: +34-94-6012739; fax: +34-94-6013220.

E-mail address: rafael.rodriguez@ehu.es

Abstract

During the progression of Alzheimer's disease, the basal forebrain cholinergic pathways progressively degenerate, leading to an irreversible impairment of memory and thinking skills. In the rat, a stereotaxic lesion with 192IgG-saporin removes basal forebrain cholinergic neurons, mimicking this process, and is used to test the effects on behavior and on neurotransmission. The modulation of cholinergic neurotransmission by the endocannabinoid system is thought to affect learning and memory processes by cannabinoid compounds. Therefore, we evaluated endocannabinoid signaling in relation to the memory impairment induced in adult male rats following a specific cholinergic bilateral lesion of the nucleus basalis magnocellularis. The lesion was further evaluated by histochemical studies, and the signaling mediated by CB_1 receptors was analyzed by both receptor and functional autoradiography and immunofluorescence. The passive avoidance test and histochemical data revealed a relationship between impaired behavior and a loss of up to 75% of cholinergic neurons in the nucleus basalis magnocellularis, accompanied by the corresponding cortical cholinergic denervation. The receptor and functional autoradiographic assays showed that there was a decrease in CB_1 receptor density in the hippocampus together with hyperactivity of endocannabinoid signaling in the cortex. Immunofluorescence studies revealed the loss of almost a third of the presynaptic GABAergic terminals in cortical and subcortical areas innervated by nucleus basalis magnocellularis cholinergic neurons. CB_1 receptors seem to be present at presynaptic GABAergic terminals in hippocampus, but in glutamatergic synapses in cortex. We propose that there is a CB_1 receptor-mediated compensation of the endocannabinoid tone to modulate the loss of cortical inhibitory terminals induced by the basal forebrain cholinergic denervation.

Keywords: nucleus basalis magnocellularis, 192IgG-saporin, memory, autoradiography, CB_1 receptors, GABA.

Abbreviations

AChE	Acetylcholinesterase
aCSF	Artificial cerebrospinal fluid
AU	Arbitrary units
BFCN	Basal forebrain cholinergic neurons
CB_1 receptor	Type-1 cannabinoid receptor
ChAT	Choline acetyltransferase
eCB	Endocannabinoid
GAD65	Glutamic acid decarboxylase isoform 65kDa
LTP	Long-term potentiation
NBM	Nucleus basalis magnocellularis
OD	Optical density
$P75^{NTR}$	Low-affinity nerve growth factor receptor
SAP	192IgG-saporin treated rats
VGLUT3	Vesicular glutamate transporter type 3

1. **Introduction**

Alzheimer's disease (AD) is a progressive neurodegenerative disorder that slowly but irreversibly impairs memory and thinking skills. Studies in humans indicate the relevance of the basal forebrain cholinergic pathways in the control of conscious awareness, attention, working memory, and a number of additional mnemonic processes (Perry et al., 1999). The first evidence of basal forebrain cholinergic damage in AD was reported in the 70s (Davies and Maloney, 1976; Perry et al., 1977; Davies, 1979; Whitehouse et al, 1982) and lead to the "cholinergic hypothesis of geriatric memory dysfunction" (Bartus et al., 1982). During the progression of AD a reduction in choline acetyltransferase (ChAT) activity (Davies, 1979) and in M_2 muscarinic acetylcholine receptor density in cholinergic innervated areas such as the hippocampus and the entorhinal cortex has been reported (Rodríguez-Puertas et al., 1997). Notwithstanding its limited efficacy, the inhibition of acetylcholinesterase (AChE) has proven to be the most viable therapeutic target for symptomatic improvement. Between 60% and 90% of AD patients develop neuropsychiatric symptoms including hallucinations, delusions, agitation/aggression, dysphoria/depression, anxiety, irritability, disinhibition, euphoria, apathy, aberrant motor behavior, sleep disturbances, appetite and eating changes and altered sexual behavior, implying alterations to multiple neurotransmission systems (Cummings et al., 2016). In this context, the endocannabinoid (eCB) system, through the modulation of the synaptic signaling pathways activated by cannabinoid receptors, is a promising target for the treatment of several neurological disorders, including AD. Thus, several studies have reported alterations in *postmortem* AD brain samples both in CB_1 (Westlake et al., 1994; Manuel et al., 2014) and CB_2 receptors (Benito et al., 2003), but also changes in the enzymatic machinery and in eCB levels (Mulder et al., 2011; D'Addario et al., 2012; Pascual et al., 2014). There is a great deal of evidence in the literature about the signaling crosstalk between cannabinoid and cholinergic systems both *in vitro*, by using cortical and hippocampal membranes (Gifford et al., 2000), and *in vivo*, by using CB_1 receptor deficient mice (Kathmann et al., 2001) or after the administration of cannabinoid synthetic agonists (Tzavara et al., 2003). Moreover, cannabinoid administration specifically reduces the turnover rate of acetylcholine in the hippocampus in a dose-dependent manner (Revuelta et al., 1980), while muscarinic cholinergic receptor activation enhances the release of eCB in this area (Kim et al., 2002). The synthesis of eCB is also increased five-fold by the simultaneous activation of NMDA and acetylcholine receptors in cortical neurons (Stella and Piomelli, 2001).

The present study analyzes eCB signaling by focusing on CB_1 receptors in a useful model with which to test the cholinergic hypothesis of AD, i.e., after inducing the specific depletion of basal forebrain cholinergic neurons (BFCN) in the nucleus basalis magnocellularis (NBM) of adult rats with the immunotoxin 192IgG-saporin. This immunotoxin is directed against the low-

affinity nerve growth factor receptor ($P75^{NTR}$) which is primarily expressed on the soma and nerve terminals of BFCN of adult rats. Firstly, we established the validity of the model by using the passive avoidance test to evaluate learning and memory. This test measures the ability of rats to recognize and avoid an environment in which they have previously received a noxious stimulus (Tulving, 2002). Following the test, the extent of the lesion in the basal forebrain cholinergic system was established by histochemical methods and CB_1 receptor-mediated eCB signaling was analyzed in the basal forebrain cholinergic pathways by using autoradiographic and immunofluorescent approaches.

2. **Materials and Methods**

2.1. Chemicals

192IgG-saporin (Batch 2441969) was acquired from Millipore (Temecula, CA, USA). [^{35}S]GTPγS (1250 Ci/mmol) and [^{3}H]CP55,940 (131.8 Ci/mmol) were purchased from PerkinElmer (Boston MA, USA), WIN55,212-2 and CP55,940 from Sigma-Aldrich (St Louis, MO, USA), SR141716A (rimonabant) from Tocris and SR144528 from Cayman-Chemicals (MI, USA). The [^{14}C] and [^{3}H]-microscales, used as standards in the autoradiographic experiments, were purchased from ARC (American Radiolabelled Chemicals, St Louis, MO, USA). Kodak Biomax MR β-radiation sensitive films, bovine serum albumine (BSA), DL-dithiothreitol (DTT), adenosine deaminase, guanosine 5´-diphosphate (GDP), guanosine5´-O-3-thiotriphosphate (GTPγS), ketamine, xylazine, oxytetracycline and Hoechst 33258 were acquired from Sigma-Aldrich. All the compounds necessary for the preparation of the different buffers, the fixation and the treatment of slides were of the highest commercially available quality.

2.2 Animals

Forty six adult male Sprague-Dawley rats, weighing 225-275 g and ranging in age from 8 to 10 weeks at the onset of the experiment, were used in this study. Rats were housed four per cage in individual 50 cm (length) x 25 cm (width) x 15 cm (height) cages at a temperature of 22ºC and in a humidity-controlled (65%) room with a 12:12 hours light/dark cycle, with access to food and water *ad libitum*. All procedures were performed in accordance with European animal research laws (Directive 2010/63/EU) and the Spanish National Guidelines for Animal Experimentation (RD 53/2013, Law 32/2007). Experimental protocols were approved by the

Local Ethical Committee for Animal Research of the University of the Basque Country (CEEA 388/2014).

2.3 Basal forebrain cholinergic lesion

All surgery was carried out under aseptic conditions. 192IgG-saporin was used to selectively eliminate cholinergic neurons in the NBM. Rats were randomly assigned to one of two groups: artificial cerebrospinal fluid as vehicle (aCSF; n = 22) and 192IgG-saporin (SAP; n = 24). The vehicle was prepared as follows: 0.15 M NaCl, 2.7 mM KCl, 0.85 mM $MgCl_2$, 1.2 mM $CaCl_2$ (pH 7.4) and sterilized by filtration with 0.4 µm-Ø filters (EMD Millipore, CA, USA). Rats were anesthetized with ketamine/xylazine (90/10 mg/kg; s.c.) and then placed in a stereotaxic instrument (Kopf, Tujunga, CA). After an incision was made in the skin along the midline of the skull, two holes were drilled and by using a 10-µl Hamilton syringe (Neuros™ Syringe, 7000 series; Bonaduz, Switzerland) with a 26-gauge needle, the intraparenchymal infusions were made into the NBM: - 1.5 mm anteroposterior from Bregma, ± 3 mm mediolateral from midline and + 8 mm dorsoventral from cranial surface (Paxinos and Watson, 2005). 192IgG-saporin was dissolved in aCSF under aseptic conditions to a final concentration of 130 ng/µl. aCSF or 192IgG-saporin was bilaterally injected (1 µl/hemisphere) at a constant rate of 0.2 µl/min. The needle was kept in for 5 min before removal to avoid a possible backflow and to allow complete diffusion. During surgery, the body temperature was controlled and the eyes were kept hydrated with warm saline solution (0.9% NaCl). After the administration was completed, the wounds were closed with braided silk sutures and a broad-spectrum antibiotic injection was given (oxytetracycline, 2.25 mg/kg; i.m.). The choice of coordinates, infusion rate, volume and dose of the immunotoxin were based on previous experiments performed in our laboratory.

2.4 Passive avoidance test

The rats were allowed seven days to recover from surgery and were then subjected to the passive avoidance test (PanLab passive avoidance box LE870/872). The apparatus consists of two methacrylate compartments separated by a guillotine door; one large white, illuminated and open-topped compartment: 31 cm (W) x 31 cm (D) x 24 cm (H), and the other small, black and closed compartment: 19.5 cm (W) x 10.8 cm (D) x 12 cm (H). Briefly, the test consists of two sessions. The first, called “the acquisition session”, was performed on day 7 after the surgery. Each animal was gently placed in the illuminated compartment and allowed to explore it for 30 sec. Then, the guillotine door was automatically opened and the animal was allowed to enter the dark compartment for 60 sec. When the rat crossed the door-way, the door closed, the acquisition latency was measured, and a scrambled foot shock (0.4 mA/2 sec) was delivered. 10 sec after the foot shock, the rat was returned to its home cage. The rats that did not enter the

dark compartment were eliminated from the study. 24 h later, in the "retention session", the rats were again placed in the illuminated compartment and allowed to explore for 30 sec. Then the door opened and the step through latency time to enter the dark compartment was measured up to a maximum cut-off time of 300 sec.

2.5 Tissue preparation

Following the passive avoidance test, the animals were anesthetized with ketamine/xylazine (90/10 mg/kg; i.p.).

Fixed tissue. Representative animals from aCSF (n = 5) and SAP (n = 5) groups were transcardially perfused with 0.1 M phosphate buffer (PB), 0.5% heparinized (37ºC, pH 7.4) followed by 4% paraformaldehyde and 3% picric acid in 0.1M PB (4ºC) (100 ml/100 g b.w.). Their brains were subsequently removed and post-fixed in the same fixative solution for 90 min at 4ºC, followed by immersion in a cryoprotective solution of 20% sucrose in PB overnight at 4ºC. Then the tissue was frozen by immersion in isopentane and kept at -80ºC. The brains were coronally cut into 10 µm slices using a Microm HM550 cryostat (Thermo Scientific) equipped with a freezing-sliding microtome at -25ºC, mounted onto gelatin-coated slides and stored at -25ºC until used.

Fresh tissue. Another group of animals was euthanized by decapitation and the brain samples from aCSF (n = 17) and SAP (n = 19) groups were quickly removed by dissection, fresh frozen and kept at -80ºC. Later they were cut into 20 µm and mounted onto gelatin-coated slides and stored at -25ºC until used.

2.6 Detection of BFCN in fresh tissue slices

Prior to histochemical or immunostaining procedures, all slices were air dried for 20 min and fresh tissue slices were post-fixed in 4% paraformaldehyde in PBS for 30 min at 4ºC and washed in 0.1 M saline phosphate buffer, pH 7.4 (PBS), for 20 min.

AChE staining and basal forebrain cholinergic neuron immunolabeling. BFCN in the NBM and cholinergic innervations were stained using the "direct coloring" thiocoline method for AChE (Karnovsky and Roots, 1964). The slices were rinsed twice in 0.1 M Tris-Maleate buffer (pH 6.0) for 10 min and incubated in complete darkness with constant, gentle agitation in the AChE reaction buffer: 0.1 M Tris-Maleate; 5 mM sodium citrate; 3 mM $CuSO_4$; 0.1 mM iso-OMPA; 0.5 mM $K_3Fe(CN)_6$ and 2 mM acetylthiocholine iodide as reaction substrate. The incubation times were from 30 min for staining cholinergic somas in NBM and 100 min for staining cholinergic fibers in the areas of innervation. Finally, the enzymatic reaction was stopped in two consecutive washes (2x10 min) in 0.1 M Tris-maleate (pH 6.0). Slices were then dehydrated in increasing concentrations of ethanol and covered with DPX as the mounting medium.

$P75^{NTR}$immunolabeling. Consecutive slices to those stained for AChE were blocked and permeabilized with 4% normal goat serum (NGS) in 0.3% Triton X-100 in PBS (0.1 M, pH 7.4) for 2 h at room temperature (22 ± 2ºC). To detect cholinergic neurons in NBM, the slices were incubated at 4ºC overnight with rabbit monoclonal anti-$P75^{NTR}$ antibody (1:750) (Cell Signaling, MA, USA) and diluted in 0.3% Triton X-100 in PBS with 5% BSA. The primary antibody was then revealed by incubation for 30 min at 37ºC in darkness with Alexa-Fluor 488 donkey-anti-rabbit (1:250) (Invitrogen, CA, USA) diluted in Triton X-100 (0.3%) in PBS. Then, slices were washed for 30 min by immersion in PBS and incubated with Hoechst 33258 for 15 min at room temperature. Finally, slices were extensively rinsed with PBS and mounted with p-phenylendiamine-glycerol (0.1%) in PBS for immunofluorescence.

2.7 CB_1 **receptor** *immunofluorescence in fixed tissue*

To label CB_1 receptors, the primary rabbit antiserum against the CB_1 receptor, PA1-743, (Affinity BioReagents, CO, USA) was diluted [1:500] in TBS (0.1 M Tris, 0.15 M NaCl, pH 7.4) containing 0.5% milk powder. Fixed 10 µm coronal slices from aCSF and 192IgG-saporin-infused rats were air dried for 20 min and washed by immersion in PBS for 15 min at room temperature. Then, the slices were blocked with 5% NGS in TBS buffer for 2 h at room temperature before being incubated with the primary antibody overnight at 4ºC. The tyramide signal amplification method was used to amplify the signal associated with the CB_1 receptor antiserum. Briefly, slices were washed for 30 min in TNT buffer (0.05% Tween 20 in TBS, pH 7.4) and blocked in TNB solution (10 ml TNT buffer, 0.05 g blocking reagent, DuPont) for 1 h at room temperature. Later, the slices were incubated with horse radish peroxidase-conjugated goat anti-rabbit secondary antibody (1:150; Perkin Elmer, MA, USA) for 1 h followed by tyramide-fluorescein-based amplification (1:100, Perkin Elmer, MA, USA) process in complete darkness for 10 min at room temperature. Slices were extensively rinsed in TBS.

2.8 Double immunofluorescence studies

To study the cellular localization of CB_1 receptors on glutamatergic or GABAergic neurons, primary guinea pig monoclonal antiserum against vesicular glutamate transporter type 3 (VGLUT3) (1:500) and mouse monoclonal anti-glutamic acid decarboxylase (GAD-65) (1:750) (EMD Millipore, CA, USA) were used respectively following the CB_1 receptor immune-detection. Primary antibodies were diluted in PBS (0.1 M, pH 7.4) containing 0.5% BSA and two consecutive 10 µm slices were incubated overnight at 4ºC. Slices were washed for 30 min in PBS and incubated with secondary Alexa-Fluor 555 donkey anti-guinea pig [1:250] or Alexa-Fluor 555 donkey anti-mouse [1:250] for 30 min at 37ºC. Then, slices were washed for 30 min at room temperature by immersion in PBS and incubated with Hoechst 33258 [$1:10^6$] for

15 min at room temperature. Finally, slices were washed for 15 min by immersion in PBS and mounted with p-phenylendiamine-glycerol (0.1%) for immunofluorescence.

2.9 Quantitative analyses of BFCN and AChE positive fibers

200-fold magnification photomicrographs from aCSF (n = 19) and SAP (n = 21) rats were acquired by using an Axioskop 2 Plus microscope (Zeiss) equipped with a CCD imaging camera (SPOT Flex Shifting Pixel). Cholinergic neurons of NBM were counted independently by two observers at three different stereotaxic levels (-1.08 mm, -1.56 mm and -2.04 mm anteroposterior from Bregma) and the total number of BFCN (N) in the whole image was obtained. The population of BFCN was expressed as N/mm^3. 200-fold magnification $P75^{NTR}$ immunofluorescence images were used to study BFCN density in the NBM. The quantification of $P75^{NTR}$ positive cells was conducted in the same manner as that performed for the AChE stained samples described above.

AChE stained slices were scanned at 600 ppi and AChE positive fiber density was quantified using Image J software (NIH, Bethesda, MD, USA). The images were converted to 8-bit grey-scale mode. This software defines the OD of an anatomical area and the background from 0 (white) to 255 (black). Background or non-specific staining values were substracted from AChE positive signal to obtain the net AChE OD in each area.

2.10 Semiquantitative analyses of GAD65 immunoreactivity

200-fold magnification photomicrographs from aCSF (n = 5) and SAP (n = 5) samples were acquired by using an Axioskop 2 Plus microscope (Carl Zeiss) equipped with a CCD imaging camera (SPOT Flex Shifting Pixel). All the images were acquired at the same brain coordinates with the same illumination and exposure time and contrasted to the same level. The GAD65 immunoreactivity was measured as arbitrary units (AU) of optical density (OD) by using Image J software (NIH, Bethesda, MD, USA). We applied the same brightness and contrast to all images, and mean intensity values were defined by the software in the selected equivalent areas from both hemispheres in all the animals. The average value from both hemispheres was calculated for each animal.

2.11 [^{3}H]CP55,940 autoradiography

Fresh 20 µm brain slices from each animal in aCSF (n = 8) and SAP (n = 8) groups were dried and submerged in 50 mM Tris-HCl buffer containing 1% of BSA (pH 7.4) for 30 min at room temperature, followed by incubation in the same buffer, but in the presence of the CB_1/CB_2 receptor radioligand, [^{3}H]CP55,940 (3 nM) for 2 h at 37ºC. Nonspecific binding was measured by competition with non-labelled CP55,940 (10 µM) in another consecutive slice. The CB_1 receptor antagonist, SR141716A (0.1 µM) and the CB_2 receptor antagonist, SR144528 (0.1

μM), were used together with [^{3}H]CP55,940 in two consecutive slices to check the CB_1 or CB_2 receptor binding specificity. Then, slices were washed in ice-cold (4ºC) 50 mM Tris-HCl buffer supplemented with 1% BSA (pH 7.4) to stop the binding, dipped in distilled ice-cold water and dried (4ºC). Autoradiograms were generated by exposure of the tissues for 21 days at 4ºC to β-radiation sensitive films and [^{3}H]-microscales were used to calibrate the optical densities to fmol/mg tissue equivalent (fmol/mg).

2.12 [^{35}S]GTPγS autoradiography

The functional coupling of cannabinoid receptors to $G_{i/o}$ proteins was performed as follows: fresh frozen 20 μm slices from each animal in aCSF (n = 9) and SAP (n = 11) groups were dried, followed by two consecutive incubations in HEPES-based buffer (50 mM HEPES, 100 mM NaCl, 3 mM $MgCl_2$, 0.2 mM EGTA and 0.5% BSA, pH 7.4) for 30 min at 30ºC. Then, slices were incubated for 2 h at 30ºC in the same buffer supplemented with 2 mM GDP, 1 mM DTT, adenosine deaminase (3-Units/l) and 0.04 nM [^{35}S]GTPγS. The [^{35}S]GTPγS basal binding was determined in two consecutive slices in the absence of the agonist. The agonist-stimulated binding was determined in the same reaction buffer in the presence of the CB_1/CB_2 receptor agonist, WIN55,212-2 (10 μM). The CB_1 receptor antagonist, SR141716A (0.1 μM), was used together with WIN55,212-2 (10 μM) in one consecutive slice to check the CB_1 receptor specific activation. Nonspecific binding was defined by competition with GTPγS (10 μM) in another section. Then, slices were washed twice in cold (4ºC) 50 mM HEPES buffer (pH 7.4) and dried. Finally, the slides were exposed to β-radiation-sensitive autoradiography films with a set of [^{14}C] standards (nCi/g tissue equivalent) to calibrate the images (gray densities) in hermetically closed cassettes. Autoradiograms were generated by exposing the tissue for 48 h with [^{14}C]-microscales, which were used as calibration standards. Then, they were scanned and quantified and the percentages of WIN55,212-2-evoked stimulations were calculated according to the following formula: ([^{35}S]GTPγS agonist-stimulated binding x 100/[^{35}S]GTPγS basal binding) - 100.

2.13 Statistical analyses

The step through latency was represented as Kaplan-Meier survival curves and for comparisons between groups the Log-rank test was used. The acquisition latency, BFCN density, percentages of agonist-evoked [^{35}S]GTPγS stimulation, [^{3}H]CP55,940 density and GAD65 OD were statistically analyzed using the two-tailed unpaired Student *t* test. Correlations between different neurochemical data were examined by linear regression analysis and the Pearson´s correlation coefficient was calculated. The statistical significance threshold was set at $p < 0.05$.

3. Results

3.1 Learning and memory impairment after basal forebrain cholinergic lesion

AChE enzymatic assay was used to stain BFCN somas and cholinergic fibers in the projecting areas, while $P75^{NTR}$ immunofluorescence assay was directed at the same target as that of the immunotoxin used (192IgG-saporin) and stained the somatodendritic compartment of BFCN. The intraparenchymal injection of 192IgG-saporin in the NBM resulted in an extensive reduction of AChE staining (1032 ± 50 cells/mm^3 in aCSF group and 270 ± 23 cells/mm^3 in SAP group; $p < 0.0001$) and $P75^{NTR}$ immunoreactive (973 ± 53 cells/mm^3 and 226 ± 25 cells/mm^3 in aCSF, and SAP group respectively; $p < 0.0001$) BFCN (Figs. 1A and B). The greatest loss of cholinergic afferents was observed in the motor (60%), somatosensory (65%) and entorhinal (40%) cortices ($p < 0.001$ vs aCSF). The linear regression analysis confirmed that a relationship exists between fewer BFCN and lower AChE fiber density in cortical areas, including the entorhinal cortex ($R^2 = 0.5536$, $p < 0.001$). There was a more modest loss of cholinergic fibers in other cortical areas such as the cingulate (20%) and piriform (15%) ($p < 0.05$ vs aCSF) and in CA3 (10%) and dentate gyrus (15%) in the hippocampus ($p < 0.05$ vs aCSF) (data not shown).

To examine learning and memory, the animals were trained and tested using the passive avoidance test. Seven days after the surgical procedure we evaluated the acquisition latency (the time that rats stayed in the open compartment) before being subjected to an aversive stimulus on entering the dark, closed compartment. No differences were observed for acquisition latency between the two groups (10.5 ± 1.7 sec and 9.78 ± 1.6 sec; aCSF and SAP, respectively) (Figure 1C). 24 h later, rats were again tested to evaluate the step through latency which was measured and represented as Kaplan-Meier survival curves to determine the estimated probability of a positive response (i.e. to reach the cut-off time). When the groups were compared, 88% of the aCSF-treated rats remembered the aversive stimulus and displayed a positive response. However, only 26% of the rats treated with 192IgG-saporin remembered the aversive stimulus ($p = 0.029$; Log-Rank/Mantel-Cox test) (Figure 1D). The median latency, i.e. the time that 50% of the animals took to cross the doorway, was 28.4 sec for 192IgG-saporin-treated rats.

Figure 1

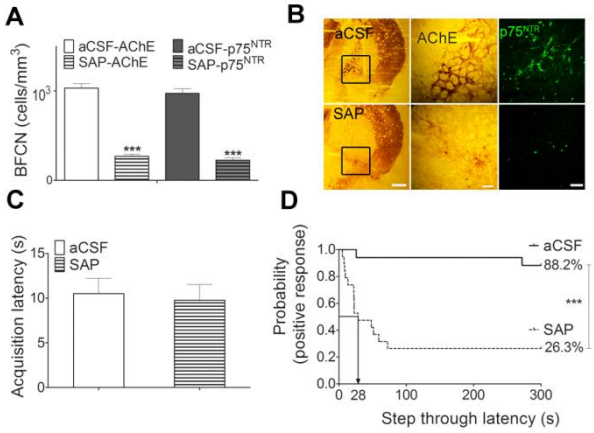

3.2 CB_1 receptor density after basal forebrain cholinergic lesion

In this study we analyzed both the density and activity of CB_1 cannabinoid receptors by using autoradiography. The rats treated with 192IgG-saporin showed no changes in [^{3}H]CP55,940 binding in the cortical areas studied, but we found an increase in [^{3}H]CP55,940 binding in the NBM (180 ± 13 fmol/mg and 364 ± 63 fmol/mg in aCSF and SAP-treated rats, respectively, $p < 0.05$) and decreases in some hippocampal subregions (oriens CA1: aCSF 1057 ± 67 fmol/mg and SAP 721 ± 92 fmol/mg, $p < 0.05$; molecular dentate gyrus: aCSF 900 ± 63 fmol/mg and SAP 603 ± 71 fmol/mg, $p < 0.01$) (Figure 2B, Table 1). CP55,940 shows high affinity for both CB_1 and CB_2 receptors. Therefore, using two different cannabinoid antagonists we checked the CB_1 receptor specificity of the results. SR141716A, a CB_1 receptor antagonist, completely blocked the binding of [^{3}H]CP55,940 (Figure 2C) while SR144528, a CB_2 receptor antagonist, failed to do so (Figure 2D), providing evidence that the changes in [^{3}H]CP55,940 binding are specifically related to CB_1 receptors.

Figure 2.

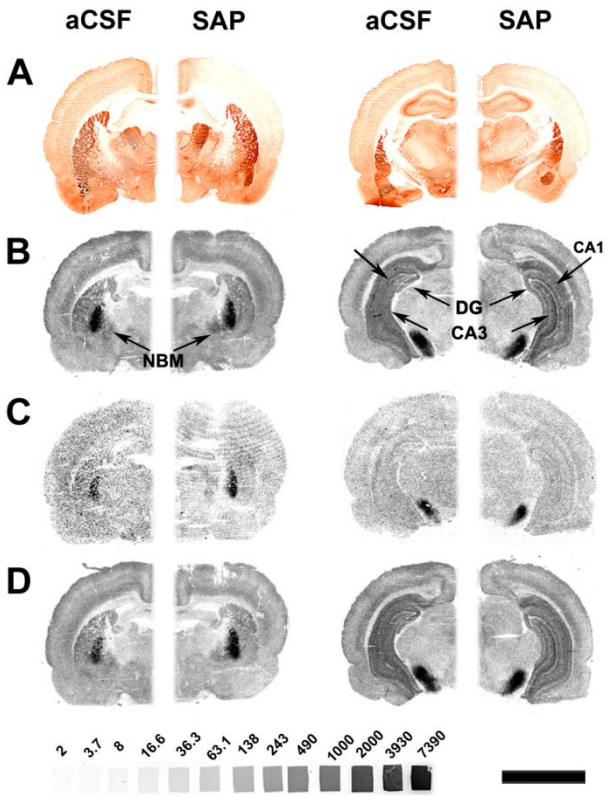

3.3 Endocannabinoid signaling deregulation in areas of cholinergic innervation

To study whether the changes in receptor density are reflected by CB_1 receptor activity mediated by $G_{i/o}$ protein signaling, we used the [^{35}S]GTPγS functional autoradiography technique. Basal binding values were similar in the two groups (aCSF and SAP) in all of the brain areas analyzed (Tables 2-3, Figure 3 A and C). The anatomical analysis of [^{35}S]GTPγS binding induced by the CB_1 receptor agonist, WIN55,212-2, revealed changes in the functional coupling of cannabinoid receptors to $G_{i/o}$ proteins. Thus, the stimulation of [^{35}S]GTPγS binding was enhanced in several cortical regions (entorhinal: aCSF 156 ± 17% vs SAP 277 ± 30%, $p < 0.01$; motor: aCSF 127 ± 20% vs SAP 203 ± 14%, $p < 0.05$; piriform: aCSF 72 ± 10% vs SAP 122 ± 9%, $p < 0.001$; somatosensory: aCSF 131 ± 29% vs SAP 218 ± 11%, $p < 0.05$), and was more evident in the inner layers, such as the layer VI of the entorhinal cortex (Table 2, Figure 3 B and D).

Also, in the striatum (aCSF 178 ± 28% vs SAP 252 ± 19%, $p < 0.05$) and in the NBM (aCSF 103 ± 18% vs SAP 142 ± 9%, $p < 0.05$) there was an increase in WIN55,212-2-induced functional coupling of CB_1 receptors to $G_{i/o}$ proteins (Table 3). However, in the hippocampus and, in accordance with the results related to CB_1 receptor density, we found a decrease in the activity in the molecular layer of dentate gyrus (aCSF 299 ± 37% vs SAP 166 ± 25%, $p < 0.05$) (Figure 3B, Table 3). SR141716A almost completely blocked WIN55,212-2-evoked binding of

[^{35}S]GTPγS which indicates that the changes in eCB signaling were due to CB_1 receptor-specific changes.

Figure 3.

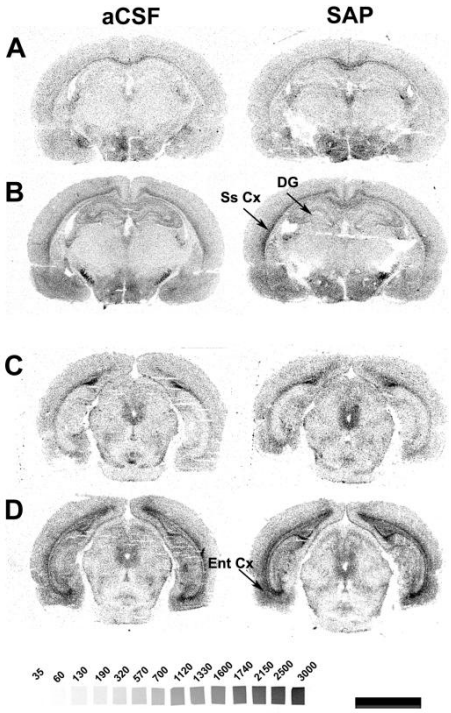

3.4 Linear regression analysis between CB_1 receptor changes and the number of surviving BFCN

To examine the relation between the results of the autoradiographic assays and BFCN density, firstly we correlated [^{3}H]CP55,940 binding (fmol/mg) with the number of cholinergic neurons in the NBM by using regression analyses. These analyses showed that 40% in NBM ($p = 0.011$), 29% in dentate gyrus ($p = 0.047$) and 36% in CA1 ($p = 0.018$) of the variation in the density of CB_1 receptors could in some way be attributable to the loss of BFCN. The lower the BFCN density, the higher the CB_1 receptor density in NBM and the lower in hippocampus, showing a different modulation depending on the brain area studied (Figure 4A). Then, we correlated the number of BFCN with CB_1 receptor activity, and similar results were obtained. Thus, the regression models showed that 39% in NBM ($p = 0.007$), 63% in striatum ($p = 0.0002$) and 40% in dentate gyrus ($p = 0.009$) of the variation in the functional coupling of cannabinoid receptors to $G_{i/o}$ proteins might be related to the loss of BFCN (Figure 4B). When we analyzed the entire cortical mantle we found the lower the number of BFCN, the higher the CB_1 receptor activity. The regression models showed that 28% in motor ($p = 0.02$), 40% in somatosensory ($p = 0.0025$), 24% in entorhinal ($p = 0.0349$) and 43% in piriform cortices ($p =$

0.002) of the increase in the CB_1 receptor activity could be related to the basal forebrain cholinergic lesion (Figure 4C).

Figure 4.

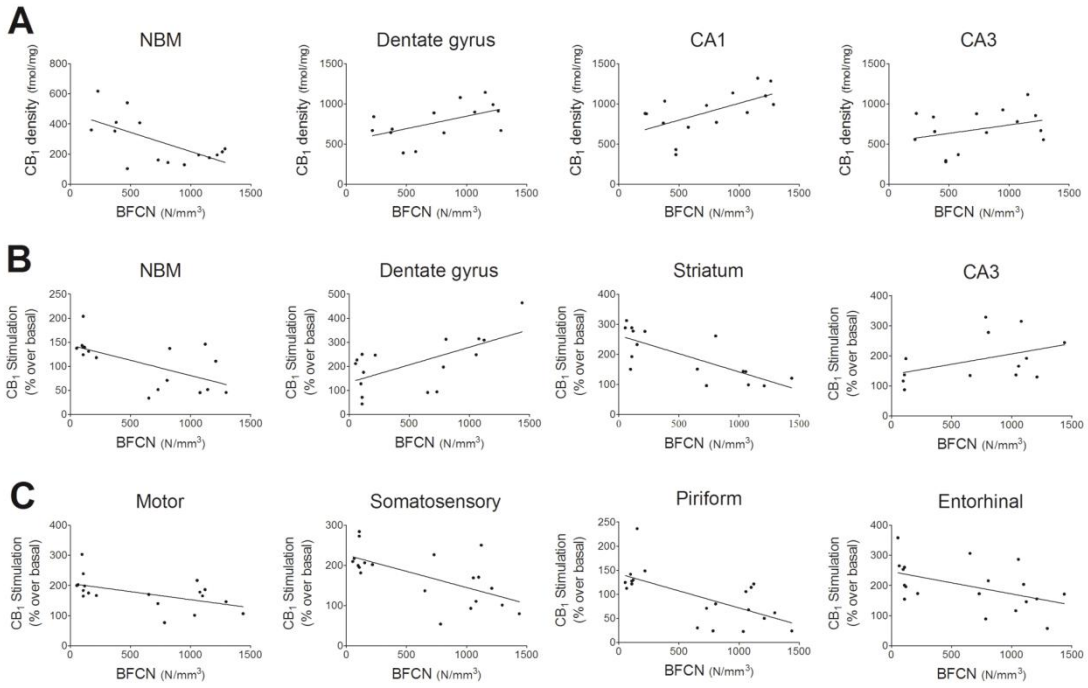

3.5 Localization of CB_1 receptor and GAD65 by immunofluorescence

The subcellular localization of CB_1 receptors was determined by immunofluorescence studies using an antiserum against the C-terminus of the human CB_1 receptor. The regional distribution pattern of immunostaining was similar to that observed in the autoradiographic studies. Some areas exhibited very high CB_1 receptor expression, such as the olfactory bulb, globus pallidus, substantia nigra, amygdala and hippocampus. The different hippocampal layers exhibited differential CB_1 receptor-immunostaining patterns and were clearly defined. We studied the co-localization of CB_1 receptors with GAD65, the smaller isoform of the enzyme glutamate decarboxylase, which is mainly associated with nerve terminals (Kash et al., 1999), and with VGLUT3, the third subtype of glutamate vesicular transporter, mainly expressed in synaptic boutons, but also in somatodendritic compartments (Herzog et al., 2004). The abundant and dense CB_1 receptor immunoreactive puncta observed suggested a predominant localization of CB_1 receptors in presynaptic terminals with similar densities in both groups of animals. Immunofluorescence assays for GAD65 and VGLUT3 and the subsequent co-localization studies allowed us to confirm the inhibitory nature of presynaptic boutons which express CB_1 receptors in the hippocampus (Figure 5A). Although GAD65 and VGLUT3 had different patterns of distribution, no differences in the immunostaining pattern were observed between

the two groups studied and therefore, the immunofluorescent images shown in figure 5 correspond to rats treated with 192IgG-saporin, in which GAD65 immunoreactivity was lower than in the aCSF-treated rats. Thus, GAD65 immunoreactivity was seen as a dense plexus of immunoreactive puncta around the pyramidal neurons and had a similar distribution to CB_1 receptors (Figure 5Ai), while VGLUT3 displayed a postsynaptic somatodendritic immunostaining (Figure 5Aii). The studies of co-localization that were performed in the Z-axis with a 0.24-µm resolution by using structured illumination revealed an optimal penetration of the antibody in the tissue. The presence of CB_1 receptors in presynaptic GABAergic terminals, with a high degree of co-immunoreactivity with GAD65 was observed (Figure 5Ai-YZ/XZ). CB_1 receptor immunostaining was found surrounding the VGLUT3-expressing somatodendritic compartment and a Z-stack analysis revealed the almost total absence of co-immunoreactivity with VGLUT3 **(**Figure 5Aii-YZ/XZ).

However, in the cortex, CB_1 receptors were not clearly located in either presynaptic GABAergic or postsynaptic glutamatergic compartments (Figure 5B). GAD65 was distributed presynaptically (Figure 5Bi), while VGLUT3 displayed a somatodendritic distribution (Figure 5Bii). Z-stack analysis revealed a similar distribution of CB_1 receptors and GAD65, but with a very low degree of co-immunoreactivity (Figure 5Bi-YZ/XZ). A higher co-expression with VGLUT3 was observed, despite the different cellular distribution (Figure 5Bii-YZ/XZ).

GAD65 immunofluorescence showed a different pattern of distribution in different cortical layers, with the highest density being in layer IV, as shown for motor cortex (Figure 6A). There was a large decrease in GAD65 positive cortical terminals in those animals lesioned with 192IgG-saporin, suggesting a down-regulation. Semiquantitative analysis in the motor cortex showed a reduction of 28%, 35% and 39% of GAD65 immunoreactivity in layers I, II-III and IV, respectively ($p < 0.05$) (Figure 6B). The somatosensory and piriform cortices were also analyzed and a similar decrease in immunosignaling was found, 28%, 32% and 32% in layers I, II-III ($p < 0.01$) and IV ($p < 0.05$) in the somatosensory cortex and 25% in the piriform cortex ($p < 0.05$) (Figure 6B). One of the most significant decreases in GAD65 immunoreactivity was registered in layer V of the entorhinal cortex (21% decrease, $p < 0.01$), but GAD65 immunoreactivity was not modified in the dentate gyrus of the hippocampus (2% decrease).

Figures 5 and 6.

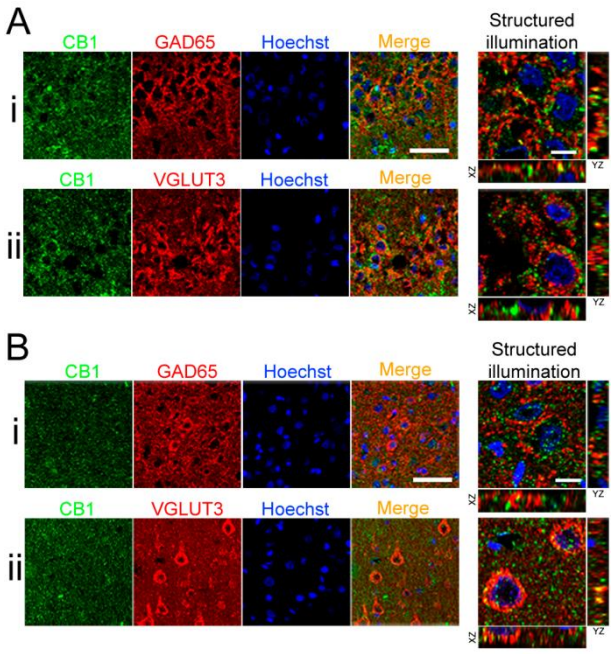

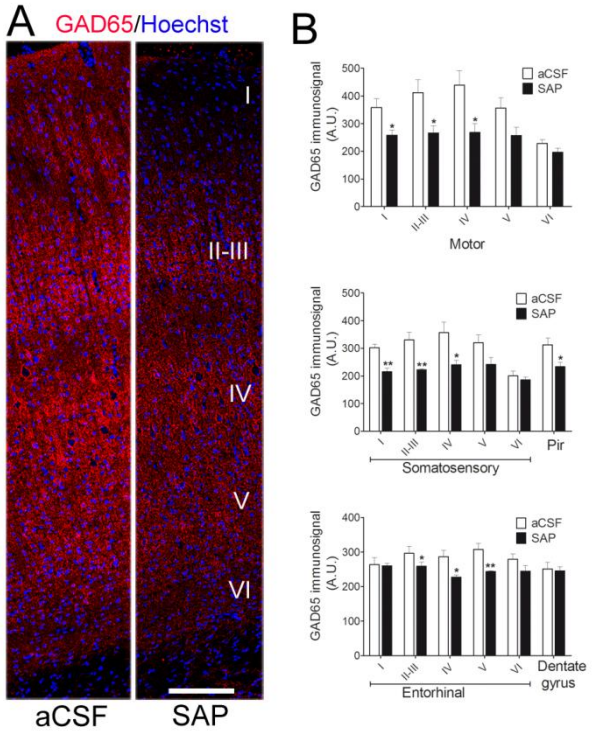

4. **Discussion**

The rat model of cholinergic dysfunction of the basal forebrain pathway to cortical and subcortical brain areas by the infusion of 192IgG-saporin in the NBM described in the present study shows a significant loss of BFCN. This specific lesion leads to cognitive impairment related to learning and memory of an aversive stimulus. The CB_1 receptor-mediated eCB signaling is modulated in the NBM and in cortical projections, which might be related to the loss of the inhibitory tone, as observed by a marked decrease in the expression of presynaptic GAD65.

4.1 192IgG-saporin infusion in the NBM impairs learning and memory

Eight days after the intraparenchymal infusion of 192IgG-saporin, at least three-quarters of BFCN had disappeared which led to memory impairment, as demonstrated by the results of the passive avoidance test. However, controversial data have been reported depending on the severity of the lesion, the dose of immunotoxin given, the stereotaxic coordinates, the needle used or the passive avoidance test conditions (see review from Myhrer, 2003). Thus, a previous study demonstrated that 50% of BFCN depletion in the NBM was not sufficient to impair memory five weeks after surgery (Wenk et al., 1994). However, our results are consistent with other studies reporting small but significant deficits associated with the NBM lesion (Torres et al., 1994). Due to the presence of censored data (cut-off time for step through latency times of 300s), Kaplan-Meier survival curves and Log-rank analysis were used to compare the behavioral responses. Based on previous reports (Barreda-Gómez et al., 2015), the statistical analysis of data carried out in the present study is the best available to analyze this type of test and represents an alternative for the right interpretation of the data. Memory evaluation under the present experimental conditions is not enough to confirm if cognitive impairment is related to acquisition, consolidation, extinction or retrieval of aversive information, but present findings provide evidence of a pivotal contribution of the cortical cholinergic denervation to learning and memory deficits. The influence of other neurotransmitter systems has been studied using the passive avoidance test. Thus, dopaminergic antagonists either impair (Lazarova-Bakarova et al., 1991; Doyle and Regan, 1993) or improve (Chugh et al., 1991) passive avoidance performance, while glutamatergic and GABAergic antagonists typically impair it (Venable and Kelly, 1990; Anglade et al., 1994), all of which suggests the involvement of multiple neurotransmission systems in cognition. In this context, the eCB system modulates the release of glutamate and GABA (Katona et al., 2001) and regulates a range of physiological processes including learning and memory (Busquets-García et al., 2011).

4.2 Endocannabinoid signaling is modulated after BFCN depletion

The present model involving BFCN depletion provides a suitable scenario in which to further our understanding of the interaction of cholinergic neurotransmission with the eCB system. The presence of CB_1 receptors in BFCN was previously established by using immunohistochemical methods. Some authors suggest that rodent BFCN are devoid of these receptors, but all basal forebrain cholinergic cells contain eCB-degrading enzymes and have a fine CB_1 receptor positive fiber meshwork surrounding the perikarya, suggesting that BFCN may utilize eCB for retrograde control of neurotransmission (Harkany et al., 2003; 2005). However, light and electron microscopy studies reported a dense labeling of CB_1 receptors in ChAT-immunoreactive neurons in monkey basal forebrain (Lu et al., 1999) and the existence of differentiated areas in the basal forebrain cholinergic system of the rat, some of them expressing CB_1 receptors (Nyíri et al., 2005).

The present autoradiographic studies revealed an increase in both density and activity of CB_1 receptors in the NBM of lesioned rats. If BFCN expresses somatodendritic CB_1 receptors, one would expect a decrease, but the results are consistent with those obtained by Harkany et al. (2003) which describe the presence of CB_1 receptors in the fiber meshwork surrounding the perikarya, but not in BFCN membranes.

The observed decrease in eCB signaling (CB_1 receptor activity) in discrete areas of the hippocampus could be a direct consequence of cholinergic denervation, but NBM mainly projects to the cortex. Immunofluorescence studies suggest an inhibitory nature of the CB_1 receptor containing GAD65 positive terminals in the hippocampus in which CB_1 receptors are mainly expressed in GABAergic interneurons (Katona et al., 1999; Tsou et al., 1999). However, further studies demonstrated that CB_1 receptors are also present in hippocampal glutamatergic synapses, albeit at much lower levels (Katona et al., 2006; Kawamura et al., 2006). In this context, despite the reported negative effects of cannabimimetics on memory in humans, the literature fails to provide strong evidence for hippocampal CB_1 receptor-mediated action (see review from Davies et al., 2002). The decrease in CB_1 receptors in the hippocampus of BFCN-lesioned rats is moderate and located mainly in GABAergic presynaptic terminals. Transgenic mice with enhanced GABAergic inhibition exhibit impairment in both hippocampal long-term potentiation (LTP) and Morris water maze performance (Gong et al., 2009). Learning deficits in these mice or in wild-type mice treated with Δ9-THC were reversed by $GABA_A$ receptor antagonists (Varvel et al., 2005; Cui et al., 2008). Thus, the decrease in eCB signaling observed in certain hippocampal regions, leading to enhanced GABAergic inhibition, may be related to the BFCN depletion-induced cognitive impairment. CB_1 receptor-mediated signaling is also affected in the hippocampus of patients diagnosed with severe AD (Manuel et al., 2014). The present animal model shows a great reduction in BFCN, which partially mimics the final Braak's stages (V-VI) of the disease described in patients who suffer a serious degeneration of

the basal forebrain cholinergic pathway which innervates the hippocampus through the entorhinal cortex (Ikonomovic et al., 2003).

The dramatic reduction of cortical cholinergic projections observed by AChE staining in rats with a lesion in BFCN, was not represented by a similar decrease in [^{3}H]CP55,940 binding in any of the different regions of brain cortex. These results are in agreement with previous studies which reported that cortical cholinergic terminals lack any detectable CB_1 receptors (Harkany et al., 2003). However, the hyperactivity of cortical CB_1 receptors that we found in BFCN lesioned-animals was similar to that described in human brain at early stages of AD. Therefore, we further explored the different regulation of CB_1 receptors in hippocampus and cortex at the subcellular level by carrying out immunofluorescence studies (see next section). CB_1 receptors are involved in the regulation of cortical glutamatergic input; CB_1 receptor agonists inhibit, while the antagonist SR141716A enhances cortical glutamatergic synaptic transmission and favors LTP (Auclair et al., 2000). CB_1 receptor–dependent activation is thought to be an early step in a protective cascade against kainic acid-induced excitotoxicity (Marsicano et al., 2003), and a CB_1 receptor-mediated decrease in TNF□-induced expression of AMPA receptors protects against excitotoxic neuroinflammation (Zhao et al., 2010). In addition, previous studies using a similar lesion in basal forebrain observed that there was a marked reduction of NMDA, □$_2$-and □-adrenoceptors and 5-HT_{2A} receptors, while AMPA, kainate and $GABA_A$ receptors were up-regulated and accompanied by a decrease in high-affinity choline uptake sites in cortical regions (Roβner et al., 1994, 1995; Schliebs et al., 1994; Heider et al., 1997). In summary, the 192IgG-saporin-induced lesion in the NBM leads to an irreversible loss of cholinergic innervation in almost the entire cortical mantle, sufficient to lead to an excess of excitatory neurotransmission that may be controlled by the observed activation of the CB_1 receptors present in cortical areas.

4.3 Cortical GABAergic dysfunction after BFCN lesion

Endocannabinoids act as retrograde synaptic messengers on presynaptic terminals and modulate the release of different neurotransmitters through the activation of CB_1 receptors (Katona et al., 2001; Ohno-Shosaku et al., 2001). Previous studies reported that almost all CB_1 receptor-positive cortical cells also express cholecystokinin and GAD65, confirming the existence of an inhibitory phenotype of CB_1 receptor containing terminals (Marsicano and Lutz, 1999). Although, the present immunofluorescence studies did not establish the precise anatomical location of CB_1 receptors in GABAergic or glutamatergic compartments, in the rat model of BFCN lesion we were able to measure a marked down-regulation of GAD65 immunoreactivity in most of the cortical areas. These results suggest that the degeneration of cortical cholinergic terminals triggers a deregulation of GABAergic neurotransmission and clearly demonstrate that BFCN terminals are devoid of CB_1 receptors. A partial loss of BFCN

induced by 192IgG-saporin was sufficient to decrease the levels of GAD65/67 and increase glutamate transporters in the prefrontal and cingulate cortices (Jeong et al., 2011; 2016). Moreover, deep brain stimulation of the remaining BFCN in the NBM improved spatial memory performance and partially restored GAD65/67 and glutamate to control levels (Lee et al., 2016). Recovery of the cortical GABAergic tone has been postulated as potentially therapeutic in AD patients (see review in Lanctôt et al., 2004). In summary, the present findings demonstrate that a 192IgG-saporin-induced BFCN lesion impairs learning and memory, activates cortical eCB signaling and provokes a significant decrease in cortical GABAergic tone.

5. Conclusions

BFCN not only represent the main source of cortical acetylcholine, but one may also speculate that they contribute to the inhibitory tone in cortical projections, and the loss of these neurons leads to a deregulation of excitatory neurotransmission which probably explains the hyperactivation of cortical CB_1 receptors located on excitatory terminals. We propose a CB_1 receptor-mediated regulation of the eCB tone as a compensatory mechanism with which to regulate a possible BFCN death-evoked glutamatergic-GABAergic imbalance, in order to maintain the control of cortical neurotransmission. The understanding of the underlying mechanisms of this regulation, could lead to the discovery of cannabinoid-based pharmacological approaches towards the treatment of common pathological features of different neurological diseases affecting neuronal survival.

6. References

Anglade, F., Bizot, J.C., Dodd, R.H., Baudoin, C., & Chapouthier, G. (1994). Opposite effects of cholinergic agents and benzodiazepine receptor ligands in a passive avoidance task in rats. *Neuroscience Letters*, 182(2):247-250.

Auclair, N., Otani, S., Soubrie, P., & Crepel, F. (2000). Cannabinoids modulate synaptic strength and plasticity at glutamatergic synapses of rat prefrontal cortex pyramidal neurons. *Journal of Neurophysiology*, 83(6):3287-3293.

Barreda-Gómez, G., Lombardero, L., Giralt, M.T., Manuel, I., & Rodríguez-Puertas, R. (2015). Effects of galanin subchronic treatment on memory and muscarinic receptors. *Neuroscience*, 293:23-34.

Bartus, R.T., Dean, R.L., Beer, B., & Lippa, A.S. (1982). The cholinergic hypothesis of geriatric memory dysfunction. Science, 217(4558):408-414.

Benito, C., Núñez, E., Tolón, R.M., Carrier, E.J., Rábano, A., Hillard, C.J., & Romero, J. (2003). Cannabinoid CB2 receptors and fatty acid amide hydrolase are selectively overexpressed in neuritic plaque-associated glia in Alzheimer's disease brains. *Journal of Neuroscience*, 23(35):11136-11141.

Busquets-Garcia, A., Puighermanal, E., Pastor, A., de la Torre, R., Maldonado, R., & Ozaita, A. (2011). Differential role of anandamide and 2-arachidonoylglycerol in memory and anxiety-like responses. *Biological Psychiatry*, 70(5):479-486.

Chugh, Y., Saha, N., Sankaranarayanan, A., & Sharma, P.L. (1991). Possible mechanism of haloperidol-induced enhancement of memory retrieval. *Methods and Findings in Experimental and Clinical Pharmacology*, 13(3):161-164.

Cui, Y., Costa, R.M., Murphy, G.G., Elgersma, Y., Zhu, Y., Gutmann, D.H., Parada, L.F., Mody, I., & Silva, A.J. (2008). Neurofibromin regulation of ERK signaling modulates GABA release and learning. *Cell*, 135(3):549-560.

Cummings, J., Lai, T.J., Hemrungrojn, S., Mohandas, E., Yun Kim, S., Nair, G., & Dash, A. (2016). Role of Donepezil in the Management of Neuropsychiatric Symptoms in Alzheimer's Disease and Dementia with Lewy Bodies. *CNS Neuroscience & Therapeutics*,1-8.

D'Addario, C., Di Francesco, A., Arosio, B., Gussago, C., Dell'Osso, B., Bari, M., Galimberti, D., Scarpini, E., Altamura, A.C., Mari, D., & Maccarrone, M. (2012). Epigenetic regulation of fatty acid amide hydrolase in Alzheimer disease. *PLoS One*, 7(6):e39186.

Davies, P. (1979). Neurotransmitter-related enzymes in senile dementia of the Alzheimer type. *Brain Research*, 171(2):319-327.

Davies, P., & Maloney, A.J. (1976). Selective loss of central cholinergic neurons in Alzheimer's disease. *Lancet*, 2(8000):1403.

Davies, S.N., Pertwee, R.G., & Riedel, G. (2002). Functions of cannabinoid receptors in the hippocampus. *Neuropharmacology*, 42(8):993-1007.

Doyle, E., & Regan, C.M. (1993). Cholinergic and dopaminergic agents which inhibit a passive avoidance response attenuate the paradigm-specific increases in NCAM sialylation state. *Journal of neural transmission. General section*, 92(1):33-49.

Gifford, A.N., Bruneus, M., Gatley, S.J., & Volkow, N.D. (2000). Cannabinoid receptor-mediated inhibition of acetylcholine release from hippocampal and cortical synaptosomes. *British Journal of Pharmacology*, 131(3):645-650.

Gong, N., Li, Y., Cai, G.Q., Niu, R.F., Fang, Q., Wu, K., Chen, Z., Lin, L.N., Xu, L., Fei, J., & Xu, T.L. (2009). GABA transporter-1 activity modulates hippocampal theta oscillation and theta burst stimulation-induced long-term potentiation. *Journal of Neuroscience*, 29(50):15836-15845.

Harkany, T., Härtig, W., Berghuis, P., Dobszay, M.B., Zilberter, Y., Edwards, R.H., Mackie, K., & Ernfors, P. (2003). Complementary distribution of type 1 cannabinoid receptors and vesicular glutamate transporter 3 in basal forebrain suggests input-specific retrograde signalling by cholinergic neurons. *European Journal of Neuroscience*, 18(7):1979-1992.

Harkany, T., Dobszay, M.B., Cayetanot, F., Härtig, W., Siegemund, T., Aujard, F., & Mackie, K. (2005). Redistribution of CB1 cannabinoid receptors during evolution of cholinergic basal forebrain territories and their cortical projection areas: a comparison between the gray mouse lemur (Microcebus murinus, primates) and rat. *Neuroscience*, 135(2):595-609.

Heider, M., Schliebs, R., Roβner, S., & Bigl, V. (1997). Basal forebrain cholinergic immunolesion by 192IgG-saporin: evidence for a presynaptic location of subpopulations of alpha 2- and beta-adrenergic as well as 5-HT2A receptors on cortical cholinergic terminals. *Neurochemical Research*, 22(8):957-966.

Herzog, E., Gilchrist, J., Gras, C., Muzerelle, A., Ravassard, P., Giros, B., Gaspar, P., & El Mestikawy, S. (2004). Localization of VGLUT3, the vesicular glutamate transporter type 3, in the rat brain. *Neuroscience*, 123(4):983-1002.

Ikonomovic, M.D., Mufson, E.J., Wuu, J., Cochran, E.J., Bennett, D.A., & DeKosky, ST. (2003). Cholinergic plasticity in hippocampus of individuals with mild cognitive impairment: correlation with Alzheimer's neuropathology. *Journal of Alzheimer's Disease*, 1:39-48.

Jeong da, U., Oh, J.H., Lee, J.E., Lee, J., Cho, Z.H., Chang, J.W., & Chang, W.S. (2016). Basal Forebrain Cholinergic Deficits Reduce Glucose Metabolism and Function of Cholinergic and GABAergic Systems in the Cingulate Cortex. *Yonsei Medical Journal*, 57(1):165-172.

Jeong, D.U., Chang, W.S., Hwang, Y.S., Lee, D., & Chang, J.W. (2011). Decrease of GABAergic markers and arc protein expression in the frontal cortex by intraventricular 192 IgG-saporin. *Dementia and Geriatric Cognitive Disorders*, 32(1):70-78.

Karnovsky, M.J., & Roots, L. (1964). A "direct-coloring" thiocholine method for cholinesterases. *Journal of Histochemistry & Cytochemistry*, 12:219-221.

Kash, S.F., Tecott, L.H., Hodge, C., & Baekkeskov, S. (1999). Increased anxiety and altered responses to anxiolytics in mice deficient in the 65-kDa isoform of glutamic acid decarboxylase. *Proceedings of the National Academy of Sciences of the United States of America*, 96:1698–1703.

Kathmann, M., Weber, B., Zimmer, A., & Schlicker, E. (2001). Enhanced acetylcholine release in the hippocampus of cannabinoid CB(1) receptor-deficient mice. *British Journal of Pharmacology*, 132(6):1169-1173.

Katona, I., Sperlágh, B., Sík, A., Käfalvi, A., Vizi, E.S., Mackie, K., & Freund, T.F. (1999). Presynaptically located CB1 cannabinoid receptors regulate GABA release from axon terminals of specific hippocampal interneurons. *Journal of Neuroscience*, 19(11):4544-4558.

Katona, I., Rancz, E.A., Acsady, L., Ledent, C., Mackie, K., Hajos, N., & Freund, T.F. (2001). Distribution of CB1 cannabinoid receptors in the amygdala and their role in the control of GABAergic transmission. *Journal of Neuroscience*, 21(23):9506-9518.

Katona, I., Urbán, G.M., Wallace, M., Ledent, C., Jung, K.M., Piomelli, D., Mackie, K., & Freund, T.F. (2006). Molecular composition of the endocannabinoid system at glutamatergic synapses. *Journal of Neuroscience*, 26(21):5628-5637.

Kawamura, Y., Fukaya, M., Maejima, T., Yoshida, T., Miura, E., Watanabe, M., Ohno-Shosaku, T., & Kano, M. (2006). The CB1 cannabinoid receptor is the major cannabinoid receptor at excitatory presynaptic sites in the hippocampus and cerebellum. *Journal of Neuroscience*, 26(11):2991-3001.

Kim, J., Isokawa, M., Ledent, C., & Alger, B.E. (2002). Activation of muscarinic acetylcholine receptors enhances the release of endogenous cannabinoids in the hippocampus. *Journal of Neuroscience*, 22(23):10182-10191.

Lanctôt, K.L., Herrmann, N., Mazzotta, P., Khan, L.R., & Ingber, N. (2004). GABAergic function in Alzheimer's disease: evidence for dysfunction and potential as a therapeutic target for the treatment of behavioural and psychological symptoms of dementia. *Canadian Journal of Psychiatry*, 49(7):439-53.

Lazarova-Bakarova, M.B., Petkova, B.P., Todorov, I.K., & Petkov, V.D. (1991). Memory impairment induced by combined disturbance of noradrenergic and dopaminergic

neurotransmissions: effects of nootropic drugs. *Acta Physiologica et Pharmacologica Bulgarica*, 17(1):29-34.

Lee, J.E., Jeong da, U., Lee, J., Chang, W.S., & Chang, J.W. (2016). The effect of nucleus basalis magnocellularis deep brain stimulation on memory function in a rat model of dementia. *BMC Neurology*, 12:16:26.

Lu, X.R., Ong, W.Y., & Mackie, K. (1999). A light and electron microscopic study of the CB1 cannabinoid receptor in monkey basal forebrain. *Journal of Neurocytology*, 28(12):1045-1051.

Manuel, I., González de San Román, E., Giralt, M.T., Ferrer, I., & Rodríguez-Puertas, R. (2014). Type-1 cannabinoid receptor activity during Alzheimer's disease progression. *Journal of Alzheimers Disease*, 42(3):761-766.

Marsicano, G., Goodenough, S., Monory, K., Hermann, H., Eder, M., Cannich, A., Azad, S.C., Cascio, M.G., Gutiérrez, S.O., van der Stelt, M., López-Rodriguez, M.L., Casanova, E., Schütz, G., Zieglgänsberger, W., Di Marzo, V., Behl, C., & Lutz, B. (2003). CB1cannabinoid receptors and on-demand defense against excitotoxicity. *Science*, 302:84-88.

Marsicano, G., & Lutz, B. (1999). Expression of the cannabinoid receptor CB1 in distinct neuronal subpopulations in the adult mouse forebrain. *European Journal of Neuroscience*, 11(12):4213-4225.

Mulder, J., Zilberter, M., Pasquaré, S.J., Alpár, A., Schulte, G., Ferreira, S.G., Köfalvi, A., Martín-Moreno, A.M., Keimpema, E., Tanila, H., Watanabe, M., Mackie, K., Hortobágyi, T., de Ceballos, M.L., & Harkany, T. (2011). Molecular reorganization of endocannabinoid signalling in Alzheimer's disease. *Brain*, 134(Pt 4):1041-1060.

Myhrer, T. (2003). Neurotransmitter systems involved in learning and memory in the rat: a meta-analysis based on studies of four behavioral tasks. *Brain Research Reviews*, 41(2-3):268-287.

Nyíri, G., Szabadits, E., Cserép, C., Mackie, K., Shigemoto, R., & Freund, T.F. (2005). GABAB and CB1 cannabinoid receptor expression identifies two types of septal cholinergic neurons. *European Journal of Neuroscience*, 21(11):3034-3042.

Ohno-Shosaku, T., Maejima, T., & Kano, M. (2001). Endogenous cannabinoids mediate retrograde signals from depolarized postsynaptic neurons to presynaptic terminals. *Neuron*, 29(3):729-738.

Pascual, A.C., Martín-Moreno, A.M., Giusto, N.M., de Ceballos, M.L., & Pasquaré, S.J. (2014). *Experimental Gerontology*, 60:92-99.

Paxinos, G., & Watson, C. (2005). The Rat Brain in Stereotaxic Coordinates, 5th Edn San Diego, Elsevier Academic Press.

Perry, E., Walker, M., Grace, J., & Perry, R. (1999). Acetylcholine in mind: a neurotransmitter correlate of consciousness? *Trends in Neurosciences*, 22(6):273-280.

Perry, E.K., Gibson, P.H., Blessed, G., Perry, R.H., & Tomlinson, B.E. (1977). Neurotransmitter enzyme abnormalities in senile dementia. Choline acetyltransferase and glutamic acid decarboxylase activities in necropsy brain tissue. Journal of the Neurological Sciences, 34(2):247-265.

Revuelta, A.V., Cheney, D.L., Costa, E., Lander, N., & Mechoulam, R. (1980). Reduction of hippocampal acetylcholine turnover in rats treated with (-)-delta 8-tetrahydrocannabinol and its 1',2'-dimethyl-heptyl homolog. *Brain Research*, 195(2):445-452.

Rodríguez-Puertas, R., Pascual, J., Vilaró, T., & Pazos, A. (1997). Synapse, 26(4):341-350.

Roβner, S., Schliebs, R. & Bigl, V. (1994). Ibotenic acid lesions of nucleus basalis magnocellularis differentially affects cholinergic, glutamatergic and GABAergic markers in cortical rat brain regions. *Brain Research*, 668:85-99.

Roβner, S., Schliebs, R., & Bigl, V. (1995). 192IgG-saporin-induced immunotoxic lesions of cholinergic basal forebrain system differentially affect glutamatergic and GABAergic markers in cortical rat brain regions. *Brain Research*, 696(1-2):165-176.

Schliebs, R., Feist, T., Roβner, S. & Bigl, V. (1994). Receptor function in cortical rat brain regions after lesion of the nucleus basalis. *Journal of Neural Transmission*, 44:195-208.

Stella, N., & Piomelli, D. (2001). Receptor-dependent formation of endogenous cannabinoids in cortical neurons. *European Journal of Pharmacology*, 17;425(3):189-196.

Torres, E.M., Perry, T.A., Blockland, A., Wilkinson, L.S., Wiley, R.G., Lappi, D.A., & Dunnet, S.B. (1994). Behavioural, histochemical and biochemical consequences of selective immunolesions in discrete regions of the basal forebrain cholinergic system. *Neuroscience*, 63(1):95-122.

Tsou, K., Mackie, K., Sañudo-Peña, M.C., & Walker, J.M. (1999). Cannabinoid CB1 receptors are localized primarily on cholecystokinin-containing GABAergic interneurons in the rat hippocampal formation. *Neuroscience*, 93(3):969-975.

Tulving, E. (2002). Episodic memory: from mind to brain. *Annual Review of Psychology*, 53:1-25.

Tzavara, E.T., Wade, M., & Nomikos, G.G. (2003). *Journal of Neuroscience*, 23(28):9374-9384.

Varvel, S.A., Anum, E., Niyuhire, F., Wise, L.E., & Lichtman, A.H. (2005). Delta(9)-THC-induced cognitive deficits in mice are reversed by the GABA(A) antagonist bicuculline. *Psychopharmacology (Berl)*, 178(2-3):317-327.

Venable, N., & Kelly, P.H. (1990). Effects of NMDA receptor antagonists on passive avoidance learning and retrieval in rats and mice. *Psychopharmacology (Berl)*, 100(2):215-221.

Wenk, G.L., Stoehr, J.D., Quintana, G., Mobley, S., & Wiley, R.G. (1994). Behavioral, biochemical, histological, and electrophysiological effects of 192 IgG-saporin injections into the basal forebrain of rats. *Journal of Neuroscience*, 14(10):5986-5995.

Westlake, T.M., Howlett, A.C., Bonner, T.I., Matsuda, L.A., & Herkenham, M. (1994). Cannabinoid receptor binding and messenger RNA expression in human brain: an in vitro receptor autoradiography and in situ hybridization histochemistry study of normal aged and Alzheimer's brains. *Neuroscience*, 63(3):637-652.

Whitehouse, P.J., Price, D.L., Struble, R.G., Clark, A.W., Coyle, J.T., & Delon, M.R. (1982). Alzheimer's disease and senile dementia: loss of neurons in the basal forebrain. *Science*, 215(4537):1237-1239.

Zhao, P., Leonoudakis, D., Abood, M.E., & Beattie, E.C. (2010). Cannabinoid receptor activation reduces TNFalpha-induced surface localization of AMPAR-type glutamate receptors and excitotoxicity. *Neuropharmacology*, 58(2):551-558.

7. Acknowledgements:

This work was supported by the Departments of Economic Development (Elkartek KK-2016/00045) and Education (IT975-16) of the Basque Government. Technical and human support was provided by General Research Services SGIker from The University of the Basque Country (UPV/EHU), co-financed by the Ministry of Economy and Competitiveness (MINECO) of the Spanish Government, European Regional Development Fund (ERDF) and the European Social Fund (ESF). A. LL. is the recipient of a fellowship from the Basque Government (BFI 2012-119). The authors declare no conflict of interest.

Table 1. Autoradiographic CB_1 densities for the specific binding of [^{3}H]CP55,940 in different brain regions from vehicle (aCSF) and 192IgG-saporin treated rats.

	Specific binding of [^{3}H]CP55,940 (fmol/mg t.e.)	
Brain region	**aCSF**	**SAP**
Cerebral cortex		
Cingulate	223 ± 27	202 ± 21
Motor	211 ± 25	197 ± 20
Somatosensory	164 ± 21	149 ± 16
Piriform	87 ± 8	112 ± 13
Perirhinal	131 ± 22	104 ± 16
Ectorhinal	155 ± 15	128 ± 26
Entorhinal	114 ± 26	96 ± 12
Diencephalon		
NBM	180 ± 13	364 ± 63*****
Rhinencephalon		
Lat.Olfact. Tract	190 ± 28	137 ± 18
Mesencephalon		
Substantia nigra	3068 ± 218	2633 ± 177
Basal ganglia		
Globus pallidus	2878 ± 264	2756 ± 303
Striatum	456 ± 33	518 ± 75
Telencephalon		
Amygdaloid nuclei		
Anterior	126 ± 13	127 ± 6
Basolateral	102 ± 15	96 ± 19
Central	146 ± 18	138 ± 10
Lateral	109 ± 15	98 ± 23
Medial	62 ± 16	55 ± 14
Hippocampus		
CA1		
Oriens	1057 ± 67	721 ± 92*****
Pyramidal	583 ± 56	340 ± 44
Radiatum	520 ± 26	384 ± 52
CA3		
Oriens	800 ± 64	550 ± 94
Pyramidal	408 ± 40	300 ± 56
Radiatum	537 ± 44	376 ± 67
Dentate gyrus		
Molecular	900 ± 63	603 ± 71******
Polymorphic	454 ± 49	305 ± 48
Granular	72 ± 18	96 ± 20
Lac. Moleculare	605 ± 42	436 ± 79
Ventral subiculum	300 ± 37	248 ± 26

Data are mean ± S.E.M values from 8 rats in each group.

*****$p < 0.05$, ****** $p < 0.01$ when compared to aCSF.

Table 2. [^{35}S]GTPγS basal binding and WIN55,212-2-induced binding (10 µM) in different cortical regions, rhinencephalon, rhomboencephalon and mesencephalon from vehicle (aCSF) and 192IgG-saporin treated animals.

	Basal binding (nCi/g t.e.)		**WIN55.212-2 stimulation (% over basal)**	
Brain region	aCSF	SAP	**aCSF**	**SAP**
Cerebral cortex				
Cingulate				
Layer I-III	351 ± 15	331 ± 20	**97 ± 22**	**120 ± 17**
Layer IV-V	395 ± 22	399 ± 22	**104 ± 25**	**116 ± 19**
Layer VI	548 ± 29	578 ± 37	**187 ± 30**	**176 ± 19**
Ectorhinal				
Layer I-III	306 ± 16	316 ± 17	**122 ± 31**	**113 ± 14**
Layer IV-V	352 ± 22	374 ± 22	**108 ± 25**	**157 ± 15**
Layer VI	386 ± 29	455 ± 22	**209 ± 36**	**195 ± 19**
Entorhinal				
Layer I-III	300 ± 25	337 ± 19	**174 ± 28**	**169 ± 20**
Layer IV-V	394 ± 26	470 ± 32	**162 ± 24**	**164 ± 14**
Layer VI	515 ± 35	531 ± 40	**156 ± 17**	**277 ± 30****
Motor				
Layer I-III	399 ± 24	386 ± 33	**71 ± 14**	**122 ± 13***
Layer IV-V	407 ± 17	420 ± 23	**110 ± 25**	**119 ± 7**
Layer VI	535 ± 33	521 ± 27	**127 ± 20**	**203 ± 14***
Perirhinal				
Layer I-III	276 ± 23	289 ± 16	**119 ± 23**	**189 ± 17**
Layer IV-V	352 ± 21	357 ± 21	**155 ± 36**	**167 ± 25**
Layer VI	388 ± 21	444 ± 25	**151 ± 24**	**218 ± 12***
Somatosensory				
Layer I-III	380 ± 23	414 ± 34	**74 ± 20**	**68 ± 11**
Layer IV-V	436 ± 30	460 ± 30	**118 ± 23**	**128 ± 7**
Layer VI	495 ± 37	512 ± 34	**131 ± 29**	**218 ± 11***
Piriform	458 ± 29	457 ± 30	**72 ± 10**	**122 ± 9****
Rhinencephalon				
Lat.Olfact. Tract nucleus	359 ± 40	364 ± 38	**55 ± 10**	**128 ± 13***
Rhomboencephalon				
Dorsal raphe	636 ± 72	665 ± 62	**59 ± 8**	**82 ± 6**
Locus coeruleus	254 ± 21	263 ± 40	**32 ± 7**	**44 ± 15**
Mesencephalon				
Periaqueductal gray	484 ± 44	503 ± 31	**69 ± 12**	**94 ± 11**
Substantia nigra	382 ± 31	463 ± 21	**835 ± 145**	**744 ± 97**

Data are mean ± S.E.M values from 9 aCSF-treated and 11 SAP-treated rats.

*$p < 0.05$, **$p < 0.01$ when compared to aCSF.

Table 3. [^{35}S]GTPγS basal binding and WIN55,212-2-induced binding (10 µM) in telencephalon and diencephalon from vehicle (aCSF) and 192IgG-saporin treated animals.

	Basal binding (nCi/g t.e.)		**WIN55.212-2 stimulation (% over basal)**	
Brain region	aCSF	SAP	**aCSF**	**SAP**
Telencephalon				
Amygdaloid nuclei				
Anterior	416 ± 50	460 ± 30	**110 ± 18**	**99 ± 12**
Basolateral	395 ± 28	457 ± 36	**223 ± 24**	**150 ± 8**
Central	586 ± 52	649 ± 53	**100 ± 19**	**92 ± 4**
Lateral	359 ± 36	442 ± 30	**157 ± 24**	**150 ± 12**
Medial	512 ± 61	636 ± 69	**116 ± 20**	**50 ± 6***
Hippocampus				
CA1				
Oriens	308 ± 27	332 ± 26	**106 ± 19**	**99 ± 17**
Pyramidal	266 ± 29	264 ± 20	**155 ± 14**	**159 ± 22**
Radiatum	384 ± 36	418 ± 28	**150 ± 28**	**178 ± 30**
CA3				
Oriens	372 ± 45	377 ± 19	**223 ± 28**	**110 ± 20**
Pyramidal	272 ± 34	241 ± 23	**198 ± 52**	**233 ± 53**
Radiatum	254 ± 25	269 ± 21	**219 ± 38**	**181 ± 28**
Dentate gyrus				
Molecular	324 ± 42	387 ± 20	**299 ± 37**	**166 ± 25***
Polymorphic	194 ± 38	200 ± 20	**168 ± 29**	**211 ± 39**
Granular	216 ± 32	204 ± 20	**122 ± 30**	**116 ± 21**
Basal ganglia				
Globus pallidus	442 ± 31	456 ± 39	**986 ± 131**	**874 ± 126**
Striatum	368 ± 25	352 ± 16	**178 ± 28**	**252 ± 19***
Diencephalon				
NBM	496 ± 57	547 ± 34	**103 ± 18**	**142 ± 9***
Horiz. diagonal band	327 ± 36	320 ± 20	**91 ± 18**	**114 ± 21**
Vertic. diagonal band	341 ± 27	393 ± 24	**145 ± 27**	**119 ± 15**
Medial septum	309 ± 27	320 ± 21	**111 ± 23**	**114 ± 18**

Data are mean ± S.E.M values from 9 aCSF-treated and 11 SAP-treated rats.

*$p < 0.05$ when compared to aCSF.

Legends

Figure 1. (A) Number of BFCN in the NBM of aCSF (n = 17) and SAP (n = 19) treated animals, quantified as AChE labelled cells and P75 ^{NTR} immunoreactive neurons. (B) AChE enzymatic staining and P75^{NTR} immunostaining in the NBM. *** $p < 0.001$ vs aCSF. Scale bars = 500 (left) and 100 µm (center and right). (C) Acquisition latency times in the learning trial of the passive avoidance test. Data are means ± SEM. (D) Step through latency times of the passive avoidance test represented as Kaplan-Meier survival curves ($p < 0.0001$ vs aCSF, log-rank test).

Figure 2. (A) AChE staining in representative fixed hemibrain slices at two different levels (right and left columns) from aCSF and SAP-treated rats. (B) [^{3}H]CP55,940 (3 nM) binding in hemibrain coronal slices from aCSF and SAP-treated rats. (C) The specificity of the binding was determined by blocking the radioligand binding in the presence of the specific CB_1 receptor antagonist, SR141716A (0.1 µM) (D) The specific CB_2 antagonist SR144528 (0.1 µM) was not able to inhibit the [^{3}H]CP55,940 (3 nM) binding to rat brain slices (D). DG: dentate gyrus; CA3: layer CA3 of hippocampus. Bottom, [^{3}H] standards (µCi/g tissue equivalent), tissue scale bar: 5 mm.

Figure 3. Representative autoradiograms including both dorsal (A, B) and ventral hippocampus (C, D) obtained from aCSF and SAP-treated rats that show [^{35}S]GTPγS basal binding (A and C) and WIN55,212-2 (10 µM) evoked activation of cannabinoid receptors (B and D). DG: dentate gyrus; Ss cx: somatosensory cortex; Ent cx: entorhinal cortex. Bottom, [^{14}C] standards (nCi/g tissue equivalent), tissue scale bar: 5 mm.

Figure 4. (A) The plots show the number of cholinergic neurons in the NBM (Number of cells/mm^3) and the density of CB_1 receptors (fmol/mg) from aCSF (n = 8) and SAP (n = 8) treated rats in different brain areas. The regression analyses reveal a decrease in the density of CB_1 receptor directly related to the depletion of BFCN in the dentate gyrus ($R^2 = 0.29$; $p = 0.047$) and CA1 ($R^2 = 0.36$; $p = 0.018$) and an increase in the NBM ($R^2 = 0.40$; $p = 0.011$). (B and C) The plots show the number of cholinergic neurons in the NBM and WIN55,212-2 (10 µM) evoked stimulation of CB_1 receptors (% activity over basal) from aCSF (n = 9) and SAP (n = 11) treated rats in different brain areas. (B) The regression analyses reveal a hyperactivity of CB_1 receptors in the NBM ($R^2 = 0.38$; $p = 0.007$) and in the striatum ($R^2 = 0.63$; $p = 0.0002$) and a decrease in the dentate gyrus ($R^2 = 0.4$; $p = 0.0089$) directly related to the loss of BFCN. (C) The regression analyses reveal a hyperactivity of CB_1 receptors in cortical areas: motor ($R^2 = 0.28$; $p = 0.0202$), somatosensory ($R^2 = 0.41$; $p = 0.0025$), entorhinal ($R^2 = 0.24$; $p = 0.0349$) and piriform ($R^2 = 0.43$; $p = 0.0018$) cortices, directly related to the depletion of BFCN.

Figure 5. Immunostaining in a representative section from a 192IgG-saporin treated rat. Immunoreactivity for CB_1 receptors in dentate gyrus (A) and in motor cortex (B), in combination with GAD65 (i) or VGLUT3 (ii). Nuclei were also stained with Hoechst. In merge images, note the CB_1 receptor co-localization in dentate gyrus with GAD65 and in cortex with VGLUT3. Triple labeling of tissue slices is shown at 200-fold magnification (merge) and at 630-fold magnification (structured illumination) in a single plane from the collecting Z-stacking. Scale bar = 50 µm and 10 µm, respectively.

Figure 6. (A) Immunoreactivity for GAD65 in the motor cortex (layers I-VI) from a aCSF and a 192IgG-saporin treated rat. (B) Note the differences in optical density of GAD65 positive presynaptic terminals in aCSF (n = 5) and SAP (n = 5) treated rats, measured as arbitrary units (A.U.) of fluorescence in motor, somatosensory and entorhinal cortical layers, and also in the total area of the piriform cortex and dentate gyrus. Data are means ± SEM; *$p < 0.05$; **$p < 0.01$. Scale bar = 150 µm.

IV

Relationship of the Cannabinoid and Muscarinic Signaling with cognitive Impairments in 3xTg-AD Mice at the Onset of Alzheimer's Disease

Alberto Llorente-Ovejero[1], Iván Manuel[1], Laura Lombardero[1], Maria Teresa Giralt[1], Catherine Ledent[2], Lydia Giménez-Llort[3], Rafael Rodríguez-Puertas[1]

[1]Department of Pharmacology, Faculty of Medicine and Nursing, University of the Basque Country (UPV/EHU), Bº Sarriena s/n, 48940 Leioa, Spain.

[2]Institut de Recherche Interdisciplinaire en Biologie Humaine et Moléculaire, Université Libre de Bruxelles, Brussels B-1070, Belgium.

[3]Department of Psychiatry and Forensic Medicine, Institut de Neurociències, Universitat Autònoma de Barcelona, 08193 Bellaterra, Spain.

---

*Corresponding author

Rafael Rodríguez-Puertas

Department of Pharmacology, Faculty of Medicine and Nursing.

University of the Basque Country. E-48940 Leioa, Vizcaya, Spain.

Tel.: +34-94-6012739; fax: +34-94-6013220.

E-mail address: rafael.rodriguez@ehu.es

Running title: **Cannabinoid and Muscarinic Signaling in 3xTg-AD Mice**

Abstract

Alzheimer's disease is characterized by a progressive decline in memory associated with selective impairment of cholinergic neurotransmission. Recently, the endocannabinoid system, which modulates emotional learning and memory through CB_1 receptors, has also been found to be deregulated. In the present study, we used the 3xTg-AD mice model harboring familial AD mutations and tau_{P301L} human transgene to identify the functional interplay of endocannabinoid and muscarinic signaling, and their cognitive behavioral correlates at the onset of disease by the passive avoidance test. Neurochemical correlates were studied with both receptor and functional autoradiography for CB_1 and muscarinic receptors simultaneously analyzed in consecutive tissue slices and regulations at the cellular level were depicted by immunofluorescence analysis. 3xTg-AD mice exhibited increased acquisition latencies and impaired memory retention compared to age-matched non-transgenic mice at the onset of disease. Neurochemical analyses showed changes in the CB_1 receptor density and functional coupling of CB_1 and muscarinic receptors to $G_{i/o}$ proteins in several brain areas, including the basolateral amygdala. Subchronic stimulation of the endocannabinoid system following repeated WIN55,212-2 (1 mg/kg) or JZL184 (8 mg/kg) administration induced a CB_1 receptor desensitization, normalizing acquisition latencies to control levels. However, cannabinoid-induced modulation of cholinergic neurotransmission in limbic areas did not significantly modify learning and memory. The CB_1 receptor-mediated decrease in the GABAergic tone in the basolateral amygdala may be controlling the limbic component of learning and memory in 3xTg-AD mice. The CB_1 receptor desensitization may be a plausible strategy to restore behavior alterations associated with genetic risk factors for developing AD.

Keywords: Alzheimer, 3xTg-AD, cholinergic, endocannabinoid, learning and memory, basolateral amygdala, autoradiography.

Abbreviations and chemical compounds

2-AG: 2-arachidonoylglycerol; 3xTg-AD: Triple transgenic mice model; Aβ: β-Amyloid; AD: Alzheimer´s disease; BLA: Basolateral amygdala; CB_1 receptor: Type-1 cannabinoid receptors; $CB_1^{-/-}$: CB_1 receptor knockout mice; eCB: Endocannabinoid; GAD65: Glutamic acid decarboxylase isoform 65kDa; GTPγS: Guanosine-5´-O-3-thiotriphosphate; mAChR: Muscarinic acetylcholine receptor; M_2 mAChR: Subtype-2 muscarinic receptor; MAGL: Monoacylglycerol lipase; Non-Tg: Non transgenic mice, VGLUT3: Vesicular glutamate transporter type 3.

R-(+)-[2,3-Dihydro-5-methyl-3-[(morpholinyl)methyl]pyrrolo[1,2,3-de]-1,4-benzoxazinyl]-(1-naphthalenyl)methanone mesylate: **WIN55,212-2***; (-)-cis-3-[2-Hydroxy-4-(1,1-dimethylheptyl)phenyl]-trans-4-(3-hydroxypropyl) cyclohexanol:* **CP55,940;** (2-Carbamoyloxyethyl) trimethylammonium chloride: **carbachol;** *4-Nitrophenyl4-(dibenzo[d][1,3]dioxol-5-yl(hydroxy)methyl)piperidine-1-carboxylate*:**JZL184;** *(Piperidin-1-yl)-5-(4-chlorophenyl)-1-(2,4-dichlorophenyl)-4-methyl-1Hpyrazole-3-carboxamide hydrochloride*: **SR141716A;** *5-(4-chloro-3-methylphenyl)-1-[(4-methylphenyl)methyl]-N-[(1S,2S,4R)-1,3,3-trimethylbicyclo[2.2.1]hept-2-yl]1pyrazole3-carboxamide*: **SR144528**

1. Introduction

Alzheimer's disease (AD), the most common cause of dementia in the elderly, is characterized by a progressive impairment of memory and thinking skills. Furthermore, 60-90% of AD patients develop neuropsychiatric symptoms including agitation, psychosis, depression, apathy, disinhibition or anxiety, which are dependent on the cholinergic deficit described in AD (Cummings and Back, 1998; Cummings et al., 2016). The cholinergic neurotransmission that controls learning and memory is specifically vulnerable in AD (Davies and Maloney, 1976; Perry et al., 1978; Bartus et al., 1982; Whitehouse et al., 1982; Rodríguez-Puertas et al., 1994, 1997). Impaired functionality of muscarinic receptors (mAChR) is found in areas that control cognitive processes, such as the amygdala and the hippocampus (Rodríguez-Puertas et al., 1997). The deregulation of neuromodulators further contributes to the alteration of cognitive and emotional processes and final outcomes. This is the case of the endocannabinoid (eCB) system, which modulates emotional learning and memory (Busquets-Garcia et al., 2011). The eCB system is deregulated in AD patients. Thus, a reduction of type-1 of cannabinoid receptors (CB_1) in different layers of the hippocampus is described at advanced Braak stages of the disease (Westlake et al., 1994), while an increase in CB_1 receptor activity and density is found at early and moderated stages of AD (Manuel et al., 2014). Endogenous and exogenous cannabinoids seem to elicit modulatory effects in multiple AD-related processes, although the biochemical mechanisms need to be further investigated. Therefore, eCB system is foreseen as a novel potential therapeutic target to counteract the disease (Bedse et al., 2015).

At the translational level, hippocampal and cortical neuritic dystrophy has been reported in the triple-transgenic mice model of AD (3xTg-AD) (Perez et al., 2011) and impairment of mAChR in other AD models, in parallel with the progression of β-Amyloid (Aβ) plaque formation (Machová et al., 2008; Manuel et al., 2016). Also, altered CB_1 receptor expression has recently been described in the 3xTg-AD mice (Bedse et al., 2014; Manuel et al., 2016). These mice harbor APP_{Swe}, $PS1_{M146V}$, and tau_{P301L} transgenes and mimic several hallmarks of familial AD (Oddo et al., 2003). While Aβ and tau neuropathologies develop in middle age (12 months), deficits in synaptic plasticity and cognition have earlier onsets, when intraneuronal accumulation of oligomeric-Aβ, is clearly established at 6 months of age (Billings et al., 2005). So far, learning and memory deficits are apparent in several cognitive paradigms such as the passive avoidance, the novel-object recognition, and the Morris water maze (Giménez-Llort et al., 2007; Filali et al., 2012). Anxiety-like behaviors have also been shown in the

open-field, the elevated plus maze, and the dark/light box (Nelson et al., 2007; España et al., 2010; Rasool et al., 2013; Pietropaolo et al., 2014). Interestingly, in 6-month-old 3xTg-AD mice, the intraneuronal Aβ accumulation in the basolateral amygdala (BLA) has been shown to enhance innate and conditioned fear as assessed in fear conditioning paradigms (España et al., 2010).

In order to elucidate the functional interplay of cannabinoid and muscarinic signaling at the onset of AD and in relation to emotional learning and memory, we examined the expression, neuroanatomical distribution, and functional coupling of CB_1 receptor and mAChR to $G_{i/o}$ proteins in seven month-old 3xTg-AD mice and age-matched non-transgenic (Non-Tg) counterparts. Behavioral correlates were depicted in the step-through passive avoidance test. Finally, behavioral outcomes and cholinergic-endocannabinoid crosstalk following the direct and indirect subchronic eCB system activation were also investigated.

2. Materials and methods

2.1. Animals

Seven-month-old male 3xTg-AD and Non-Tg mice were obtained from Universitat Autonòma de Barcelona, in collaboration with Dr Lydia Giménez Llort. The 3xTg-AD mice harboring $PS1_{M146V}$, APP_{Swe}, and Tau_{P301L} transgenes were genetically engineered as previously described (Oddo et al., 2003). Also, nine-week-old male $CB_1^{-/-}$ and $CB_1^{+/+}$ mice were used, provided by C. Ledent of the University of Brussels.

All the animals were housed (4-5 animals per cage) and maintained under standard laboratory conditions of 12 hours light-dark cycle with light from 8 am to 8 pm and availability of food/water *ad libitum*. All procedures were performed in accordance with European Directive 2010/63/EU and the Spanish National Guidelines for Animal Experimentation and the Use of Genetically Modified Organisms (Real Decreto 1205/2005) and 178/2004; Ley 32/2007 and 9/2003). Experimental protocols were approved by the local Committee for Animal Research at the University of the Basque Country (CEIAB/21/2010/Rodríguez-Puertas).

2.2. Drugs and treatments

WIN55,212-2, CP55,940 and carbachol were acquired from Sigma-Aldrich (St Louis, MO, USA); JZL184 and SR144528 from Cayman-Chemicals (MI, USA) and SR141716A from Tocris (Bristol, UK). WIN55,212-2 and JZL-184 were administered intraperitoneally, once daily, in a volume of 5 ml/kg for seven consecutive days. Both cannabinoid compounds were dissolved in pure DMSO and diluted with Kolliphor EL (Sigma-Aldrich) and 0.9% saline to a final proportion of (1:1:18) respectively, as vehicle. Two independent sets of mice were randomly assigned to one of the following five groups (n = 9-10): [1]-Non-Tg-vehicle, [2]-3xTg-AD-vehicle, [3]-3xTg-AD-WIN55,212-2 (0.1 mg/kg), [4]-3xTg-AD-WIN55,212-2 (1 mg/kg) and [5]-3xTg-AD-JZL184 (8 mg/kg) (Figure 1).

2.3. Behavioral test

On the two days following the last dose, the behavioral effects of cannabinoid administration in the step-through passive avoidance were studied (PanLab, passive avoidance box LE872). During the acquisition session, the animals were placed in the open and illuminated compartment with heads facing the door, and then allowed to explore for 30 s. Then, the door was opened, allowing the mice to enter the dark compartment. The acquisition latency, with a cut-off time of 60 s, was recorded. When the animals crossed the door it was closed and a foot shock (0.4 mA/2 s) was delivered. Twenty-four hours later, during the retention session, the animals were

placed again into the illuminated chamber and allowed to explore for 30 s. Then, the door was opened and the step-through latency before entering the dark chamber, with a maximum cut-off time of 300 s, was recorded. No foot shock was delivered in the retention session.

2.4. Tissue preparation

For immunohistochemical studies, Non-Tg and 3xTg-AD mice (n = 3/group) were anesthetized with ketamine:xylazine (90:10 mg/kg), and transcardially perfused via the ascending aorta with 50 ml warm (37ºC), calcium-free Tyrode's solution (0.15 M NaCl, 5 mM KCl, 1.5 mM $MgCl_2$, 1 mM $MgSO_4$, 1.5 mM NaH_2PO_4, 5.5 mM Glucose, 25 mM $NaHCO_3$; pH 7.4), 0.5% heparinized, followed by 4% paraformaldehyde and 3% picric acid in 0.1M PB (4ºC) (100 ml/100 g b.w.). Brains were removed, post-fixed for 90 min at 4ºC, and cryoprotected in 20% phosphate buffer-sucrose solution overnight. The tissue was immersed in isopentane (-80ºC). 10 µm coronal slices were obtained in a cryostat, mounted onto gelatin-coated slides, and stored (-25ºC). The remaining brain samples from Non-Tg and 3xTg-AD mice (*n* = 7/group) and those from $CB_1^{-/-}$ and $CB_1^{+/+}$ mice (including spleen samples) were removed, fresh frozen, cut into 20 µm slices, mounted onto gelatin-coated slides and stored (-25ºC).

2.5. Radioligands and chemical reagents

[^{35}S]GTPγS (1250Ci/mmol) and [^{3}H]CP55,940 (131.8Ci/mmol) were purchased from PerkinElmer (Boston MA, USA). The [^{14}C] and [^{3}H]-microscales used as standards were purchased from American Radiolabelled Chemicals (Saint Louis, MO, USA). The β-radiation sensitive films were purchased from Carestream. Bovine Serum Albumine (BSA), DL-dithiothreitol (DTT), adenosine deaminase (ADD), guanosine-5´-diphosphate (GDP), and guanosine-5´-O-3-thiotriphosphate (GTPγS) were acquired from Sigma-Aldrich. Finally, all the compounds necessary for the preparation of the different buffers were of the highest quality commercially available.

2.6. Cannabinoid receptor autoradiography

Fresh slices from 3xTg-AD and Non-Tg mice (*n* = 6/group) and from $CB_1^{-/-}$ and $CB_1^{+/+}$ mice (including brain and spleen) were dried and submerged in 50 mM Tris-HCl buffer containing 1% of BSA (pH 7.4) for 30 min at room temperature, followed by incubation in the same buffer in the presence of the CB_1/CB_2 radioligand, [^{3}H]CP55,940 (3 nM) for 2 h at 37ºC. Nonspecific binding was measured by competition with non-labelled CP55,940 (10 µM) in another consecutive slice. The CB_1 receptor antagonist, SR141716A (0.1 µM) and the CB_2 receptor antagonist, SR144528 (0.1 µM), were used

together with [^{3}H]CP55,940 in two consecutive slices to check the CB_1 or CB_2 receptor binding specificity. Then, slices were washed in ice-cold (4ºC) 50 mM Tris-HCl buffer supplemented with 1% BSA (pH 7.4) to stop the binding, followed by dipping in distilled ice-cold water and drying (4ºC). Autoradiograms were generated by exposure of the tissues for 21 days at 4ºC to β-radiation sensitive film together with [^{3}H]-microscales used to calibrate the optical densities to fmol/mg tissue equivalent (fmol/mg t.e.).

2.7. Labeling of activated $G_{i/o}$ proteins by [^{35}S]GTPγS binding assay

Fresh slices (n = 7/group), were dried, followed by two consecutive incubations in HEPES-based buffer (50 mM HEPES, 100 mM NaCl, 3 mM $MgCl_2$, 0.2 mM EGTA and 0.5% BSA, pH 7.4) for 30 min at 30ºC. Briefly, slices were incubated for 2 h at 30ºC in the same buffer supplemented with 2 mM GDP, 1 mM DTT, ADD (3-Units/l), and 0.04 nM [^{35}S]GTPγS. The [^{35}S]GTPγS basal binding was determined in two consecutive slices in the absence of agonist. The agonist-stimulated binding was determined in the same reaction buffer in the presence of the CB_1/CB_2 receptor agonist, WIN55,212-2 (10 µM). Nonspecific binding was defined by competition with GTPγS (10 µM) in another section. Then, slices were washed twice in cold (4ºC) 50 mM HEPES buffer (pH 7.4), dried, and exposed to β-radiation sensitive film with a set of [^{14}C] standards.

A similar procedure was followed for mAChR in the presence of the non selective cholinergic agonist carbachol (100 µM).

After 48 h, the films were developed, scanned, and quantified by transforming optical densities into nCi/g tissue equivalence units using a calibration curve defined by the known values of the [^{14}C] standards (NIH-IMAGE, Bethesda, MD, USA). Nonspecific binding values were subtracted from both agonist-stimulated and basal-stimulated conditions. The percentages of agonist-evoked stimulation were calculated from both the net basal and net agonist-stimulated [^{35}S]GTPγS binding densities according to the following formula: ([^{35}S]GTPγS agonist-stimulated binding x 100/[^{35}S]GTPγS basal binding)-100.

2.8. Immunofluorescence

Fixed 10 µm coronal slices from Non-Tg and 3xTg-AD mice were air dried for 20 min and washed by immersion in PBS for 15 min at room temperature. Then, the slices were blocked with 5% normal goat serum in PBS buffer for 2 h at room temperature before being incubated with the primary antibody overnight at 4ºC.

To label CB_1 receptors, the primary rabbit antiserum against the CB_1 receptor, PA1-743, (Affinity BioReagents, CO, USA) was diluted [1:500] in TBS (0.1 M Tris, 0.15 M

NaCl, pH 7.4) containing 0.5% milk powder. The tyramide signal amplification method was used to amplify the signal associated with the CB_1 receptor antiserum. Briefly, slices were washed for 30 min in TNT buffer (0.05% Tween 20 in TBS, pH 7.4) and blocked in TNB solution (10 ml TNT buffer, 0.05 g blocking reagent, DuPont) for 1 h at room temperature. Later, the slices were incubated with horse radish peroxidase-conjugated goat anti-rabbit secondary antibody (Perkin Elmer, MA, USA) for 1 h followed by tyramide-fluorescein-based amplification (Perkin Elmer, MA, USA) process in complete darkness for 10 min at room temperature. Slices were extensively rinsed in TBS.

To label the subtype-2 muscarinic receptor (M_2 mAChR), rabbit anti- M_2 mAChR (EMD Millipore, CA, USA) was diluted in PBS (0.1 M, pH 7.4). Then, the primary antibody was revealed by incubation (30 min at 30ºC) with donkey anti-rabbit CY3. To study the cellular localization of CB_1 receptor and M_2 mAChR on glutamatergic or GABAergic neurons, tissue slices were incubated with primary guinea pig anti-vesicular glutamate transporter 3 (VGLUT3) and mouse anti-glutamic acid decarboxylase isoform 65kDa (GAD65) (EMD Millipore, CA, USA) diluted in PBS (0.1 M, pH 7.4), and revealed by incubation (30 min at 30ºC) with secondary Alexa488 or Alexa555 [1:250] donkey anti-guinea pig and FITC [1:80]**,** or Alexa 555 donkey anti-mouse. Then, slices were incubated with Hoechst [$1:10^6$] for 15 min, washed, and mounted with p-phenylendiamine-glycerol.

Slices were screened with an Axioskop microscope (Zeiss). 630-fold magnification images for colocalization were acquired on an Axioskop Observer A1 inverted microscope (Zeiss) by optical sectioning (0.24 µm/X-Y-Z-resolution) using structured illumination (ApoTome-Zeiss). Images were created with ZEN2014 software (Zeiss) and defined as signal being present without physical separation.

2.9. Statistical analysis

The two-tailed unpaired Student's *t*-test was used for differences between genotypes (Non-Tg *versus* 3xTg-AD) and one-way analysis of variance (ANOVA) for comparisons between treatments, followed by Bonferroni or Dunn's *post hoc* tests. The step-through latencies were represented as Kaplan-Meier survival curves, and for comparisons the nonparametric Log-rank/Mantel-Cox test was used which is appropriate when censored data must be analyzed, as explained in Barreda-Gómez et al., (2015). The existence of animals that reached the cut-off time of 300 s was the reason to choose this rigorous statistical analysis. Behavioral correlations with neurochemical data were analyzed with Pearson's correlation. Statistical significance was set at $p < 0.05$.

3. Results

3.1. Learning and memory impairment

3xTg-AD and Non-Tg mice clearly differed during the training and testing sessions on the passive avoidance test. 3xTg-AD mice took significantly longer to enter the dark compartment than Non-Tg mice ($p = 0.0002$, Student's *t*-test) (Figure 2A). Moreover, 40% of them failed to remember the foot shock as compared to the positive response shown in 100% of Non-Tg mice ($p = 0.029$, Log-Rank/Mantel-Cox test) (Figure 2B).

3.2. Deregulated endocannabinoid signaling

Quantitative densitometry showed increased density of CB_1 receptors (specific [^{3}H]CP55,940 binding sites) in the BLA of 3xTg-AD mice ($p = 0.0008$) and the lateral olfactory tract nucleus ($p = 0.0274$), but a decrease in the glomerular olfactory bulb ($p < 0.0001$; Student's *t*-test) (Figures 2 and 5) (Tables 1 and S1). SR141716A and SR144528, well-known selective antagonists for CB_1 and CB_2 receptors respectively, were used in combination with brain and spleen samples from $CB_1^{+/+}$ and $CB_1^{-/-}$ mice to check the specific subtype of cannabinoid receptor involved in the observed changes. SR141716A blocked [^{3}H]CP55,940 binding in brain slices from 3xTg-AD and $CB_1^{+/+}$ mice, but failed in spleen. SR144528 completely blocked [^{3}H]CP55,940 binding in spleen slices but failed in brain samples. $CB_1^{-/-}$ mice showed an almost completely absence of [^{3}H]CP55,940 binding in the brain, whereas displayed similar binding levels in the spleen to those obtained in $CB_1^{+/+}$ mice, demonstrating the selectivity of both antagonists and the specific deregulation of the CB_1 subtype in 3xTg-AD mice (Figure 3). [^{35}S]GTPγS autoradiography allows anatomically localizing and quantifying receptor-dependent $G_{i/o}$ protein activity directly in tissue. Basal activity was similar in the two genotypes. The activity of CB_1 receptors evoked by WIN55,212-2 (10 µM), was higher in the BLA of 3xTg-AD ($p = 0.0303$) but lower in several areas such as the striatum ($p = 0.0285$), the glomerular olfactory bulb ($p = 0.0043$), and the molecular layer of hippocampal dentate gyrus ($p = 0.0040$; Student's *t*-test) (Figure 4) (Tables 2 and S2).

3.3. Subchronic cannabinoid administration restores acquisition latencies

The subchronic administration of direct or indirect cannabinoid agonists in 3xTg-AD mice reduced the increase in acquisition latencies observed in the vehicle-treated 3xTg-AD group (one-way ANOVA, Dunn's multiple comparison test), restoring the latencies to Non-Tg levels (see Figure 2A). Thus, WIN55,212-2 elicited a behavioral

dose-response with slight (0.1 mg/kg, reduction 35%) and marked (1 mg/kg, reduction 50%, $p < 0.05$) reductions in acquisition latency as compared with those observed in the vehicle-treated 3xTg-AD animals. JZL184 (8 mg/kg), a monoacylglycerol lipase (MAGL) inhibitor, also induced such an effect (reduction 42%, $p < 0.05$) (Figure 2C). The treatments elicited subtle variations in memory (step-through latency) in 3xTg-AD mice, as shown in the Kaplan-Meier representation, although they did not reach statistical significance (Figure 2D).

3.4. CB_1 receptor desensitization induced by direct and indirect cannabinoids

[^{3}H]CP55,940 autoradiography revealed specific modifications in cerebral CB_1 receptor density following the subchronic eCB system activation. WIN55,212-2 (0.1 mg/kg) did not modify CB_1 receptor density, but WIN55,212-2 (1 mg/kg) induced a significant decrease in BLA (22%). Furthermore, the administration of JZL184 dramatically reduced the CB_1 receptor density, including cortical, hippocampal, and amygdaloid regions (Figures 2 and 5) (Tables 1 and S1). Functional [^{35}S]GTPγS autoradiography of CB_1 receptor activation showed a decrease of 24% and 32% in the BLA following treatment with WIN55,212-2 (1 mg/kg) and JZL184 (8 mg/kg), respectively (Figures 4 and 5) (Tables 2 and S2). The basal binding of [^{35}S]GTPγS was not modified by the different cannabinoid compounds, which probably indicates the absence of changes in the constitutive activity of G protein-coupled receptors (GPCR).

The regression analyses showed that 50% and 33% of the variation in the acquisition latencies recorded in 3xTg-AD mice were related to changes in CB_1 receptor density ([^{3}HCP55,940 binding) in the BLA ($r^2 = 0.5096$, $p = 0.0091$) and/or to changes in CB_1 receptor activity (evoked by WIN55,212-2) ($r^2 = 0.3299$, $p = 0.0508$), respectively (Figure 5). No statistically significant correlations were found when other brain areas were compared such as the lateral olfactory tract nucleus and glomerular olfactory bulb (p = ns). Both treatments, JZL184 (8 mg/kg) and WIN55,212-2 (1 mg/kg), decreased the acquisition latencies of 3xTg-AD mice to Non-Tg mice control values due to the pharmacological desensitization of CB_1 receptors to levels even lower than those observed in Non-Tg mice. When the groups were compared all together, a positive and statistically significant correlation between CB_1 receptor density in the BLA and acquisition latencies was found, showing that 25% of the acquisition latency variation may be explained by changes in CB_1 receptor density ($r^2 = 0.2499$, $p = 0.013$), but not by changes in CB_1 receptor activity (Figure 5).

3.5. Decreased M_2/M_4 mAChR-mediated activity in 3xTg-AD is modulated by cannabinoid administration

We analyzed the functional coupling of mAChR to $G_{i/o}$ proteins evoked by carbachol (100 µM) in both genotypes and in cannabinoid-based treated 3xTg-AD mice. Transgenic mice showed decreased functional coupling in the BLA ($p = 0.0258$), in the lateral amygdala ($p = 0.0303$) and hippocampal pyramidal CA1 ($p = 0.0227$). Moreover, increased M_2/M_4 mAChR receptor activity was found in the glomerular olfactory bulb ($p = 0.0095$) of 3xTg-AD mice. The administration of 1 mg/kg of WIN55,212-2 was able to increase the M_2/M_4 mAChR-mediated activity to similar values of Non-Tg mice; up to 60% in the BLA ($p < 0.05$ vs 3xTg-AD vehicle) and up to 100% in the lateral amygdala ($p < 0.01$ vs 3xTg-AD vehicle) (Figure 4). No modulation of M_2/M_4 mAChR-mediated activity was observed in other brain areas (Tables 3 and S3).

3.6. CB_1 receptors in BLA and M_2 mAChR in hippocampus colocalize with GABAergic terminals

The different nuclei of the amygdala exhibited distinct CB_1 receptor immunostaining patterns and were clearly defined. The dense CB_1 receptor immunoreactive puncta observed at the BLA suggested a presynaptic localization of CB_1 receptor. Immunofluorescence assays for VGLUT3 and GAD65 and the subsequent colocalization studies suggested the inhibitory nature of CB_1 receptor containing presynaptic boutons (Figure 6).

M_2 mAChR immunoreactivity was differentially localized along the hippocampal formation. The pyramidal neurons of CA1-CA3 displayed a dense network of fibers delineating the perikarya in basket-like formations. VGLUT3 displayed a somato-dendritic immunostaining, but GAD65 immunoreactivity was present as a dense plexus of fibers around pyramidal neurons with a similar distribution to M_2 mAChR. Colocalization studies showed the presence of M_2 mAChR in presynaptic GABAergic terminals with a high degree of co-immunoreactivity with GAD65, and an almost total absence of expression on VGLUT3 positive cells (Figure 7).

4. Discussion

Altered cannabinoid and muscarinic signaling is correlative to emotional learning and memory impairment in seven month-old 3xTg-AD mice

Changes in CB_1 receptors have recently been described in several brain areas of 3xTg-AD mice which are similar to the changes found in the brains of AD patients, rendering this model suitable for the study of the neuronal correlates (Bedse et al., 2014; Manuel et al., 2016). In the present study, we provide evidence of neuroanatomical and neurochemical modifications related to the eCB neuromodulatory system and muscarinic cholinergic signaling in the 3xTg-AD mice model, and of behavioral modifications at the onset of disease (7 months of age), when cognitive impairment is clearly established and is concurrent with limbic system mediated symptoms. The results point to the eCB system as a key element controlling neuronal homeostasis as well as the limbic component of cognition.

The results of behavioral assessment during the passive avoidance test, one typically used to evaluate learning and memory under anxiogenic conditions, may also be indicating the presence of fear and diminished motivation to explore as shown in a lesion rat model of AD (Babalola et al., 2012). 3xTg-AD mice had higher acquisition latency times than did controls. This is in agreement with the reduced exploratory activity and increased freezing behavior shown in the contextual fear-conditioning test, in the open field and in the passive avoidance test in this same transgenic mouse model of AD at 6 months of age (Gimenez-Llort et al., 2007; España et al., 2010; Filali et al., 2012). In addition, anxiety, fear, agitation and phobias may help to create a state of confusion which contributes to other behavioral disorders observed in AD patients, including learning and memory impairment (Ferretti et al., 2001; Aso and Ferrer, 2014).

The eCB system has emerged as a promising target for the treatment of several neurodegenerative disorders and has received a good deal of attention in AD. In this study, we report specific changes in density and in activity of CB_1 receptors, indicative of a potentiation of cannabinoid signaling in the BLA and an attenuation in the olfactory bulb and hippocampal dentate gyrus of transgenic mice. The specificity for CB_1 receptors was demonstrated by the anatomical pattern of distribution of [^{3}H]CP55,940 binding sites in brain, in comparison with that of spleen. [^{3}H]CP55,940 binding in 3xTg-AD and $CB_1^{+/+}$ mice was blocked by SR141716A and totally absent in $CB_1^{-/-}$ mouse brain. Indeed, SR144528, a specific CB_2 receptor antagonist, failed to block the binding in the brain but completely inhibited it in the spleen (where the CB_2 subtype is predominant) of both $CB_1^{+/+}$ and $CB_1^{-/-}$ mice. On the other hand, up-regulation of CB_2 receptors is reported to occur during neuroinflammation associated with

neurodegenerative processes (Benito et al., 2003; Tolón et al., 2009; Schmöle et al., 2015). Therefore, the absence of a CB_2 receptor-mediated signal in the CNS of seven month-old 3xTg-AD mice, is in agreement with the lack of neuritic plaque-associated neuroinflammation at the onset of disease. Our results coincide with those of studies which report a significant increase in CB_1 receptor density in BLA when only intracellular Aβ accumulation can be detected, and which may be related to the symptoms of fear and anxiety observed in these mice (España et al., 2010; Bedse et al., 2014).

Behavioral outcomes of 3xTg-AD mice after the subchronic administration of synthetic cannabinoids. Possible functional interplay with muscarinic cholinergic signaling

The present study examines for the first time the neurochemical effects of cannabinoid agonism in 3xTg-AD mice and their behavioral correlates in a learning and memory task, which may be relevant in terms of clinical interventions in humans at the onset of disease. The results provide evidence that CB_1 receptor activation, following repeated cannabinoid administration, was able to decrease the acquisition latency times in 3xTg-AD mice to Non-Tg levels during the learning trial, which may be related to the CB_1 receptor density desensitization recorded in the BLA. Stressing factors can result in a modulation of the endocannabinoid levels in the amygdala, and can also induce a subsequent CB_1 receptor-mediated suppression of GABA release in the BLA (Jenniches et al., 2015; Di et al., 2016; Morena et al., 2016). Interestingly, we observed both a down-regulation of CB_1 receptors and an attenuation of their functional coupling to $G_{i/o}$ proteins induced by the subchronic administration of JZL-184, comparable to the results obtained in a previous study, but at different doses (Kinsey et al., 2013). Moreover, the administration of WIN55,212-2 (1 mg/kg), decreases the acquisition latency times without significantly changing CB_1 receptor functionality in the BLA. Our results confirm previous findings which showed that JZL184 selectively increased brain 2-AG and also indicated that the inhibition of MAGL could be promising as a way to indirectly potentiate the activation of CB_1 receptors or CB_2 receptors (Busquets-Garcia et al., 2011; Kinsey et al., 2011). In this context, the pharmacological blockade or genetic deletion of MAGL dramatically raises brain 2-AG levels, down-regulates CB_1 receptor, and modulates synaptic plasticity, learning, memory and anxiety-like behavior (Pan et al., 2011). Accordingly, URB597, an AEA degrading enzyme inhibitor, induced CB_1 receptor-mediated anxiolytic effects in the elevated plus maze (Moise et al., 2008). Moreover, a recent study shows that the intra-BLA administration of both AEA and 2-AG hydrolysis inhibitors is able to attenuate anxiety-like responses, which are dependent on deregulated levels of eCB in the amygdala (Morena et al., 2016).

Conversely, chronic CB_1 receptor blockade induced up-regulation of CB_1 receptor expression, down-regulation in hippocampus, and modified anxiety-like behavior (Tambaro et al., 2013).

Depending on the specific location of CB_1 receptors in inhibitory or excitatory neurons, the functional and physiological outcomes of this deregulated endocannabinoid signaling may be useful to understand the present results. In order to address this issue immunochemical studies were performed and we found that in the BLA CB_1 receptor are more frequently located in GABAergic than in glutamatergic compartments, even though they have previously been detected in both of them (Kodirov et al., 2009; Ruehle et al., 2013; Shonesy et al., 2014; Robinson et al., 2016). The CB_1 receptors in BLA were located in the proximity of GAD65 (the enzyme glutamate decarboxylase; GAD, associated with inhibitory nerve termini) (Kash et al., 1999). In addition, the detection of VGLUT3 (the third subtype of glutamate vesicular transporter) has been used to identify both excitatory presynaptic boutons and glutamatergic somatodendritic compartments (Herzog et al., 2004). Although CB_1 receptors are present in both GABAergic and glutamatergic cellular compartments in areas such as the hippocampus, their activity could be lower in the inhibitory terminals (Steindel et al., 2013). However, in the BLA, CB_1 receptors are highly expressed in axon terminals of GABAergic neurons which modulate GABA release via a presynaptic mechanism (Katona et al., 2001). Some authors have related a long-lasting increase in anxiety-like behavior with a hyperactivity of BLA, as a consequence of a decrease in the inhibitory synaptic transmission (Almeida-Suhett et al., 2014). Thus, eCB-mediated suppression of inhibitory inputs to BLA neurons is involved in the cellular mechanism for stress-induced increases in anxiety-like behavior (Roozendaal et al., 2009). The genetic deletion of MAGL or GAD65 triggers an excitatory-inhibitory imbalance leading to increased anxiety-like responses (Imperatore et al., 2015; Müller et al., 2015). The glucocorticoid-induced suppression of inhibitory synaptic inputs to BLA principal neurons has recently been proposed as playing a pivotal role in the regulation of emotional disorders (Di et al., 2016). Globally, the present findings suggest that an up-regulation of the eCB tone in areas such as the BLA alters the local excitatory–inhibitory balance, and may be an underlying mechanism involved in the observed differences in cognitive behavior. Furthermore, a reversion to Non-Tg mice behavioral parameters was recorded after the attenuation of eCB signaling mediated by a pharmacological desensitization of CB_1 receptors. We propose that there is a CB_1 receptor-induced enhancement of the excitatory drive in brain areas such as the BLA due to the suppression of inhibition mediated by up-regulated CB_1 receptor signaling, which, by decreasing GABAergic neurotransmission, is an important component of the

neurobiological mechanisms that control some cognitive deficits observed in 3xTg-AD mice (acquisition latency).

Moreover, the administration of WIN55,212-2 (1 mg/kg), but not JZL-184, was able to induce a significant increase in the activity mediated by mAChR in the BLA, revealing a possible interaction between both systems in limbic areas. This specific CB_1 receptor-driven modulation of cholinergic neurotransmission in the amygdala could also be involved in the behavioral outcomes recorded with the passive avoidance test. In addition, these results support those of previous studies in which the role of the BLA cholinergic system, via mAChR, in memory retrieval in fear-induced learning was described (Malin et al., 2006; Nazarinia et al., 2017). Further behavioral studies are necessary in order to understand the meaning of CB_1 receptor-induced modulation of muscarinic control and its influence on acquisition latency, and to verify its validity as a possible indicator of anxiety, attention, agitation or states of confusion.

Regarding memory, step-through latency clearly distinguished the cognitively impaired AD-phenotype of 3xTg-AD mice, in accordance with previous studies (Clinton et al., 2007; Filali et al., 2012). Thus, 40% of 3xTg-AD mice did not remember the aversive stimulus received, while all the Non-Tg control mice did. However, under the present experimental conditions, we cannot rule out the possibility that the differences found in acquisition, or even putatively in consolidation, may also contribute to the performance of step-through latency. The desensitization of CB_1 receptors by means of subchronic administration of direct and indirect agonists failed to induce significant modifications in this variable. However, the analgesic effects of CB_1 receptor activation are well known (Meng et al., 1998). Subsequently, the pain threshold of the foot-shock in the passive avoidance test may be increased (Abush and Akirav, 2010). Therefore, the subtle variations in step-through latencies recorded after cannabinoid administration could be biased by the cannabinoid-induced analgesia. Further behavioral analyses by means of non-aversive stimulus-based learning and memory tests will help to clarify this question since 3xTg-AD mice do not seem to differ from Non-Tg in terms of pain thresholds (Filali et al., 2012; Baeta-Corral et al., 2015). However, the limbic system which is involved in cholinergic neurotransmission may be controlling specifically controls the consolidation and extinction of aversive or traumatic memories (Vazdarjanova and McGaugh, 1999).

3xTg-AD mice present deficits in cognition and synaptic plasticity associated with intraneuronal Aβ accumulation (Oddo et al., 2003). Muscarinic activation, through the M_2 mAChR subtype, promotes a rise in AMPA receptor sensitivity to glutamate, which finally leads to the so-called ‘muscarinic long term potentiation’ essential to explain hippocampal neuronal plasticity (Segal and Auerbach, 1997). Behavioral and

neurochemical studies in M_2 mAChR knockout mice showed that the lack of receptors was accompanied by cognitive impairment in the passive avoidance test (Tzavara et al., 2003). The present immunofluorescence studies revealed the presynaptic localization of M_2 mAChR in GABAergic terminals, presumably making contact with postsynaptic VGLUT3 immunoreactive pyramidal neurons in CA1-CA3. The present findings in 3xTg-AD mice are similar to those reported in rat brain, suggesting that ACh via M_2 mAChR may reduce GABA release from presynaptic inhibitory terminals, leading to increased activity in the dendritic region of pyramidal neurons (Levey et al., 1995; Hájos et al., 1998). The significant reduction in choline acetyltransferase activity described in hippocampus from middle-aged 3xTg-AD mice, but not associated with the loss of cholinergic neurons, may be related to the observed decrease in mAChR functionality (Perez et al., 2011). We suggest that intraneuronal accumulation of Aβ, beginning at 4 months of age, may trigger an early deregulation of the hippocampal muscarinic neurotransmission at the onset of disease, as observed in seven month-old 3xTg-AD mice, thereby contributing to the cognitive impairment observed in this model (Billings et al., 2005). Moreover, an excitatory/inhibitory imbalance mediated by a deregulated presynaptic muscarinic neurotransmission in the hippocampus may underlie the impaired synaptic plasticity, i.e. the neurobiological substrate for creating and maintaining new memories.

Conclusions.

We provide evidence that muscarinic and cannabinoid signaling is altered in seven month-old 3xTg-AD mice, showing a specific regional and neuronal distribution in vulnerable limbic areas at the onset of disease. CB_1 receptor-mediated hyperactivity in some specific brain areas may have behavioral correlates that correspond with the restoration to control levels after direct and indirect pharmacological desensitization of CB_1 receptors. Finally, decreased muscarinic neurotransmission may be involved in memory-related impairment in 3xTg-AD mice. We propose that CB_1 receptor desensitization is a plausible strategy to palliate specific behavioral impairment associated with genetic variants of AD.

6. *Tables*

Table 1. [^{3}H]CP55,940 binding in different brain areas of seven month-old Non-Tg and 3xTg-AD mice expressed in fmol/mg t.e. of CB_1 receptors.

	Non-Tg Vehicle	3xTg-AD Vehicle	3xTg-AD WIN55,212-2 [0.1 mg/kg]	3xTg-AD WIN55,212-2 [1 mg/kg]	3xTg-AD JZL184 [8 mg/kg]
Telencephalon					
Amygdala					
Anterior	209 ± 16	269 ± 16	240 ± 20	244 ± 19	209 ± 11
Basolateral	386 ± 12	497 ± 19***	469 ± 20	385 ± 32$	247 ± 14###a,b,c,d
Central	169 ± 6	216 ± 17	190 ± 27	211 ± 24	172 ± 12
Lateral	230 ± 10	253 ± 10	272 ± 29	246 ± 23	182 ± 16#c
Medial	121 ± 8	174 ± 16	155 ± 23	178 ± 24	122 ± 14
Hippocampus					
CA1	593 ± 38	607 ± 28	542 ± 30	473 ± 32	410 ± 25
Oriens	541 ± 36	592 ± 37	584 ± 30	486 ± 18	366 ± 28**b,c
Pyramidal	924 ± 75	909 ± 69	878 ± 42	679 ± 47$	529 ± 56**b,c
Radiatum	603 ± 56	613 ± 51	559 ± 29	482 ± 34	434 ± 44
CA3	591 ± 40	599 ± 19	543 ± 36	496 ± 24	396 ± 27
Oriens	545 ± 51	481 ± 39	499 ± 59	378 ± 32	394 ± 27
Pyramidal	885 ± 70	818 ± 65	763 ± 80	618 ± 67	599 ± 26*a,b
Radiatum	630 ± 89	596 ± 43	591 ± 58	487 ± 59	419 ± 45
Dentate gyrus	473 ± 37	487 ± 17	454 ± 26	434 ± 40	348 ± 22
Granular	922 ± 75	855 ± 49	836 ± 50	711 ± 27	574 ± 35**a,b,c
Molecular	569 ± 55	544 ± 48	489 ± 32	404 ± 30	371 ± 32
Polymorphic	272 ± 25	267 ± 33	224 ± 25	233 ± 19	189 ± 11
Subiculum	861 ± 86	909 ± 38	866 ± 53	712 ± 48	449 ± 56***a,b,c;*d
Cerebral cortex					
Cingular	286 ± 17	316 ± 15	332 ± 25	308 ± 15	247 ± 10*c
Ectorhinal	291 ± 28	321 ± 17	331 ± 32	308 ± 31	220 ± 16*b, c
Entorhinal	254 ± 21	276 ± 18	271 ± 17	254 ± 19	164 ± 12*b, c
Frontal	499 ± 17	427 ± 16	501 ± 22	415 ± 17	310 ± 10**a, c
Motor	340 ± 8	314 ± 13	347 ± 24	317 ± 20	241 ± 11**a, c; *b, d
Perirhinal	278 ± 32	302 ± 9	280 ± 23	271 ± 32	195 ± 13*b
Rhinencephalon					
Lat. olf. tract N	281 ± 40	424 ± 38*	389 ± 32	327 ± 22	239 ± 17##b,#c
Glom. olf. bulb	470 ± 8	304 ± 9***	293 ±15***	308 ± 19***	276 ± 12***

Data are expressed as mean ± S.E.M. *p<0.05, ***p<0.001 vs Non-Tg (vehicle). #p<0.05, ##p<0.01, ###p<0.001 vs Non-Tg (vehicle) (**a**); 3xTg-AD (vehicle) (**b**); 3xTg-AD (0.1 mg/kg WIN55,212-2) (**c**); 3xTg-AD (1 mg/kg WIN55,212-2) (**d**). $p<0.05 vs 3xTg-AD (vehicle).

Table 2. [^{35}S]GTPγS binding in different brain areas of seven-month-old Non-Tg and 3xTg-AD mice evoked by WIN55,212-2 (10 µM) expressed as percentage of stimulation over the basal binding.

	Non-Tg Vehicle	3xTg-AD Vehicle	3xTg-AD WIN55,212-2 [0.1 mg/kg]	3xTg-AD WIN55,212-2 [1 mg/kg]	3xTg-AD JZL184 [8 mg/kg]
Brain region					
Telencephalon					
Amygdala					
Anterior	82 ± 16	79 ± 16	68 ± 14	98 ± 16	89 ± 24
Basolateral	168 ± 24	281 ± 41*****	311 ± 42	213 ± 25	191 ± 31
Central	76 ± 28	61 ± 14	66 ± 17	58 ± 19	63 ± 21
Lateral	156 ± 26	197 ± 36	167 ± 45	159 ± 26	123 ± 23
Medial	35 ± 13	56 ± 9	100 ± 15	77 ± 20	89 ± 20
Hippocampus					
CA1	114 ± 17	63 ± 13	64 ± 6	61 ± 9.9	59 ± 8
Oriens	183 ± 40	164 ± 14	132 ± 11	178 ± 16	110 ± 19
Pyramidal	142 ± 23	165 ± 49	157 ± 15	151 ± 20	112 ± 22
Radiatum	144 ± 32	141 ± 34	105 ± 16	109 ± 16	53 ± 7$^{\#}$
CA3	154 ± 14	104 ± 19	105 ± 11	96 ± 15	116 ± 25
Oriens	143 ± 18	161 ± 17	134 ± 21	143 ± 16	121 ± 21
Pyramidal	94 ± 21	117 ± 22	135 ± 25	141 ± 23	82 ± 13
Radiatum	189 ± 51	123 ± 35	94 ± 19	89 ± 13	93 ± 13
Dentate gyrus	119 ± 17	70 ± 8	65 ± 8	62 ± 10	68 ± 12
Granular	293 ± 71	143 ± 20	193 ± 12	186 ± 36	152 ± 25
Molecular	199 ± 34	108 ± 18*****	99 ± 13	113 ± 8	112 ± 20
Polymorphic	261 ± 24	146 ± 20	104 ± 14	134 ± 13	112 ± 13
Ventral subiculum	162 ± 37	130 ± 21	106 ± 15	125 ± 18	127 ± 19
Cerebral cortex					
Cingular	90 ± 10	110 ± 14	102 ± 14	98 ± 10	69 ± 7
Ectorhinal	159 ± 37	131 ± 12	141 ± 21	115 ± 25	93 ± 19
Entorhinal	154 ± 27	165 ± 36	135 ± 22	180 ± 17	149 ± 20
Frontal	101 ± 14	114 ± 20	99 ± 13	115 ± 17	107 ± 15
Motor	108 ± 10	127 ± 18	93 ± 17	88 ± 6	87 ± 5
Perirhinal	168 ± 41	146 ± 29	127 ± 21	107 ± 21	85 ± 12
Striatum	134 ± 19	81 ± 8*****	80 ± 6	102 ± 10	73 ± 13
Rhinencephalon					
Lat. olf. tract N	221 ± 58	232 ± 71	230 ± 44	325 ± 61	326 ± 60
Glom. olf. bulb	580 ± 61	343 ± 18******	317 ± 41	391 ± 50	331 ± 22

Data are expressed as mean ± S.E.M.

*****p < 0.05 vs NonTg-vehicle; ******p < 0.01 vs NonTg (vehicle).

# p < 0.05 when compared to 3xTg-AD (vehicle).

Table 3. [^{35}S]GTPγS binding in different brain areas of seven-month-old Non-Tg and 3xTg-AD mice evoked by carbachol (100 µM) expressed as percentage of stimulation over the basal binding.

	NonTg Vehicle	3xTg-AD Vehicle	3xTg-AD WIN55.212-2 [0.1 mg/kg]	3xTg-AD WIN55.212-2 [1 mg/kg]	3xTg-AD JZL-184 [8 mg/kg]
Brain region					
Telencephalon					
Amygdala					
Anterior	89 ± 18.0	92 ± 21.1	128 ± 19.9	116 ± 9.7	82 ± 17.4
Basolateral	102 ± 13.7	55 ± 10.5*****	68 ± 16.0	97 ± 12.6#	71 ± 11.0
Central	43 ± 7.6	31 ± 9.5	40 ± 8.5	43 ± 5.9	53 ± 15.1
Lateral	96 ± 18.3	41 ± 11.3*****	43 ± 11.9	84 ± 9.1##	55 ± 8.1
Medial	66 ± 5.8	49 ± 14.6	31 ± 6.7	54 ± 10.0	46 ± 11.2
Hippocampus					
CA1	42 ± 6.6	21 ± 3.0*****	38 ± 8.5	39 ± 12.0	28 ± 7.6
Oriens	33 ± 6.9	29 ± 9.2	36 ± 7.6	59 ± 11.0	26 ± 8.7
Pyramidal	30 ± 6.0	16 ± 6.8*****	23 ± 6.1	34 ± 7.0	14 ± 4.8
CA3	43 ± 9.1	33 ± 6.4	43 ± 5.4	47 ± 15.1	46 ± 9.3
Oriens	30 ± 11.9	24 ± 9.9	27 ± 8.0	49 ± 11.7	27 ± 4.6
Pyramidal	34 ± 14.4	29 ± 5.2	28 ± 10.2	53 ± 15.0	33 ± 7.3
Dentate gyrus	34 ± 7.6	21 ± 4.7	28 ± 6.4	21 ± 5.2	21 ± 4.1
Granular	23 ± 8.8	26 ± 9.4	32 ± 10.5	19 ± 5.6	21 ± 6.4
Molecular	21 ± 6.2	19 ± 4.4	16 ± 13.2	17 ± 4.2	8 ± 3.1
Polymorphic	16 ± 15.1	24 ± 5.2	3 ± 12.3	23 ± 13.2	11 ± 5.7
Cerebral cortex					
Cingular	62 ± 12.2	64 ± 13.0	54 ± 9.6	68 ± 10.9	58 ± 9.5
Ectorhinal	39 ± 14.8	42 ± 11.7	38 ± 12.8	46 ± 8.7	37 ± 5.2
Entorhinal	41 ± 12.9	30 ± 13.6	27 ± 9.2	37 ± 11.3	34 ± 8.8
Frontal	54 ± 17.9	57 ± 11.8	42 ± 8.9	68 ± 11.9	57 ± 9.6
Motor	59 ± 10.9	56 ± 12.1	50 ± 10.7	59 ± 11.5	46 ± 8.5
Perirhinal	46 ± 6.7	40 ± 4.7	43 ± 9.8	45 ± 5.4	51 ± 12.5
Rhinencephalon					
Lat. olf. tract N	173 ± 22.3	107 ± 15.9*****	125 ± 14.3	140 ± 19.9	112 ± 8.2
Glom. olf. bulb	193 ± 25.9	295 ± 14.9*****	312 ± 45.0	279 ± 53.7	266 ± 37.6

Data are expressed as mean ± S.E.M.
*****p < 0.05 compared to Non-Tg (vehicle)
#p < 0.05; ##p < 0.01 when compared to 3xTg-AD (vehicle).

7. References

Almeida-Suhett, C.P., Prager, E.M., Pidoplichko, V., Figueiredo, T.H., Marini, A.M., Li, Z., Eiden, L.E., Braga, M.F., 2014. Reduced GABAergic inhibition in the basolateral amygdala and the development of anxiety-like behaviors after mild traumatic brain injury. PLoS One 9(7), e102627.

Abush, H., Akirav, I., 2010. Cannabinoids modulate hippocampal memory and plasticity. Hippocampus 20(10),1126-1138.

Aso, E., Ferrer, I., 2014. Cannabinoids for treatment of Alzheimer's disease: moving toward the clinic. Front. Pharmacol. 5:37.

Babalola, P.A., Fitz, N.F., Gibbs, R.B., Flaherty, P.T., Li, P.K., Johnson, D.A., 2012. The effect of the steroid sulfatase inhibitor (p-O-sulfamoyl)-tetradecanoyl tyramine (DU-14) on learning and memory in rats with selective lesion of septal-hippocampal cholinergic tract. Neurobiol. Learn. Mem. 98(3), 303-310.

Baeta-Corral, R., Defrin, R., Pick, C.G., Giménez-Llort, L., 2015. Tail-flick test response in 3×Tg-AD mice at early and advanced stages of disease. Neurosci. Lett. 600,158-163.

Barreda-Gómez, G., Lombardero, L., Giralt, M.T., Manuel, I., Rodríguez-Puertas, R., 2015. Effects of galanin subchronic treatment on memory and muscarinic receptors. Neuroscience 293, 23-34.

Bartus, R.T., Dean, R.L., Beer, B., Lippa, A.S., 1982. The cholinergic hypothesis of geriatric memory dysfunction. Science 217(4558), 408-414.

Bedse, G., Romano, A., Cianci, S., Lavecchia, A.M., Lorenzo, P., Elphick, M.R., Laferla, F.M., Vendemiale, G., Grillo, C., Altieri, F., Cassano, T., Gaetani, S., 2014. Altered expression of the CB1 cannabinoid receptor in the triple transgenic mouse model of Alzheimer's disease. J. Alzheimers Dis. 40(3), 701-712.

Bedse, G., Romano, A., Lavecchia, A.M., Cassano, T., Gaetani, S., 2015. The role of endocannabinoid signaling in the molecular mechanisms of neurodegeneration in Alzheimer's disease. J. Alzheimers Dis. 43(4), 1115-1136.

Benito, C., Núñez, E., Tolón, R.M., Carrier, E.J., Rábano, A., Hillard, C.J., Romero, J., 2003. Cannabinoid CB2 receptors and fatty acid amide hydrolase are selectively overexpressed in neuritic plaque-associated glia in Alzheimer's disease brains. J. Neurosci 23(35), 11136-11141.

Billings, L.M., Oddo, S., Green, K.N., McGaugh, J.L., LaFerla, F.M., 2005. Intraneuronal Abeta causes the onset of early Alzheimer's disease-related cognitive deficits in transgenic mice. Neuron 45, 675-688.

Busquets-Garcia, A., Puighermanal, E., Pastor, A., de la Torre, R., Maldonado, R., Ozaita, A., 2011. Differential role of anandamide and 2-arachidonoylglycerol in memory and anxiety-like responses. Biol. Psychiatry 70(5), 479-486.

Clinton, L.K., Billings, L.M., Green, K.N., Caccamo, A., Ngo, J., Oddo, S., McGaugh, J.L., LaFerla, F.M., 2007. Age-dependent sexual dimorphism in cognition and stress response in the 3xTg-AD mice. Neurobiol. Dis. 28(1):76-82.

Cummings, J.L., Back, C., 1998. The cholinergic hypothesis of neuropsychiatric symptoms in Alzheimer's disease. Am. J. Geriatr. Psychiatry 6(2 Suppl 1), S64-78. Review.

Cummings, J., Lai, T.J., Hemrungrojn, S., Mohandas, E., Yun Kim, S., Nair, G., Dash, A., 2016. Role of donepezil in the management of neuropsychiatric symptoms in Alzheimer's disease and dementia with Lewy bodies. CNS Neurosci. Ther. 1-8.

Davies, P., Maloney, A.J., 1976. Selective loss of central cholinergic neurons in Alzheimer's disease. Lancet 2, 1403.

Di, S., Itoga, C.A., Fisher, M.O., Solomonow, J., Roltsch, E.A., Gilpin, N.W., Tasker, J.G., 2016. Acute Stress Suppresses Synaptic Inhibition and Increases Anxiety via Endocannabinoid Release in the Basolateral Amygdala. J. Neurosci. 36(32), 8461-8470.

España, J., Giménez-Llort, L., Valero, J., Miñano, A., Rábano, A., Rodriguez-Alvarez, J., LaFerla, F.M., Saura, C., 2010. Intraneuronal beta-amyloid accumulation in the amygdala enhances fear and anxiety in Alzheimer’s disease transgenic mice. Biol. Psychiatry 67, 513-521.

Ferretti, L., McCurry, S.M., Logsdon, R., Gibbons, L., Teri, L., 2001. Anxiety and Alzheimer's disease. J. Geriatr. Psychiatry Neurol. 14, 52–58.

Filali, M., Lalonde, R., Theriault, P., Julien, C., Calon, F., Planel, E., 2012. Cognitive and non-cognitive behaviors in the triple transgenic mouse model of Alzheimer’s disease expressing mutated APP, PS1, and Mapt (3xTg-AD). Behav. Brain Res. 234, 334–342.

Giménez-Llort, L., Blázquez, G., Cañete, T., Johansson, B., Oddo, S., Tobeña, A., LaFerla, F.M., Fernández-Teruel, A., 2007. Modeling behavioral and neuronal

symptoms of Alzheimer's disease in mice: a role for intraneuronal amyloid. Neurosci Biobehav. Rev. 31, 125-147.

Hájos, N., Papp, E.C., Acsády, L., Levey, A.I., Freund, T.F., 1998. Distinct interneuron types express m2 muscarinic receptor immunoreactivity on their dendrites or axon terminals in the hippocampus. Neuroscience 82(2), 355-376.

Herzog, E., Gilchrist, J., Gras, C., Muzerelle, A., Ravassard, P., Giros, B., Gaspar, P., El Mestikawy, S., 2004. Localization of VGLUT3, the vesicular glutamate transporter type 3, in the rat brain. Neuroscience 123(4), 983-1002.

Imperatore, R., Morello, G., Luongo, L., Ulrike, T., Romano, R., De Gregorio, D., Belardo, C., Maione, S., Di Marzo, V., Cristino, L., 2015. Genetic deletion of monoacylglycerol lipase leads to impaired cannabinid receptor CB_1R signaling and anxiety-like behavior. J. Neurochem. 135, 77-813.

Jenniches, I., Ternes, S., Albayram, O., Otte, D.M., Bach, K., Bindila, L., Michel, K., Lutz, B., Bilkei-Gorzo, A., Zimmer, A., 2015. Anxiety, stress, and fear response in mice with reduced endocannabinoid levels. Biol. Psychiatry 79, 858-868.

Kash, S.F., Tecott, L.H., Hodge, C., Baekkeskov, S., 1999. Increased anxiety and altered responses to anxiolytics in mice deficient in the 65-kDa isoform of glutamic acid decarboxylase. Proc. Natl. Acad. Sci. USA 96, 1698–1703.

Katona, I., Rancz, E.A., Acsady, L., Ledent, C., Mackie, K., Hajos, N., Freund, T.F., 2001. Distribution of CB1 cannabinoid receptors in the amygdala and their role in the control of GABAergic transmission. J. Neurosci. 21(23), 9506-9518.

Kinsey, S.G., O'Neal, S.T., Long, J.Z., Cravatt, B.F., Lichtman, A.H., 2011. Inhibition of endocannabinoid catabolic enzymes elicits anxiolytic-like effects in the marble burying assay. Pharmacol. Biochem. Behav. 98(1), 21-27.

Kinsey, S.G., Wise, L.E., Ramesh, D., Abdullah, R., Selley, D.E., Cravatt, B.F., Lichtman A.H., 2013. Repeated low-dose administration of the monoacylglycerol lipase inhibitor JZL184 retains cannabinoid receptor type 1-mediated antinociceptive and gastroprotective effects. J. Pharmacol. Exp. Ther. 345(3), 492-501.

Kodirov, S.A., Jasiewicz, J., Amirmahani, P., Psyrakis, D., Bonni, K., Wehrmeister, M., Lutz, B., 2009. Endogenous cannabinoids trigger the depolarization-induced suppression of excitation in the lateral amygdala. Learn. Mem. 17(1), 43-49.

Levey, A.I., Edmunds, S.M., Koliatsos, V., Wiley, R.G., Heilman, C.J., 1995. Expression of m1-m4 muscarinic acetylcholine receptor proteins in rat hippocampus and regulation by cholinergic innervation. J. Neurosci. 15(5 Pt 2):4077-4092.

Machová, E., Jakubík, J., Michal, P., Oksman, M., Iivonen, H., Tanila, H., Dolezal, V., 2008. Impairment of muscarinic transmission in transgenic APPswe/PS1dE9 mice. Neurobiol. Aging 29(3), 368-378.

Malin, E.L., McGaugh, J.L., 2006. Differential involvement of the hippocampus, anterior cingulate cortex, and basolateral amygdala in memory for context and footshock. Proc. Natl. Acad. Sci. USA 103(6), 1959-1963.

Manuel, I., González de San Román, E., Giralt, M.T., Ferrer, I., Rodríguez-Puertas, R., 2014. Type-1 cannabinoid receptor activity during Alzheimer's disease progression. J. Alzheimers Dis. 42(3), 761-766.

Manuel, I., Lombardero, L., LaFerla, F.M., Giménez-Llort, L., Rodríguez-Puertas, R., 2016. Activity of muscarinic, galanin and cannabinoid receptors in the prodromal and advanced stages in the triple transgenic mice model of Alzheimer's disease. Neuroscience 329, 284-293.

Meng, I.D., Manning, B.H., Martin, W.J., Fields, H.L., 1998. An analgesia circuit activated by cannabinoids. Nature 395(6700), 381-383.

Moise, A.M., Eisenstein, S.A., Astarita, G., Piomelli, D., Hohmann, A.G., 2008. An endocannabinoid signaling system modulates anxiety-like behavior in male Syrian hamsters. Psychopharmacology (Berl) 200(3), 333-346.

Morena, M., Leitl, K.D., Vecchiarelli, H.A., Gray, J.M., Campolongo, P., Hill, M.N., 2016. Emotional arousal state influences the ability of amygdalar endocannabinoid signaling to modulate anxiety. Neuropharmacology 111:59-69.

Müller, I., Çalışkan, G., Stork, O., 2015. The GAD65 knock out mouse – a model for GABAergic processes in fear- and stress-induced psychopathology. Genes Brain Behav. 14(1), 37-45.

Nazarinia, E., Rezayof, A., Sardari, M., Yazdanbakhsh, N., 2017. Contribution of the basolateral amygdala NMDA and muscarinic receptors in rat's memory retrieval. Neurobiol. Learn. Mem. 139, 28-36.

Nelson, R.L., Guo, Z., Halagappa, V.M., Pearson, M., Gray, A.J., Matsuoka, Y., Brown, M., Martin, B., Iyun, T., Maudsley, S., Clark, R.F., Mattson, M.P., 2007. Prophylactic treatment with paroxetine ameliorates behavioral deficits and retards the development of amyloid and tau pathologies in 3xTgAD mice. Exp. Neurol. 205(1), 166-176.

Oddo, S., Caccamo, A., Shepherd, J.D., Murphy, M.P., Golde, T.E., Kayed, R., Metherate, R., Mattson, M.P., Akbari, Y., LaFerla, F.M., 2003. Triple-transgenic model

of Alzheimer's disease with plaques and tangles: intracellular Abeta and synaptic dysfunction. Neuron 39, 409-421.

Pan, B., Wang, W., Blankman, J.L., Cravatt, B.F., Liu, Q.S., 2011. Alterations of endocannabinoid signaling, synaptic plasticity, learning, and memory in monoacylglycerol lipase knock-out mice. J. Neurosci. 31(38), 13420-13430.

Perez, S.E., He, B., Muhammad, N., Oh, K.J., Fahnestock, M., Ikonomovic, M.D., Mufson, E.J., 2011. Cholinotrophic basal forebrain system alterations in 3xTg-AD transgenic mice. Neurobiol. Dis. 41(2), 338-352.

Perry, E.K., Tomlinson, B.E., Blessed, G., Bergmann, K., Gibson, P.H., Perry, R.H., 1978. Correlation of cholinergic abnormalities with senile plaques and mental test scores in senile dementia. Br. Med. J. 2, 1457-1459.

Pietropaolo, S., Feldon, J., Yee, B.K., 2014. Environmental enrichment eliminates the anxiety phenotypes in a triple transgenic mouse model of Alzheimer's disease. Cogn. Affect. Behav. Neurosci. 14(3), 996-1008.

Rasool, S., Martinez-Coria, H., Wu, J.W., LaFerla, F., Glabe, C.G., 2013. Systemic vaccination with anti-oligomeric monoclonal antibodies improves cognitive function by reducing Aβ deposition and tau pathology in 3xTg-AD mice. J. Neurochem. 126(4), 473-482.

Robinson, S.L., Alexander, N.J., Bluett, R.J., Patel, S., McCool, B.A., 2016. Acute and chronic ethanol exposure differentially regulate CB1 receptor function at glutamatergic synapses in the rat basolateral amygdala. Neuropharmacology 108, 474-484.

Rodríguez-Puertas, R., Pazos, A., Zarranz, J.J., Pascual, J., 1994. Selective cortical decrease of high-affinity choline uptake carrier in Alzheimer's disease: an autoradiographic study using 3H-hemicholinium-3. J. Neural Transm. Park. Dis. Dement. Sect 8, 161-169.

Rodríguez-Puertas, R., Pascual, J., Vilaró, T., Pazos, A., 1997. Autoradiographic distribution of M1, M2, M3, and M4 muscarinic receptor subtypes in Alzheimer's disease. Synapse 26, 341-350.

Roozendaal, B., McReynolds, J.R., Van der Zee, E.A., Lee, S., McGaugh, J.L., McIntyre, C.K., 2009. Glucocorticoid effects on memory consolidation depend on functional interactions between the medial prefrontal cortex and basolateral amygdala. J. Neurosci. 29, 14299 –14308.

Ruehle, S., Remmers, F., Romo-Parra, H., Massa, F., Wickert, M., Wörtge, S., Häring, M., Kaiser, N., Marsicano, G., Pape, H.C., Lutz, B., 2013. Cannabinoid CB1 receptor in

dorsal telencephalic glutamatergic neurons: distinctive sufficiency for hippocampus-dependent and amygdala-dependent synaptic and behavioral functions. J. Neurosci. 33(25), 10264-10277.

Schmöle, A.C., Lundt, R., Ternes, S., Albayram, Ö., Ulas, T., Schultze, J.L., Bano, D., Nicotera, P., Alferink, J., Zimmer, A., 2015. Cannabinoid receptor 2 deficiency results in reduced neuroinflammation in an Alzheimer's disease mouse model. Neurobiol. Aging 36(2), 710-719.

Segal, M., Auerbach, J.M., 1997. Muscarinic receptors involved in hippocampal plasticity. Life Sci. 60(13-14), 1085-1091.

Shonesy, B.C., Bluett, R.J., Ramikie, T.S., Báldi, R., Hermanson, D.J., Kingsley, P.J., Marnett, L.J., Winder, D.G., Colbran, R.J., Patel, S., 2014. Genetic disruption of 2-arachidonoylglycerol synthesis reveals a key role for endocannabinoid signaling in anxiety modulation. Cell Rep. 9(5), 1644-1653.

Steindel, F., Lerner, R., Häring, M., Ruehle, S., Marsicano, G., Lutz, B., Monory, K., 2013. Neuron-type specific cannabinoid-mediated G protein signalling in mouse hippocampus. J. Neurochem. 124(6), 795-807.

Tambaro, S., Tomasi, M.L., Bortolato, M., 2013. Long-term CB_1 receptor blockade enhances vulnerability to anxiogenic-like effects of cannabinoids. Neuropharmacology 70, 268-277.

Tolón, R.M., Núñez, E., Pazos, M.R., Benito, C., Castillo, A.I., Martínez-Orgado, J.A., Romero, J., 2009. The activation of cannabinoid CB2 receptors stimulates in situ and in vitro beta-amyloid removal by human macrophages. Brain Res. 1283, 148-154.

Tzavara, E.T., Bymaster, F.P., Felder, C.C., Wade, M., Gomeza, J., Wess, J., McKinzie, D.L., Nomikos, G.G., 2003. Dysregulated hippocampal acetylcholine neurotransmission and impaired cognition in M2, M4 and M2/M4 muscarinic receptor knockout mice. Mol. Psychiatry 8(7), 673-679.

Vazdarjanova, A., McGaugh, J.L., 1999. Basolateral amygdala is involved in modulating consolidation of memory for classical fear conditioning. J. Neurosci. 19(15), 6615-6622.

Westlake, T.M., Howlett, A.C., Bonner, T.I., Matsuda, L.A., Herkenham, M., 1994. Cannabinoid receptor binding and messenger RNA expression in human brain: an in vitro receptor autoradiography and in situ hybridization histochemistry study of normal aged and Alzheimer's brains. Neuroscience 63(3), 637-652.

Whitehouse, P.J., Price, D.L., Struble, R.G., Clark, A.W., Coyle, J.T., Delon, M.R., 1982. Alzheimer's disease and senile dementia: loss of neurons in the basal forebrain. Science 215, 1237-1239.

8. Acknowledgements

This work was supported by the Departments of Economic Development (Elkartek KK-2016/00045) and Education (IT975-16) of the Basque Government. Technical and human support provided by General Research Services SGIker from University of the Basque Country (UPV/EHU), co-financed by Ministry of Economy and Competitiveness (MINECO) of the Spanish Government, European Regional Development Fund (ERDF), and European Social Fund (ESF). Dr. Frank M LaFerla, University of California Irvine, Irvine, CA, (USA) for kindly providing the progenitors of the Spanish colonies of 3xTg-AD and non-transgenic mice. A. LL. is the recipient of a fellowship from the Basque Government (BFI 2012-119). The authors declare no conflict of interest.

9. Figure captions

Figure 1. Synopsis of the experimental design including treatment schedule and behavioral assessment.

Figure 2. Passive avoidance test and CB_1 receptor binding sites. (A) Acquisition latency times during the learning trial in both genotypes in the absence of treatment; ***p < 0.01 vs Non-Tg. (B) Step-through latency times in both genotypes represented as Kaplan-Meier survival curves. (C) 3xTg-AD mice treated with different cannabinoid agonists. The subchronic administration of WIN55,212-2 (1 mg/kg) and JZL184 (8 mg/kg) for seven consecutive days triggered a statistically significant decrease in the acquisition latency compared to that obtained in the Non-Tg group; * p < 0.05 vs 3xTg-AD mice treated with vehicle. (D) Step-through latency times in 3xTg-AD mice represented as Kaplan-Meier survival curves. The probability is plotted over the step-through latency in 3xTg-AD mice after different cannabinoid-based treatments. (E) [^{3}H]CP55,940 binding autoradiography in representative brain coronal slices from both genotypes treated with vehicle and from 3xTg-AD treated with either WIN55,212-2 (1 mg/kg) or JZL184 (8 mg/kg). Note that both pharmacological treatments decreased the density of receptors in the whole grey matter including the basolateral amygdala (BLA) (boxed area). [^{3}H]-microscales used as standards in µCi/g t.e. (n = 9-10 mice/group). Scale bar: 5 mm.

Figure 3. [^{3}H]CP55,940 binding autoradiography in brain and spleen. The image show the cannabinoid receptor distribution in brain and spleen samples from 3xTg-AD, CB_1 receptor knockout ($CB_1^{-/-}$) and wild type ($CB_1^{+/+}$) mice. The total binding is shown in the top row, displaying the characteristic and well-described distribution of cannabinoid receptors in the brain, and surrounding the lymphatic nodules (white pulp) in the spleen. In the presence of 0.1 µM of SR141716A, a CB_1 receptor specific antagonist, binding is almost completely blocked in the brain but not in the spleen (middle row) while 0.1 µM of SR144528, a CB_2 receptor specific antagonist, completely displaced the [^{3}H]CP55,940 binding in the spleen without affecting the binding in the brain (bottom row). Note the absence of binding in the brain from $CB_1^{-/-}$ and the identical distribution in the spleen from both Non-Tg and knockout mice, revealing the preponderance of CB_1 receptors in the brain and CB_2 receptors in spleen tissue, and the specificity of the cannabinoid antagonists. Scale bar = 5 mm.

Figure 4. [^{35}S]GTPγS autoradiography. [^{35}S]GTPγS binding evoked by both WIN55,212-2 (10 µM) for cannabinoid receptors (A-D) and carbachol (100 µM) for M_2/M_4 muscarinic acetylcholine receptors (mAChR) (E-H), in representative coronal brain slices from Non-Tg and 3xTg-AD mice treated with vehicle and cannabinoid agonists. The highest CB_1 receptor stimulation was found in the hippocampus, the most caudal portion of the globus pallidus, the deeper layers of the cortex, and the amygdaloid complex. Thus, in the amygdala, the latero-basolateral region (boxed area) (A-D) seems to be the most activated, displaying a hyperactivation in 3xTg-AD (B) mice, which is attenuated with both cannabinoids (C-D). Moreover, deregulation of mAChR functionality in 3xTg-AD mice was found. Note the decrease in the latero-basolateral region and in the pyramidal layer of the hippocampal CA1 region (boxed areas) (F) and the potentiation of muscarinic signaling in the amygdala following the subchronic administration of 1 mg/kg of WIN55,212-2 (G). [^{14}C]-microscales used as standards in µCi/g t.e. Scale bar: 5 mm.

Figure 5. CB_1 receptor-mediated signaling and behavior. [^{3}H]CP55,940 binding in the BLA in both genotypes treated with vehicle (A) and in 3xTg-AD mice treated with WIN55,212-2 (0.1 mg/kg or 1 mg/kg) or JZL184 (8 mg/kg) (B). Correlation analyses between the CB_1 receptor density in the BLA and the acquisition latency times of both genotypes (C) and of 3xTg-AD mice after cannabinoid treatments (D). Note that data are grouped according to both, genotype and treatment. Quantification of CB_1 receptor stimulation (% over basal activity) evoked by WIN55,212-2 (10 µM) in the BLA of both genotypes (E) and of 3xTg-AD mice treated with WIN55,212-2 (0.1 mg/kg or 1 mg/kg) or JZL184 (8 mg/kg) (F). Correlation analyses between the endocannabinoid signaling in the BLA and the acquisition latency times of both genotypes (G) and of 3xTg-AD mice after cannabinoid treatments (H). Note that data are grouped according to genotype and not to treatment (n = 6 mice/group). *****$p < 0.05$; ******$p < 0.01$ and ****** $p < 0.001$; two-tailed unpaired Student's *t* test.

Figure 6. Localization of CB_1 receptors in the BLA. Double labeling of tissue slices including the amygdaloid complex from seven month-old 3xTg-AD mice processed for CB_1 receptor (in green) and vesicular glutamate transporter type 3 (VGLUT3) (A2 and C2 in red) as a glutamatergic marker, and glutamic acid decarboxylase isoform 65kDa (GAD65) (B2 and D2 in red) as a GABAergic presynaptic marker. The different amygdaloid nuclei exhibited specific CB_1 receptor-immunostaining patterns. VGLUT3 was distributed presumably in postsynaptic somatodendritic compartment (A2 and C2) while GAD65 immunostaining was clearly delineated presynaptic inhibitory boutons (B2

and D2). In low magnification images, note the distribution of CB_1 receptors surrounding positive glutamatergic neurons (A3) and sharing localization with GAD65 (B3); scale bar: 150 µm. High magnification images showed the intracellular localization of VGLUT3 (C2) closely surrounding the nuclei stained with Hoechst (C3 in blue) revealing the almost complete lack of colocalization with CB_1 receptors (C4). Conversely, CB_1 receptors were located on GAD65-positive terminals (D4), revealing its presynaptic localization on inhibitory synaptic boutons. Scale bar = 10 µm. Bregma -1.82 mm. CeL central amygdaloid nucleus, lateral division; La lateral amygdaloid nucleus; BLA basolateral amygdaloid nucleus, anterior part; BLP basolateral amygdaloid nucleus, posterior part; BMP basomedial amygdaloid nucleus, posterior part.

Figure 7. Localization of M_2 mAChR in the hippocampus. Double labeling of tissue slices including the CA1 field of the hippocampus from a representative 7-month-old 3xTg-AD mouse processed for M_2 mAChR (in red) and VGLUT3 (A1 and C1 in green) as a glutamatergic marker, and GAD65 (B1 and D1 in green) as a GABAergic presynaptic marker (B). The different hippocampal subfields exhibited specific M_2 mAChR-immunostaining patterns delineating the perikarya of the large pyramidal neurons in basket-like formations. VGLUT3 was distributed near the nucleus (A1 and C1), presumably in the somatodendritic compartment of pyramidal neurons, while GAD65 immunostaining (B1 and D1) clearly delineated presynaptic inhibitory boutons. In low magnification images, note that M_2 mAChR-immunoreactivity showed a complementary distribution to VGLUT3, surrounding the pyramidal neurons (A3), and was localized in GAD65-positive presynaptic terminals (B3); scale bar: 150 µm. High magnification images revealed the intracellular localization of VGLUT3 (C1) closely surrounding the nuclei stained with Hoechst (C3 in blue) and the almost complete lack of colocalization with M_2 mAChR (C4). Conversely, M_2 mAChR was distributed in GAD65-positive terminals, revealing the presynaptic localization on inhibitory synaptic boutons (C4). Scale bar = 10 µm. Bregma -3.08 mm. Alv alveus of the hippocampus; Or oriens layer of the hippocampus; Py pyramidal cell layer of the hippocampus; Rad radiatum layer of the hippocampus; LMol lacunosum molecular layer of the hippocampus.

10. Figures

Figure 1

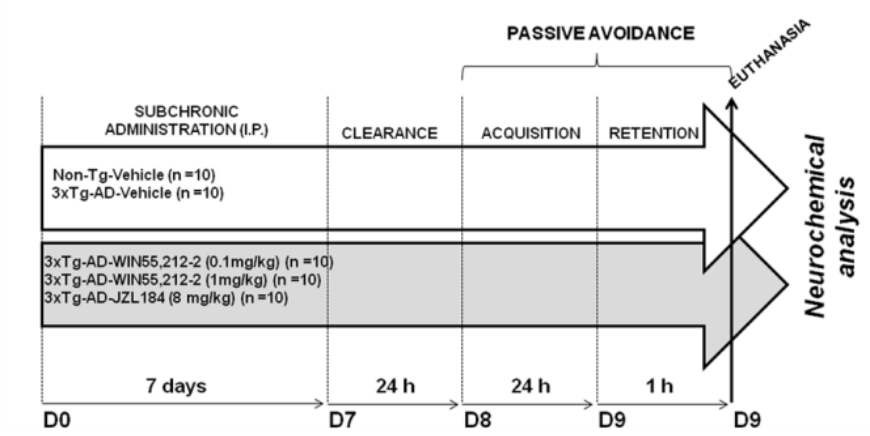

Figure 2

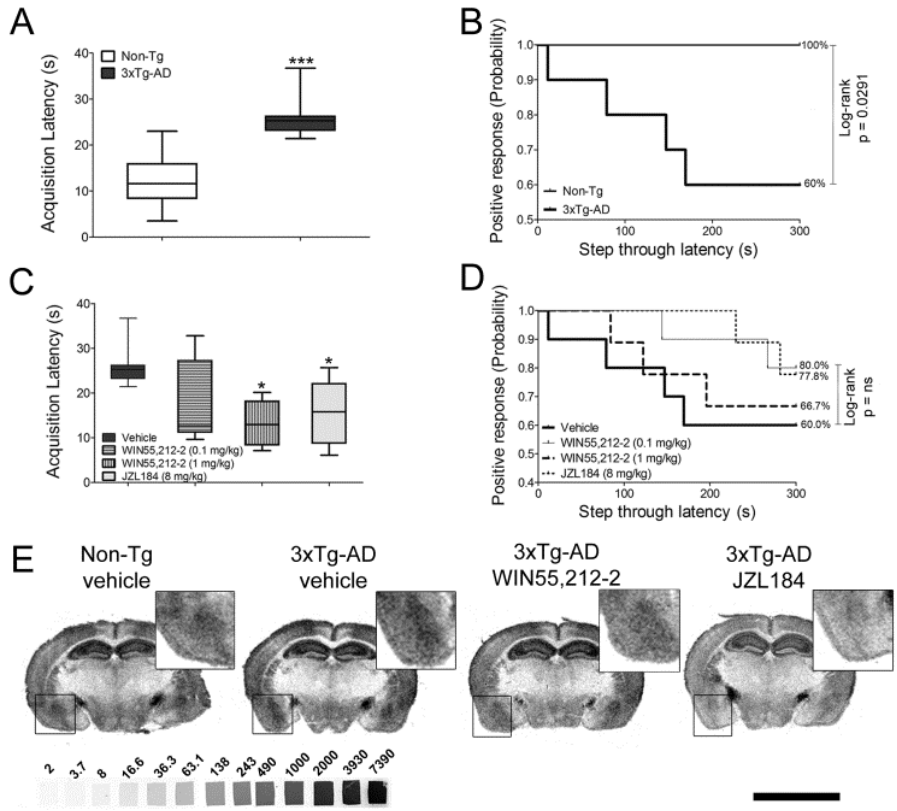

Figure 3

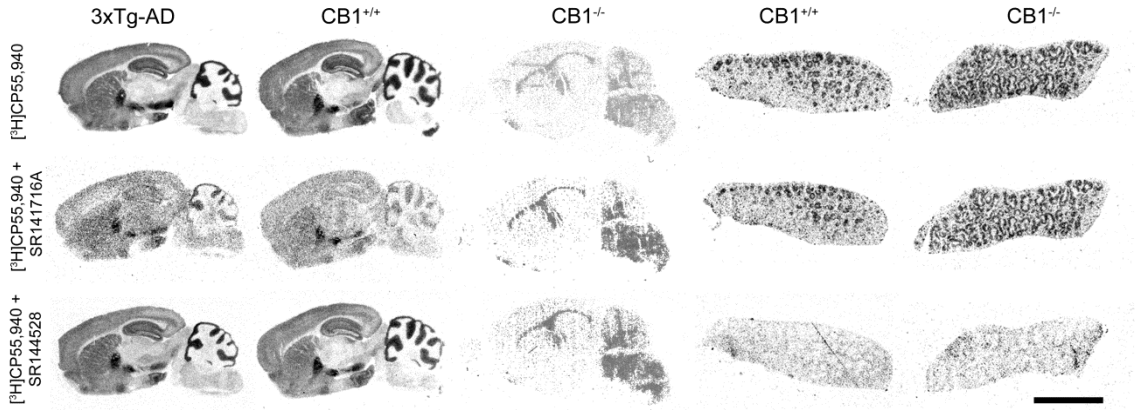

Figure 4

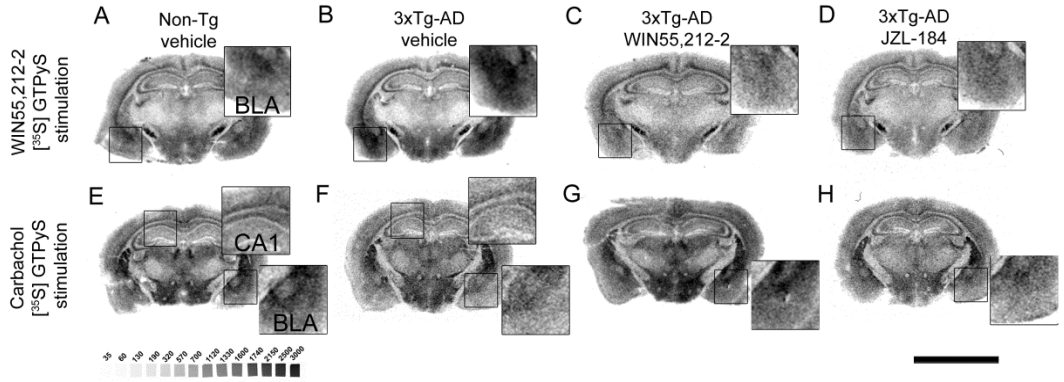

Figure 5

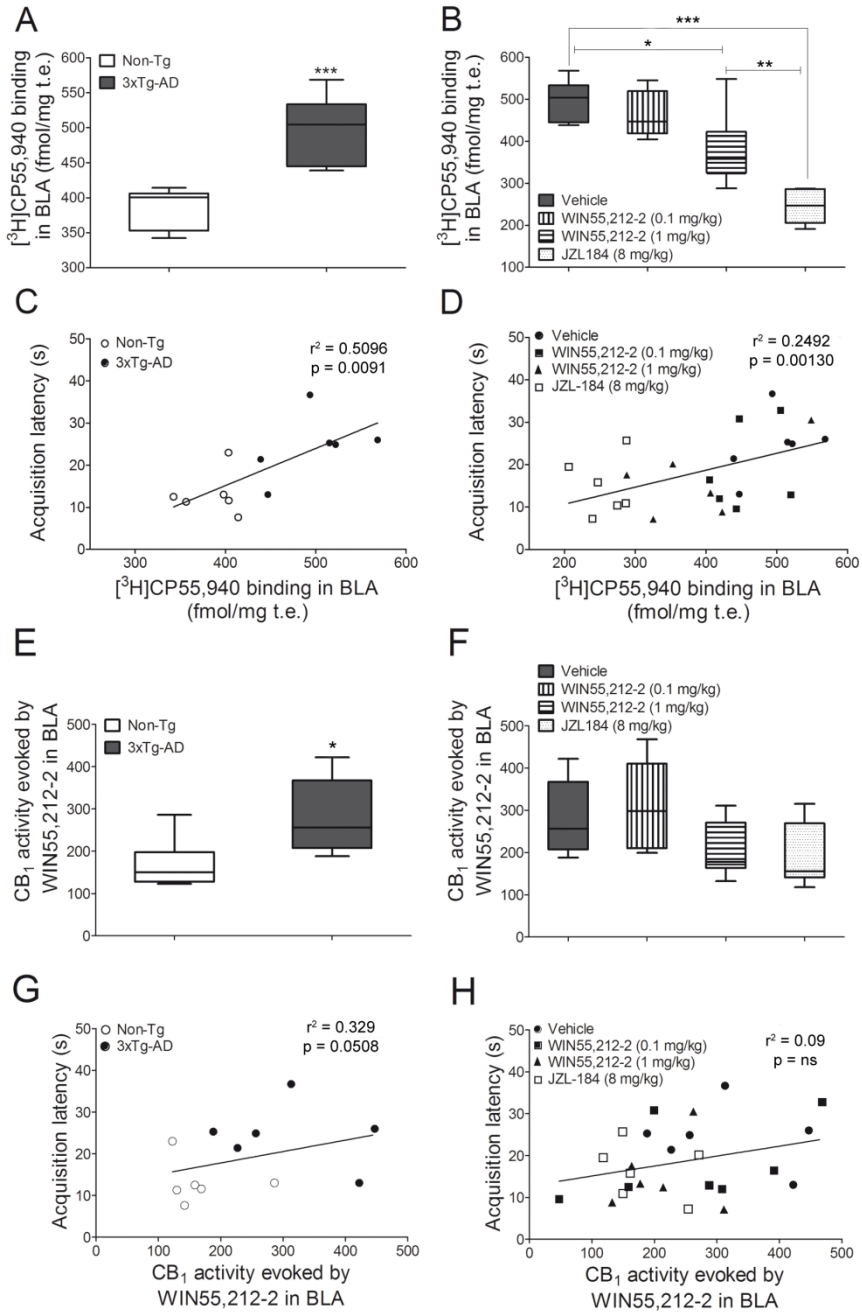
A
[3H]CP55,940 binding in BLA (fmol/mg t.e.)
Non-Tg
3xTg-AD
***
B
[3H]CP55,940 binding in BLA (fmol/mg t.e.)
***
*
**
Vehicle
WIN55,212-2 (0.1 mg/kg)
WIN55,212-2 (1 mg/kg)
JZL184 (8 mg/kg)
C
Acquisition latency (s)
Non-Tg
3xTg-AD
r2 = 0.5096
p = 0.0091
[3H]CP55,940 binding in BLA (fmol/mg t.e.)
D
Acquisition latency (s)
Vehicle
WIN55,212-2 (0.1 mg/kg)
WIN55,212-2 (1 mg/kg)
JZL-184 (8 mg/kg)
r2 = 0.2492
p = 0.00130
[3H]CP55,940 binding in BLA (fmol/mg t.e.)
E
CB1 activity evoked by WIN55,212-2 in BLA
Non-Tg
3xTg-AD
*
F
CB1 activity evoked by WIN55,212-2 in BLA
Vehicle
WIN55,212-2 (0.1 mg/kg)
WIN55,212-2 (1 mg/kg)
JZL184 (8 mg/kg)
G
Acquisition latency (s)
Non-Tg
3xTg-AD
r2 = 0.329
p = 0.0508
CB1 activity evoked by WIN55,212-2 in BLA
H
Acquisition latency (s)
Vehicle
WIN55,212-2 (0.1 mg/kg)
WIN55,212-2 (1 mg/kg)
JZL-184 (8 mg/kg)
r2 = 0.09
p = ns
CB1 activity evoked by WIN55,212-2 in BLA

Figure 6

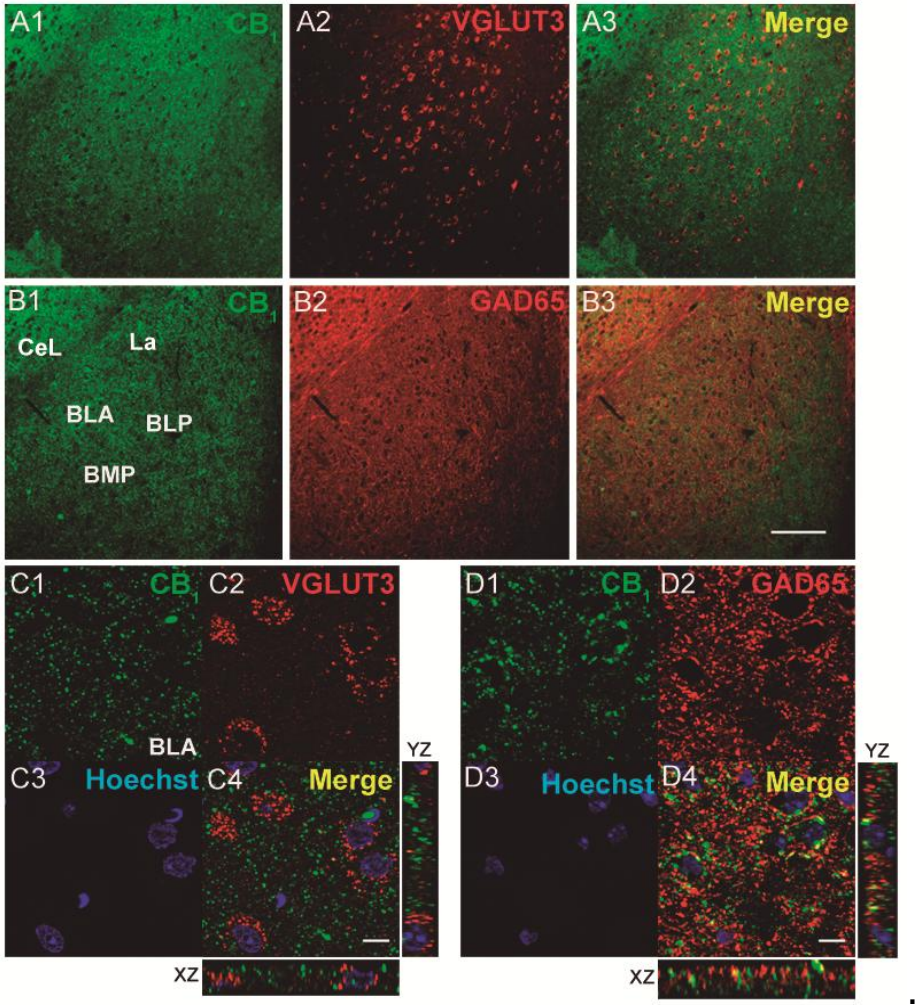
A1
CB1
A2
VGLUT3
A3
Merge
B1
CB1
CeL
La
BLA
BLP
BMP
B2
GAD65
B3
Merge
C1
CB1
C2
VGLUT3
BLA
C3
Hoechst
C4
Merge
YZ
XZ
D1
CB1
D2
GAD65
D3
Hoechst
D4
Merge
YZ
XZ

Figure 7

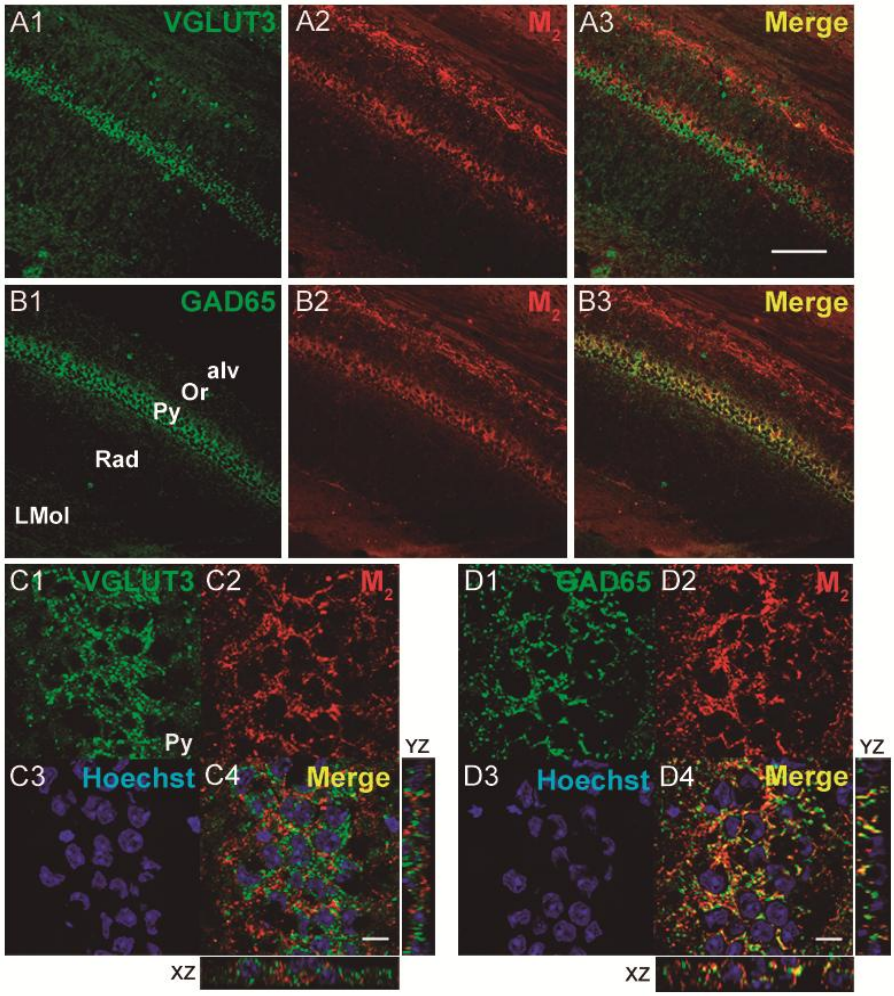
A1
VGLUT3
A2
M2
A3
Merge
B1
GAD65
alv
Or
Py
Rad
LMol
B2
M2
B3
Merge
C1
VGLUT3
C2
M2
Py
YZ
C3
Hoechst
C4
Merge
XZ
D1
GAD65
D2
M2
YZ
D3
Hoechst
D4
Merge
XZ